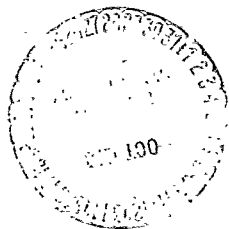NASA TM X- **6534**

SUPER-HIGH-FREQUENCY (SHF) COMMUNICATIONS SYSTEM PERFORMANCE ON ATS

VOLUME 2: DATA AND ANALYSIS

AUGUST 1970

GSFC ——— **GODDARD SPACE FLIGHT CENTER** ———
GREENBELT, MARYLAND

SUPER-HIGH-FREQUENCY (SHF)

COMMUNICATIONS SYSTEM

PERFORMANCE ON ATS

VOLUME 2: DATA AND ANALYSIS

Prepared by:
Westinghouse Electric Corporation
and
The ATS Project Office

August 1970

GODDARD SPACE FLIGHT CENTER
Greenbelt, Maryland

This report consists of two volumes. Volume 1, System Summary (X-460-70-299), contains section 1 only (section 2 was deleted). Volume 2, Data and Analysis (X-460-70-300), contains sections 3, (4 deleted), 5, 6, and 7.

TABLE OF CONTENTS

TABLE OF CONTENTS (Continued)

LIST OF ILLUSTRATIONS

LIST OF TABLES

3. DATA ANALYSIS

Contained within this section are detailed analyses of the various SHF experiments. These experiments were performed at the three ground stations, utilizing both ATS-1, ATS-3, and ATS-5, and the test results were recorded during actual test runs.

Subsequent paragraphs contain individual analyses of these experiments. The analyses are based on an evaluation of large quantities of data obtained under various controlled and uncontrolled conditions. The statistical approach used in obtaining meaningful conclusions is described in detail in section 7.3 of this report.

3.1 PATH-LOSS EXPERIMENTS

3.1.1 RF SIGNAL POWER LEVELS AND PROPAGATION LOSSES (J. G. McGillen)
(MA-AT-1.1, MA-AT-1.2, FT-AT-1.1, MA-RF-1.1, MA-RF-1.2, MA-RF-1.3, FT-RF-1.1, FT-RF-1.2)

3.1.1.1 Description and Test Results

The objective of this experiment is to evaluate and obtain accurate methods for determining path losses (uplink and downlink) for both modes of the ATS-SHF system. Measuring techniques will be different for the SSB/PhM mode than for the Frequency-Translation mode. A secondary objective is to evaluate the importance of antenna beam position on the path-loss calculation.

In the analysis of the test data, a computation of the path-loss factor is performed using the line-of-sight range between the ground station and the satellite, and the uplink and downlink operational frequencies. These computed values are called the predicted path-loss factors, and the path-loss values determined from the test data are called the measured path-loss factors. The parameters in this experiment are:

1) Transmitter Output $(P_t + G_t)_g$ - Effective radiated power per test tone (MA mode-SSB); Effective total radiated power (FT mode-FM)

2) Satellite Received Power $(P_r - G_r)_s$ - Test-tone power at satellite antenna (MA mode), total power at satellite antenna (FT mode)

3) Uplink Path Loss (U_u)

4) Satellite Transmitter Power $(P_t + G_t)_s$ - Effective total radiated power (both modes)

5) Ground-Receiver Input Power $(P_r - G_r)_g$ - Total power at receive antenna

6) Downlink Path Loss (U_d).

The relationship between transmitted and received powers in a communications link is as follows:

$$P_r = \frac{P_t \ G_t \ G_r \ \lambda^2}{16_\pi{}^2 \ R^2 \ L} = \frac{P_t \ G_t \ G_r}{U}$$

where:

P_r = Received power at the receiver input terminals

P_t = Transmitted power at the power amplifier output terminals

G_t = Transmitting antenna gain, including losses between the power amplifier and the antenna

G_r = Receiving antenna gain, including losses between the antenna and the receiver input (e.g., parametric amplifier input for the ground receiver)

λ = Wavelength

R = Range

$\dfrac{16\pi^2 R^2}{\lambda^2}$ = Free space loss

L = Other path losses, such as rain

$U = \dfrac{16\pi^2 R^2 L}{\lambda^2}$ = Total path loss

In decibels, the equation can be written

$$P_r = P_t + G_t + G_r - U$$

where U is regarded as a positive number (e.g., 150 db). From this equation

$$U_u = (P_t + G_t)_g - (P_r - G_r)_s \text{ and}$$
$$U_d = (P_t + G_t)_s - (P_r - G_r)_g$$

If R is expressed in nautical miles and the operating frequency in MHz, free space loss can be predicted as follows:

Free space loss = 37.85 + 20 log R + 20 log f

While the path losses should be identical for the SSB/PhM and FT modes, the results have been separated due to the difference in power measurement techniques for P_{rg}. Data is also presented on an individual station and satellite basis as the path-loss values should vary slightly due to variations in range.

The satisfactory test results obtained to date are presented by station, satellite, and operational mode (MA or FT) in table 3.1. The table also shows the calculated mean value of uplink and downlink path loss obtained from the measured transmitted and received power levels for the specified number of test runs. This calculated value is used as the best estimate of the measured path-loss value. The predicted values are obtained from the free space-loss calculation. The predicted values do not take into account atmospheric losses of free oxygen absorption and vapor absorption. These losses are a function primarily of elevation angle, as well as weather conditions. Also, the atmospheric losses are an increasing function with frequency in C-band.

3.3

3.1.1.2 Analysis

In the limited number of test runs on ATS-1 from Rosman and Mojave, the deviation between measured and predicted values for the uplink path loss is generally greater than that obtained by Cooby Creek. This may be expected, however, when it is noted that Cooby Creek has over 40 test runs for both the FT and MA mode from which the mean may be determined. For both ATS-1 and ATS-3, the maximum deviation from any station between the computed measured mean value and the predicted value is 3.0 db. The single measurement on ATS-5 in the MA mode shows correlation within 1.3 db.

In the uplink path-loss calculation, satellite received power (P_{rs}) is measured in the FT mode by a power detector in the spacecraft and its value transmitted to ground via telemetry. In the MA mode, P_{rs} is measured indirectly by monitoring the peak-to peak amplitude of a received tone at the output of the ground receiver. A calibration curve that relates the above amplitude to P_{rs} is employed for this measurement. This technique is possible because of the unique manner (SSB/PhM) in which the uplink MA mode of operation is instrumented. To date, the data shown in table 3.1 does not show any consistent difference between the two modes.

P_{rs} is measured in the MA mode on ATS-5 which has a spinning antenna, by noting the deviation of the PhM downlink during the burst of received signal measured when the S/C antenna is pointing towards the earth. The technique involves synchronizing a spectrum analyzer to sweep only during the peak of the spacecraft antenna beam pattern. When the first sideband equals the carrier power of the IF downlink spectrum, the modulation index is equal to 1.435 radians. By knowing the spacecraft modulator deviation constant, the spacecraft-received signal power may be calculated.

The downlink path-loss values for Cooby Creek are shown in table 3.1. Starting with test data acquired January 19, 1968, spacecraft Antenna Beam Position (ABP) for ATS-1 in most cases is recorded. From this, the off-beam center allowance can be calculated for any ground station. This telemetry data is available only for the ATS-1 spacecraft.

From knowledge of the spacecraft ABP, the off-beam center allowance may be determined by finding the stations position in the beam cross-section pattern. While the inflight spacecraft three-dimensional transmit antenna beam pattern has not been measured, an adequate approximation can be obtained by assuming a parabola in both elevation and azimuth sections and an ellipse in cross section. Where the ABP data has been available, the correction for assumed antenna gain has been modified and used to correct measured downlink path-loss values. As shown in table 3.1, the use of this correction factor increases correlation in both the FT and MA modes from 2 db to within 1 db.

The lack of ABP data on ATS-3 makes an accurate determination of the off-beam center allowance impossible. An allowance of up to 2 db is made when it is indicated that the stations have not optimized the beam prior to running the test. This could account in part for the somewhat higher path-loss values measured for ATS-3.

While an ABP readout was not considered essential on ATS-3 due to the complexity and resultant size and weight of such a system, it is apparent from the above data that such a system is required in order to realize accurate results. This is more true in the case of ATS-3 than ATS-1 in that on ATS-3,both the transmit and receive antennas are oriented by the same control system. Errors, therefore, are reflected in both the measured uplink and downlink path losses. On ATS-1, with its broad beam from the collinear receive array, the full antenna gain is easily realized.

Excellent correlation has been attained on downlink measurements on ATS-5,to date, using the synchronizing technique mentioned above. The mean value is only 0.6 db higher than the predicted.

Measured path-loss variations, within a test run, of approximately 1 db have been observed in manual and automated tests. These variations are due to variations in P_{rs} and P_{rg}. Time records for these two factors show a distinct 1.6-Hz frequency component exists in the continuous plot. This frequency is equal to the spin rate of the satellite. The P_{rg} variations within a test run are caused by variations in G_{ts}. This latter factor is supposed to be held constant by the PACE or MACE system which nullifies the spinning effects of the satellite. The one-db variation in P_{rg} can be taken as a figure of merit for the PACE and MACE Antenna Control Systems.

3.1.1.3 Conclusions

The best estimates for uplink and downlink path losses for ATS-1, ATS-3, and ATS-5 are presented in table 3.1. For ATS-1, the data from the Cooby Creek ground station shows excellent correlation between measured and predicted values with a maximum deviation of 0.6 db for the uplink path loss and 0.8 db for the downlink value. Correlation of the down-link measured values has been enhanced by correcting for off-beam center allowance.

On ATS-1 for the uplink path loss, the main reason for the deviations has been the inaccuracies in measuring P_{tg} and P_{rs}. The indirect method of measuring P_{rs} in the MA mode and AGC method in the FT mode,both show comparable measurement errors.

Test results on ATS-3 show a slightly larger deviation than ATS-1 data. Rosman shows 3.0-db maximum deviation on the uplink and 2.5-db maximum on the downlink. Mojave measurements indicate 1.9 db on the uplink and 3.0 db on the downlink.

The larger deviation for the ATS-3 uplink data is due in part to the assumed value for G_{rs}. The much narrower receiving antenna beam on ATS-3 results in a loss of gain when not positioned properly. With the broad receiving beam on ATS-1, the actual maximum gain is truly being realized.

For the downlink path loss, the measurement errors in P_{rg} and the assumed value for G_{ts} are the main cause of the deviations. The present method of employing C/N

measurements to obtain P_{rg} in place of AGC calibration readings shows an improved correlation between measured and predicted values for this parameter. The lack of ABP data makes an accurate determination of G_{ts} impossible.

Good correlation has been obtained between the predicted and measured path loss values when operating with ATS-5.

TABLE 3.1. SUMMATION OF MEASURED AND PREDICTED PATH-LOSS VALUES
FOR MANUAL TESTS (ATS-1, ATS-3, AND ATS-5)

Station	Satel-lite	Mode	Uplink Path Loss		90% Confidence Interval (db)	Number of test Runs	Downlink Path Loss		90% Confidence Interval	Number of test Runs
			Predicted* (db)	Mea. Mean (db)			Predicted* (db)	Mea. Mean (db)		
Rosman	1	FT	200.8	202.0	±2.36	5	197.1	196.9	±1.85	5
Rosman	1	MA	200.8	202.5	±0.79	6	197.1	197.5	±3.6	3
Mojave	1	FT	200.3	199.7	±0.925	7	196.6	197.9	±2.92	6
Mojave	1	MA	200.3	201.3	±1.38	9	196.6	198.5	±1.69	10
Cooby	1	FT	200.6	201.2	±0.39	47	196.9	199.0	±0.42	49
								197.7**	±0.54	32
Cooby	1	MA	200.6	200.8	±0.36	45	196.9	198.9	±0.50	42
								197.7**	±0.74	20
Rosman	3	FT	200.0	203.0	±0.46	20	196.3	198.6	±0.545	22
Rosman	3	MA	200.0	202.7	±0.76	18	196.3	198.8	±0.66	17
Mojave	3	FT	200.2	202.1	±0.66	12	196.5	199.5	±0.24	18
Mojave	3	MA	200.2	201.7	±0.88	13	196.5	197.5	±0.86	11
Mojave	5	MA	199.9	201.2		1	196.3	196.9		1

*Predicted values are based upon frequencies of 6301-MHz uplink and 4179-MHz downlink for Rosman, otherwise frequencies of 6212-MHz uplink and 4120-MHz downlink are used.
**Corrected for Off-Beam Center Allowance.

3.2 MULTIPLEX IF/RF AND BASEBAND PERFORMANCE EXPERIMENTS

3.2.1 BASEBAND NOISE POWER RATIO (MA-BB-1.1 and FT-BB-1.1) (E.E. Crampton)

3.2.1.1 Description and Test Results

OBJECTIVE

      The objectives of this experiment are to: (1) Determine the noise characteristics of the SSB-FDMA/PhM (multiple access, MA) and FM-FDM/FM (frequency translation, FT) modes of operation, and (2) Determine the optimum test tone-to-noise (TT/N) for the various ATS earth station/spacecraft configurations.

      The optimum TT/N ratios, the noise power ratio (NPR) should be maximum; therefore, the following relationships are developed to evaluate the effect of various system parameters on optimum system performance:

    1) Test tone-to-noise due to modulation ($TT/(I + \triangle$) and test tone-to-idle noise $TT/R + N_i$) as a function of channel loading and baseband frequency for the ATS system configurations listed below:

      a) Earth station antennas: 85 feet at Rosman, and 40 feet at Mojave and Cooby Creek.

      b) Spacecraft EIRP: ranges from 49.4 dbm to 56.5 dbm.

    2) Optimum channel test tone level for most efficient use of spacecraft/earth station configurations.

TEST CONDITIONS

      The following test conditions are applicable to this analysis:

    1) Mode of operation - Each test was performed in one of two modes; multiple access SSB-PhM (MA), or frequency translation (FT).

    2) System Configuration - All experiments were separated into various ground station-satellite groups (e.g., Rosman and ATS-3). Each group provides manual test data for single station tests. The data varies between groups due to differences in ground station G/T values and satellite radiated power (EIRP).

    3) Controlled parameters - Table 3.2 lists the nominal system parameters which were controlled for the FDM tests.

    4) Uncontrolled variables - The uncontrolled variables that have the most significant effect on system performance are path loss variations, S/C antenna pointing, and system noise temperature. The effect of these variables may be partially offset by normalizing NPR and TPR data to a particular

carrier-to-noise ratio, (C/N), as discussed in paragraph 7.6.1. Also weekly system noise temperature is presented as supplementary data to this section.

STANDARDS

The recommended standards relating to user requirements for an FDM telephone channel are defined in terms of channel test tone (TT)-to-noise ratio which is related to the NPR of the multiplex channel by system constants; namely, channel bandwidth, channel loading, and channel bandwidth weighting. Therefore, no conclusions regarding user requirements will be presented in this paragraph. For an equivalent TT/N (F1A weighted) of 50 db, the NPR is: Rosman, 30.5 db, Mojave and Cooby Creek, 30.8 db. These values are obtained by using the equations given in subsection 7.5.2.

TABLE 3.2. NOMINAL SYSTEM PARAMETERS FOR FDM BASEBAND TESTS

Parameter	Station	
	Rosman (85-Ft antenna) (See Note 1)	Mojave and Cooby Creek (40-Ft antenna)
Channel Spectrum (No. of channels)	1200	240
Baseband Channel Spectrum (kHz)	316-5564	316-1300
Channel Loading* (dbm0)	15.8	8.8
Receiver IF Bandwidth		
(3 db) (MHz)	30 nominal	12 nominal
(Noise Bandwidth) (MHz)	35.5	15.5
FDM Channel Bandwidth (kHz)	3.1	3.1
Channel Weighting (F1A) (db)	3.0	3.0
Peak Deviation of Carrier (FT Mode)		
per channel (kHz)	690	1230
Total Baseband** (MHz)	9.6	7.6
Spacecraft Received Power		
SSB-PhM Mode (Per Channel) (dbm)	-87.0	-87.0
FT Mode (Total) (dbm)	-73.0	-73.0
Peak Test Tone Modulation Index		
At Spacecraft (SSB-PhM Mode)		
(Per Channel) (Radians)	0.35	0.35
Total Baseband (Radians) **	4.84	2.12

NOTE 1 - Mojave is also capable of 1200 channel operation with ATS-3.

 * The CCIR recommended noise loading for N channels is applied to a baseband spectrum of N channels. Refer to paragraph 7.6.3 (System Loading) for a complete discussion of the FDM Multiplex System Loading.

** Calculation assumes a peak to rms factor of 10 db.

TEST RESULTS

NOISE CHARACTERISTICS

Following is a list of figures which show the baseband noise characteristics in both the FT and MA modes. Both idle (no modulation) and loaded (with modulation) conditions are included.

Figure 3.1   (FT Mode, idle noise spectrum at various
                      C/N ratios)

Figure 3.2   (FT Mode, loaded noise spectrum with sinusoidal
                      modulation at various C/N ratios)

Figure 3.3   (FT Mode, effect of CCIR 240 and 1200 channel
                      telephony de-emphasis on idle noise spectrum)

Figure 3.4   (FT Mode, 1200 channel intermodulation noise
                      spectrum derived from multitone testing)

Figures 3.5   (MA Mode, noise spectrum for idle and nominal 1200
and 3.6   channel white noise modulation)

Figures 3.7   (MA Mode, individual noise spectrums at various
through 3.9   C/N ratios for sinusoidal modulation)

Figure 3.10   (MA Mode, 1200 channel intermodulation noise
                      spectrum derived from multitone testing)

The following list of figures show the results of several one tone, two tone, and three tone tests for the MA mode as well as the FT mode which were performed on ATS-3. These figures show the harmonic or intermodulation products relative to the power of the fundamental tones used in these tests.

Figure 3.11   (Mojave, MA, two station – two-tone test)

Figure 3.12   (Rosman, MA Mode two station – two-tone test)

Figures 3.13   (Rosman, MA Mode, one, two, and three-tone tests)
through 3.15

Figures 3.16   (Mojave, MA Mode, one, two, and three-tone tests)
through 3.18

Figures 3.19   (Rosman, FT Mode, one-and two-tone tests)
and 3.20

Figures 3.21   (Mojave, FT Mode, two-and three-tone tests)
and 3.22

Figures 3.23 and 3.24 show typical group delay measurements through ATS-3 repeaters for the Mojave and Rosman earth stations. Also shown in these figures are the first two terms of the group delay expansion continuous function about 70 MHz.

SYSTEM OPTIMIZATION

SSB-PhM (MA) MODE

The figures in the following list show the loaded noise power ratio (NPR), idle noise power ratio (TPR), and test tone-to-noise ratio (TT/N) (idle and loaded conditions) as a function of test tone power for various channels across the baseband. Also shown, as a function of test tone power, is the test tone-to-intermodulation noise plus △ noise (the △ noise component is only significant at low carrier-to-noise ratios). The ordinate of these curves represent the mean values of several test runs. A single curve representing the channel frequencies is shown whenever the mean NPR or TPR were within ±0.5 db for several channels.

Figures 3.25 and 3.26	(Cooby Creek, ATS-1, 52.2 dbm EIRP)
Figures 3.27 and 3.28	(Mojave, ATS-1, 52.2 dbm EIRP)
Figures 3.29 and 3.30	(Mojave, ATS-3, 54.6 dbm EIRP)
Figure 3.31	(Rosman, ATS-1, 52.2 dbm EIRP)
Figure 3.32	(Rosman, ATS-3, 52.2 dbm EIRP)

The following figures show the NPR values versus the variation of test tone power for five different values of loaded baseband bandwidth (B_n) corresponding to 180 channels, 240 channels, 600 channels, 960 channels, and 1200 channels. Also shown is the optimum operating point for each B_n.

Figures 3.33 and 3.34	(Rosman, ATS-3)
Figure 3.35	(Mojave, ATS-1)
Figure 3.36	(Cooby Creek, ATS-1)

Figures 3.37, 3.38, 3.39, and 3.40 show the relative signal power spectrums as well as the SSB transmitter power output at the optimum test tone level for each loading bandwidth, B_n.

Table 3.3 presents a summary of link performance limitations. The table indicates whether the system is uplink or downlink limited (or optimized, arbitrarily defined

for purposes of this analysis as when the uplink and downlink test tone-to-noise performances are within 2 db of each other). The table also indicates whether intermodulation or thermal noise is the limiting factor within the channel. Table 3.4 presents a summary of baseband performance, at both optimum test tone power as well as nominal test tone power. Also shown in this table is the change in test tone power from nominal required to optimize the system for the various conditions tested. Measured downlink C/N ratios for various test conditions are also given (S/C antenna is beamed to the sub-satellite point for these tests).

FT MODE

The figures presented in this section represent the mean values of numerous tests. The following is a list of figures which show the NPR/TPR ratios, TT/N ratio, and TT/(I + $\triangle$) ratio as a function of test tone level. The optimum test tone level is also shown.

Figures 3.41	(Mojave, ATS-3)
and 3.42	
Figures 3.43	(Mojave, ATS-1)
and 3.44	
Figures 3.45	(Rosman, ATS-3)
and 3.46	

Figure 3.47 shows a typical comparison between FM (with and without pre/de-emphasis) and PhM using the FT mode on ATS-3.

Table 3.5 presents a summary of link performance limitations. The table indicates whether the system is uplink or downlink limited (or optimized when the uplink and downlink test tone-to-noise performances are within 2 db of each other). The table also indicates which noise component is the limiting factor in the total link for either the high or low channel. The user requirements as they apply to the ATS system are discussed extensively in paragraph 3.4.1, and are directly applicable to this analysis.

Table 3.6 summarizes TT/N (loaded) and NPR performance in both the high and low channels for nominal and optimum test tone level. In these tables the change in test tone power necessary to optimize system performance is also included. Table 3.6 presents a summary of performance with and without CCIR recommendation 275-1 (Oslo, 1966) for pre/de-emphasis circuits.

SYSTEM NOISE TEMPERATURE

The figures presented in this section are a time record on a weekly basis of the noise temperature for the three stations. Figure 3.48 is the time plot for the three stations when operating with ATS-1. Figure 3.49 gives the time plot for Mojave and Rosman when operating with ATS-3.

3.2.1.2 Analysis

This analysis is divided into three sections: NOISE CHARACTERISTICS, SYSTEM OPTIMIZATION, and SYSTEM NOISE TEMPERATURE. In the NOISE CHARACTERISTICS section the significant types of noise in the ATS system are presented and discussed. The SYSTEM OPTIMIZATION section presents test tone-to-noise ratios as a function of test tone level and discusses variations of the noise characteristics as the test tone level approaches the point at which maximum test tone-to-noise is reached (optimum operating point). Also included in this section is system optimization for other than 240 and 1200 channel loading. The SYSTEM NOISE TEMPERATURE section presents the system noise temperature variation over approximately a 3-year period on a weekly basis.

NOISE CHARACTERISTICS

In theory, the output noise characteristics of an FM or PhM receiver are developed in terms of an input carrier-to-noise (C/N) ratio to the discriminator and system non-linearities. Practically, C/N ratio is dependent on several factors, but primarily spacecraft EIRP and earth station G/T ratio. In the ATS system, spacecraft EIRP ranges from 49.4 dbm to 56.5 dbm while the earth stations obtain G/T theoretical ratios of 32.2 and 39.6 db for parabolic antennas of 40 feet and 85 feet in diameter, respectively. At the extremes, for example, in a multi-station configuration using ATS-1 (EIRP of 52.2 dbm) with 1200-channel loading, both Cooby Creek and Mojave (G/T ratios of 32.2 db) operate with a C/N ratio near 7 db. Rosman (G/T ratio of 39.6), on the other hand, when using ATS-3 (EIRP of 56.6 dbm) operates with a C/N ratio near 20 db. To analyze the FT and SSB-PhM (MA) modes of operation over this range of C/N ratios, the noise characteristics are discussed in terms of four significant components. These components are intermodulation noise (I), thermal noise (R) and threshold noises (N_i) and ($\triangle$) and are defined as follows:

(I)   =   Intermodulation noise which varies with the degree and form of modulation and is caused by system non-linearities, but is not a function of C/N ratio.

(R)   =   Thermal noise which varies linearly with decreasing C/N_o (carrier-to-noise density ratio).

(N_i) =   Threshold noise due to impulse (or "click") noise that is a function of C/N and varies in a non-linear manner with C/N.

($\triangle$) =   Threshold noise due to impulse noise that is not only a function of C/N (varies in a non-linear manner with C/N ratio) but also the degree and form of modulation employed.

At low C/N ratios (7 to 10 db), the threshold components (N_i) and ($\triangle$) or ($N_i + \triangle$) are predominant in the lower portion of the baseband. In the intermediate range of C/N ratios,

3.13

which for the ATS system is 11 to 15 db, thermal noise (R) predominates. At high C/N ratios (20 db), intermodulation noise (I) predominates since the other noise components, which are a function of the C/N ratio, become insignificant. In the following analysis, the measured noise characteristics are presented and their effect on multiplex channel performance is discussed in more detail.

THERMAL NOISE

In an angle modulated system, basic theory shows that the spectral characteristics of the thermal noise power at the output of the detector or FM discriminator varies as the square of the baseband frequency, ω, for high C/N ratios. Stated mathematically, noise power density (N_D) is given by,

$$N_D = \frac{k\omega^2}{\frac{C}{n_o}}$$

where C/N_o is the input to the discriminator defined in a unit bandwidth and K is the discriminator constant. The resulting output baseband noise power spectrum is commonly termed parabolic and is characteristic of the FT mode of operation at high C/N ratios.

In the SSB-PhM (MA) mode, this parabolic spectrum is passed through a de-emphasis network with a transfer function of $1/(1 + \omega/\omega_a)$, where ω_a is the frequency at which the response is down 3 db. When $\omega/\omega_a \gg 1$, the noise density output of the de-emphasis network is independent of ω, and the resulting flat noise spectrum is characteristic of the SSB-PhM (MA) mode at high C/N ratios.

Figure 3.1 shows the baseband idle noise characteristics (no modulation) in the FT mode without de-emphasis. At C/N ratios above 10 db, the primary contributor to the noise spectrum in the 316 kHz to 5564 kHz baseband is thermal noise (R). It can be seen that the R component increases approximately as the square of the baseband frequency. As expected, the measured results are consistent with the FM theory previously discussed.

System signal-to-noise performance can be improved at the high end of the baseband with the use of de-emphasis to equalize the noise component R across the baseband. Figure 3.3 shows the equalization of the baseband idle noise based on the standard CCIR 1200 channel de-emphasis network (Recommendation 275-1, Oslo, 1966), as well as the CCIR 240 channel de-emphasis network. Characteristically, the noise is increased at the low end of the baseband, while at the high end, it is decreased relative to the idle noise without de-emphasis.

Optimum de-emphasis for the FT mode depends on the amount of increase in noise which can be tolerated in the low end of the baseband to improve the high end and must

3

take into account any increase in non-linear noise in the low end of the baseband due to system non-linearities. For the particular case shown, a maximum improvement of 4 db is realized at the high end while the low-end degradation does not exceed 4 db for the 1200-channel network. On the basis of the 240-channel de-emphasis network the noise is equalized such that a maximum test tone-to-idle noise improvement of 4 db is realized at the high end of the baseband, while the low-end degradation does not exceed 3 db.

The flat noise spectrum which describes the thermal noise characterisitics of the SSB-PhM (MA) mode is shown in figure 3.5. It can be seen that for C/N ratios above 10 db, the measured noise spectrum is essentially flat across the 316 kHz to 5564 kHz baseband.

THRESHOLD NOISE

ATS earth station/spacecraft configurations provide a variety of C/N ratios, as mentioned previously. At C/N ratios of 10 db or less, it was noted that the noise level increased in the lower end of the baseband (342 kHz, 768 kHz region) for both the FT and MA modes above that expected by the equation for thermal noise given previously. This phenomenon of increased low frequency noise in the baseband noise spectral characteristics at the FM discriminator output for the threshold region has been analyzed in a number of publications (42, 44). It is explained by noting that the baseband noise consists not only of thermal (parabolic) noise, but also a flat noise which is a critical function of C/N. This flat noise spectrum is sometimes called impulse (or "click") noise because the amplitude is proportional to the number of impulses ("clicks") per second. The flat noise spectrum arises from the fact that the frequency response of the baseband filter is essentially flat within the regions of interest for an impulse input. For this analysis this flat noise has been divided into two components: N_i, the threshold noise which is only a function of C/N, and Δ, the threshold noise which is due to the degree and form of modulation as well as C/N ratio. At low C/N ratios (below 10 db), the threshold noise components become dominant in the low end of the baseband relative to the thermal noise.

It can be seen in figure 3.1 that as C/N is decreased, the N_i component causes the noise spectrum to become flat in the low end of the baseband as discussed above. In going from a C/N ratio of 18 db to 8 db, the N_i threshold component increased the total idle noise approximately 1 db at 342 kHz.

When modulation is applied, the Δ component is present and this case is shown in figure 3.2. In going from a C/N ratio of 18 db to 8 db, both threshold components $(N_i + \Delta)$ now increase the total noise approximately 13 db at 342 kHz. Thus the Δ component contribution is approximately 11.5 db above the idle noise terms at this baseband frequency. To arrive at the above results, single tone modulation (10-MHz peak deviation) was used so that baseband intermodulation products would not contribute to the increase in noise with

modulation. Although the form of modulation used to simulate multichannel telephony is different from that used for this test, the significant Δ noise component contribution discussed above is indicative of the presence of this component when a white noise-like signal is used for modulation.

Also it can be pointed out that the rms frequency deviation used for 1200 channel telephony is about 3.8 MHz while the sinusoidal modulation rms frequency deviation used for this test was about 7 MHz. Thus for 1200-channel telephony the Δ noise component should not be as great as shown in figure 3.2.

Noise characteristics for the PhM (MA) mode downlink were determined by noise loading the test modulator (316 kHz to 5564 kHz). The PhM detector is configured by employing an FM discriminator followed by a 6 db per octave de-emphasis network. At high C/N ratios (above 10 db), the discriminator output noise spectrum is parabolic, thus the de-emphasis network output noise spectrum is flat. At low C/N ratios (below 10) , the noise spectrum which is flat prior to the de-emphasis network is equalized such that the de-emphasis network output noise spectrum increases as a function of decreasing baseband frequency. These conditions are shown in figures 3.5 and 3.6.

A further indication of the threshold noise effects in the SSB-PhM (MA) mode is shown in figures 3.7, 3.8, and 3.9. The Δ component shown in these figures was measured by applying a 40 kHz tone to the FM modulator. The peak frequency deviation was set at 10 MHz. The measured data at the output of the FM discriminator was analytically altered by the PhM de-emphasis network transfer function to determine the shape of the noise spectrum for the output of the PhM receiver.

It can be seen that at a C/N ratio of 20 db (figure 3.7) both threshold components are about 6 db below the thermal noise at 316 kHz. As the C/N ratio decreases, both N_i and Δ components increase. However, at a C/N ratio of 8 db (figure 3.9) the Δ component is dominant and in the worst case (at 316 kHz) it is about 14 db above the thermal noise. Basically, these figures show that both thermal noise and the threshold component N_i are independent of modulation and are present regardless of the type of modulation. It can also be seen that the Δ component contributes the larger amount of noise at a low C/N ratio. Although the degree and form of modulation used to determine Δ shown in figures 3.7, 3.8, and 3.9 are different from the nominal SSB-PhM (MA) mode signal characteristics, these figures clearly indicate the presence of the component in the baseband spectrum. It can be noted, however, that the effective frequency deviation for this test is somewhat larger compared to the effective frequency deviation of the SSB-PhM (MA) mode for 1200-channel operation. For example, the effective frequency deviation was 7 MHz for this test, while the effective frequency deviation for 1200-channel loading in the MA mode is approximately 5 MHz, thus the Δ component is expected to be less for 1200-channel loading than shown in

these figures. This conclusion of $\triangle$ noise increasing with modulation has been shown analytically by Rice [46]

NON-LINEAR NOISE

Intermodulation and harmonic non-linear baseband distortion using the various ATS earth station/spacecraft configurations is generated from several sources. In the FT mode (for single carrier operation) and the downlink portion of the SSB-PhM (MA) mode there are essentially three separate sources of baseband distortion caused in the IF-RF transmission medium; amplitude response non-linearities, phase response non-linearities, and spectrum truncation of the modulated signals. These affect the modulated signal spectrum in such a way that linear distortion occurs. It is not until the demodulator operates on the IF-RF signal spectrum that new frequencies or non-linear distortion is generated in the baseband. Also in these modes, the non-linearity of the FM or PhM modulators and demodulators create non-linear distortion. In the uplink portion of the SSB-PhM (MA) mode and the baseband amplifiers of both modes, the chief cause of non-linear distortion is the non-linear dynamic amplitude transfer characteristic.

The sensitivity of the system to amplitude response deviations of the phase modulated downlink signals (SSB-PhM (MA) mode) and the frequency modulated signals (FT mode) is reduced as the index of modulation is increased [48]. Since for nominal 1200-channel conditions the modulation index is large, the importance of amplitude response deviations is greatly reduced and thus is not considered significant for the ATS modes of operation.

It should be noted that harmonic distortion is insignificant compared to intermodulation when a white noise-like signal is used for modulation. The harmonic distortion is insignificant for two reasons: (1) the number of harmonic products of any particular order is at least an order of magnitude less than intermodulation products of the same order; and (2) the magnitude of the harmonic products is several db below the level of the intermodulation products of the same order. Therefore, intermodulation distortion will be used instead of non-linear distortion in the following analysis, except where harmonic distortion is specifically included. When considering baseband non-linear distortion in terms of its effect in a multiplex channel, it is present as additional noise regardless of whether or not the channel is being used. Thus the term noise will replace the term distortion in the subsequent analysis.

The non-linear noise is determined by two techniques; multitone tests and noise loading tests. In the noise loading test, the system is modulated with a white noise-like signal (which simulates multichannel telephony) in a manner which follows CCIR Recommendation 353-1, Oslo, 1966. A Marconi Noise Test Set OA2090 is used to determine the signal density-to-total noise density ratio (NPR) as well as the signal density-to-idle noise density ratio (TPR). The signal for this analysis is the reference level measured with the Marconi Test Set.

3.17

The use of NPR and TPR is used extensively in this section as a basis for analysis and therefore these terms will be defined as follows:

NPR - The ratio of the noise in a slot channel in the baseband when the system is noise loaded to the noise in the slot channel when noise loading is removed from that channel. This ratio is a measure of the total noise present in the slot channel.

TPR - The ratio of the noise in a slot channel in the baseband when the system is noise loaded to the noise in the slot when noise loading is removed from the system. This ratio is a measure of the idle noise present in the channel.

By removing the contribution of the idle noise from the total noise the signal density-to-intermodulation noise density ratio (K) may be determined from the following:

$$K = \frac{(NPR)\ (TPR)}{(TPR)-(NPR)} \qquad \text{(numeric)}$$

This equation applies whenever the C/N ratio is above threshold. In the threshold region it should be noted that the above equation yields the signal-to-intermodulation plus $\triangle$ density ratio, since the equation essentially removes the effect of idle noise components from the total noise leaving only the noise which can be attributed to modulation from all sources in the system.

In the SSB-PhM (MA) mode care must be taken in analyzing the NPR/TPR results. In this mode there is an attenuation roll-off of approximately 3 db at the highest baseband frequency (5.6 MHz) in the SSB uplink. This rolloff causes less equivalent frequency deviation for the highest baseband channels on the PhM downlink which can cause the signal density-to-intermodulation density to be in error up to 3 db in the lowest portion of the baseband. This error results from the fact that the second order intermodulation spectrum in the low end of the baseband is changed when a net baseband roll-off is present at the input to the S/C modulator. This same type of error is also present either in the uplink due to the third order intermodulation spectrums caused by transmitter non-linearity (amplitude) and other non-linearities in the downlink (phase or amplitude).

In the MA mode there is no practical way of measuring group delay of the PhM downlink. However by assuming typical group delay coefficients measured through the link in the FT mode for the MA mode PhM downlink phase non-linearity, additional conclusions can be drawn from the two tone test results. These group delay coefficients should represent a maximum value since the earth station IF-RF receiving equipment is the same in each mode as well as the transmitter sections of the S/C repeater. For the FT mode additional group delay is introduced in the ground transmitter and input sections of the S/C transponders.

The amplitudes of intermodulation products in multitone tests in the MA mode are a function of the frequency of the fundamental tones when these products are caused by downlink phase non-linearity or discriminator non-linearity. However, when the cause of the intermodulation products are from amplitude non-linearities in the uplink or the S/C modulator, these products are not frequency dependent. These results are arrived at in sub-section 7.7. Similarly, in the FT mode the intermodulation products in a multitone test caused by phase non-linearities in the total link are dependent upon the baseband frequency at which these products are measured.

Figures 3.11 and 3.12 show the results of a two tone multi-station test in the SSB-PhM (MA) Mode. Mojave and Rosman each transmitted one tone at 12.8 dbm0 (3 db below the nominal aggregate of 15.8 dbm0 for 1200 channel operation). This test was conducted on ATS-3 with a spacecraft EIRP of 54.6 dbm. The results show the magnitudes of the various orders of intermodulation and harmonic products relative to the fundamental tones. The results are then compared to the SSB-PhM (MA) mode one, two, and three tone single station tests shown in figure 3.13 through 3.18.

These SSB-PhM (MA) mode tests show that the third order $2f_1-f_2$ type products were the largest in magnitude on single station tests while in the multistation tests this type of product is not present. Fifth order products also follow this trend although the fifth order products are not as significant in amplitude as the third order. At Rosman the third order products measured in a two tone single station test are approximately 33 db below the total fundamental power. At Mojave the $2f_1-f_2$ third order products are approximately 39 db below the total fundamental power. From the foregoing, it can be concluded that the $2f_1 - f_2$ third order and $3f_1-2f_2$ fifth order intermodulation products in the single station test are caused solely by the SSB earth station transmitter. Third and fifth order products such as $2f_1 + f_2$, $3f_1$ or $3f_1 + 2f_2$ cannot be generated in the SSB transmitter since these products fall out of band.

Using the fundamental frequencies shown in figures 3.11, 3.12, 3.14, or 3.17 (and the equations in sub-section 7.7), the calculated second order products caused by non-linear phase response in the IF-RF portions of the PhM downlink are negligible when compared to the measured values shown in these figures. This fact follows because the frequency of the fundamental tones are relatively low in the baseband. Therefore, the measured intermodulation products are not expected to be caused primarily by phase non-linearities. The frequency of the fundamental tones must be in the upper portion of the baseband for second order intermodulation products caused by IF-RF non-linear phase response to be approximately the value of those shown in figures 3.11, 3.12, and 3.17.

3.19

It can be noted that in the multistation tests (figures 3.11 and 3.12) the second order products are approximately the same level measured at either station. It has also been observed that when the frequency of the fundamental tones is reduced from those used in these figures, the amplitude of the intermodulation products did not reduce in value. Thus, it can be concluded that the second order intermodulation products shown in these multistation two tone tests are primarily caused by the S/C modulator. This follows since these products were not a function of fundamental frequency, which eliminates phase non-linearities and the earth station demodulator as the sources of these intermodulation. Furthermore these products could not be generated in the earth station transmitter since each station transmitted only one tone.

When a two-tone multistation test (both stations receive) is performed such that both fundamental frequencies (in upper portion of baseband, 3.886 MHz and 5.34 MHz) are transmitted by a single station and the test tone deviation is increased above nominal a significance difference in level (10 db or greater) is noted in measurements of second order products made at Rosman and Mojave earth stations. The second order products measured at Mojave were 12 db above the products measured at Rosman. Since the transmitting earth station and spacecraft were the same for each measuring earth station, it can be concluded that the Mojave earth station non-linearities (phase in IF-RF region or discriminator) are greater than at Rosman. From group delay measurements (see figures 3.23 and 3.24) it can be been that the measurements made at Mojave show the total parabolic group delay as well as the linear group delay to be less than the measurements at Rosman. From the above, it appears that the Mojave discriminator non-linearity is the source of these intermodulation products.

Figures 3.19 through 3.22 show the results for two and three tone single station tests at Mojave, and one and two tone single station tests at Rosman in the FT mode. The intermodulation products shown in these figures are a function of baseband frequency. As an example, for the same type of product (third order) shown in figure 3.21, the amplitude of $2f_1 - f_2$, $2f_2 - f_1$, $2f_1 + f_2$ and $2f_2 + f_1$ increase monotonically with baseband frequency. From the equations in subsection 7.7, it is shown that the amplitude of intermodulation products when caused by phase non linearities in the IF-RF portion of the total links are a function of the baseband frequency at which the products are measured. It is also shown that the intermodulation products caused by non-linearities of the modulator and discriminator in the FT mode are not a function of baseband frequency. Thus, it is concluded that the dominant source of the intermodulation products shown in these figures is the IF-RF phase non-linearity.

There is a definite relationship between the results of two tone tests and signal-to-intermodulation noise ratio determined from the NPR/TPR results. These relationships are quite complex from the standpoint that the relative spectrums of various orders of

intermodulation noise must be determined for all significant causes of intermodulation noise, the sum total of which combines into the total nonlinear noise spectrum that exists at the baseband output of the earth station receiver. These relationships have been developed in several papers for most of the causes of nonlinear noise previously discussed [39, 26, 43, 49] Typical relationships are given in subsection   7.7.

Based on theoretical equations, calculated spectrums, and results of multitone single-station and multistation tests, the predominant second and third order 1200 channel intermodulation spectrums are shown in figures 3.4 and 3.10 for the FT and SSB-PhM (MA) modes, respectively. The amplitudes of intermodulation products caused by various sources in the system are determined by varying the conditions of multitone tests. For example, the frequencies of the fundamental tones are varied and multistation two tone tests are used to isolate the source of particular orders of intermodulation products. Next, the second and third order intermodulation spectrums are computed for a white Gaussian noise input. These spectrums are computed by taking the Fourier transform of the autocorrelation function of the output of the system for which white Gaussian noise is the input. Quasi-stationary assumptions are made in these computations. Using expressions given in subsection

7.7 the measured intermodulation products and spectrums are normalized to a common reference. These spectrums are shown in figures 3.4 and 3.10. These figures also show the combination of these spectrums added on a power basis to yield the total intermodulation spectrum from the multitone test results. Also the intermodulation spectrums computed from NPR/TPR results are shown for comparison. It can be seen in these figures that the total intermodulation spectrums based upon multitone tests and the NPR/TPR measurements agree within ±2 db.

SYSTEM OPTIMIZATION

The curves presented in this analysis are based on typical SSB-PhM (MA) mode and FT mode NPR/TPR test runs from each ATS station. Utilizing various earth station/ spacecraft configurations, C/N ratios above and below threshold are obtained. At C/N ratios above 10 db, the threshold noise components are negligible, thus only thermal noise (R) and intermodulation (I) determine total noise. At C/N ratios below 10 db, both N_i and Δ threshold noise components contribute to the total noise, particularly at the lower end of the baseband. For a particular configuration, the contribution of all noise components to the total noise can be determined by noting their variation with respect to test tone level. In particular, the combination of $TT/(R+N_i)$ and $TT/(I+\Delta)$ at low C/N ratios or TT/R and TT/I at high C/N ratios determines the optimum operating test-tone level.

System $TT/(R+N_i)$ and $TT/(I+\triangle)$ ratios are derived from measured NPR and TPR data. The $TT/(R+N_i)$ ratio is given by:

$$TT/(R+N_i) = TPR \text{ (db)} + 10 \log Y \text{ (db)}$$ and the $TT/(I+\triangle)$ ratio is given by:

$$TT/(I+\triangle) = \frac{(Y)\,(TPR)}{\left(\dfrac{TPR}{NPR} - 1\right)} \quad \text{(all numeric)}.$$

where N_i and $\triangle$ are negligible at high C/N ratios, and Y is given by,

$$Y = \frac{B}{bK}$$

where K is a function of the number of channels being loaded, b is the channel bandwidth (FIA weighted), and B is the noise loading bandwidth. The constant Y for the ATS earth stations is as follows:

$10 \log (Y) = 19.5$ db at Rosman (K = 15.8 db)

$10 \log (Y) = 19.2$ db at Mojave and Cooby Creek (K = 8.8 db)

In addition, at low C/N ratios, the relatively high level of the total noise causes the reference level for the NPR and TPR ratios to be in error, thus measured values are also in error. Corrected NPR and TPR are derived as follows:

$$(NPR)_m = \frac{(RL) + R + N_i + \triangle + I}{R + N_i + \triangle + I} \tag{1}$$

$$(TPR)_m = \frac{(RL) + R + N_i + \triangle + I}{R + N_i} \tag{2}$$

$$(NPR)_c = \frac{(RL)}{R + N_i + \triangle + I} \tag{3}$$

$$(TPR)_c = \frac{(RL)}{R + N_i} \tag{4}$$

where:

$(NPR)_m$ = Measured NPR value

$(TPR)_m$ = Measured TPR value

$(NPR)_c$ = Correct NPR value

$(TPR)_c$ = Correct TPR value

RL = Correct reference level

Using equations (1), (2), (3), and (4) it can be shown that

$$(NPR)_c = (NPR)_m - 1$$

and

$$(TPR)_c = TPR_m \left[1 - \frac{1}{(NPR)_m} \right]$$

SSB-PhM (MA) MODE

Figures 3.25 through 3.32 show the variation of TT/N (loaded), TT/N (idle) and TT/(I + $\triangle$) ratios (all FIA weighted) as a function of test tone level for various earth station/spacecraft configurations, hence various C/N ratios. Noise variation in terms of NPR and TPR as well as the equivalent test tone to noise are shown so that station performance can be compared for different channel loading and baseband bandwidths. For each configuration, the point at which system operation is optimum is clearly evident.

As shown in figures 3.25 through 3.32, TT/N (idle) and TT/N (loaded) increase linearly with increased system test tone power until the (I + $\triangle$) noise term becomes significant with respect to the (R+N$_i$) term. At this point the TT/N (loaded) begins to level off, and then deceases with further increase in the (I+$\triangle$) noise term. At all earth station/spacecraft configurations utilizing 240 channel loading the (I+$\triangle$) noise term was not dominant at nominal test tone level. This can be seen from the fact that at nominal test tone level the TT(I +$\triangle$) ratio is much greater (more than 3 db) than the TT/N (idle) ratio.

The effect of the (I +$\triangle$) noise term at C/N ratios below 10 db is seen in figures 3.26 and 3.28. The low channels at both Cooby Creek and Mojave, each using 30 MHz IF filters and 240 channel loading, have degraded in TT/N performance because of the threshold effects previously discussed. For Cooby Creek with a C/N ratio of 7.3 db, the degradation is 3 db at nominal (TT/N decreased from 36 db to 33 db), and at the optimum operating point the degradation is 4 db (38 db to 34 db). At the higher C/N ratio of 9.0 db at Mojave, the degradation is approximately 1 db (36.5 db to 35.0 db at nominal; 38 db to 37 db at the optimum operating point).

Figure 3.30 shows TT/N performance at Mojave with 1200 channel loading using ATS-3. Figures 3.31 and 3.32 show similar performance at Rosman using ATS-1 and ATS-3. In the case of Mojave, optimum performance requires a 2-db increase in test tone power. It can also be seen that intermodulation noise as a function of test tone power is frequency dependent for both stations above nominal test-tone power. The I + $\triangle$ noise distribution is such that it is greatest in the low frequency baseband channels and decreases with increasing baseband frequency. For example, in figure 3.32, when test tone at Rosman is increased 4 db above nominal, TT/N drops 1 db at 1248 kHz relative to 5340 kHz (39.5 db to 38.5 db) while

at 342 kHz TT/N decreases another 1.5 db relative to 1248 kHz (38.5 db to 37.0 db), resulting in a spread in TT/N of 2.5 db between the 342-kHz and 5340-kHz channels. It was shown previously that the composite intermodulation spectrum is essentially flat across the baseband for nominal test tone level (see figure 3.10). When operating above nominal as shown in figures 3.30, 3.31, and 3.32 the intermodulation spectrums combine such that this frequency dependence is evident.

The effect on TT/N performance of varying the IF filter may be seen in figures 3.25 through 3.28. In these figures, Cooby Creek and Mojave NPR/TPR performance is given with the 12-MHz and 30-MHz IF filters. For the higher baseband frequencies, at the optimum operating point, the TT/N for 12-MHz and the 30-MHz filters are approximately equal. For example, in figure 3.27 and 3.28, at the optimum operating point, Mojave using ATS-1 has a TT/N of 38.5 db with the 12-MHz filter and TT/N of 38.0 db with the 30-MHz filter. Also, in figures 3.25 and 3.26, Cooby Creek, at the optimum operating point, has a TT/N of 37.5 db for either the 12-MHz or 30-MHz filter. However, the overall C/N in the receiver IF is decreased as a result of more noise due to the wider IF filter bandwidth. This reduction in C/N ratio (below 10 db) degraded TT/N performance in the low frequency channels because of threshold effects at both Mojave and Cooby Creek.

Figures 3.33 through 3.40 further summarize optimum earth station performance on the basis of channel loading and SSB transmitter power output. These figures also show the NPR variation with respect to test tone level for loaded baseband bandwidths (B_n) other than 240 and 1200 channel loading.

Figure 3.33 shows the NPR values versus the variation in transmitter power output per channel for five different values of B_n. In each case, the reference power level was determined according to the CCITT recommendations based upon the number of channels N, contained within B_n. The NPR data was measured in the 342-kHz baseband slot (Rosman, ATS-3). The optimum operating point was determined by locating the point at which the NPR was maximum.

Figure 3.37 shows the baseband signal power spectrum which exists for the optimum operating point shown in figure 3.33. It should be noted that the total earth station power output required for the optimized condition varies only 3 db for optimization of 180 to 1200 channels; however, the signal power density undergoes a total change of 6.7 db.

The foregoing optimization was based on NPR measurements made in the 342 kHz slot. Figures 3.34 and 3.38 show the corresponding curves for measurements made in the 1248 kHz slot. In this case the total earth station power output changes 2.6 db for optimum performance from 240 to 1200 channels. Similar results were obtained for channel optimization based upon the NPR measurements at other baseband slot frequencies.

Figures 3.35 through 3.40 show the results of similar optimization at Mojave and Cooby Creek both operating with the ATS-1 spacecraft. In both cases the optimization was performed based upon NPR measurements made in the 342-kHz baseband slot. In all cases as B_n is decreased, the SSB transmitter power output is only slightly affected (for optimum operation), thus indicating that the increase in TT level required is essentially offset by the corresponding decrease in B_n.

Table 3.4 summarizes the results of optimization tests performed for a variety of earth station/spacecraft configurations under maximum loading conditions (the test data presented in figures 3.33 through 3.40 was not used to compile table 3.4, however, close agreement is seen to exist between corresponding system configurations). The measured NPR and TT/N ratios are listed for nominal conditions as well as the corresponding optimum conditions. Also shown is the increase in test-tone level required to achieve these optimum ratios. Table 3.3 summarizes which link, uplink or downlink, limits performance and which noise component causes this limitation.

FT MODE

Figures 3.41 through 3.46 show the variation of test tone-to-idle-intermodulation and-total noise for several typical ATS earth station/spacecraft configurations, hence for various C/N ratios. Also shown for several configurations is the effect of de-emphasis on the low and high frequency channels in the baseband.

As shown in figures 3.41, 3.43, and 3.45, TT/N in the low channel (342 kHz), without de-emphasis, exceeds the CCIR recommendation of 50 db. Characteristically, TT/N decreases with increasing baseband frequency and for a baseband loaded from 316 kHz to 1300 kHz, figures 3.42 and 3.44 show that the high channel (1248 kHz) TT/N is about 4 db below the recommended TT/N of 50 db. For a baseband loaded from 316 kHz to 5564 kHz figure 3.46 shows that high channel (5340 kHz) TT/N is about 15 db below the 50-db recommendation.

Table 3.6 summarizes the results previously discussed. The measured NPR is listed for specific earth station/spacecraft configurations as well as the corresponding optimum NPR. It is evident that the largest improvement realized by increasing TT level occurs for those configurations where C/N ratio is at or below threshold.

When C/N is low (below 15 db), TT/N can be improved by increasing test tone level. For example, in the case of Mojave with ATS-1 and 1200-channel loading (table 3.6) an increase in test-tone level increases TT/N about 2 db.

Table 3.5 summarizes link performance and shows whether the uplink or down-link limits performance and which noise component causes this limitation.

The addition of pre/de-emphasis improves the TT/N in the high channels at least 3 db with a corresponding 3 db decrease in the low channels. These results are also shown in figure 3.41 through 3.46, as well as table 3.6. In order to meet a 50-db TT/N across the entire baseband, compandors are required for the high channels when 1200 channel loading is used.

Figure 3.3 shows the relative thermal noise spectrum for 240-and 1200-channel bandwidths. As indicated in the figure, the noise density increases with baseband frequency. Consequently, the noise is highest in the channel which is highest in the baseband. Figure 3.3 also shows the effect of de-emphasis (based on CCIR recommendation 275-1 Oslo) on the noise spectrum across the baseband. It is seen that this effect is to substantially flatten the noise across the baseband.

The effect of pre/de-emphasis is further illustrated in figure 3.47 for several types of pre/de-emphasis (FM without pre/de-emphasis is shown as a reference). The CCIR pre/de-emphasis lowers the test tone-to-noise ratio in the lower channels relative to no pre/de-emphasis, yet raises the test tone-to-noise ratio in the upper channels. Since PhM is equivalent to FM with a 6 db/octave pre/de-emphasis, it is shown also. It can be seen that the CCIR pre-emphasis circuit lowers the test tone-to-noise at 342 kHz by 4 db, while increasing the test tone-to-noise at 5340 kHz by 4 db. On the other hand a straight 6 db per octave pre/de-emphasis (PhM) lowers the test tone-to-noise ratio at 342 kHz by 19 db relative to no emphasis FM, while raising the test tone-to-noise ratio at 5340 kHz by about 5 db. It would appear from the figure that pre/de-emphasis circuits which would optimize the greatest number of channels having 50 db test tone-to-noise ratio or close to it would require pre/de-emphasis circuits somewhere between the CCIR 1200 channel pre/de-emphasis and the 6 db pre/de-emphasis (PhM).

SYSTEM NOISE TEMPERATURE

Figures 3.48 and 3.49 show plots of the earth station system noise temperature (T_R) for each station operating with ATS-1 and ATS-3 respectively. The plots present T_R with the earth station antenna pointed in the approximate vicinity of the S/C. Each point represents the mean of several tests conducted during a one week time interval. It should be noted that, due to the low elevation angle, the T_R value for Rosman using ATS-1 is considerably greater than for any other system configuration (approximately 105°K versus 70°K). The curves are presented to give an indication of the variation of T_R over a long time interval. The T_R value is also recorded each time a test is performed; thus the actual value is available for consideration when the data is analyzed.

3.2.1.3   Conclusions

The results of the (SSB-PhM) MA mode tests have been summarized in tables
3.3 and 3.4 with typical performance characteristics plotted in figures 3.25 through 3.32.

The optimum test-tone power is reached when NPR is a maximum. This con-
dition is essentially attained at nominal test tone power of 15.8 dbm0 at Rosman using either
ATS-1 or ATS-3. At Mojave, optimum operation is reached on ATS-1 for 240 channel loading
at a test tone level of +4 db from nominal, while on ATS-3 for 240 channel loading optimum
operation is reached at a test tone power of +2 db from nominal. At Cooby Creek, an increase
in test tone power of +4 db would be required to achieve optimum operation.

At Mojave, where one of the test conditions results in a C/N ratio of 9.0 db,
threshold effects were noticed (the degration in the 342 kHz channel NPR was 1 db relative
to the 1248-kHz channel). At Cooby Creek, threshold effects caused by a low C/N ratio of
7.3 db in one of the test conditions showed a degradation of 3 db in the 342-kHz channel re-
lative to the 1248 kHz channel.

At all stations in the SSB-PhM (MA) mode the downlink was the limiting link for
all channels, except Rosman using ATS-1. However at Rosman (using ATS-1, EIRP of
49.6), the uplink (TT/N) and the downlink (TT/N) are within 2 db of each other. For
practical purposes, this link is optimum.

For 240 channel loading NPR has no dependency upon baseband frequency with
increased test tone power, assuming C/N is above 10 db. When 1200 channel loading is
used, then intermodulation noise which varies with frequency is apparent above nominal
test tone power. For example, at Rosman on ATS-3 when the test tone power is increased
+4 db, there is a spread of 2.5 db between the 342-kHz slot and the 5340-kHz slot.

The FT mode results have been summarized in tables 3.5 and 3.6 with typical
performance characteristics presented in figures 3.41 through 3.46. In this mode, the
thermal noise power, R, increases approximately as the square of the baseband frequency
(as expected from theory). The intermodulation noise power, I, is very dependent upon
baseband loading, and is also dependent upon baseband frequency. Because the baseband
noise spectrum is a function of frequency, it is generally not possible to optimize the
performance of the high and low channels simultaneously by adjustment of test-tone level.
For 240 channels loading the CCIR recommended pre/de-emphasis networks equalize the
noise such that the test tone-to-noise is almost uniform across the baseband. However, for
higher channel loading the spread between the upper and lower baseband channel test tone-
to-noise ratios, when the CCIR recommended pre/de-emphasis networks are used, indicates
that more optimum networks could be employed.

TABLE 3.3. SUMMARY OF LINK PERFORMANCE LIMITATION, SSB-PhM MODE

Station	Satellite	Satellite EIRP (dbm)	$\left(\frac{TT}{N}\right)_{up} - \left(\frac{TT}{N}\right)_{down}$ (Based on System Calculations)	① Limiting Link D Downlink U Uplink O Optimum	② Noise Limitation $R + N_i$ I + O Optimum System
Rosman	ATS-1	49.4	-0.7	O	$(I + \Delta)$
		52.2	-2.3	U	$(I + \Delta)$
	ATS-3	52.2	3.1	D	$(I + \Delta)$
		54.6	2.4	D	$(I + \Delta)$
		56.5	2.4	D	$(I + \Delta)$
Mojave	ATS-1	49.4	5.9	D	$(R + N_i)$
		52.2	4.5	D	$(R + N_i)$
	ATS-3	52.2	7.0	D	$(R + N_i)$
		54.6	5.0	D	$(R + N_i)$
		56.5	4.0	D	$(R + N_i)$
Cooby Creek	ATS-1	52.2	4.5	D	$(R + N_i)$

① By definition, the system performance is downlink limited when $\left(\frac{TT}{N}\right)_{up} - \left(\frac{TT}{N}\right)_{down} > 2\,db$
Uplink limited when $\left(\frac{TT}{N}\right)_{down} - \left(\frac{TT}{N}\right)_{up} > 2\,db$, Optimum when $\left| \left(\frac{TT}{N}\right)_{up} - \left(\frac{TT}{N}\right)_{down} \right| \leq 2\,db$

② By definition the link is R limited when $(R + N_i) - (I + \Delta) > 2\,db$, I limited when $(I + \Delta) - (R + N_i) > 2\,db$
and Optimum when $\left| (R + N_i) - (I + \Delta) \right| \leq 2\,db$

TABLE 3.4. SUMMARY OF BASEBAND PERFORMANCE AT NOMINAL AND OPTIMIZED TEST-TONE LEVEL (SSB-PhM (MA) MODE) (1)

Station	S/C	S/C EIRP (dbm)	Loading (Channels)	IF Bandwidth (MHz)	Nominal				Optimum				Optimum Test Tone Power from Nominal (3)		Mean C/N (2) (db)
					Low Channel		High Channel		Low Channel		High Channel		Low Channel (db)	High Channel (db)	
					NPR (db)	TT/N (db)	NPR (db)	TT/N (db)	NPR (db)	TT/N (db)	NPR (db)	TT/N (db)			
Rosman	ATS-1	52.2	1200	30	20	39	20	39	20	39	20	39	0.0	0.0	14.8
	ATS-3	54.6	1200	30	24	43	24	43	24	43	24	43	+0.4	+0.4	19.7
Mojave	ATS-1	52.2	240	12	19	38	19	38	20	39	20	39	+2.5	+2.5	13.0
			240	30	16	35	17	36	17	36	19	38	+3.0	+3.6	9.0
	ATS-3	54.6	240	30	21	40	21	40	23	42	23	42	+4.8	+4.8	11.6
			1200	30	18	38	20	39	18	38	20	40	+2.0	+2.0	11.6
Cooby Creek	ATS-1	52.2	240	12	18	37	18	37	19	38	19	38	+2.0	+2.0	10.6
			240	30	14	33	17	36	15	34	19	38	+4.1	+4.2	7.3

(1) NPR and (TT/N) have been rounded off to the nearest whole db. The high-channel baseband frequency is 5340 kHz at Rosman and 1248 kHz at Mojave and Cooby Creek. The low-channel baseband frequency is 342 kHz at all stations. NPR and (TT/N) for intermediate channel frequencies generally fell between the values for the high and low channels. (TT/N) includes a 3 db F1A weighting.

(2) These values are the measured downlink (C/N)'s.

(3) Optimum occurs when the NPR is a maximum, which is the point where $TT/(I + \Delta)$ and idle (TT/N) are equal.

TABLE 3.5. SUMMARY OF LINK PERFORMANCE LIMITATION, FT MODE

Station	Satellite	Satellite EIRP (dbm)	$(C/N_o)_{up} - (C/N_o)_{down}$ (Based on System Calculations)	① Limiting Link D = Downlink U = Uplink O = Optimum	② Noise Limitation $\frac{R + N_i}{I + \Delta}$ O = Optimum System Low Channel	High Channel
Rosman	ATS-1	49.4	5.3	D	$R + N_i$	$R + N_i$
		52.2	2.5	D	O	$R + N_i$
	ATS-3	52.2	1.6	O	$R + N_i$	$R + N_i$
		54.6	-0.8	O	$R + N_i$	$R + N_i$
		56.5	-2.2	U	O	$R + N_i$
Mojave	ATS-1	49.4	11.3	D	$R + N_i$	$R + N_i$
		52.2	8.5	D	O	O
	ATS-3	52.2	9.0	D	$R + N_i$	$R + N_i$
		54.6	6.6	D	$R + N_i$	$R + N_i$
		56.5	5.2	D	O	O
Cooby Creek	ATS-1	52.2	8.5	D	O	O

① By definition, the system performance is downlink limited when $(C/N_o)_{up} - (C/N_o)_{down} > 2$ db
Uplink limited when $(C/N_o)_{down} - (C/N_o)_{up} > 2$ db, and optimum when $\left|(C/N_o)_{up} - (C/N_o)_{down}\right| \leq 2$ db

② The channel is $R + N_i$ limited when $(R + N_i) - (I + \Delta) > 2$ db, I limited when $(I + \Delta) - (R + N_i) > 2$ db,
and optimum when $(R + N_i) - (I + \Delta) \leq 2$ db
Low Channel = 316 to 342 kHz
High Channel = 5340 or 5560 at Rosman and 1248 or 1296 at Mojave and Cooby Creek

TABLE 3.6. SUMMARY OF BASEBAND PERFORMANCE AT NORMAL AND OPTIMIZED TEST TONE LEVEL (FT MODE)

Station	S/C	S/C EIRP (dbm)	Loading (Channels)	IF Bandwidth (MHz)	Nominal				Optimum				Optimum Uplink Test Tone Power From Nominal		Mean C/N (db)
					Low Channel		High Channel		Low Channel		High Channel				
					NPR (db)	TT/N (db)	NPR (db)	TT/N (db)	NPR (db)	TT/N (db)	NPR (db)	TT/N (db)	Low Channel (db)	High Channel (db)	
Rosman	FLAT ATS-3	54.6	1200	30	39	58	16	35	40	59	16	35	-0.4	+1.4	17.2
	FLAT ATS-3	56.5	1200	30	40	60	16	36	40	60	17	36	1.0	+2.5	20.2
	EMPH ATS-3	56.6	1200	30	37	.56	20	40	37	56	21	40	1.0	+2.5	20.2
	EMPH ATS-3	54.6	1200	30	37	56	20	39	37	56	21	40	0.0	+1.0	17.2
Mojave	FLAT ATS-1	52.2	240	12	37	56	27	46	37	56	27	46	0.0	+1.0	12.3
	FLAT ATS-1	52.2	1200	30	31	50	10	29	32	51	12	31	+2.0	+3.0	9.7
	FLAT ATS-3	54.6	240	12	38	57	30	49	40	59	30	49	-1.0	0.0	14.3
	FLAT ATS-3	54.6	1200	30	36	56	12	31	37	56	14	33	+0.8	+3.0	12.1
	EMPH ATS-1	52.2	240	12	31	50	31	50	33	52	31	50	-2.0	+1.0	12.3
	EMPH ATS-1	52.2	1200	30	28	47	13	32	29	48	16	35	+2.0	+4.0	9.6
	EMPH ATS-3	54.6	240	12	32	51	33	52	36	55	33	52	-2.0	0.0	14.3
	EMPH ATS-3	54.6	1200	30	31	50	15	34	35	54	17	36	+4.0	+4.0	10.1
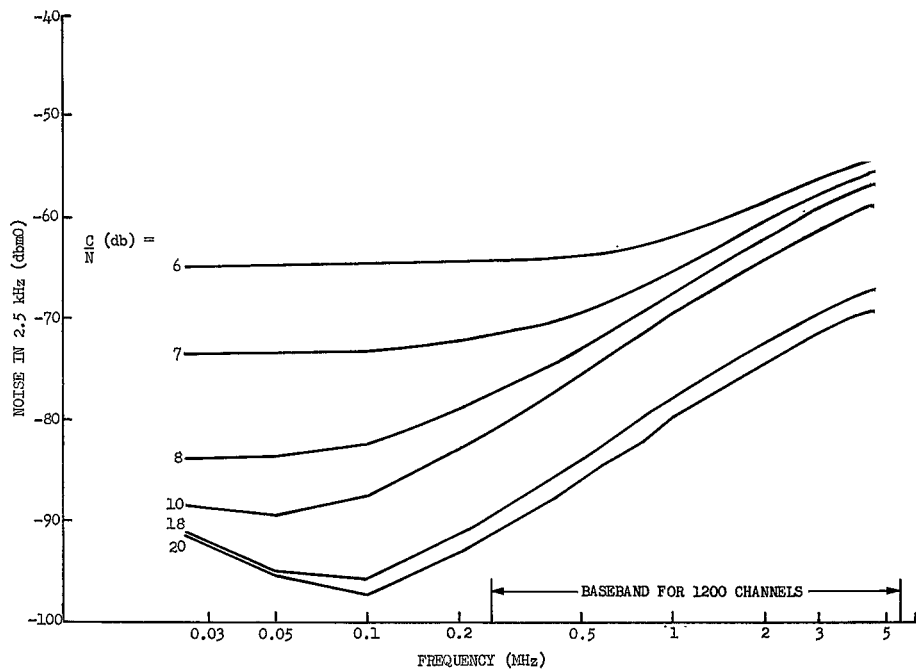
Figure 3.1. Idle Baseband Noise Spectrum (FT, Mode)
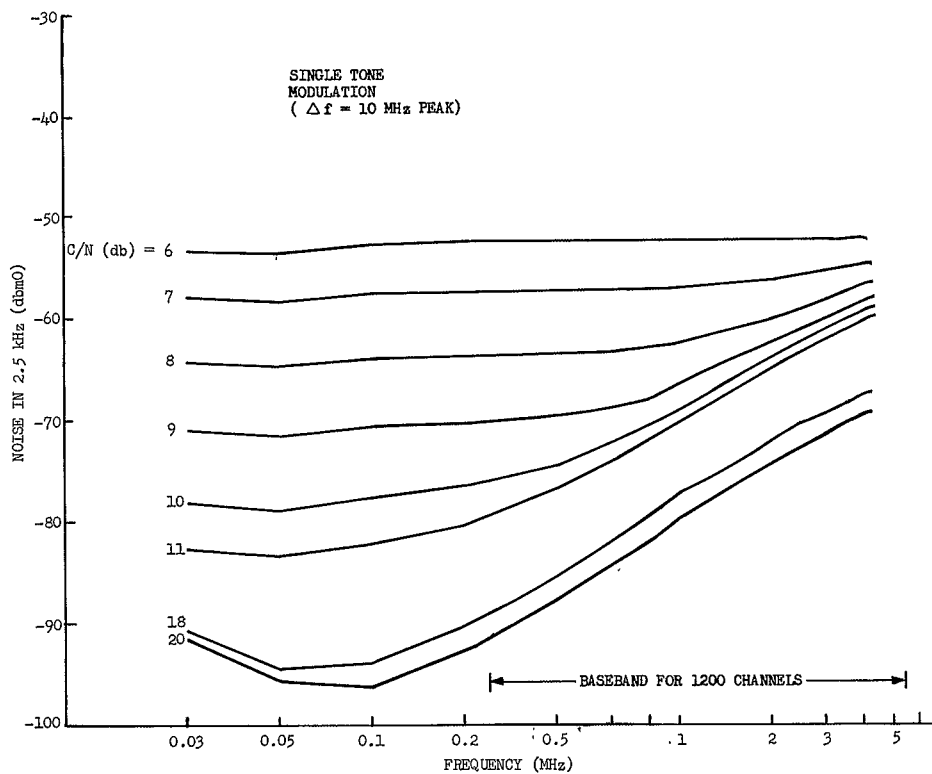
Figure 3.2. Loaded Baseband Noise Spectrum (FT, Mode)
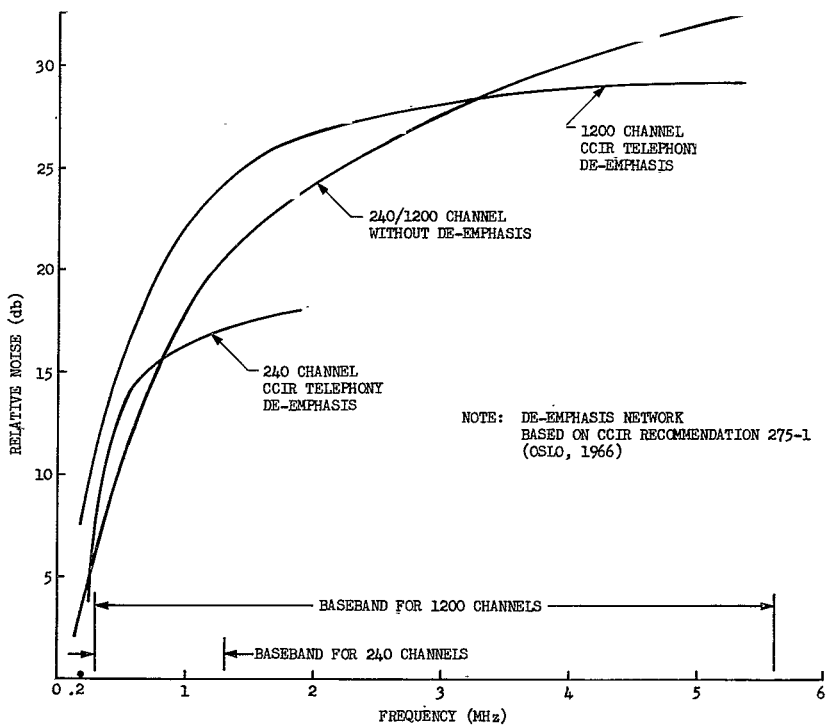
Figure 3.3. Baseband Idle Noise Spectrum with/without De-Emphasis
(FT Mode, High C/N)
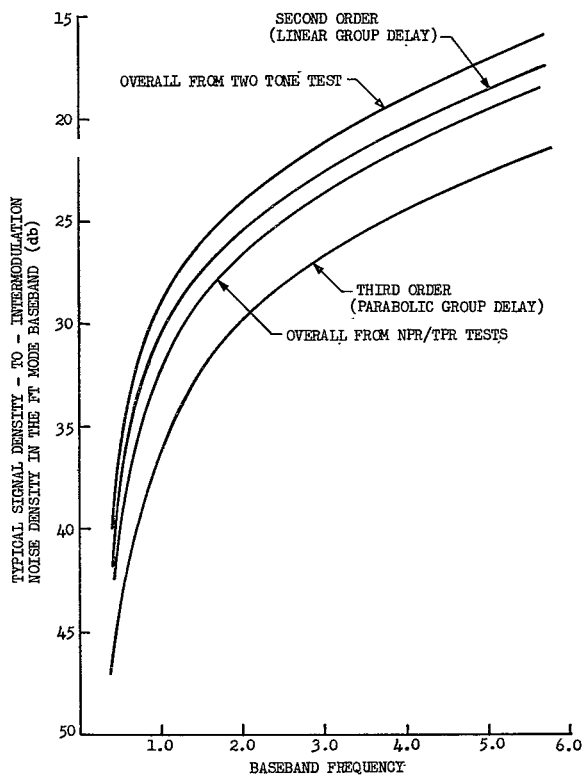
Figure 3.4. Second and Third Order Intermodulation Noise Spectrums
(FT Mode, 1200 Channels, ATS-3)
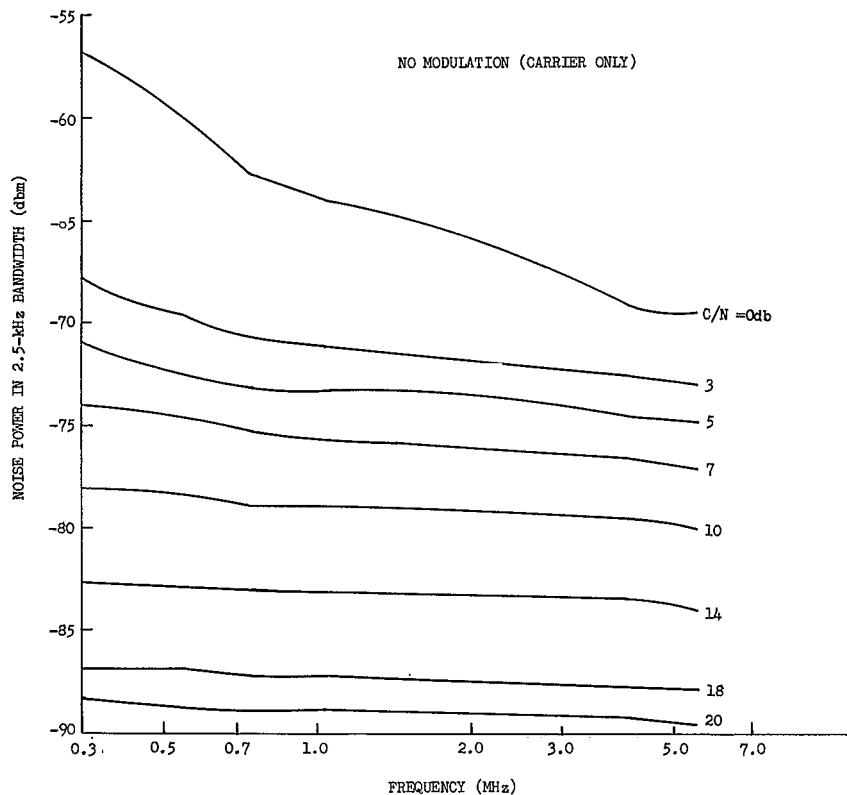
Figure 3.5. Idle Noise Spectrum of the SSB-PhM (MA) Mode (No Modulation)
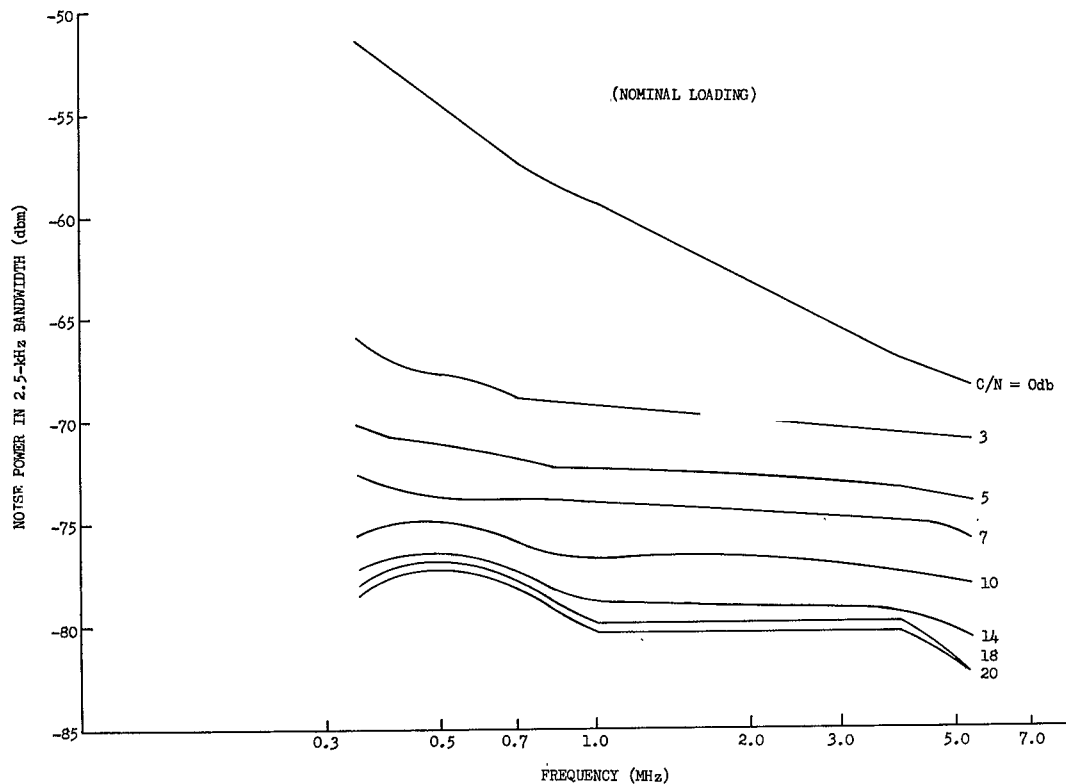
Figure 3.6. Loaded Noise Spectrum of the SSB-PhM (MA) Mode (1200 Channel Noise Modulation)
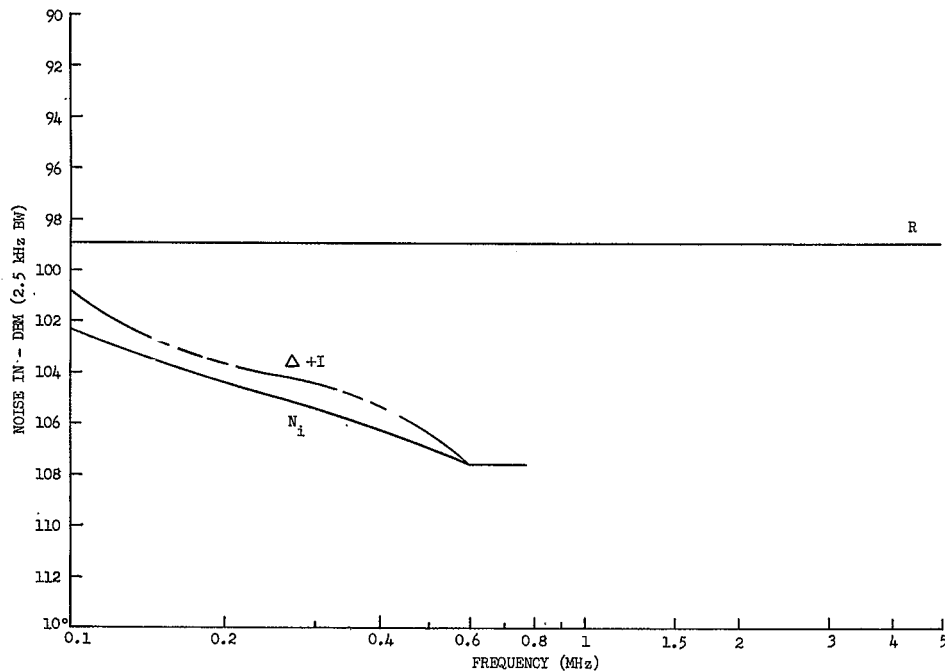
Figure 3.7. SSB-PhM (MA) Mode Baseband Noise Spectrum (C/N = 20 db)
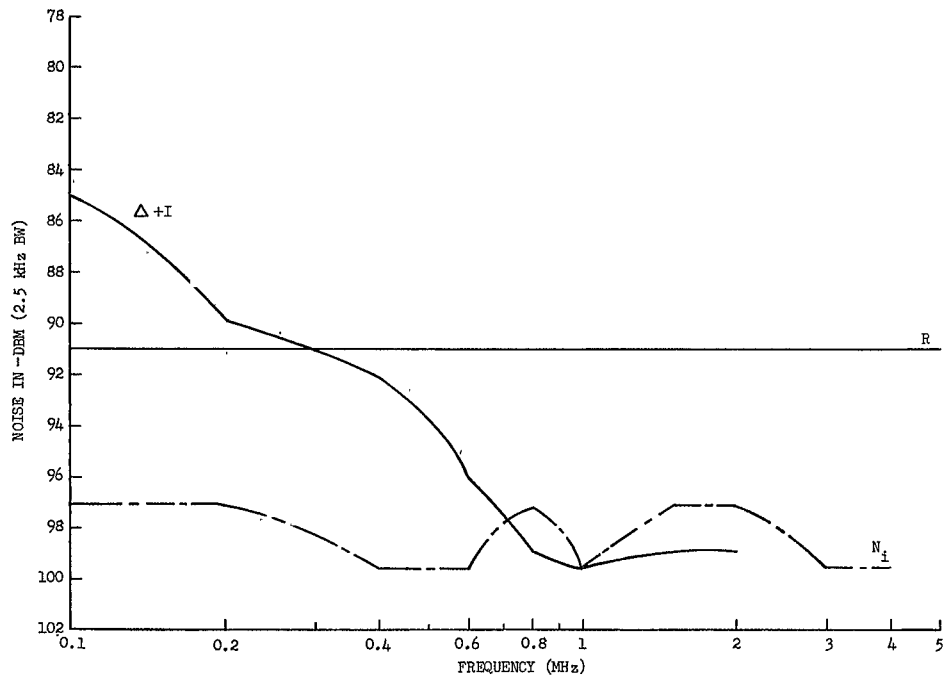
Figure 3.8. SSB-PhM (MA) Mode Baseband Noise Spectrum (C/N = 12 db)

3.39
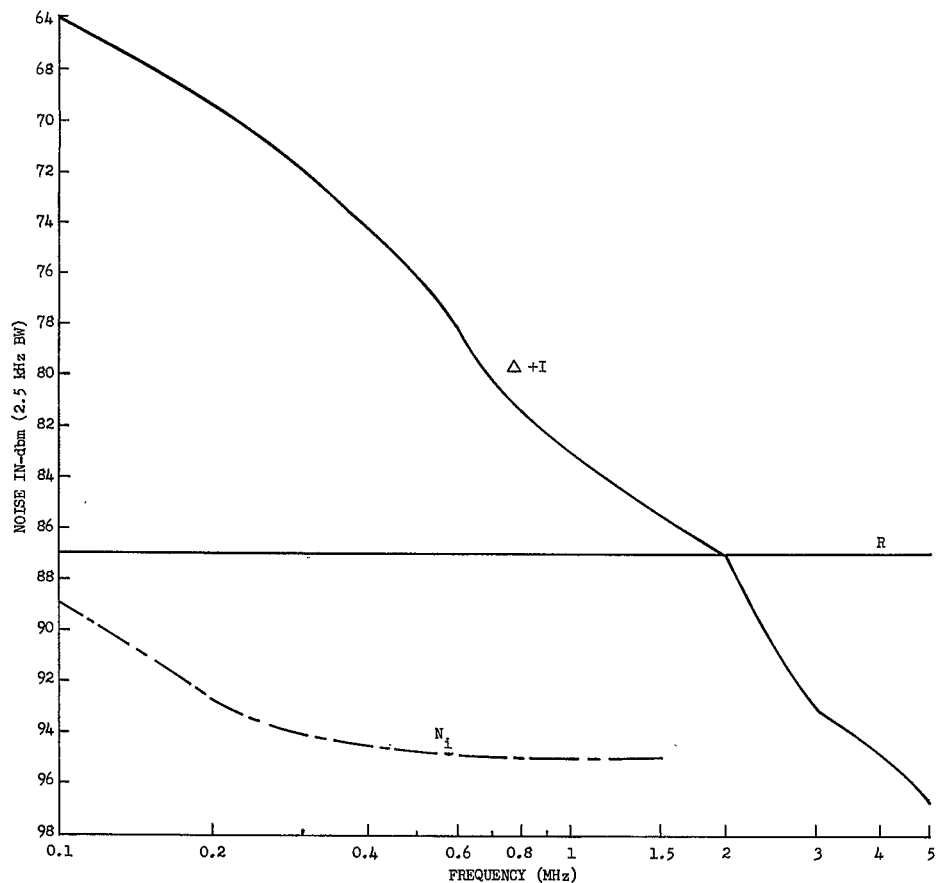
Figure 3.9. SSB-PhM (MA) Mode Baseband Noise Spectrum (C/N = 8 db)
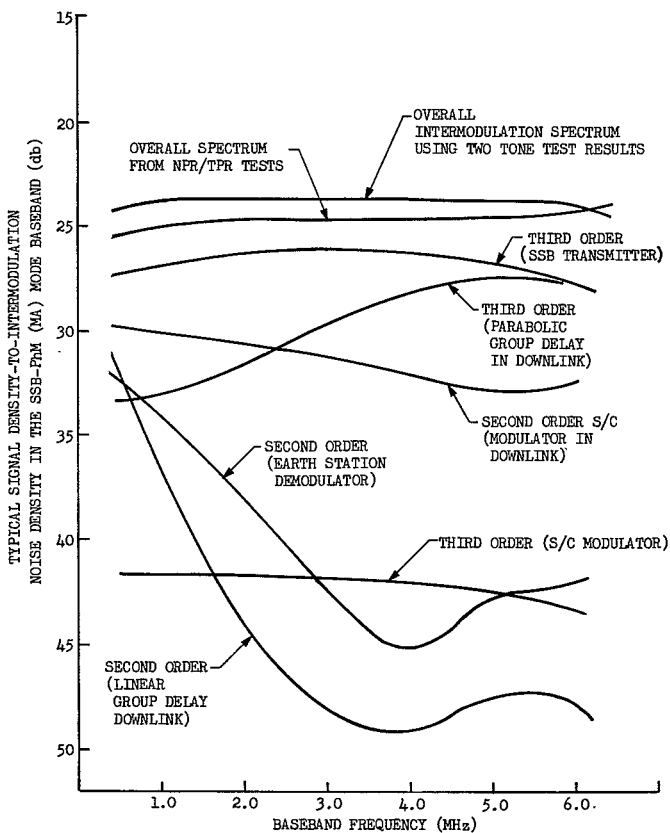
Figure 3.10. Second and Third Order Intermodulation Noise Spectrums (MA Mode, 1200 Channels, ATS-3)
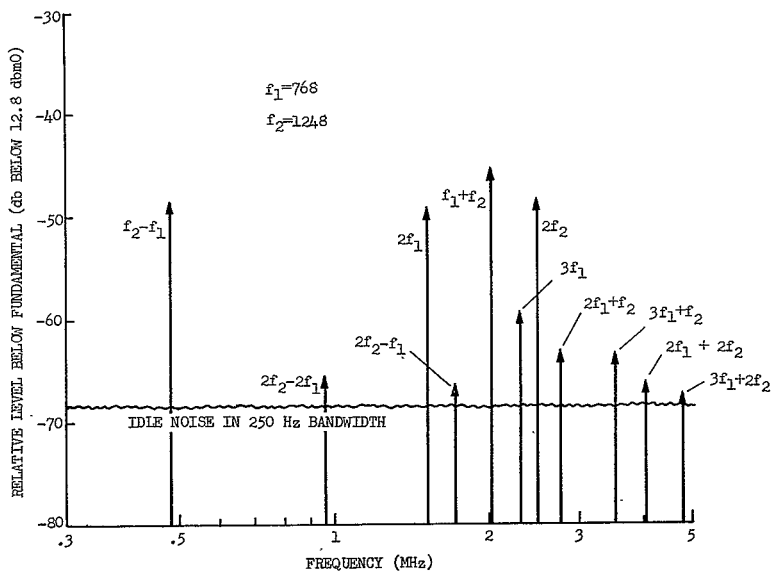
Figure 3.11. Two-Station Two-Tone Test, Mojave Receiving Earth Station
(ATS-3, EIRP = 54.6 dbm, MA Mode)
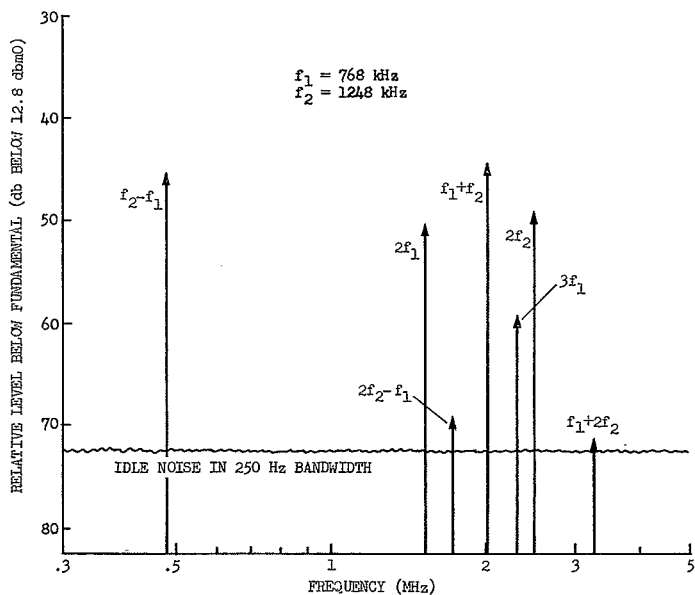
Figure 3.12.   Two-Station Two-Tone Test, Rosman Receiving Earth Station
(ATS-3 EIRP = 54.6 dbm, MA Mode)

3.43
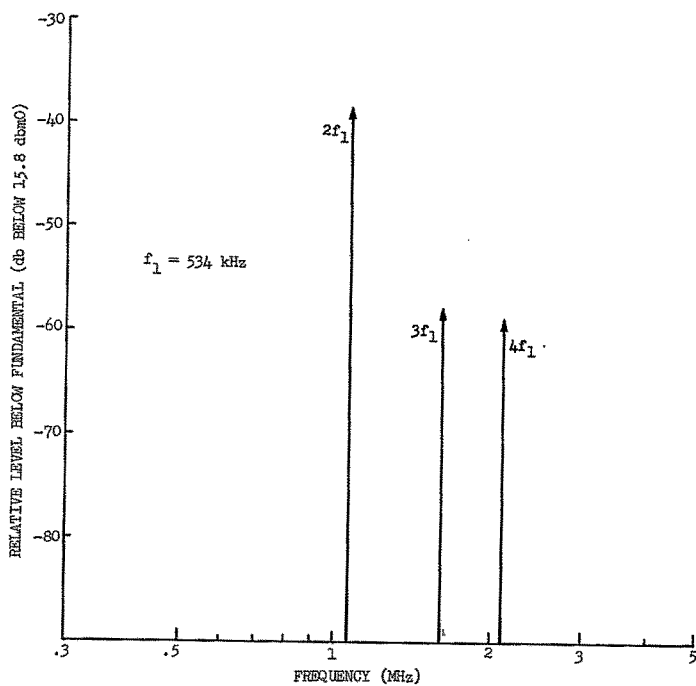
Figure 3.13.   One-Tone Test (Rosman, MA Mode, ATS-3)
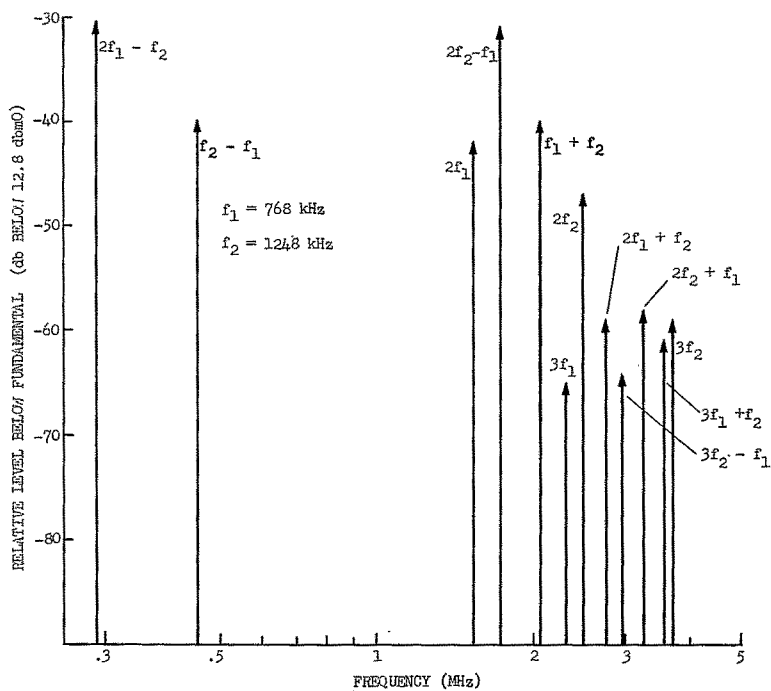
Figure 3.14. Two-Tone Test (Rosman, MA Mode, ATS-3)
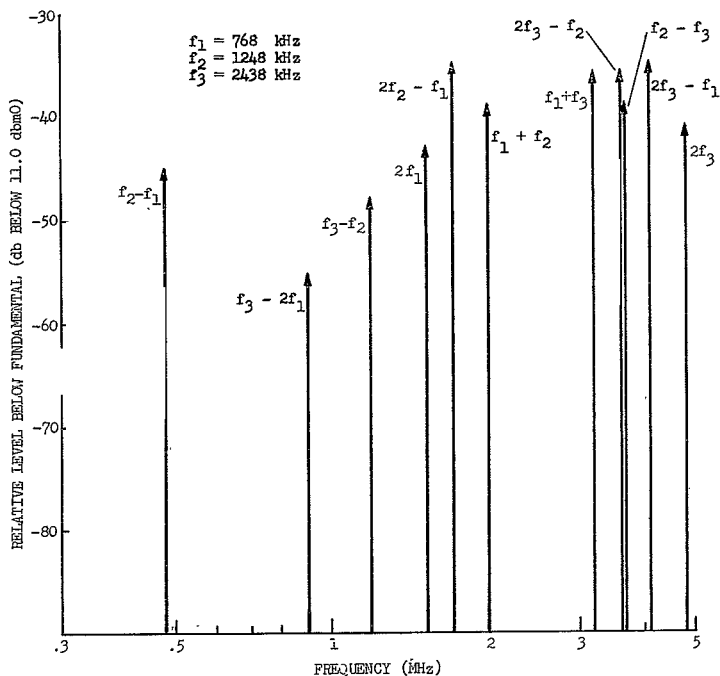
Figure 3.15. Three-Tone Test (Rosman, MA Mode, ATS-3)
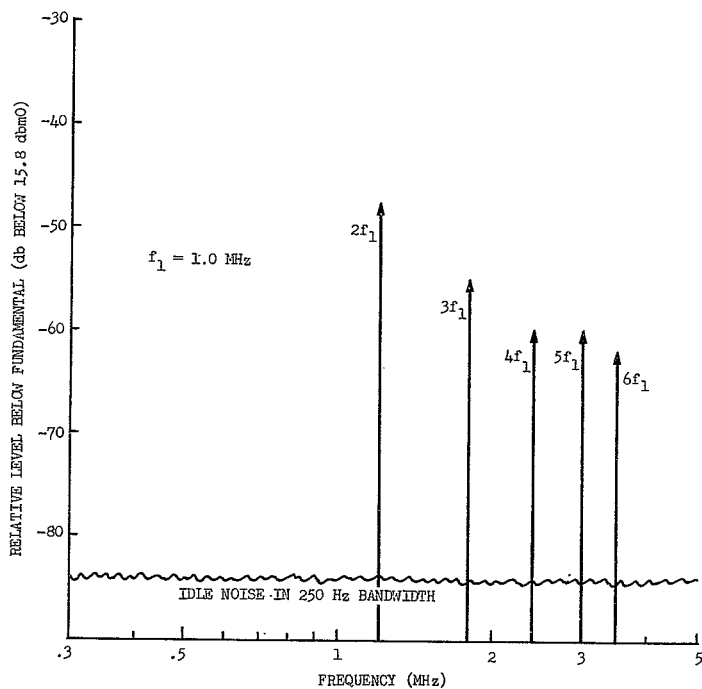
Figure 3.16. One-Tone Test (Mojave, MA Mode, ATS-3)
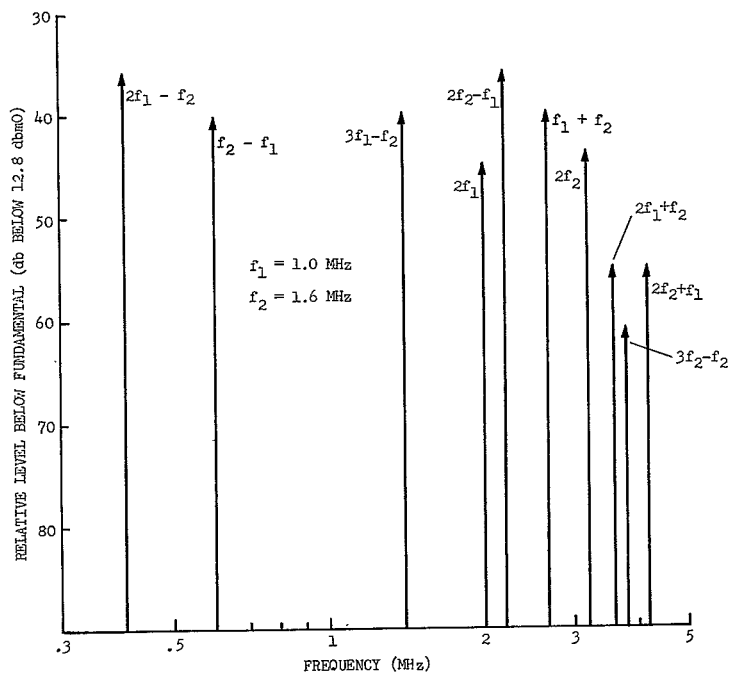
Figure 3.17. Two-Tone Test (Mojave, MA Mode, ATS-3)
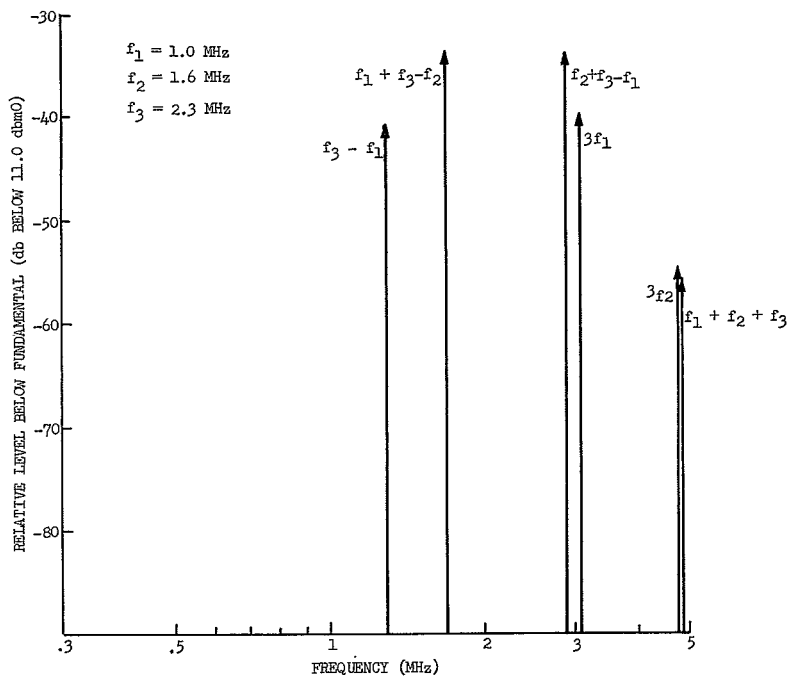
Figure 3.18. Three-Tone Test (Mojave, MA Mode, ATS-3)

3.49
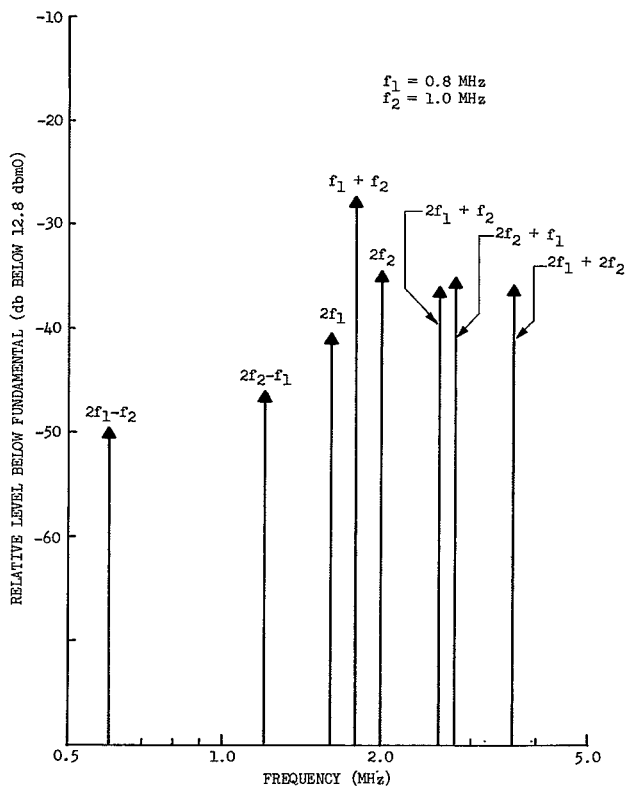
Figure 3.19. Two-Tone Test (Rosman, FT Mode, ATS-3)
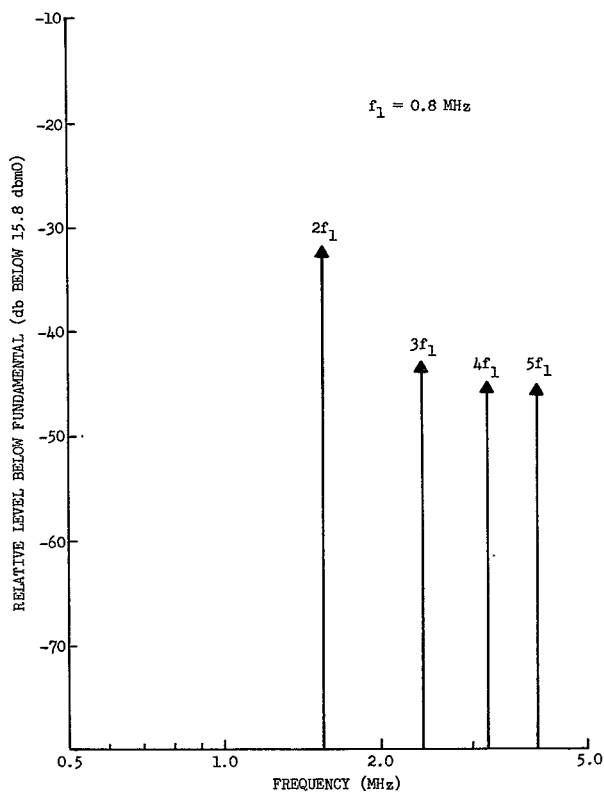
Figure 3.20. Three-Tone Test (Rosman, FT Mode, ATS-3)
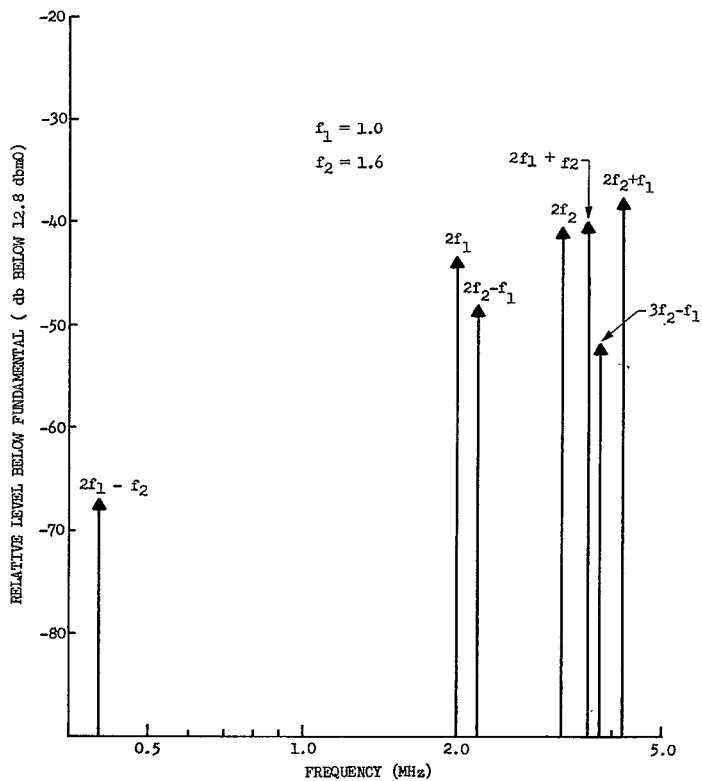
Figure 3.21. Two-Tone Test (Mojave, FT Mode, ATS-3)

3.52
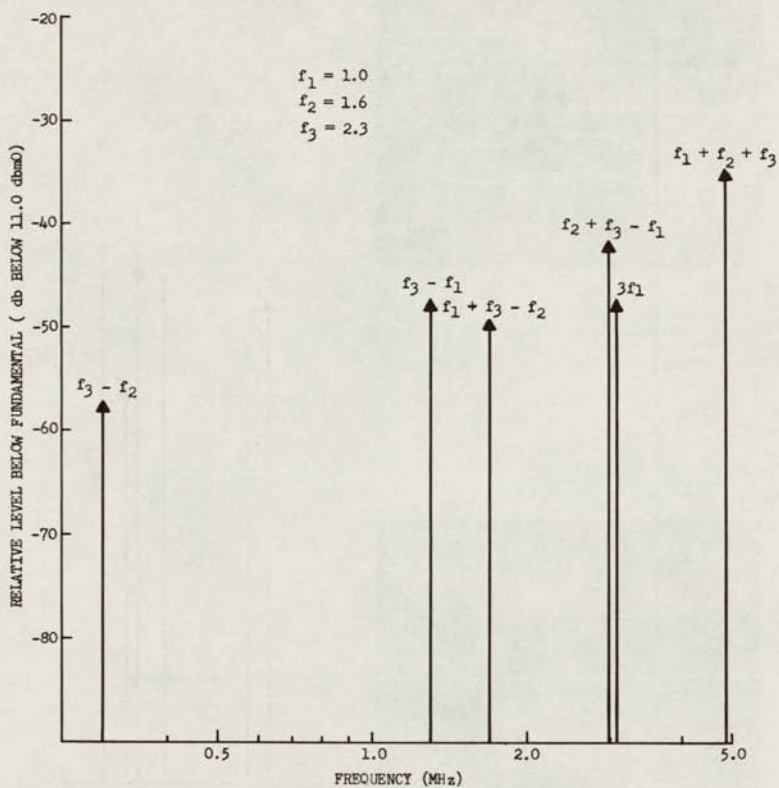
Figure 3.22. Three-Tone Test (Mojave, FT Mode, ATS-3)
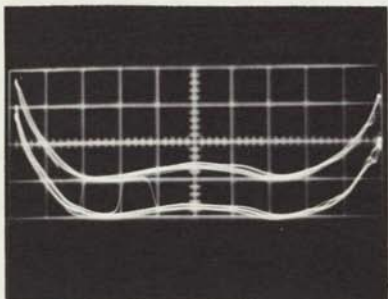
$$G.D. = .31\omega + .27\omega^2$$

S/C Loop - Group Delay (T)
Vertical - 30 Nanoseconds/cm
Horiz. - 3 MHz/cm
Total Freq. Deviation $\pm$ 15 MHz

Figure 3.23. IF/RF Group Delay Measurements for FT Mode
(Mojave, ATS-3, B_{IF} = 30 MHz)
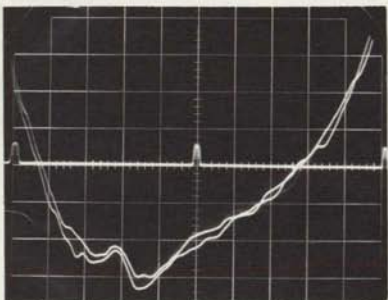
$$G.D. = 1.2\omega + .27\omega^2$$

S/C Loop - Group Delay (T)
Vertical - 30 Nanosecond/cm
Horiz. - 3 MHz/cm
Total Freq. Deviation $\pm$ 15 MHz

Figure 3.24. IF/RF Group Delay Measurements for FT Mode
(Rosman, ATS-3, B_{IF} = 30 MHz)

3.54
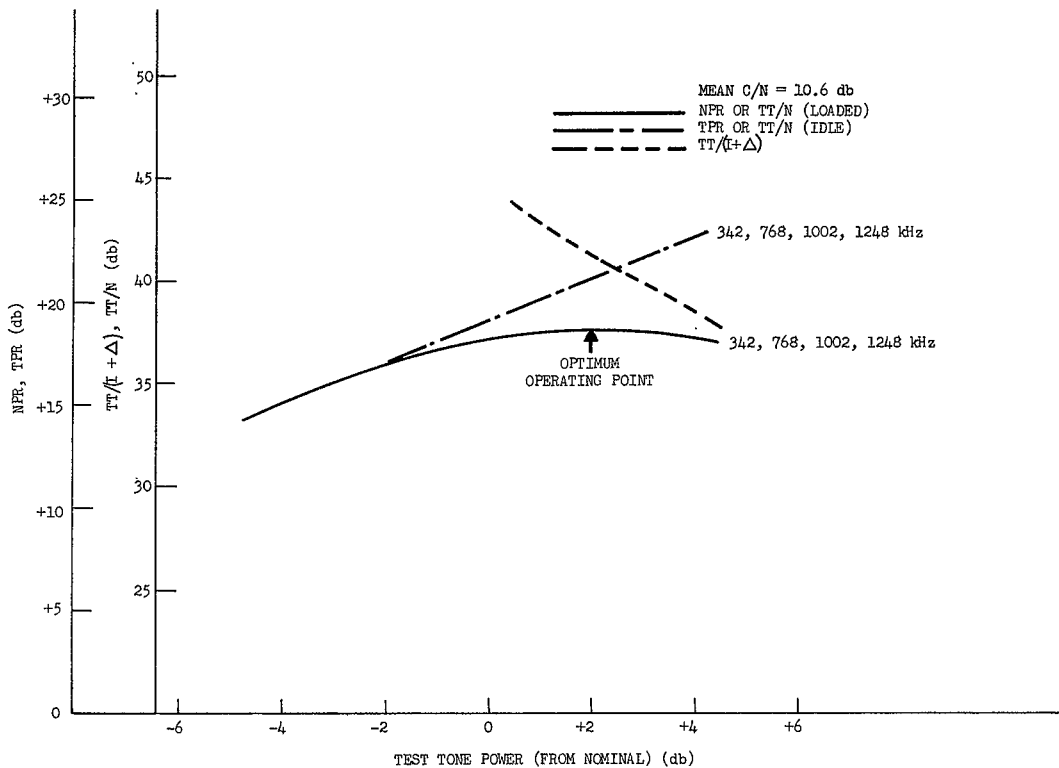
Figure 3.25. Mean NPR/TPR, TT/N, and TT/(I + Δ) Versus Test Tone Power (Cooby Creek, SSB-PhM ATS-1, 52.2 dbm EIRP, 12 MHz IF Filter)
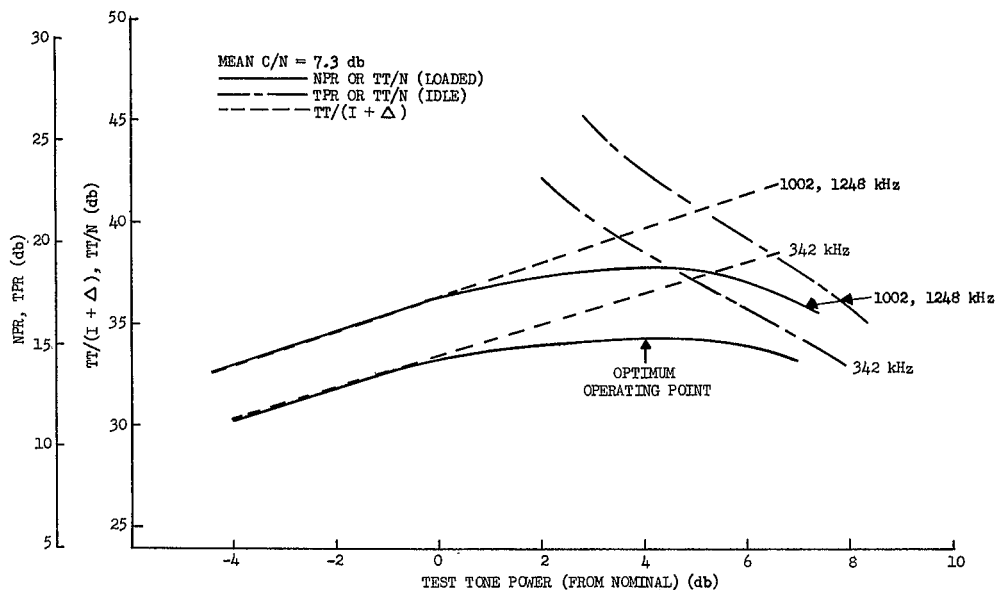
Figure 3.26. Mean NPR/TPR, TT/N and TT/(I + Δ) Versus Test Tone Power (Cooby Creek, SSB-PhM ATS-1, 52.2 dbm EIRP, 30 MHz IF Filter, 240 Channels)
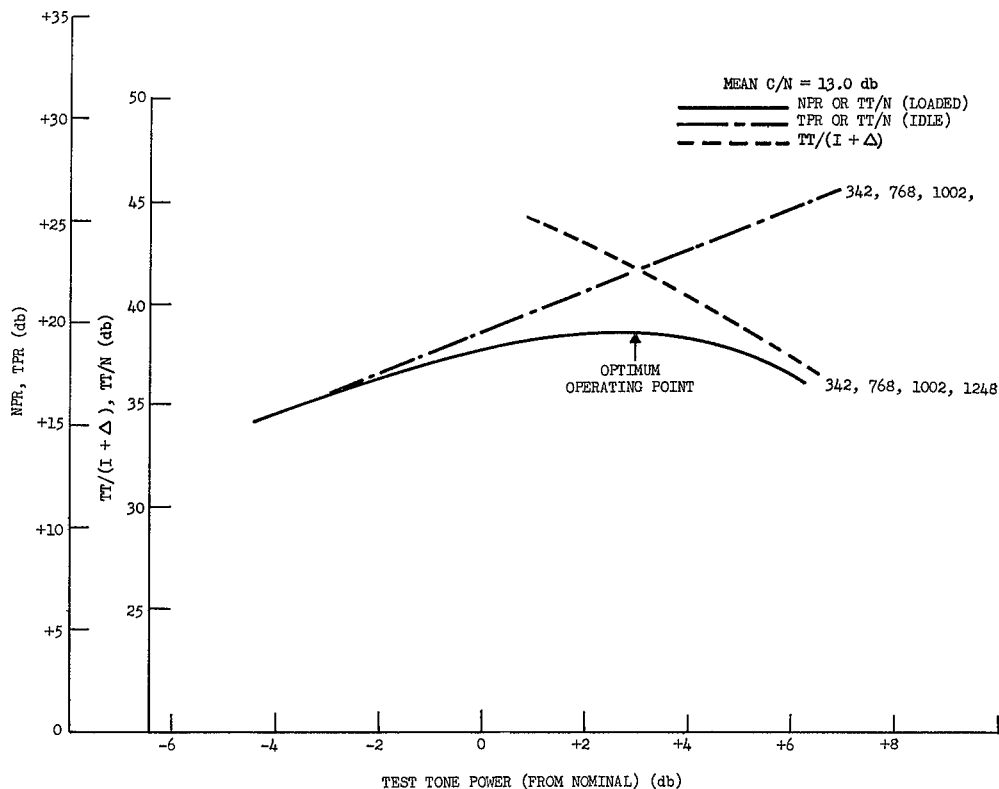
Figure 3.27. Mean NPR/TPR, TT/N and TT/(I + Δ) Versus Test Tone Power (Mojave, SSB-PhM, ATS-1 52.2 dbm EIRP, 12 MHz IF Filter)

3.57

3.58
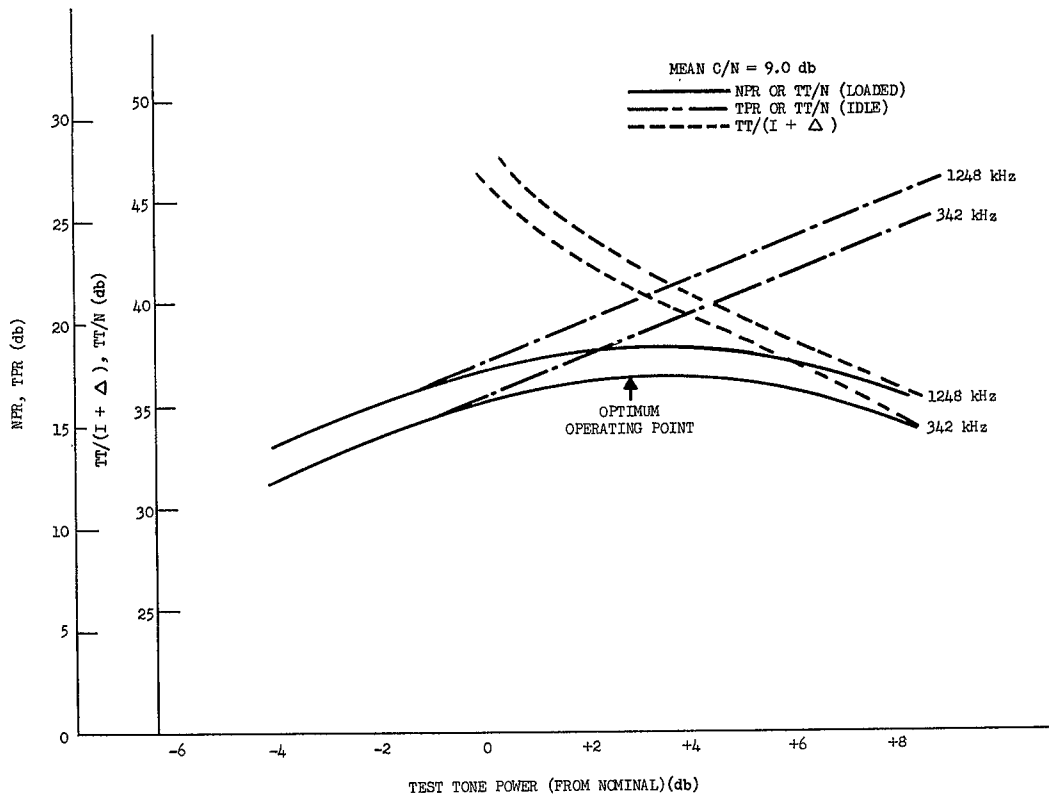
Figure 3.28. Mean NPR/TPR, TT/N and TT/(I+△) Versus Test Tone Power (Mojave SSB-PhM ATS-1
52.2 dbm EIRP, 30 MHz IF Filter, 240 Channels)
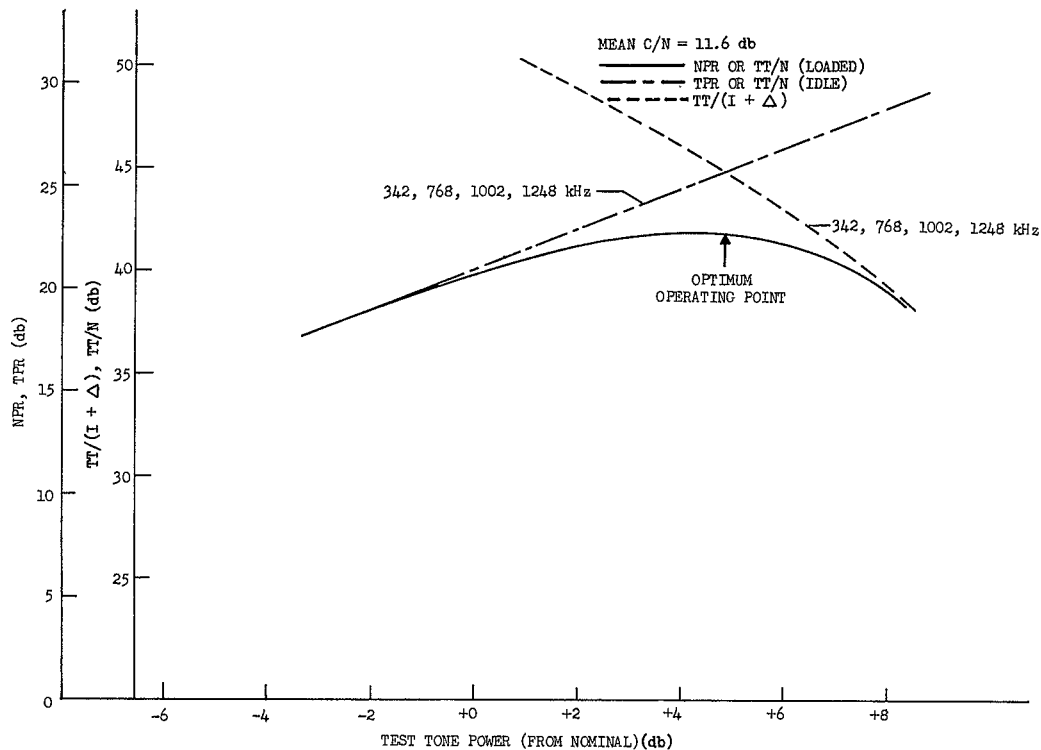
Figure 3.29. Mean NPR/TPR, TT/N and TT/(I+△) Versus Test Tone Power (Mojave SSB-PhM ATS-3 54.6 dbm EIRP, 30 MHz IF Filter, 240 Channels)
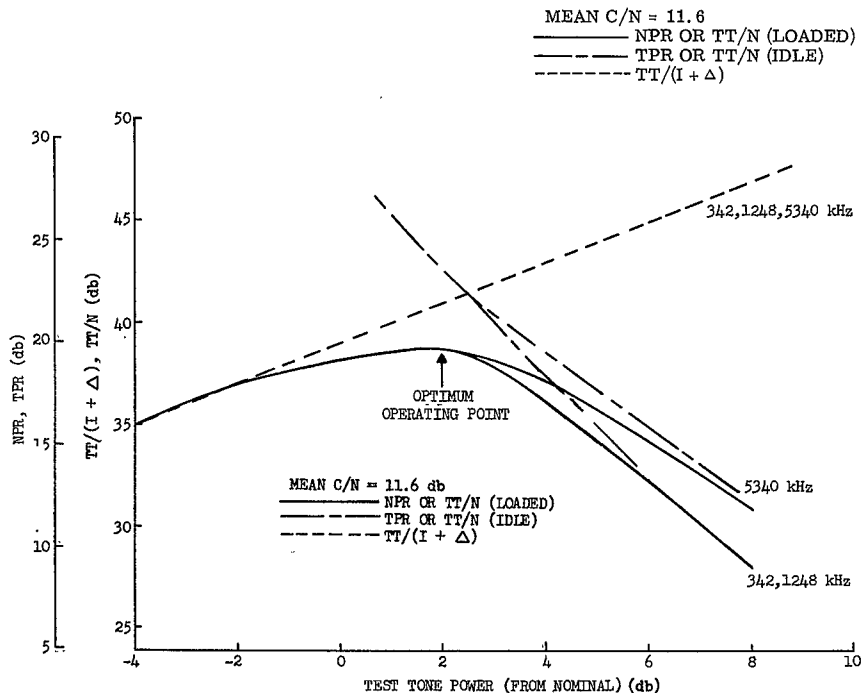
Figure 3.30. Mean NPR/TPR, TT/N and TT/(I+△) Versus Test Tone Power (Mòjave, SSB-PhM ATS-3, 54.6 dbm EIRP, 30 MHz IF Filter, 1200 Channels)
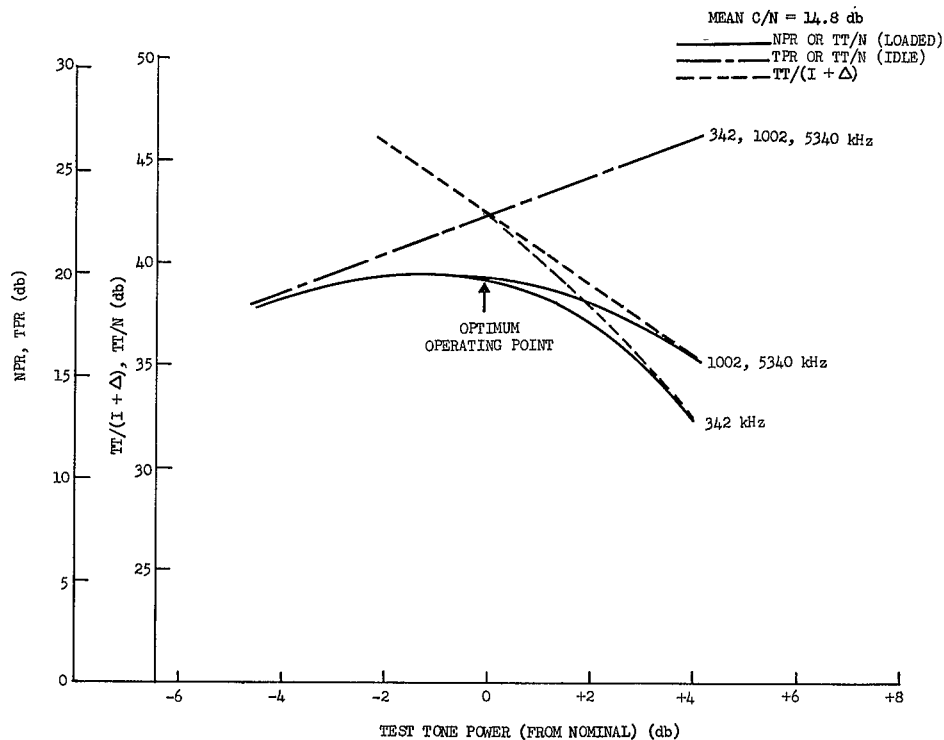
Figure 3.31. Mean NPR/TPR, TT/N, and TT/(I + △) Versus Test Tone Power (Rosman SSB-PhM, ATS-1, 52.2 dbm EIRP, 30 MHz IF Filter, 1200 Channels)
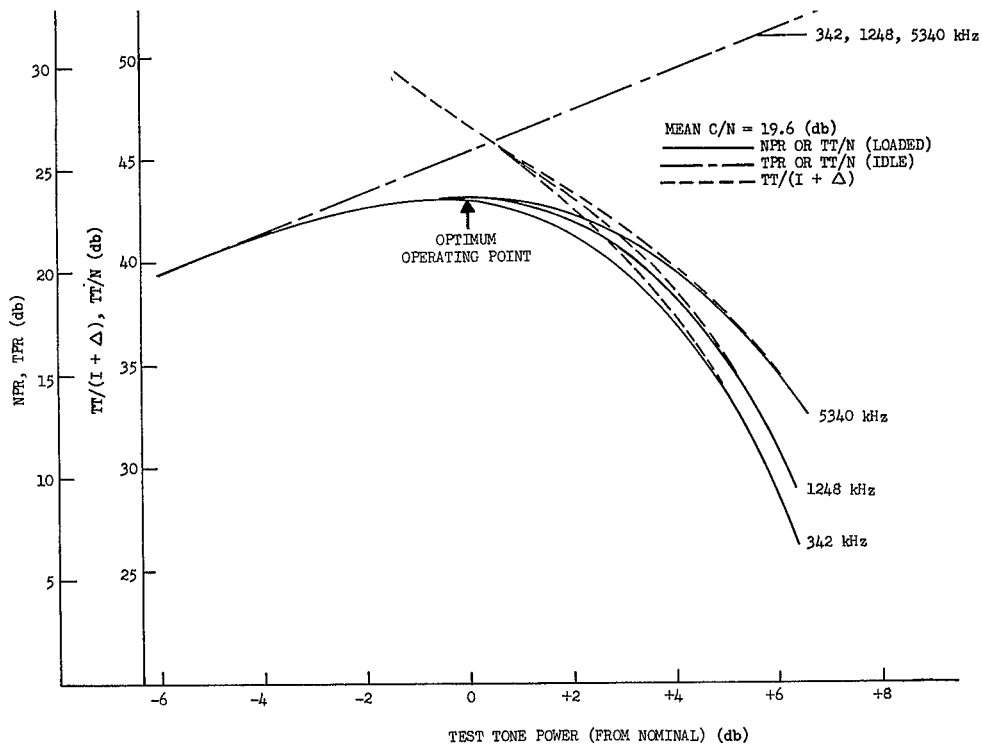
Figure 3.32. Mean NPR/TPR, TT/N, and TT/(I + Δ) Versus Test Tone Power (Rosman, SSB-PhM, ATS-3, 54.6 dbm EIRP, 30 MHz IF Filter, 1200 Channels)
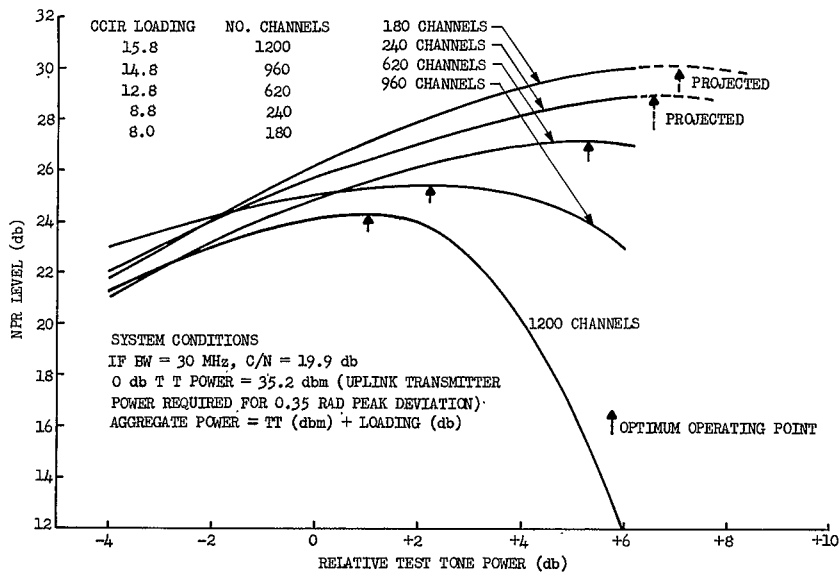
Figure 3.33. NPR Versus TT Power For Various Channel Loading (Rosman, ATS-3, 342 kHz)

CCIR LOADING   NO. CHANNELS
   15.8   1200
   14.8   .960
   12.8   620
    8.8   240

240 CHANNEL
620 CHANNEL
960 CHANNEL
1200 CHANNEL

SYSTEM CONDITIONS

IF BW =30 MHz, C/N = 19.9 db
0 db TT TONE POWER = 35.2 dbm
(UPLINK TRANSMITTER POWER REQUIRED
FOR 0.35 RAD. PEAK DEVIATION)
AGGREGATE POWER = TT (dbm) + LOADING (db)

↑ OPTIMUM OPERATING POINT

RELATIVE TEST TONE POWER (db)

3.64
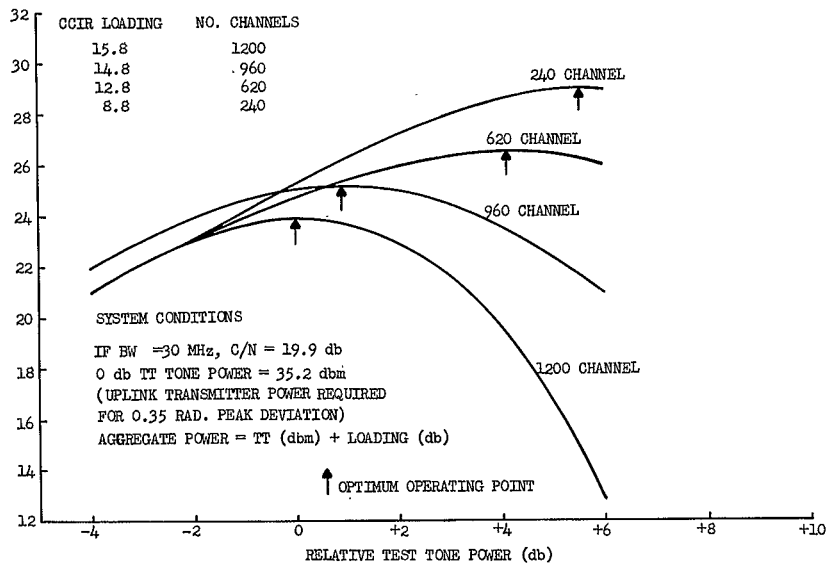
Figure 3.34. NPR Versus TT Power For Various Channel Loading (Rosman, ATS-3, 1248 kHz)
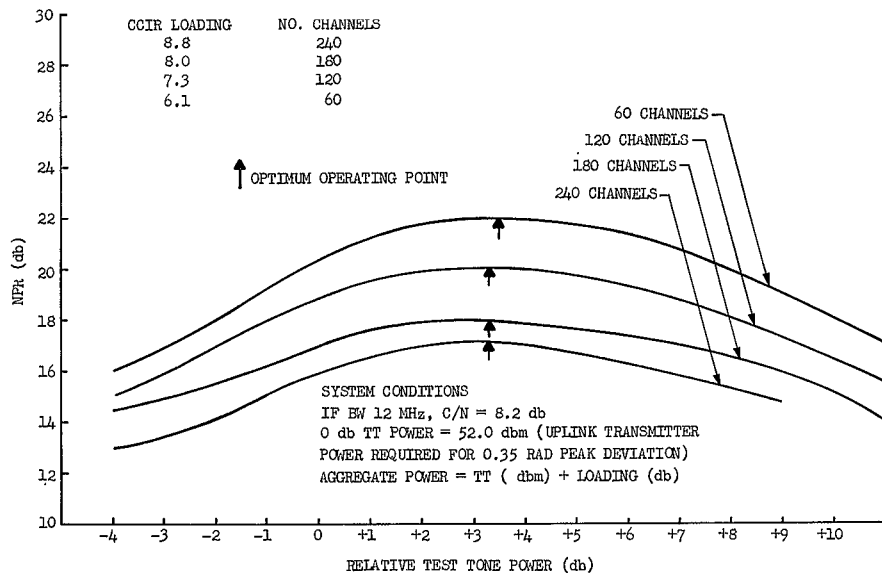
Figure 3.35. NPR Versus TT Power For Various Channel Loading (Mojave, ATS-1, 342 kHz)

CCIR LOADING   NO. CHANNELS
8.8   240
8.2   200
7.3   120
6.1   60

↑ OPTIMUM OPERATING POINT

60 CHANNEL

120 CHANNELS

200 CHANNELS

240 CHANNELS

SYSTEM CONDITIONS

IF BW = 12 MHz, C/N = 8.2 db
0 db TT POWER = 52.0 dbm (UPLINK TRANSMITTER
POWER REQUIRED FOR 0.35 RAD PEAK DEVIATION)
AGGREGATE POWER = TT (dbm) + LOADING (db)

RELATIVE TEST TONE POWER (db)

NPR (db)
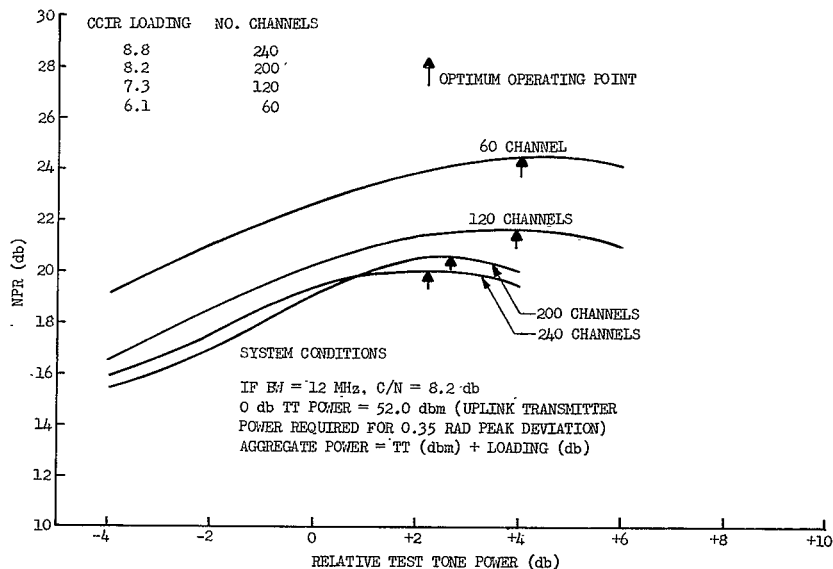
Figure 3.36. NPR Versus TT Power For Various Channel Loading
(Cooby Creek. ATS-1. 342 kHz)

3.66
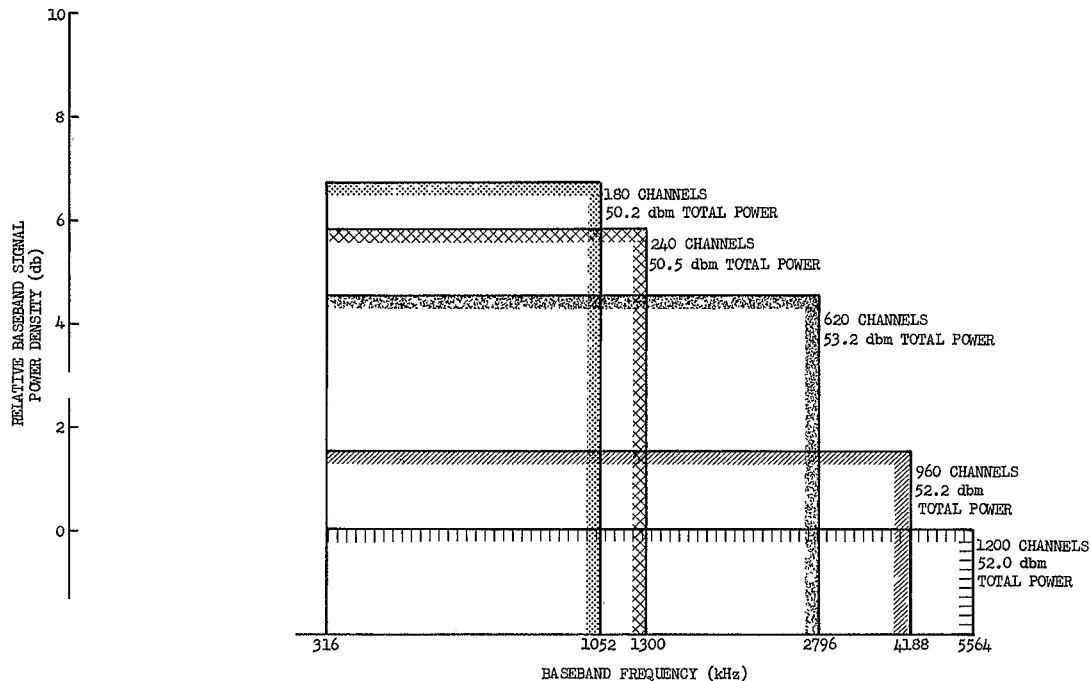
Figure 3.37. Baseband Signal Power Spectrum For Optimized TT Power (Rosman, ATS-3, 342 kHz)
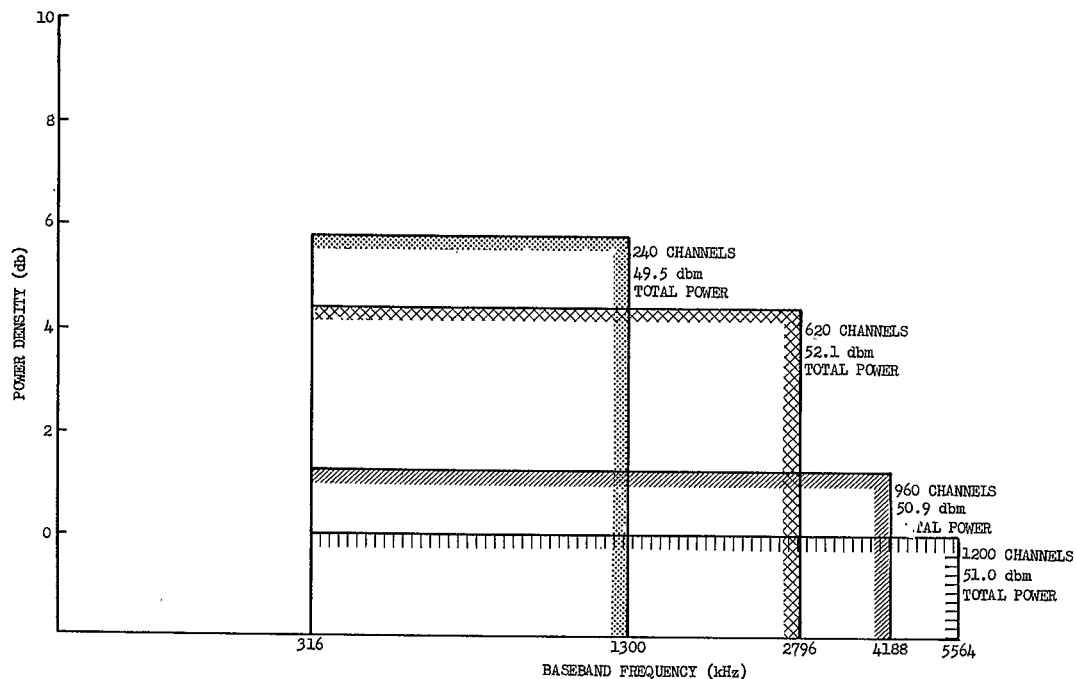
Figure 3.38. Baseband Signal Power Spectrum For Optimized TT Power (Rosman, ATS-3, 1248 kHz)
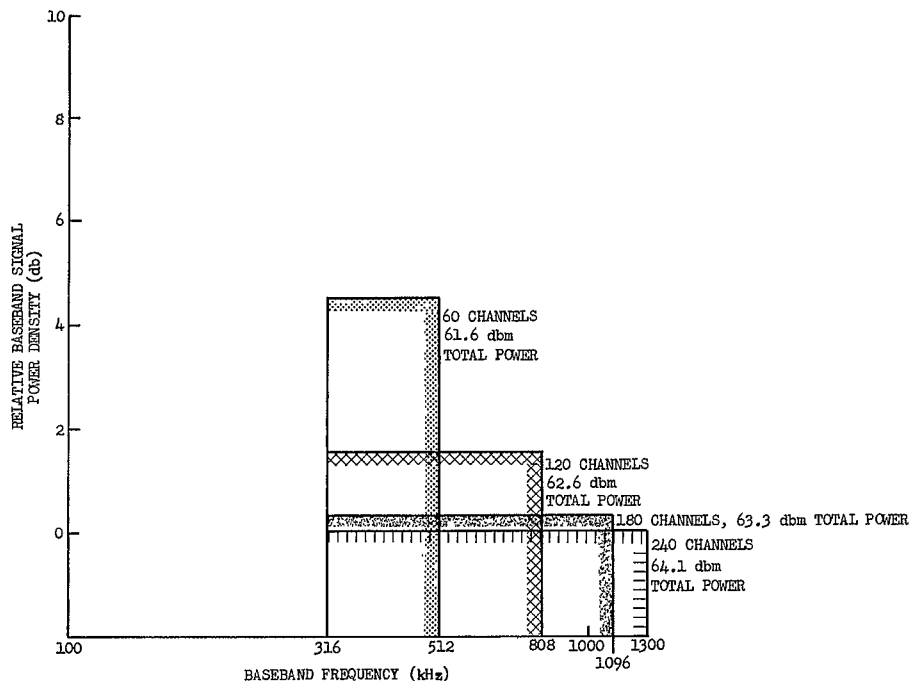
Figure 3.39. Baseband Signal Power Spectrum For Optimized TT Power (Mojave, ATS-1, 342 kHz)
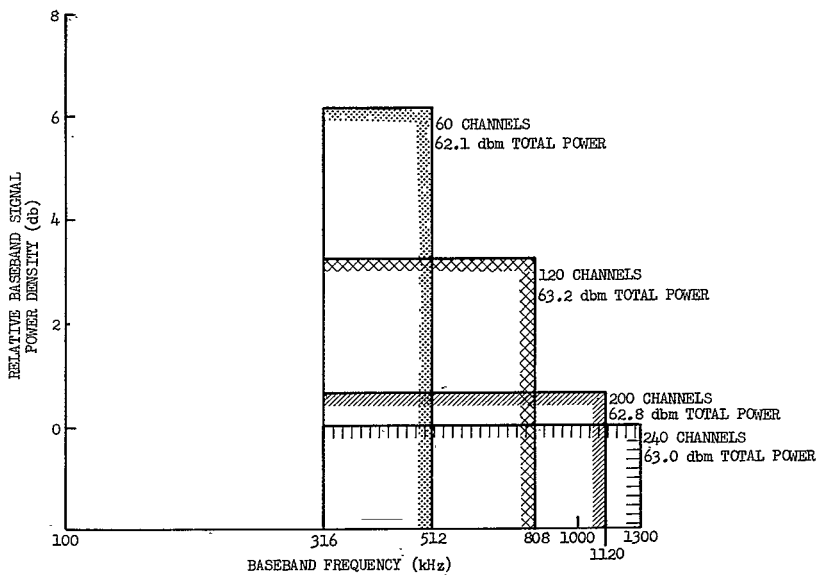
Figure 3.40. Baseband Signal Power Spectrum For Optimized TT Power
(Cooby Creek, ATS-1, 342 kHz)
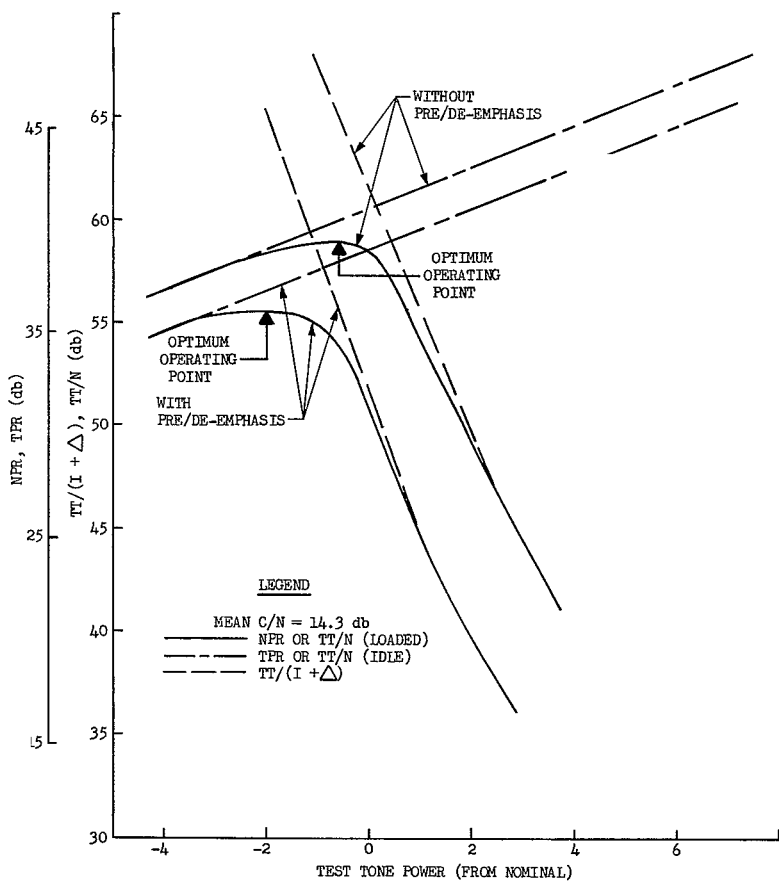
Figure 3.41. Mean NPR/TPR, TT/N and TT/(I+△) Versus Test-Tone Power
(Mojave, FT Mode, ATS-3, With and Without Pre/de-emphasis, 342 kHz)

3.71
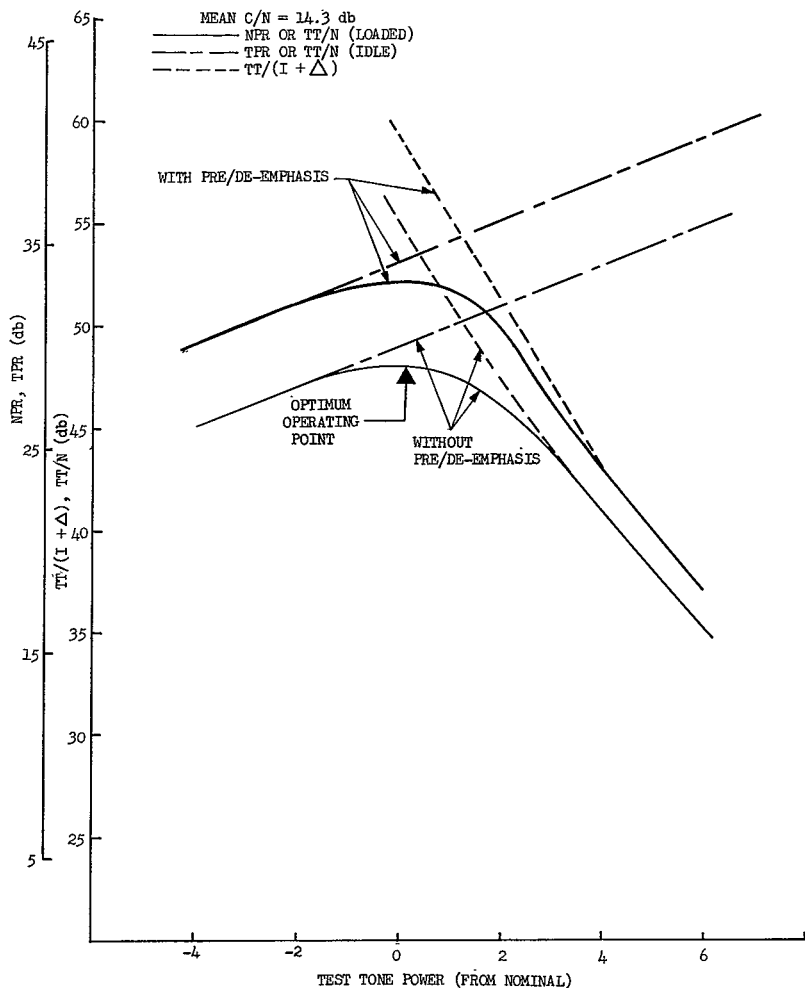
Figure 3.42. Mean NPR/TPR, TT/N and TT/(I+△) Versus Test-Tone Power
(Mojave, FT Mode, ATS-3 With and Without
Pre/de-emphasis, 1248 kHz)

3.72
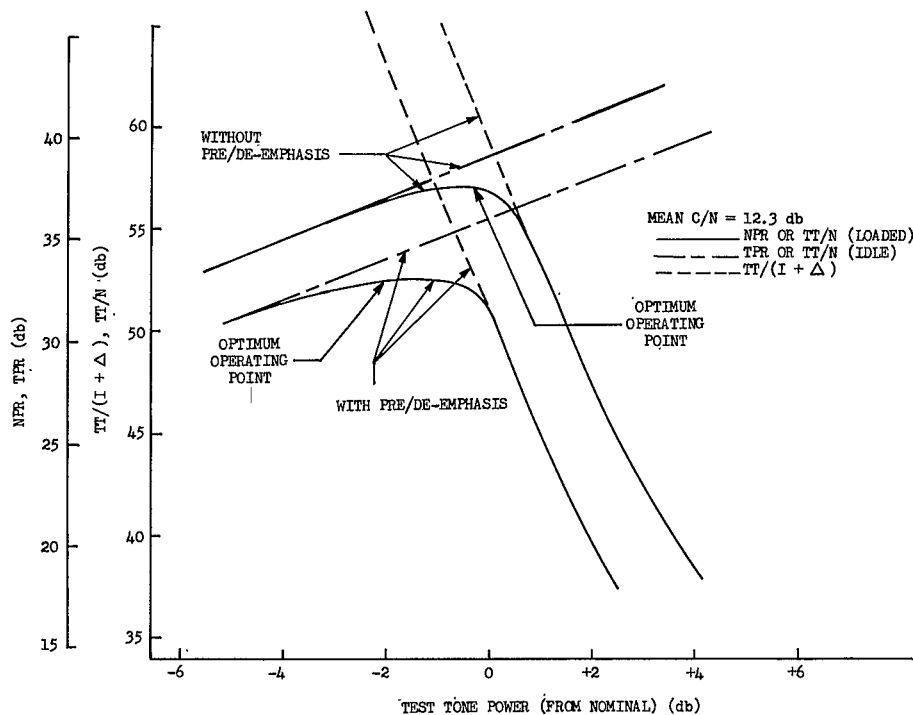
Figure 3.43. Mean NPB/TPR, TT/N, and TT/(I + Δ) Versus Test-Tone Power (Mojave, FT Mode ATS-1 52.2 dbm EIRP, With and Without Pre/de-emphasis, 342 kHz)

Figure 3.44. Mean NPR/TPR, TT/N and TT/(I + △) Versus Test-Tone Power (Mojave, FT Mode ATS-1
52.2 dbm EIRP, With and Without Pre/de-emphasis, 1248 kHz)
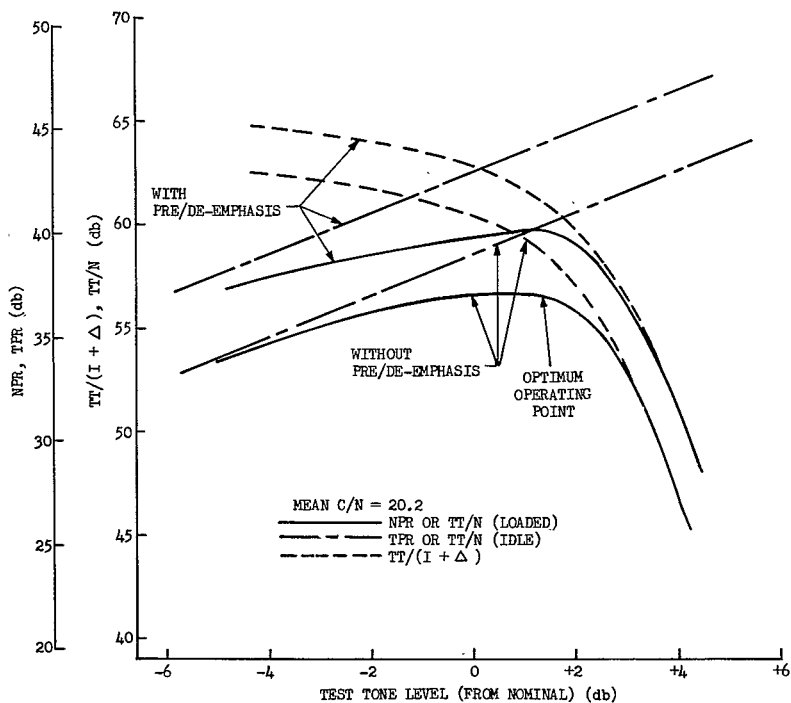
Figure 3.45.   Mean NPR/TPR, TT/N and TT/(I + Δ) Versus Test-Tone Power
(Rosman, FT Mode, ATS-3, 56.5 dbm EIRP, With and Without
Pre/de-emphasis, 342 kHz)
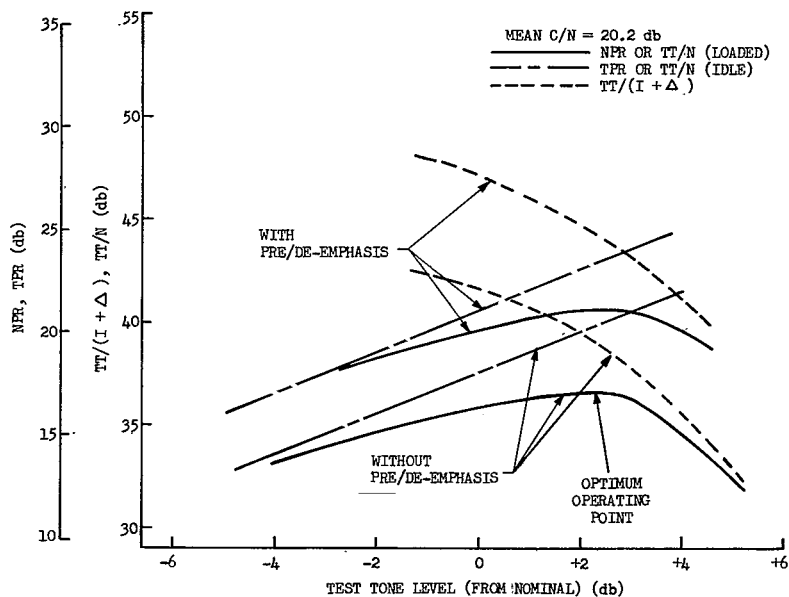
Figure 3.46. Mean NPR/TPR, TT/N and TT/(I+△) Versus Test Tone Power
(Rosman, FT Mode, ATS-3, 56.5 dbm EIRP, With and Without
Pre/de-emphasis, 5340 kHz)
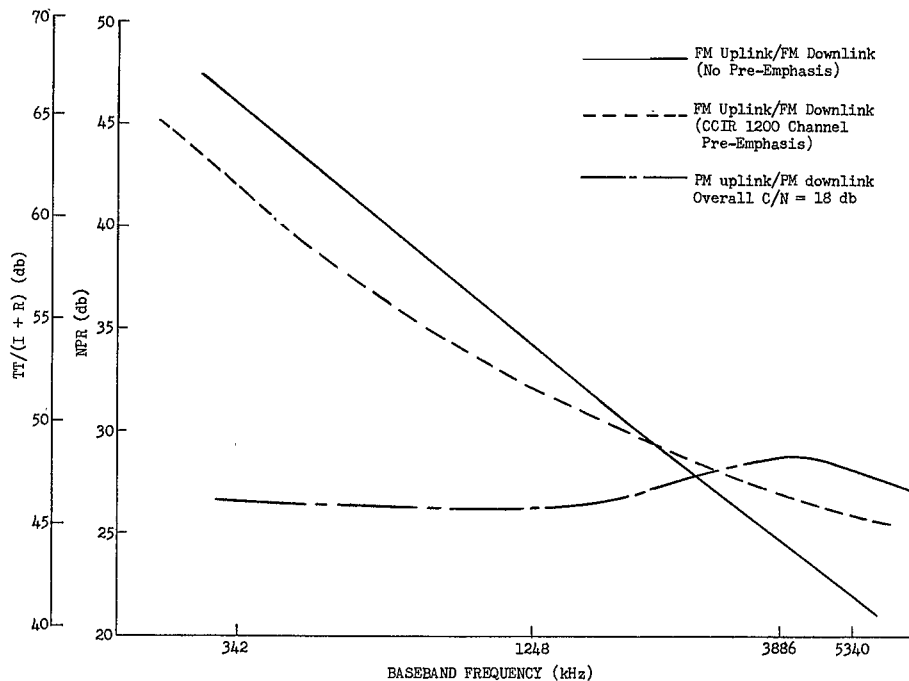
Figure 3.47. Comparison of Pre-emphasis in the FT Mode (ATS-3, in 1200-Channel Loading)
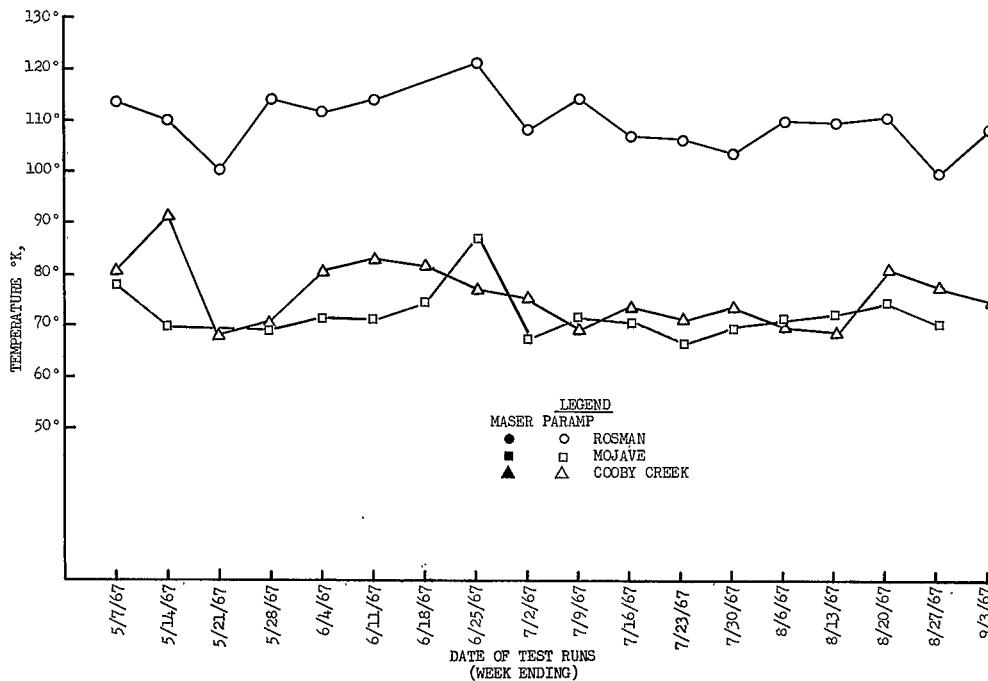
Figure 3.48. Operational System Noise Temperature (ATS-1) (Sheet 1 of 9)
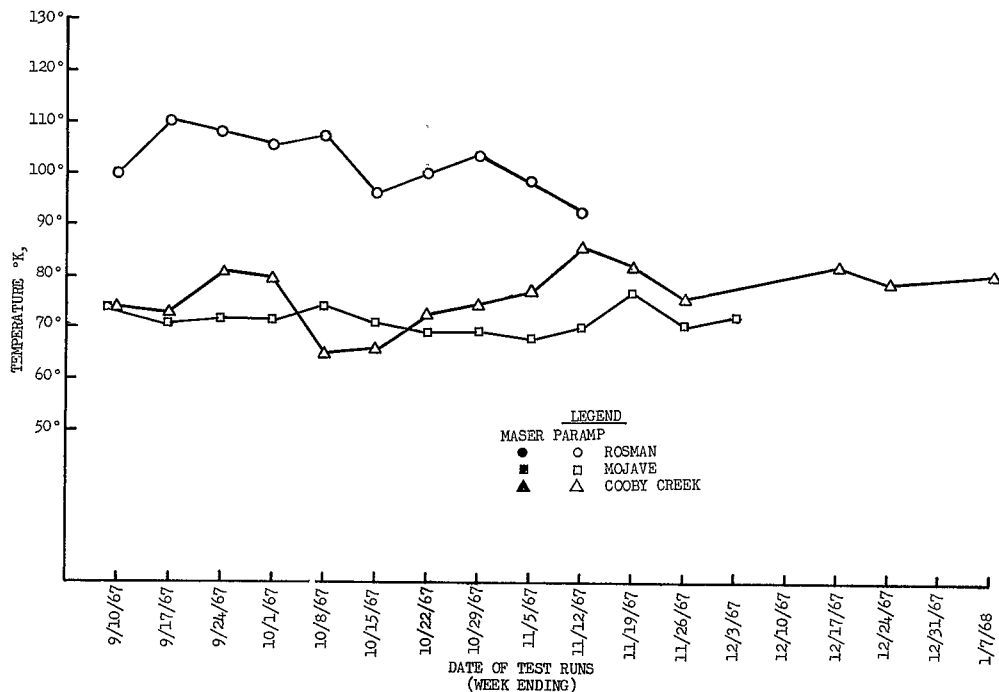
Figure 3.48. Operational System Noise Temperature (ATS-1) (Sheet 2 of 9)
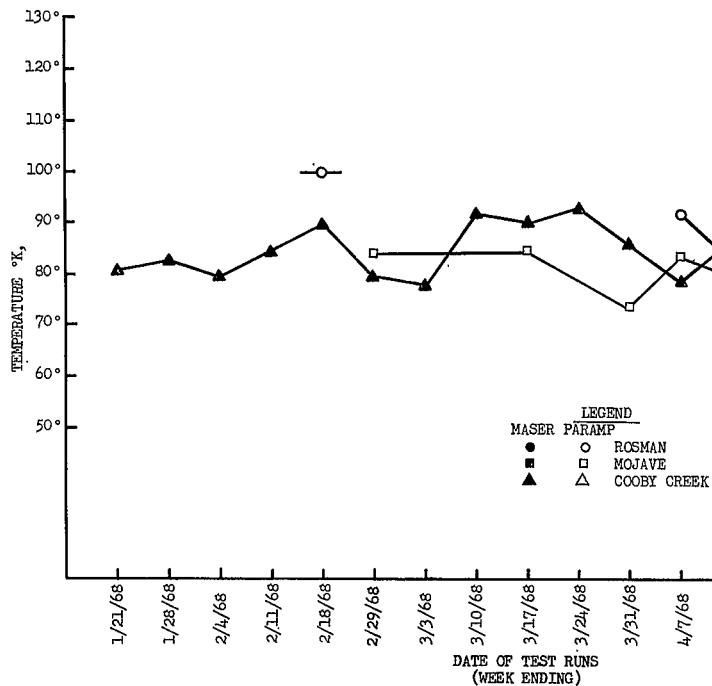
Figure 3.48. Operational System Noise Temperature (ATS-1) (Sheet 3 of 9)
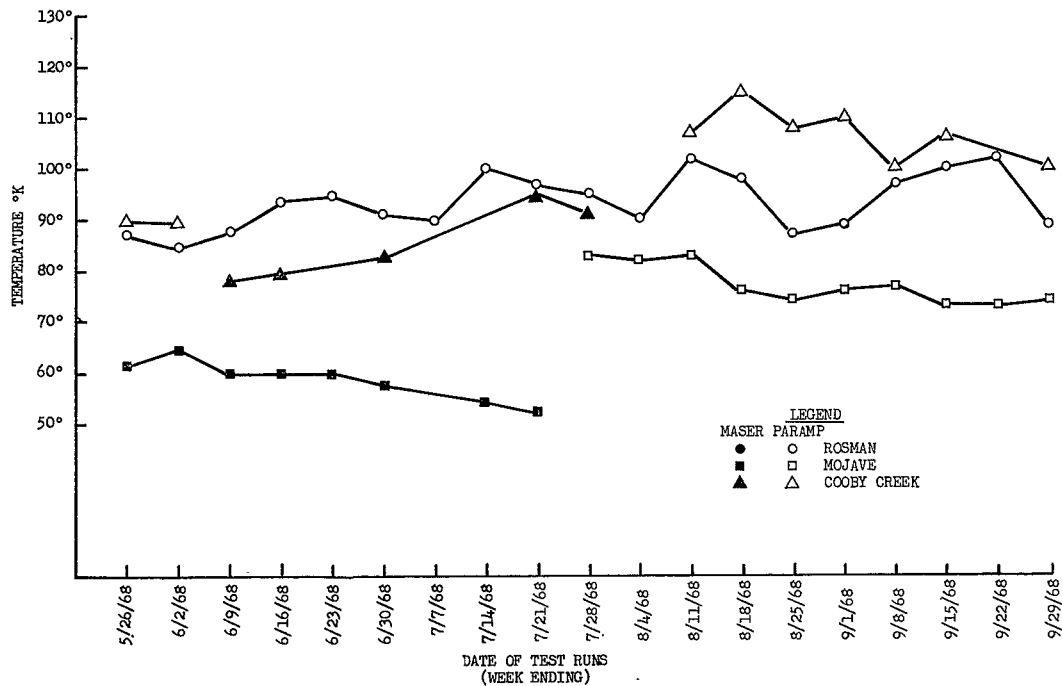
Figure 3.48. Operational System Noise Temperature (ATS-1) (Sheet 4 of 9)
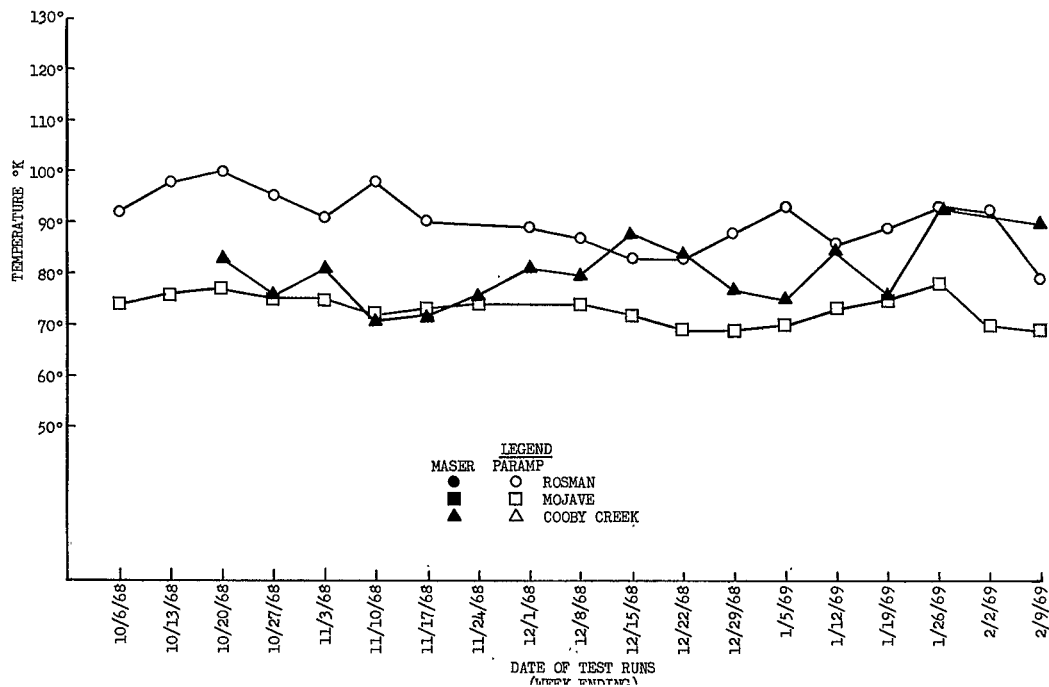
Figure 3.48. Operational System Noise Temperature (ATS-1) (Sheet 5 of 9)

3.82
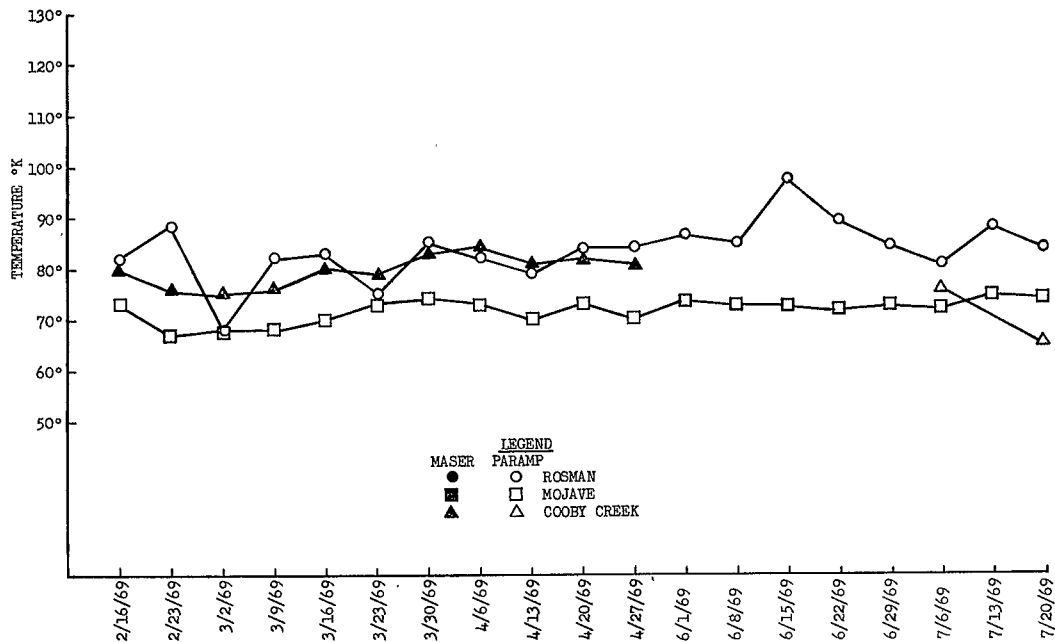
Figure 3.48. Operational System Noise Temperature (ATS-1) (Sheet 6 of 9)
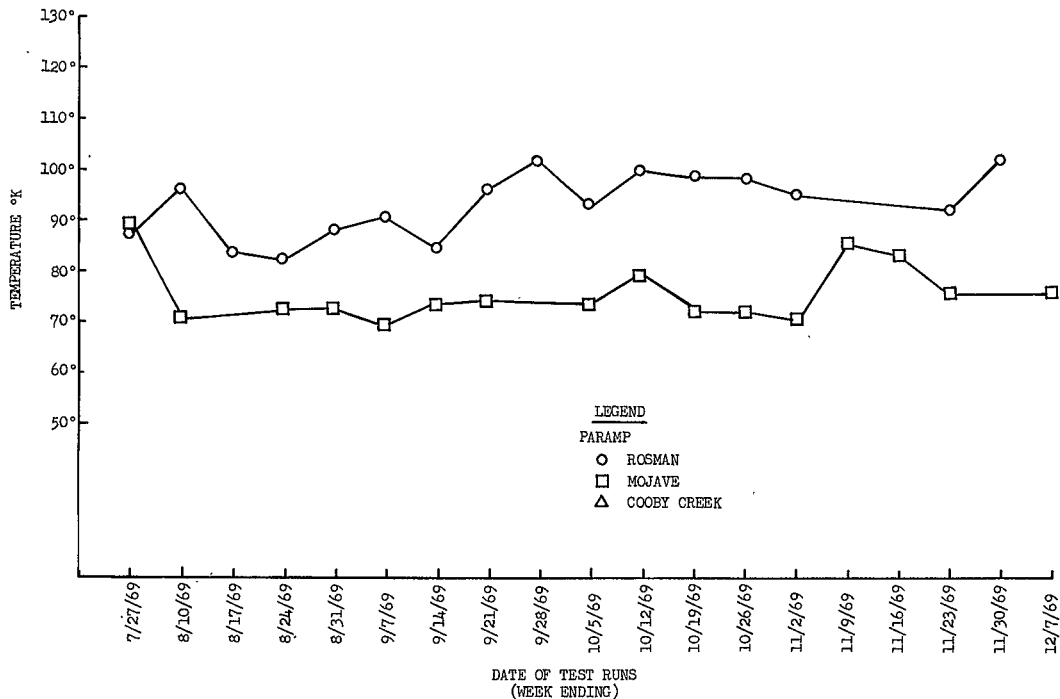
Figure 3.48. Operational System Noise Temperature (ATS-1) (Sheet 7 of 9)
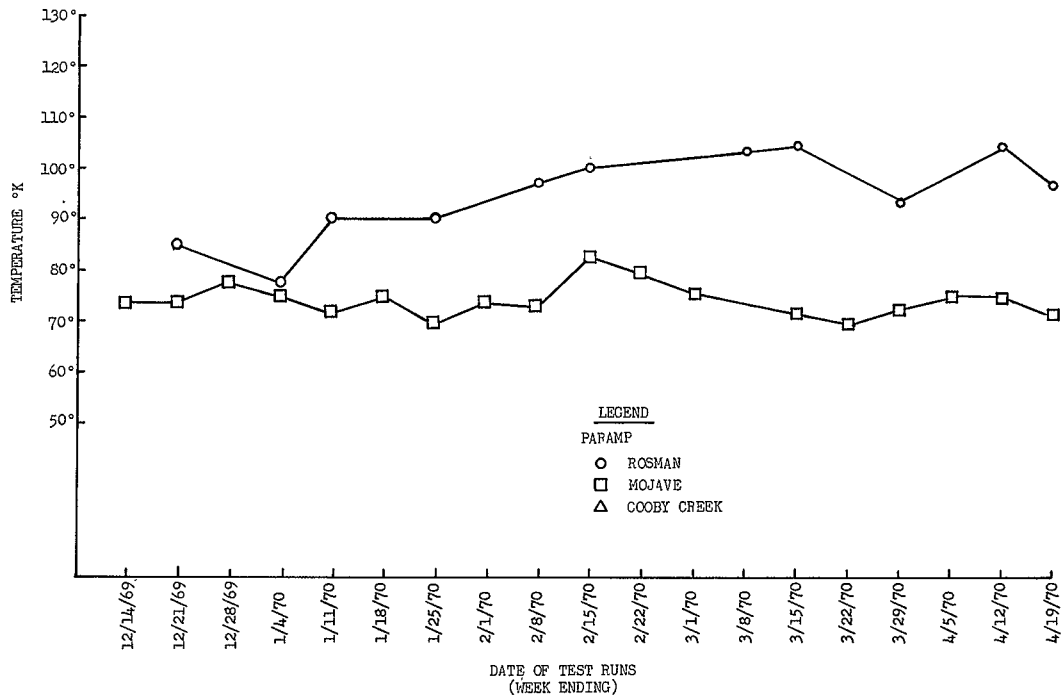
Figure 3.48. Operational System Noise Temperature (ATS-1) (Sheet 8 of 9)
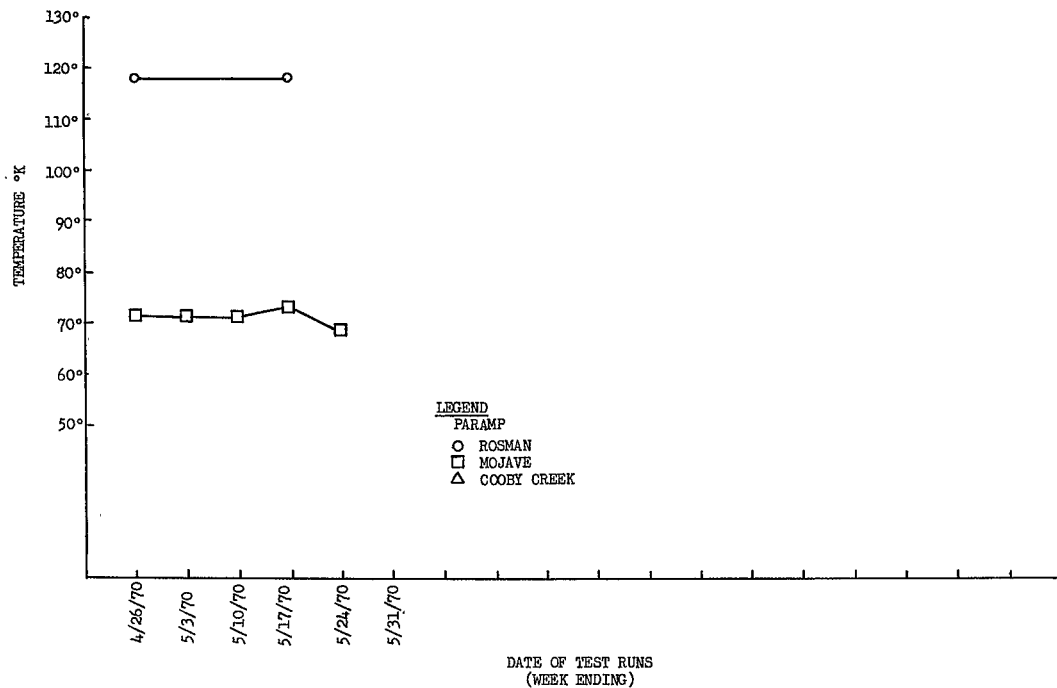
Figure 3.48. Operational System Noise Temperature (ATS-1) (Sheet 9 of 9)
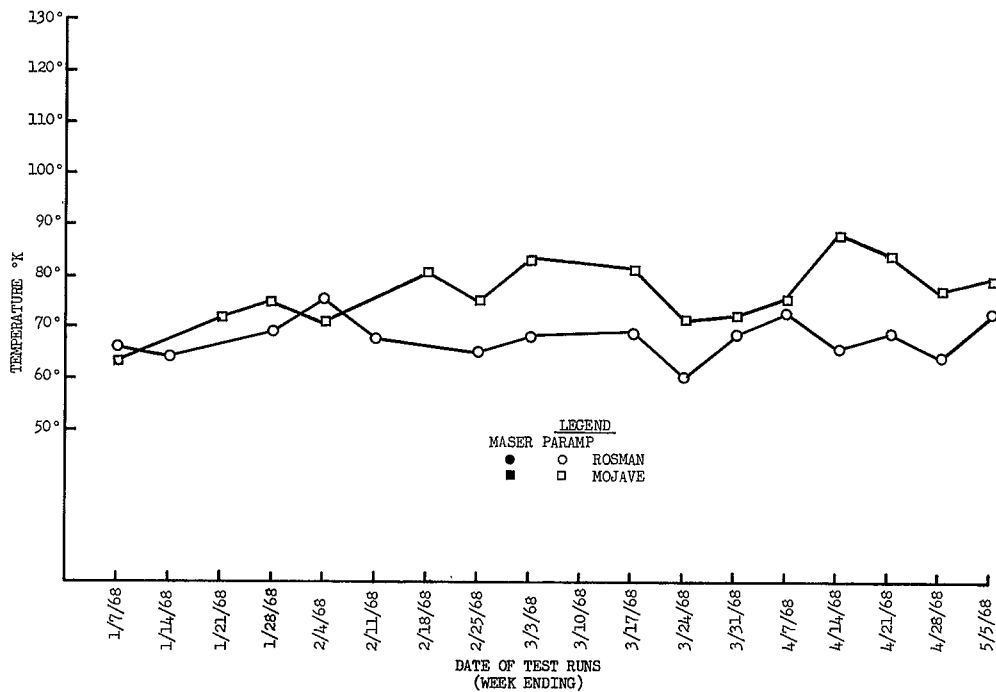
Figure 3.49. Operational System Noise Temperature (ATS-3) (Sheet 1 of 7)
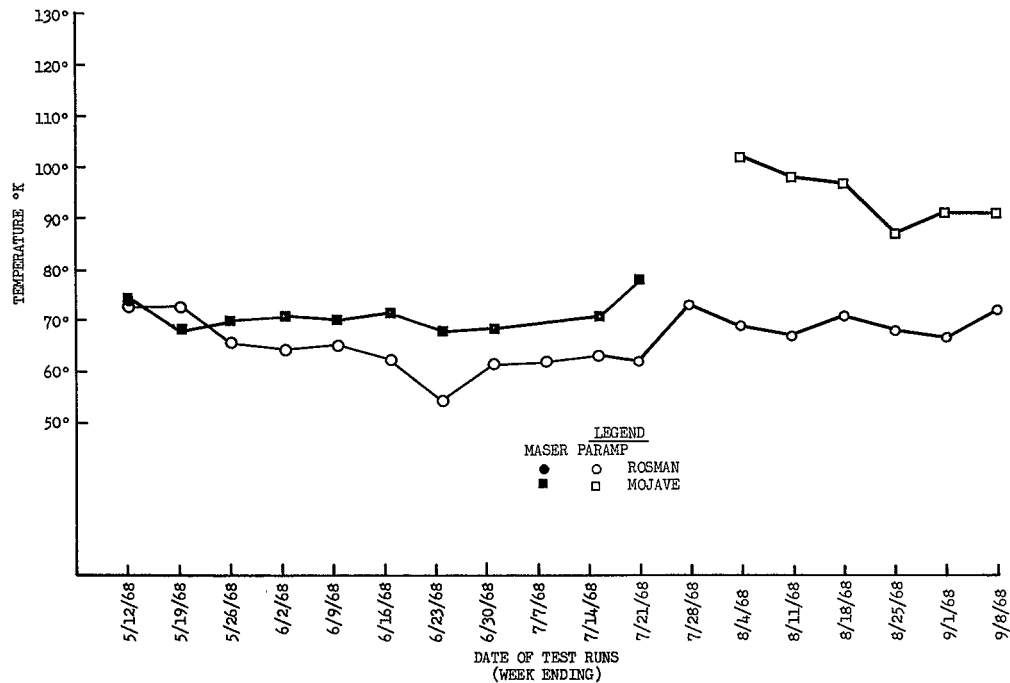
Figure 3.49. Operational System Noise Temperature (ATS-3) (Sheet 2 of 7)
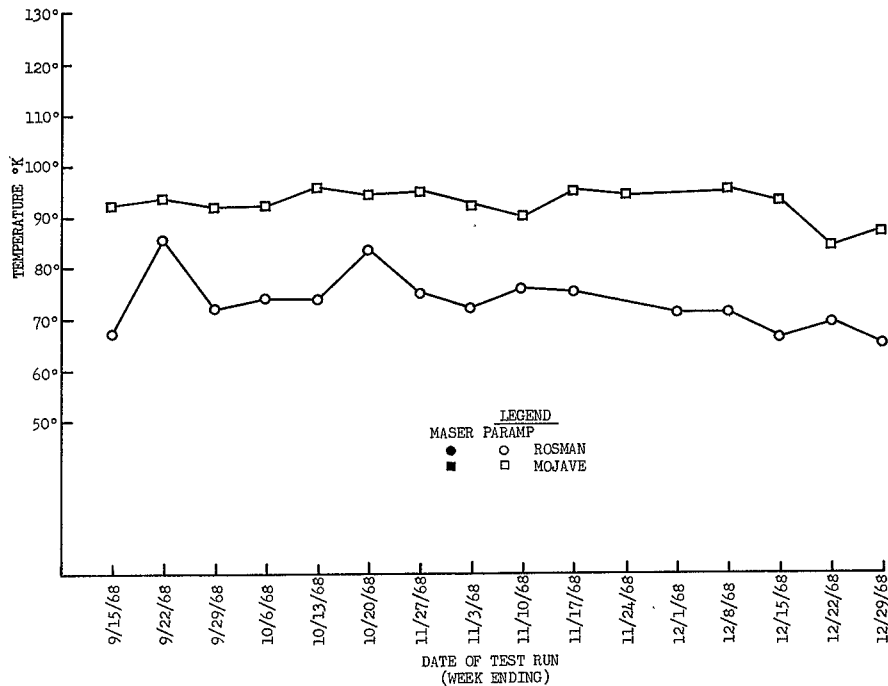
Figure 3.49. Operational System Noise Temperature (ATS-3) (Sheet 3 of 7)
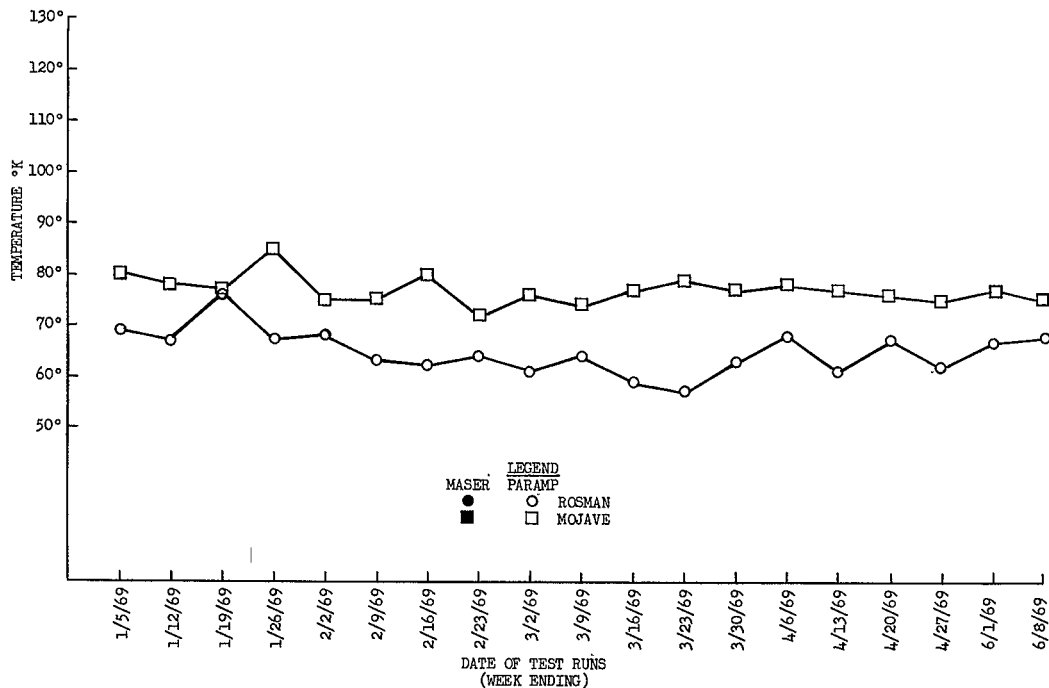
Figure 3.49. Operational System Noise Temperature (ATS-3) (Sheet 4 of 7)

3.90
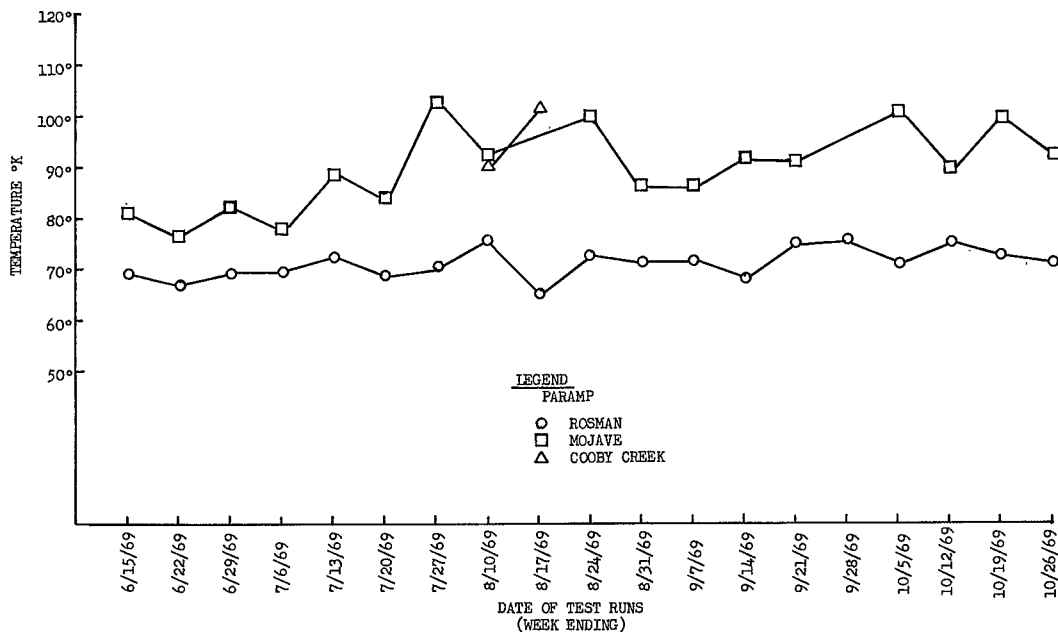
Figure 3.49. Operational System Noise Temperature (ATS-3) (Sheet 5 of 7)
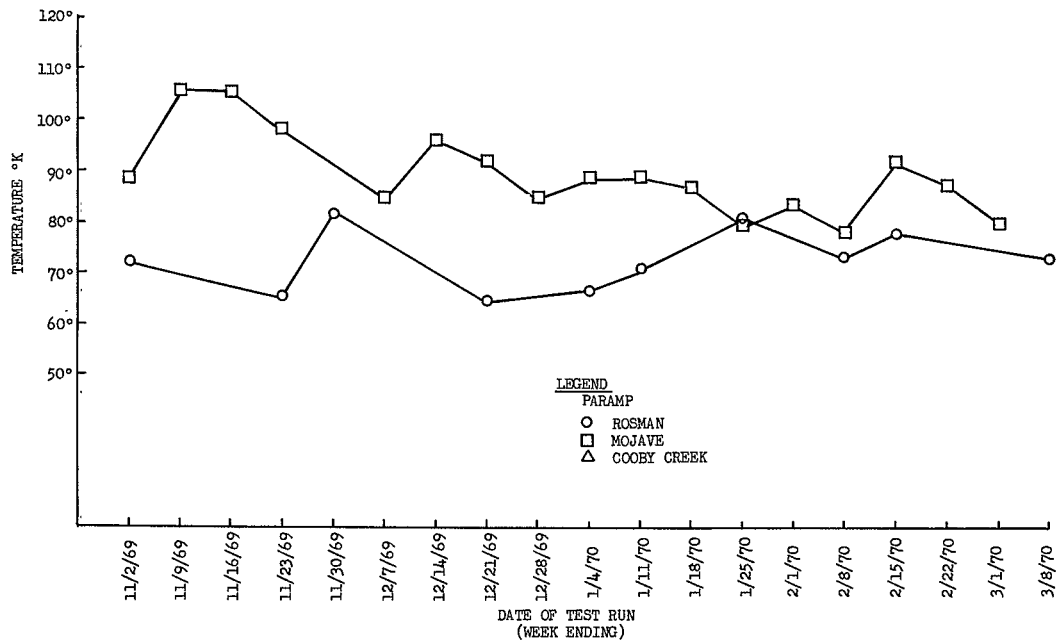
Figure 3.49. Operational System Noise Temperature (ATS-3) (Sheet 6 of 7)
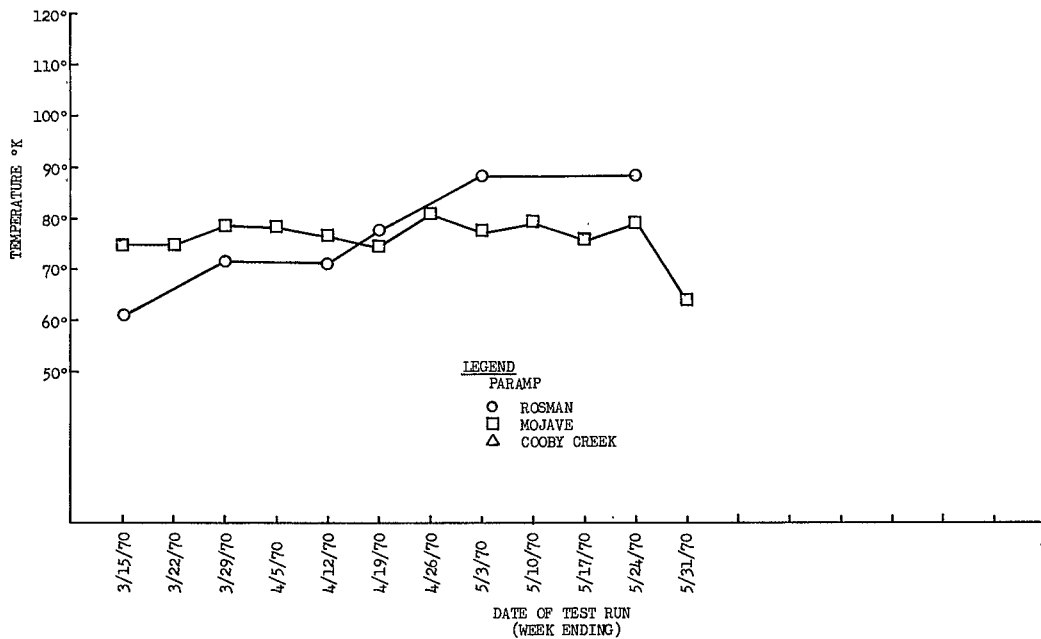
Figure 3.49. Operational System Noise Temperature (ATS-3) (Sheet 7 of 7)

3.2.2 FDM BASEBAND ATTENUATION VERSUS FREQUENCY (BASEBAND FREQUENCY RESPONSE) (J.W. Bedinger) (MA-BB-2.1)

3.2.2.1 Description and Test Results

OBJECTIVE

The objective of this experiment is to determine the baseband frequency response for the SSB/PhM mode from the transmitter baseband input to the receiver baseband output for system conditions utilizing the ATS-1 and ATS-3 satellites. The response covers a frequency range of 300 kHz to 6 MHz and employs two methods of collecting data: (1) a sweep technique above 1 MHz that is supplemented by a point-to-point technique below 1 MHz, (2) a point-to-point measurement over the whole frequency band (300 kHz to 6 MHz).

TEST CONDITIONS

The baseband frequency response is measured by a sweep oscillator, covering the baseband frequency range of 300 kHz to 6 MHz, connected to the SSB transmitter baseband input. The receiver is terminated in the receiver detector unit of the test set. The output of the detector is connected to the vertical deflection input of a calibrated strip chart recorder which has its horizontal deflection input synchronized with the oscillator sweep rate. The resulting strip chart recordings are a permanent record of the baseband frequency response. The normal method of obtaining data is by the sweep technique which is supplemented between 300 kHz and 1 MHz by the point-to-point measurement. For this report only data taken over the whole frequency band by a normal point-to-point measurement will be presented. The reason for this is the poor repeatability of the results from the sweep response technique. The amplitude versus baseband frequency curves are normalized relative to the response at 1 MHz and also corrected for any cable losses in the system. Frequency scale expansion between 300 kHz to 1 MHz is necessary to accurately plot the response. The SSB/PhM receiver has a 315-kHz to 5.8-MHz bandpass filter with a response which is nominally flat between 500 kHz to 5 MHz.

STANDARDS

No applicable standards exist for FDM operation.

RESULTS

The response curves presented in this analysis are typical SSB/PhM test runs from each station. For a particular satellite, each station has a similar response; therefore, a composite response curve may be representative for all stations using that satellite. The response curves for this experiment are shown in figures 3.50 and 3.51 depicting data from ATS-1 and ATS-3. The plots shown in figure 3.50 are derived from tests at 3 stations (Rosman, Cooby Creek, Mojave) and are typical of the results obtained from the three

stations. The response labelled, "AVG PM RCVR Response" is the average measured response in a test loop that only includes the PM receiver and a test modulator. This response is given as a standard for comparing the S/C loop results.

Figure 3.51 shows the results of a multistation test performed with Rosman and Mojave on ATS-3. The test was performed by Rosman transmitting the test frequencies and both Rosman and Mojave measuring the response. It was repeated with Mojave transmitting the test frequencies. The responses for the two conditions were almost identical, hence, only one response is presented. A comparison of the baseband frequency response with filter characteristics as specified by the baseband filter manufacturer is given in table 3.7.

3.2.2.2 Analysis of Test Results

As shown in figure 3.50, good correlation exists between the various responses for the stated system conditions in the flat portion of the baseband frequency range. Hence in this frequency interval the response is mainly determined by the baseband filter in the PM receiver. This would normally be expected. Response deviations occur between stations and the filter manufacturer's roll-off characteristics in the upper and lower skirt regions as shown in table 3.51 for the ATS-1 test loop. These variations are due to the following factors: (1) Rate of change of the response in the skirt regions is quite high; consequently second order effects on the response would be more pronounced. These effects would include such things as the response variations in the SSB transmitter and the effect of the S/C circuitry on the overall response. (2) Measurement accuracy of the response is more critical in the skirt regions. This accuracy will depend on the stability of the measuring unit and the magnitude of the signal-to-noise ratio. Noise impinging on the test signal will definitely degrade the measurement accuracy.

Results of the multistation test shown in figure 3.51 (ATS-3 test loop) shows a more pronounced roll-off at the high end of the band relative to the response for the ATS-1 test loop. Quantitative measurements shown in table 3.7 at test frequencies of 5.6 MHz and 5.8 MHz give the actual response differences. Since Mojave and Rosman both measured this excessive roll-off when each was the transmitting station, it can be concluded that the circuitry in ATS-3 definitely effects the response at the high end of the band. The response degradations at the skirts will adversely effect the NPR/TPR measurements. This follows from the fact that the measurement accuracy of the above factors depends on a uniform noise reference level that exists over a frequency interval of 316 kHz to 5.5 MHz. Tests have shown that a 2 db error results from the degradations in the baseband frequency response.

3.2.2.3 Conclusions

Good correlation exists between the response plots shown in figure 3.50 for the RF, S/C (ATS-1) and receiver test loops. Response deviations occur between stations and

the filter manufacturer's roll-off characteristics in the upper and lower skirt regions of the response. These deviations are due to second order system effects on the response and the limitations on the measurement accuracy of the test frequencies. From the multistation test results on ATS-3, it was concluded that the roll-off at the high end of the test frequency band is affected by the circuitry in the spacecraft.

Degradations in the response at the upper and lower frequency regions effects the measurement accuracy of the NPR and TPR factors by as much as 2 db.

TABLE 3.7. COMPARISON OF BASEBAND CHARACTERISTICS

	315 kHz	320 kHz	5.6 MHz	5.8 MHz
Rosman, ATS-1	-2.2 db	-1.8 db	-1.0 db	-3.35 db
Cooby Creek, ATS-1	-4.8 db	-4.3 db	-1.47 db	-4.7 db
Mojave, ATS-1	-5.5 db	-4.8 db	-1.75 db	-4.3 db
Mojave and Rosman, ATS-3	-2.6 db	-0.7 db	-4.4 db	-7.3 db
Filter Mfr's stated roll-off characteristics	-3 db	-1 db	-1 db	-3 db
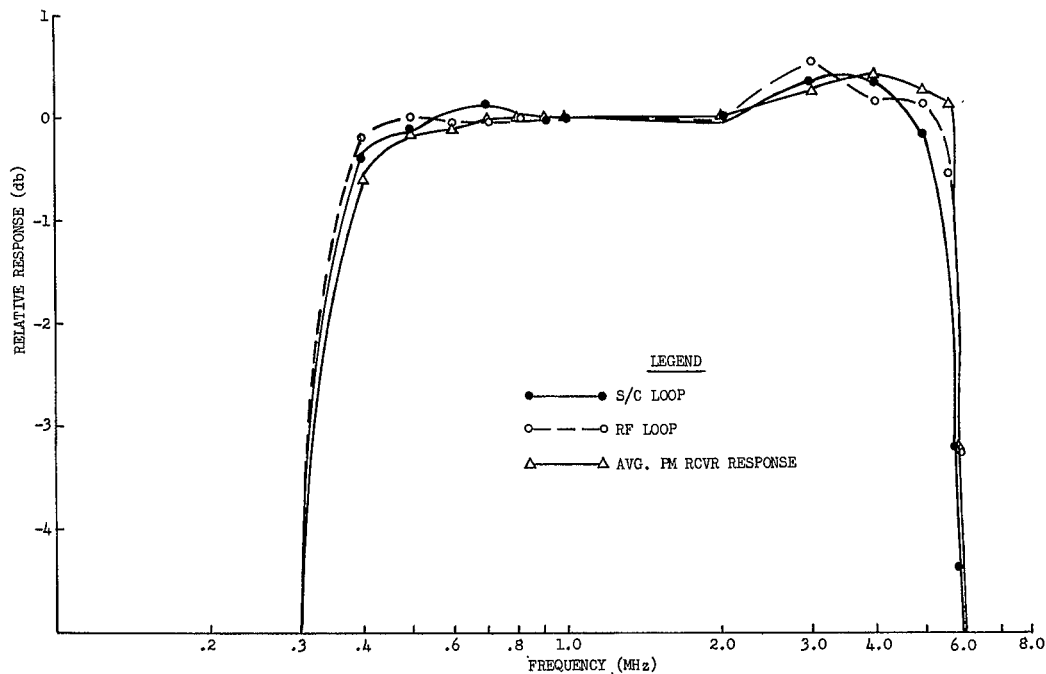
Figure 3.50. Typical Baseband Amplitude Versus Frequency, ATS-1, MA Mode, (Rosman, Mojave, and Cooby Creek)
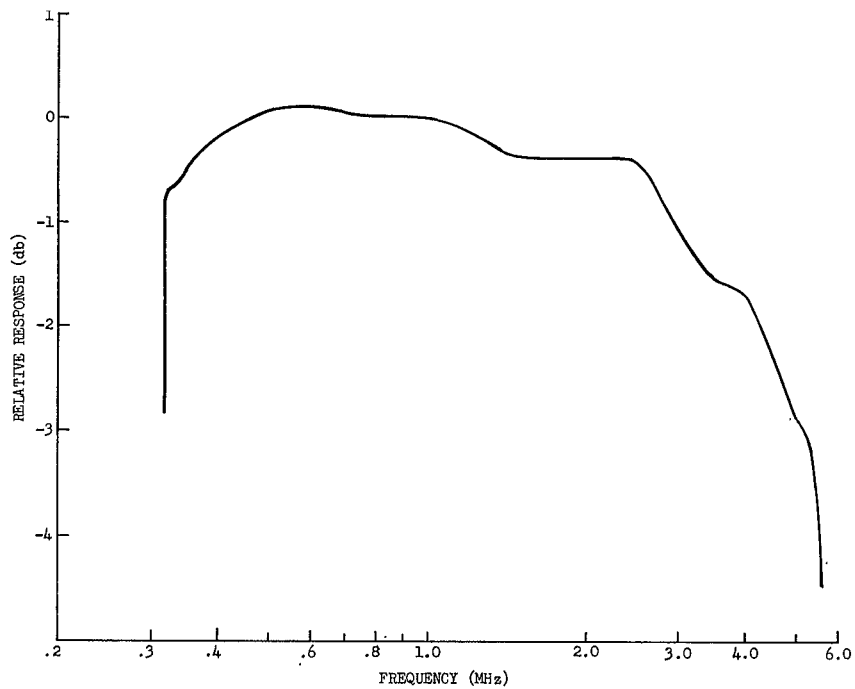
Figure 3.51. Baseband Amplitude Versus Frequency Response, ATS-3, Multistation Test, (Mojave and Rosman)

3.3 CONTROL LOOP AND STABILITY EXPERIMENTS

3.3.1 MULTIPLEX-CHANNEL FREQUENCY STABILITY (L. K. Harman)

3.3.1.1 Description and Test Results

OBJECTIVES

The primary objective of this experiment is to determine the frequency stability characteristics of a test tone in a 4-kHz multiplex channel and the degree of compensation achieved by the SSB/PhM AFC unit on the instabilities of the test tone. Another objective is to determine the frequency stability characteristics that affect voice intelligibility and error rates on a digital signal. The above signal types are transmitted over the SSB/PhM system.

A complete discussion of the overall AFC system is given in section 1 of this report. In general, the system consists of a primary AFC loop and an open-loop system defined as an error correction loop (E). The primary AFC system is type zero unit with an open-loop gain of 60-db and 3-db closed-loop bandwidth of 0.32 Hz. This low bandwidth is required for loop stability because of the abnormally high transport lag value (T) of 0.27 second. The E unit operating by itself applies an inverse frequency correction only to the FDM signal in the SSB transmitter to insure that this signal will arrive at the S/C receiver at the correct frequency.

The various factors that affect the test tone frequency stability will be divided into two categories: (1) Factors that define the short term stability characteristics; and (2) factors that define the long term frequency stability characteristics. The first category will be defined as those factors that cannot be reduced or eliminated by the AFC unit. The second category will be defined as those factors that can be eliminated or substantially reduced by the AFC unit.

TEST CONDITIONS

To determine the factors that affect the long- and short-term frequency stability characteristics of the test tone in a multiplex channel, various tests were performed in a number of test loop configurations. The test loops employed were: (1) Multiplex back-to-back (b-b) loop; (2) S/C loop on both ATS-1 and ATS-3 (performed with and without the E loop inserted); and (3) collimation tower test loop with and without the E loop inserted. The multiplex b-b loop test was utilized to determine the effects of thermal noise on the short term stability characteristics of the test tone. The collimation tower tests were utilized to determine the effects of the S/C transport lag (0.27 second) on the operation of the E loop and its ultimate effect on the short term frequency stability factors.

Spacecraft and multiplex b-b loop tests were also performed on a method developed to reduce the short term stability factors called the carrier reference technique.

This technique is discussed in detail in paragraph 5.1.13 of the report. This technique involves transmitting a reference carrier along with a specified group of multiplex channels. The carrier is then employed to demodulate the channels in the multiplex receive unit. The basic idea is to demodulate the channels with a carrier that contains aberrations which are identical to those imposed on the channels. The resulting frequency distortion will only be a function of the differential distortion and relative time delay between the carrier and the multiplex channels.

Various methods were employed to determine the factors that affect the short term frequency stability. A Marconi TF 2330 wave analyzer with a search bandwidth of 6 Hz was swept through a typical multiplex channel to determine the presence and relative amplitudes of distinct spurious frequencies. Also strip-chart recordings of the received test tone were employed. Both of these methods were utilized with the various loop configurations presented above.

Due to the resolution and bandwidth limitations of the above measurement technique another method utilizing Fourier techniques was developed. This technique presented an amplitude spectrum and a frequency histogram of the output signal from a discriminator that was tuned to the received test tone frequency. The resulting spectrum shows the various frequency components that cause the instabilities down to a resolution of 0.1 Hz. The histogram gives a quantitative measure of the frequency instability. It follows that the standard deviation (σ) of the histogram is a good measure of the frequency instability of the received tone.

The long-term frequency stability characteristics are based on the results of an automated test which calculates statistical factors (mean, median, etc.) based on secondly averages of the frequency errors. These tests are performed through the spacecraft with the system normally configured, and the results for the conditions of baseband noise loading on and off are averaged.

STANDARDS

For evaluating the long-term frequency stability, the RETMA TR-141 specification and the CCITT Recommendation G. 225 are used.

The RETMA specification states that the frequency error shall not exceed 10 Hz in a multiplex voice channel (with seasonal oscillator adjustment of 1 per year) for voice application and shall not exceed ±3 Hz per year with the same seasonal adjustment for data application. The CCITT specification, which is a general specification designed to suit most user requirements, simply states that the frequency error shall not exceed 2 Hz in a multiplex voice channel.

RESULTS

The following figures and tables are presented to show the stability characteristics of the received test tone and the effects of the AFC unit on these characteristics:

Figure	Data
3.52	Frequency spectrum for Collimation Tower Loop, (0 - 200 Hz) (σ for E loop in 3.65 Hz, σ for E loop out 3.31 Hz,
3.53	Frequency spectrum for Collimation Tower Loop, 0-20 Hz
3.54	Frequency spectrum for ATS-1 loop (0-200 Hz) (σ for E loop in 4.02 Hz, σ for E loop out 3.39 Hz.
3.55	Frequency spectrum for ATS-1 loop (0-20 Hz)
3.56	Frequency spectrum for ATS-3 loop (0-200 Hz)
3.57	Frequency spectrum for ATS-1 loop (0-600 Hz with Supergroup Correction

Table	
3.8	Reference Carrier Test Results (ATS-1)
3.9	Summary of Automated Tests
3.10	Test Time Availability
3.11	Automated Test Long-Term Observations
3.12	Frequency Stability Test Results
3.13	Thermal Noise Effects on the σ factor.
3.14	Carrier Offset Data
3.15	P_e vs. Pk-to-Pk Frequency Jitter on the Receiver L.O.

3.3.1.2 ANALYSIS

GENERAL

Utilizing the Marconi TF 2330 wave analyzer, it was possible to detect harmonics of the 1-kHz test tone plus 60-Hz components and multiples thereof when operating with the ATS-1 S/C loop. Of the two components measured, the harmonic levels were negligible relative to the 60-Hz component levels. When operating with the ATS-3 loop, the above components were detected along with large spurious components in the 130-Hz to 200-Hz region. Frequency spectrums obtained from the Fourier measurement technique give the same results as stated above. Figures 3.54 and 3.55 show that relatively, large components

3.102

occur at the S/C spin rate and 60-Hz components and multiples thereof when operating with ATS-1. For ATS-3 operation, the large components in the 130-Hz to 200-Hz region are quite evident in figure 3.55.

From the above measurement techniques, it was determined that the following factors affect the test-tone frequency stability:

1) 60-Hz sidebands and multiples thereof (Incidental modulation).

2) Spin-modulation components (approx 1.6 Hz) due to S/C spin effect.

3) Oscillator 1/f phase noise.

4) Quadrature component of the normally distributed thermal noise.

5) Spurious frequencies at high end of frequency test band (ATS-3).

6) Frequency offsets of the system oscillators.

7) Doppler shifts.

AFC UNIT

Due to the extremely low bandwidth of the AFC loop (0.32 Hz), it follows that only very low-frequency rates can be handled by the loop. It has been found that items (6) and (7) fall into this low rate category; hence, the AFC loop can negate their effect. However, the effect of the other 5 factors cannot be negated so they cause short term variations of the test tone frequency. The σ values computed from the frequency histograms are a direct measure of the magnitude of these factors. The values of σ obtained from the various test configurations are listed in table 3.12.

Thermal noise (factor 4) is present in all systems. It can cause short-term frequency variations of the test tone by the vector addition of the signal vector and the quadrature component of the noise vector. In order to determine the thermal noise effect on stability, tests were performed in the multiplex b-b loop at various S/N values. For each of the values a value of σ was measured. Because of the test loop employed, the thermal noise was the chief contributor to the σ value. The results are shown in table 3.13. The operational S/N values vary in a range of 34 db to 40 db (flat-weighted). Therefore, the above σ values set an absolute lower limit on the test-tone short-term frequency stability that can be obtained from the system.

ERROR CORRECTION LOOP (E LOOP)

The effect of the E loop is to increase the σ factor for any given test loop configuration. This is clearly shown in table 3.12 and in figures 3.54 and 3.56. The spectrum plots show that, in general, the E loop amplifies the factors that affect the short-term frequency instability.

As explained in paragraph   5.5.1 of the report, the E loop varies the test tone error spectrum in a sinusoidal manner. This is shown in figure 3.55. Specifically, the transfer function is 2 sin π ft. T is the time delay between the residual frequency errors that are present in the E loop and the AFC loop. For a S/C loop test configuration, T would be the S/C loop transport lag, 0.27 seconds. For this value of T it can be shown that frequency errors will be cancelled if they fall at multiples of 3.7 Hz. Also, the frequency components at 1.85 Hz and multiples thereof, will be increased by a factor of 6 db (figure 3.55). In the 60 Hz region, the sinusoid will peak at 61.05 Hz. From the above it can be concluded that the E loop actually amplifies the spin modulation and incidental modulation components.

The effect of reducing T on the E loop performance is shown in figures 3.52 and 3.53. In the latter figure the spectrum is basically flat over the 0 to 20 Hz range; hence, it can be concluded that T is low enough to obtain a nearly constant value for the sinusoidal transfer function. As shown in figure 3.52, the E loop is effective in reducing the error spectrum in the lower part of the 0 to 200 Hz spectrum. However, in the 30 to 70-Hz region, the E loop amplifies the components of the spectrum. It can be concluded that the E loop has an added property of an amplification effect on noise in addition to its sinusoidal response characteristic. This amplification effect is probably due to the fact that the E loop is instrumented by utilizing a mixer and other associated circuitry. Evidently when mixing two noisy signals that have the same noise characteristics but are displaced in time, the resultant noise level on the output signal is an amplified version of the noise level at the input to the mixer. This amplification effect could be due to the fact that the noise components at the inputs to the mixer are narrow band and highly correlated. The correlation coefficient for thermal noise is largely dependent on the bandwidth of the noise signals. As the bandwidth decreases, the correlation between the input noise signals increases for a given time displacement between the signals.

REFERENCE CARRIER STABILIZATION TECHNIQUE

This technique was developed for reducing the magnitude of the components that effect short term frequency stability. A detailed discussion of the technique is given in paragraph   5.1.13 of the report. Figure 3.57 shows the effect of the above technique on a 0 to 600-Hz error spectrum. As shown, the technique substantially reduces the spectrum in the lower end of the frequency band. In the 360-Hz region, the response with the reference carrier technique approaches the response obtained with normal system operation with the E loop off. The thermal noise contribution to the error spectrum is defined by the line which defines the error spectrum for a multiplex b-b loop with thermal noise inserted to obtain the same S/N value that is realized in the S/C loop.

3.104

Table 3.8 shows the σ values for various test loop configurations when operating with a normal system and with the reference carrier unit inserted in the system. The σ values for the multiplex b-b loop show the effect of thermal noise on the normal and reference carrier test configurations. As shown the reference carrier technique has an amplification effect on the thermal noise. It is noticed that for both S/N values, the σ values for the reference carrier condition are essentially equal for the multiplex b-b loop and the S/C loop (e.g., for an S/N of 37 db, σ = 2.36 Hz and 2.31 Hz). Therefore, it can be concluded that the reference carrier technique reduces the effects of all components causing the short term instability other than thermal noise. It is shown in paragraph 5.1.13 that these components are reduced by a factor that is greater than 40 db. This fact supports the above statement.

Since thermal noise is the main factor in determining σ for the reference carrier technique, it follows that the effect on σ of the incidental modulation factors, the spin modulation component and the $1/f$ phase noise can be obtained by comparing the σ values for the normal system and reference carrier test configurations in the S/C loop. For a S/N of 37 db the difference is 0.85 Hz. For an S/N of 43 db it is 1.88 Hz. From the above results it can be concluded that thermal noise is the main limiting factor in reducing the short term frequency instability for operation with ATS-1.

LONG TERM FREQUENCY STABILITY

In assessing the long term frequency stability of the ATS system, the CCITT G.225 Recommendation is used for comparison. Site operation and method of testing multiplex channel frequency stability preclude direct application of the previously stated RETMA specification.

The results of the automated tests (tables 3.9 through 3.11), based on secondly averages of the multiplex channel frequency errors, show that in nearly 100 percent of the tests considered, the test mean and median frequency errors were less than 2 Hz. The RMS variation of the test means was less than 2 Hz in all cases. Generally, about 25 percent of the automated tests showed worst case minutely means greater than 2 Hz, with a median worst case minutely mean at Cooby Creek in the order of 0.6 Hz. Perhaps the most meaningful statistic from a user point of view is the time availability. This statistical value, for all test data from all stations, shows that when the system is operating normally, less than 10 percent of secondly frequency errors will be greater than 2 Hz. It is concluded, then, that the AFC system in the SSB transmitter is sufficient for meeting the CCITT G.225 specification, and will probably also meet the RETMA TR-141 specification.

EFFECT OF CARRIER FREQUENCY OFFSET ON VOICE INTELLIGIBILITY

An important source of distortion with regard to voice usage is the condition of unequal L. O. frequencies in the transmit and receive multiplex units.

This distortion was first noticed in carrier telephone circuits using SSB suppressed carrier modems, and involves destruction of harmonic relationships, best explained by an example. In table 3.14, the sender's suppressed carrier frequency is precisely 400 kHz. For this example, suppose the receiver, after mixing, must insert a 400 kHz signal for demodulation in the receive multiplex unit. In the demodulated output, the harmonic relationships are preserved. In the next condition, the receiver L. O. frequency is 20 Hz higher than the sender's suppressed carrier. For this case, it is seen that the harmonic relationships of the 1-kHz modulating frequency are destroyed.

Fletcher, et al [22] found through a series of subjective tests that naturalness of speech is maintained for carrier frequency offsets up to 20 Hz, and that for 90% phonetically-balanced word list intelligibility, a receiver L. O. offset of -200 Hz to +325 Hz could be tolerated.

Needless to say, transmission of music is very sensitive to harmonic relation-ships. Just a few cycles of carrier frequency offset is detrimental to this type of trans-mission.

EFFECT OF SPACECRAFT FREQUENCY INSTABILITIES ON FSK DATA ERROR RATE IN THE MA MODE

Subjective tests have shown that the frequency jitter and S/C spin modulation of the ATS system do not impair voice and music transmission, but these instabilities, plus random noise, produce errors in the transmission and reception of FSK data.

An experiment was performed on ATS-1 with Cooby Creek and Mojave which helps to answer the question as to the relation of error rate to the ratio E/N_o, where E is the bit energy and N_o is the spectral noise density which could be jitter noise, white Gaussian noise, or a mixture of the two.

The following is a synopsis of the test format, and results.

TEST FORMAT

A narrowband FSK modem was used at three different bit rates, 50, 100 and 200 bauds. The peak deviations were 30, 60, and 120 Hz, respectively. The test was performed under the following system configurations:

1) The normal spacecraft loop, in the SSB/PhM mode.

2) The spacecraft loop, with Gaussian noise inserted along with the FSK signal at the input to the transmitter MUX.

3) MUX back-to-back loop with Gaussian noise inserted as in condition 2.

4) MUX back-to-back with a Gaussian noise source FM modulating a frequency synthesizer, tuned to the receive MUX carrier frequency.

In the first configuration, the combined effects of S/C spin modulation, ambient noise, and jitter noise affect the error rate.

The second and third configurations provide the framework for comparing identical E/N_0 values for the cases of N_0 being the sum of ambient noise and S/C oscillator jitter noise (case 2), and N_0 being white Gaussian noise alone (case 3).

The fourth configuration isolates the effect of various amounts of oscillator frequency jitter on data error rate.

TEST RESULTS

Comparing the results to the theoretical values of error probability versus E/N_0, obtained from the relation $P_e = (1/2) e^{-1/2 (E/N_0)}$

where P_e = probability of error.

E = average bit energy.

N_0 = average Gaussian noise energy.

it was found that under configurations 2 and 3, for the same error probability, the corresponding E/N_0 value was on the average 1 db greater than the theoretical for measurements in both the S/C and baseband loops, for each of the three bit rates tested. This was caused possibly by: (1) accurate S/N measurements are relatively difficult to perform in the S/C loop due to spin modulation; (2) impulse noise is not taken into account; and (3) the discriminator used did not have an ideal filter associated with it. The close agreement of these results with the theoretical values for Gaussian noise alone shows that total system oscillator frequency jitter, and in particular the S/C oscillator frequency jitter, is minimal when compared to overall ambient noise.

In the normal S/C loop configuration, when no additional noise is introduced in the ground transmitter, no errors were counted at either of the bit rates used. The MUX channel TT/N was 39 db for this configuration (configuration 1).

The results of testing under configuration 4 show the effect of frequency jitter alone on FSK modem data error rate

for the cases of no baseband loading and for the worst case of a continuous

space in one adjacent channel and a continuous mark in the other adjacent channel. Table 3.15 summarizes the results of this test.

For the same P_e, the difference between frequency jitter for the loaded and unloaded cases was in the order of 30 Hz for each of the bit rates tested. If a P_e of 10^{-5} is desired, the amount of tolerable jitter at 50 bauds is 100 Hz, at 100 bauds is 120 Hz, and at 200 bauds is 190 Hz.

3.3.1.3 CONCLUSIONS

The overall system AFC unit consists of a primary AFC-loop and an open-loop system defined as an error correction (E) loop. The latter loop has a sinusoidal response that is a function of the S/C transport lag, T. For a T of 0.27 second, it can be shown that the E loop amplifies the spin-modulation components (1.6 Hz) and the 60-Hz components (incidental angle modulation). It also attenuates the $1/f$ phase noise. From the test data obtained, it has been shown that the overall AFC unit can compensate only for long-term frequency drifts (S/C oscillator drifts and/or doppler shifts). Incidental angle-modulation components, S/C spin-modulation components and thermal noise are the chief contributors to the short-term test-tone frequency instability for ATS-1 operation. For ATS-3 operation, the above factors cause short-term frequency instability in addition to large spurious frequency components in the 130-Hz to 200-Hz region. Because of these latter components, the σ value for ATS-3 operation is approximately double the value that is realized for ATS-1 operation (4 Hz for ATS-1, and 9.45 Hz for ATS-3).

The E loop and the reference-carrier stabilization technique has an amplification effect on thermal noise. Because of this, thermal noise is the limiting factor in reducing the short-term test-tone instability for ATS-1 operation. Thermal noise and the spurious frequency components are the limiting factor for ATS-3 operation.

Assessment of long-term frequency stability, or frequency drift is based on automated test data which calculates statistical factors on the basis of secondly averages of frequency errors. In nearly 100 percent of the tests considered, the test-mean and median frequency errors were less than 2 Hz. In 75 percent of the tests, the worst-case minutely mean was less than 2 Hz, and the cumulative time availability shows that less than 10 percent of the secondly average frequency errors were greater than 2 Hz. It is then concluded that the AFC system in the SSB transmitter is sufficient for meeting the CCITT 2-Hz frequency error limit.

The frequency characteristic that is most detrimental to voice intelligibility is the destruction of the harmonic relationship of the various tones that make up a voice signal. The destruction can be realized by a fixed-frequency offset of the local oscillator in the receive multiplex unit relative to the local oscillator frequency in the transmit multiplex unit.

The error rate (P_e) of an FSK digital signal was found to be relatively insensitive to the peak-to-peak frequency jitter impressed on the signal. For a 30-Hz frequency deviation of a 50-baud signal, a peak-to-peak jitter value of 100 Hz is required to produce a P_e of 10^{-5} This is equivalent to a σ of 16 Hz. If the adjacent multiplex channels are loaded with a continuous mark and space frequency in different channels, it was found that a peak-to-peak jitter of 50 Hz is required to produce a P_e of 10^{-5}. This is equivalent to a σ of 8 Hz. This critical condition would not be realized in an operational system. The 8-Hz value is only given to define the lower limit for σ for the 50-baud case which utilizes a frequency deviation of 30 Hz.

TABLE 3.8. REFERENCE CARRIER TEST RESULTS (ATS-1)

Test Loop	Multiplex Channel TT/N (db)	Normal System (σ-Hz)	Reference Carrier (σ-Hz)
Multiplex back-to-back loop	37	1.66	2.36
S/C	37	3.16	2.31
Multiplex back-to-back loop	43	0.91	1.23
S/C	43	3	1.12
S/C	37	3.74*	

*With E loop in, all other cases E loop was not in system.

TABLE 3.9. SUMMARY OF AUTOMATED TESTS

Station	Number of Tests Represented	% Of Tests For Which Mean Freq. Error Was > 2 Hz		% Of Tests For Which Median Freq. Error >2 Hz		% Of Tests For Which The Worst Case Minutely-Average Freq. Error Was > 2 Hz	
		High Chan.	Low Chan.	High Chan.	Low Chan.	High Chan.	Low Chan.
Cooby Creek	37	0	2.7	0	0	29.8	27.0
Rosman	9	0	0	0	0	22.2	11.1

TABLE 3.10. TEST-TIME AVAILABILITY

	High Channel	Low Channel
Cooby Creek	8.1	15.6
Rosman	22.2	22.2

TABLE 3.11. AUTOMATED TEST LONG-TERM OBSERVATIONS

Station	RMS Variation of Test Mean Freq.		Overall % of Errors Less Than 2 Hz		Median of Worst Case Minutely Means			
	Low Chan.	High Chan.	Low Chan.	High Chan.	Low Channel		High Channel	
					Max.	Min.	Max.	Min.
Cooby Creek	0.643	0.117	95	92	0.50	-0.67	0.50	-0.70
Rosman	1.35	1.80	92	93	3.75	-2.78	0.50	-2.47

TABLE 3.12. FREQUENCY STABILITY TEST RESULTS

Test Configuration	σ (Hz)	TT/N (db)
Collimation Tower Loop E Loop In	3.65	40
Collimation Tower Loop E Loop Out	3.31	40
ATS-1 E Loop In	4.02	33.5
ATS-1 E Loop Out	3.39	33.5
ATS-3 E Loop In	9.45	37
ATS-3 E Loop Out	8.45	37

TABLE 3.13. THERMAL NOISE EFFECTS ON THE σ FACTOR

TTs/N (db)	σ (Hz)
28	5.05
30	4.01
32	3.17
34	2.51
36	1.96
38	1.56
40	1.24
68	0.17

TABLE 3.14. CARRIER OFFSET DATA

Transmitted Freq. (kHz)	Receiver L.O. Freq. (kHz)	Demodulated Output (Hz)
401.0, 402.0, 403.0	400.000 ±0 Hz (Normal Case)	1000, 2000, 3000
401.0, 402.0, 403.0	400.02 (carrier offset of 20 Hz)	980, 1980, 2980

Example of the effect on a received tone of a mismatch between the Suppressed Carrier and Receiver L.O. Frequencies in SSB Transmission. Assume a suppressed carrier frequency of 400 MHz and a modulating frequency of 1 kHz.

TABLE 3.15. P_e VERSUS PK-PK FREQUENCY JITTER ON THE RECEIVER L.O.

Bit Rate (Bauds)	P_e for a pk-pk jitter of				
	50 Hz	100 Hz	150 Hz	200 Hz	
50	-	10^{-5}	10^{-1}	-	Adjacent Channels Unloaded
100	-	-	5×10^{-3}	-	
200	-	-	-	10^{-4}	
50	10^{-5}	10^{-2}	-	-	Adjacent Channels Unloaded
100	-	10^{-4}	5×10^{-2}	-	
200	-	-	5×10^{-5}	5×10^{-3}	

3.113
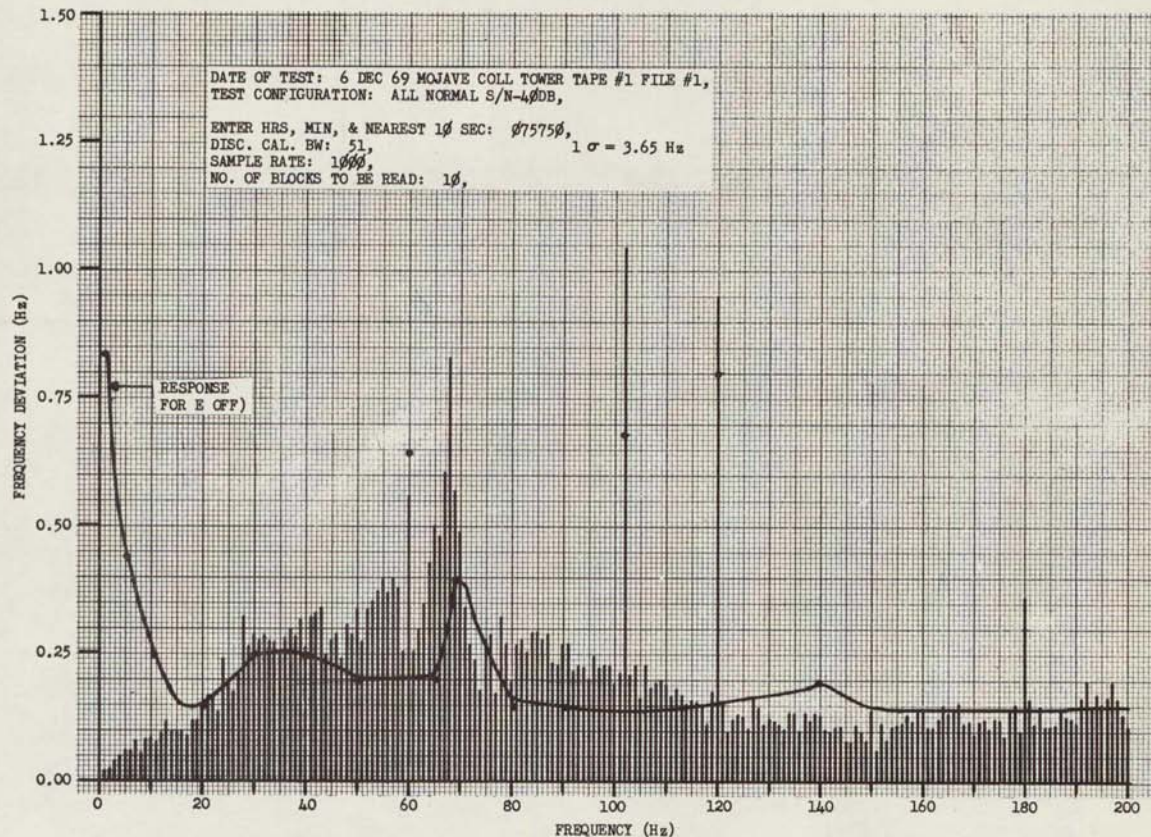
Figure 3.52. Frequency Spectrum For Collimation Tower Loop (0-200 Hz) (σ for E Loop In 3.65 Hz, σ for E Loop Out 3.31 Hz)

DATE OF TEST: 6 DEC 69 MOJAVE COLL TOWER TAPE #1 TILE #2,
TEST CONFIGURATION: ALL NORMAL, E LOOP IN.

ENTER HRS, MIN, & NEAREST 1Ø SEC: Ø8Ø1ØØ,
DISC. CAL. BW: 51,
SAMPLE RATE: 1ØØ,
NO. OF BLOCKS TO BE READ: 1Ø,

3.114
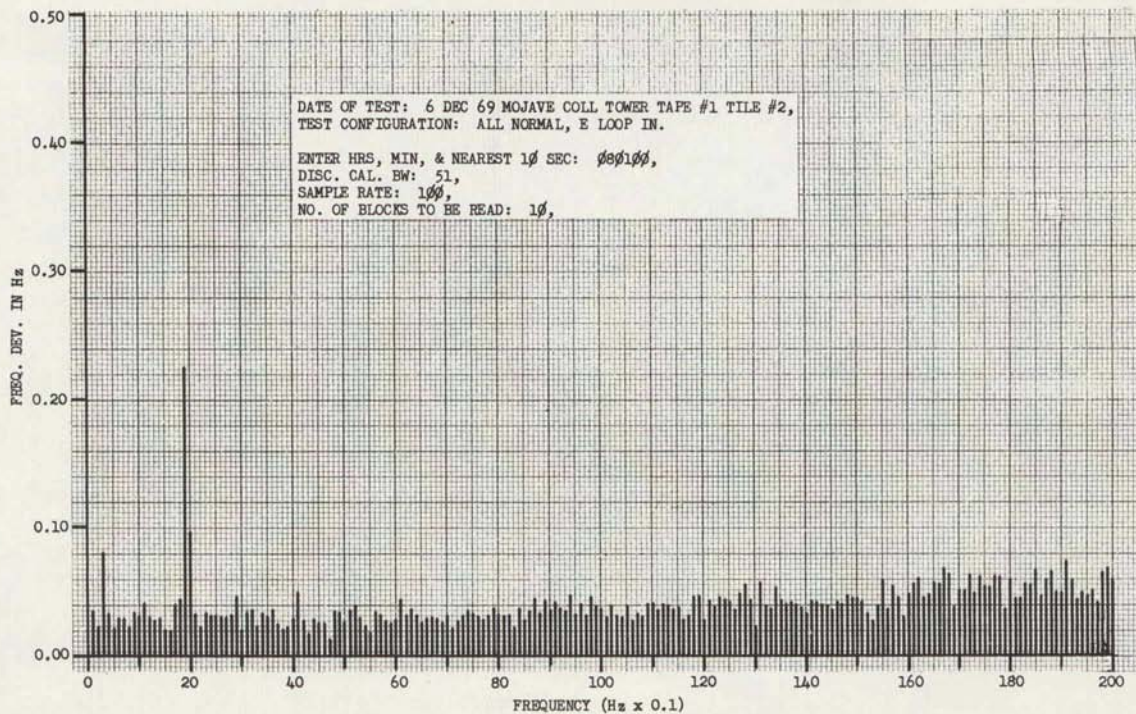
Figure 3.53. Frequency Spectrum For Collimation Tower Loop (0-20 Hz)
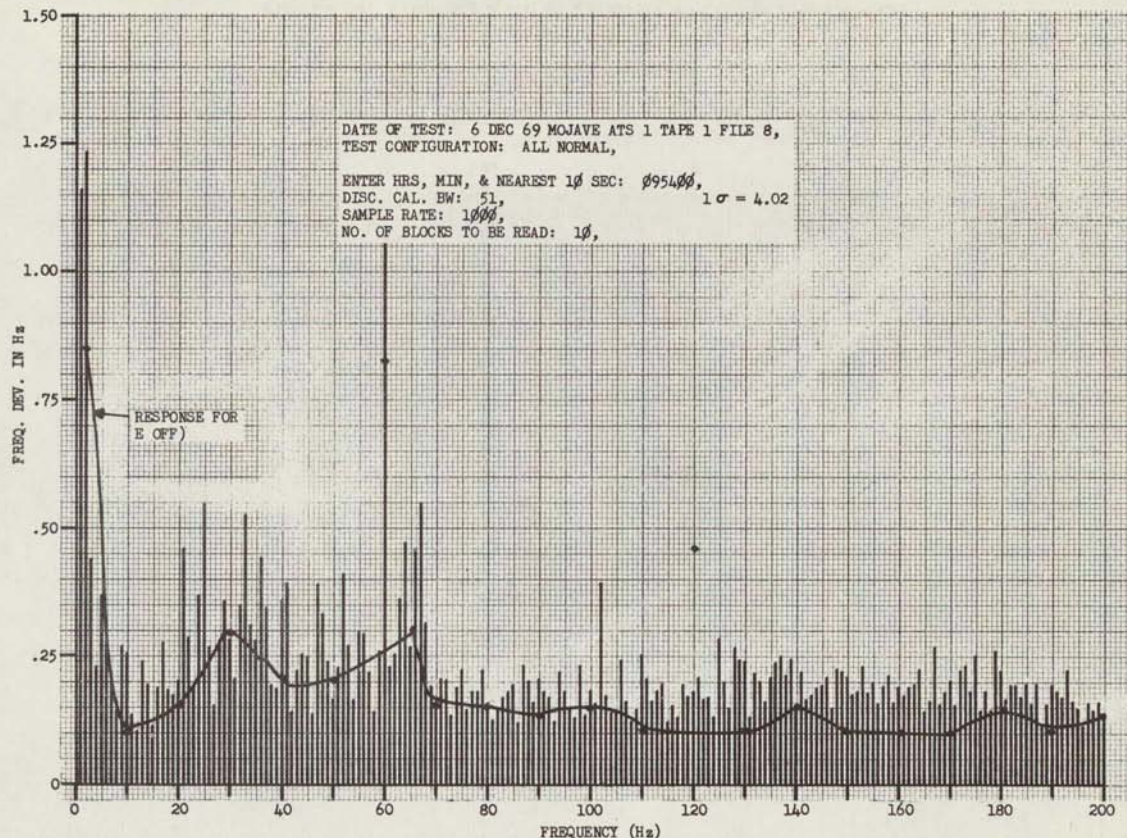
Figure 3.54. Frequency Spectrum For ATS-1 Loop (0-200 Hz) (σ for E Loop in 4.02 Hz, σ for E Loop Out 3.39 Hz)

DATE OF TEST: 6 DEC 69 MOJAVE ATS 1 TAPE 1 FILE 8,
TEST CONFIGURATION: ALL NORMAL,

ENTER HRS, MIN, & NEAREST 1∅ SEC: ∅9540∅,
DISC. CAL. BW: 51,   1 σ = 4.02
SAMPLE RATE: 100∅,
NO. OF BLOCKS TO BE READ: 1∅,

RESPONSE FOR
E OFF)

Axis labels: FREQ. AMP. IN HZ (vertical), FREQUENCY (Hz) (horizontal)

3.115
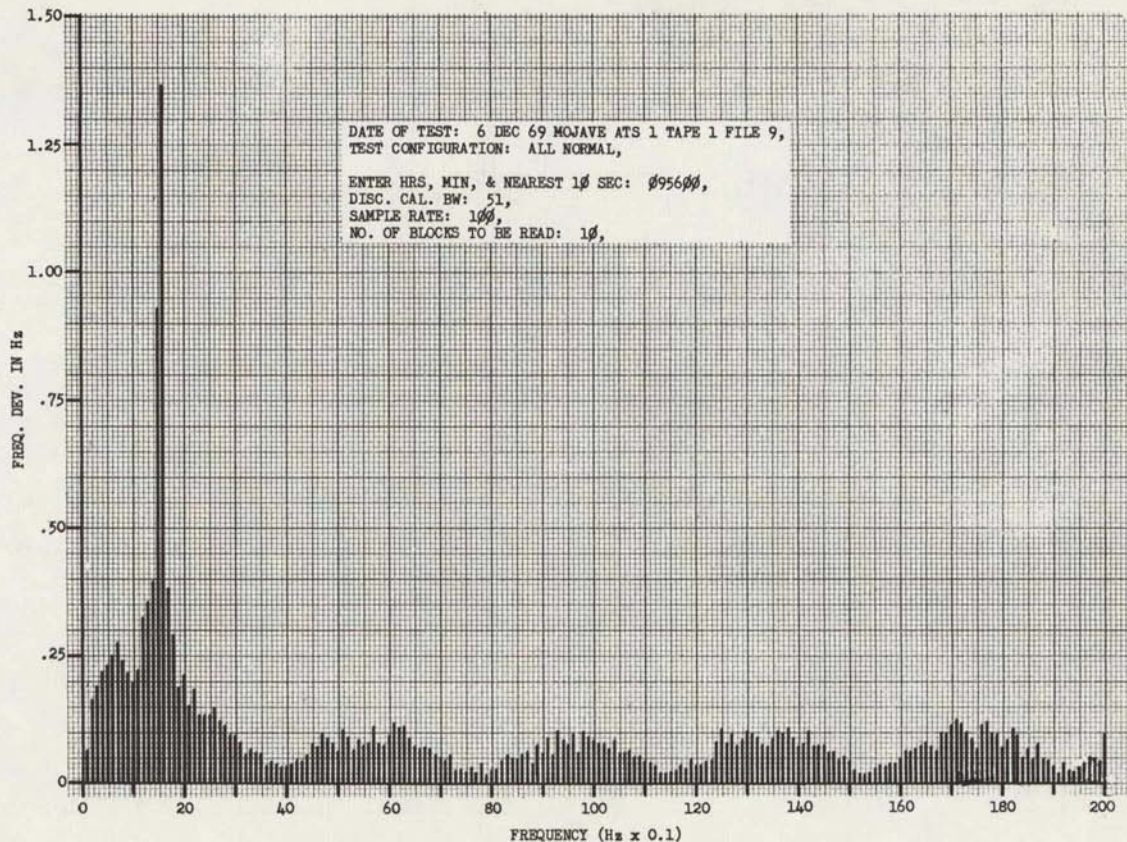
Figure 3.55. Frequency Spectrum for ATS-1 Loop (0-20 Hz)
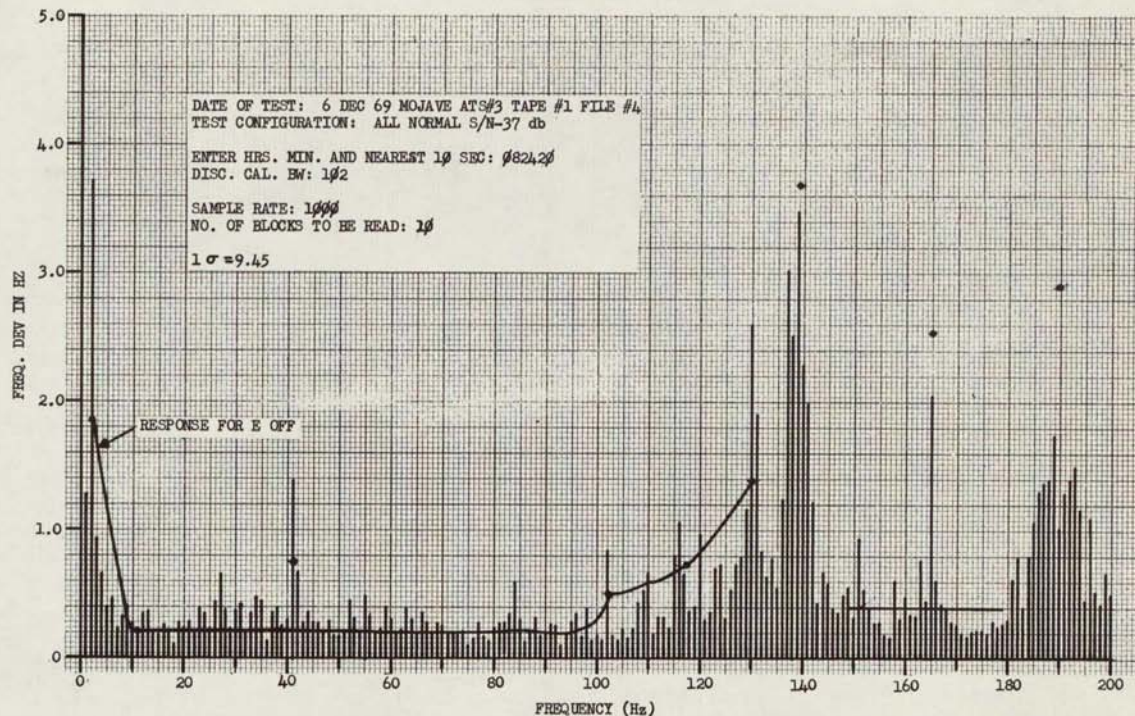
Figure 3.56. Frequency Spectrum for ATS-3 Loop (0-200 Hz) (σ for E Loop in 9.45 Hz, σ for E Loop Out 8.45 Hz)

3.118
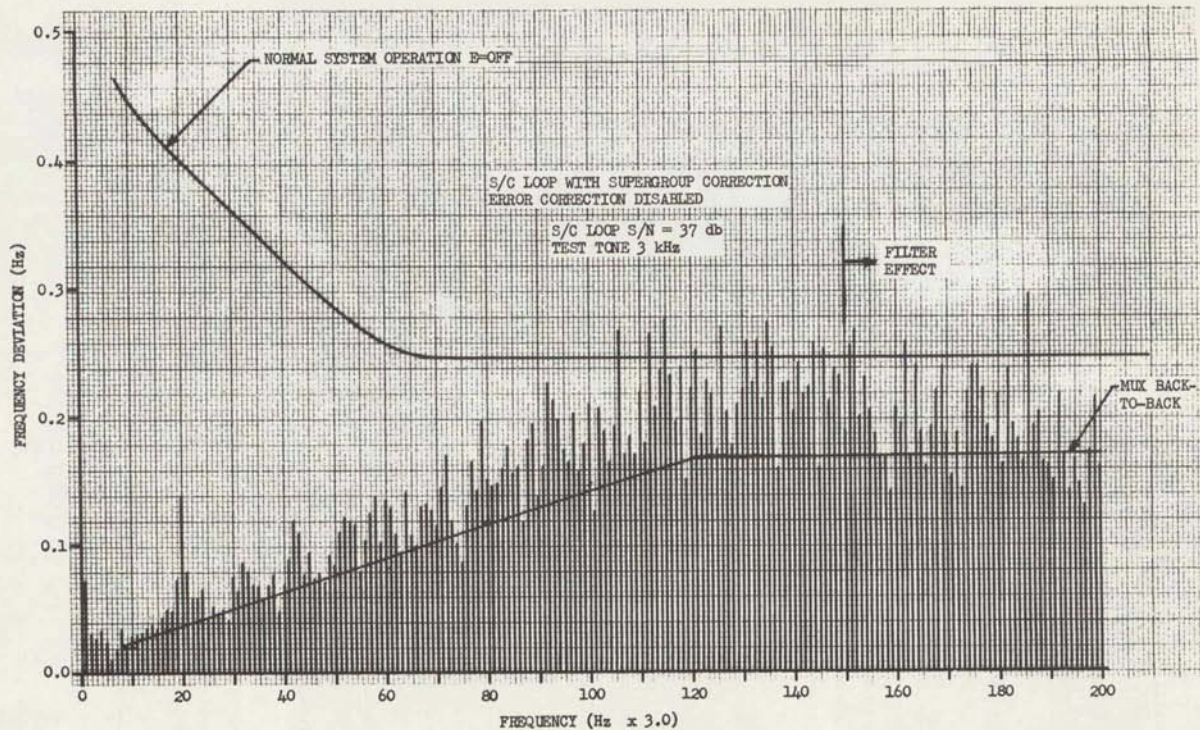
Figure 3.57. Frequence Spectrum for ATS-1 Loop (0-600 Hz) With Supergroup Correction

3.3.2 MULTIPLEX-CHANNEL LEVEL STABILITY (L.K. Harman), (MA-MX 2.1, MA-AT-1.1, MA-AT-1.2)

3.3.2.1 Description and Test Results

OBJECTIVES

The objective of this experiment is to determine the effect of the entire SSB/PhM satellite communications system, including the ALC subsystem, on the long and short-term level stability of signals in multiplex channels across the baseband.

The test parameters are: 1) Short-term level instability, which occurs over periods up to one second, (including the effects of random variations and 1.6-Hz modulation caused by misalignment of the spacecraft receive antenna; and 2) Long-term level instability, which are level variations occuring over periods greater than one second and through several test periods.

The short-term parameters are the prime reason for level instability in a multi-plex channel in the MA mode. This affects the multiplex channel voice telephone user because there is a subjective limit to the amount of cyclic level fluctuation and random noise that can be tolerated for voice communication. The long-term level drift, caused by pro-pagation changes (e.g., due to weather) or caused by relatively slow variations in system gain can be corrected by the ALC loop in the SSB transmitter.

TEST CONDITIONS

Level stability tests were performed only in the S/C loop. The short-term level stability measurements are taken in a high-and a low-multiplex channel on a single-station basis with noise loading off. Two tests are used to assess short term level stability: 1) Strip-chart recordings of multiplex channel test-tone level versus time. In this test, a 1-kHz tone is transmitted through the spacecraft in the SSB/PhM mode. Strip-chart recordings are then made of the received multiplex channel test-tone level variations. 2) A Fourier analysis test, in which level changes in the 1-kHz tone are detected. The output signal of the detector is fed into an A/D converter and then into a computer where a Fourier spectrum is computed.

STANDARD

Directly applicable specifications are not readily available for either the long or short term level stability evaluation. However, the CCITT Recommendation G. 121 and the results of research into the subjective effect of level changes are used for comparison.

RESULTS

Short Term Level Stability

        The results of the short-term level stability strip-chart tests are summarized in table 3.16. A typical strip-chart recording of level variations versus time is presented in figure 3.58. The rms error is estimated by using values on the strip chart recording. It should be pointed out when comparing this test to the Fourier analysis test in paragraph 3.6.2, that the limiting bandwidth in the strip-chart test is the strip-chart channel (3 Hz). The Fourier analysis test should be weighted more heavily, since higher frequency effects can be assessed.

        Table 3.16 represents the results of a typical test run at each station. The values listed apply to both satellites ATS-1 and ATS-3, since no noticeable difference exists in the parameters listed. Since there is close correlation between the high and low channels, (see table 3.17) the above values apply to both channels.

        Reference to figure 3.38 shows that the maximum level excursions on the strip-chart recording occur at the spacecraft spin rate, so that in table 3.16 the recorded maximum values (column 4) contain the effects of thermal noise plus 1.6-Hz S/C spin modulation. In general, the average fluctuation at the S/C spin rate is ±0.5 db. The level variations occurring at a rate greater than 1.6 Hz are seen qualitatively on the recording but no quantitative assessment, except on a general basis has been made. One noticeable difference between ATS-1 and ATS-3 strip-chart records is in an increased amount of higher frequency fluctuations through ATS-3. This fact is verified by the Fourier analysis test and discussed in paragraph 3.6.2.

Long Term Level Stability

        Table 3.17 contains a summary of automated test results. The statistical factors given are calculated by the computer on the basis of secondly samples.

        The overall percent of level errors within 2 db, based on secondly samples of multiplex channel test-tone power is shown in table 3.18.

        The channel level correlation coefficients (table 3.17) are better than 0.96 Hz for each station, indicating equal level changes across the band.

3.3.2.2 Analysis

        The method of analysis must, of necessity, follow two lines of approach. For the short term level stability evaluation, no specifications can be found in the literature. Use is therefore made of the results of subjective listener tests performed at the Bell Telephone Laboratory.* On the basis of these tests it appears that for multiplex channel voice

---

*Fletcher: "Speech and Hearing", D. Van Nostrand Co., Vol. 1, pg. 145.

communication, the 1.6-Hz level variation will be the most detrimental to listener tolerance. Conclusions can be drawn, then, by comparing the observed 1.6-Hz level fluctuation of the ATS system with the above subjective test results. For evaluating the long-term level stability and ALC loop operation, results of the automated and manual level stability tests will be used for comparison with the CCITT Recommendation G.121, and the above subjective test results.

Short-Term Level Stability

It was found as a result of the subjective tests carried out at Bell Laboratories (27) that the ear was most sensitive to fluctuations in intensity when these fluctuations occurred a rate between 1 and 6 Hz. In their experimental work, the 3-Hz rate was chosen as being best for perceiving small differences in intensity. At this rate, it was found that for a 1000-Hz tone of power greater than 50 db above the threshold of perception (-122 dbm), the minimum fractional variation in tone power barely perceptible to the average listener was found to be from 5 to 10 percent of the nominal tone level. It is pointed out that these results were obtained under conditions of minimal background noise. Also, these test results do not provide information on the subjective effect of level fluctuations on speech intelligibility and listener tolerance.

Since the ATS spin rate (1.6 Hz) is very close to the level-variation rate chosen for the above subjective tests, and since the nominal multiplex channel test tone power is >50 db above the threshold of perception as determined in the above subjective tests, the results of these tests may be used for comparison with the short term level instability observed through the ATS. The average fractional variation due to the observed 1 db peak-to-peak level variations of the 1 kHz multiplex channel test tone at 1.6 Hz is $(1.2/5) \times 100 = 20$ percent. This is well above the 10 percent limit stated above. It is concluded, then, assuming negligible background noise, and no other significant level variations within the 1 to 6 Hz band that the normal level fluctuations occurring at the S/C spin rate will be perceived by the multiplex voice telephone user. Reference to table 3.16 shows that peak-to-peak fluctuations in excess of 1 db are experienced in a 2-second interval. These represent fractional variations in the order of 35 percent, but are not in the frequency range of greatest listener sensitivity to level variations. The research at Bell Laboratories showed that variations occurring at less than 0.2 Hz or greater than 25 Hz had about one-third the effect of changes at a 1 to 6-Hz rate. Level variations occurring over a period greater than 5 seconds, and higher frequency variations such as those seen in the ATS-3 data, will have a secondary

effect on the multiplex voice telephone user. Figure 3.128 of paragraph 3.6.2 shows a 14-Hz component (8th harmonic) 1.5 times the magnitude of the spin-component (1.6 Hz).

It is pointed out that the tests by Fletcher were performed under S/N conditions much higher than the ATS multiplex channel S/N total in the range of 40 db. It is felt that the total effects of other short term variations plus thermal noise is the limiting factor, rather than this 20 percent level fluctuation.

Long Term Level Stability

In assessing the long term stability of the ATS system, CCITT Recommendation G.121 is used for comparison. This specification applies to four wire telephone transmission on metallic lines and states that, for a 1000-Km circuit, the standard deviation of overall loss with time should be less than 1.0 db for circuits routed over automatically regulated groups.

Table 3.16 shows the rms level error to be on the order of 0.3 db on the basis of the strip chart recordings. Table 3.17 shows the rms variations of test minutely means is less than 1 db in all cases. Thus it is concluded that the overall system (including the SSB transmitter ALC circuit) long term level variations meet the above CCITT Recommendation. Time availabilities have been calculated on the basis of a 2 db spread and are presented in table 3.18. They indicate that on the basis of secondly samples, approximately 81 percent of the test tone power level samples will show variations of less than 2 db from the mean level. The above analysis applies to all channels in the baseband, since the high and low channel correlation coefficients are nearly 1 for all stations (table 3.17).

3.3.2.3 Conclusions

The manual level stability tests indicate a test tone level variation of between 0.5 to 1 db as a result of the satellite antenna spin rate. From subjective testing, it is concluded that this fluctuation alone would be barely perceptible under conditions of large S/N as a cyclic level variation when the channel is used for voice communication. However, other short term effects observed in the Fourier analysis tests (paragraph 3.6.2) contribute to the overall level fluctuations in a multiplex channel. The total of these components will give the effect of increased noise in a multiplex channel.

For the long-term level stability, the rms channel level error is below the CCITT G.121 Recommendation of 1 db. The rms variation of minutely means of secondly channel level samples also shows a value below 1 db. About 80 percent of the secondly samples show power level variations of less than 2 db from the average. It is concluded that on a long-term basis, the overall ATS system level instabilities, including effects of the transmitter ALC loop, are sufficient to meet the CCITT G.121 Recommendation, and that

level correlation between multiplex channels is nearly unity for all stations. Further, it is concluded that short-term level fluctuations will not be perceived by the average multiplex voice telephone user as a cyclic variation, because this effect will be masked by the total noise in a multiplex channel. The subjective effect can therefore be ascertained by multiplex channel S/N measurements, since this parameter will be the limiting parameter on voice intelligibility.

TABLE 3.16. SHORT-TERM LEVEL STABILITY TEST RESULTS

Station	Overall RMS Error (db) For a 10 Minute Interval	Max. Variation in Any 2 Second Interval	Max. Variation in Any 2 Minute Interval	Mean Test Tone Power (dbm)
Cooby Creek	0.3	1.8 db	2.3 db	7.0
Rosman	0.26	1.0 db	1.2 db	7.4
Mojave	0.28	1.5 db	2.5 db	7.0

TABLE 3.17. LONG TERM LEVEL STABILITY TEST RESULTS**

No. of Tests Rep-resented	Station	RMS Variation of Test Mean Chan. Level***		RMS Variation of Test Minutely Means*		% Tests With Worst Case Power Var. < 2 db	Worst Case Chan. Level Corr. Coeff.
		Low Chan	High Chan	Low Chan	High Chan		
36	Cooby Creek	1.04	1.08	0.24	0.51	86.4	0.967
9	Rosman	1.75	1.43	0.20	0.14	65.0	0.987
8	Mojave	1.43	2.24	0.40	0.31	70.6	0.994

*These values are based on the results of one 3-station automated test.
**The computer calculates the mean tone level for each test, and the average tone level for each minute of each test. Also, the greatest deviation from nominal test-tone level is printed out. The channel level correlation coefficient is calculated for each two-minute interval by the following method:

$$C_r = \frac{L_1 H_1 + L_2 H_2 + \cdots + L_n H_n}{L_1^2 + L_2^2 + \cdots + L_n^2}$$

where,

$$L_1 = \log^{-1} \frac{\ell_1 - \overline{\ell}_1}{10} \quad \ell_1, \quad \ell_2 \text{ --- } \ell_n = \text{ individual data points (db) for the low channel.}$$

$$\overline{\ell} = \text{ average of low channel data points for 2-minute period.}$$

H_1, H_2 - - - H_n is similarly defined for the high channel.

***The values in this column do not reflect relative level variations, but variations in the mean level from test to test.

TABLE 3.18. PERCENT OF LEVEL ERRORS

Station	No. of Sec. Samples	% Sec. Samples of TT Level Var. < 2 db
Cooby Creek	8640	78.2
Rosman	5760	76.3
Mojave	7200	87.2
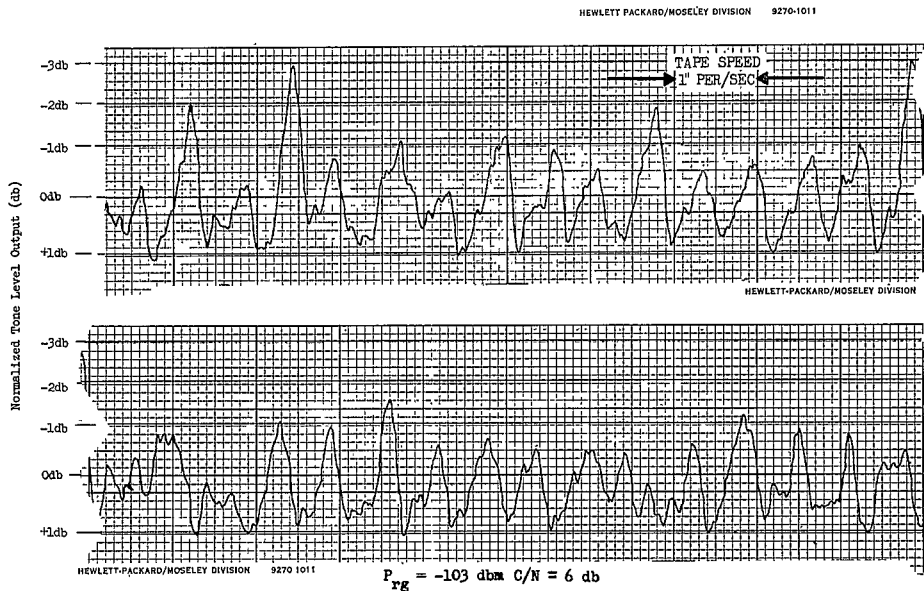
Figure 3.58. Typical Strip-Chart Recording of Level Variations vs. Time

3.3.3 GROUND-TRANSMITTER AUTOMATIC-LEVEL CONTROL LOOP (J. G. McGillen) (MA-SP-3.1)

3.3.3.1 Description and Test Results

OBJECTIVES

The objective of this experiment is to evaluate the performance of the automatic level control (ALC) system for the SSB Transmitter.

In the MA mode, the satellite may receive SSB signals from many ground stations with variable but unique path attenuations between each ground station and the satellite. These variable path attenuations can result from range variations, rainfall, gain changes in the SSB transmitter, and gain changes in the spacecraft receiver. In addition, spacecraft antenna pointing inaccuracies occur when the spacecraft is in eclipse. During this period an unsensed increase in angular velocity occurs, causing the despun antenna beam to move off the subsatellite point which changes the satellite received antenna gain for ATS-3.

TEST CONDITIONS

The test-tone PhM deviation produced in the satellite SSB/PhM transponder is, ideally, proportional to the received SSB signal amplitude. To provide uniform deviation for all FDM channels, each ground station must individually, precorrect its transmitter power. ALC systems at each ground station operate by local measurement of deviation produced remotely at the satellite, for their respective assigned pilot signal, F_p. The ALC adjusts the RF drive to the SSB power amplifier to compensate for long-term variations in test tone PhM.

STANDARD

The design specification for the ALC loop states that the loop will sense and correct level changes +6 db and -20 db about the nominal operating condition. The received pilot is to be maintained within 0.2 db of its normal value and should be corrected by the loop at a rate of 0.1 db per second.

RESULTS

The results of two RF loop tests performed by Cooby Creek are summarized in table 3.19. Figure 3.59 explains graphically the response parameters given in the table. Figure 3.60 is a sample strip-chart recording of the ALC loop response. The following is a verbal definition of the control-loop parameters presented:

1) Loop Delay or Dead Time, T_p - The point at which the response is equal to one-half its final value is visually determined, and the associated point on the horizontal time axis is designated T_p. The time at which the step function is introduced is the reference origin $(t = 0)$. This parameter, then, includes the transport time to and from the S/C.

2) Rise Time, T_r - Commonly defined as the time interval between the 10-percent and 90-percent points (of the steady-state value) on the response.

3) Overshoot, O_S - With the initial value of the transient response taken as the reference level, the maximum value of the response and the steady-state value of the response are designated M and A, respectively. The percent overshoot, O_S, is then given by

$$O_S = \frac{M-A}{A} \times 100$$

4) Total Settling Time, T_S - The time interval between the input perturbation and the point at which the response transient has decayed to ±5 percent of its steady-state value.

5) The Effective System Velocity Constant, K_V - Defined on the basis of a step input as

$$K_V = \frac{Log^{-1}(S/20)}{T_r}$$

where S is the db value of the step input perturbation and T_r is as defined above.

3.3.3.2 Analysis

It should be noted that the transmitters at Mojave and Cooby Creek when operating with ATS-1 under a fully loaded condition are at their maximum rated power. Any level changes at this point would cause the intermediate power amplifier to overdrive the power amplifier with a resultant rise in intermodulation. In the case of ATS-3, however, the ground transmitter is operating some 10 db below maximum power. The ALC loop, therefore, would be readily able to compensate for such an increase in attenuation without affecting overall system performance.

From the design specifications and the possible causes of level changes mentioned above, it can be seen that the loop is not required to overcome rapid large variations. For this testing program the maximum perturbations have been limited to 6 db.

From the results of the two RF loop tests, the ALC loop meets the specification of response rate perturbations. For a 1.0-db step the correction rates were 0.14 and 0.09 db per second. For a 3.0-db step, they were 0.11 db per second; and for a 6.0-db step they were 0.09 and 0.1 db per second. In both tests there was no observable overshoot. These results show that due to the finite speed limitation of the motor driven attenuator, the ALC loop acts like a perfect integrator to step changes, and controls the loop within the response rate specification.

3.3.3.3 Conclusions

The two ALC loop tests were performed in the RF loop-test configuration, the results indicate that performance is essentially in agreement with the design objectives. The median value of test runs shows a response rate of 0.1 db per second. The principal conclusion to be drawn from the tests is that slope of the transient response is essentially constant (i.e., independent of the magnitude of the step input). Also, from observation of the strip chart recording, the overshoot of the response was not significant, thus indicating a well-damped system.

TABLE 3.19. GROUND-TRANSMITTER, AUTOMATIC
LEVEL CONTROL-LOOP TEST RESULTS (MA-SP-3.1)

Station		Cooby Creek	Cooby Creek		
Date		11-29-67	12-3-67		
Test Time		0800Z	0635Z		
Duration (minutes)		30	26		
Station Pilot, F_p (kHz)		292	292		
Loop Configuration		RF	RF		
Rise Time T_r (Seconds)	0.2-db STEP	①	①		
	1.0-db STEP	7.2	11		
	3.0-db STEP	28.0	27		
	6.0-db STEP	66.0	63		
Percent Over Shoot	0.2-db STEP	①	①		
	1.0-db STEP	①	①		
	3.0-db STEP	①	①		
	6.0-db STEP	①	①		
Delay Time, T_p (Seconds)	0.2-db STEP	①	①		
	1.0-db STEP	8.0	7.0		
	3.0-db STEP	20.0	21.0		
	6.0-db STEP	40.0	42.0		
Settling Time, T_s (Seconds)	0.2-db STEP	①	①		
	1.0-db STEP	14.0	17.0		
	3.0-db STEP	35.0	45.0		
	6.0-db STEP	92.0	84.0		
Carrier-to-Noise Ratio		31.4 db	128.0 db		
Computed Velocity Constant, K_v (H_z)	0.2-db STEP	①	①		
	1.0-db STEP	0.156	0.102		
	3.0-db STEP	0.050	0.052		
	6.0-db STEP	0.303	0.318		

① Not Discernible
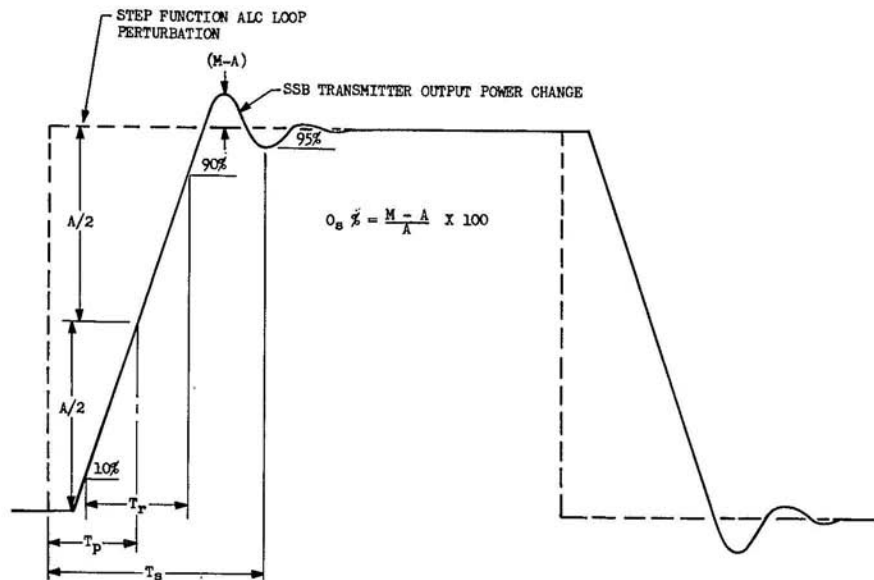
Figure 3.59.   ALC Loop Response Parameters Defined

3.130
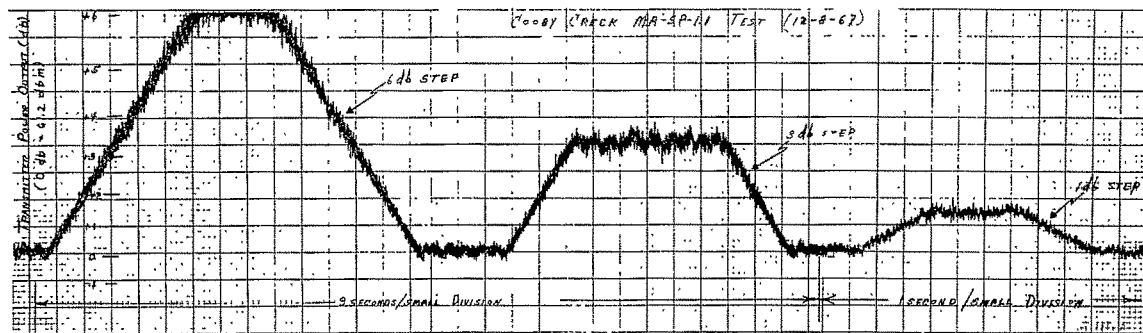
Figure 3.60.   ALC Loop Transient Response, MA-SP-1.1 (Cooby Creek, 3 Dec 67)

3.131

3.4 MULTIPLEX PERFORMANCE EXPERIMENTS

A series of tests are employed to evaluate the performance capabilities of the ATS system in the transmission of multi-channel FDM (frequency division multiplex). These tests include both operating modes of the SHF radio equipments: namely, FT (FM/FM frequency translation), and SSB/PhM (SSB uplink and PhM downlink).

These tests are performed under the following conditions unless stated otherwise under the individual subparagraph:

1) FT or SSB - PhM mode as applicable.

2) Earth station antenna "peaked" on satellite.

3) Spacecraft antenna positioned for maximum earth station received signal strength, except for multistation tests. .

4) Earth station AFC in "AVG" position with FM transmitter.

.5) RF carrier deviation (FM) or S/C mod index.for TT level (SSB/PhM)

$$FT \begin{cases} 690\text{-kHz peak,Rosman} \\ 1230\text{-kHz peak,Mojave and Cooby Creek} \end{cases}$$

SSB/PhM 0.35-radian peak (spacecraft)

6) Receiver IF bandwidth set to 30 MHz (nominal) at Rosman, and 12 MHz (nominal) at Cooby Creek and Mojave, except 30 MHz is used whenever more than 240 channel spectrum is received, eg., for multistation tests.

7) Audio test-tone levels set for -16 dbm at the input to the multiplex equipment and the receive output is set to +7 dbm (unweighted).

8) Baseband test-tone levels set at -30 dbm send and receive.

3.4.1 CHANNEL TT/N RATIO (MA-AT-1.1, MA-AT-1.2, MA-MX-7.1, MA-MS-2.1, FT-MX-6.1 (D. F. Maguire, E. E. Crampton)

3.4.1.1 Description and Test Results

OBJECTIVES

The primary objectives of the channel test tone-to-noise (TT/N) ratio experiment are to evaluate the capability of the ATS system to provide useful frequency division multiplex (FDM) telephone service and to obtain the experimental data necessary to establish realistic user requirements for such a system.

The following specific relationships will be developed to obtain these two broad objectives:

1) Multiplex voice channel TT/N performance will be compared to the nominal CCIR recommendation of 50 db and the nominal EIA recommendation of 45 db.

3.132

2) Multiplex voice channel TT/N performance will be determined as a function of:
   a) SSB-PhM (MA) and FT modes.
   b) Earth station antenna (85 feet at Rosman and 40 feet at Mojave and Cooby Creek).
   c) Satellite EIRP (over a range of 49.4 to 56.5 dbm)
   d) Channel frequencies (low channel,316 kHz to 342 kHz at Rosman, Mojave, and Cooby Creek; high channel, 5340 kHz and 5560 kHz at Rosman; 1248 kHz and 1296 kHz at Mojave and Cooby Creek)
   e) Single and multiple earth station access to the satellite
3) Multiplex voice channel TT/N performance will be related to the abnormal conditions during an eclipse (satellite in Earth's shadow) and closest con-conjunction (satellite in a direct line between Earth and sun.)

In addition to the primary objectives, the TT/N data will be used for correlation to other experiments, specifically Data Error Rate (par. 3.4.2) and Noise-Power Ratio (NPR/TPR) (par. 3.2.1).

TEST CONDITIONS

The following test conditions are applicable to this analysis:

1) Mode of Operation - Each test is performed in one of the two modes; multiple access SSB-PhM (MA) or frequency translation (FT). Basically, selected channels are noise-loaded and measurements obtained; the loading is removed and measurements are again made. An evaluation is then made to determine the intermodulation noise and how the TT/N varies as a function of baseband frequency.
2) System Configuration - The experiments are separated into two earth station - satellite groups; a) single station (e.g., Rosman and ATS-3) and, b) multi-station (e.g., all three earth stations and ATS-1). This is done to evaluate differences due to earth station antenna size, satellite transmitter power , and earth station performance as well as multistation access to the satellite.
3) Uncontrolled Variables - The uncontrolled variables that have the most signifi-cant effect on system performance are path loss variations, S/C transmitter power output, S/C antenna pointing, and system noise temperature. The effect of these variables may be partially offset by normalizing TT/N data to the mea-sured mean carrier-to-noise ratio of the test runs.
4) Controlled Variables - The following listed system parameters have been con-trolled for the FDM tests.

3.133

PARAMETER	STATION	
	ROSMAN (85' Antenna)	MOJAVE and COOBY CREEK (40' Antenna)
Channel Bandwidth (unweighted) (kHz)	3.1	3.1
Weighting Improvement (FIA) (db)	3.0	3.0
Channel Spectrum	1200	240
*Channel Loading (noise on) (db)	15.8	8.8
Receiver IF Bandwidth (signal) (MHz) (noise bandwidth) (MHz)	30 nominal 35.5	12 nominal 15.5
FDM Channel Spacing	4.0	4.0
Peak Deviation of Carrier (FT Mode) per channel (kHz) Total baseband (MHz)	690 9.5	1230 7.6
Spacecraft Received Power SSB-PhM Mode (per channel) (dbm) FT Mode (total) (dbm)	−87.0 −73.0	−87.0 −73.0
Peak Test-Tone Modulation Index at Spacecraft (SSB-PhM Mode) (per channel) (radians) Total baseband (radians)**	0.35 4.84	0.35 2.12

*The CCIR recommended noise loading for channels is applied to a baseband spectrum of N channels. Refer to paragraph 7.6.3 (System loading) for a complete discussion of the FDM multiplex system loading.

**Based on a peak-to-rms factor of 10 db.

STANDARDS

     In this analysis, the user requirements are presented that are applicable to all system configurations and conditions.

     These requirements have been developed from the recommendation contained in EIA TR-141 para. 2.7 "Standards for Multiplex Telephone Channels" and CCIR XI Plenary Assembly. These recommendations are presented in paragraph 7.6.2 FDM Multiplex user requirements.

     The test tone-to-noise (TT/N) recommendations which are applicable to the ATS system consist of the following:

EIA (RETMA)   45 db (F1A weighted)

CCIR   50 db (Psophometrically weighted, 50.5 db F1A weighted)

RESULTS

SSB-PhM (MA) Mode, Single Station Access

MA mode test results are summarized in table 3.20 for the low-baseband channel (336 kHz or 342 kHz at all earth stations and for the high-baseband channel (5340 kHz at Rosman and 1248 kHz at Mojave and Cooby Creek). This table lists the mean TT/N (noise loading on) and TT/R (noise loading off) ratios as a function of ATS-1 and ATS-3 EIRP. The mean ratios were determined after the measured ratios were normalized to mean C/N also listed in table 3.20. The noise loading on ratios are for 1200 channel loading (15.8 dbm0) at Rosman and 240 channel loading (8.8 dbm0) at Mojave and Cooby Creek. In addition, the predicted TT/N and TT/R ratios are listed as a basis for comparison.

Table 3.21 summarizes a number of automated tests performed at the Mojave earth station. The automated feature provides a system/computer interface such that the mean of TT/N and TT/R (12 samples) is computed each minute. This data indicates the variation of these ratios over the test interval as well as the rate of variation. Typical examples of the data printout are illustrated in figures 3.61 and 3.62.

SSB-PhM (MA) Mode, Multistation Access

Two comprehensive series of multistation tests were performed in the SSB-PhM mode. The results of the first series, which included some automated tests, are presented in figures 3.63 through 3.70 and in table 3.22 for the different multistation system configurations.

Figures 3.63 and 3.64 show the variation of TT/N in two (341 kHz to 1247 kHz) multiplex channels at each earth station as a function of the number of channels loading the satellite. The variation of TT/N across the baseband (test channels slots from 342 kHz to 5340 kHz) as a function of C/N ratio at each earth station is shown in figures 3.65 through 3.69 for 240, 640, 940, and 1200 channels loading the satellite. Figure 3.70 shows the effect of overdeviating the low-frequency channels at the medium station as well as medium station TT/N improvement. Finally, the measured mean TT/N for the various system configurations and loading conditions are summarized in table 3.22. Results of this first test series are presented with no attempt to normalize the measured TT/N to mean C/N. Thus, figures 3.63 through 3.70 and table 3.22 include any variation in C/N during the test interval.

The second series of multistation tests was expanded to include over-deviation of the high-frequency channels and to show any multistation effect relative to medium station channel group placement within the baseband spectrum. In addition, specific tests were.

3.135

performed to measure TT/N variation across the baseband as a function of C/N ratio. Since all tests were at 1200-channel loading, the measured parameter, NPR, is presented to show this variation rather than TT/N.

Figure 3.71 shows the variation of NPR across the 316-kHz to 5564-kHz baseband as a function of C/N ratio to further emphasize degradation in the low-frequency channels when receiver operation is in the threshold region. Figures 3.72 and 3.73 summarize the effects of medium station overdeviation of the low-and high-frequency channels,respectively. The data shown in these figures is at 1200-channel loading of ATS-1. Figures 3.74 and 3.75 indicate system limitations from intermodulation noise contributed by the spacecraft and earth station receiver (K_{ov}) and the earth station transmitters (K_2) as a function of baseband noise loading.

FT MODE, SINGLE STATION ACCESS

FT mode test results are summarized in the same manner as those shown for the MA mode. Table 3.23 presents the mean of the TT/N and TT/R ratios measured without pre-emphasis/de-emphasis as well as the corresponding predicted ratios. Measured and predicted ratios with pre-emphasis/de-emphasis are presented in table 3.24.

SPECIAL CONJUNCTION EXPERIMENT

Special tests were conducted at the Mojave and Rosman earth stations to measure multiplex-channel received test tone and noise levels during conjunction of the earth, spacecraft,and sun. Measurements made in selected multiplex channels at the Mojave earth station are presented in figure 3.76 and are considered representative of the variation of these two parameters during the period of conjunction. In addition, the variation of carrier plus noise during the conjunction period, also measured at the Mojave earth station, is shown in figure 3.77.

3.4.1.2 Analysis

Test tone-to-noise (TT/N) or (TT/R) ratios discussed in this analysis are derived from measured test tone plus noise-to-noise ratios. For high ratios (above 15 db), (TT+N)/N and (TT+R)/R ratios are, for all practical purposes, identical to TT/N and TT/R, respectively. (N) consists of four types of noise terms which are intermodulation (I), thermal (R), and threshold noises (N_i) and ($\triangle$). These noise components and their significance with respect to C/N ratio are fully described in section 3.2.1. In the idle condition (noise off), the noise consists of (N_i) and (R) and in the loaded condition (noise on) all noise terms are present. However, in this analysis, the (R) term only is used to denote idle noise and the (I) term to denote all noise terms except idle noise. (N) then, denotes idle noise plus all other noise terms in the noise-loaded condition.

Predicted TT/N and TT/R ratios provide the reference for comparing measured ratios. Predicted ratios were derived from an overall system analysis, based on SSB and FM theory, using pre-launch system design parameters either unmodified or modified by post-launch measurements. Thus, the system parameters, used to calculate the predicted ratios, are known to an acceptable degree of accuracy. These ratios define multiplex channel operational performance in both the SSB-PhM and FT modes. However, the comparison between predicted and measured TT/N and TT/R ratios is valid only if the C/N ratio is above threshold. Evaluation of multiplex-channel performance for the SSB-PhM and FT modes is based on the above theory, and the measured and predicted ratios should essentially agree for above threshold operation.

SSB-PhM (MA) MODE, SINGLE STATION ACCESS

Characteristically, TT/N and TT/R ratios measured in the SSB-PhM mode of operation should be essentially constant over the operating baseband, provided the received C/N ratio is above threshold. With the received C/N ratio at or below threshold, there is a noise build-up in the low end of the baseband (see section 3.2.1 for analysis) and in fact, in the threshold region, a one db decrease in C/N ratio will cause the 342 kHz channel TT/N to decrease about 2 db. Thus, the TT/N and TT/R summary presented in table 3.20 is for earth station/spacecraft configurations that provide C/N ratios above the threshold level of about 10 db. However, measurements were made in low-and high-baseband channel to show any variation. It is seen that this variation does not exceed 2 db which occurs at Cooby Creek with a C/N ratio of 10.9 db.

The TT/N summary in table 3.20 shows that measured ratios are within 2.8 db of the predicted ratios. However, none of the earth station/spacecraft configurations shown can provide a TT/N ratio to meet either the 45 db EIA standard or the 50 db CCIR recommendation. In fact, only the Rosman earth station (85-foot antenna) with ATS-3 (54.6 dbm EIRP) can meet the EIA standard and this is based on TT/R (F1A weighted) at the nominal spacecraft received test tone power (P_{rs}) of -87 dbm.

At this nominal P_{rs} condition, figure 3.75 shows that the best TT/I the earth station transmitter, with a 40-foot antenna and using ATS-1 (240-channel loading), can provide is approximately 46 db. On the other hand, this same earth station, using ATS-3 (1200-channel loading), yields a TT/I of 54 db; however, the spacecraft now limits TT/I such that the best overall system TT/I is still about 46 db. The earth station transmitter, with an 85-foot antenna and using ATS-1 (see figure 3.74) provides a TT/I of approximately 43 db. This earth station with ATS-3 is again limited by the spacecraft such that the system TT/I is still about 46 db. Based on this 46 db TT/I ratio and the TT/R ratio of about 46 db, shown in table 3.20, the best TT/N is 43.3 db and this occurs at the Rosman earth station (85-foot antenna) using

ATS-3 (56.5 dbm EIRP), also indicated in table 3.20. In order to meet a 50 db TT/N ratio without compandors, both TT/I and TT/R should be increased to 53 db.

An increase in earth-station transmitter output power will increase uplink TT/R and this can improve the overall TT/N for those configurations that are thermally limited. These configurations include all earth stations with 40-foot antennas. The overall improvement in TT/N is limited by the increase in intermodulation noise caused by the system non-linearities. Referring to section 3.2.1, table 3.3, shows the limiting noise factors, i.e., uplink and downlink thermal and intermodulation noise for the SSB-PhM (MA) mode. Table 3.4 shows that it is possible to obtain a one to two db improvement in overall TT/N relative to the nominal operating point.

Table 3.20 shows that the measured TT/R ratios are generally lower than predicted TT/R ratios. This shows the effects of the uncontrolled variables discussed under test conditions which caused measured C/N ratios to be somewhat lower than those used to obtain the predicted ratios.

Table 3.21 provides an indication of the variation of measured TT/N and TT/R with time. Each test covered a continuous time period of one hour. The observed maximum deviation from the mean of the measured TT/N ratios is plus 0.2 db/minus 0.5 db and this occurs within a 13-minute period. Short term TT/R variations are somewhat larger, the maximum being a 1.1-db total excursion in a 2-minute period. The larger variation in TT/R is reflected in TT/N since the TT/I, which is relatively constant, and TT/R are the same order of magnitude as previously discussed. Although these test results are somewhat limited, they provide an indication of both long and short term TT/N and TT/R variation. These measured variations do not appear to be significant with respect to the operating system TT/N and probably no more than a one db margin for variations with time, is required to compensate for the uncontrolled variables listed under test conditions.

In addition, tests were performed under extreme weather conditions. During a heavy rainstorm and with the earth station antenna at a low elevation angle (approximately 7°), a maximum decrease of 4 db from nominal multiplex TT/N was observed. At higher elevation angles (approximately 36°), the maximum observed decrease in multiplex channel TT/N was 2 db. In another test, a maximum decrease of 2 db was observed when the earth station antenna was covered with snow.

The statistical nature of these weather conditions depends on geographical location. This fact must be considered along with the measured data to arrive at the proper system margin to compensate for these conditions. Based on the location of the ATS earth stations, and considering TT/N variation due to uncontrolled parameters stated above, a system margin of 2 db appears adequate to realize the mean TT/N ratios shown in table 3.20, in any hour.

This analysis shows that for the earth station/spacecraft configurations shown in table 3.20, the best TT/N ratio is obtained with the Rosman earth station (85-foot antenna) using ATS-3 (56.5 dbm EIRP). This TT/N ratio is 43.3 db which is practically equal to the predicted ratio. However, it is 1.7 db below the EIA standard and 6.7 db below the CCIR recommendation. TT/N ratios for the thermally limited earth station/spacecraft configurations can be improved by 2 db, however, this improvement is not sufficient to meet the EIA standard. The fact that TT/N ratios in the SSB-PhM mode do not meet either the EIA standard or the CCIR recommendation is also reflected in the predicted ratios. To overcome the system limitations, compandors can be used to increase TT/N somewhere between 13 db and 22 db. The overall improvement will then depend on the number of compandors and in general their use will allow the system TT/N to subjectively meet the CCIR recommendation of 50 db. The variation of multiplex channel TT/N due to the uncontrolled parameters appears minimal. Considering a one db margin (exclusive of weather effects), both TT/I and TT/R should be at least 54 db to provide a TT/N of 50 db without compandors.

SSB-PhM (MA) MODE, MULTISTATION ACCESS

Figures 3.63 through 3.69 show measured TT/N as a function of satellite loading and baseband frequency for the various multistation system configurations. This data taken during the first series of tests is summarized in table 3.22 for 640 and 1200 channel loading for the high (5339 kHz and 1247 kHz) and low (341 kHz) telephone channels. Table 3.22 also shows the results of automated multistation tests indicative of TT/N variation as a function of time. No attempt was made to normalize the multistation test TT/N to the mean C/N.

With 1200-channel loading at ATS-1, measured TT/N in the 341 kHz channel at both Cooby Creek and Mojave drops to unacceptable levels. Multistation operation requires that all earth stations receive the entire baseband signal which in turn requires an IF filter bandwidth of 30 MHz nominal. The penalty is low C/N ratio (7.4 db to 9.1 db) at the medium earth stations (40 ft. antennas). Positioning of the ATS-1 antenna beam to provide equal C/N ratios at these two stations as opposed to positioning the beam for optimum C/N ratio at an individual station, also contributes to the lower C/N ratio in multistation operation. The variation of earth station C/N ratio with respect to the ATS-1 antenna beam position is shown in figure 3.78. The net result is operation in the receiver threshold region, leading to noise build-up (N_i and $\triangle$ become dominant), thus low TT/N and the unacceptable performance.

This effect, although less severe, also occurs at Rosman (85 ft. antenna and ATS-1). In this case, C/N ratio is some 3 db to 5 db higher which provides a 2-db to 3-db margin above an assumed threshold level of 10 db. It appears that a larger margin is

required to completely eliminate the threshold noise effects. This is further substantiated by the Mojave/ATS-3 system configuration (C/N of 11.8 db, TT/N of 34.1 db) which compares to Rosman/ATS-1 (C/N of 12.4 db, TT/N of 34.8 db).

Figures 3.65 and 3.66 show that measured TT/N in the high channel (5339 kHz) shows little or no decrease due to threshold effects at low C/N ratios (7.4 db to 9.1 db). This compares to single station data for the same system conditions (Mojave and ATS-1), where TT/N varies about 1.0 db for the worst case. The TT/N ratio of 36.5 db at Cooby Creek and Mojave for 1200-channel loading at ATS-1 is about 1.0 db less than the predicted TT/N ratio of 38.3 db for 240-channel loading.

The Rosman ATS-3 system configuration provides the largest C/N ratio, approximately 20.0 db. At this level, measured TT/N ratio remains fairly constant over the baseband as shown in figure 3.69 and compares favorably to single station predicted TT/N ratio.

Figure 3.70 shows the improvement obtained at a medium station as a result of overdeviating the medium station 60-channel spectrum (316 kHz to 552 kHz). Overdeviation is accomplished by increasing the loading level above nominal 2.8 dbm0 for 60 channels until NPR measurements show that intermodulation noise due to spectrum truncation or SSB transmitter non-linearities limits improvement in the overdeviated channels. Approximately 5.0-db improvement is realized in the 341-kHz channel at a load factor 6.0 db above nominal. At the same time, about 2.0-db improvement is realized in the 341-kHz channel at the large station. Since the large station thermal noise is low compared to the medium station, it should and does see the effects of increased intermodulation noise due to overdeviation sooner, consequently the improvement will be less. There is negligible degradation on the channels (e.g., 767 kHz) outside the 60-channel spectrum.

Measured TT/N ratios derived from the multistation automated tests (see table 3.22) show the same results as the above data, i.e., the threshold noise effect at low C/N ratios. Variation of TT/N with time is essentially the same as that discussed for single-station access, as shown in table 3.21.

The second series of tests were performed with nominal 1200-channel loading (15.8 dbm0 per CCITT recommendation G222). Various stations, through the process of mixing and filtering, were allocated 60, 120 and 240 channel groups at different portions of the baseband spectrum, but with the large station supplying the necessary channels to provide full 1200-channel loading at the satellite. The average of some 27 test runs showed that TT/N over the 316-kHz to 5564-kHz baseband was consistent (±1.0 db) with the 1200-channel curves shown in figures 3.66 through 3.68 for comparable C/N ratios. During the second series of tests, C/N varied from 8.1 db to 8.9 db at the medium station and from

13.0 db to 15.2 at the large station, from ATS-1. Thus, these curves reflect expected system performance under the given conditions in either a fixed or random assignment of channels. They also show that the medium station with its low C/N ratio can avoid the threshold effect at the low end of the baseband and realize some 10 db to 12 db TT/N improvement when it receives its multiplex channel group at the high end of the baseband. This restriction limits the random access feature but may be necessary for satisfactory communications to the medium station.

A further indication of the threshold characteristic at low C/N ratios is seen in figure 3.71, which shows the medium station TT/N variation over the 316-kHz to 5564-kHz baseband as a function of C/N ratio. That TT/N is a critical function of C/N ratio below threshold operation, particularly at the low-baseband frequencies, is quite apparent, since a 2-db change in C/N ratio causes TT/N to change 6 db in the 342-kHz channel. This data tends to confirm that threshold for the SSB-FDMA/PhM mode is in the neighborhood of 10 db. The drop in TT/N at the low and high ends of the curve for the 10 db C/N ratio, is attributed to baseband frequency response which is down about one db at 342 kHz and 2 db to 3 db at 5340 kHz. From the standpoint of complete random access, this data indicates system design should require all stations, regardless of classification, to operate above threshold.

The variation of TT/N over the baseband at low C/N ratios suggests the possibility of overdeviation at the low end of the baseband to improve TT/N ratio when the medium station is receiving a group of channels in this portion of the baseband. This means that the transmitting station must be given a larger share of the satellites available power by permitting overdeviation of this same channel group, to improve TT/N at the medium station. It also means that SSB transmitter linearity must be able to support this over-deviation without generating excessive intermodulation noise. Depending on the mix of medium and large stations and on the links between stations, overdeviation at the trans-mitting station to improve medium station TT/N would become quite complex and is not considered a practical solution. However, a practical solution would be to have proper pre-emphasis in the satellite. It follows that this solution would reduce station transmitter-power requirements as well as more stringent transmitter linearity requirements. These effects were investigated but were restricted to overdeviation in a link between two medium stations, both occupying the low end of the baseband, and with the large station making up the total of 1200 channels loading the satellite. In addition, the effects of overdeviation at the high end of the baseband were investigated.

Figure 3.72 summarizes the results of medium station 60-and 120-channel overdeviation at the low end of the baseband. Sixty-channel (316 kHz to 552 kHz) over-deviation shows practically a 1-to 1-db TT/N improvement at the medium receiving station

up to 9 db of overdeviation at the medium transmitting station. Reception at the large station also shows an improvement which begins to limit and then decrease at about 6-db overdeviation with the medium station transmitting. Since the large station thermal noise is low (high C/N ratio) compared to the medium station, it begins to see the effects of inter-modulation noise build-up sooner than the medium station. In this case, the intermodulation noise is most likely due to the medium station transmitter. This data essentially confirms that shown in figure 3.70, obtained during the first multistation test series. During both series of tests, no noticeable degradation was observed outside the overdeviated (9 db) 60-channel spectrum.

Figure 3.72 also shows that by increasing the number of channels overdeviated at the medium transmitting station to 120 (316 kHz to 808 kHz), the effect of intermodulation noise build-up is now seen at the medium station at about 6 db compared to 2 db at the large station. In addition to transmitter intermodulation noise, the increased rate of intermodulation noise build-up observed when 120 channels are overdeviated, follows from the fact that with PhM the lower modulating frequencies contribute less to the overall width of the frequency spectrum than the higher modulating frequencies. This can be seen in figure 3.79 which shows the equivalence between phase and frequency deviation with noise loading measured at Cooby Creek. In the event a medium station must receive at the low end of the baseband, overdeviation improvement, if allowed, also becomes a function of the number of low-frequency channels being overdeviated.

As pointed out, overdeviation at the higher baseband frequencies increases the rate of intermodulation noise build-up and is caused by IF passband spectrum truncation. Figure 3.73, which summarizes the results of 60-channel (5322 kHz to 5558 kHz) and 120-channel (5066 kHz to 5558 kHz) overdeviation at the high-baseband frequencies, clearly shows this effect. This data shows that transmission level is critical for any station transmitting at the high end of the baseband. In this case, the intermodulation noise buildup degrades all channels outside the overdeviated spectrum at both the medium and large stations. The total noise in any channel is now proportional to the magnitude of the intermodulation noise caused by the overdeviation, and either the magnitude of the thermal noise at the high C/N ratio (14 db - large station) or the magnitude of the threshold noise at the low C/N ratio (8.6 db - medium station). Data for the large station shows that the intermodulation noise predominates. It increases with decreasing baseband frequency and thus TT/N degradation is most severe in the low-frequency (342 kHz) channel. At the medium station, however, threshold noise predominates in the 342-kHz channel. Threshold noise decreases with increasing baseband frequency. Its level in the 534-kHz channel is sufficiently low so that as the intermodulation noise increases with increased overdeviation levels, TT/N begins to decrease at a faster rate relative to the 342-kHz channel. It is also dependent on the number of channels being overdeviated. Figure 3.73 shows that 120-channel overdeviation at the high end of the baseband causes the intermodulation noise to increase two to four times faster than for 60-channel overdeviation.

3.142

In an ideal FDM FM system, the relationship between thermal noise and baseband frequency is given by $R = Kf^2$ (where K is a constant), provided C/N is above threshold. The expected difference in channel TT/R ($\triangle$ TT /R) is:

$$\triangle TT/R = 20 \log \frac{(f_2)}{(f_1)}$$

where f_2 = high-channel baseband frequency (5340 kHz at Rosman and 1248 kHz at Mojave and Cooby Creek)

f_1 = low-channel baseband frequency (342 kHz at all earth stations)

Based on the above equations, the predicted $\triangle$TT/R is 23.8 db for Rosman and 11.2 db for Mojave and Cooby Creek. Referring to table 3.23, it can be seen that the measured $\triangle$TT/R ratios are within 1.9 db of the predicted ratios for all earth station/ spacecraft configurations. Since these configurations provide C/N ratios above 13 db, the FM demodulator output thermal noise spectrum should be parabolic and this is confirmed by the measured $\triangle$ TT/R. $\triangle$TT/N also has the same characteristic for C/N ratios above 13 db.

Considering TT/N, the measured ratios in the low-frequency channel for all earth station/spacecraft configurations are within 3.8 db of the predicted ratios. The high-frequency channels show a maximum difference of 1.6 db between measured and predicted TT/N ratios. This variation is expected and is evident from figure 7.5 in paragraph 7.2, which shows the variation of K_{ov} (overall TT/I at any channel within the baseband). Predicted TT/N ratios, presented in table 3.23, particularly for the low-frequency channel, used the more optimistic values of K_{ov} shown in figure 7.5, thus, the measured ratios are more realistic in terms of normal system operation. The TT/R ratios shown in table 3.23 define the upper limit of TT/N.

Although measured TT/N ratios in the low-frequency channel are somewhat lower than the predicted ratios, for all configurations TT/N exceeds the CCIR recommendation of 50 db by at least 4.4 db. Characteristically, TT/N decreases across the baseband and at 1248 kHz (240 channel total loading), TT/N is 4 db below the CCIR recommendation in the worst case, while at 5340 kHz (1200-channel total loading) the difference is 15.8 db. This again follows from the fact that both I and R increase with increasing baseband frequency.

TT/N in the high-frequency channel can be improved with the use of standard CCIR pre-emphasis/de-emphasis networks. Table 3.24 shows this improvement for representative earth station/spacecraft configurations. For 240-channel total loading, it can be seen that both the low-and high-channel TT/N ratios are slightly above 50 db. De-emphasis reduces the $\triangle$TT/N from about 9 db to 2 db or less. This indicates that the pre-emphasis/de-emphasis networks are essentially optimum for this condition. In fact the 50-db TT/N ratio is realized without using compandors.

With 1200-channel loading, pre-emphasis/de-emphasis improves TT/N in the 5340-kHz channel about 4 db. At the same time, it is noted that the low channel TT/N is decreased about 3 db, but is still some 4 db above the 50-db TT/N ratio. In this case, de-emphasis reduced $\triangle$ TT/N from about 22 db to 14 db, thus a further reduction appears desirable. This indicates that for this condition, pre-emphasis/de-emphasis is not necessarily optimum. A further decrease in low-channel TT/N could be tolerated in order to further improve high-channel TT/N. In either case, compandors are required to realize a 50 db TT/N ratio across the entire baseband. The number of compandors required can be minimized by using optimum pre-emphasis/de-emphasis with this condition of 1200-channel total loading. The results of experiments with different pre-emphasis/de-emphasis networks for 1200-channel loading are discussed in section 3.2.1.

SPECIAL CONJUNCTION EXPERIMENT-SSB-PhM (MA) MODE

The results of the special conjunction experiment are shown in figures 3.76 and 3.77. The test was conducted by monitoring a tone in the high-and low-FDM channel outputs on a strip-chart recorder as the S/C went into conjunction with the sun (earth station, S/C, and sun in line with each other). In order to obtain a measure of the noise alone, channels at the high and low ends of the baseband, adjacent to the tone-carrying channels, were also monitored. The earth station RCVR AGC was monitored in order to obtain a measure of the magnitude of the received carrier plus noise during the conjunction period.

Figure 3.76 shows the high-and low-channel tone plus noise and noise only curves (TT + N, N). It should be noted that the noise is significantly higher (approximately 9 db) in the low channel during the time that the receiver is operating below the threshold point of the discriminator. This is in agreement with previous observations that, at low C/N, the threshold noise in the low channels is significantly greater than in the high channels.

Figure 3.77 shows the plot of RCVR AGC (calibrated in terms of receiver input power) during the conjunction period. It is seen that the communication system is completely out of service during most of the conjunction period (system operation is below threshold for five minutes of the nine-minute period).

At operation above threshold, the T + N output consists essentially of tone power only; however, as the threshold point of operation is reached, the channel noise power increases until it becomes appreciable and eventually exceeds the tone power. As shown in figure 3.76, the tone power is seen to decrease as the threshold point is reached. The tone and noise powers are equal at a total power output of about -6 dbm for the high channel and +2 dbm for the low channel (corresponding to -9 dbm and -1 dbm levels for the high and low tone, respectively).

It should be noted that the tone only curve has been approximated over a portion of the eclipse period. This is because the calculation of the tone power becomes inaccurate

as the T + N and N terms become nearly equal. This inaccuracy is compounded by the fact that separate FDM channels are used to measure T+N and N, each with slightly different gain and noise bandwidth characteristics, thus no accurate measurement can be made of signal suppression in either the high or low channels.

3.4.1.3 Conclusions

SSB-PhM (MA) MODE

Depending on earth station/spacecraft configuration, in the SSB-PhM (MA) mode, measured TT/N ratios vary from 36.7 db to 43.3 db based on single-station access. The 43.3-db TT/N ratio is realized at the Rosman earth station (85-foot antenna) using ATS-3 (56.5 dbm EIRP) and this ratio is within 0.4 db of the predicted ratio or expected performance. However, it is 1.7 db below the EIA standard of 45 db and 6.7 db below the CCIR recommendation of 50 db. The system is thermally limited on the basis of 240 channel operation while inter-modulation noise limits 1200-channel operation relative to nominal operation. Although a 2-db improvement is possible for the thermally limited configurations, this improvement is not sufficient to meet the EIA standard. These system limitations can be overcome with the use of compandors. Overall improvement will depend on the number of compandors and in general, they will allow the multiplex channel to subjectively meet the CCIR requirement of 50 db.

The results of the multistation tests show that predicted channel TT/N ratios at the low end of the baseband frequency spectrum cannot be obtained with the present mix of earth stations and the ATS-1 spacecraft operating at full 1200 channel system capacity. The system configuration utilizing 40-foot antennas at Cooby Creek and Mojave with ATS-1 (52.2 dbm EIRP), give C/N ratios in the receiver threshold region, resulting in TT/N ratios of about 24 db, which are unacceptable.

Performance can be improved by limiting system capacity. For example, with 640 channel loading some 8-db to 12-db improvement in TT/N is realized in the low-frequency channels. By assigning the high end of the baseband spectrum to the two earth stations with 40-foot antennas, TT/N ratio may be improved by some 12 db. If the medium station must receive a channel group at the low end of the baseband, performance can also be improved by allowing the transmitting station to overdeviate this same channel group. There is practically a one db increase in TT/N for each db increase in overdeviation relative to nominal. However, a limit exists when intermodulation noise due to transmitter non-linearity and/or spectrum truncation tends to negate this improvement. This same overdeviation effect could be realized with the proper pre-emphasis at the satellite and is considered the more practical solution for future similar SSB-PhM (MA) systems.

At high C/N ratios, TT/N performance compares favorably to predicted performance and is reasonably consistent across the baseband. It follows that design of a random-access multiple-access system using a SSB-FDMA/PhM mode, requires a high C/N ratio (adequate margin above threshold at each earth station to provide an acceptable TT/N ratio).

In the SSB-PhM (MA) mode, the variation of multiplex TT/N due to uncontrolled variables appears to be minimal. Considering a one-db margin based on the 1.1-db total measured excursion in the automated tests (exclusive of weather effects), both TT/I and TT/R should be at least 54 db to provide a TT/N ratio of 50 db without compandors. Based on the Rosman earth station (85-foot antenna) and a nominal 30 MHz RF-IF bandwidth, a C/N ratio of 27 db is required to realize a TT/R ratio of 54 db.

FT MODE

The various ATS earth station/spacecraft configurations provide C/N ratios above threshold in the FT mode of operation. As a result, TT/N ratios measured across the baseband without pre-emphasis/de-emphasis vary in accordance with the parabolic noise spectrum characteristic of FM systems. With 240-channel loading, TT/N ratio in the low channel (342 kHz) varies from 54.5 db to 57.7 db while in the high channel (1248 kHz), it varies from 46.0 db to 49.0 db. In this case, the use of standard CCIR pre-emphasis/de-emphasis networks will allow the system to meet the CCIR recommendation of 50 db without the addition of compandors.

For the case of 1200-channel loading, TT/N ratio in the low channel (342 kHz) varies from 54.6 db to 58.4 db while in the high channel (5340 kHz), it varies from 34.2 db to 38.1 db. In this case, standard CCIR pre-emphasis/de-emphasis networks improve the high channel about 4 db with less than 3-db decrease in low-channel TT/N. This indicates that the pre-emphasis/de-emphasis is not necessarily optimum for 1200-channel loading. In order to realize a 50-db TT/N ratio across the baseband, compandors are required. The number of compandors required can be minimized by using optimum pre-emphasis/de-emphasis for this case.

TABLE 3.20. TT/N AND TT/R SUMMARY, SSB-PhM (MA) MODE (SINGLE-STATION ACCESS, MANUAL TESTING)

Station	Satellite	EIRP (dbm)	Loading (Channels)	IF Bandwidth (MHz)	MEAN OF MEASURED RATIOS NORMALIZED TO MEAN C/N				PREDICTED RATIOS		Mean Downlink C/N (db)
					TT/N (db)		TT/R (db)		TT/N (db)	TT/R (db)	
					Low Ch:	High Ch:	Low Ch:	High Ch:			
Rosman (85' ANT.)	ATS-1	52.2	1200	30	40.2	41.1	42.4	44.0	40.3	45.4	14.7
	ATS-3	52.2	1200	30	42.2	42.1	43.7	43.3	42.9	45.6	16.1
		54.6	1200	30	43.0	43.0	45.6	45.4	43.3	46.6	19.6
		56.5	1200	30	43.3	43.3	46.3	46.3	43.7	47.5	20.5
Mojave (40' ANT.)	ATS-1	52.2	240	12	37.4	38.7	38.1	39.8	39.5	40.5	12.9
	ATS-3	52.2	240	12	37.9	38.2	38.5	39.5	40.5	40.5	14.9
		54.6	240	12	39.9	40.9	40.7	41.2	42.3	42.5	15.4
Cooby Creek (40' ANT.)	ATS-1	52.2	240	12	36.7	38.7	37.6	39.2	39.5	40.5	10.9

NOTES:

(1) Low channels are 336 kHz or 342 kHz at all earth stations. High channels are 5340 kHz at Rosman and 1248 kHz at Mojave and Cooby Creek. All ratios are F1A weighted.

TABLE 3.21. TT/N AND TT/R SUMMARY SSB-PhM (MA) MODE (ONE HOUR TEST RUNS)
(SINGLE-STATION ACCESS, AUTOMATED TESTING)

Channel	Test Serial No.	Meas. C/N (db)	Noise Loading On			Noise Loading Off		
			Mean of Measured Ratios			Mean of Measured Ratios		
			TT/N (db)	Deviation from Mean (db)	Time Between Max. & Min. Dev.	TT/R (db)	Deviation from Mean (db)	Time Between Max. & Min. Dev.
Low (341 kHz)	M3003B	11.7	38.9	+0.1 -0.2	16	39.2	+0.1 -0.2	3
	M3004*	11.7	38.1	+0.2 -0.4	55	41.4	+0.2 -0.7	21
Center (758 kHz)	M3303B	11.7	41.7	+0.2 -0.1	14	42.2	+0.2 -0.1	2
	M3004*	11.7	38.2	+0.2 -0.5	13	41.2	+0.2 -0.9	2
High (1248 kHz)	M3003B	11.7	40.7	±0.2	43	41.1	+0.1 -0.4	1
	M3004*	11.7	38.5	+0.1 -0.5	53	41.3	+0.1 -0.4	8

* Noise loading on 1200 channels (15.8 dbm0), all other test runs on 240 channels (8.8 dbm0)

TABLE 3.22. TT/N AND TT/R SUMMARY SSB-PhM (MA) MODE,
(MULTISTATION ACCESS)

MANUAL TESTS - TELEPHONE CHANNEL-MEASURED MEAN TT/N RATIO IN DB

Station	Sat.	Sat. EIRP dbm	C/N db	640-Channel Loading at Satellite - 13.1 dbm0		1200-Channel Loading at Satellite - 15.8 dbm0	
				341 kHz Ch:	1247 kHz Ch:	341 kHz Ch:	5339 kHz Ch:
Cooby Ck	ATS-1	52.2	7.4-9.1	36.4	37.9	24.5	36.5
40' Ant.							
Mojave	ATS-1	52.2	7.5-8.8	31.2	36.1	23.7	36.5
40' Ant.	ATS-3	54.6	11.8	39.4	40.4	34.1	37.5
Rosman	ATS-1	52.2	12.4-14.2	39.2	40.2	34.8	40.0
85' Ant.	ATS-3	54-6	20.7	43.5	44.9	·41.8	43.9

AUTOMATED TESTS - TELEPHONE CHANNEL-MEASURED MEAN
TT/N AND TT/R RATIO IN DB

Station	Sat.	Sat. EIRP dbm	No. of Sta.	C/N db	Test Interval	1200-Channel Loading at Satellite - 15.8 dbm0							
						341 kHz Channel				1247 kHz Channel			
						TT/N	σ	TT/R	σ	TT/N	σ	TT/R	σ
Cooby Ck	ATS-1	52.2	3	6.2-7.4	1 Hr 45 Min	28.5	0.90	46.8	0.84	32.3	0.52	39.5	0.37
40' Ant.													
Mojave	ATS-3	52.2	3	7.7	2 Hr 0 Min	23.3	0.41	35.2	0.31	33.2	0.45	39.3	0.22
40' Ant.	ATS-3	54.6	2	11.7	3 Hr 31 Min	41.2	0.15	42.7	0.14	36.9	0.40	41.0	0.26
Rosman	ATS-1	52.2	3	13.0	1 Hr 46 Min	39.9	0.26	44.1	0.26	42.0	0.14	45.4	0.26
85' Ant.	ATS-3	54.6	2	20.0	3 Hr 31 Min	43.3	0.44	44.7	0.50	45.0	0.60	47.3	0.71

3.149

TABLE 3.23. TT/N AND TT/R SUMMARY, FT MODE WITHOUT PRE-EMPHASIS/DE-EMPHASIS
(SINGLE-STATION ACCESS)

Station	Satellite	EIRP dbm	Mean of Measured Ratios Normalized to Mean C/N				Predicted Ratios			
			TT/N (db)		TT/R (db)		TT/N (db)		TT/R (db)	
			Low Ch:	High Ch:	Low Ch:	High Ch:	Low Ch:	High Ch:	Low Ch:	High Ch:
Rosman (85' Ant.)	ATS-1	52.2	56.4	34.2	56.4	34.2	58.1	35.5	60.7	36.9
	ATS-3	52.2	56.8	36.4	58.6	36.7	60.1	36.9	61.7	37.9
		54.6	57.6	37.8	60.2	38.1	61.0	37.9	63.0	39.2
		56.5	58.4	38.1	62.3	39.9	61.6	38.8	64.1	40.3
Mojave (40' Ant.)	ATS-1	52.2	56.8	47.3	60.6	49.1	58.2	47.6	61.0	49.8
	ATS-3	52.2	56.1	47.7	59.6	49.4	59.7	48.7	61.1	49.9
		54.6	57.7	49.6	62.5	51.3	61.0	50.1	63.1	51.9
Cooby Creek (40' Ant.)	ATS-1	52.2	54.4	46.0	58.9	47.4	58.2	47.6	61.0	49.8

NOTE: TT/N and TT/R ratios based on 1200-channel loading at Rosman and 240-channel loading at Mojave and Cooby Creek. Low channel is 342 kHz at all earth stations. High channels are 5340 kHz at Rosman and 1248 kHz at Mojave and Cooby Creek.

TABLE 3.24. TT/N AND TT/R SUMMARY, FT MODE WITH PRE-EMPHASIS/DE-EMPHASIS
(SINGLE STATION ACCESS)

Station	Satellite	EIRP dbm	Mean of Measured Ratios Normalized to Mean C/N				Predicted Ratios			
			TT/N (db)		TT/R (db)		TT/N (db)		TT/R (db)	
			Low Ch:	High Ch:	Low Ch:	High Ch:	Low Ch:	High Ch:	Low Ch:	High Ch:
Rosman (85' Ant.)	ATS-1	52.2	52.8	38.7	53.2	39.6	54.1	39.5	56.7	40.9
	ATS-3	52.2	54.2	40.5	55.2	41.6	56.1	40.9	57.7	41.9
		54.6	55.3	41.5	56.5	41.9	57.0	41.9	59.0	43.2
		56.5	55.6	42.5	58.5	43.5	57.8	42.8	60.1	44.3
Mojave (40' Ant.)	ATS-1	52.2	50.3	51.5	56.6	51.6	55.2	51.6	58.0	53.8
	ATS-3	52.2	50.2	50.7	57.5	52.0	56.7	52.7	58.1	53.9
		54.6	51.6	53.7	59.6	55.6	58.0	54.1	60.1	55.9

NOTE: TT/N and TT/R ratios based on 1200-channel loading at Rosman and 240-channel loading at Mojave. Low channel is
342 kHz at both earth stations. High channels are 5340 kHz at Rosman and 1248 kHz at Mojave.
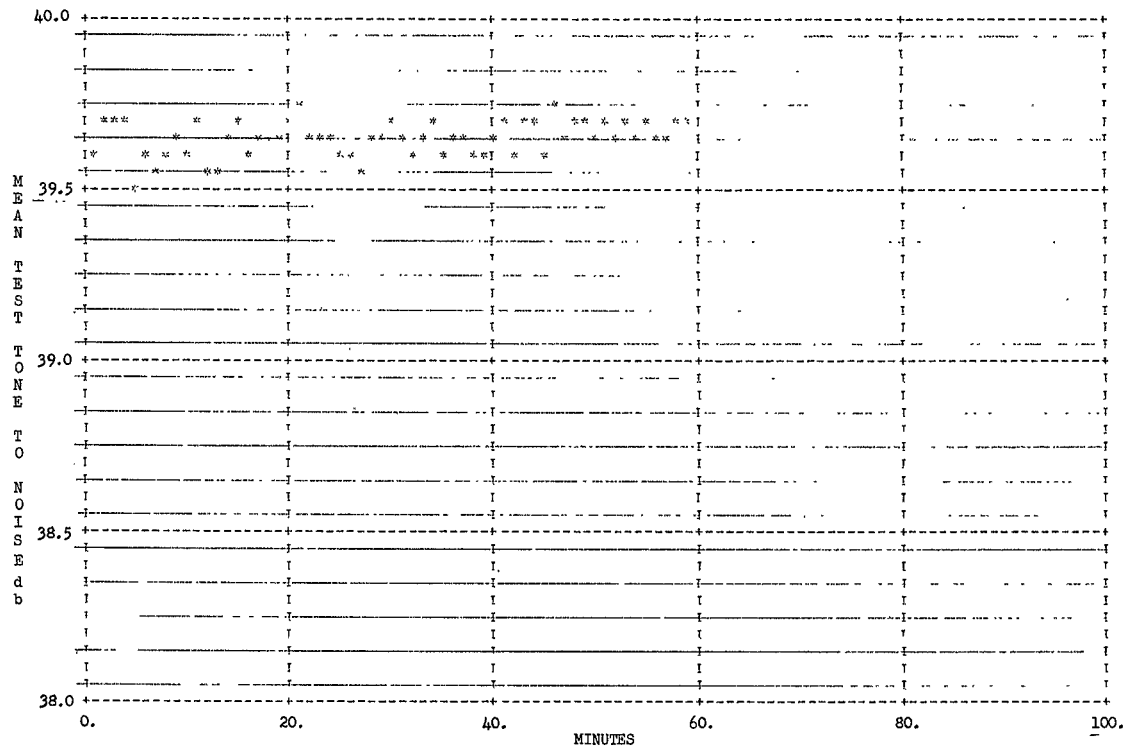
C/N = 11.7 db, 30 MHz IF FILTER
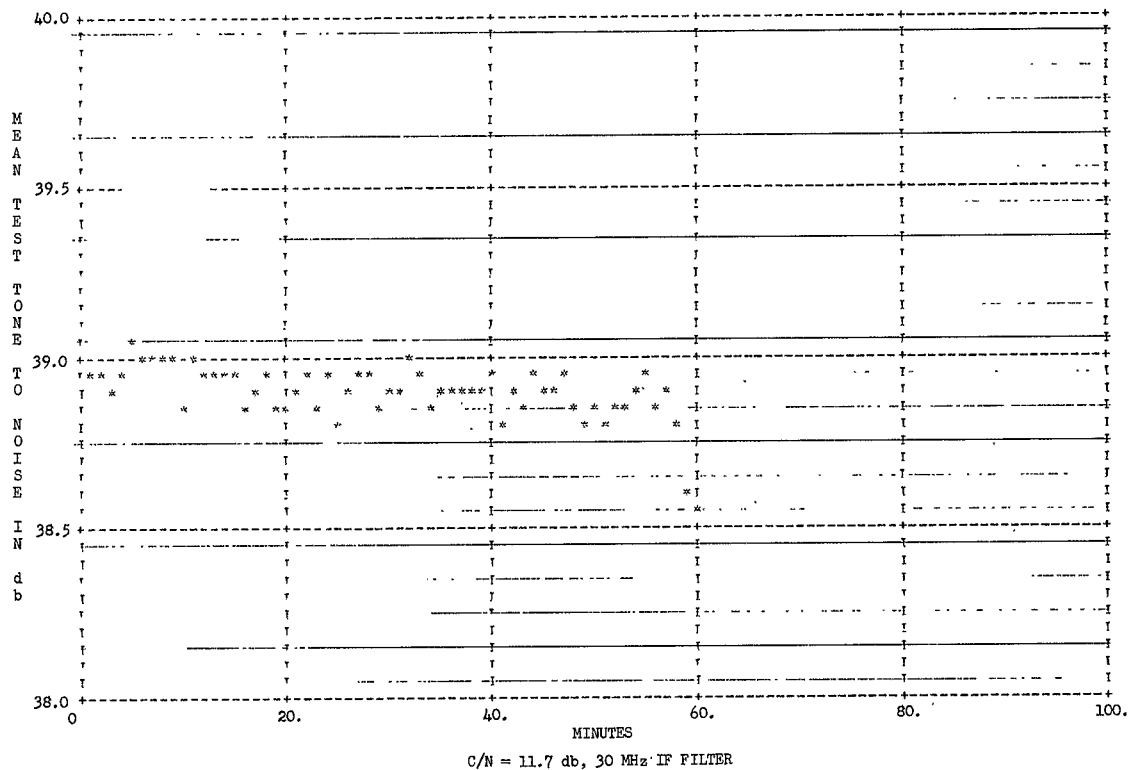
Figure 3.62.   Minutely Mean Test Tone-to-Noise, Mojave Automated Test (341 kHz, 1200-Channel Loading (15.8 dbm))
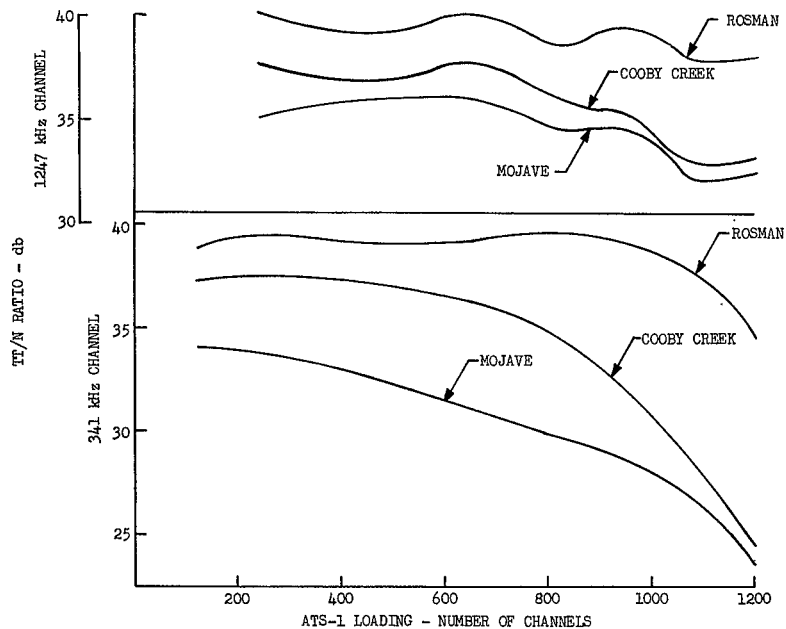
Figure 3.63.   Multiplex-Channel TT/N Ratio Versus ATS-1 Loading, Multistation Operation, for C/N Between 7.4 db and 14.3 db
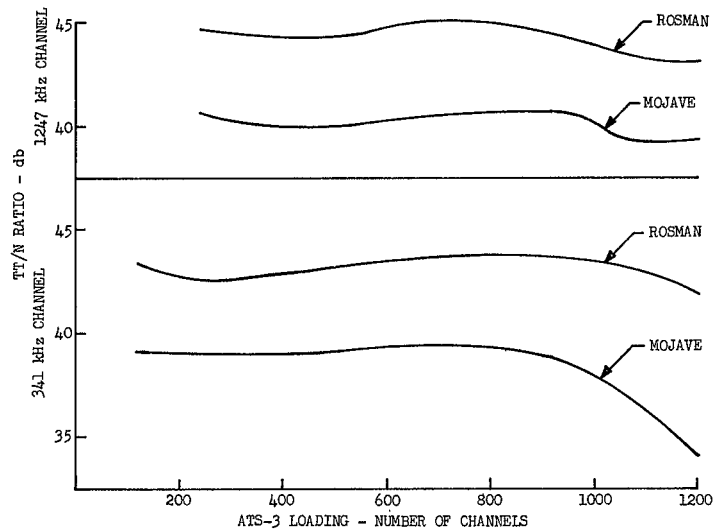
Figure 3.64. Multiplex-Channel TT/N Ratio Versus ATS-3 Loading, Multistation Operation Mojave
C/N Ratio of 11.8 db; Rosman C/N Ratio of 20.7 db
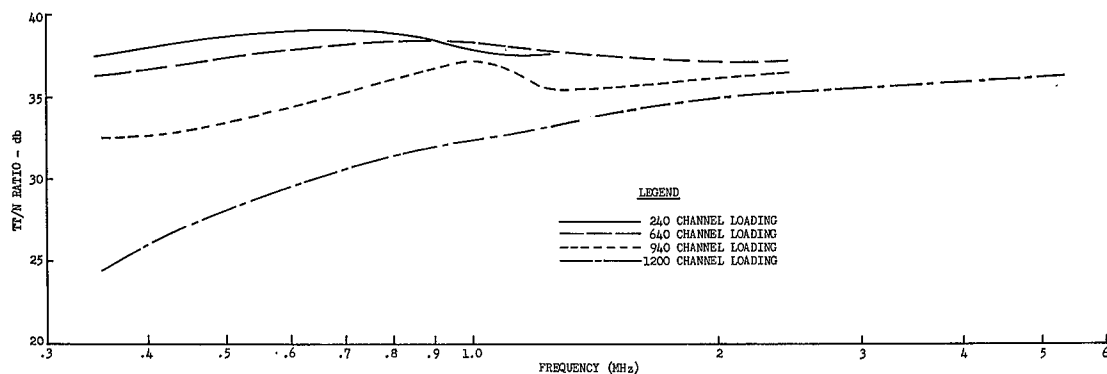
Figure 3.65. Multiplex-Channel TT/N Ratio Versus Baseband Frequency (ATS-1) for C/N Ratios
Between 7.4 db and 9.1 db
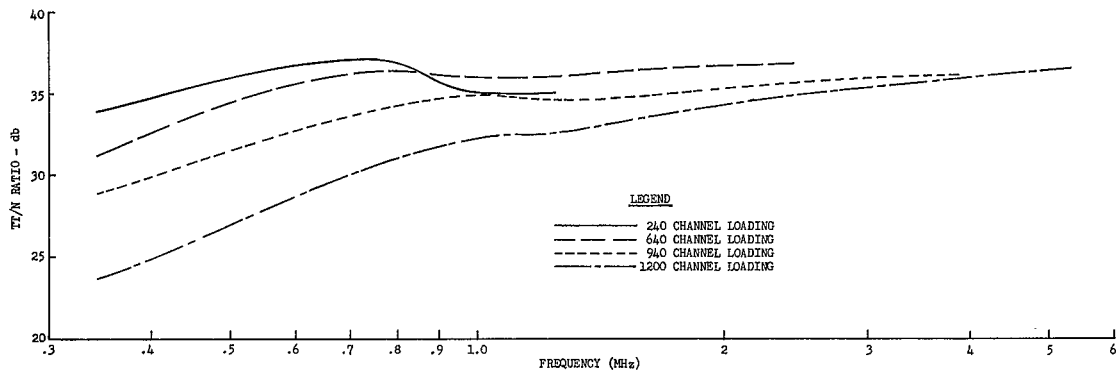
Figure 3.66. Multiplex-Channel TT/N Ratio Versus Baseband Frequency (ATS-1)
for C/N Ratio Between 7.5 db and 8.8 db
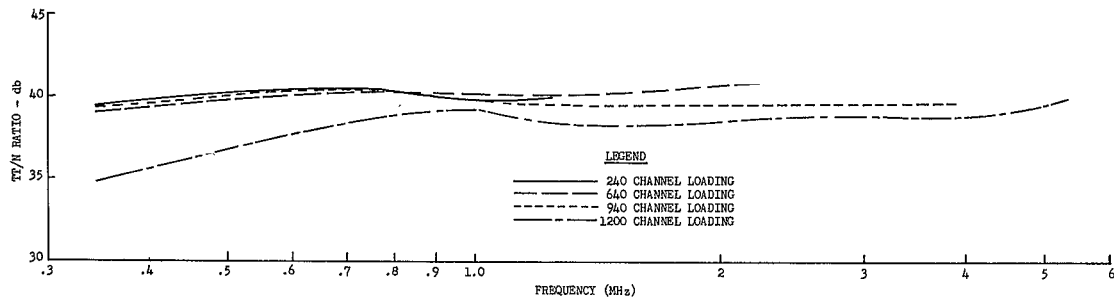
Figure 3.67. Multiplex-Channel TT/N Ratio Versus Baseband Frequency (ATS-1) for C/N
Ratios Between 11.8 db and 14.3 db
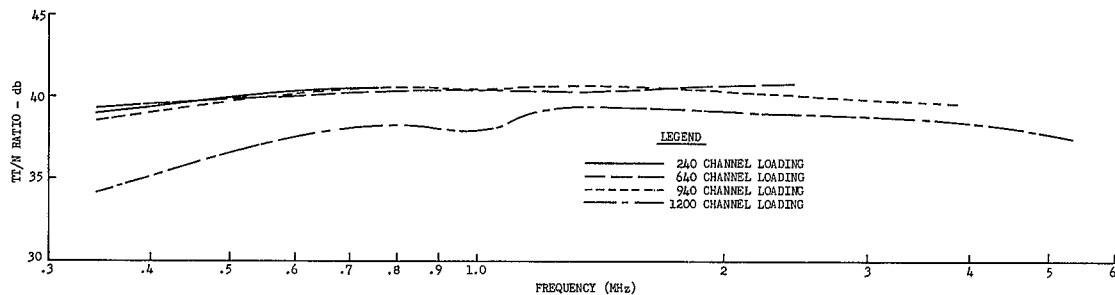
Figure 3.68.   Multiplex-Channel TT/N Ratio Versus Baseband Frequency, Mojave Earth
Station and ATS-3, for C/N Ratio of 11.8 db
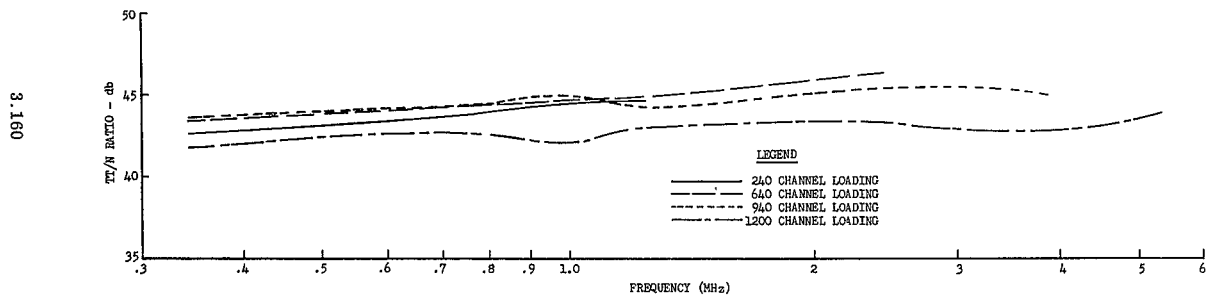
Figure 3.69. Multiplex-Channel TT/N Ratio Versus Baseband Frequency, (ATS-3) for a C/N Ratio of 20.7 db
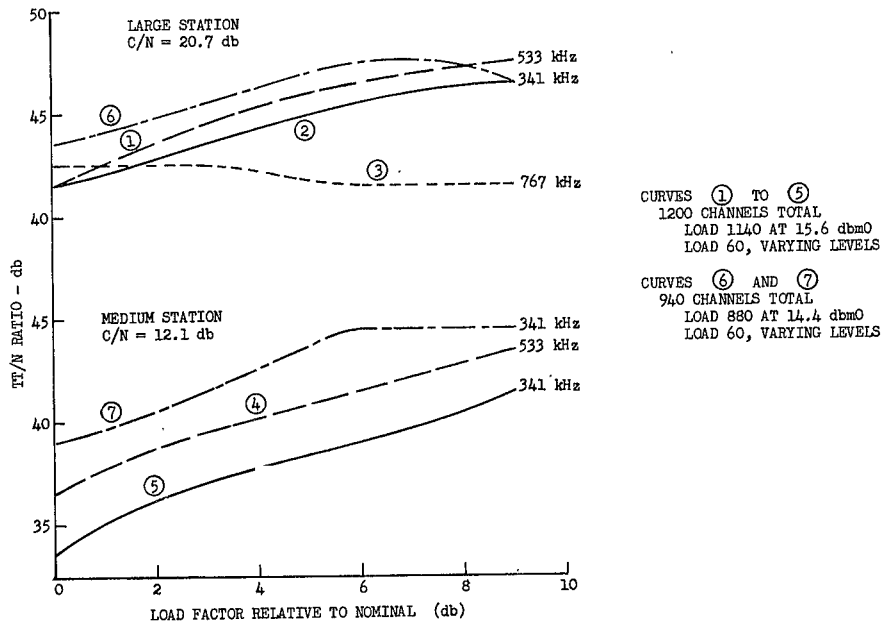
Figure 3.70. Medium Earth Station Over Deviation Improvement
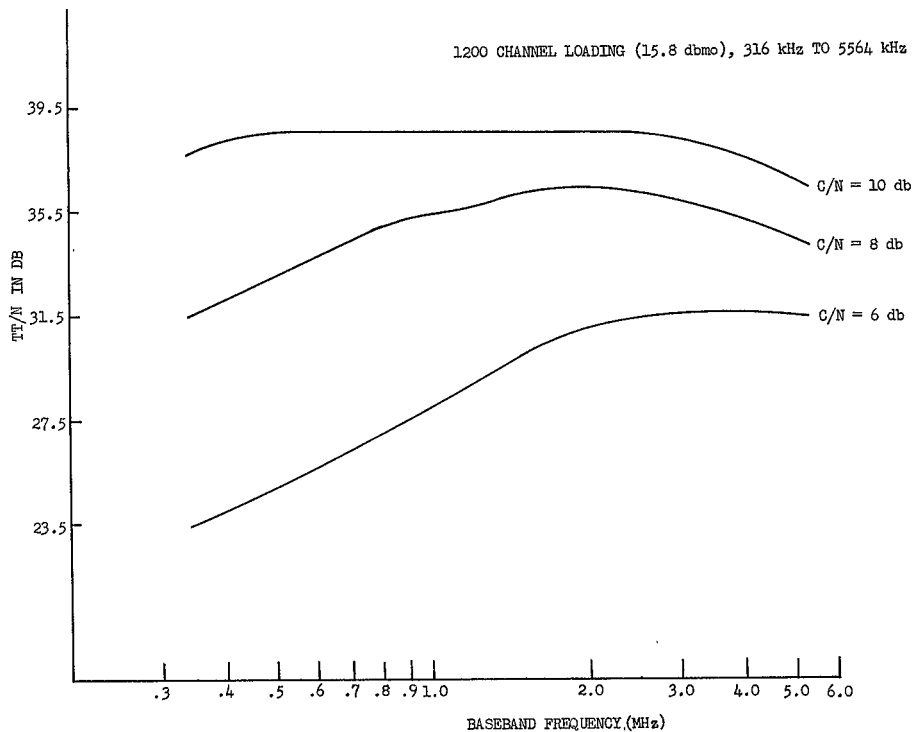
Figure 3.71.   Medium Station NPR Versus Baseband Frequency
as a Function of C/N Ratio
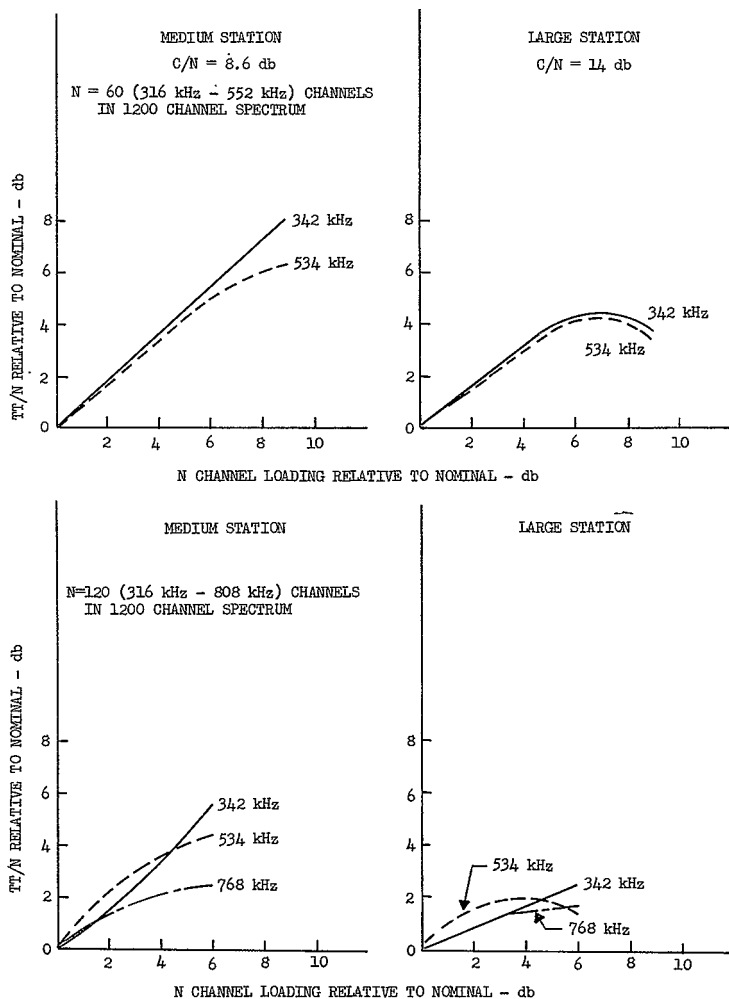
Figure 3.72. Effects of Medium Station Overdeviation At Low-
Baseband Frequencies

3.163
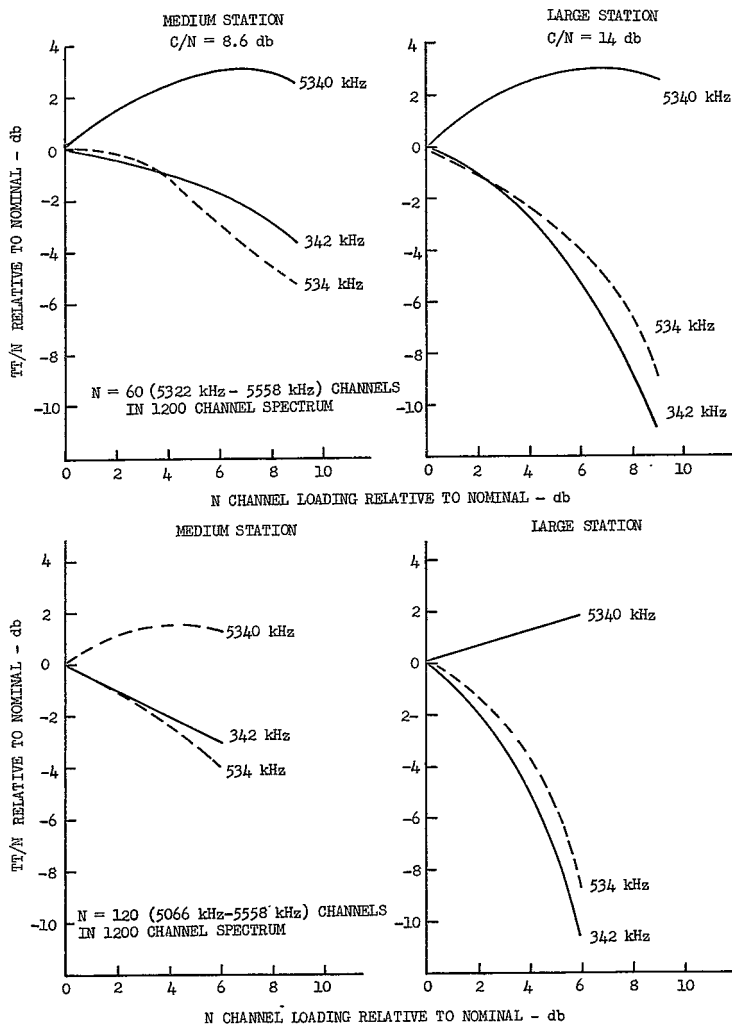
Figure 3.73. Effects of Medium Station Overdeviation at High-Baseband Frequencies

3.164
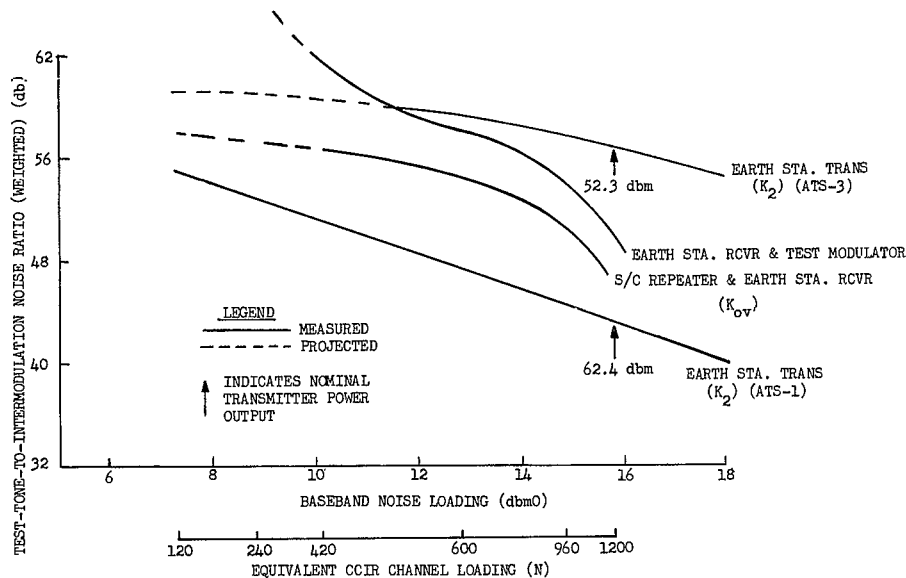
Figure 3.74. System Test-Tone to Intermodulation Noise (85' Antenna)
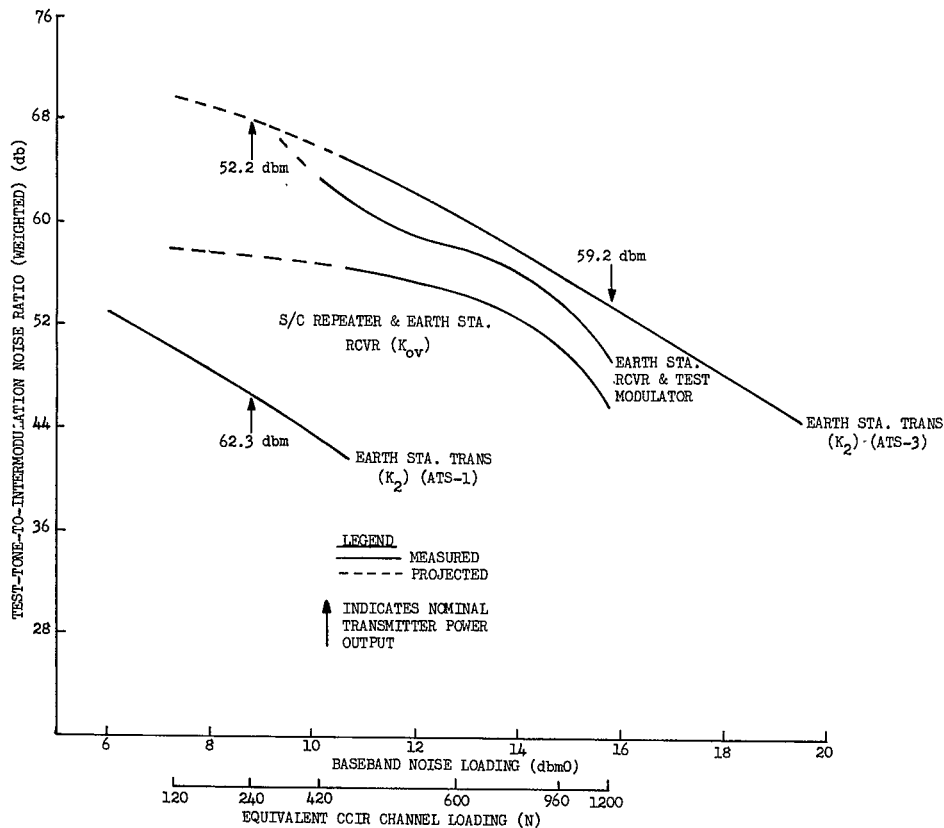
Figure 3.75. System Test-Tone to Intermodulation Noise (40' Antenna)
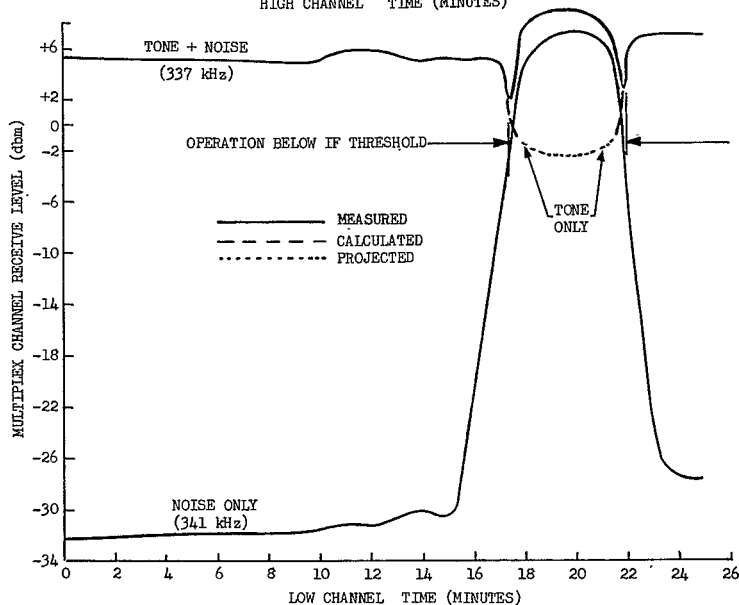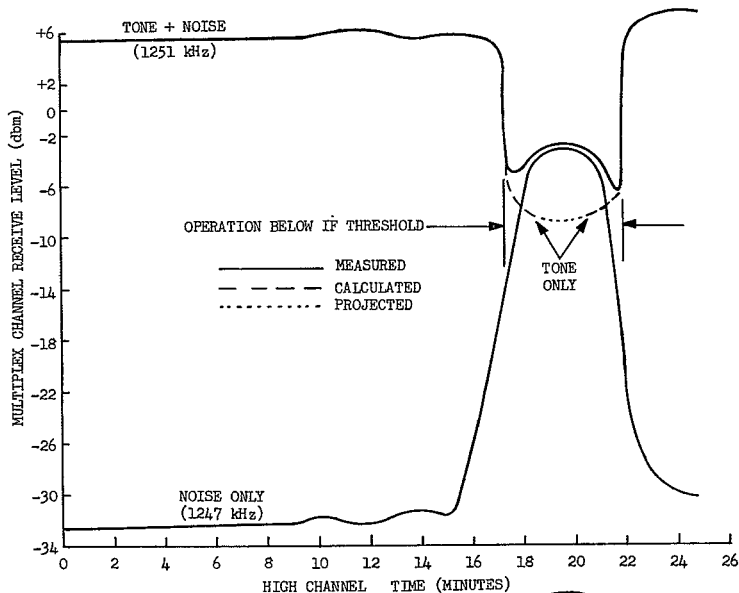
Figure 3.76.   Conjunction Test, Multiplex Channel Test-Tone and Noise Variation
(Mojave; ATS-3)

3.167
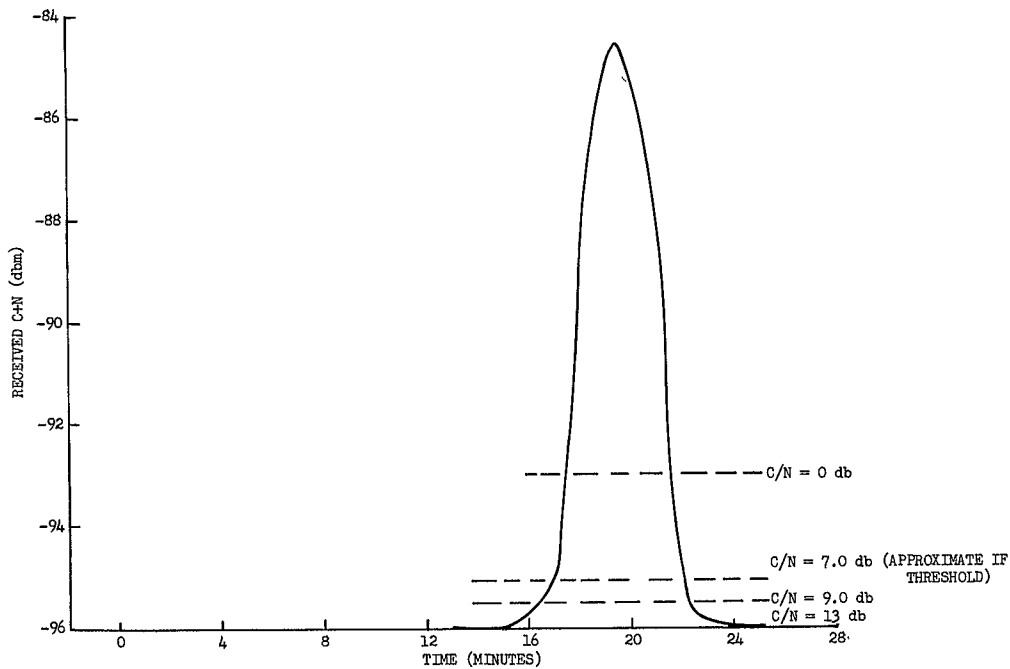
Figure 3.77. Conjunction Test, Received Carrier Plus Noise Variation (Mojave, ATS-3)
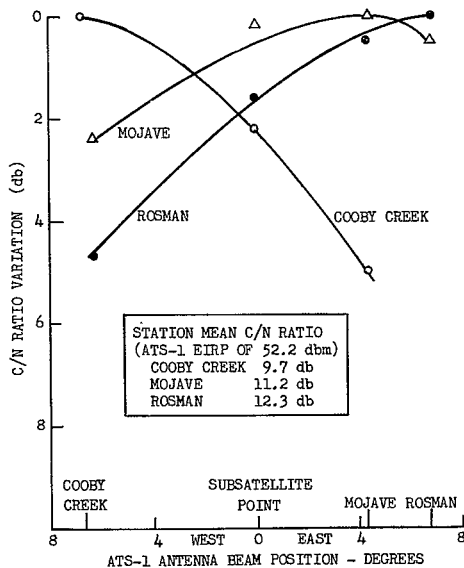
Figure 3.78. Earth-Station C/N Ratio Variation Vs ATS-1 Antenna Beam Position

3.169
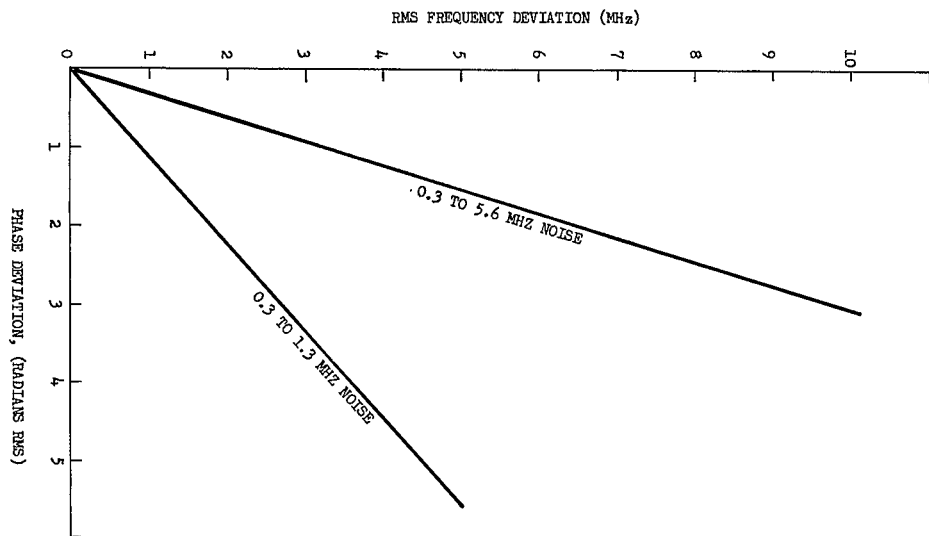
Figure 3.79. Equivalence Between Phase and Frequency Deviation with Noise-Loading

3.4.2 DIGITAL DATA ERROR RATE (F.J. Kissel) (MA-AT-1.1, FT-AT-1.1)

3.4.2.1 Description and Test Results

OBJECTIVES

The objective of this test is to determine the bit error rate of a FSK digital signal transmitted by means of an FDM voice channel. Separate tests are performed to obtain data in the SSB-PhM (MA) mode and in the frequency translation (FT) mode using automated testing at one or more earth stations in either single or multistation operation. The results of these tests are analyzed to provide the following ATS performance characteristics:

1) Bit error rate under nominal system conditions

2) Bit error rate as a function of multiplex channel S/N.

TEST CONDITIONS

1) Mode of operation

Each test is performed in one of two system conditions, SSB-PhM (MA) or frequency translation (FT). The data and analysis of each mode is presented separately.

2) System Configuration

All experiments are separated into various earth station - satellite groups. Each group is capable of providing automated test data for both single and multistation tests.

3) Controlled Variables

The following system parameters have been established for the FDM tests:

a) Type of data — Pseudo random, word length 2047 bits

b) Data rate - 1200 bits/sec

c) Modulation — non-coherent FSK

d) FSK "Space" pulse frequency - 1232.5 Hz

e) FSK "Mark" pulse frequency - 2252.5 Hz

f) FDM data channel bandwidth — 3.1 kHz

g) FDM data channel group location — 80 kHz

h) FDM data channel baseband location — 336 kHz

i) Channel deviation of RF carrier in FT mode - 490-kHz rms (1200-channel spectrum) and 870-kHz rms (240-channel spectrum)

j) S/C received power (SSB/PhM mode) — minus 87 dbm per test tone

k) S/C peak deviation per channel (SSB/PhM mode) - 0.35 radians per test tone

---

*Peak factor = 1.

· 4) Uncontrolled Variables

The uncontrolled variables which have the most significant effect on
system performance are impulse noise and signal fading; however, at
normal system signal levels, only interference which is in excess of
20-25 db above the noise level will cause measurable degradation.

THEORY OF ANALYSIS

The theory of analysis consists of determining the bit error rate as a function
of the energy contrast factor (E/N_o) of the data channel. The (E/N_o) factor is directly
related to the data channel S/N, bandwidth and bit rate (discussed in paragraph 3.4.2.2).
The data channel S/N is determined from the measured S/N in a voice channel adjacent to
the test channel.

RESULTS

1) MA Mode (SSB/PhM)

a) Normal Tests

Due to the high S/N ratios (approx 35 db) for all single or multistation
test runs, no bit errors were recorded during the test intervals. An
average test interval is 30 minutes with 1.44×10^6 bits compared
for errors.

b) Special Tests

Table 3.25 shows the data error rate as a function of test-tone
signal-to-noise ratio. As expected, no errors were detected during the
15-minute test duration when the S/N was held at 32.5 db since the
channel is virtually error-free at this S/N level.

A special bit error test was performed at Cooby Creek and Mojave using the MUX
back-to-back configuration. The S/N was varied in steps and the number of errors occurring
during each step was recorded. The test was performed for data bit rates of 1200 bps and
1500 bps.

Figure 3.81 shows the results of the foregoing tests plotted against the FDM
channel energy contrast value. The notable item from figure 3.81 is that the filters
employed in the multiplex units limit the bit rate to around 1200 bps.

2) FT Mode

    a) Normal Tests

Due to the high S/N ratios for all single or multistation test runs, zero-bit errors were recorded during the test intervals. An average test interval is 30 minutes with 1.44×10^6 bits compared for errors.

    b) Special Tests

Figure 3.80 shows the results of the FT-AT-1.1 test performed at the Rosman station during an eclipse period of the ATS-3 satellite. The test results show zero errors detected during all but two of the 46 one-minute test periods. All of the errors were detected during a time that the high-and low-channel S/N values were out of limits (too low to be recorded). During the last 33 minutes of the test, 1.58×10^6 bits were transmitted without error, thus establishing the bit-error rate to be less than 6.3×10^{-7}

3.4.2.2 Analysis

MA MODE (SSB/PhM)

Because of the high signal-to-noise ratios obtained at the standard test-tone levels (35 to 45 db, depending upon earth station, S/C, S/C EIRP, etc), the bit-error rate is essentially zero. To determine the error rate as a function of test-tone S/N, a special test (T1020) was performed at the Cooby Creek ground station. This was accomplished by attenuating the transmitted FSK digital signal level 20, 25, and 30 db to provide S/N ratios of 12.5; 7.5 and 2.5 db, respectively. The results of this test are shown in table 3.25 and figure 3.81 where the ideal curve for non-coherent FSK is also plotted. It should be noted that the ideal curve is based upon a statistical noise distribution which may be somewhat different from the noise distribution which actually exists in the FDM channel. Such is apparently the case since, as shown in Figure 3.81, the measured MUX back-to-back test results indicate performance slightly better than that predicted under-ideal conditions.

The actual error rate, P_e, at a specified test-tone level is a function of the energy contrast factor, E/N_0, which is defined as the ratio of the energy per bit to the normalized spectral noise density, N_0. The relation of E/N_0 to the channel S/N value is as follows:

$$\frac{E}{N_0} = \frac{S}{N} \cdot \frac{B}{H}$$

where:

    B is the bandwidth in which the S/N ratio is defined (3.1 kHz = 34.9 db/Hz)

    H is the bit rate (nominal 1200 bits/sec = 30.8 db)

E/N_o values corresponding to the test S/N ratios are also shown in table 3.25. This provides a comparison to the ideal curve for non-coherent FSK which plots E/N_o versus bit-error rate, as shown in figure 3.81.

Considering the above values of B and H, the nominal S/N ratio of 32.5 db with the 20-db attenuation factor, corresponds to an E/N_o value of 16.6 db. At this relatively high level, the corresponding P_e value is so low that excessive test time would be required to obtain a bit-error sample.

For the 25-db attenuation factor, the corresponding E/N_o is 11.6 db. For this value, a 9-minute test period produced an error rate less than 2.1×10^{-5}. For the 30-db attenuation factor, the E/N_o value is 6.6 db. In this case, the bit-error rate was 0.120. Thus bit-error-rate performance was acceptable at S/N ratios above 7.5 db.

Observed modem performance at a 1200-bps rate shows that at a S/N ratio of 17 db, an error rate not in excess of 1×10^{-6} can be expected. At a S/N ratio of 12.5 db, an error rate less than 2.1×10^{-5} was measured. A comparison of bit rates shows that an increase in bit rate yields a corresponding increase in error rate for a given energy contrast factor due to the bandwidth limitation of the multiplex channel. This limitation causes a decrease in E as the bit rate is increased.

Included in figure 3.81 are the results of a special bit-error-rate test conducted at Cooby Creek and Mojave, for different S/N levels at two different bit-error rates with the multiplex equipment in a back-to-back test configuration. In these tests, the S/N level was varied by changing the level of noise injected in the MUX channel. The MUX back-to-back configuration was used to determine what bit-rate limitation was imposed on the system by virtue of the multiplex transmit and received units. As shown in figure 3.81, the back-to-back loop imposes a limit on the error rate somewhere between 1200 bps and 1500 bps. The limitation is readily apparent when the error rates at an E/N_o of 13 db are considered (2×10^{-5} error rate at 1200 bps versus 6.5×10^{-4} error rate at 1500 bps). This limiting effect is even more pronounced at higher values of E/N_o. Data taken at bit rates lower than 1200 bps showed essentially no change in error rate from that observed at 1200 bps.

FT MODE

Significant bit error rate data was obtained from a single test (FT-AT-1.1, R3-004) using ATS-3 performed at the Rosman earth station on 18 March 1968. A total of 1,584,000 bits were transmitted without error, establishing a bit error rate less than 6.3×10^{-7}. As a matter of interest, an eclipse of the ATS-3 satellite occurred during this test.

When the satellite went into the eclipse position (within the earth's shadow) the MACE lost its sun-synchronization pulses, with the result that the mechanically despun antenna (MDS) shifted its boresight away from the earth. This shift continued until about the 15th minute of the test, when the sun was reacquired. Figure 3.80 shows a partial history of this eclipse. The S/N of the low and high multiplex channels decreased rapidly from nominal during the first portion of the eclipse period. During the 12th and 13th minute test periods, the values of S/N were out of limits (too low to be measured). It is during this interval that bit errors were in evidence. The S/N slowly returned to nominal during the remaining 33 minutes of the test. A total of five errors were detected during the last 15 seconds of the 12th one-minute test period, and 36 errors were detected during the first 20 seconds of the 13th one-minute test period.

3.4.2.3 Conclusions

In the foregoing analysis, the following conclusions have been made:

1) The bit error rate of the FDM FSK digital channel at nominal S/N levels is less than 6.3×10^{-7}, based on no errors received in 1.584×10^{6} bits transmitted.

2) Reasonably good bit error rate performance (1 part in 10^{-6}) will be realized at a S/N ratio as low as 10 db (corresponding to an energy contrast level of 14 db) for a 1200-bps rate.

3) Bandwidth restrictions of the multiplex units limit the bit rate to about 1200 bps.

TABLE 3.25. DIGITAL DATA-ERROR RATE VERSUS
CHANNEL S/N COOBY CREEK (T1020), 2 AUG. 1967

Data Channel S/N (db) (Calculated)	Energy Contrast Factor $(E/N_o(db))$	Error Rate, P_e	Number of BITS Transmitted
32.5	36.6	$<5.6 \times 10^{-6}$	180,000
12.5	16.6	$<2.1 \times 10^{-5}$	48,000
7.5	11.6	6.0×10^{-3}	108,000
2.5	6.6	0.120	108,000
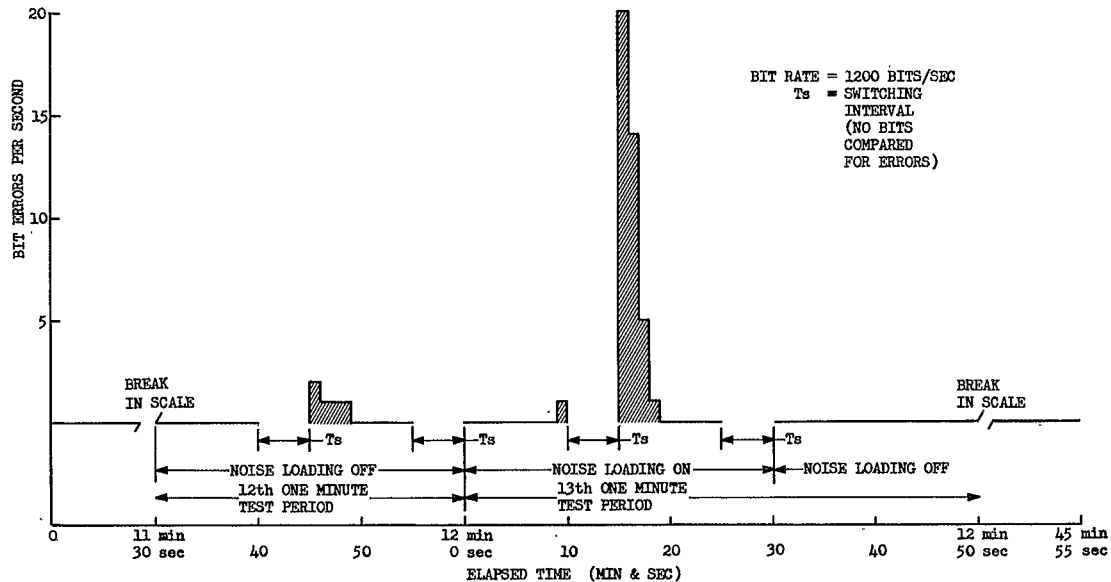
Figure 3.80. BIT Errors vs Time During Satellite Eclipse (FT Mode, Rosman, ATS-3, 3/18/68)
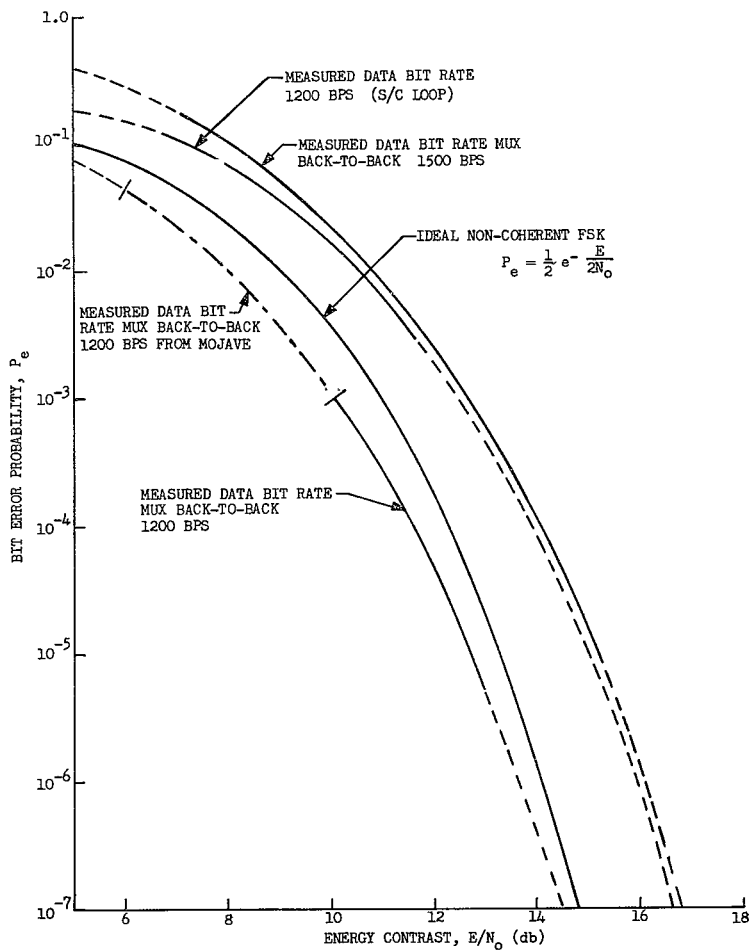
Figure 3.81. Data Error Rate Versus Energy Contrast (Cooby Creek, ATS-1)

3.178

3.4.3 MULTIPLEX-CHANNEL LINEARITY (M. E. STRONG) (FT-MX-3.1/MA-MX-4.1)

3.4.3.1 Description and Test Results

OBJECTIVE

       The objective of this experiment is to determine the amplitude linearity characteristics and overload compression point of a voice frequency multiplex channel. This test is performed using the SHF equipment on a single station basis for both the MA and FT modes to establish the operating range of the multiplex system and the range of input signal levels that can be handled by the equipment.

TEST CONDITIONS

       The significant conditions of this experiment are:

       1) Tests are run in both FT and MA modes utilizing both S/C and RF loops. The RF loop is run primarily as a comparison for evaluating the satellites contribution to the parameter.

       2) The "reference" is established by setting the channel output level at + 7 dbm with an input of –16 dbm at 1000 Hz. This is the system nominal operating level.

       3) The tests were performed in a high-and low-multiplex channel at each of the three test stations.

       4) Tests are run over a range of levels from –32 dbm to –4 dbm at discrete intervals.

STANDARDS

       Specifications and user requirements applying to the overall multiplex SHF systems of this type are not readily available. The reports of CCIR and CCITT omit the parameter completely. EIA Standard 2.4.2 of TR-141 denotes the overload level* and 6 db above test-tone level (or at –10 dbm input when applied to the ATS system).

*Overload level is defined here according to ASA 65.08.048 which states that "overload level is that level which operation ceases to be satisfactory as a result of signal distortion, overheating, damage, etc.".

RESULTS

In figure 3.82, a representative curve for all test conditions is presented. Individual test data has shown sufficient uniformity to justify a typical curve. No significant differences were observed relating to frequency, mode, satellite, or station.

3.4.3.2 Analysis of Test Results

Amplitude linearity is a measurement of incremental increases of output power levels corresponding to discrete increments of input signal level. Ideal linearity is obtained when the incremental rise in output power equals the incremental rise in input level. At some value of input level, the multiplex equipment will begin to limit the output level, an effect referred to as overload compression. When compression occurs, the signal ceases to be satisfactory as a result of signal distortion. Economics dictate that equipment be operated in the upper portion of its linear range, but with sufficient margin to enable optimum signal-to-noise without compression.

The respresentative curve of figure 3.82 shows the multiplex channel test-tone level to be about 2 db down at + 6 dbm0 input level. The gain reduction at + 3.5-dbm0 input is in the order of 0.5 db, and the gain reduction at + 12 dbm0 is about 8 db. For all practical purposes these results represent the channel response of the multiplex equipment itself. It is seen that the EIA specification is met, since the gain reduction is about 2 db at + 6 dbm0 (-10 dbm).

3.4.3.3 Conclusions

On an individual channel basis, the linearity characteristics of the multiplex equipment are adequate for any mode of transmission within the ATS system capabilities.
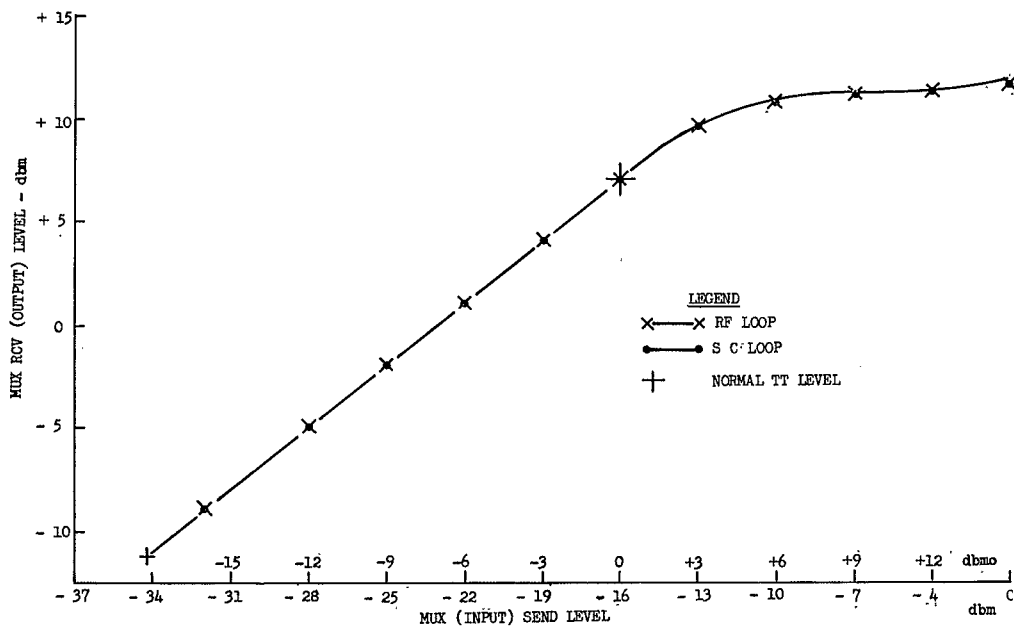
Figure 3.82. Typical Multiplex-Channel Linearity

3.4.4 MULTIPLEX-CHANNEL AUDIO-ENVELOPE DELAY (FT-MX-4.1, MA-MX-5.1, FT-MS-1.1, MA-MS-1.1) (M.E. STRONG)

3.4.4.1 Description and Test Results

OBJECTIVES

This experiment is conducted to determine the relative audio-frequency envelope delay in a multiplex channel. It is performed with the SHF equipment on either a single or multi-station basis in either the MA or FT modes to determine the capability of the ATS system in the handling of digital data. Signal distortions produced by variations of time delay affect the wave shape of digital signals but are not critical for voice and teletype signals. In the ATS system, a digital rate of 1200 bauds is employed. When sending a digital signal at a 1200-baud rate, there will be components of the signal distributed across the voice channel passband. Differential time delays between these components will cause envelope distortion of the received bits, and, for a given S/N ratio, could increase the error rate.

TEST CONDITIONS

The significant conditions for this experiment are:

1) Tests are run in both MA and FT modes utilizing both S/C and RF loops. The RF loop is run primarily as a comparison for evaluating the satellite's contribution to the parameter.

2) The "reference" is established by determining the frequency of minimum delay using an Acton 453-B delay measuring test set.

3) The tests were performed in high-and low-multiplex channels at each of the three test stations.

4) Delay measurements are made at frequencies of 500 Hz, 800 Hz, 2000 Hz, 2400 Hz, 3000 Hz, and 3400 Hz.

STANDARDS

CCITT Recommendation G131, paragraph F, is used for comparison and is applicable to international telephone circuits.

RESULTS

A typical multiplex-channel audio-envelope delay versus channel frequency is presented in figure 3.83.

3.4.4.2 Analysis of Test Results

Reference to figure 3.33 shows that the multiplex-channel audio-envelope delay versus frequency response is within the manufacturer's stated limits. Also, no difference attributable to mode (FT or MA), loop (S/C or ground RF), station, or satellite has been observed.

The effect of the observed multiplex channel envelope delay will be most pronounced when transmitting data. In terms of the harmonic relationships involved, the digital signal f(t) (which can be represented as a rectangular wave) may be expressed as the sum of an infinite series

$$f(t) = \sum_{n \text{ odd}}^{\infty} \frac{2A}{n\pi} \quad \sin \frac{n\pi t}{t_0}$$

where A is the amplitude of the rectangular wave, n is the harmonic of the fundamental frequency $\frac{\pi}{t_0}$, and t_0 is the bit length in seconds. Assuming a 1200-baud signal, the fundamental frequency in the Fourier expansion is $\omega_0 = \frac{\pi}{t_0} = 600 \ (2\pi)$ Hz, and $t_0 = 8.34 \times 10^{-4}$ seconds. Substituting into the previous equation:

$$f(t) = \frac{2A}{\pi} \left[\sin \left(\frac{10^4 \pi t}{8.34} \right) + 1/3 \sin \left(\frac{3 \times 10^4 \pi t}{8.34} \right) + 1/5 \sin \left(\frac{5 \times 10^4 \pi t}{8.34} \right) + \text{--------} \right]$$

Only the first 3 terms in the expansion lie in the channel passband. These are the fundamental, third, and fifth harmonics, lying at 600, 1800, and 3000 Hz, respectively. The envelope delay at these frequencies, relative to the lowest value of envelope delay in the channel passband is 0.37 msec, 0.03 msec, and 0.15 msec, respectively. The envelope delay relative to the 600-Hz fundamental is then 0.03-0.37 = -0.34 msec for the third harmonic, and 0.15 - 0.37 = -0.22 msec for the fifth harmonic. The relative phase delay of each harmonic is given by $\Delta\phi = (360°)f\tau$

where $\Delta \phi$ is the phase delay relative to the fundamental in degrees

τ is the envelope delay at the harmonic frequency of interest

f is the frequency of the harmonic of interest.

then, $\Delta \phi \Big] = -(0.34 \times 10^{-3}) \ 360 \ (1800) = -220°$
3rd Harmonic

and $\Delta \phi \Big] = -(0.22 \times 10^{-3}) \ 360 \ (3000) = -238°$
5th Harmonic

These harmonics can now be added in the proper phase in order to determine the shape of the received data signal. It is pointed out that data is transmitted through the ATS system by means of FSK. The above development is presented as a means of interpreting the observed multiplex-channel audio-envelope delay.

3.4.4.3 Conclusions

The multiplex-channel audio-envelope delay is entirely satisfactory for voice usage. Data transmission will be somewhat impaired because of bandwidth limitation and the above phase shift of each harmonic.
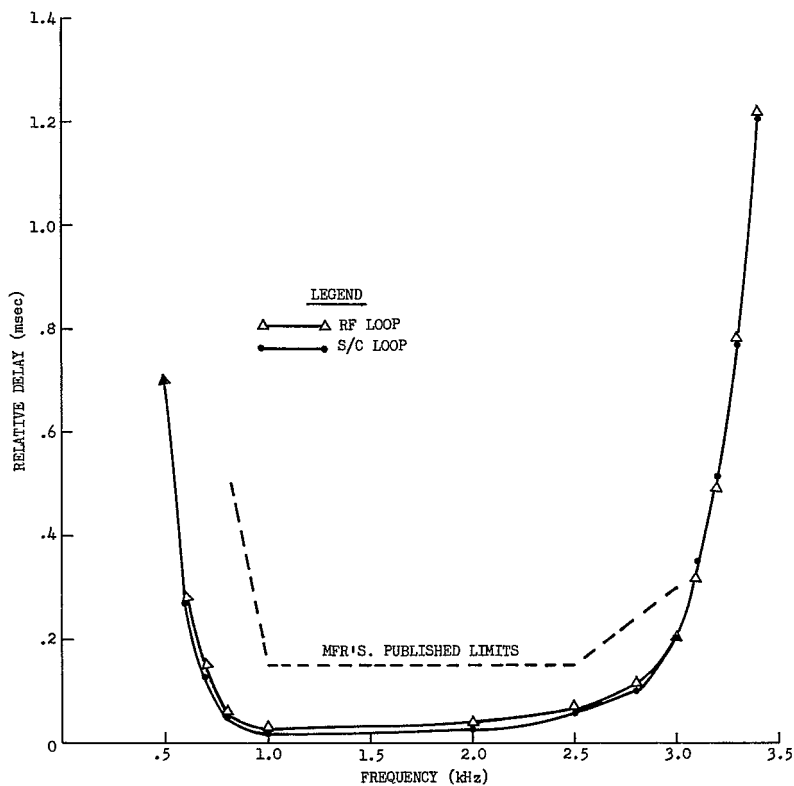
Figure 3.83. Typical Multiplex-Channel Audio-Envelope Delay

3.4.5 MULTIPLEX-CHANNEL TOTAL DISTORTION (FT-MX-7.1, MA-MX-6.1)
E.E. Crampton

3.4.5.1 Description and Test Results

OBJECTIVE

The objective of this experiment is twofold: (1) to measure the magnitude of the multiplex-channel total distortion, and (2) to determine the nature of the distortion.

TEST CONDITIONS

The significant conditions applicable to this experiment are:

1) Mode of operation-Tests are conducted in both the MA (SSB-PhM) and FT modes of operation. The data and analysis of each mode is presented separately.

2) The tests utilize both the S/C and earth RF loops. RF loop tests are performed primarily as a comparison for evaluating the satellite's contribution to the total distortion level.

3) The tests are performed at two test-tone frequencies (500 Hz and 1000 Hz).

4) Harmonic and spurious tones are measured with a Marconi TF 2330 Wave Analyzer.

THEORY OF ANALYSIS

The theory of analysis is based upon determining the total distortion from the combination of harmonic and non-harmonic distortion terms. The amplitudes of the harmonic components are identified and measured with the wave analyzer, and then these amplitudes are combined in an RMS manner to yield the total harmonic distortion. Similarly, the amplitudes of the non-harmonic signals are measured and combined in an RMS manner to yield another distortion term.

STANDARDS

User specifications applying to the overall multiplex-radio system of this type are not presently available. However, EIA Standard TR-141, Sec 3.2 and CCITT Recommendation G:531 (f) of the Plenary Assembly in New Delhi, December 1960, states that the telephone channel (Voice and Teletype) harmonic distortion should not exceed 5 percent (26 db below test tone). It should be noted that in systems for which these recommendations were written, harmonic distortion was the predominate distortion. Therefore, the recommendations should be used cautiously with regard to the SSB-PhM (MA) Mode where harmonic distortion

is not the predominate distortion. The manufacturers' specification for the multiplex equipment states that 1 per cent (40 db below test tone) is the limit for the total multiplex-channel distortion.

RESULTS

Average percent distortion values, based on test results from Cooby Creek, Mojave, and Rosman are presented in tables 3.26 and 3.27.   Signal-to-distortion noise ratio values are shown for each condition that the distortion percentage is given. Table 3.26 shows the results of the FT mode operation for the 500 Hz and 1000 Hz input test tones. Table 3.27   shows the harmonic distortion and the 60 Hz sideband distortion levels measured for the (SSB-PhM) MA mode using the 500 Hz and 1000 Hz input test tones. Table 3.28 shows the results of two tests conducted at Mojave for various test loops and with both ATS-1 and 3 satellites.

3.4.5.2 Analysis of Test Results

FT MODE

Total distortion includes 60-Hz sidebands on the signal tone, but these components were negligible with respect to the predominate harmonic distortion. The FT system does not contribute significantly to the multiplex equipment distortion. Since the carrier which is used for demodulation goes through the same perturbations as the signal, this mode has an intrinsic self cancellation characteristic for frequency instabilities.

When operating in the FT mode, the system performance is well within the CCITT/EIA recommendation of 5 percent total harmonic distortion since it rarely exceeded 1.2 percent. Since the total distortion is mainly comprised of harmonic distortion, only this factor is shown in table 3.26.

MA MODE

The Marconi TF 2330 wave analyzer with a search bandwidth of 6 Hz was utilized to determine the levels of the spurious frequencies and test tone harmonics present in a typical multiplex channel. In addition to the test-tone harmonics, frequency components that are related to the S/C spin modulation harmonics and frequency components caused by incidental FM modulation of the frequency standard in the SSB transmitter were measured in the multiplex channel. Also components that can be related to the S/C master oscillator and its related circuitry in the case of ATS-3 were also measured.

From the results shown in tables 3.27 and 3.28, it is apparent that the test tone harmonic distortion is mainly caused by the non-linearities in the transmit and receive multiplex units. This conclusion is reasonable when comparing the corresponding S/N values for the various test loops with the multiplex-unit back-to-back loop. Since no

appreciable S/N degradation is apparent when the test results are compared between the basic multiplex loop and the S/C loop, it is reasonable to conclude that the multiplex units are the main cause of the levels measured for the test tone harmonic distortion. Also, it can be concluded that the multiplex units meet the manufacturer's standard for multiplex equipment which is an S/N of 40 db.

For the test results given in table 3.27, it is apparent that for the Cooby Creek data, the 60 Hz components and multiples thereof (produced by incidental modulation of the frequency standard) emanating from the SSB transmitter define the limit on the maximum signal-to-total noise ratio (S/N) that can be obtained when operating with ATS-1. As shown, this value is 34 db which meets the EIA/CCITT total link recommendation of 26 db. The same conclusions can be obtained from the data obtained from Rosman when operating with both ATS-1 and ATS-3. For the Rosman case, it is apparent that the levels produced by incidental modulation in the SSB transmitter are about 7 db worse than the levels produced at Cooby Creek. Also, these levels are the limiting factor for the maximum S/N value that can be realized at Rosman.

As shown in table 3.28, the test results from the ATS-1 and collimation tower test loops are generally consistent, that is, they produce an S/N of about 42 db. These results show that multiples of the spin modulation fundamental component are not important in their contribution to the total distortion level. The significant components measured for these test configurations were mainly multiples of the 60-Hz component and not the actual fundamental component. In comparing the Mojave results with Cooby Creek, and Rosman for the ATS-1 test condition, it is apparent that the levels of the incidental modulation components (60 Hz and multiples thereof) at Mojave are at least 8 db better relative to Cooby Creek and 15 db better relative to Rosman. Since the S/N value for idle noise is 10 db less than the S/N value for spurious frequencies at Mojave for ATS-1, it follows that the thermal noise level is the limiting factor in defining the total distortion level.

For the ATS-3 test case, it is noticed that the resulting S/N value for the spurious frequencies is about 8 db less (≈ 34 db) than the corresponding value (≈ 42 db) for the ATS-1 collimation tower test loops. Hence, it can be concluded that for ATS-3 operation, the dominant spurious frequency levels are produced by either multiples of the spin modulation component or by components emanating from the S/C master oscillator and/or related circuitry. From the wave analyzer measurements, it was shown that this increase in the spurious frequency components occurs at frequencies of 130 Hz or greater. Because of this relatively high-frequency range, it is not reasonable to conclude that these components are being generated by a higher order multiple of the eighth harmonic of the spin-modulation frequency. This eighth factor results from the modulation produced by the eight VHF whip antennas crossing the SHF beam while the S/C is spinning. Therefore, it must be concluded

that the high-frequency components being generated are produced by the S/C master oscillator or related circuitry. Also, it is shown in table 3.28 that for ATS-3 operation, the spurious frequency and idle S/N ratios are essentially equal. Hence the spurious frequencies and idle noise contribute equally to the overall noise level.

3.4.5.3 Conclusion

For the FT mode of operation, performance is well within the CCITT/EIA recommendation of a S/N of 26 db. The lowest S/N value (mainly due to harmonic distortion) measured was 39.2 db for a test-tone input of 1 kHz. In the MA mode of operation, the test-tone harmonic levels are negligible compared to the spurious frequency levels.

For the MA mode of operation at Cooby Creek and Rosman the spurious 60-Hz sidebands and multiples thereof, caused by incidental angle modulation of the master oscillator in the SSB transmitter, produce the highest components in the multiplex channel. The corresponding S/N for Cooby Creek is 34 db and for Rosman it is about 27 db for both ATS-1 and ATS-3 operation. For Cooby Creek, the 60-Hz components contribute about equally with idle noise to the total multiplex-channel noise level. For Rosman, the 60-Hz components are the limiting factor.

At Mojave, for ATS-1 operation, the idle noise level is the limiting factor since its measured S/N value was about 32 db and was 10 db lower than the spurious frequency S/N value. For ATS-3 operation, frequency components at 130 Hz and higher were measured. These components caused the corresponding spurious frequency S/N value to decrease to about 34 db. It was concluded that these components are being generated by the S/C master oscillator or related circuitry. Since the spurious frequency and idle S/N ratios are essentially equal, both factors contribute equally to the overall noise level.

TABLE 3.26. FT MODE MULTIPLEX-CHANNEL TOTAL DISTORTION

Condition	Test Frequency (Hz)	Average Harmonic Distortion	EIA/CCITT Total Link Recommendation	Manufacturer's Standards for Multiplex Equipment
Representative of Actual Conditions Cooby Creek ATS-1	500	Percent 0.51 S/N (db) 45.8	5.0 26	1.0 40
	1000	Percent 0.33 S/N (db) 49.5	5.0 26	1.0 40
Representative of Actual Conditions Rosman ATS-3	500	Percent 0.90 S/N (db) 40.9	5.0 26	1.0 40
	1000	Percent 1.10 S/N (db) 39.2	5.0 26	1.0 40
Representative of Actual Conditions Mojave ATS-1	500	Percent 0.75 S/N (db) 42.5	5.0 26	1.0 40
	1000	Percent 0.64 S/N (db) 43.9	5.0 26	1.0 4.0

TABLE 3.27. MA MODE MULTIPLEX-CHANNEL TOTAL DISTORTION

Condition	Test Frequency (Hz)	Average Harmonic Distortion	Average 60 Hz Sideband Distortion	EIA/CCITT Total Link Recommendation	Manufacturer's Standards for Multiplex Equipment
Representative of Actual Conditions Cooby Creek ATS-1	500 Hz	Percent 0.30 S/N (db) 50.2	2.0 34.0	5.0 26	1.0 40
	1000 Hz	Percent 0.22 S/N (db) 53.1	1.9 34.2	5.0 26	1.0 40
Representative of Actual Conditions Rosman ATS-3	500 Hz	Percent 0.33 S/N (db) 49.5	4.5 26.9	5.0 26	1.0 40
	1000 Hz	Percent 0.26 S/N (db) 51.8	4.9 26.3	5.0 26	1.0 40
Representative of Actual Conditions Rosman ATS-1	500 Hz	Percent 0.26 S/N (db) 51.8	4.9 26.3	5.0 26	1.0 40
	1000 Hz	Percent 0.22 S/N (db) 53.1	4.2 27.5	5.0 26	1.0 40

TABLE 3.28.   MA MODE MULTIPLEX-CHANNEL DISTORTION (MOJAVE)

Test Loop	Test Freq. (Hz)	Harmonic Distortion S/N (DB)	Spurious Sidebands S/N (DB)	Signal to Idle Noise Ratio (DB)	EIA/CCITT Total Link Recommenda-tion S/N (DB)	Manufacturer's Stan-dards for Mux. Equipment S/N (DB)
MUX. B to B 12/6/69	500	53.2				40
	1000	55.4				
ATS-1 S/C 12/6/69	500	51.4	41.3	33.5	26	40
	1000	53.2	41.5			
ATS-3 S/C 12/6/69	500	NOISE	35.6	35	26	40
	1000	53.1	35.6			
MUX B to B 12/13/69	500	52.2				40
	1000	55.5				
COLL. TOWER 12/13/69	500	54.2	42.6	38.6		
	1000	56	41.2			
ATS-1 S/C 12/13/69	500	56	43.5	31.5	26	40
	1000	56	43			
ATS-3 S/C 12/13/69	500	NOISE	33	34.6	26	40
	1000	NOISE	33			

3.4.6 MULTIPLEX-CHANNEL AMPLITUDE VERSUS FREQUENCY RESPONSE (FT-MX-2.1, MA-MX-3.1) (M.E. Strong)

3.4.6.1 Description and Test Results

OBJECTIVE

The objective of this experiment is to measure the multiplex-channel amplitude versus frequency response to determine the bandwidth of a channel and the amplitude variations as a function of frequency within the channel. The ideal amplitude versus frequency response is a constant output level at all frequencies within the multiplex-channel bandwidth, assuming a constant input level. In a multiplex voice channel, the response is dependent upon the channel bandwidth filters, and to a lesser degree by the transmission system.

TEST CONDITIONS

The significant conditions of this experiment are:

1) Tests conducted in both the FT and MA modes utilizing both S/C and ground RF loops. The RF loop is run primarily to evaluate the spacecraft's contribution to this parameter.

2) The reference point is established by setting the channel input level to -16 dbm and the output to +7 dbm at 1000 Hz. This represents the nominal operating level of the system.

3) The tests are conducted in the 317-kHz, 509 kHz, and 1247-kHz channels at Mojave and Cooby Creek, and in the 319-kHz, 511-kHz,and 3895-kHz channels at Rosman.

4) The frequency response is obtained for the range of frequencies from 250 Hz to 3600 Hz in the multiplex channel.

STANDARDS

CCITT Recommendation G. 511 paragraph 5.1, EIA Standard TR-141, paragraph 3.1, and the multiplex manufacturer's specification TCS-600/1200 are used for comparison. The CCITT limits apply to international telephone circuits, and the EIA Standard applies to microwave relay systems. The CCITT Standard is shown in figure 3.84.

RESULTS

A typical response curve indicative of the results of many tests under all conditions is presented in figure 3.84.

3.4.6.2 Analysis

The typical response curve in figure 3.84 shows that the amplitude versus frequency response of the SHF multiplex channels is virtually flat (between 0.5 db and -0.5 db)

from 300 to 3500 Hz, with a sharp roll-off above and below this band. This roll-off characteristic is integral to the multiplex equipment design. Since the transmission system has minor influence on the multiplex-channel responses, the curve of figure 3.84 can be considered the frequency response of the multiplex equipment itself.

3.4.6.3 Conclusions

The multiplex-channel amplitude versus frequency response characteristic is virtually flat from 300 to 3500 Hz, indicating that the amplitude fidelity for all modes and conditions of transmission should be excellent and the sharply defined bandwidth provides for good channel separation.
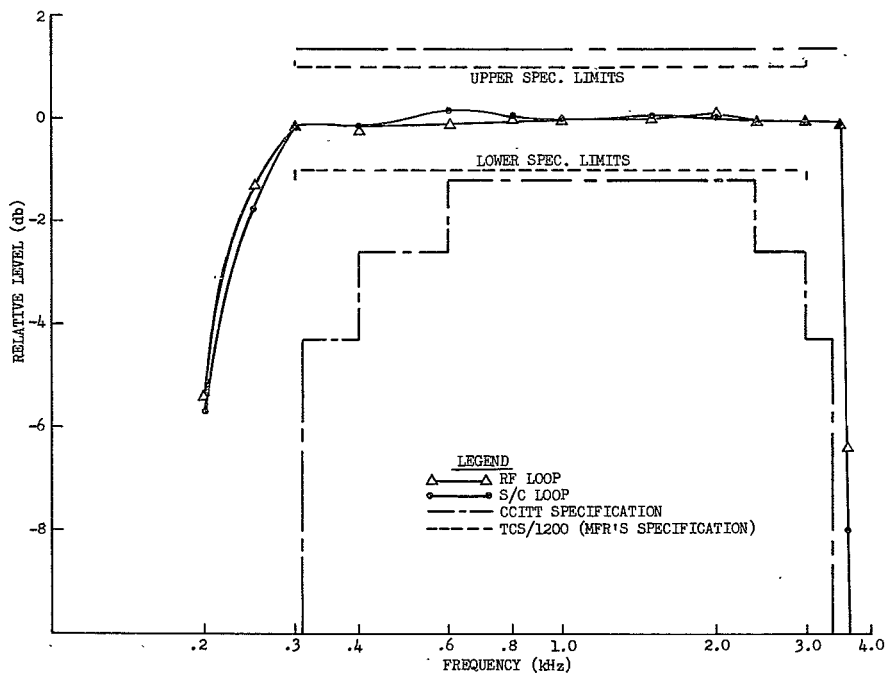
Figure 3.84. Typical Multiplex-Channel Amplitude Versus Frequency

3.5 TELEVISION PERFORMANCE EXPERIMENTS

INTRODUCTION

A series of tests are employed to evaluate the performance of both the video and audio channels of the system. The audio tests cover frequency response; video-to-audio crosstalk; hum and other periodic noise components; channel S/N ratio, and distortion. The video tests include insertion gain stability; differential gain; low-and high-frequency responses; hum and other periodic noise components; color-vector transmission analysis; and video S/N. In addition, intermodulation distortion is measured in the video baseband above 100 kHz for correlation with other experiments.

TEST CONDITIONS

These tests are performed under the following conditions unless otherwise stated:

1) Frequency Translation (video) mode

2) Ground antenna peaked on satellite

3) Spacecraft antenna positioned for maximum received signal strength at the earth station.

4) Ground station transmitter AFC switch in "Sync Tip" position for those test signals that include the horizontal (line)-sync pulses. If sync pulses are not present then the "AVG" position is used.

*5) Pre-emphasis network removed from transmitter for both video and audio.

*6) De-emphasis network removed from receiver for both video and audio.

7) RF carrier deviation: ±10-MHz peak (video)
   ±1-MHz peak (subcarrier).

8) 6-MHz audio-subcarrier deviation: ±200 kHz peak.

9) Receiver IF bandwidth set to 30 MHz.

10) 4.5-MHz filter in video-baseband output.

*Several tests include comparative data with and without the inclusion of pre-emphasis.

3.5.1 CONTINUOUS RANDOM NOISE (TV WEIGHTED NOISE) (M. E. Strong) (FT-TV-1.1):

3.5.1.1 Description and Test Results

OBJECTIVES

       The objective of this experiment is to measure the video channel signal-to-noise ratio and correlate this measured value with the values obtained from calculations based on measured carrier-to-noise ratios and link calculations.

TEST CONDITIONS

       The test conditions are as stated in paragraph 3.5, with the addition of a 10-kHz high-pass filter and a video noise-weighting network (per CCIR Recommendation 421-1) in the video baseband.

STANDARDS

       The standard used for comparison is the CCIR Recommendation 421-1, paragraph 3.3.1. This recommendation states that for 525-line systems, in Canada and the USA, the peak-to-peak amplitude of the picture to the rms amplitude of the noise within the range between 10 kHz and the nominal upper limit of the video frequency band of the system (4 MHz) must be at least 56 db. This recommendation applies to intercontinental transmission and transmission through active communication satellites (see CCIR working group IV-A, amendment of recommendation 354, question 2/IV). In addition, the EIA Standard RS-250A paragraph 5.7 calls for an overall signal-to-noise ratio of 56 db in multihop systems. However, this figure includes the sync pulse which is excluded in the CCIR recommendation, and the EIA standard calls for a noise weighting filter of 7 db instead of the 10.2 db of the CCIR. These two factors nearly cancel each other, so the net result is that the EIA standard is nearly equal to the CCIR, where the requirements apply to the video terminals. However, Prosser and Allnatt[21] have conducted extensive subjective viewer tests and have concluded that adequate viewer performance is attained at signal-to-weighted triangular noise ratios of about 39 to 41.5 db. (See section   1.3 of this report for a summary of their results) It may be concluded that the ATS communications systems can logically be judged on their ability to attain the performance level computed as the "system calculated" in table 3.29, since this value is in keeping with the above referenced subjective test results. This value is calculated from the system design parameters (i.e., transmitter powers, receive noise figures, antenna gains, etc.).

RESULTS

       Since evaluation of the video channel signal-to-noise ratio depends on individual station parameters, such as antenna gain and look angle, and on individual satellite parameters, such as EIRP, receiving antenna gain, and noise figure, the results are presented separately for

each station and satellite in table 3.29. The "mean-measured" signal-to-noise values given are based on the indicated number of observations, each normalized to the mean station receiving system noise temperature of 76°K (except for Rosman on ATS-1 which is normalized for 105°K) and corrected for the satellite antenna off beam position. The "predicted from measured C/N" values of S/N ratio are calculated by adding a system bandwidth and deviation adjustment factor to the mean measured carrier to noise figures given for each station and satellite. The "system calculated" values are based on link calculations as previously mentioned. (See section   7.1.) This value of video channel weighted signal-to-noise ratio can be considered as the optimum value for the respective stations, since it is calculated from system design parameters and operating conditions. The 90-percent confidence interval (or the interval, assuming random error, in which we are 90 percent confident the true mean lies) is given for each "measured" value of S/N. Table 3.30   presents a summary of comparative measurements both with and without the inclusion of the CCIR recommended emphasis networks.

3.5.1.2 Analysis

COOBY CREEK

          The data summary for Cooby Creek shows close agreement (within 1.4 db) between the system calculated, predicted, and measured values of video S/N. The 90-percent confidence interval of ±0.9 db from 11 tests indicates a relatively close grouping of data points. The close agreement among the three recorded values indicates that the system parameters as assumed to compute the "system calculated" S/N value are in fact valid and correct as verified by the two measured values. The correlation shown by the predicted value indicates that the system parameters assumed in calculating uplink and downlink carrier-to-noise ratios are correct and valid. The correlation shown by the measured value indicates that the system parameters of bandwidth ratios and FM improvement (deviation) factors are correct and valid.

ROSMAN

          As expected, the highest video channel S/N values were obtained with the 85-foot dish at Rosman on ATS-3. Table 3.29 shows compatibility among the system calculated, C/N predicted, and measured S/N values of 1.2 db, and a 90-percent confidence interval among the 5 measured values of ±1.5 db. The observed video-channel S/N ratio at this station is in the order of 5 db below the CCIR Recommendation of 56 db. However, the results are in keeping with the system-calculated values, and are sufficient to produce a high-quality television picture.

MOJAVE

        Results through ATS-1 and ATS-3 at the Mojave station are presented in table 3.29. For ATS-1, the "predicted" and "measured" video S/N values for conditions of one and two satellite TWT's are within 0.7 db in the worst case and each agree with the "system calculated" or optimum value within 0.8 db in the worst case. The 90-percent confidence interval given for the measured video S/N values for the case of one satellite TWT indicates that a substantial portion of the time, the video-channel S/N will be below the 39-db minimum viewer tolerance limit. This case (i.e., ATS-1 with one TWT and a 40-foot earth receiving antenna) is seen to represent a marginal system from the standpoint of acceptable viewer tolerance to noise influences. Even the 2 TWT case (ATS-1) at this station is not far above marginal performances since the mean measured C/N is less than 2 db above the idle threshold value (7.5 db) for this station. For 2 TWT's the video S/N is above the subjective limits stated under the "Standards" of paragraph 3.4.1.1, but taking into account the 1.8-db confidence interval, it appears that even with two satellite TWT's operating, the video S/N will be marginal a small percentage of the time.

        On ATS-3, there is close agreement (within 1.1 db) between the system calculated, predicted, and measured S/N. It appears that the video channel S/N through ATS-3, with one or two satellite TWT's operating will be sufficient to produce a good picture from a subjective point of view.

PRE-EMPHASIS

        Table 3.30   summarizes the results obtained from several comparative tests. These measurements were performed to evaluate the effect of adding the CCIR recommended pre-emphasis/de-emphasis networks. The receiving equipment de-emphasis curve is shown in figure 3.85. When this curve is applied to the parabolic spectrum of FM noise it is found that the calculated improvement in video S/N is 2.6 db. This differential is therefore shown in the "System Calculated" column of table 3.30. The mean of the three sets of measurements at Mojave show a S/N improvement of 2.3 db via the ATS-3 satellite, and an improvement of 2.2 db when checked in the RF Loop configuration. The measured values are thus seen to correlate with the theoretical values within less than 0.5 db. The measurements at Rosman show an improvement of 1.8 db via ATS-1 and 2.6 db via ATS-3. An RF loop measurement has shown an improvement of 3 db. The relatively small reduction in noise is primarily obtained in the upper portion of the frequency spectrum where the eye is more tolerant of thermal noise in the video display. This accounts for the fact that a video transmission system is frequently operated without use of the pre-emphasis techniques. However, systems such as the ATS where the audio is carried on a sub-carrier can benefit considerably by the use of video pre-emphasis. This fact is illustrated by other portions of this document. (See paragraphs 3.5.6 and 3.5.9.)

3.5.1.3 Conclusions

The conclusions drawn from the foregoing discussion are summarized below:

1) On the basis of thorough subjective viewer testing, adequate video performance is attained at signal-to-weighted triangular noise ratios of about 39 to 41.5 db. (See section   1.3.)

2) Comparing to the above subjective tests, results from the Cooby Creek Station are generally acceptable, but at times may produce a marginal picture.

3) Results from Rosman, with the 85-foot dish and high C/N through ATS-3, are some 10 db higher than necessary to produce an adequate picture, under the above assumption; but is approximately 5 db below the CCIR and EIA recommendation for video channel S/N.

4) The Mojave results show unacceptable response through ATS-1 with one satellite TWT and marginal results with two TWT's. The system calculated, or optimum value, based on design parameters, receiver noise figures, antenna gains, etc., show that these results are in keeping with the system capability.

5) The Mojave results through ATS-3 show a S/N in the video channel which is sufficient to give good picture quality.

6) The measurements with pre-emphasis at Mojave and Rosman show that approximately 2-db improvement is attainable. While not large, this improvement is sufficient to be noticeable and desirable in a marginal system.

TABLE 3.29. VIDEO WEIGHTED SIGNAL-TO-IDLE NOISE RATIO

| Station and No. of observations | Satellite | | | Station Mean Measured C/N (normalized to Station Mean Noise temp) | S/N Values in db, Normalized to System Mean Noise Temp. | | | 90% Confidence Interval for Mean Measured Value |
	ATS No.	E.I.R.P (dbm)	No. of TWT's		System Calculated	Mean of Values Predicted from Measured C/N	Mean of Measured Values	
Mojave(5)	1	52.2	2	8.7	43.2	42.4	42.4	±1.8
Mojave(5)	1	49.4	1	7.4	*39.6	40.1	39.4	±1.9
Mojave(4)	3	54.6	2	10.6	45.4	44.3	45.5	±0.8
Mojave(3)	3	56.5	1	12.7	47.1	46.4	46.9	±1.4
Rosman(5)	3	56.5	1	17.0	51.9	50.7	51.1	±1.5
Cooby(11)	1	52.2	2	8.1	43.2	41.8	42.5	±0.9

*Value given is at threshold.

TABLE 3.30. EFFECTS OF PRE-EMPHASIS ON VIDEO S/N RATIO

| | Satellite | | | Station Mean Measured C/N (normalized to Station Mean Noise temp) | S/N Values in db, Normalized to System Mean Noise Temp. | | | 90% Confidence Interval for Mean Measured Value |
	ATS No.	E.I.R.P (dbm)	No. of TWT's		System Calculated	Mean of Values Predicted from Measured C/N	Mean of Measured Values	
Mojave; average of 3 test measurements								
without emphasis	3	54.6	2	11.2	45.4	44.9	46.0	±0.5
with pre-emphasis					48.0	47.5	48.3	±0.4
without emphasis	RF	Loop		12.1	N/A	45.8	47.0	±2.0
with pre-emphasis						48.4	49.2	±1.6
Rosman								
without emphasis	1	52.2	2	14.0	48.1	47.7	48.5	N/A
with pre-emphasis					50.7	50.3	50.3	N/A
without emphasis	RF	Loop		18.7	N/A	52.4	54.1	N/A
with pre-emphasis						55.0	57.1	N/A
Rosman without emphasis	3	54.6	2	18.0	50.7	51.7	50.6	N/A
with emphasis					53.3	54.3	53.2	N/A
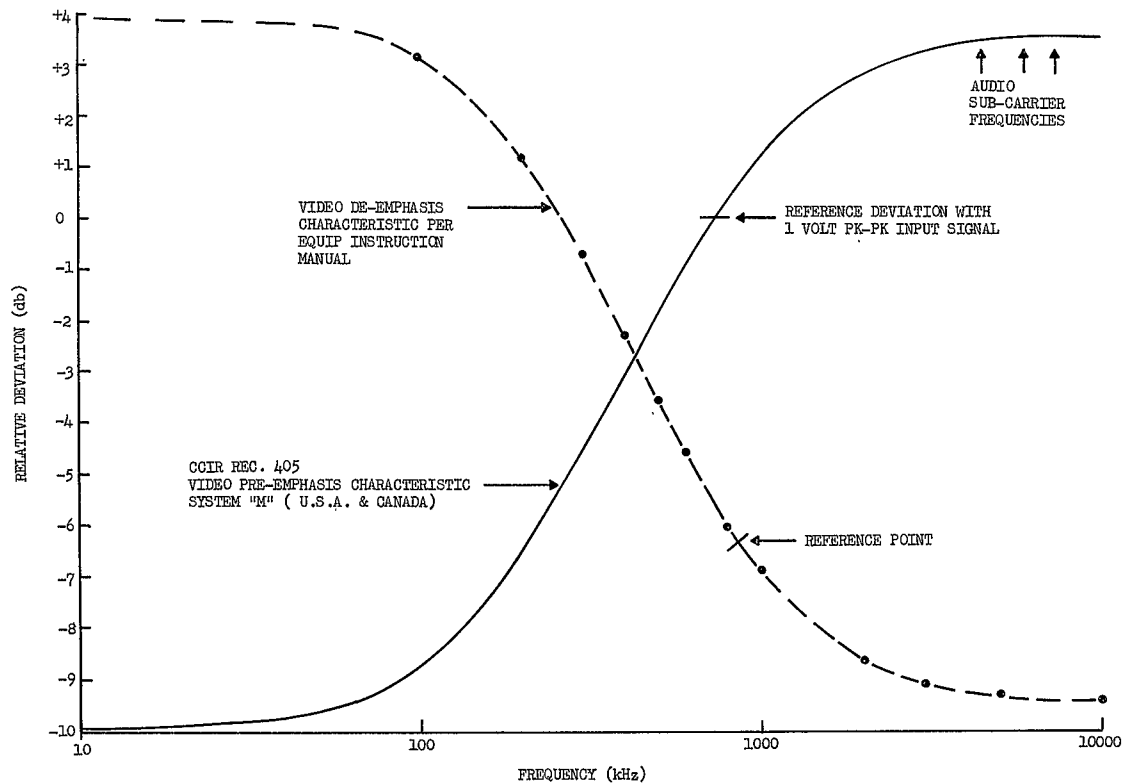
Figure 3.85. Video Pre- and De-emphasis Curves

3.5.2 VIDEO-CHANNEL PERIODIC NOISE AND TWO-TONE INTERMODULATION
       DISTORTION (M. E. Strong) (FT-TV-4.1)

3.5.2.1 Description and Test Results

OBJECTIVE

This experiment is conducted to evaluate periodic noise due to single-frequency spurious signals, and power-supply hum, including the fundamental and lower harmonics.

Periodic noise is measured with an idle channel to determine if spurious signals or power-supply hum meet CCIR and EIA standards. If these standards are not exceeded, periodic noise should have no effect on picture quality or stability of synchronization.

The primary quantity of interest is the ratio of the peak-to-peak picture signal to peak-to-peak power-supply hum plus its harmonics. Expressed analytically,

$$R(db) = 10 \log_{10} \left[\frac{\frac{0.714^2}{4}}{\sum\limits_{n=1} \left(V_{60_n} \right)^2} \right]$$

where $R(db)$ = ratio of interest in db

   0.714 = peak-to-peak picture signal voltage (less sync)

   V_{60_n} = peak-to-peak voltage of the nth harmonic of the power-supply ripple.

The fourth harmonic is generally the highest harmonic of significance in the measurement.

The results of the power-supply hum tests may vary slightly between earth stations, but the measurements at a given earth station should not vary between the S/C and RF loop. This is because the S/C does not contain any 60-Hz power sources.

TEST CONFIGURATIONS

While power supply hum occurs at the lower baseband frequencies, spurious signals are likely to occur at the higher baseband frequencies. A spectrum analyzer is used to search for spurious signals in the baseband when the carrier is unmodulated. This search is conducted between 100 kHz and 4.9 MHz.

TEST CONDITIONS

The test conditions are as stated in paragraph 3.5. Results are presented for both earth RF and S/C loops.

STANDARDS

The applicable standards for the periodic noise measurement are CCIR Recommendation 421-1, paragraph 3.3.2, and EIA Standard RS-250A, paragraph 5.8. The CCIR Recommendation states that the ratio of the peak-to-peak picture signal to peak-to-peak

periodic noise, including harmonics, should be at least 35 db. The EIA Recommendation is 37 db for this ratio. In addition, the CCIR Recommendation states that on a similar basis the ratio be at least 59 db for periodic noise between 1 kHz and 2 MHz, and decrease linearly to a final value of 43 db at the 4-MHz cutoff frequency.

RESULTS

The results of tests to determine the magnitude of the power-supply hum and its harmonics are presented in tables 3.31 and 3.32. Table 3.32 presents comparative results with and without the inclusion of pre-emphasis networks.

3.5.2.2 Analysis

POWER SUPPLY HUM

The data from Cooby Creek and Mojave confirms expected results and provides a reliable basis for evaluating ATS system performance. It can be seen from table 3.31 that the total power of the hum components for Cooby Creek (44.7 db) was virtually the same for the S/C loop and the ground RF loop, as expected. The value is nearly 8 db better than the EIA Standard and 10 db better than the CCIR recommendation for frequencies below 1 kHz. Although not listed in the table, there were two spacecraft loop tests that reported a total of five spurious periodic noise components between 1.0 kHz and 1.5 kHz. These same tests noted one similar component each in the earth RF loop tests. All the observations were within a few cycles of being multiples of 60 Hz and were better than 55 db below the picture signal reference. Four of the seven observations were not within the CCIR recommendation of 59 db. The source of these components cannot be confirmed from the data; however, since they were multiples of 60 Hz and the particular tests involved contained numerous other harmonics between 240 Hz and 1 kHz, it is suspected that the source is possible leakage by cable crosstalk from lines carrying the field synchronizing pulses of the TV signal. It will also be noted in the data that 180-Hz and 240-Hz harmonics are in many cases not as low as might be expected if the source was strictly power supply hum wherein 60 Hz and 120 Hz (from full wave rectification) would predominate. This also tends to support the cable crosstalk theory. However, since these components were only observed on two out of seven tests and were very nearly within the rather strict CCIR limits, it is not felt that this is a serous problem worthy of further analysis.

The power-supply hum and its harmonics measured at Mojave show generally decreasing amplitude with successive harmonics as do those at Rosman. These test results showed no significant periodic components above 1 kHz.

The sum of the power-supply hum and its harmonics (up to the fourth) meet the above stated CCIR and EIA recommendations. Also, the periodic components above 1 kHz in the video baseband were greater than 60 db below picture signal level.

The measurements of power supply hum components as shown in table 3.32 illustrate the effect of applying pre-emphasis techniques to a video transmission system. The fact that the hum level increases nearly 10 db indicates that the major portion of the hum components are introduced into the system after the transmitter pre-emphasis network and/or before the receiver de-emphasis network. Any hum introduced into the system prior to pre-emphasis and after de-emphasis is unaffected by whether the networks are inserted or not. However, when the receiver de-emphasis network is switched into the circuit, all frequencies below 10 kHz are boosted in level by 10.2 db as compared to their former level. Thus it is seen that care is required in system and hardware design to avoid hum problems when applying pre-emphasis. A balanced design would require that hum introduced into the system between the pre- and de-emphasis networks should be held to at least 10 db less than that hum generated before and after the networks. This problem can be minimized by locating the transmitting pre-emphasis as near as possible to the modulator and the receiving de-emphasis as near as possible to the demodulator.

The measurements at Mojave (table 3.32) reveal that the system becomes marginal when pre-emphasis is employed. The measured value of 33 db is 2 db below the CCIR recommendation, and 4 db below that of the EIA. Investigation at the site revealed that the larger part of the hum originates in a baseband amplifier immediately following the receiver demodulator, but preceding the de-emphasis network.

SPURIOUS SIGNALS

The video baseband appears to be free from spurious signals. Several tests did indicate the presence of such signals, but, since the test results could not be duplicated later, the signals were assumed to have been generated within the test equipment.

3.5.2.3 Conclusions

The results from performing the power-supply hum and spurious signal tests may be summarized as follows:

FOR THE NON-EMPHASIZED BASEBAND

1) The sum of the power supply hum and its harmonics up to 240 Hz meets the the CCIR and EIA Recommendations of 35 db and 37 db below picture signal level (0.714 volt peak-peak). In general, the harmonics above 240 Hz are greater than 60 db below this signal level.

2) The periodic components observed between 1 kHz and 2 MHz, except in a few cases, meet the CCIR Recommendation of 59 db below picture signal level.

3) There appears to be no spurious components in the video baseband above 100 kHz.

FOR THE BASEBAND WITH PRE-EMPHASIS

A measurement at Mojave has shown that the 60-Hz hum in the ATS ground equipment is about 2 db greater than the CCIR recommendation. If the system is to be used with pre-emphasis, a change in the receiving baseband equipment is required.

TABLE 3.31. PERIODIC NOISE (POWER-SUPPLY·HUM) FT-TV-4.1

| Satellite & Ground Station | Freq. Hz | Level below Peak-to-Peak Picture Signal (less synch) db | |
| | | RF Loop | S/C Loop |
		Mean	Mean
ATS-1 Cooby Creek (7 Observations)	60	49.5	49.6
	120	52.1	53.0
	180	49.1	48.3
	240	56.3	55.4
	R(db)	44.9	44.7
ATS-1 & ATS-3* Mojave (5 Observations)	60	46.8	43.2
	120	59.2	43.2
	180	57.6	57.4
	240	52.0	59.4
	R(db)	46.2	42.8
ATS-3 Rosman (4 Observations)	60	45.3	49.3
	120	45.1	49.4
	180	51.2	51.5
	240	54.9	59.8
	R(db)	43.0	45.0

Note: All values in this table were adjusted to picture signal peak-to-peak of 0.714 volt from test signal peak-to-peak of 0.5 volts.

*The mean values for Mojave are based on 3 tests through ATS-1 and 2 tests through ATS-3.

TABLE 3.32. MEASUREMENTS WITH PRE-EMPHASIS

| Satellite and Ground Station | Frequency in Hz | Level below Peak-to-Peak Picture Signal (less synch) db | |
		No Emphasis	With Pre and De-Emphasis
ATS-3 Mojave	60	42	33
	120	62	51
	180	59	51
	240	57	47
	300	–	57
	360	62	52
	R(db)	41.7	32.6

3.5.3 FIELD-TIME AND LINE-TIME LINEAR WAVEFORM DISTORTION (VIDEO LOW-FREQUENCY RESPONSE) (G.I. Shriver) (FT-TV-2.3)

3.5.3.1 Description and Test Results

OBJECTIVE

   The objective of this experiment is to evaluate the video-amplitude and phase-response characteristics of the ATS system at the field rate of 60 Hz and at the line rate of 15,750 Hz. Deviation from uniform amplitude response and linear phase shift characteristics throughout the passband of the video transmission system must be limited. This is done to prevent distortion of the relative luminous intensity of the various picture elements as well as objectionable picture streaking or smearing.

   Field-time and line-time linear waveform distortion is measured by employing a 60-Hz square wave and the white-level portion of a standard test window pattern, respectively. Photographs of CRT presentations are examined to determine percentage tilt. Overshoots and undershoots are overlooked in determining this value. (See figure 3.86) Overshoots and undershoots are, however, considered in the analysis since they cause streaking and smearing.

TEST CONDITIONS

   This test is performed under the conditions stated in paragraph 3.5.

STANDARDS

   The CCIR (Recommendation 421-1 paragraphs 3.5.1 and 3.5.2) suggests a 10-percent limit (signal unclamped) at the field rate, and a 5-percent limit at the line rate for international television circuits for this type of distortion; 5-percent limit (signal unclamped) at the field rate and 1-percent limit at the line rate for system M (Canada and United States).

RESULTS

   Table 3.33 shows the test results from the various stations. The mean-percent tilt and 90-percent confidence is shown for both line and field rates. The aggregate values are also shown on this table for all stations combined. Table 3.34 gives the results of comparative measurements both with and without the recommended CCIR pre-emphasis/de-emphasis networks.

3.5.3.2 Analysis

   Uniform amplitude response and linear phase shift throughout the passband of the video-transmission system are characteristics to be desired. Failure to attain these characteristics can cause many different impairments to picture transmission, but are generally manifested in the form of relative luminous intensity distortion, and picture streaking or smearing. Streaking is caused by frequency distortion up to approximately 200 kHz, while smearing is generally caused by somewhat higher frequencies. These impairments affect both monochrome and color video transmission almost equally.

Amplitude response and phase-linearity tolerances at the very low end of the video band, generally below half-line frequency, are not too critical. In fact, the amplitude response at 60 Hz can be allowed to vary considerably, and when the signal is clamped, it can be adjusted to depart from a uniform response at 60 Hz or other points below half-line frequency to provide phase correction at line frequency and its harmonics.

Luminous intensity distortion manifests itself in the following manners, if impairments are of sufficient magnitude: at the field rate (60 Hz), a noticeable change in contrast between the top and bottom portions of picture elements occurs: at the line rate, the change occurs between the left and right portions of a picture element. Such changes are objectionable to the viewer and are most prominent for a very light, or very dark picture element:

Distortion in the region of the 15,750-Hz line rate, or its first few harmonics, will cause streaking as evidenced by a sharp luminance transition starting at some point in the picture and extending toward the right edge. Streaking is highly objectionable when the transition is from a high luminance to a low luminance or vice-versa. An increase in low-frequency gain causes the black to white (or white to black) transition of the window pattern to appear rounded and the white level amplitude tends to have a positive slope. A decrease in low-frequency gain causes long duration overshoots at the transitions and the white-level amplitude tends to have a negative slope.

Photographs of received window patterns were studied with respect to the above characteristics. The transmitted waveform, at field rate appeared slightly rounded instead of flat. The received waveforms at both line and field rate have essentially the same shape as the transmitted waveforms, however, some negative tilt or droop usually occurs. Since some of the transmitted waveforms are not flat and noise is present on the received waveforms, an accurate analysis is not possible. However, at line rate a slight overshoot is often observed thus indicating a very small amount of negative streaking.

The data presented in table 3.33 indicates the field-time and line time linear waveform distortion is well within the CCIR limit. There is no significant difference between RF loop and S/C loop data. This indicates that the satellites are not appreciably contributing to this parameter.

The data listed in table 3.34 would appear to show that a considerable improvement in linear waveform distortion is attainable at the field rate through the use of pre-emphasis. However, the data shown for the 15.75-kHz line rate refutes this assumption. Investigation reveals that the field rate data is distorted by the presence of 60-Hz hum in the displayed signal waveform. This distortion of the waveform makes accurate data reduction nearly impossible, and the listed results are really a "best estimate" of the true values as

seen in a Polaroid snapshot of the test waveforms. The non-emphasized data is free of this hum distortion because the transmitted signal in this case is 10 db greater than it is when operating with pre-emphasis. (Measurements and a discussion of this problem are given in paragraph 3.5.2.) It is therefore concluded that Linear Waveform Distortion, either at field or line rate, is largely unaffected by the presence (or absence) of video pre-emphasis/de-emphasis networks.

3.5.3.3 Conclusions

The data indicates that the ATS system is well within the 10-percent CCIR limit for field-time linear waveform distortion and the five percent limit for line-time distortion for the international television circuits. It is also well within the five-percent CCIR limit for field-time linear waveform and slightly exceeds the one percent CCIR limit for line-time waveform distortion. Satellite contribution to these parameters is negligible.

TABLE 3.33. LINEAR WAVEFORM DISTORTION (VIDEO LOW-FREQUENCY RESPONSE)

Station	ATS No.	No. of Tests RF/S/C	U.S. CCIR Standard (%)	Field Rate RF Loop		Field Rate S/C Loop		No. of Tests RF/S/C	U.S. CCIR Standard (%)	Line Rate RF Loop		Line Rate S/C Loop	
				Avg. % Tilt	90% Confidence Interval	Avg. % Tilt	90% Confidence Interval			Avg. % Tilt	90% Confidence Interval	Avg. % Tilt	90% Confidence Interval
Cooby Creek	1	8/7	5	3.29	±0.61	2.80	±0.84	3/3	1	1.87	±1.59	1.77	±1.85
Rosman	1	3/4	5	4.43	±0.09	4.20	±1.85	2/2	1	0.55	*	0.70	*
Mojave	1	3/3	5	2.28	±1.61	3.08	±1.43	1/1	1	0	-*	0	*
Rosman	3	2/5	5	5.75	*	3.32	±0.47	2/5	1	1.05	*	0.75	±0.47
Mojave	3	3/3	5	1.67	±1.56	1.40	±1.66	3/3	1	0.60	±0.51	0.53	±0.78
Aggre-gate	1 & 3	19/22	5	3.31	±0.65	3.02	±0.47	11/14	1	1.18	±0.59	1.03	±0.40

*Less than 3 test runs

TABLE 3.34.   MEASUREMENTS WITH PRE-EMPHASIS/DE-EMPHASIS NETWORKS

| Station | Field Rate (60 Hz) | | | | Line Rate (15750 Hz) | | | |
| | RF Loop | | S/C Loop | | RF Loop | | S/C Loop | |
	No Emphasis	With Emphasis	No Emphasis	With Emphasis	No Emphasis	With Emphasis	No Emphasis	With Emphasis
Mojave ATS-3	1.24%	0.15%	2.6%	.62%	.62%	1.1%	1.1%	1.1%
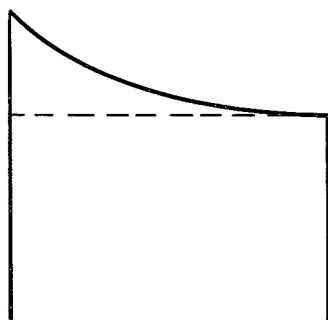
OVERSHOOT
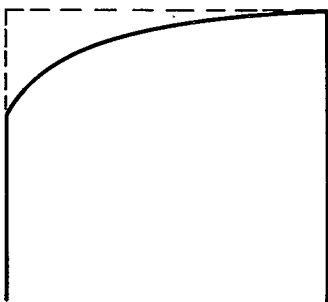
UNDERSHOOT

Figure 3.86.   Waveform Distortion (Shows departure from ideal waveform)

3.5.4 SHORT-TIME LINEAR WAVEFORM DISTORTION (VIDEO TRANSIENT RESPONSE)
(G. I. Shriver) (FT-TV-3.1)

3.5.4.1 Description and Test Results

OBJECTIVE

The objective of this experiment is to determine the ATS video system short-time linear waveform distortion. This characteristic is significant in that excessive distortion will cause an undesirable "edge effect" and may even reach the point of ringing or smearing.

TEST CONDITIONS

This test is performed under the conditions stated in paragraph 3.5.

STANDARD

CCIR Recommendation 421-1, paragraph 3.5.3, suggests that where a test signal comprising a sine-squared pulse of half amplitude duration is used, the output signal should have a first overshoot amplitude (negative), leading or trailing, not greater than 13 percent of the peak amplitude of the pulse.

RESULTS

Short-time linear waveform distortion test results are summarized in table 3.35 Results are given by earth station and S/C. Aggregate test results are also given. Table 3.36 shows a comparison of this parameter with and without CCIR recommended pre-emphasis/de-emphasis.

3.5.4.2 Analysis

This analysis is concerned only with the overshoot, or excessive response to a sudden change in signal, generally caused by excessive gain at high frequencies. An overshoot of the trailing edge of the sync pulse, if it extends above black level, may be visible in the picture as a gray vertical bar due to illuminating portions of the horizontal return traces. An overshoot of the transition from picture to blanking, if of sufficient magnitude, may cause improper triggering, or clamping, which could result in serious tearing or complete loss of picture. Either overshoots (or the inability of the system to follow rapid amplitude transition accurately) if sufficiently severe, will also cause edge effect, streaking, or smearing. In a monochrome system streaking and smearing appear as contrast distortion, but in a color system they appear as saturation distortions. If overshoots tend to oscillate, ringing will also appear in the picture.

"Edge effect" is displayed as a light border following a dark picture element, or a dark border following a light picture element. Ringing appears as additional lines on either or both sides of a picture element. The test is performed using a sine-squared pulse

of half-amplitude duration ($1/2f_c$, where f_c is the high-frequency cutoff point). This experiment is another means of evaluating video baseband-amplitude response.

Table 3.35 shows the mean percent T-pulse overshoot for both S/C to be well within the CCIR recommendation of 13 percent. The maximum overshoot for an individual test was 11 percent, thus, none of the values determining the mean exceeded the CCIR standard. Where values are present for both the RF loop and S/C loop configuration, those for the S/C loop are slightly higher. This seems to indicate that the satellites are adding to the short-time linear waveform distortion. The average amount of distortion added by the satellites, according to the aggregate test results, is about 1.1 percent.

Table 3.36 shows the results from one comparative test with the without the use of the CCIR recommended pre-emphasis/de-emphasis networks. The readings in each of the three test-loop configurations indicate a small increase in overshoot with the inclusion of the emphasis networks. This would suggest that the networks cause a small boost in the high-frequency amplitude response. A test run of this latter parameter as recorded in paragraph 3.5.12 tends to verify this conclusion. The test result is seen to be well within the CCIR recommended limit of 13 percent. It also verifies the obvious hypothesis that the use of video pre-emphasis and de-emphasis networks have little or no effect upon the system transient response.

3.5.4.2 Conclusions

The test results indicate that the ATS video system will easily remain within the 13-percent limit recommended by the CCIR.

TABLE 3.35. SHORT-TIME LINEAR WAVEFORM DISTORTION (VIDEO TRANSIENT RESPONSE)

Station	ATS-1			ATS-3		
	Number of Tests	Mean % * T-Pulse Overshoot	90% Confidence Interval	Number of Tests	Mean % * T-Pulse Overshoot	90% Confidence Interval
Cooby Creek						
RF Loop	6	4.05	±0.69	ATS-3 not visible at		
S/C Loop	6	5.67	±2.42	Cooby Creek		
Rosman						
RF Loop	5	4.74	±1.28	2	5.55	±2.83
S/C Loop	6	6.65	±2.02	5	5.16	±1.22
Mojave						
RF Loop	5	5.90	±1.92	3	3.00	±0
S/C Loop	5	6.80	±1.70	3	3.67	±1.94

Aggregate Results

Loop Configuration	Number of Tests	Mean % T-Pulse Overshoot *	90% Confidence Interval
RF Loop	21	4.65	±0.68
S/C Loop	25	5.79	±0.77

*13% CCIR Recommended Limit

3.216

TABLE 3.36.   TRANSIENT RESPONSE WITH PRE-EMPHASIS (T-Pulse)

Station and Test Loop	C/N Ratio	No Emphasis* % T-Pulse Overshoot	With Pre & De-Emphasis * % T-Pulse Overshoot
Mojave Hi-Level RF Loop	35.0	5.9	6.5
Lo-Level RF Loop	12.8	6.0	8.6
ATS-3 S/C	10.2	8.6	10.2

* 13% CCIR Recommended Limit

3.5.5 INSERTION GAIN (AND VARIATIONS) (VIDEO INSERTION GAIN) (STABILITY) (G. I. Shriver) (FT-TV-2.2)

3.5.5.1 Description and Test Results

OBJECTIVE

The objective of this experiment is to determine the transmission gain stability of the ATS system, in the FT mode, over a given time period. System gain variations are reflected as a change in contrast of the received picture. Excessive contrast changes in a short period of time are objectionable to the viewer, and therefore must be held to specified limits.

TEST CONDITIONS

This test is performed under the conditions specified in paragraph 3.5.

STANDARDS

CCIR recommendation 421-1, paragraph 3.2, establishes the limits for short-term (1-second interval) gain variations at ±0.3 db (±0.2 db for Canada and the U.S.A.). Limits of ±1.0 db are also suggested for medium-term variations (1-hour time period). Because of the time required to perform the test, no medium-term observations were made.

RESULTS

The results of the short-term gain variation tests appear in table 3.37. The table shows the number of tests which equal or exceed the CCIR limit in both the RF and S/C loop configurations. The tests are separated according to earth station and the results for both satellites are combined. Only two variations were observed during these tests, and the maximum variation (0.2 db) did not exceed the CCIR recommended limit. Since the inclusion of video pre-emphasis has no effect upon this parameter, no measurements were made in this configuration.

3.5.5.2 Analysis of Test Results

For the purpose of this analysis the test results from the different earth stations and satellites are grouped together. This is considered valid since the satellites are essentially the same, and the earth stations have identical equipment with the exception of the antenna system.

This test is performed by observing amplitude changes on a waveform monitor for a period of 60 seconds. The maximum change that occurred during any 1-second time period is then recorded as the short-term insertion gain value. Although medium-term insertion gain was not measured, no indication of drift has been noted over the 60-second time period.

Only two variations of short-term insertion gain were reported and they did not exceed the CCIR limit. It is essential to maintain correct video levels in a video-transmission system, since any rapid changes in insertion gain, if of sufficient

magnitude ($>$ ±0.2 db), would result in rapid changes in picture brightness and contrast which would be disturbing to the viewer. Very large changes ($\gg$ ±0.2 db) could even result in frame rolls or momentary picture tearing. The test results indicate that the ATS system will not create disturbances of this type.

3.5.5.3 Conclusions

It is concluded that the short-term video insertion gain characteristic of the ATS system is within the CCIR recommended limits.

TABLE 3.37. INSERTION GAIN (AND VARIATIONS) (VIDEO· INSERTION GAIN) (STABILITY)

Station and Loop Configuration	Short–Term Variations (CCIR International Standard ±0.3 db) (CCIR Standard ±0.2 db in USA and Canada)	
	Number of Tests Within Standard	Number of Tests Exceeding Standards
Mojave		
RF Loop	5	0
S/C Loop	5	0
Rosman		
RF Loop	5	0
S/C Loop	5	0
Cooby Creek		
RF Loop	2	0
S/C Loop	1	0

3.5.6 LINE-TIME NON-LINEARITY DISTORTION (VIDEO DIFFERENTIAL GAIN)
(G.I. Shriver) (FT-TV-2.1)

3.5.6.1 Description and Test Results

OBJECTIVE

This test measures the line-time non-linearity distortion as a function of average
picture level (APL). This is accomplished by transmitting a stairstep line pattern (10-step
sawtooth) with a low-level 3.58-MHz subcarrier superimposed on each step. The received
test signal is passed through a high-pass filter to eliminate the sync pulses and stairsteps,
and displayed on a waveform monitor (A-scope). The maximum and minimum amplitudes of
the 3.58-MHz bursts are determined, and the percent line-time non-linearity distortion is
computed as,

$$100 \left(1 - \frac{m}{M}\right) \%:$$ where m and M are as shown in figure 3.87.

The test parameter is measured at 10-percent, 50-percent, and 90-percent average picture
levels (APL). Fifty-percent APL is attained with the above described waveform transmitted
on every horizontal line. Ten-percent APL is obtained by transmitting the stairstep pattern
on every fifth line with the four intervening lines being sent at "blank" level. Ninety-percent
APL is the same as above except that the four intervening lines are sent at "white" level.
Thus, it is seen that the percent APL is also a measure of the video system loading; 10 per-
cent being lightly loaded and 90 percent being heavily loaded.

Excessive line-time non-linearity variation in a monochrome transmission system
will distort the gray scale of the displayed image. In a color-transmission system, line-time
non-linearity causes an error in color saturation of the received image. This distortion is
more noticeable, and thus more objectionable to the viewer, when transmitting images in the
lower APL ranges (i.e., 10 to 50 percent).

TEST CONDITIONS

This test is conducted under the conditions stated in paragraph 3.5.

STANDARDS

The CCIR (Recommendation 421-1 Paragraph 3.4.2) states "the non-linearity
distortion should be expressed as a percentage" and "should not be more than 20 percent".
The CCIR also states "for system M (Canada and the U.S.A.), the non-linearity distortion
should not be more than 13 percent, and "for color in system M (Japan), . . . the differential
gain should not exceed 10 percent".

RESULTS

Video-Differential Gain is largely controlled by the phase and amplitude response in the system I.F. Since the effective EIRP's from the different ground stations and satellites should have no effect on this performance characteristic, and as the remaining equipment characteristics are essentially the same, test results from all stations and both satellites have been combined. The aggregate-mean and 90-percent confidence interval for each APL is given below for several test runs on a flat, or non-emphasized baseband.

APL	Mean %	90% Confidence Interval
10%	19.0 (Based on 11 values)	±6.3%
50%	19.5 (Based on 21 values)	±3.1%
90%	18.7 (Based on 11 values)	±4.2%

A special series of four test runs were conducted in order to specifically compare system performance with and without the inclusion of the recommended pre-emphasis networks. The results of these tests are given below:

Test Configuration (All in RF Loop)	Percent Line-Time Non-linearity Distortion		
	At 10% APL	AT 50% APL	AT 90% APL
No Pre-emphasis	15%	14.5%	14.2%
With Pre-emphasis	6.3%	7%	4.3%

3.5.6.2   Analysis

Difficulties were encountered in obtaining test data for this experiment. The signal-to-noise levels, especially for the earth stations equipped with 40-foot antennas, are not high enough to obtain a noise-free CRT presentation of the 3.58-MHz subcarrier when using the standard bandpass filters in the waveform monitors. This results in presentations lacking a distinct outline. This problem is further amplified at 10-and 90-percent APL, because the stairstep is being transmitted only 20 percent of the time, and the CRT presentation is not only masked by noise, but also lacks contrast. The severity of the latter effect can be reduced by either increasing the brilliance on the oscilloscope, or by increasing the exposure on the camera (slower shutter speed or larger aperture).

However, the noise masking effect illustrates a deficiency in the test method when applied to systems operating at relatively low carrier-to-noise ratios. For example, the 85-foot Rosman station with ATS-3 operates with a C/N ratio around 18 db. The ratio of peak signal-to-noise peaks exceeded 1 percent of the time is about 20 db. Thus, it is seen that the oscilloscope presentation of the 3.58-MHz subcarrier envelope will be masked by a

noise envelope whose amplitude is up to 10 percent or more of the desired signal under scrutiny. As a result, the values obtained from the various tests are limited to best estimates. Due to poorer CRT presentation at 10-and 90-percent APL, a distortion value could not be evaluated for many tests. For some tests, due to the high noise level, no distortion value was obtained for any APL. This problem is also largely instrumental in causing the large spread in the 90-percent confidence interval seen in the above results.

   The average values of line-time non-linearity distortion, and the 90-percent confidence intervals, indicate that the non-emphasized ATS system will operate near, or slightly below the CCIR recommended international limit of 20 percent. The distortion values in only a small percentage of the tests are within the 13-percent CCIR limit recommended for Canada and the U.S.A. On the other hand, the values shown above for the special test series illustrate the large improvement attainable when applying pre-emphasis techniques to the system. The transmitter pre-emphasis network reduces the deviation from the large level, low frequency signal components below 100 kHz by at least 9 to 10 db. Thus the system loading by the horizontal line sync pulses and the 10-step sawtooth is reduced by up to 90 percent of its former value. System deviation from the 3.58-MHz color subcarrier is increased about 3 db. Thus the effective "modulation" of the subcarrier by the low-frequency components is greatly reduced, and the distortion introduced by RF/IF phase and amplitude non-linearities is largely overcome.

3.5.6.3 Conclusion

   The test data indicates that the line-time non-linearity distortion, when measured on a non-emphasized baseband, should average slightly below the CCIR 20-percent international limit. Based on the test data, it is expected that this limit will be exceeded occasionally. The 13-percent USA/Canadian limit will nearly always be exceeded. The measured data points have a large spread in value because of the masking effects of noise. This results in a rather large confidence interval.

   The test data taken with video pre-emphasis applied to the system shows that the more stringent U.S./Canadian limit of 13 percent is easily attainable. This data also indicates the dependence of this parameter on the RF/IF group delay and amplitude-response characteristics of the system.
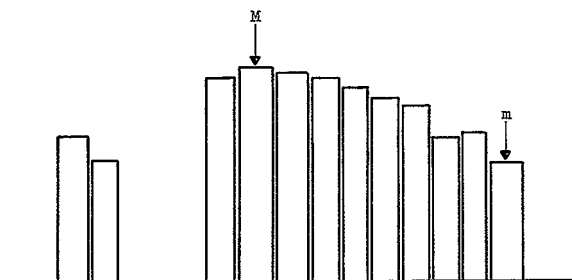
Figure 3.87.   Line-Time Non-Linearity Distortion

3.5.7 COLOR VECTOR AMPLITUDE AND PHASE DISTORTION (FT-TV-5.2) (G.I. Shriver)

3.5.7.1 Description of Experiment

OBJECTIVES

This experiment is conducted to evaluate the ATS video system with respect to the transmission of color TV signals.

The visual sensation of color results from the combination of three characteristics known as hue, saturation, and luminance (brightness). Brightness is the only characteristic of the image that can be transmitted over a monochrome system. (This parameter is not considered in the analysis section of this experiment, but is included in the analysis section of the line-time non-linearity distortion experiment (FT-TV-2.1).) To produce a color image, provisions must be made to transmit all three of these color characteristics. Although color television signals are affected by the same impairments as monochrome, color signals may also be seriously impaired by conditions that do not affect monochrome signals. Thus, the ATS video system "color fidelity", or ability to reproduce colors which are realistic and pleasing to most viewers, must be known.

TEST CONDITIONS

This experiment is performed under the conditions stated in paragraph 3.5.

STANDARDS

Each transmitted color can be represented by a color vector. In the National Television System Committee system, a standard color phase vector diagram has been specified for six colors: red, green, blue, yellow, magenta, and cyan. The hue of each color is identified by the vector angular (phase) displacement with respect to the color sub-carrier reference vector. The magnitude (or amplitude) of each vector corresponds to the saturation of its respective hue. FCC Regulations [Sec. 73.682 (20)(vii)] specify the allowable variation in phase and amplitude of each vector with respect to its standard phase and amplitude on the vector diagram and is applicable to this test. CCIR Report 407* (part A1.1.6) also covers this requirement and gives the same allowable variations as the FCC. The minimum variations specified are ±10 degrees for phase, and ±20 percent for amplitude.

RESULTS

The results of this experiment in terms of the measured mean color vector phase and amplitude variations are shown in figure 3.88. This data is also summarized in table 3.38 along with the 90-percent confidence interval about the measured mean values. The data is based on the results of five tests with ATS-3.

---

*XIth Plenary Assembly, Oslo, 1966, Volume V.

3.5.7.2 Analysis

Figure 3.88 and table 3.38 show that both the color vector amplitude and phase are well within the recommended limits. The reproduction of colors by the ATS video system should suffer only small errors in saturation and hue. The mean phase variation shows a small lag for all colors except blue, and the mean amplitude variation shows an increase in amplitude for all colors except blue. If the hue and saturation controls on the receiver are adjusted to minimize the errors for most colors, the distortion in the blue area will be amplified. The use of pre-emphasis/de-emphasis networks results in improved phase and amplitude response.

3.5.7.3 Conclusions

Both amplitude and phase variations appear to be well within the CCIR recommended limits, and only minimal errors in hue and saturation should occur within the ATS system. Pre/de-emphasis networks make these parameters better yet.

TABLE 3.38.   COLOR VECTOR AMPLITUDE AND PHASE DISTORTION
(COLOR VECTOR ANALYSIS) (FT-TV-5.2)

(Spacecraft Loop) (5 Tests) (Flat Baseband)

Color Vector	Phase Variation (Degrees) CCIR Rec. ±10°		Amplitude Variation (Percent) CCIR Rec. ±20%	
	Mean	90% Confidence Interval	Mean	90% Confidence Interval
Red	-0.6	±2.37	+0.4	±4.43
Green	-1.6	±3.45	+3.0	±4.95
Blue	+1.0	±2.62	-1.2	±5.50
Yellow	-2.4	±3.58	+5.6	±8.08
Magenta	-0.8	±1.38	+1.0	±4.88
Cyan	-1.6	±3.51	+2.8	±5.52

(Spacecraft-Loop) (1 Test) (Pre/de-emphasized Baseband)

Color Vector	Phase Variation (Degrees) CCIR Rec. ±10°		Amplitude Variation (Percent) CCIR Rec. ±20%	
	No Emphasis	With Emphasis	No Emphasis	With Emphasis
Red	+2.0	0	+2.2	-1.3
Green	+3.3	-0.2	+3.2	0
Blue	+4.2	-0.3	0	-1.2
Yellow	+0.5	+0.5	-2.3	-2.3
Magenta	+3.7	+0.7	+1.0	-1.8
Cyan	+1.0	-0.5	+0.9	-0.6
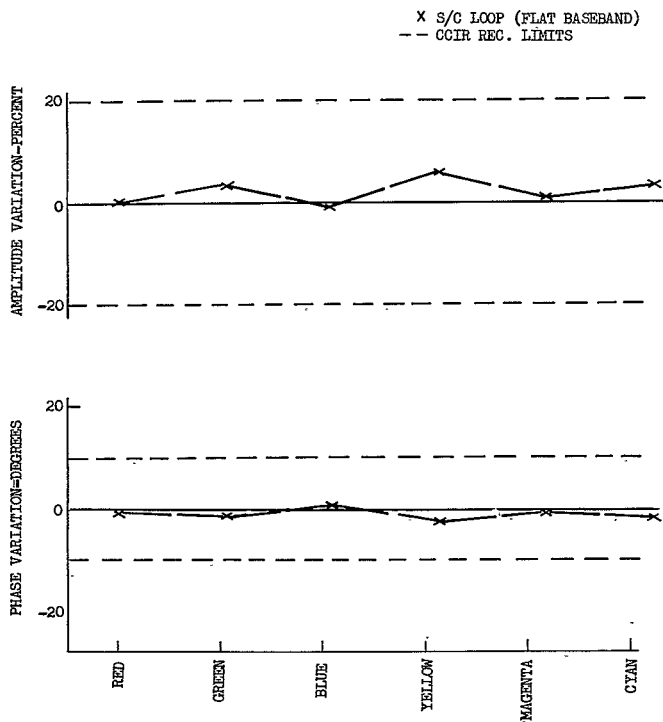
Figure 3.88. Color-Vector Mean-Phase and Amplitude
Variation (FT-TV-5.2)

3.5.8 TV AUDIO CHANNEL IDLE NOISE (M.E. Strong)

3.5.8.1 Description and Test Results

OBJECTIVE

        The objective of this experiment is to measure and establish the signal-to-idle noise ratio in the audio channel of the ATS Television sub-system operating in the FT mode. Idle noise is a combination of thermal noise, power-supply hum, and any spurious components present in the unmodulated TV relay subsystem.

TEST CONDITIONS

        This experiment is performed under the conditions stated in paragraph 3.5.

STANDARDS

        The CCIR has proposed that in the 50-to 15,000-Hz frequency band, the absolute rms noise voltage level, measured at the end of the circuit without a weighting network, and referred to a zero relative level, should not be more than -52 db.[25] This recommendation is applicable to the normal program circuit, Type A, defined in CCITT Recommendation J.21 for carrier systems. EIA Standard RS-250-A recommends that the audio signal-to-noise ratio (rms signal to rms noise) at the output terminals of a multi-hop relay system shall be at least 55 db (58 db for a single hop-relay system) where noise is any extraneous output voltage in the frequency band from 50 Hz to 15 kHz. Both of these recommendations are considered applicable to the analysis of the ATS Television subsystem audio channel.

RESULTS

        The satellite EIRP will vary according to the spacecraft and transponder used. This variation is noted in the test results contained in tables 3.39 and 3.40.

3.5.8.2 Analysis

        With respect to the standards used in this analysis, both are based on total noise measured in the audio channel instead of idle noise, thus neither standard is directly applicable. The CCIR proposed recommendation (S/N = 61 db) is for a common carrier circuit, not a satellite relay system, but is significant in that the circuit is described as "very-high-quality". The EIA Standard (S/N = 58 db for single hop systems, S/N = 55 db for multi-hop systems) references circuits utilizing equipment common to the audio and video signals. Thus, to meet the CCIR Recommendation, a signal-to-total noise ratio of not less than 61 db can be realized if the signal-to-idle noise and signal-to-crosstalk noise are each not less than 64 db. To meet the EIA Standard for multi-hop relay systems, the S/N ratios must be 58 db. Based on the above and the assumption that the crosstalk products are at least 6 to 10 db below idle channel noise, a 55 db signal-to-idle noise ratio is suggested as the standard for evaluating the audio channel of the ATS Television Subsystem.

3.229

Based on system calculations, for a "Flat" or non-emphasized configuration, table 3.39 shows that the Rosman station (85-foot antenna) is capable of achieving a signal-to-idle noise ratio of 55 db or greater for all system conditions using the ATS-3 satellite. The corresponding measured S/N ratios support the system calculations quite well.

The Rosman station with its 85-ft antenna is also able to achieve a 55-db signal-to-thermal noise ratio via ATS-1 when it is in the 8-watt mode (two TWT's). The "System Calculations" and the measured values both show that the 4-watt mode of ATS-1 cannot be expected to produce the desired 55-db S/N ratio. As before, the measured values of S/N ratio support the accuracy of the calculations.

The ATS-1 measurements from Mojave illustrate the system incapability to attain a 55-db S/N ratio with the 40-ft earth-station antenna at the E.I.R.P levels attainable with this satellite. This is largely because the receiver G/T ratio for Mojave is approximately 6 db less than that of the Rosman station. The influence of the uplink noise contribution is responsible for the observation that there is less than 6-db difference in the calculated S/N values between Rosman and Mojave employing ATS-1 for the two TWT condition.

The data listed in table 3.40 illustrates the advantage to be gained by using the recommended 75-microsecond pre-emphasis and de-emphasis networks. The values listed in the "System Calculated" column are obtained by use of the formula:

$$\rho \text{ (db)} = 10 \log \frac{(2 \pi \, fm \, \tau)^3}{3 \, (2 \pi \, fm \tau - \tan^{-1} 2 \pi \, fm \tau)},$$

where ρ is the calculated value of improvement, τ is the 75-μsec time constant of the emphasis network, and fm is taken as 13,000 Hz. This value of 13 kHz for the audio-channel bandwidth was determined by the frequency response curves plotted subsequent to the addition of the 15.75-kHz notch filter. (See paragraph 3.5.10.) Using these values in the above equation yields an expected improvement in signal-to-noise of about 12 db.

However, the actual improvement gained through use of audio pre-emphasis is only about 8.5 db as seen in the column of measured values. This discrepancy is explained when the curve of channel response with pre-emphasis is examined for this station. This curve (see paragraph 3.5.10) shows that the audio channel effective bandwidth is reduced to about 7 or 8 kHz when emphasis is employed. Using a value of 8 kHz for fm in the above formula yields an expected noise improvement factor of 8.6 db. Thus the actual improvement as measured is verified, and the value of 64.5 db listed as the "System Calculated" signal-to-noise ratio really becomes approximately 60 to 61 db. A more exact determination would require a more detailed analysis of the channel response and effective noise bandwidth under the effect of the emphasis networks. However, the theoretical

improvement of 12 db remains in table 3.40 because this is the value which should be attained if the pre-emphasis and de-emphasis responses were complementary to each other.

3.5.8.3 Conclusions

The audio channel S/N of 55 db, as specified by the EIA, cannot be attained in the ATS system with earth station antennas 40 feet in diameter (G/T ratio of 32.2 db). To accomplish this level on a "Flat" or non-emphasized basis requires a satellite EIRP of 57.5 dbm or more. Changes to system parameters such as deviations and uplink power levels can also vary the thermal noise level, but only at the expense of other conditions such as intermodulation and harmonic distortion overloads. On the other hand, use of the recommended 75-microsecond pre-emphasis will allow the 55-db signal-to-noise ratio to be attained for all conditions of satellite EIRP for the ATS System (minimum is 49.5 dbm EIRP).

TABLE 3.39. TV AUDIO-CHANNEL IDLE NOISE

Station	Satellite			Station Mean Measured C/N (Normalized to Station Mean Noise Temp.) (db)	S/N ratio in db, normalized to System Mean Noise Temperature		
	ATS No.	EIRP (dbm)	No. of TWT's		System[1] Calculated	Mean of ratios Predicted from Measured C/N	Mean of Measured ratios
Rosman	3	52.2	1	17.1	56.4	58.5	56.3
	3	54.6	2	14.4	57.8	55.2	57.6
	3	56.5	1	17.2	59.0	58.0	57.6
Rosman	1	49.4	1	12.2	53.1	53.1	53.5
	1	52.2	2	13.7	55.2	54.5	54.7
Mojave	1	49.4	1	6.8	46.7[2]	45.8	45.0
	1	52.2	2	9.6	50.3	50.4	52.8

[1] Reference Section   1.3 for system calculations.

[2] Allows 1-db degradation for assumed threshold operation

TABLE 3.40. EFFECTS OF EMPHASIS ON AUDIO S/N RATIO

Station	Satellite			Station Mean Measured C/N (Normalized to Station Mean Noise Temp.) (db)	S/N ratio in db, normalized to System Mean Noise Temperature		
	ATS No.	EIRP (dbm)	No. of TWT's		System [1] Calculated	Mean of ratios Predicted from Measured C/N	Mean of Measured ratios
Mojave							
with Emphasis	3	54.6	2	11.1	64.5	63.9	58.5
without Emphasis					52.5	51.9	50.0
with Emphasis	RF Loop			11.0	N/A	63.8	59.5
without Emphasis						51.8	51.0

3.5.9.1 Description and Test Results

OBJECTIVES

This experiment is conducted to evaluate the periodic and crosstalk noise in the TV audio channel of the ATS television subsystem. Periodic noise, in contrast to idle noise (measured in another experiment), results primarily from power-supply hum, while the crosstalk noise is usually caused by the field and line synchronizing pulses in the video signal.

TEST CONDITIONS

This experiment is performed under the conditions stated in paragraph 3.5.

STANDARDS

The criteria for this evaluation will be based on the CCIR proposed[25] change to CCITT Recommendation J-21 pertaining to international program circuits, and EIA Standard RS-250A pertaining to television relay facilities.

Before proceeding with the analysis, it will be necessary to discuss the standards to be used in the evaluation. Multiplexing sound with video on international radio relay circuits using satellites is being studied by the CCIR. Thus, the CCIR does not have specific recommendations for crosstalk in such systems. The nearest applicable recommendation is the CCIR proposed change to CCITT No. J21* pertaining to program channels carried on international telephone networks. This recommendation states that the unweighted noise (which includes both random and periodic noise) should not exceed minus 52 db relative to a zero reference level at the extremity of an international Normal Program Circuit, Type A. (Type A circuits are those transmitting a frequency band of 50 Hz to 10 kHz and are the highest grade circuit covered by CCITT for international telephone systems.) However, the recommendation was never intended to cover a satellite TV relay system with a multiplexed audio channel. In this analysis, the above recommendation is considered mainly as a guide to a reasonable performance level. However, it is suggested that EIA Standard ** RS-250A, "Electrical Performance Standard for Television Relay Facilities," is a more appropriate standard since it deals with radio relay equipment for an application similar to the satellite relay system and specifically notes that it applies to circuits that are "common to the audio and video signals". This standard sets a minimum S/N ratio of 58 db in single hop systems and 55 db in multi-hop systems where the noise is any extraneous output voltage in the frequency band from 50 Hz to 15 kHz. The EIA standard requires that the audio S/N measurements shall be made while

_____
*(CCITT Red Book Volume III)
**Electronic Industries Association, Feb. 196

relaying a standard composite picture signal under standard input and output conditions. Since the satellite system is capable of bridging long distances equivalent to multi-hop systems, the 55-db standard will be considered the criteria for evaluating the ATS system. This means that the periodic (power-supply hum) and the video-to-audio crosstalk S/N ratios should each be greater than 60 db (assuming that thermal and periodic/crosstalk are approximately equal).

RESULTS

The results of the tests performed at Rosman, Cooby Creek and Mojave are summarized in table 3.41. It should be recognized that the 60-Hz and 120-Hz field-rate crosstalk listed in the table is actually the total periodic noise at these frequencies, which includes the power-supply hum. However, this does not lead to difficulty in analysis since the power supply hum level is generally several db lower in level; a fact which permits the field rate crosstalk to be readily identified. Table 3.42 lists the results of a special test performed to specifically evaluate the effects of the video and audio pre-emphasis on the video-to-audio crosstalk.

3.5.9.2 Analysis

The analysis of the results of this experiment is divided into three parts, based on the source of the periodic noise. The first is the idle 60-Hz power-supply hum in the audio channel itself. The other two result from the intermodulation crosstalk from the active video channel wherein the 60-Hz field rate and 15.75-kHz line-rate synchronization provide the predominant sources of crosstalk products. Only the second harmonic of the 60-Hz sources is considered in the analysis since the appearance of the higher order harmonics was not consistent and was usually 60 db or more below the test-tone level.

POWER SUPPLY HUM

This source arises from the TV audio-channel equipment in the ground stations and is not expected to be affected by the spacecraft transponder. It can be seen in table 3.41 that at the Rosman and Mojave stations the 60-Hz and 120-Hz power-supply hum is consistently low, (greater than 55 db). At Cooby Creek the hum was generally low; but there has been an occasional observation of -50 db in the satellite loop. However, the RF loop recordings at this site show that the hum level is very low. Since Cooby Creek operates at the lowest C/N ratio, it is believed that this factor was responsible for masking the proper reading in the S/C loop.

Many of the test measurements did not list a specific numeric quantity for the 60-Hz and 120-Hz power-supply hum components. The test data merely recorded the components as "greater than 55 db below test-tone level." (Examples are seen in table 3.41 under Rosman and Mojave via ATS-1.) However, many other tests did record a

numeric value, and it was found that the 60-Hz hum and its 120-Hz harmonic were each down at least 60 db or more. From the above, it is concluded that power supply hum levels in the idle audio channel are probably at least 60 db below test tone. This is seen to be satisfactory in accordance with the criteria developed in the section above.

FIELD RATE CROSSTALK

The vertical synchronizing pulses in the video signal are a source of 60-Hz crosstalk into the accompanying audio channel. The results listed in table 3.41 indicate that this parameter has been observed to be from 36 db to over 70 db below test-tone level. Furthermore, the majority of readings are seen to be considerably below the target of minus 60 db. All of these test measurements were made on a flat baseband (i.e., with no video or audio pre-emphasis/de-emphasis). Thus, it is concluded that the field-rate (60 Hz) crosstalk into the audio channel is excessive in the ATS system, and will not permit the desired 55-db signal-to-total noise to be obtained. This crosstalk problem is caused by the group delay characteristic of the IF passband which introduces intermod products within the sub-carrier channel passband.

LINE RATE CROSSTALK

The horizontal synchronizing pulses of the video signal are a source of 15.75-kHz crosstalk into the audio channel. However, since the audio channel contains a 15-kHz low pass filter in the receiver output circuitry, the crosstalk component is technically an "out-of-band" interference. The filter specification calls for not more than 3 db down at 14.5 to 15 kHz, with a roll-off of 36 db per octave above the 3-db down frequency. This means that the channel response is probably no more than about 5 or 6 db down at the 15.75-kHz line rate. Even with this "out-of-band" attenuation advantage, the line-rate crosstalk component was measured at levels as high as -37 db (see Rosman via ATS-1 in table 3.41). This 37 db is a 6-test average containing a low of 35 db and a high of 39 db. Other averages are seen to run between 40 to 58 db, all of which do not meet the target of more than 60 db below test-tone level.

Since the interfering signal is technically, if not actually, out-of-band, a large scale effort to locate the exact source of the crosstalk was not initiated. A notch filter tuned to 15.75 kHz was procured and installed in the receiver audio-output circuitry. Subsequent measurements indicated that the line rate crosstalk was reduced to well over 60 db. The effect upon the audio channel amplitude versus frequency response was minimal. The 3-db down point is now about 13 kHz instead of the former 15 kHz. This is considered to be a relatively insignificant degradation in the channel bandwidth.

However, the 60-Hz field rate and 15.75-kHz line rate components are not the only parts of the total crosstable problem. When the video channel is actively carrying a test pattern or other video waveforms, there is a general interference, or random noise level introduced into the audio channel. The phenomena is shown in lines one and two of table 3.42 where the rms noise level without video pre-emphasis is seen to rise at least 6 to 8 db when a video signal is transmitted. However, a narrowband wave analyzer search in the audio channel failed to reveal any distinct periodic interference components; at least in sufficient numbers and levels to account for the observed increase in the channel rms noise level. When video pre-emphasis is applied to the system it is seen from lines 3 and 4 of table 3.42 that the former crosstalk problem disappears. The very small increase in noise level when video is applied means that the crosstalk noise components are at least 8 to 10 db below the idle system noise level (thermal plus power supply hum). Thus, it is seen that the incorporation of video pre-emphasis and de-emphasis techniques is most effective in eliminating the crosstalk problem. The observed 8 db or so improvement from lines 1 to 2 and from lines 3 to 4 in the table are indicative of gains made by utilizing audio pre-emphasis. This subject is discussed in paragraph 3.5.8 of this report.

3.5.9.3 Conclusions

All identifiable noise sources in the ATS TV audio channel (i.e., idle channel continuous random noise from thermal limitations, power supply hum components, and crosstalk from the video field and line rate sync pulses) must be considered for their contribution to total noise. Generally, this experiment shows that the contributions from power supply hum are sufficiently well suppressed as to be relatively insignificant in their effect upon the total noise level. Video crosstalk, however, is severe enough as to preclude meeting the goal of 55-db signal-to-total noise on a flat baseband basis. The line rate crosstal can be eliminated by the addition of a 15.75-kHz notch filter. The remaining crosstalk components are still capable of defeating the 55-db S/N goal. The use of video pre-emphasis and de-emphasis was found to be effective in eliminating video crosstalk into the audio channel Measurements indicate that the video crosstalk is at least 8 to 10 db below idle channel noise. Furthermore, the use of emphasis techniques in the audio channel was found not to be detrimental to power-supply hum components. Thus the limitation to achieving the desired channel S/N ratio of 55 db becomes primarily dependent on the thermal noise level.

TABLE 3.41. TV AUDIO-CHANNEL PERIODIC AND CROSSTALK NOISE (FT-TV-6.1)

Station, Satellite, and Dates	Component	db Below Test Tone Level			
		S/C Loop		RF Loop	
		Idle Channel Hum	Video Crosstalk	Idle Channel Hum	Video Crosstalk
Cooby, ATS-1	60 Hz	≥ 50	36.0	≥ 70	52.5
7/2/67 thru	120 Hz	> 50	46.2	> 70	62.2
6/10/68 (6 tests)	15.75 kHz		40.9		46.1
Rosman, ATS-1	60 Hz	> 55	> 55	> 55	≥ 50
7/23/67 thru	120 Hz	> 55	> 55	> 55	≥ 48
9/21/67 (6 tests)	15.75 kHz		37.1		39.8
Rosman, ATS-3	60 Hz	59.0	54.6		
8/2/68 thru	120 Hz	67.2	61.5		
9/6/68 (8 tests)	15.75 kHz		57.9		
Mojave, ATS-1	60 Hz	> 55	45.5	58.5	46.5
7/25/68 thru	120 Hz	> 70	39.0	> 70	50.0
10/8/68 (2 tests)	15.75 kHz		40.5		46.8
Mojave, ATS-3	60 Hz	> 70	47.3	> 70	45.0
12/20/67 thru	120 Hz	> 70		> 70	52.3
10/8/68 (3 tests)	15.75 kHz		54.2		54.2
Mojave, ATS-3	60 Hz	> 70	70	69	70
12/8/68* (1 test)	120 Hz	None	72	72	None
	15.75 kHz		None		None

*Measurements made with 15.75-kHz notch filter in receiver output.

TABLE 3.42.   EFFECTS OF EMPHASIS ON VIDEO-TO-AUDIO CROSSTALK

| | db Below Test Tone Level | | | |
| | Satellite Loop | | RF Loop | |
	Idle Channel Noise	Video Crosstalk Noise	Idle Channel Noise	Video Crosstalk Noise
Mojave, Dec. 1969, ATS-3				
No Video or Audio Emphasis	50.0	43.0	51.0	45.0
No Video Emphasis, but with Audio Emphasis	58.5	50.0	59.5	53.0
With Video Emphasis, but No Audio Emphasis	50.0	49.5	50.5	50.0
With Video and Audio Emphasis	58.5	58.0	59.5	57.5

3.5.10 TV AUDIO-CHANNEL AMPLITUDE VERSUS FREQUENCY RESPONSE (M. E. Strong)
(FT-TV-6.2)

3.5.10.1 Description and Test Results

The objective of this experiment is to establish the amplitude versus frequency response of the TV Audio Channel in the ATS television subsystem. The significance of this response characteristic resides in the fact that it is one of the important characteristics which defines the fidelity of the audio channel.

TEST CONDITIONS

This experiment was performed under the conditions stated in paragraph 3.5.

STANDARDS

The ATS television subsystem audio channel will be evaluated in the context of contemporary program channels employed in common carrier systems. The CCIR proposed* change to CCITT Recommendation J-21, pertaining to Type A program circuits on common carrier telephone circuits, is considered applicable to the ATS TV audio channel and is considered in the analysis of the experiment. Briefly, CCIR recommends that the frequency band effectively transmitted should extend from 30 Hz to 15,000 Hz and the response curve should be within limits as shown in figures 3.89 through 3.94 where the slope of the curve should not exceed 6 db per octave in the 10,000-Hz to 15,000-Hz frequency band.

RESULTS

The TV audio channel amplitude versus frequency response characteristics was measured at each of the earth stations, using either ATS-1 or ATS-3, during the period December, 1966, through October, 1968. The results of these measurements are shown in figures 3.89, 3.90 and 3.91. Subsequent to October, 1968, a 15,750-Hz notch filter was installed in the audio channel output to reduce line rate crosstalk appearing in the audio channel. The resulting audio channel response characteristic, is shown in figures 3.92 through 3.94.   In December 1969 and February 1970, the effect of adding the 75-microsecond pre- and de-emphasis networks was ascertained. These results are seen in figures 3.95 through 3.98.

3.5.10.2 Analysis

NON-EMPHASIZED CHANNEL

CCIR studies covering circuits for monophonic program transmission have resulted in recommended changes to CCITT Recommendation J.21 for normal program circuits, Type A. This recommendation pertains to a very high-quality circuit and is considerably more stringent than the existing CCITT Recommendation J.21.

---

*Study Program 5A/CMTT, Addendum No. 1 to Volume V of the documents of the XIth Plenary Assembly of the CCIR, Oslo, 1966.

Examination of the above referenced figures shows that the audio channel amplitude response consistently falls below the Oslo 1966 recommendation of the CCIR in the 50- to 100-Hz frequency range. However, it is also true that even the worst of these curves is well within the limits of CCITT Recommendation J-21 dated December 1960. This latter guideline was the one in effect at the time of equipment procurement and installation. The high-frequency response appears to be somewhat marginal for Cooby Creek and Mojave in the vicinity of 8 to 10 kHz. On the other hand, the curves for Rosman (without pre-emphasis) show an adequate high-frequency response. As before, even the worst curve (Mojave) is well within the earlier limits of CCITT Recommendation J-21.

Figures 3.92, 3.93, and 3.94 show the amplitude response after the installation of the aforementioned 15.75-kHz notch filter. As expected, the high-frequency response is seen to have a very sharp roll-off above 12 kHz because of the presence of the notch filter. The relative amplitude at 15 kHz is over 20-db down, referenced to the output at 1 kHz. However, the output at 13 kHz is down only 3 db or less. Thus the effective 3-db bandwidth transmitted is found to be approximately 40 to 13,000 Hz. This response does not quite meet the suggested criteria of the Oslo 1966 meeting of the CCIR. However, it is well within the limits recommended by CCITT Rec. J-21 of Dec. 1960.

EFFECTS OF PRE-EMPHASIS

Figures 3.95 through 3.98 illustrate the result of adding the 75-microsecond pre-emphasis and de-emphasis networks to the audio subsystem. It is seen that the response with emphasis is degraded at both stations, (Mojave and Rosman) when compared to the "Flat" or non-emphasized conditions. The high frequency roll-off at Mojave is considerably worse than that of Rosman. This is probably caused by the difference that exists in the audio input circuits at the two sites. At Rosman the audio input signals are first applied to a switch which selects either a fixed attenuator or a 75-microsecond pre-emphasis network. At Mojave the pre-emphasis is inserted in an audio feedback loop which is primarily used for control over modulation linearity and audio harmonic distortion reduction. Nevertheless, it is evident at both sites that the pre-emphasis and de-emphasis network responses are not exact complements to each other. The feedback loop circuit as used at Mojave is seen to be inferior at matching the receiver de-emphasis network.

3.5.10.3 Conclusions

It is concluded that the "Flat" or non-emphasized ATS audio channel frequency response will not meet the modern CCIR recommended limits for a small portion of the low frequency end of the audio band (approximately 50 Hz to 100 Hz) and will not meet the high-frequency limits (13 kHz to 15 kHz) because of the 15.75-kHz notch filter. However, the observed deviations from the recommended requirements are relatively small and should not materially affect the audio-channel fidelity.

When the 75-microsecond pre-emphasis and de-emphasis is added to the system, the high-frequency response is degraded. The modified input circuit as used at Rosman improves the response characteristic, but additional improvement is needed to make the emphasis curves more exact complements of each other.
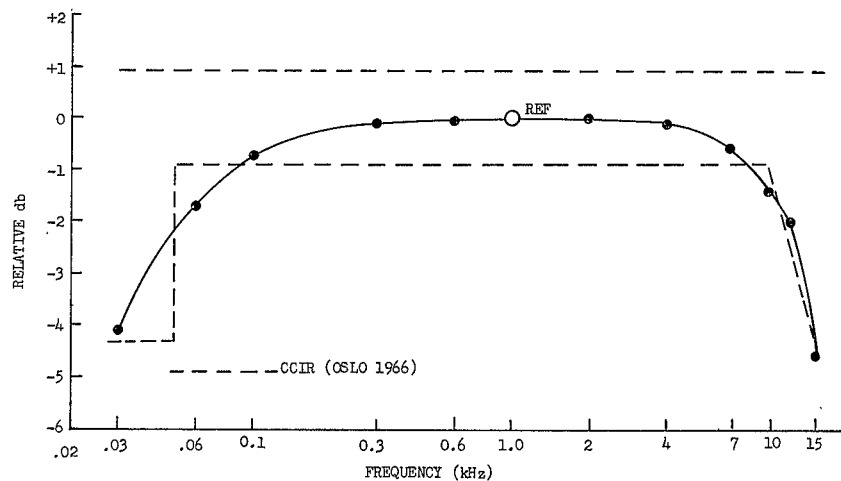
Figure 3.89. TV Audio-Channel Frequency Response, Cooby Creek
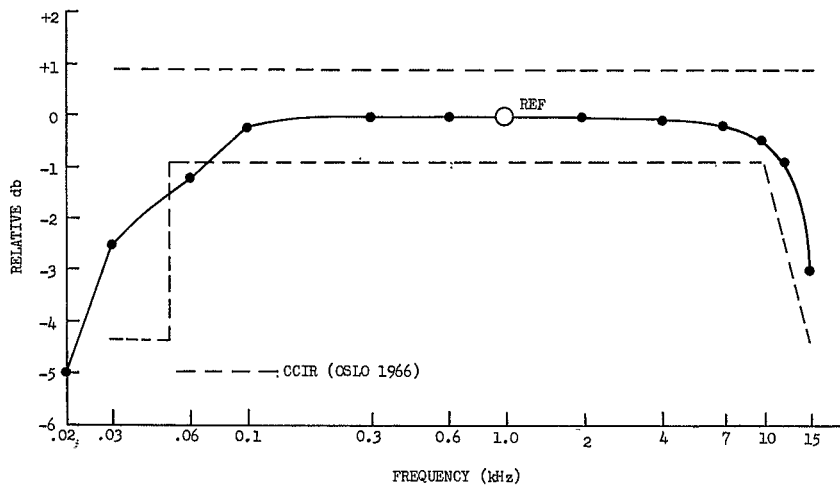
Figure 3.90.   TV Audio-Channel Frequency Response, Rosman
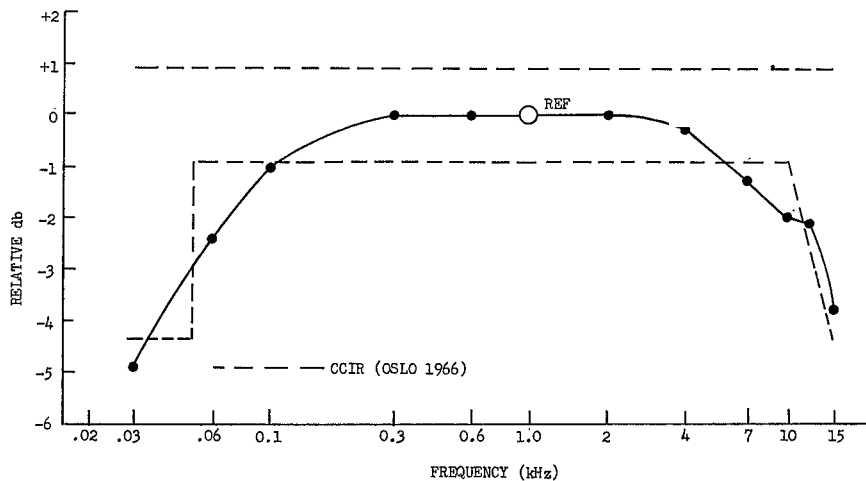
Figure 3.91. TV Audio-Channel Frequency Response, Mojave
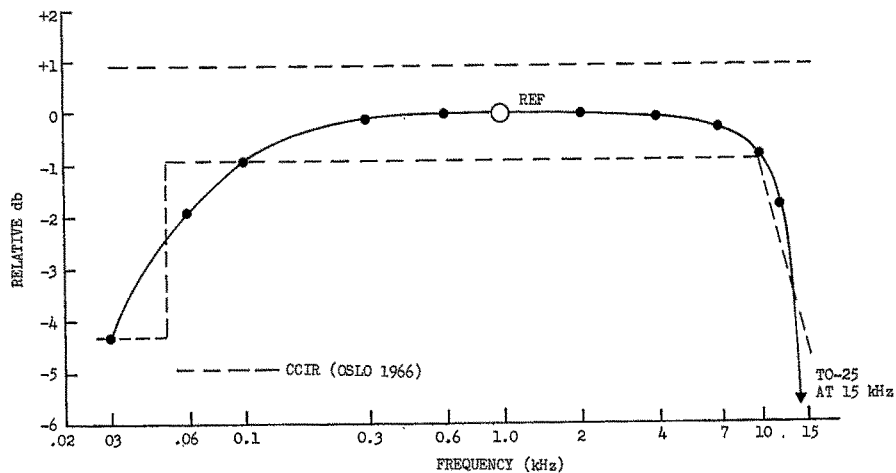
Figure 3.92. TV Audio-Channel Frequency Response, Cooby Creek with 15.75-kHz Notch Filter
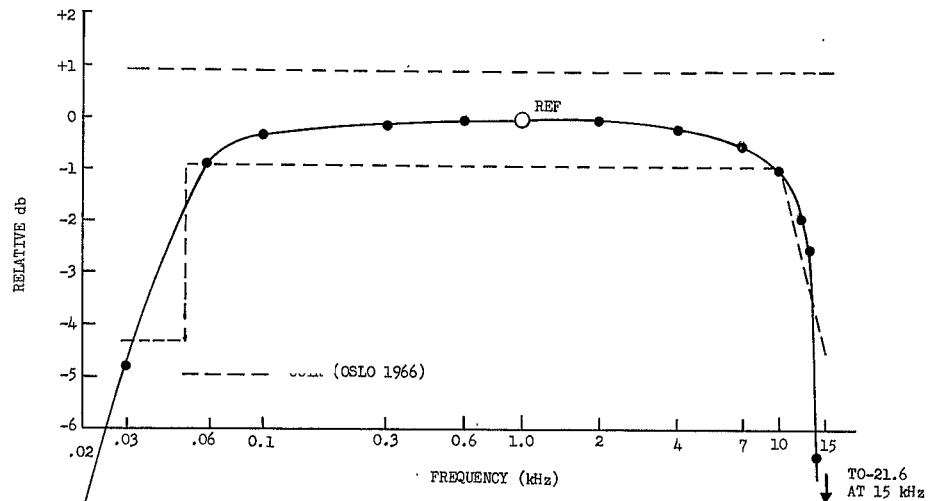
Figure 3.93.   TV Audio-Channel Frequency Response, Rosman with 15.75-kHz Notch Filter
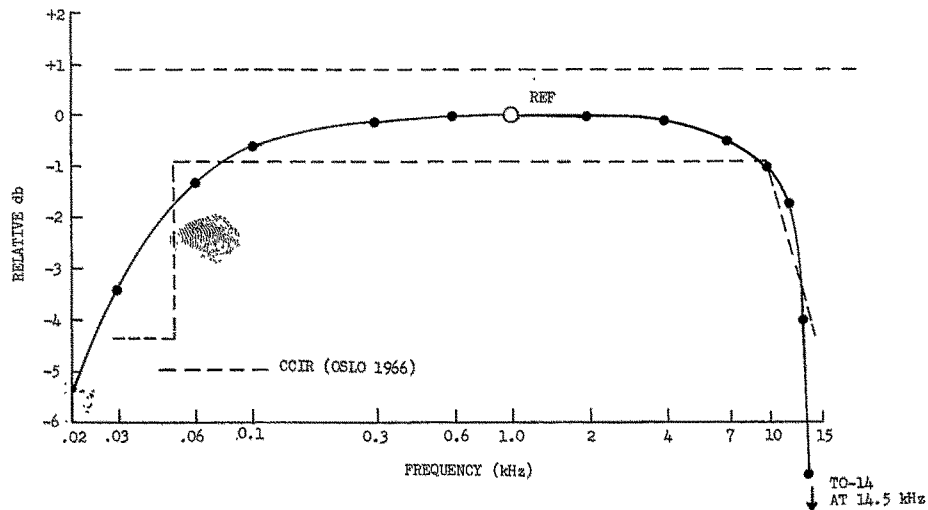
Figure 3.94. TV Audio-Channel Frequency Response, Mojave with 15.75-kHz Notch Filter
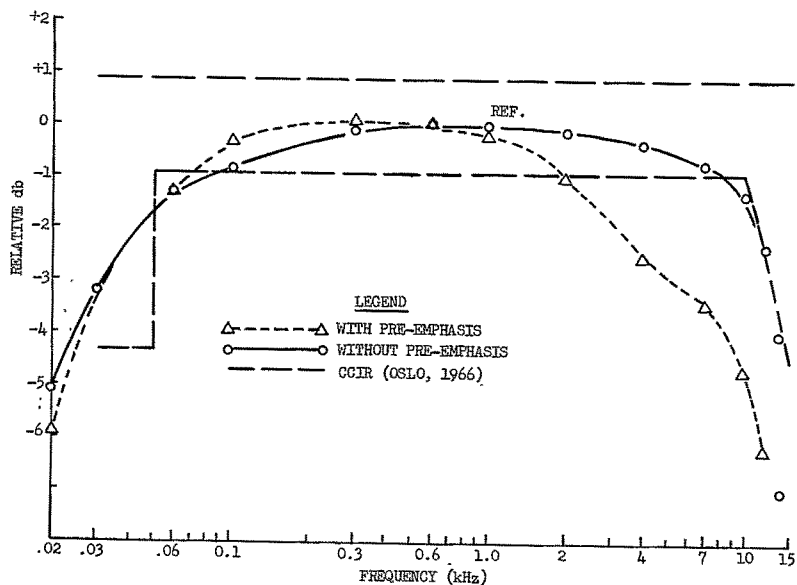
Figure 3.95.   TV Audio-Channel Frequency Response (With 15.75-kHz Notch Filter and
Pre-Emphasis) - Mojave, Dec 1969 via ATS-3
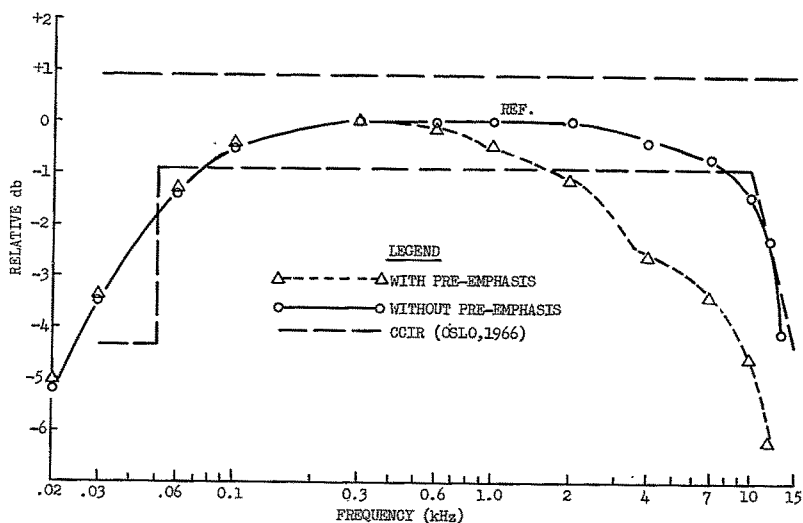
Figure 3.96. TV Audio-Channel Frequency Response (With 15.75-kHz Notch Filter and Pre-Emphasis) - Mojave, Dec 1969 via RF Loop
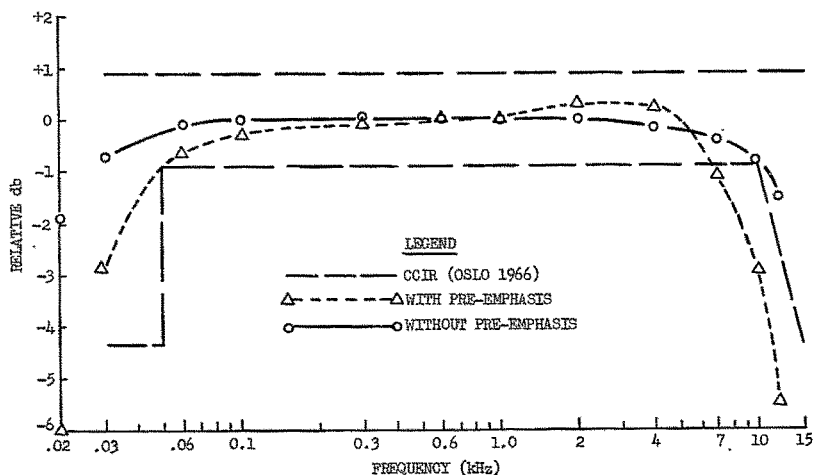
Figure 3.97. TV Audio-Channel Frequency Response (With 15.75-kHz Notch Filter and
Pre-Emphasis) - Rosman, Feb. 1970, via RF Loop
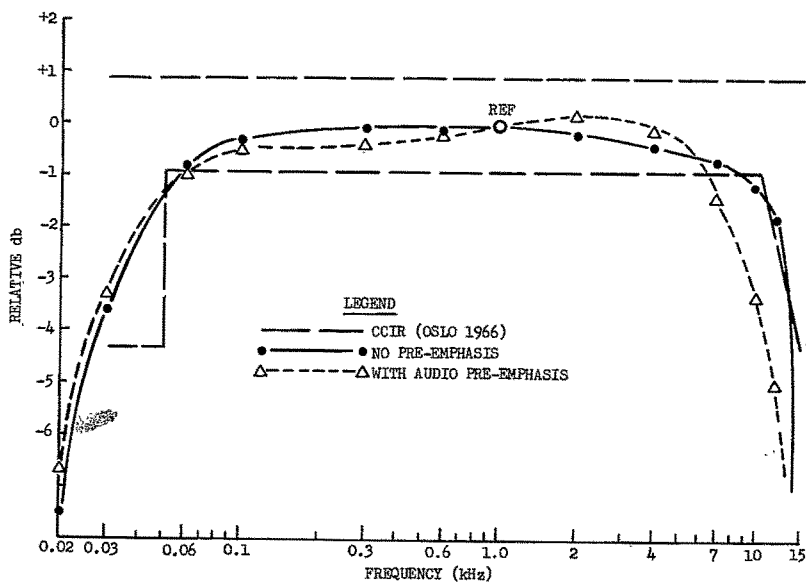
Figure 3.98. TV Audio-Channel Frequency Response (With 15.75kHz Notch Filter and
Pre-Emphasis) – Rosman, April 1970, via ATS-3

3.5.11 TV AUDIO-CHANNEL NON-LINEAR DISTORTION (M.E. Strong) (FT-TV-6.4)

3.5.11.1 Description and Test Results

OBJECTIVE

        The objective of this experiment is to establish the harmonic distortion character-istics of the television audio channel portion of the FM video transmission system. Harmonic content and components are determined because they are a direct measure of amplitude non-linearities occuring in the system.

TEST CONDITIONS

        The experiment is performed under the conditions stated in paragraph 3.5. Dis-tortion characteristics are evaluated for test tone fundamentals below 100, 1000, and either 4000 or 5000 Hz.

STANDARDS

        The ATS television subsystem audio channel will be evaluated in the context of contemporary program channels employed in common carrier systems.

        One standard applicable to systems, similar to the ATS, is the EIA Standard RS-250A. This document is primarily intended to cover studio-to-transmitter links, but it is specifically stated to apply to facilities where the audio program material is transmitted along with the video signal over common equipments and carriers. This standard is dated February 1967, and allows the following levels of harmonic distortion:

Fundamental	Harmonic Distortion
50 to 100 Hz	1.5%
100 to 7500 Hz	1.0%
7500 to 15000 Hz	1.25%

        Another applicable document is CCITT Recommendation J-21 dated December 1960. This document was published and in force at the time of ATS equipment procurement and installation. As such, it is considered more directly applicable to the system under discussion. This recommendation allows harmonic distortions of 4 percent or less, but suggests that a more modern design objective would be for distortions of 3 percent or less for fundamentals below 100 Hz and 2 percent or less for fundamentals above 100 Hz.

        Finally, at the Oslo 1966 meeting, the CCITT proposed a revision to their Recommendation J-21* which suggested the following tolerances on harmonic distortion:

Fundamental	Harmonic Distortion
50 to 100 Hz	3%
100 to 7500 Hz	1%
7500 to 15000 Hz	3%

---

* Study Program 5A/CMTT Addendum No. 1 to Vol. V of documents of the XIth Plenary Assembly of the CCIR, Oslo 1966.

RESULTS

The results of harmonic-distortion measurements are shown in tables 3.43 and 3.44 for satellites ATS-1 and 3, respectively. Table 3.45 shows the results of comparative measurements made both with and without the use of audio pre-emphasis and de-emphasis networks.

3.5.11.2 Analysis

From an examination of the results shown in the tables, it would appear that the satellite was a contributing factor to the determination of overall audio channel harmonic distortion. This apparently anomolistic behavior can be at least partially attributed to the fact that many of the distortion measurements were made with an instrument which operates on the principal of nulling out the fundamental and measuring the remaining signals within the channel passband. This of course means that noise and all other in-band components are recorded as well as the desired harmonics of the fundamental signal. Since the satellite loop circuits are generally considerably more noisy than the RF loop configurations, it is expected that the spacecraft harmonic distortion readings would be slightly greater than those of the RF loops.

The various entries in the tables for each site show a large degree of variation in the measurements. The differentials between readings are seen to cover ratios from two to four or more. This points up the difficulty and sensitivity of the audio channel to system alignment and adjustments.

The distortion measurements tabulated in tables 3.43 and 3.44 were taken at the normal test-tone level of +9 dbm. A few measurements made at test tone levels one or two db greater resulted in greatly increased harmonic distortion. Likewise, measurements taken at a test tone level of +6 dbm showed harmonic distortion levels only a few tenths of one percent. This indicates that the test tone level of +9 dbm is close to the system "crash-point".

The measurements from Mojave in table 3.45 were also taken at maximum rated subcarrier deviation. The data from Rosman in the non-emphasized configuration was obtained at maximum level (+9 dbm). These results show that the CCITT proposed recommendation can nearly be attained. However, of more interest in this latter table is the indication that pre-emphasis and de-emphasis is effective in further reducing the amount of harmonic distortion. Actually, it is the effects of the de-emphasis network that is instrumental in reducing harmonic distortion. As seen from the table the harmonic suppression is greater for the higher frequency fundamentals. This is caused by the increasing amplitude reductions for signals above 1000 Hz. In any event, the results shown in table 3.45 indicate that the CCITT recommended limits for harmonic distortion can be attained when pre-emphasis is applied to the audio channel.

The tables do not show any distortion values for fundamentals above 5000 Hz. In particular, they show no measurements in the 7500-to 15000-Hz range of the referenced standards. However, measurements actually have been conducted in this region, but practically no harmonic distortion could be detected for fundamentals above 7500 Hz, and very little distortion could be detected between 5000 to 7500 Hz. This is caused by the fact that the channel has a fairly sharp cut-off above 14 or 15 kHz. Therefore, the harmonic distortion measurements were limited to an upper limit of 5 kHz, so that at least the second and third harmonics were still within the channel passband.

3.5.11.3 Conclusions

With careful adjustment, the ATS system is capable of performance at reasonably low harmonic-distortion levels. The system can be operated at a lower test-signal level with less attention to adjustments. The use of the standard 75-microsecond pre-emphasis and de-emphasis technique is effective in reducing the level of harmonic distortion to within the CCITT recommended limits.

TABLE 3.43   TV Audio–Channel Harmonic Distortion (ATS-1)

Station, Date, & Serial No.	C/N in db		Percent total harmonic distortion					
	RF Loop	S/C Loop	RF Loop			S/C Loop		
			100 Hz	1 kHz	5 kHz	100 Hz	1 kHz	5 kHz
Cooby Creek, T1001 7 April 1968	31	6.5	3.6	3.6	3.6	3.8	5.6	4.5
Cooby Creek, T1008 11 November 1968			1.5	1.3	0.3	1.7	1.7	1.1
Mojave, M-block 25 July 1968	17	9.6	1.8	1.7	2.1	1.7	1.3	1.2

TABLE 3.44   TV Audio–Channel Harmonic Distortion (ATS-3)

Station, Date, & Serial No.	C/N in db		Percent total harmonic distortion					
	RF Loop	S/C Loop	RF Loop			S/C Loop		
			100 Hz	1 kHz	5 kHz	100 Hz	1 kHz	5 kHz
Rosman, R3003 22 August 1968		17.5				5.0	3.7	
Mojave, M3001 8 December 1968			4.2	2.4	10 kHz 0.1	4.3	3.1	10 kHz 2.5

TABLE 3.45 EFFECTS OF EMPHASIS ON AUDIO DISTORTION

Station and Date	Frequency in Hz	Percent total harmonic distortion			
		RF Loop		S/C Loop	
		No Pre-Emphasis	With Pre-Emphasis	No Pre-Emphasis	With Pre-Emphasis
Mojave (ATS-3) 11 December 1969	75	1.45	1.25	1.55	1.38
	1000	1.25	0.8	1.4	0.9
	4000	1.54	0.76	1.6	0.84
Rosman February 1970	75	1.21	<1.0	–	–
	1000	1.02	0.42	–	–
	4000	1.61	0.6	–	–

3.5.12 VIDEO BASEBAND ATTENUATION VERSUS FREQUENCY (BASEBAND FREQUENCY RESPONSE) (G.I. Shriver) (FT-BB-5.1)

3.5.12.1 Description and Test Results

OBJECTIVE

The objective of this experiment is to determine the video baseband attenuation versus frequency characteristic of the ATS system in the FT (television) mode. Picture deterioration of several types may be observed if this transmission parameter is excessively degraded.

TEST CONDITIONS

This test is performed under the conditions stated in paragraph 3.5.

STANDARDS

CCIR Recommendation 421-1, paragraph 3.6, gives the following design-objective limits for system "M", and recommends a reference frequency of 160 kHz. The limits, for Canada and the U.S.A., are ±0.16 db between 10 kHz and 300 kHz with a linear increase between 300 kHz and 4 MHz to ±0.63 db. The international limits allow a variations of ±1.0 db between 160 kHz and 800 kHz, with a linear increase in level to +2.5 db at 4 MHz, and linear decreases in level to -2.0 db at 3.2 MHz and -4.0 db at 4 MHz.

RESULTS

Results from this experiment are shown in figures 3.99 and 3.100. Rosman test means are shown in figure 3.99. The plots on this figure were obtained from test information on ATS-1 and ATS-3. No significant difference was observed in the test results from the two S/C. Figure 3.100 shows test results for Cooby Creek on ATS-1 only. These two figures show the mean, maximum, and minimum values obtained from numerous tests. Figure 3.101 shows the results of a special test run at Mojave on ATS-3. This figure shows test results with and without pre/de-emphasis. The Canadian - U.S.A. and the international CCIR design-objective limits are also shown on all figures.

3.5.12.2 Analysis of Test Results

The attenuation versus baseband frequency curves in figures 3.99 and 3.100 are normalized to 200 kHz instead of 160 kHz as recommended by the CCIR. This change in the normalization frequency has little or no effect on the displayed curves.

There appears to be no significant difference in test results from the three earth stations or from the two spacecraft. Deviations from a nominally flat response occur at both ends of the frequency band. A low frequency boost was intentionally added in the receiver video amplifier to prevent a decrease in gain at the lower frequencies. In most

cases the bandpass is essentially flat between 200 Hz and 200 kHz. A gain increase does occur at very low frequencies but this is far below the lowest frequency covered by the CCIR Recommendation. At 30 Hz, (the lowest frequency component of a television signal) the level is generally within 1 db of the level at 200 kHz. A high frequency roll-off exceeds the CCIR Recommendation for the USA and Canada at about 2 MHz (1 MHz at Mojave with ATS-3 on the special test performed on 27 April 68). The system does, however, meet the CCIR international limits. From typical filter response test data, about half of this high frequency roll-off can be attributed to the video low-pass filter. Excessive loss of gain at the higher video frequencies could result in a loss of picture detail. However, these losses are not considered excessive since subjective tests and TV demonstrations indicate a high resolution picture is possible. (See section   1 of this report.)

Figure 3.101 shows the results of a special test performed at Mojave on ATS-3 (27 April 68). The test was performed in the normal manner with pre-emphasis and de-emphasis removed. Then the test was repeated with pre-emphasis and de-emphasis networks installed. The test results indicate essentially no difference in attenuation at the lower frequencies, but a more rapid roll-off as frequency increases when pre/de-emphasis networks are used. The maximum difference in attenuation between the two tests is in the order of 0.5 db. This indicates that the pre/de-emphasis networks are not exact complements of each other.

3.5.12.3 Conclusions

The video baseband attenuation versus frequency curve shown in figure 3.99 is typical of test results at the three earth stations and for spacecraft. The baseband attenuation increases with frequency and exceeds the CCIR USA-Canadian limits at about 2 MHz. The system does not exceed the CCIR international limits.

The results of limited testing indicates no change at the low frequencies, but a more rapid roll-off at higher frequencies when pre-emphasis and de-emphasis networks are not removed for test execution. This roll-off is approximately 0.5 db greater, at the upper end of the frequency spectrum, when the measurement is made with pre/de-emphasis.
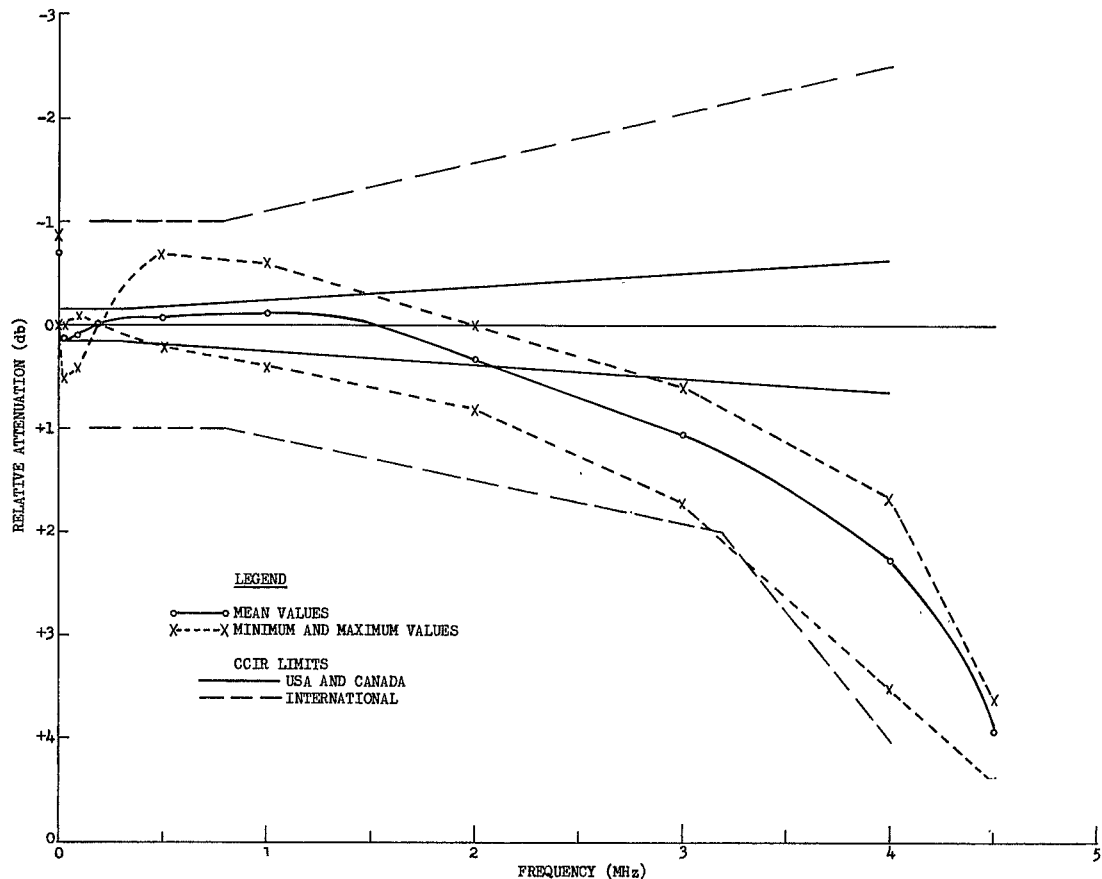
Figure 3.99. Video Baseband Attenuation Versus Frequency (Rosman ATS-1 and ATS-3)
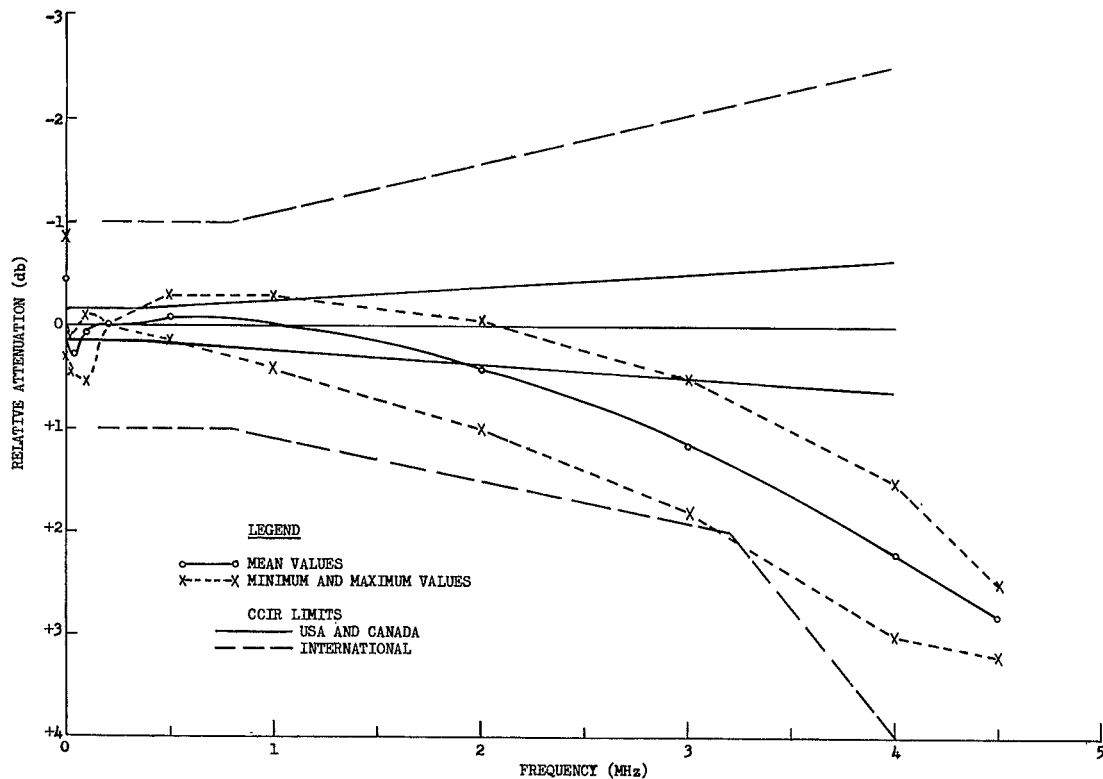
Figure 3.100. Video Baseband Attenuation Versus Frequency (Cooby Creek, ATS-1)
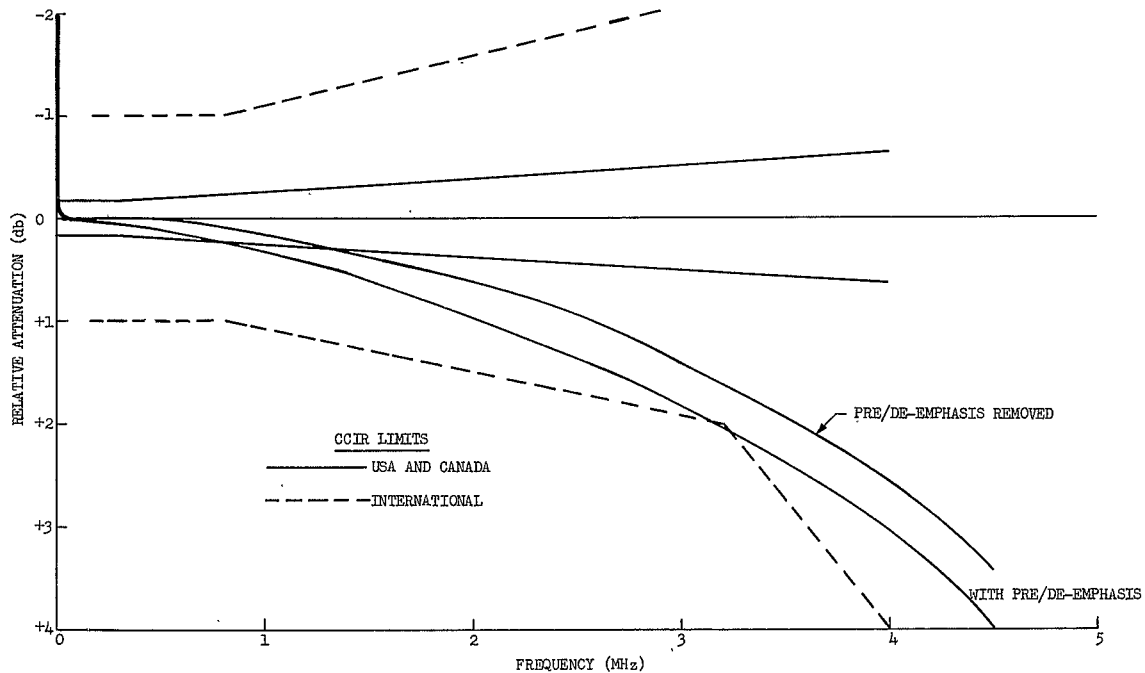
Figure 3.101. Video Baseband Attenuation Versus Frequency (Mojave ATS-3, 27 April 68)

3.5.13 ENVELOPE DELAY VERSUS BASEBAND FREQUENCY (ENVELOPE DELAY
DISTORTION) (G.I. Shriver) FT-BB-4.1)

3.5.13.1 Description and Test Results

OBJECTIVE

This experiment is performed to determine the envelope delay characteristic
of the ATS satellite system. Envelope delay versus baseband frequency in this experiment,
refers to a departure from flatness in the envelope delay of the FT mode transmission
system as a function of the baseband frequency. This departure can cause waveform distor-
tion of complex signals and is of more importance to the transmission of wideband digital
data and television signals rather than FDM multiplex signals. This experiment is also
performed with and without pre-emphasis/de-emphasis to determine the effect of the
emphasis circuits on envelope delay.

TEST CONDITIONS

This test is performed under the conditions stated in paragraph 3.5.

STANDARD

CCIR Recommendation 421-1, paragraph 3.6 is applicable to this experiment.
This recommendation allows a variation of ±32 nsec from 10 kHz to 3 MHz, and from 3 MHz to
4 MHz, a linear increase to ±63 nsec is permitted.

RESULTS

Some typical envelope delay versus baseband frequency curves are shown in
Figures 3.102 through 3.105. Figures 3.106 and 3.107 show the results of this
test performed with and without pre-emphasis/de-emphasis on the S/C and RF loop configura-
tions.

3.5.13.2 Analysis

The test equipment used in the experiment limited the measurements to above
100 kHz which does not include the lower end of the spectrum to 10 kHz covered by the CCIR
Recommendation. Also, the reference frequency used in the test set was 200 kHz instead of
the 160 kHz recommended by CCIR. It is considered that these factors do not materially
affect the results of the test nor the conclusions that may be drawn from them. The theory
of envelope delay distortion and its effect on television signals is well documented in literature
and will not be covered here. [24]

The 4.5-MHz video low-pass filter is the primary factor determining the
envelope delay characteristic. Secondary factors affecting the results of this experiment
include the FM modulator/demodulator transfer characteristics and video-baseband amplifiers
and circuitry. A minor contributor is the IF/RF group delay.

In performing the tests, it was found that the resolution and stability of the measurements were highly dependent on the baseband signal-to-noise ratio. This was traced to the fact that the test equipment used (which is typical of that available today) requires a rather high baseband signal-to-noise ratio. As a result of this, measurements made on ATS-1 or at the stations with a 40-foot antenna tended to be very "noisy" and un-repeatable. (See figures 3.103 and 3.104.) Tests performed employing the RF loop were somewhat better due to the use of a simulated carrier level some 10 db higher than that from the spacecraft (see figure 3.105). The best results were obtained at Rosman (85-foot antenna) using, ATS-3 (12 watt transponder). (See figure 3.102.) This configuration provided a C/N ratio of 20.5 db resulting in a baseband S/N ratio of 37.5 db. These results indicate that measurements obtained using the available test equipment must have a baseband S/N of better than 30 db or so in order to obtain satisfactory results. Therefore, this tends to limit this test to the Rosman and Mojave Stations when utilizing ATS-3.

The test was run at three deviation levels to determine if the envelope delay distortion would improve if a narrower TV signal spectrum were used (lower deviation). Figures 3.104 and 3.105 are examples of the typical results which indicate that the envelope delay distortion became worse at the high end of the spectrum when the deviation was decreased. This is contrary to expectation since the lower deviation occupies the more linear portion of the transfer characteristic and should show improvement. These apparently anomalous results may be explained, however, in the following manner. Since pre-emphasis/de-emphasis is not used, the baseband noise is parabolic. Therefore, the S/N ratio at the high end of the baseband is considerably poorer than at the low end. When the test signal is swept in this region, the resultant phase measurement is subjected to a larger error which is reflected in a noisy, less reliable plot. This theory tends to be supported by the fact that the test at Rosman where the best overall baseband S/N ratio was obtained, the three deviations tended to produce nearly identical results.

On all tests, at the high end of the frequency spectrum, increasing envelope delay is indicated. This delay increases very rapidly between 4 and 4.5 MHz, and is attributed to the 4.5-MHz video low-pass filter. The manufacturers instruction book indicates a 1-db drop at 4 MHz and a 3-db drop at 4.5 MHz. This indicates a rapid increase in group delay in this portion of the frequency spectrum. This instruction book also allows a filter delay tolerance at 4 MHz that is almost as great as the tolerance recommended by the CCIR for the entire system.

On a high percentage of tests from all stations, some indication of discontinuity is present. This discontinuity manifests itself in the form of one or more narrow spikes, either positive or negative, on the envelope delay versus baseband plot. These spikes were originally attributed to noise bursts. Later consistent test results show that these spikes

are not random, but in fact, tend to be repetitive at specific points within the frequency spectrum. The spikes are shown in figure 3.106 but do not appear in the other figures showing spacecraft loop test results due to the smoothing technique employed in plotting the data. Figure 3.107 shows the results of an RF loop test performed on the same day, at. the same site, and under the same conditions as the spacecraft loop test results shown in figure 3.106. Since these spikes are present in the spacecraft loop, but not in the RF loop, it is concluded that spikes on the envelope delay distortion versus baseband frequency plot are introduced by the spacecraft transponder. There is some speculation that this distortion is present only during the test because of transponder sensitivity to the characteristics of the test signal employed to measure envelope delay. Whether or not these spikes in the envelope delay response are actually present while a television signal is being transmitted is unknown. However, no degradation in picture quality that might be attributed to envelope delay discontinuity has been reported from the many TV demonstrations performed with the ATS-1 and ATS-3 satellites.

CCIR Recommendation 421-1 applies to the transmission of television signals over long distance international television circuits and is representative of the quality of performance that may be expected by users of a satellite system such as ATS. The limits contained in the recommendation as they apply to a 525 line TV system defined as System M (USA) are shown on the figures for reference. The general shape of the plots indicates the system should operate within these limits, yet the limits are often exceeded by the sharp spikes

This experiment was performed with and without the video pre-emphasis/ de-emphasis networks in the earth station equipment to determine the effects of these networks on envelope delay. Figure 3.106 shows typical results of a test performed with and without pre/de-emphasis in the spacecraft loop. Since the discontinuities introduced by the spacecraft make this figure somewhat difficult to analyze , figure 3.107 may be substituted. Both of these figures show the results of the same test run at the same site on the same day at the same peak to peak signal levels. The only difference being that figure 3.107 was run in the RF loop and figure 3.106 was run in the spacecraft loop. . Except for the spikes introduced by the spacecraft, the figures are essentially the same. The figures show that the emphasis networks cause a greater relative delay variation at the low end of the frequency band (below 1.5 MHz), while in the remainder of the frequency band of interest (1.5 MHz to 4.0 MHz), the delay variations are essentially the same. A vertical shift in the entire envelope delay curve is of no significance; only the relative variations in envelope delay with respect to frequency can cause signal distortion.

3.5.13.3 Conclusions

The results of this experiment have shown the following:

1) An overall baseband S/N ratio of about 30 db or more is required in order to obtain satisfactory test results with the available test equipment.

2) The degree of envelope delay distortion is, to a first order, not dependent on the deviation of the test signal, but the measurement accuracy is probably seriously affected by the fact that the S/N ratio, in the detector of the test equipment, is reduced at the high end of the baseband spectrum.

3) The test results show that the spacecraft transponders cause abrupt changes in envelope delay with respect to frequency. It is not presently known whether this distortion is generated at all times or just during testing. However, no degradation in picture quality that might be attributed to envelope delay discontinuity, has been reported from the many TV demostrations performed with ATS-1 and ATS-3.

4) The addition of the video pre/de-emphasis networks causes envelope delay variation to increase at frequencies below 1.5 MHz, but delay variation in the remainder of the frequency band is essentially unchanged.

5) Except for the narrow spikes, the measured envelope delay is within the limits recommended by the CCIR for the US and Canada. At no time have the spikes exceeded the less stringent CCIR recommended international limits.
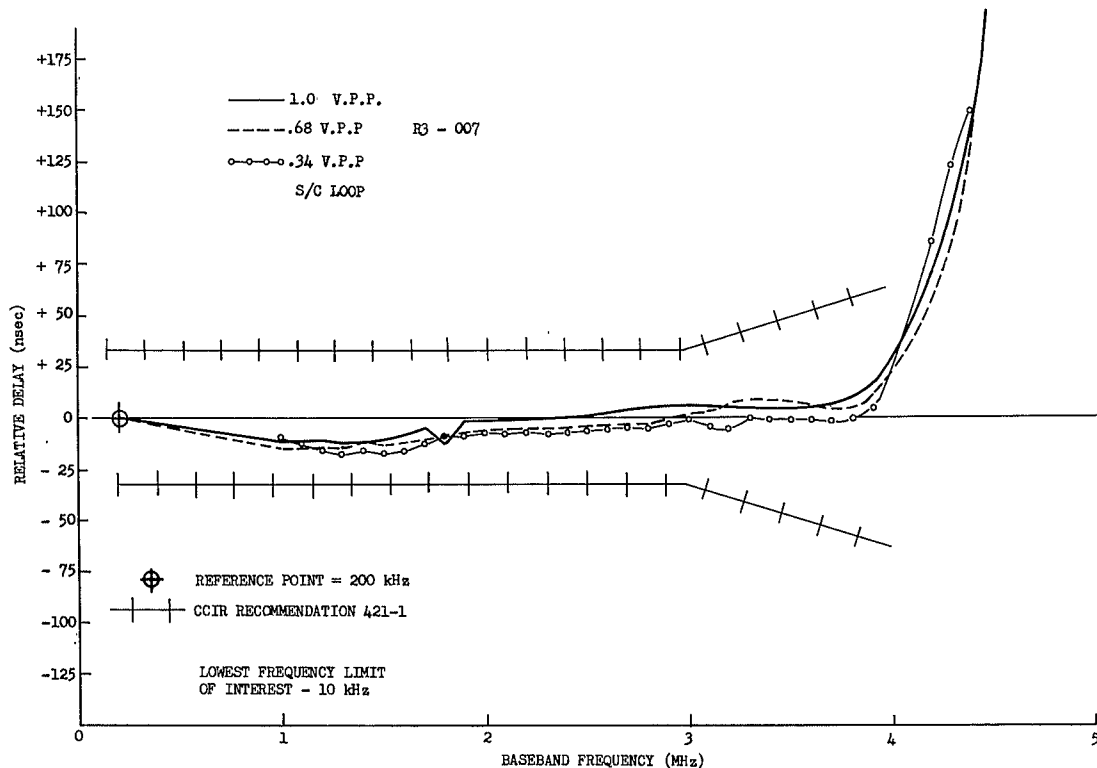
Figure 3.102. Baseband Envelope Delay Response, ATS-3, S/C Loop, FT Mode, FM Discr. (Rosman, 9 Aug. 68)
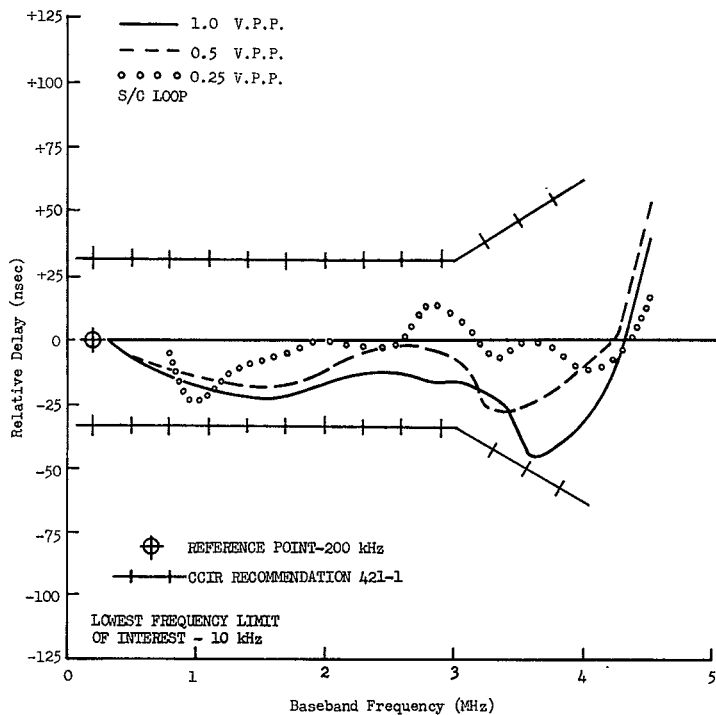
Figure 3.103. Baseband Envelope Delay Response, ATS-1, S/C Loop, FT Mode, FM Discr.
(Cooby Creek, 10 Feb. 68)

3.267
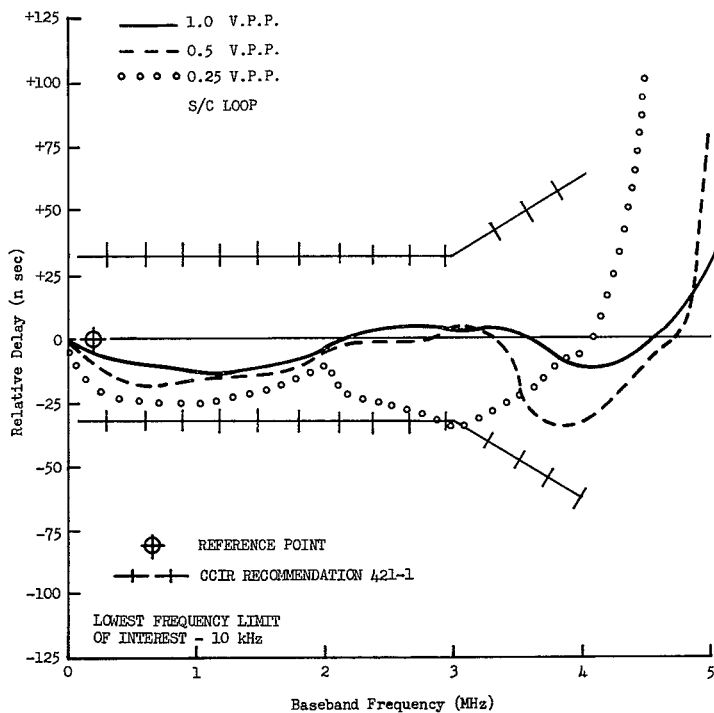
Figure 3.104. Baseband Envelope Delay Response, ATS-3, S/C Loop, FT Mode, FM Discr.
(Mojave, 26 Dec. 67)

3.268
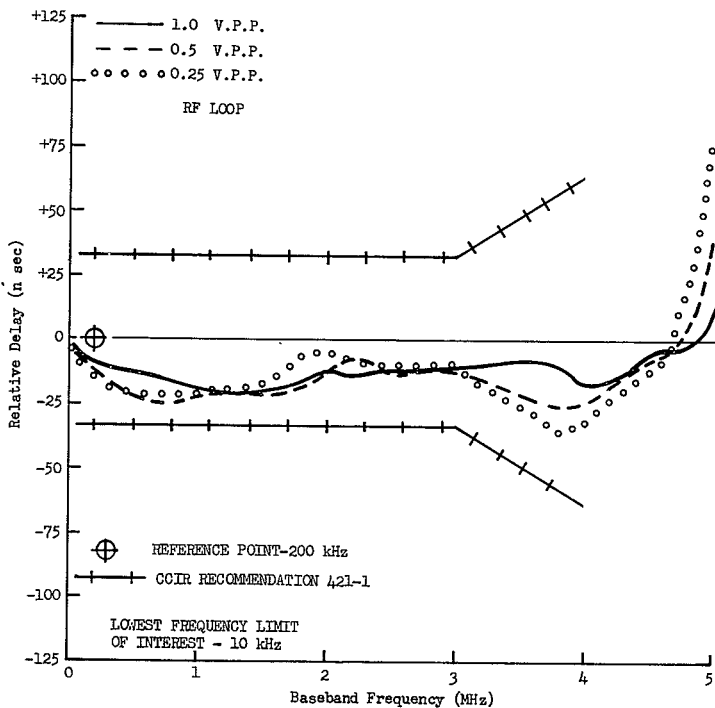
Figure 3.105.   Baseband Envelope Delay Response, RF Loop, FT Mode, FM Discr.
(Mojave, 26 Dec. 67)
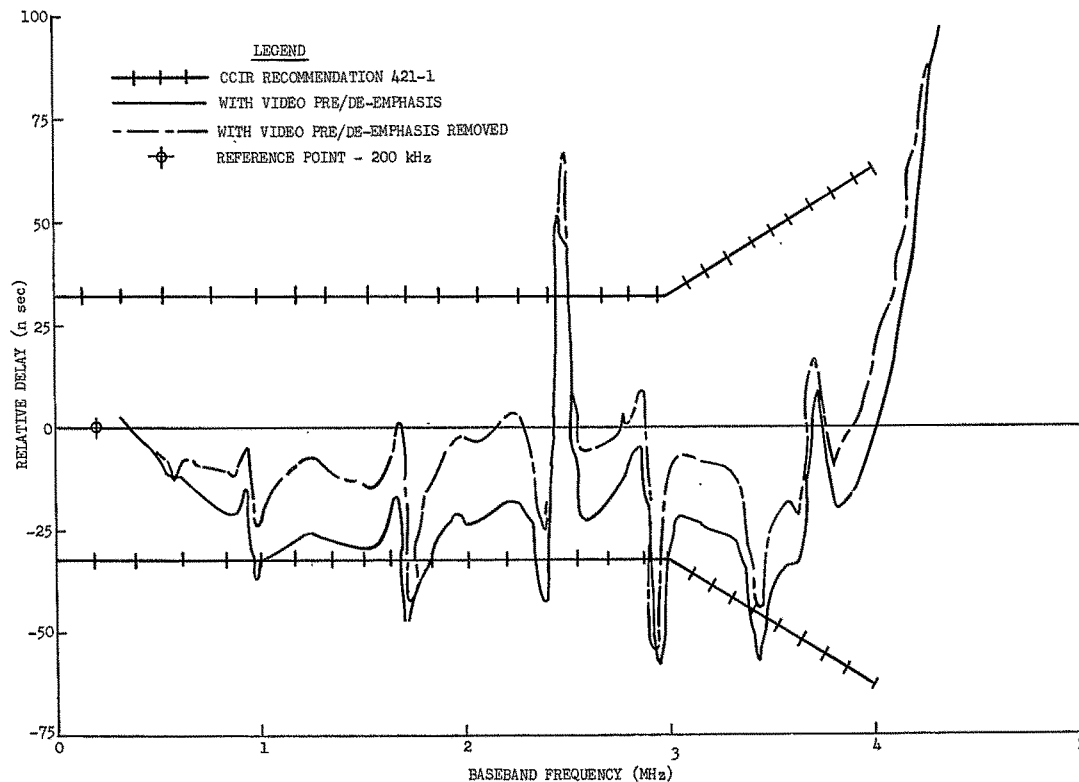
Figure 3.106   Baseband Envelope Delay With and Without Pre/De-emphasis
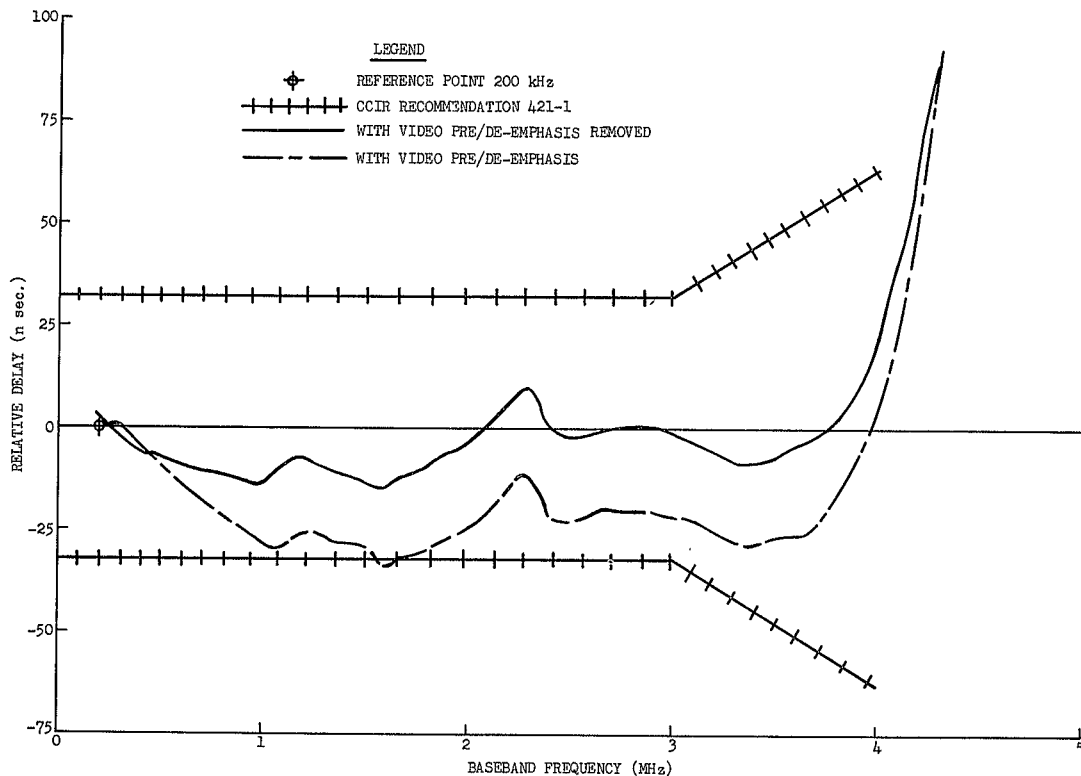
Figure 3.107. Baseband Envelope Delay in RF Loop With and Without Pre/De-emphasis

3.6 SPACECRAFT EXPERIMENTS

3.6.1 SPACECRAFT ANTENNA PATTERNS (R. L. Baldridge)

3.6.1.1 Description and Test Results

OBJECTIVE

The objective of this experiment is to verify that spacecraft antenna patterns can be measured at an earth station, and to determine the value of the technique. Only conical cuts of the antenna patterns are obtained. If full three dimensional patterns with a spin-stabilized spacecraft are desired, the spin axis would have to be placed in the earth's equatorial plane.

BACKGROUND

ATS-1 AND ATS-3

To make antenna pattern measurements from the ground it is necessary to vary the antenna pattern position in time and measure signal power received at the spacecraft and also at the ground. This is conveniently done in the case of the spin stabilized ATS-1 and ATS-3 spacecrafts. The transmit antenna pattern is measured by recording the power received at an earth station (AGC voltage) as the transmit pattern is made to precess, relative to the earth, about the spacecraft spin axis, with constant spacecraft transmitter power. The receive antenna pattern is measured by recording the spacecraft received power as the received antenna is made to precess about the spacecraft spin axis with constant ground transmitter power. For this purpose, a single sideband pilot tone is transmitted to the spacecraft in the MA mode. The pilot level received at the spacecraft is determined by measuring the pilot level at the ground station after phase demodulating the signal from the spacecraft. (In the MA mode the spacecraft phase modulates the single sideband AM signal received from the ground.) The transmit and receive antenna patterns can in this way be recorded simultaneously.

The spacecraft antenna patterns are made to rotate about the spacecraft by changing the despin rate of the antenna pattern while the spacecraft spin rate remains constant. The precession rate is equal to the difference between the spacecraft spin rate and the antenna pattern despin rate. Each 360-degree rotation of the beam provides a complete conical cut of the antenna pattern at the antenna angle, which is the complement of the aspect angle. The antenna geometry is shown in figure 3.108. In the normal attitude, the aspect angles from which available earth stations can view the spacecraft are about 94 degrees from Cooby Creek and about 84 degrees from both Rosman and Mojave for ATS-3. Therefore, only Rosman and Mojave are capable of obtaining ATS-3 antenna patterns. These aspect angles vary slightly within a 24-hour period. All stations can view the ATS-1 spacecraft.

Although, ATS-5 was to be gravity-gradient stabilized, technical difficulties prevented deployment of the gravity gradient stabilization system. ATS-5 is presently spinning at a rate of approximately 76.2 rpm and has no despun antennas like ATS-1 and ATS-3.

Due to this relatively rapid antenna spin rate, certain changes in the test procedure are necessary to record the antenna patterns. The same test procedure as used on ATS-1 and ATS-3 was used with the following two exceptions. First, since the antennas on ATS-5 are already spinning with respect to the earth, it is no longer necessary (or possible, since the antennas cannot be despun) to make the antennas precess, relative to the earth, about the spacecraft spin axis. Secondly, since the strip-chart recorder used to record ATS-1 and ATS-3 is not capable of following the rapid changes in level. (due to the rapid spin rate) it is replaced by a Honeywell 1508 Visicorder.

RESULTS

The measured transmit and receive antenna patterns for ATS-3 are shown in figures 3.109 and 3.110, respectively. These are shown in polar form in figures 3.111 and 3.112. These patterns were taken with an antenna precession period of about 5 minutes. The width of the lines in figures 3.109 and 3.111 indicate the level of spin modulation on the pattern. In figure 3.112, the front 230 degrees of the received pattern are reproduced. The absolute levels shown in these figures are arbitrary. The levels relative to isotropic cannot be determined from isolated conical cuts, so the antenna gains cannot be determined from these results. Replication of only the transmit antenna pattern has been achieved.

A measured transmit antenna pattern for ATS-1 is shown in figure 3.115. This pattern was obtained by recording the AGC of the SHF tracking receiver utilizing an AGC time constant of three seconds. Figure 3.116 shows the preflight transmit antenna pattern. It should be noted that other transmit antenna patterns have been obtained and the results are very similar to the preflight transmit antenna pattern.

The ATS-1 receive antenna pattern cannot be measured since it is omidirectional.

Figures 3.117 and 3.118 show the ATS-5 transmit antenna patterns for the planar array and the omni antenna, respectively. The ATS-5 planar array receive antenna pattern is shown in figure 3.119. All of these patterns were derived from measurements made at Mojave with the S/C spinning at about 76 revolutions per minute. This means that signal transmission to and from the satellite is possible for approximately 50 milliseconds per revolution (3-db beamwidth) when using the planar array antennas. Due to the measuring technique used, only about 40 percent of the planar array receive pattern can be measured. However, the main lobe is included in this 40 percent.

For comparison, prelaunch antenna patterns for each of the above cases are shown in figures 3.120 through 3.122.

3.6.1.2 Analysis

 To verify that orbiting spacecraft antenna patterns can be measured from the ground it must be shown that the recorded variations in signal levels are indeed produced by the antenna gain variation with antenna beam attitude and not by some other mechanism. This can be shown by repeating the measurements on separate occasions. The level variations due to the antenna pattern rotation will be reproduced but other variations will not.

 Replication of the ATS-3 transmit antenna pattern has been achieved on different occasions and with different antenna pattern precession rates so the pattern presented is an accurate representation of the actual pattern.

 Replication of the ATS-1 transmit antenna pattern has also been performed with a fair degree of correlation with the preflight transmit pattern.

 Replication of the ATS-3 receive antenna pattern has not been achieved, but there is reason to believe that the pattern presented is an accurate representation of the actual pattern. Note that the in-orbit measured transmit antenna pattern closely resembles the preflight measured transmit pattern. (See figure 3.113.) It would be expected that the in-orbit measured receive antenna pattern would likewise resemble the preflight receive antenna pattern because the transmit and receive antenna patterns are of the same design and are constructed on the same assembly. These receive patterns are very similar. (See figures 3.112 and 3.114.)

 No replication of the ATS-5 antenna patterns has been achieved. However, the measurements do appear to be quite similar to measurements made prior to launching the spacecraft.

A comparison between the ATS-1 transmit antenna pattern and the preflight pattern indicates that good correlation exists (see figures 3.115 and 3.116).This is especially noted in comparing the beamwidths, depth of nulls and sidelobe gains.

The value of measuring ATS spacecraft antenna patterns in orbit is twofold. The technique provides a means of determining changes in the pattern due to the launch or to the space environment, and the technique provides a good measure of the antenna nulls, side lobes, and back lobes, free from reflection and near field effects present on a ground test range. Note that these effects are present in the preflight antenna patterns and not in the patterns made while in orbit. In other space systems there may be other applications of this technique.

There is an additional advantage of the inflight patterns over the preflight antenna patterns. The inflight patterns display well-defined spin modulation. The mechanism that produces this spin modulation was present when the preflight patterns were measured, but it was not controlled. If the preflight patterns were obtained by rotating the antenna reflector and the spacecraft body, the actual patterns could be either higher or lower than the preflight measurement by the amount of the spin modulation. If the preflight patterns were obtained by rotating the antenna reflector while holding the spacecraft body fixed, the actual patterns could be both higher and lower than the preflight measured pattern. The result is that the preflight pattern may be in error by plus or minus the spin amplitude modulation. This advantage of the inflight measurement could have been realized on preflight pattern measurements by altering the procedure to provide for spacecraft spin-up.

3.6.1.3 Conclusions

The ATS-3 transmit antenna pattern and partial receive antenna pattern have been measured after launch at an aspect angle of 84 degrees, and are shown in figures 3.109 through 3.112.   The patterns are similar to the preflight measured patterns but provide a more accurate measure of the far field pattern free from reflection distortions.

The same condition exists for the ATS-1 transmit antenna patterns. In comparing the ATS-1 transmit antenna pattern with the preflight transmit pattern it is seen that these patterns are quite similar.

ATS-5 antenna patterns are also quite similar to preflight patterns.

Figure 3.108 Antenna System Coordinates for Spin-Stabilized Satellites ATS-1 and ATS-3
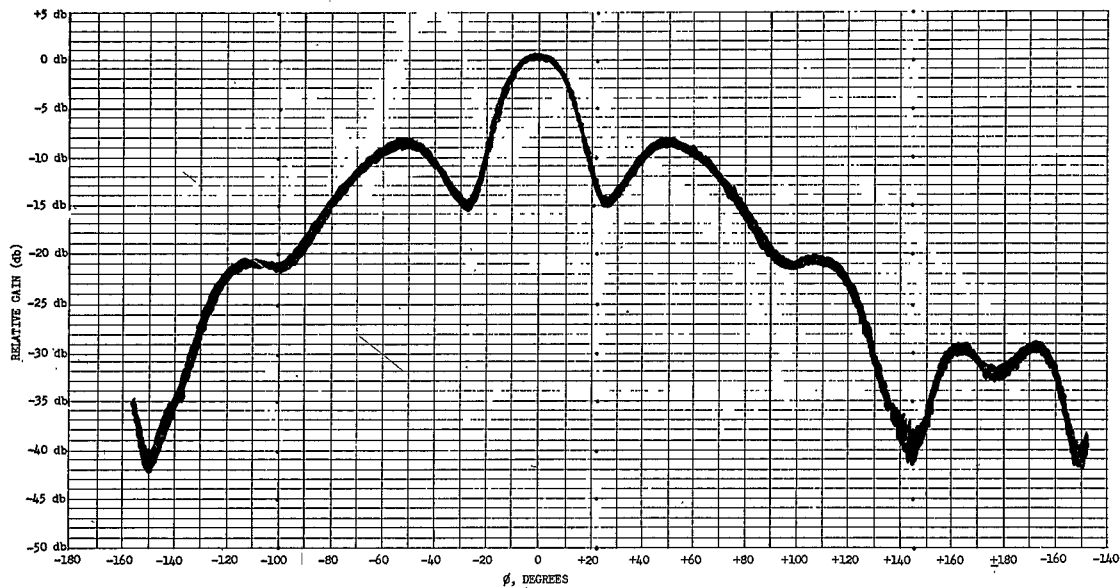
Figure 3.109. ATS-3 Transmit Antenna Pattern, Aspect Angle 84 Degrees
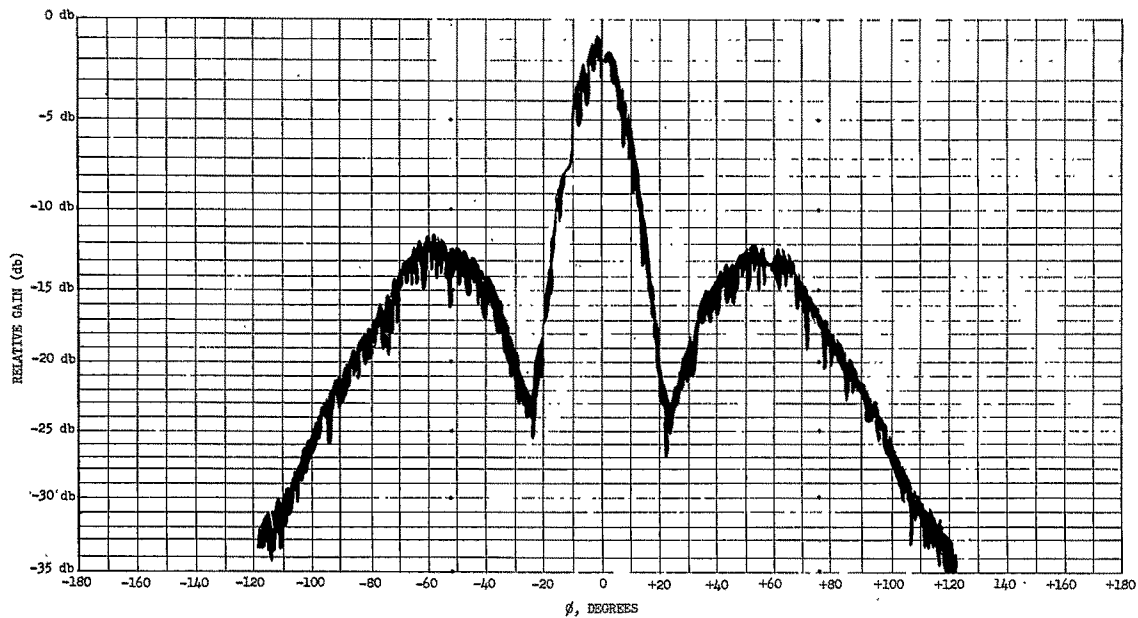
Figure 3.110   ATS-3 Receive Antenna Pattern, Aspect Angle 84 Degrees
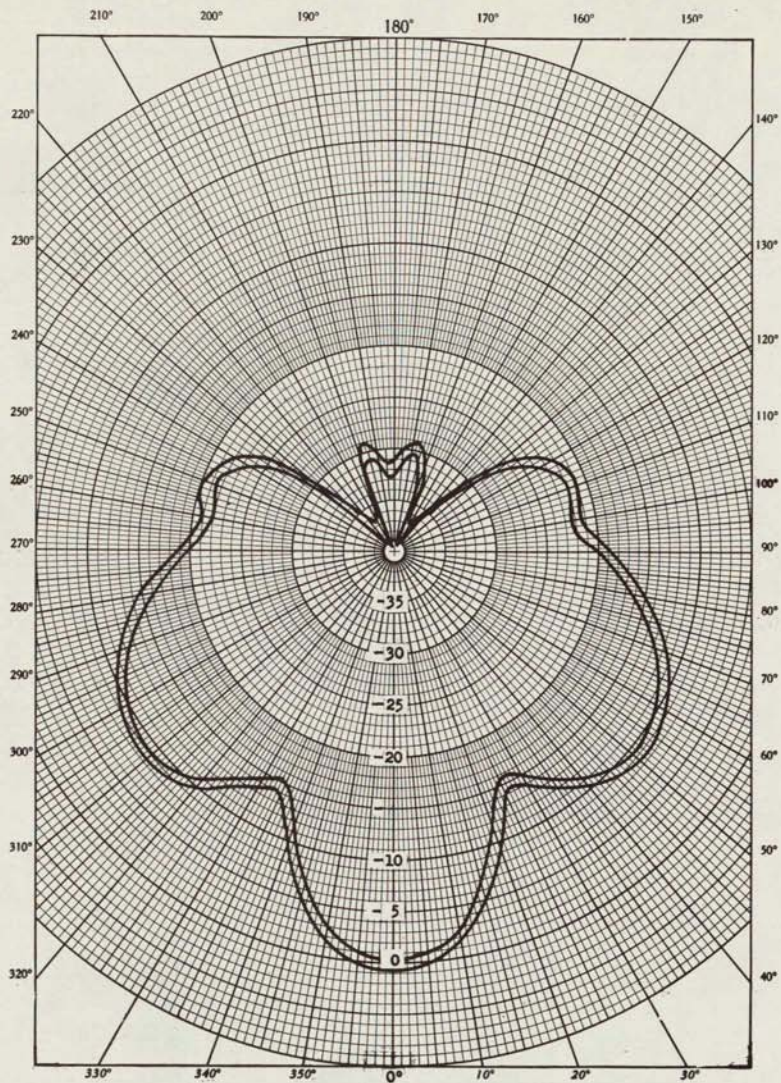
Figure 3.111 ATS-3 Transmit Antenna Pattern, Aspect Angle 84 Degrees

VI
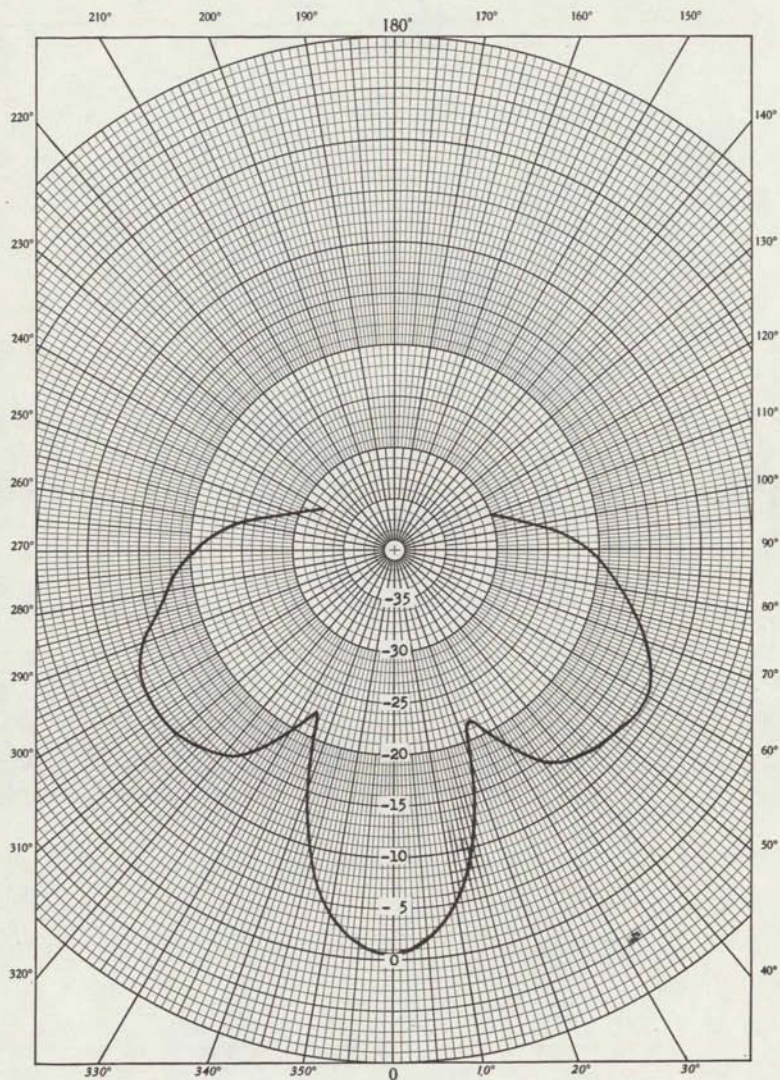
Figure 3.112 ATS-3 Receive Antenna Pattern, Aspect Angle 84 Degrees

3.280
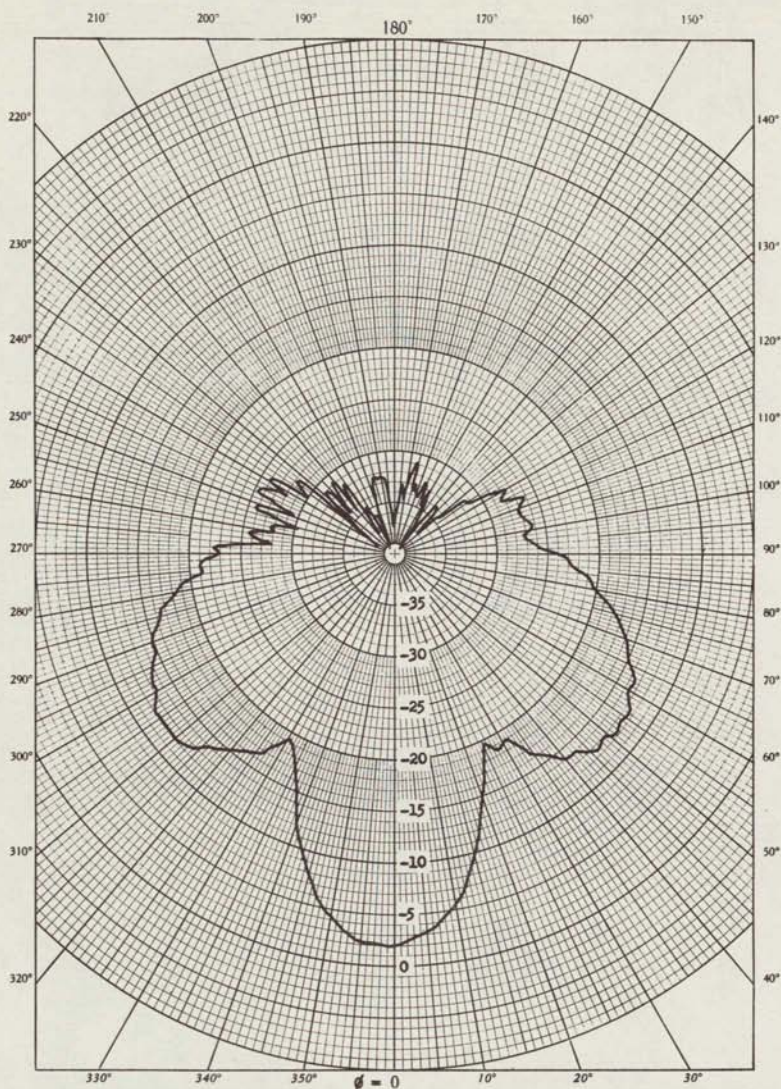
Figure 3.113 ATS-3 Preflight Transmit Antenna Pattern, Aspect Angle 85 Degrees

3.281
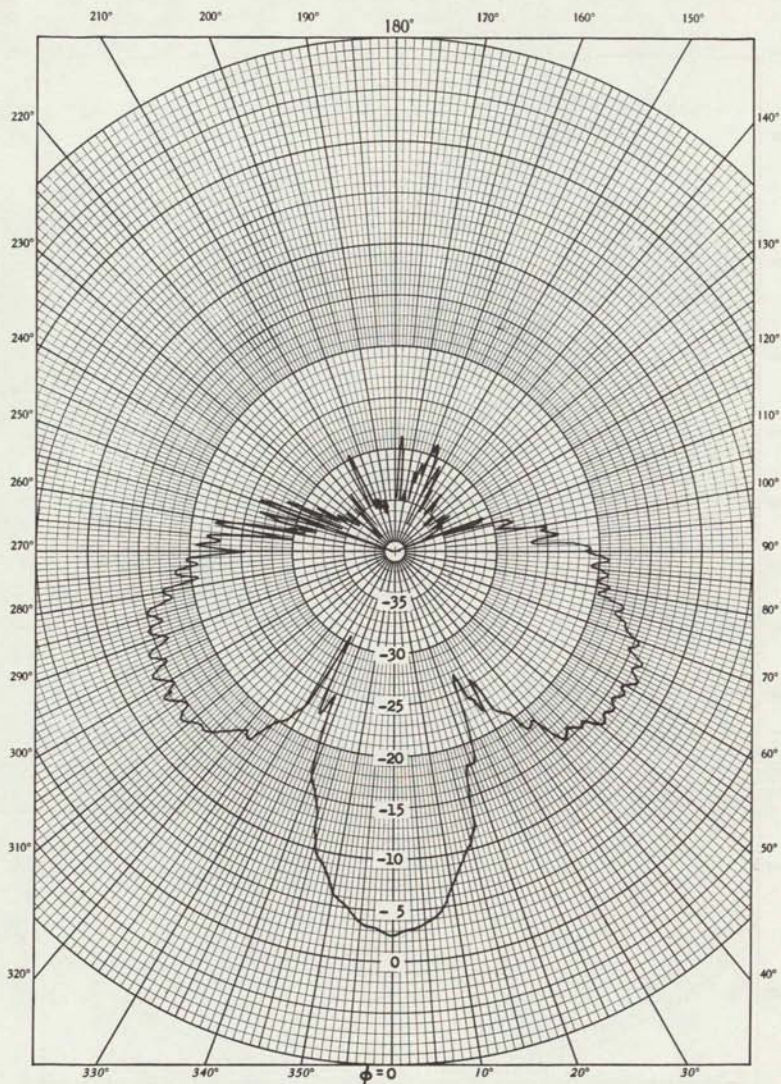
Figure 3.114 ATS-3 Preflight Receive Antenna Pattern, Aspect Angle 85 Degrees
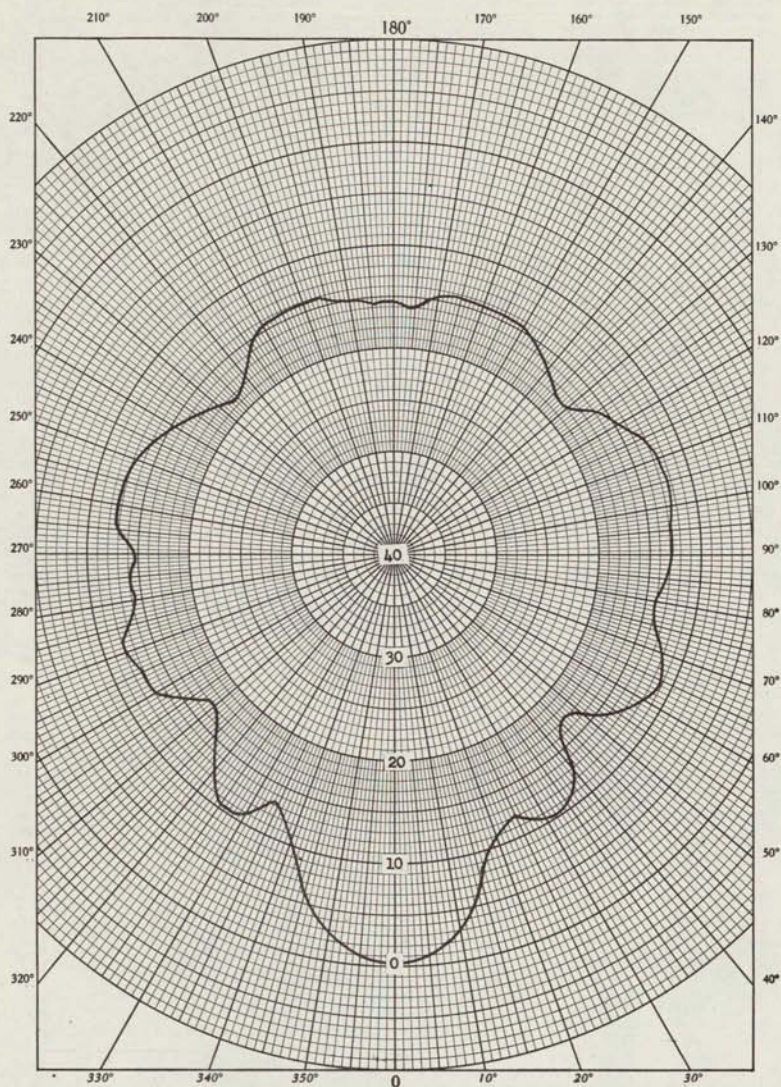
Figure 3.115. ATS-1 Transmit Antenna Pattern, Aspect Angle 85 Degrees

3.283
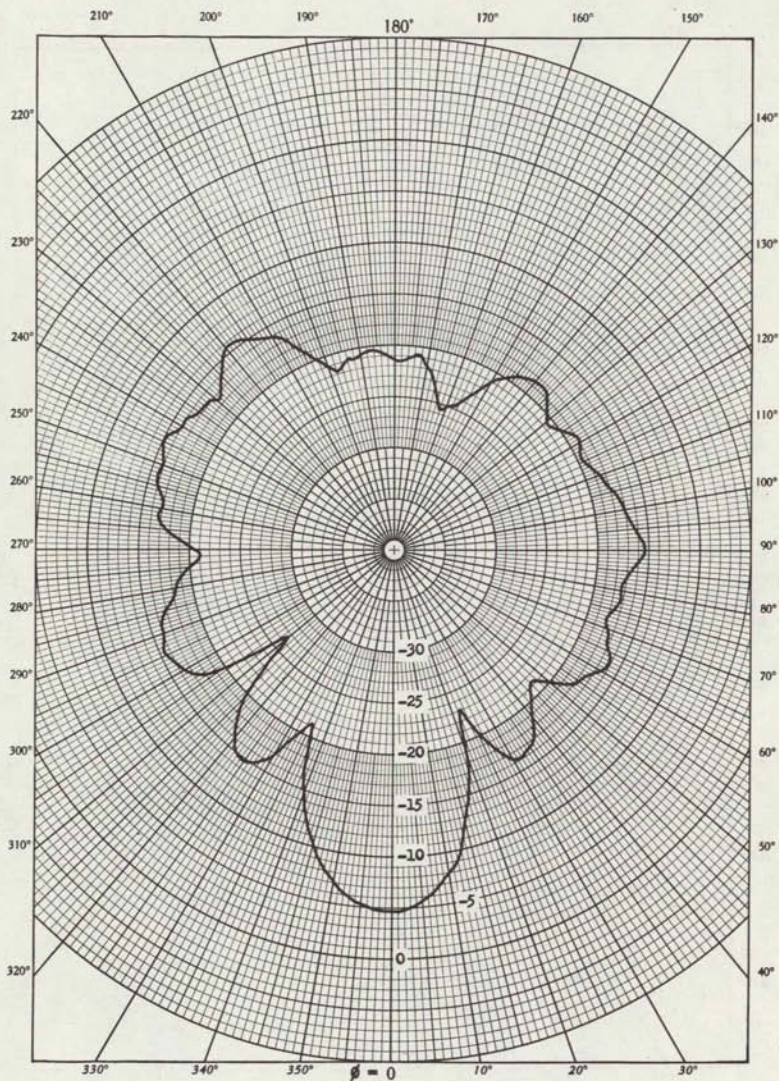
Figure 3.116. ATS-1 Preflight Directional Transmit Antenna
Pattern, Aspect Angle 95°, θ = 85°

3.284
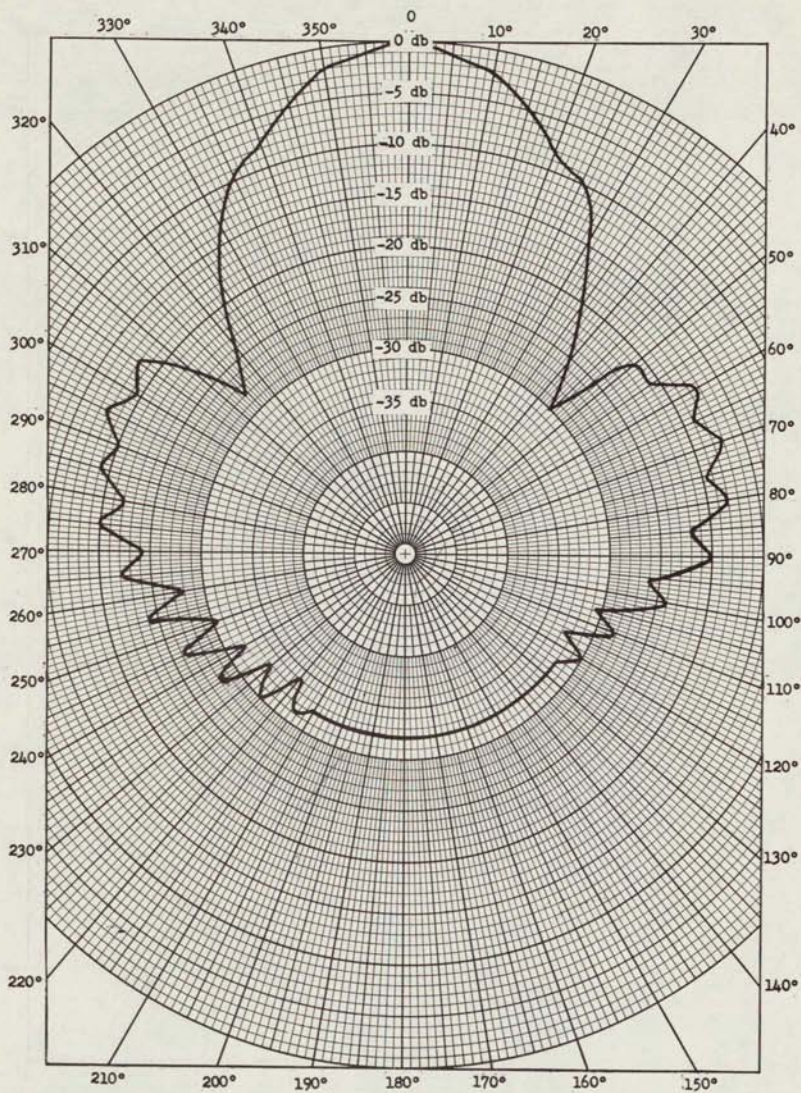
Figure 3.117. ATS-5 Transmit Antenna Pattern (Planar Array) (Measured at Mojave)

3.285
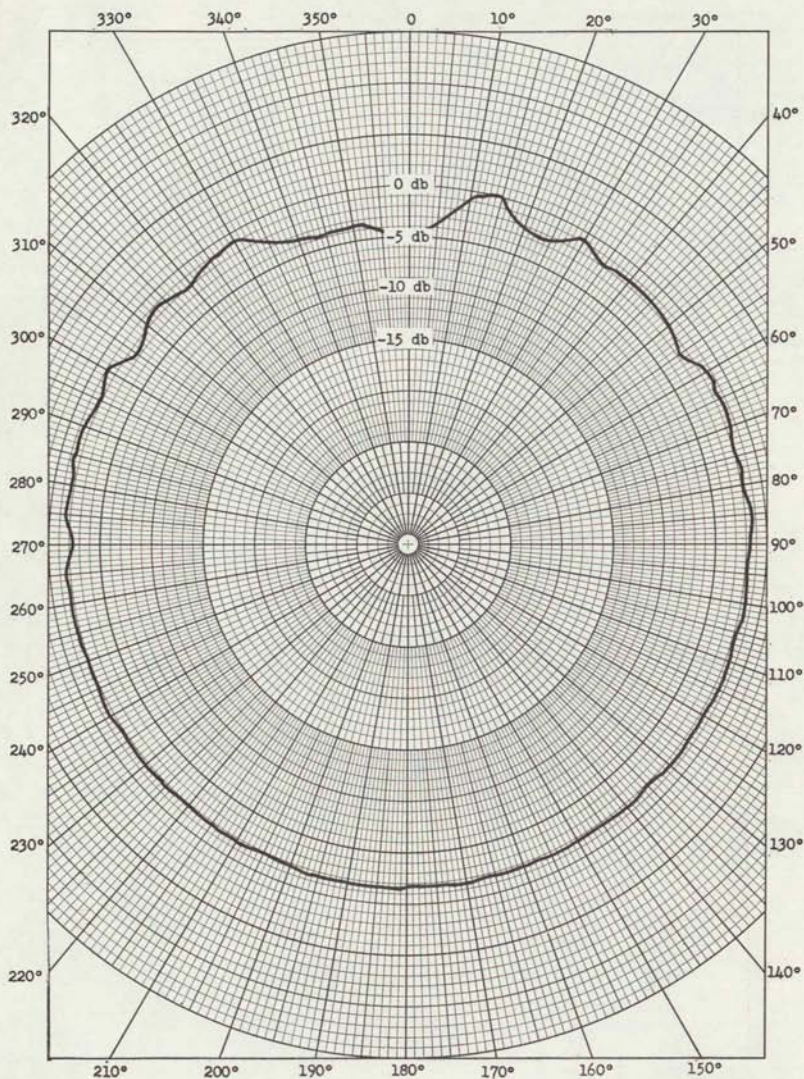
Figure 3.118. ATS-5 Transmit Antenna Pattern (Omni Antenna) (Measured at Mojave)
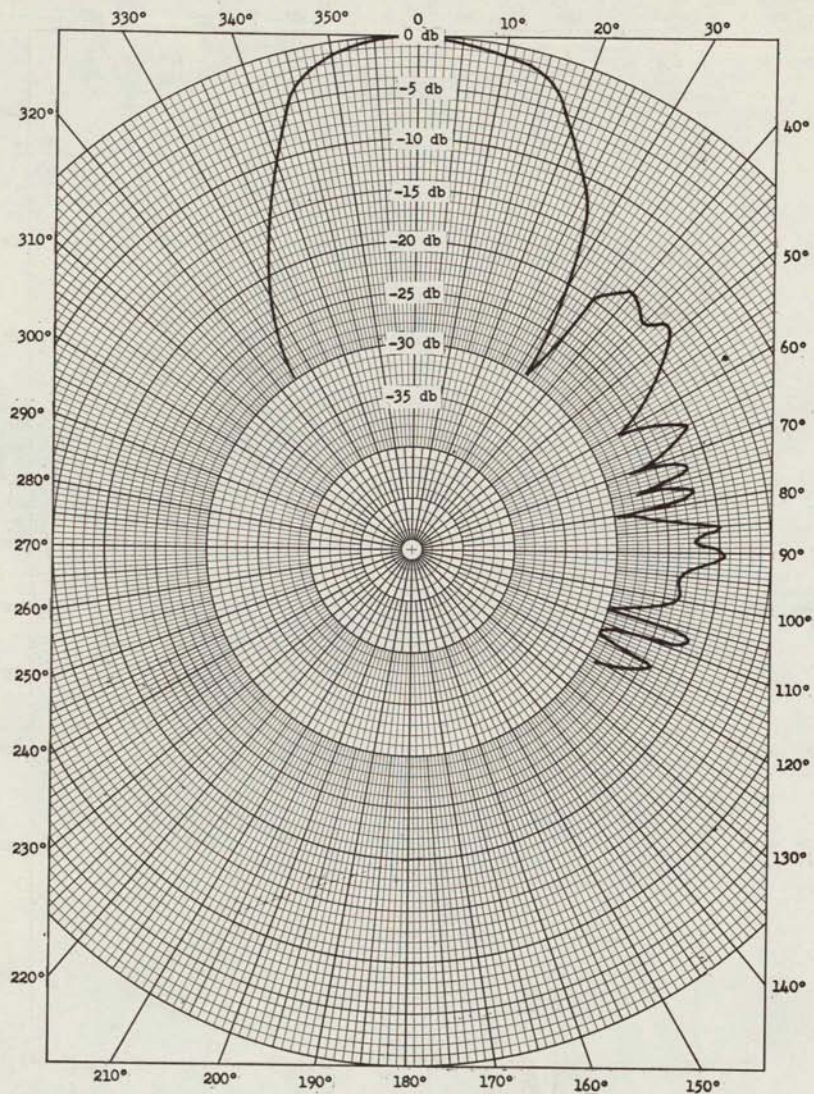
Figure 3.119. ATS-5 Receive Antenna Pattern (Planar Array) (Measured at Mojave)

3.287
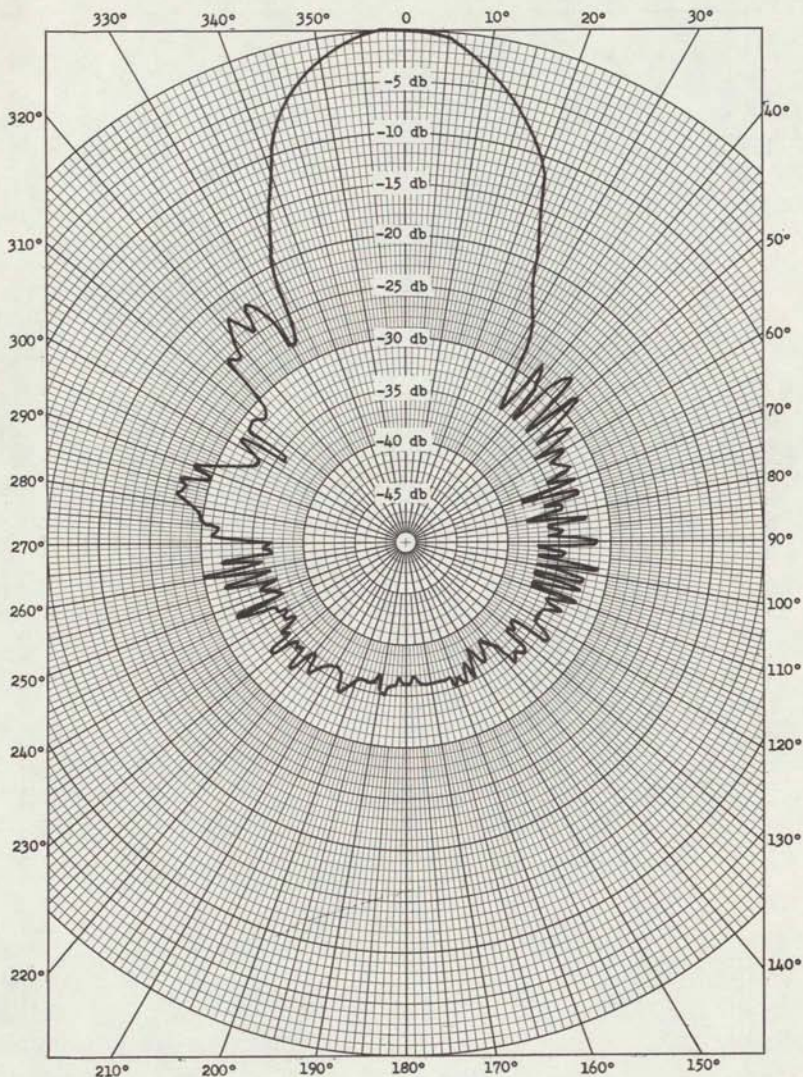
Figure 3.120. ATS-5 Transmit Antenna Pattern (Planar Array) (Measured Prior to Launch)
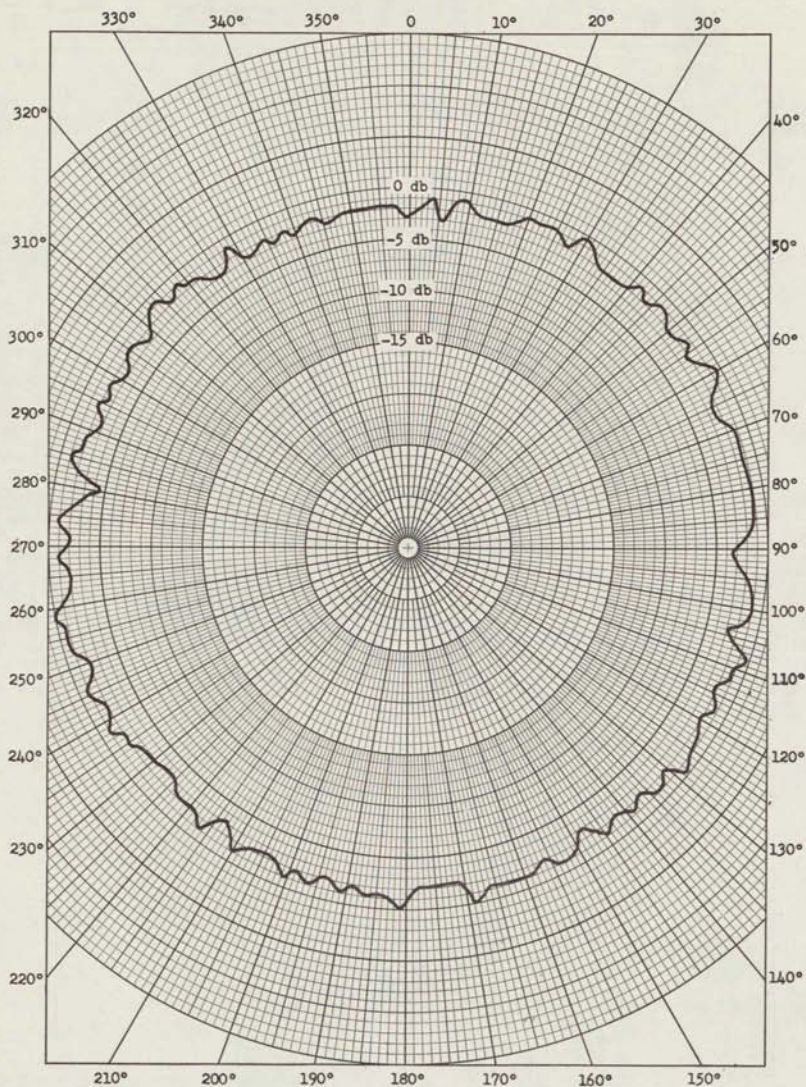
Figure 3.121. ATS-5 Transmit Antenna Pattern (Omni Antenna) (Measured Prior to Launch)
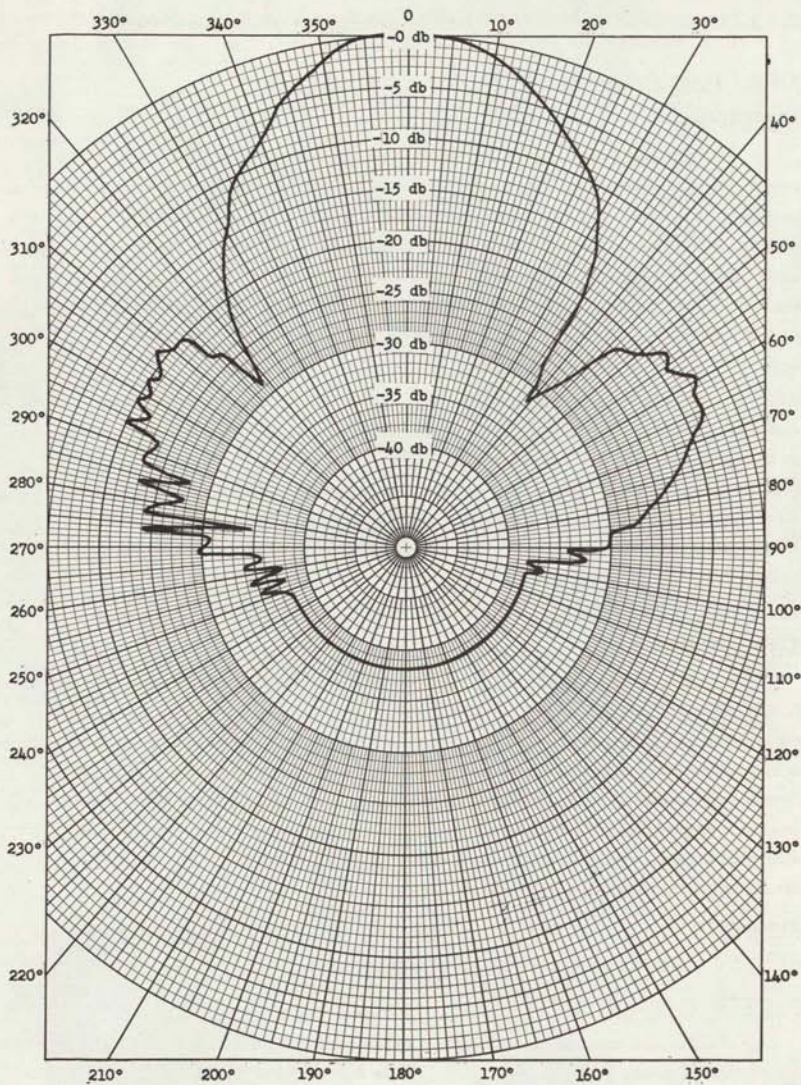
Figure 3.122. ATS-5 Receive Antenna Pattern (Planar Array) (Measured Prior to Launch)

3.6.2 CARRIER MODULATION DUE TO SPIN (MA-SP-1.1) (R. L. Baldridge and
G. K. Kuegler)

3.6.2.1 Description and Test Results

OBJECTIVES

The major objective of this experiment is to measure the modulation at the
spacecraft spin frequency and its harmonics produced upon reception and upon transmission
of signals at the spacecraft as a result of the spacecraft's spinning, and to determine,
where possible, the probable cause of the modulation. Since this modulation is introduced
by the spacecraft antennas, and because of the approach of this experiment in measuring
the modulation, the experiment is an antenna subsystem rather than a communication
system experiment. In this experiment, four antenna subsystems of three different types
are considered.

A secondary objective of this experiment, which is more in the nature of a
communication test objective, is to determine the effect of the automatic level control loop
on the spin amplitude modulation produced by the satellite receiving antenna. The pilot
tone for level control will undergo the same spin modulation effect as the 1-kHz tones;
therefore, when using the automatic level control, the 1-kHz tones will contain the effect of
any automatic adjustments of the single-sideband transmitted power. This effect is evalu-
ated by comparing the amplitude modulation on the received 1-kHz tone measured with
automatic level control, with that measured without automatic level control.

TEST CONDITIONS

To determine the spin modulation produced by the spacecraft antennas, the test
is performed in the MA mode. An AM detector is placed at the output of a multiplex
receive channel to determine the amount of amplitude modulation present on a 1-kHz or a
3-kHz submultiplexed tone,transmitted and received at the Mojave ground station. The
frequency modulation on a similarly multiplexed tone is also recorded. These modulations
are the spin modulation produced by the spacecraft receiving antennas. To determine the
spin amplitude modulation produced by a spacecraft transmitting antenna, the amplitude
variations of the carriers received from the spacecraft are measured.

STANDARDS

There are no known standards which are applicable to this experiment.

RESULTS

The measured spin modulation characteristics for the ATS-1 collinear array and
for the phased array antenna are shown in figures 3.123 through 3.126. The spin amplitude

modulation characteristic for the ATS-3 mechanically despun receive antenna is shown in figures 3.127 through 3.129.

3.6.6.2 Analysis

The three types of antennas considered are the ATS-1 receive antenna, a spinning collinear array; the ATS-1 transmit antenna, an electronically despun-phased array; and the ATS-3 transmit and receive antennas, which are both mechanically despun antennas. The parameters required to determine the spin amplitude and angle modulation produced by the receive antennas on both satellites and the spin amplitude modulation produced by the transmit antennas on both satellites are measured in this experiment. The spin angle modulation produced by the transmit antennas is not measured because the results of such a measurement are not significant to the communications experiments on the ATS program.

ATS-1 COLLINEAR ARRAY SPIN AMPLITUDE MODULATION

In the ATS-1 receive antenna spin amplitude modulation shown in figure 3.123, the spin frequency of the spacecraft and twice the spin frequency of the spacecraft are apparent. The peak-to-peak variation is approximately 1 db.

The results of the Fourier Analysis is depicted in the amplitude spectrum of figure 3.124. The 1st, 2nd, 3rd, 4th, 5th, and 8th harmonics of the spin rate are evident. The frequency and magnitude of the 1st and 2nd harmonic have been resolved[47] to 1.5613 and 3.12295 Hz, and 0.071 and 0.1025-volt peak, respectively. The 8th harmonic has a level of 0.02-volt peak. These levels can be converted to percent modulation using the curves of figure 3.130. The curves in this figure are the calibration of the AM detector output as a function of percent modulation. The primary curve was obtained from a 10-Hz modulating signal by varying the percent modulation from 2 to 6 percent. The family of curves was obtained by inserting different modulating frequencies from 1 to 10 Hz at a constant 5-percent modulation and graphically extrapolating the curves associated with each modulating frequency.

From this figure, it can be seen that the levels of the 1st and 2nd harmonics of the spin frequency correspond to 4 percent modulation. The 8th harmonic corresponds to 1 percent modulation.

The automatic level control loop has no apparent effect on the spin-amplitude modulation produced by the spacecraft receiving antenna. This is expected because of its low-response time.

ATS-1 COLLINEAR ARRAY SPIN-ANGLE MODULATION

The receive antenna spin frequency modulation for ATS-1, shown in figure 3.125, agrees with the model developed in section   5.1 of this report which considers the effect of the phase center being offset from the spin axis. It is seen from the figure that the peak frequency variation, Δf is about 1.0 Hz. This produces a peak-phase deviation of 0.635 radians. (For sinusoidal modulation μ is given by Δf divided by the modulation frequency which is, in this case, the spin frequency, 1.58 Hz.) Recalling equation 56 from section   5.1 which relates the phase deviation to the misalignment, it can be determined that such a phase modulation could result if there were a misalignment of only 0.246 cm between the S/C spin axis and the electrical phase center of the spacecraft receiving antenna.

ATS-1 PHASED ARRAY SPIN AMPLITUDE MODULATION

The transmit phased array antenna on ATS-1 consists of eight phase shifters driving sixteen elements. Misalignment in the radiation elements or in the phase shifters could cause strong harmonics in the spin amplitude modulation characteristic of this antenna up to eight or sixteen times the basic spin frequency. A second possible source of 8th harmonic and multiples of the 8th harmonic modulation is the telemetry whip antenna which pass between the antenna and the ground eight times per revolution. Although the eighth harmonic is not the only harmonic in this characteristic, its presence is apparent. (See figure 3.126.) The maximum and minimum points lie very nearly 45 degrees apart, as can be seen in figure 3.126, in which the spacecraft transmit spin amplitude modulation characteristic is shown along with a graph of its maximum and minimum points. Four of these points are not true maximum or minimum in that their first derivatives are not equal to zero, but they are so identified because there is an apparent trend to a maximum or minimum where these maximums and minimums are expected for pure eighth harmonic. The technique of recording the modulation on a stripchart will diminish eighth harmonics considerably and will completely remove multiples of the eighth harmonic due to the low frequency response of the stripchart.

ATS-3 RECEIVE MECHANICALLY DESPUN ANTENNA SPIN AMPLITUDE MODULATION

Figure 3.127 is a stripchart recording of the detected AM on a 3-kHz submultiplexed tone. The peak-to-peak variations appear to be approximately 1 db. The eighth harmonic of the S/C spin rate is clearly visible.

Unfortunately, the data was not calibrated and the percent modulation of each frequency component cannot be determined.

Figures 3.128 and 3.129 indicate the relative magnitude of the various harmonics of the S/C spin rate. The x's indicate the resolved levels at the spin rate and harmonics. A comparison of these figures with figure 3.124 indicate that ATS-3 is much richer in harmonic content than ATS-1. Particularly the multiples of the eighth harmonic which are much more severe with the mechanical despun antenna than with the collinear array antenna (ATS-3 and ATS-1 respectively).

3.6.2.3 Conclusions

The following conclusions can definitely be made.

First, the ATS-1 collinear receive antenna spin phase modulation is large (±0.635 radians) and free of harmonics. This means that the antenna phase center is not on the spin axis. In fact, on 11 November 1967, it was 0.246 cm off axis. Whether this is due primarily to a tilt of the spacecraft and/or antenna, or to an electrical misalignment is not clear.

Second, the ATS-1 collinear receive antenna spin amplitude modulation is about 1 db peak-to-peak. The AM consists of harmonics of the S/C spin rate. The first and second S/C harmonic frequencies are probably present because of an asymetrical receiving antenna radiation pattern. The eighth harmonic is probably due to the interaction with the eight telemetry whip antennas that are fixed about the SHF receive antenna.

Third, the ATS-1 phased array transmit antenna spin-amplitude modulation is small (0.4 db peak-to-peak) and contains strong harmonics of the spin frequency, most notably the eighth. This could be due to the eight phase shifters or to the light telemetry antennas.

Fourth, the ATS-3 mechanically despun receive antenna spin amplitude modulation has a large eithth harmonic and is rich in multiples of the eight harmonic of the S/C spin rate. There is also a notable first and second harmonic of the S/C spin rate. This is probably due to the telemetry whips revolving in front of the SHF antenna. Because of the large number of multiples of the eighth harmonic present, it can be concluded that there is an abrupt change in the radiation pattern at 8 times the spin frequency. The cause of the large fundamental component is more difficult to ascertain. Since ATS-3 has a mechanical despun antenna for both the receive and transmitted signal, the only way to alter the radiation pattern at the S/C spin rate is to change the relative position between the feed and the reflector. This change of focus will deteriorate the radiation pattern and therefore change the gain of the antenna as a function of S/C rotation.

Fifth, the ALC loop in the MA mode has no effect on the spin-amplitude modulation produced by the collinear-array receiving antenna.
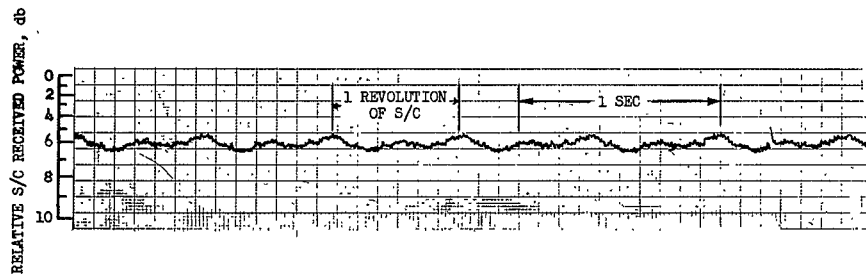
Figure 3.12
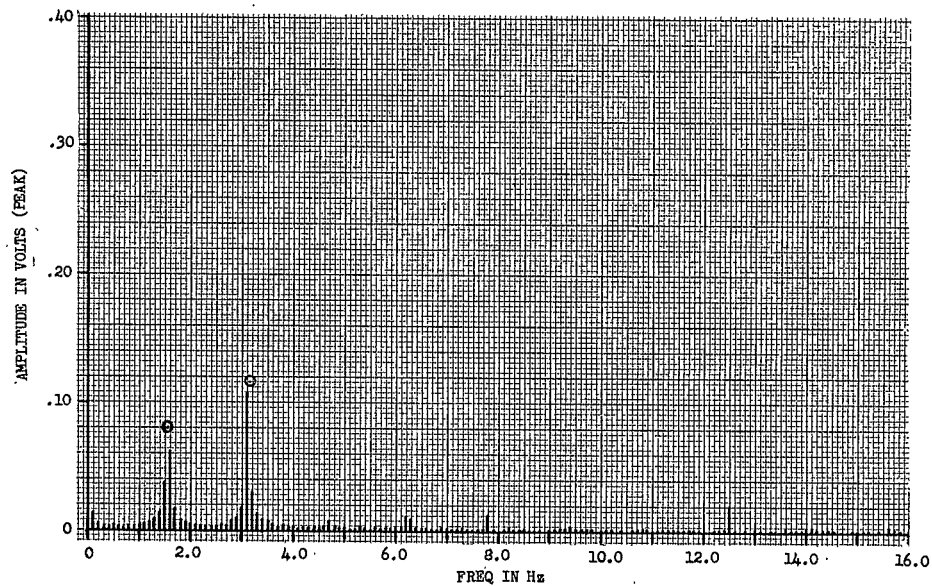
Figure 3.124. ATS-1 Receive-Antenna Spin-Amplitude-Modulation Spectrum
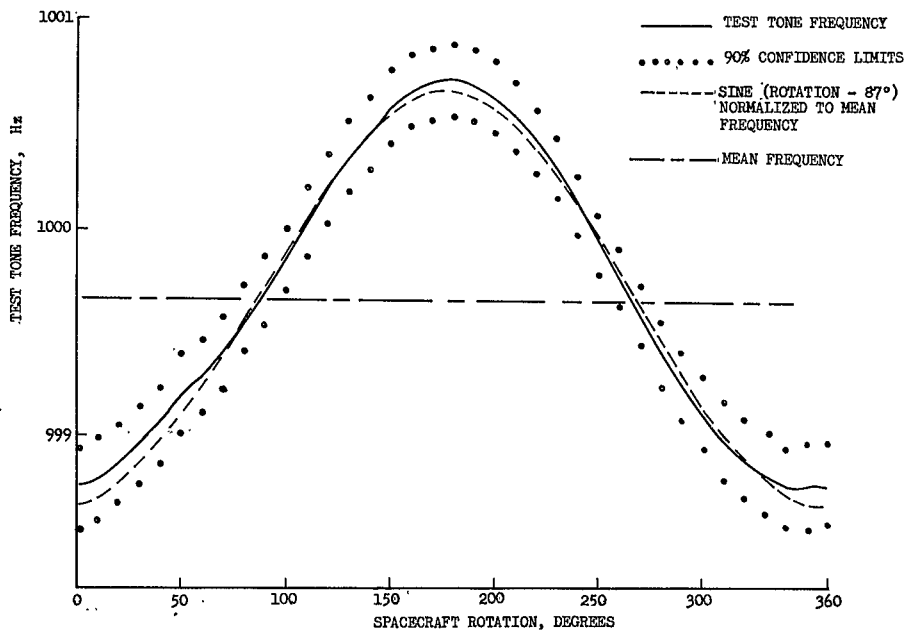
Figure 3.125. ATS-1 Receive-Antenna Spin-Frequency Modulation

3.298
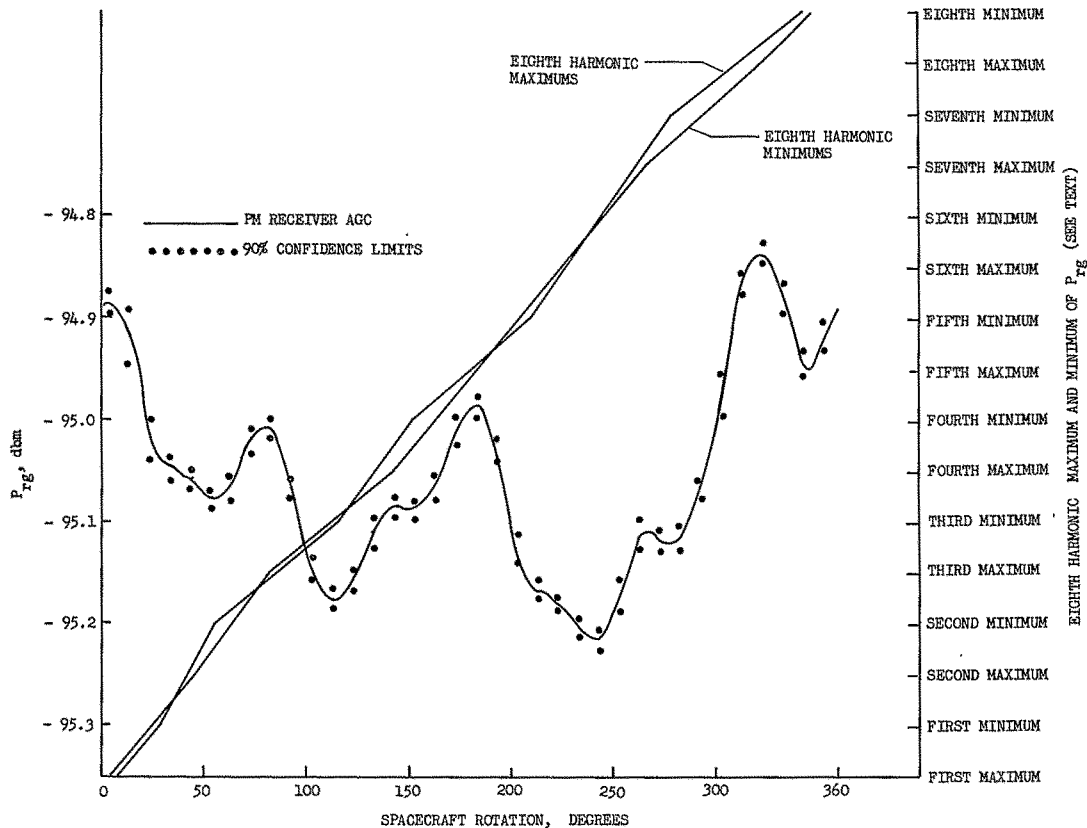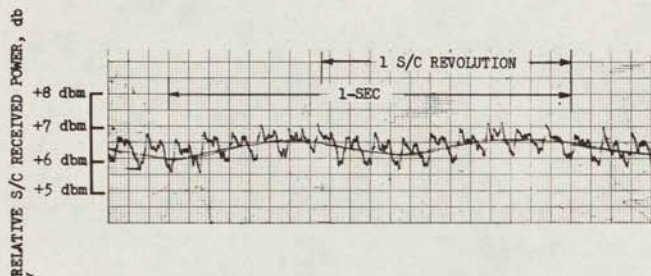
Figure 3.127. ATS-3 Receive Antenna Spin-Amplitude Modulation

3.300
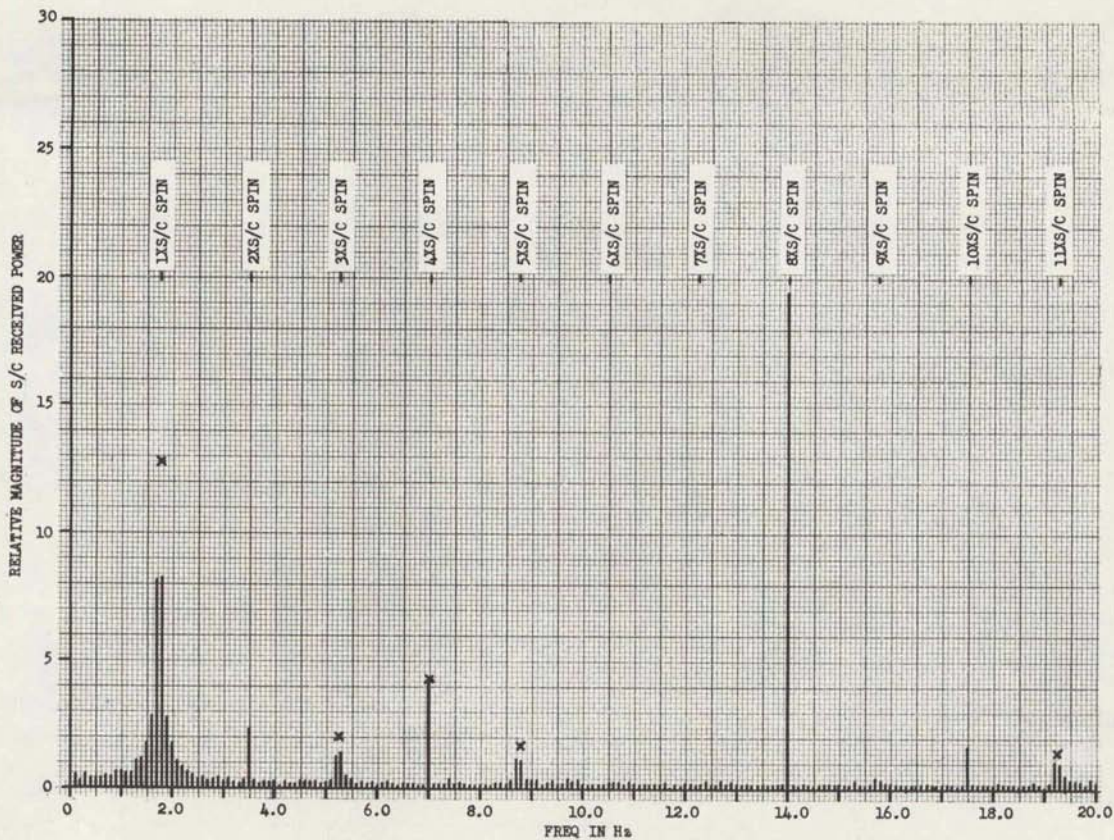
Figure 3.128. ATS-3 Receive-Antenna Spin-Amplitude-Modulation Spectrum
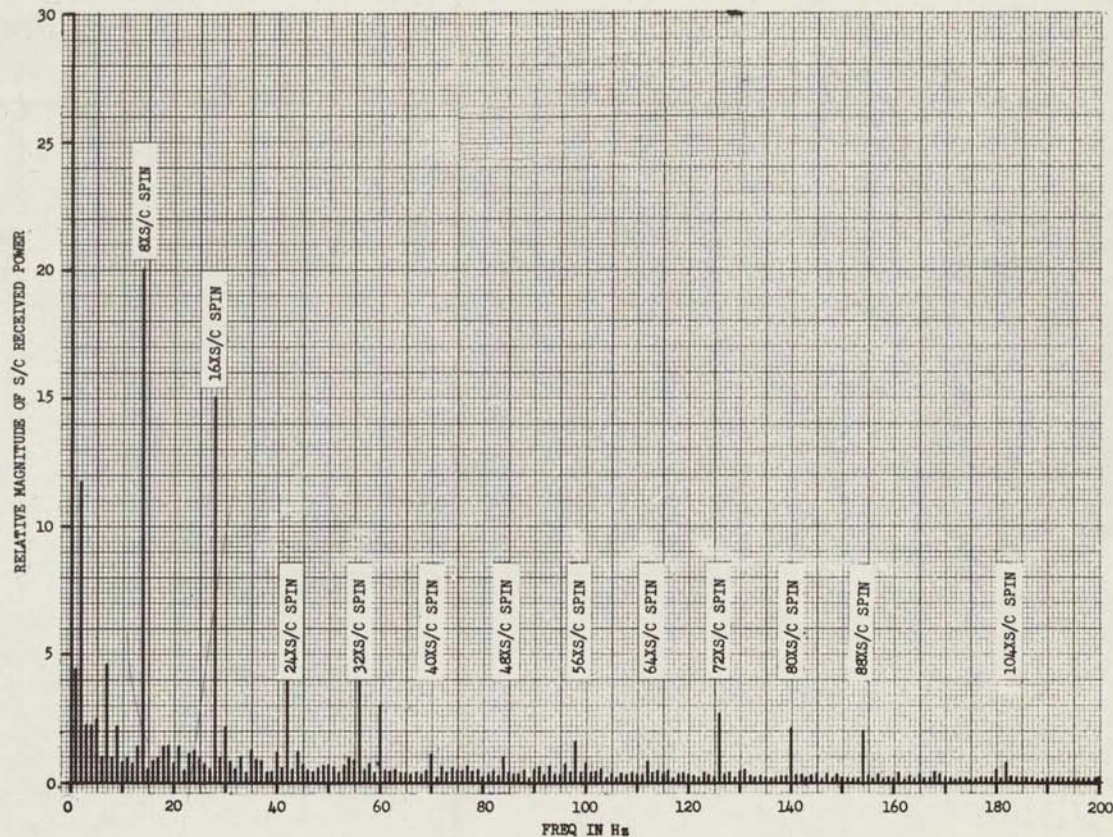
Figure 3.129. ATS-3 Receive-Antenna Spin-Amplitude-Modulation Spectrum

3.301
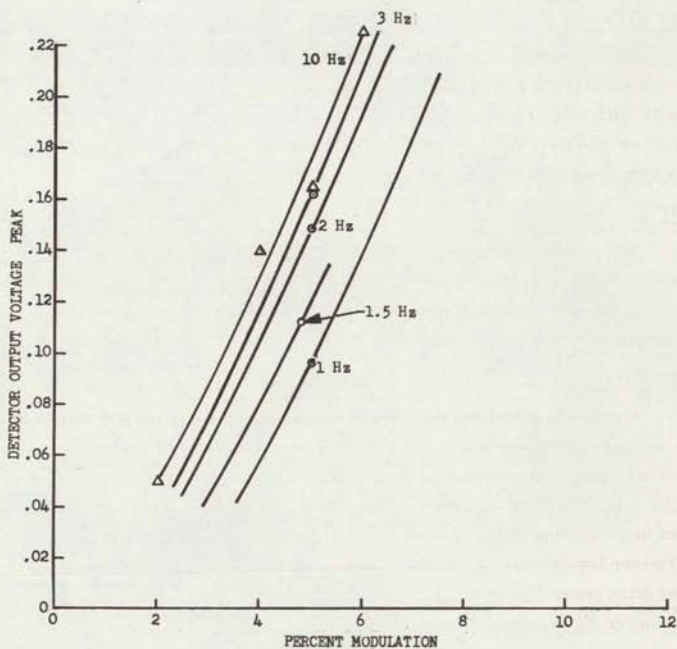
Figure 3.130. AM Detector Output as a Function of Percent Modulation

3.6.3 REPEATER-SATURATION CHARACTERISTICS (FT-SP-1.1) (E. E. Crampton)

3.6.3.1 Description and Test Results

OBJECTIVES

The major objectives of this experiment are to determine the repeater-saturation characteristics of the FT mode in terms of (1) spacecraft carrier-output power versus space-craft received power and (2) total link carrier-to-noise density as a function of spacecraft-received power.

TEST CONDITIONS

The two ATS-1 transponders and ATS-3 transponder 1 can be configured to provide 4 watts (1 TWT) or 8 watts (2 TWT's) output power. ATS-3 transponder 2 provides 12 watts (TWT) output power. Specific test configurations included all transponder configurations on ATS-3 while on ATS-1 only the 8-watt output power configuration was used. All tests were conducted with the Rosman earth station.

RESULTS

The resulting normalized saturation curves for each of the transponder configura-tions were within ±1.0 db of each other. A typical saturation curve is presented in fig-ure 3.131. Also shown with this typical saturation curve are the uplink, downlink, and overall carrier-to-noise density ratios (C/N_o) for the ATS-3, 12-watt repeater.

3.6.3.2 Analysis

In order to determine the saturation characteristics in the S/C test configuration, the received carrier plus total noise (C + N) is measured in a 2.16-MHz noise bandwidth. At the earth station, this received carrier is then translated (10 MHz) at IF such that it is outside the 2.16-MHz filter bandwidth. This allows the total received noise power to be measured in the absence of the carrier. This process is repeated at various spacecraft received power levels obtained by varying earth station transmitter output power. When measured noise power (N), is subtracted from (C + N), this method provides an indirect measurement of the variation of transponder carrier output power.

The downlink carrier-to-noise ratio is determined at a high spacecraft received carrier-to-noise density (greater than 90 db) by first measuring the carrier plus total noise at the earth station. The earth station antenna is then moved 10° off the spacecraft and the downlink noise power measured. Since the downlink noise is constant, the downlink carrier-to-noise density is a direct function of the S/C carrier output power. Thus at low values of spacecraft received power, the downlink carrier-to-noise density ratio follows the S/C output-carrier power.

The uplink carrier-to-noise density is defined as the carrier-to-noise density at the output of the spacecraft transponder. This ratio was determined by removing the downlink carrier-to-noise density contribution from the total carrier-to-noise density ratio.

In the normal use of the FT mode, the repeaters are operated in a saturated condition (spacecraft received power (P_{rs}) equals -73 dbm). However, figure 3.131 shows that if the P_{rs} is reduced approximately 22 db (assuming a peak-to-rms factor of 10 db for a noise-like signal), the repeaters can be operated linearly. However, lowering the P_{rs}, results in a lower overall carrier-to-noise density ratio, thus utilization of full system bandwidth is not realized. This indicates that multiple-access in the FT mode, i.e., multiple carriers which require greater transponder linearity, is possible, but the number of operational voice channels would be reduced.

For the conditions shown in figure 3.131, the improvement in carrier-to-noise density from the S/C limiter begins to increase this uplink carrier-to-noise density at a P_{rs} equal to -83 dbm. At nominal P_{rs} of -73 dbm, full 3 db theoretical limiter improvement is realized. This 3-db realization is also true for all other test configurations at this P_{rs}.

In addition, for the configuration shown in figure 3.131, if the uplink carrier-to-noise density is increased by increasing P_{rs} 10 db from the nominal -73 dbm, the overall C/N ratio will increase by approximately 3 db. This follows from the fact that at the nominal level, the uplink and downlink carrier-to-noise densities are essentially equal. Since down-link carrier-to-noise density is a function of (1) repeater EIRP and (2) earth station G/T, it would be reduced either by using one of the transponder configurations other than ATS-3, 12 watt output power or by using an earth station with a lower G/T ratio such as Mojave, for example. In the other configurations where the downlink carrier-to-noise density is lower, less improvement in overall C/N ratio would result from an increase in uplink carrier-to-noise density.

The saturation point is defined as that spacecraft input power level which when increased by two db, results in a one-db increase in spacecraft power output (also referred to as the one-db compression point). The one-db compression point, was found to be about -85 dbm, and it is an indication of the non-linearity of the transponder.

3.6.3.3 Conclusions

It can be concluded that at nominal -73 dbm spacecraft received power, the full theoretical 3 db limiter improvement is obtained in the uplink carrier-to-noise density. Non-linear operation of the transponder is indicated by the one db compression point and occurs at a spacecraft input power of about -85 dbm. For the configuration shown in figure 3.131, an improvement of 3 db in overall carrier-to-noise ratio can be obtained by

increasing the uplink carrier-to-noise density approximately 10 db. The amount of improvement in the overall carrier-to-noise ratio with other earth station-repeater configurations, based upon an increased uplink carrier-to-noise density, will depend on the repeater EIRP and earth station G/T.
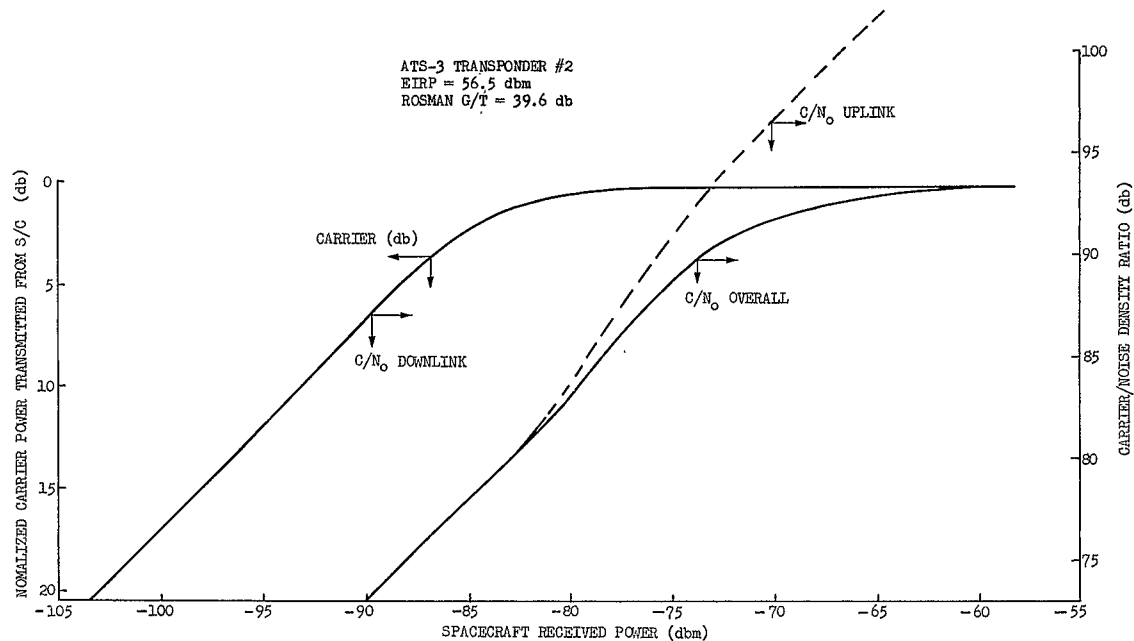
Figure 3.131. Repeater-Saturation Characteristic

3.7 EARTH-STATION EXPERIMENTS

3.7.1 EARTH TERMINAL G/T (AN-SP-1.2) (H. J. Kochevar)

3.7.1.1 Description and Test Results

OBJECTIVE

The purpose of this experiment is to determine accurately the G/T ratio of the earth terminal antennas by utilizing a radio star of known radiating power density as a signal source. Where an earth station which is capable of performing this measurement has established its G/T value, it becomes the standard with which other stations can determine their G/T ratio by a comparison method of their C/N ratio measurements performed with an ATS satellite.

With the establishment of the G/T ratio of an antenna, the gain can be obtained by simply measuring the system noise temperature and adding it (in db) to the G/T value.

TEST CONDITIONS

The establishment of the G/T ratio of an earth station antenna by utilizing a radio star was performed at the Rosman station. With an 85 foot antenna, only this station has sufficient gain to provide the minimum signal plus noise-to-noise ratio required from the low radiation level emitted by the radio stars. If the S+N/N ratio is less than 2 db, the measurement accuracy is degraded considerably.

The radio star Cassiopeia A was selected for this measurement because it provides the larger power density level at the 4-GHz frequency than two other possible sources (Cygnus A and Taurus A). Radiation level of the latter two stars is appreciably lower than Cassiopeia A and therefore they are not suitable for use in this test.

The G/T for the Rosman antenna was determined by first measuring the S+N signal with the antenna pointing at the Cassiopeia A star. With the antenna fixed in its position relative to earth, the earth's rotation moved the antenna beam approximately 10 degrees away from the star's position in space. At this antenna position the system noise temperature was measured. With the measured S+N/N value and a calculated constant containing the established radiated power density of the star, the G/T ratio was determined.

After the G/T measurement was completed for theRosman antenna, the next step was to measure the carrier-to-noise ratio of the signal received from one of the ATS satellites. The Rosman antenna was centered on the ATS satellite (in this case the ATS-3) and the satellite's antenna beam centered on the earth station antenna for a maximum received signal. The latter function was performed to normalize all parameters that may effect the measured carrier-to-noise ratio. An unmodulated carrier was provided by the satellite for this measurement. After the carrier plus noise-to-noise ratio of received satellite

signal was measured, the Rosman antenna was moved about 10 degrees away from the satellite to allow the system noise temperature to be measured. During this process, the elevation angle was kept constant to minimize the measuring errors.

The next procedure was to measure the carrier-to-noise ratio at the Mojave station antenna. This procedure required the Mojave antenna to be centered onto the same satellite and the satellite antenna to be centered onto the Mojave antenna for a maximum received signal. The carrier-plus-noise-to-noise ratio and the system noise temperature for the Mojave station were measured by following the same procedure as that performed on the Rosman antenna.

With the data measured at Rosman and Mojave, the G/T value and the antenna gain for both stations were computed.

STANDARDS

There are no standards for the G/T ratio because of its dependence on the antenna system noise temperature which is a variable function. However, the antenna gain determined from the measured G/T ratio is compared with the theoretical value which is used as a standard. The standard value of the antenna gain does not have variables because its deviation is based strictly from the geometry of the antenna and the operating frequency.

RESULTS

The G/T ratio and the gain of the earth station antennas at Rosman and Mojave were determined from measured parameters and are presented in tables 3.46 and 3.47. In addition to the measured parameters, the theoretical gain of the antennas is shown in the tables for comparative purposes.

3.7.1.2 Analysis

The measured gain of 57.2 db obtained for the Rosman antenna by the radio star method compares closely to the theoretical value of 58.4 db shown in table 3.46. This close agreement of the antenna gain to the ideal value indicates the accuracy in the use of the radio star method of measurement. However, this accuracy cannot be achieved unless a minimum signal plus noise-to-noise ratio (r) of 2 db is obtained. To achieve this minimum ratio, the earth station antenna must have a G/T value of at least 36 db when using the radio star Cassiopeia A. The test performed at the Rosman station met these minimum requirements with values of 37.3 db for the G/T ratio and 2.46 db for the "r" ratio which are indicated in table 3.46. A relatively higher system noise temperature of 97°K was measured resulting from the low-elevation pointing angle of 15 degrees to the radio star.

When the signal plus noise-to-noise ratio "r" has been measured, the G/T value for the Rosman antenna is calculated in accordance to the CCIR standards. The G/T value is determined from the following formula:

$$G/T = \frac{8 \pi \ K \ (r - 1)}{\lambda^2 \ \phi_n} \qquad \text{(antenna figure of merit)}$$

where

$\qquad$ G = Gain of earth-station antenna

$\qquad$ T = System noise temperature of earth station

$\qquad$ K = Boltzman's Constant = 1.38×10^{-23} joules/°K

$\qquad$ r = Signal plus noise-to-noise ratio measured = $\dfrac{P_{st} + P_n}{P_n}$

$\qquad$ P_{st} = Noise power received from radio star

$\qquad$ P_n = Noise power of earth station corresponding to system noise temperature T_s

$\qquad$ (r - 1) = Signal-to-noise ratio = $\dfrac{P_{st}}{P_n}$

$\qquad$ λ = Wavelength of receiving frequency = 0.0718 meter (4.178 GHz)

$\qquad$ ϕ_f = Flux density radiated from radio star Cassiopeia A at measured frequency = 1030×10^{-26} Watts/Meter^2 /Hz (4.178 GHz)

$\qquad$ ϕ_n = Flux density of ϕ_f corrected for time elapsed from January 1, 1968, to February 14, 1970.

The flux density of ϕ_f or noise power radiated from the radio star Cassiopeia A was extracted from the graph of figure 3.132 for the receive frequency of 4.178 GHz. This value of flux density is based on established data which is dated January 1, 1968. Radio star Cassiopeia A has a flux density which decreases in level with time as shown in figure 3.135. A correction for the flux density must therefore be made based on a time elapse from January 1, 1968, to February 2, 1970, amounting to 2.2 years. The new flux value is determined from the following expression;

$\qquad$ $\phi_n = \phi_f (0.989)^n$

$\qquad$ n = Number of years from Jan. 1, 1968 = 2.2 yrs

$\qquad$ $\phi_n = 1030 \times 10^{-26} (0.989)^{2.2} = 1006 \times 10^{-26}$ W/M^2/Hz (time corrected)

The same value of time corrected flux density can also be obtained from the graph in figure 3.135. A signal-to-noise ratio (r- 1) is now determined from the measured value of "r".

$$r = 2.46 \text{ db} = 1.76$$

$$(r - 1) = 1.76 - 1.0 = 0.76 = -1.21 \text{ db}$$

A G/T ratio for the Rosman antenna is obtained by substituting all of the known parameters into the above formula:

$$G/T = \frac{8\pi K}{\lambda^2 \phi_n} (r-1) = \frac{8\pi (1.38 \times 10^{-23}) (r-1)}{(0.0728)^2 (1006 \times 10^{-26})}$$

In terms of db the above expression becomes:

$$G/T = 38.2 + 10 \log(r-1) = 38.2 - 1.21 = 37.0 \text{ db}$$

There are two correction factors that must be applied to the calculated G/T ratio in order to achieve an accurate value by minimizing all of the effective errors. These correction factors consist of atmospheric attenuation and angular extension of ratio stars. The atmospheric attenuation is dependent upon the frequency and the antenna elevation angle. This value was derived from the following formula and can also be extracted from the graph shown in figure 3.133 for an elevation angle of 15 degrees:

$$C_1 = \text{Atmospheric Attenuation} = \frac{0.036}{\sin \alpha} \text{ (db)}$$

where

α = Antenna elevation angle to radio star Cassiopeia A = 15'

$$C_1 = \frac{0.036}{\sin 15°} = \frac{0.036}{0.26} = 0.14 \text{ db}$$

Flux emanating from the radio star Cassiopeia A is considered a source represented by a disc subtending an angle of 4.3 minutes. The effective beamwidth of the earth antenna for receiving the star radiation is based on the half power level. Since the distribution of the star flux is not uniform over the antenna beamwidth, a correction factor must be applied. With a beamwidth of 0.20 degree or 12 minutes at the -3 db point for the Rosman antenna, a correction factor of 0.18 db is obtained from the graph in figure 3.134 and is presented as:

$$C_2 = 0.18 \text{ db}$$

By applying the two correction factors C_1 and C_2 to the G/T value, the resultant ratio for the Rosman antenna becomes:

$$G/T = 37.0 + C_1 + C_2 = 37.0 + 0.14 + 0.18 = 37.3 \text{ db}$$

With a measured system noise temperature of 97°K for the star-pointing condition the Rosman antenna gain becomes:

$$T_s = 97°K = 19.9 \text{ db Rosman System Noise temperature}$$

$$G = G/T + T_s = 37.3 + 19.9 = 57.2 \text{ db Rosman antenna gain}$$

When the Rosman antenna was directed towards an ATS satellite, optimum values of the carrier-to-noise ratio and systems noise temperature had to be measured to determine accurately the Mojave antenna characteristics. One condition required was the centering of the satellite antenna beam to the Rosman antenna for a maximum received signal level. Another condition utilized to minimize errors was to measure the system noise temperature with the earth station antenna pointed to the satellite and the downlink carrier removed. This procedure maintained the propagation conditions the same by not altering the earth antenna pointing angle. The measured carrier-to-noise ratio and system noise temperature values shown in table 3.46 are nominal values and agree closely to previous measured results.

The Mojave antenna G/T ratio is derived from the Rosman antenna G/T value after it is first normalized to the measured system noise temperature when the Rosman antenna is pointing to the ATS satellite. The normalized G/T now becomes:

$$\Delta T_S = \frac{97°}{77°} = (19.87 - 18.87) \text{ db} = 1.0\text{-db correction for normalizing to } 77°\text{K}$$

$$G/T = 37.3 + 1.0 = 38.3 \text{ db}. \quad \text{Rosman antenna normalized to } 77°\text{K}$$

When the parameters were measured at Mojave for the G/T determination, the satellite beam was centered to the Mojave antenna for the purpose of minimizing errors. Before the conversion of the G/T ratio from Rosman to Mojave can be accomplished, the measured carrier-to-noise ratio at Mojave must be normalized to the Rosman antenna receiving conditions. To perform this normalization, three factors must be considered and consist of: the difference in the range and atmospheric attenuation between the two earth stations and the satellite; and the difference in the system noise temperatures between the two earth stations. The range correction is proportional to the square of the range and becomes:

$$(\Delta R)^2 = \left(\frac{38,887}{37,292}\right)^2 = (91.79 - 91.43) \text{ db} = 0.36 \text{ db Correction for range difference}$$

To correct for atmospheric attenuation, the attenuation factor for each earth station is first obtained from the graph of figure 3.133 by using the associated elevation angle for each station antenna as follows:

(Rosman) $C_1 = 0.05$ db $(\alpha = 48°)$

(Mojave) $C_1 = 0.07$ db $(\alpha = 31°)$

The correction factor to be applied is the difference in the atmospheric attenuation between the two stations and becomes:

$$\Delta C_1 = 0.07 - 0.05 = 0.02 \text{ db correction for atmospheric attenuation}$$

3.311

To normalize the Mojave carrier-to-noise ratio to the Rosman system noise temperature, the following correction factor is determined. This factor is negative because normalization is performed to a higher system noise temperature.

$$\Delta T_s = \frac{(74)}{(77)} = (18.69 - 18.87)\,db = -0.17\,db$$

The Mojave carrier-to-noise ratio is normalized to the Rosman receiving system conditions by applying the three correction factors relating to the range, atmospheric attenuation and system noise temperature. The normalized value is obtained as follows:

$$C/N = C/N + (\Delta R)^2 + \Delta C_1 + \Delta T_s = 14.0 + 0.36 + 0.02 - 0.17 = 14.2\,db$$

The Mojave G/T ratio can now be simply achieved by taking the difference between the normalized carrier-to-noise ratios of the two earth stations and applying it to the Rosman G/T value as follows:

$$\Delta C/N = 20.5 - 14.2 = 6.3\,db$$

$$G/T = G/T\,(ROS) - \Delta C/N = 38.3 - 6.3 = 32.0\,db\ \text{Mojave antenna}$$

By applying the Rosman system noise temperature to the Mojave G/T ratio, the antenna gain for Mojave becomes:

$$T_s = 77°K = 18.9\,db\,(Rosman)$$

$$G = G/T + T_s = 32.0 + 18.9 = 50.9\,db\ \text{Mojave antenna gain}$$

A comparison of the measured Mojave antenna gain of 50.9 db indicates a close agreement to the calculated value of 51.8 db. Accurate results are feasible only if all of the effective errors occurring in measured parameters are considered and minimized. The most significant characteristics of the Mojave antenna are presented in table 3.47.

3.7.1.3 Conclusion

The results obtained in measuring the G/T ratio of an earth station antenna by the radio star method verifies the accuracy of this technique. Greater accuracy is achieved with the radio star method because it can be considered to be a point source of radiation whose power density is well established. By using the radio star method the near field effects and multipath effects for the earth station antennas are essentially eliminated.

In addition to the accuracy that this method provides, it has another advantage of requiring only one simple and quick measurement, the S + N/N ratio (r), to determine the G/T value. If the gain of the antenna is required it is simply achieved by measuring the system noise temperature and applying it to the G/T value.

A desirable feature of this technique is that once an earth station has established its G/T ratio by the radio star method, it can be used as a standard for other earth-station antennas who do not have the capability of using the radio star method of measurement. By utilizing a geostationary satellite, any number of earth-station antennas can have their G/T ratios and their gain determined accurately from the established standard G/T value.

TABLE 3.46. ROSMAN ANTENNA CHARACTERISTICS

Radio Star Cassiopeia A					Satellite				
$\frac{S+N}{N} = r$	T_s	G/T	Meas G	Calc G	C/N	T_s	G/T	Range	El. Angle
2.46 db	97°K	37.3 db	57.2 db	58.4 db	20.5 db	77°K	38.3 db	37,292 KM	48°

TABLE 3.47. MOJAVE ANTENNA CHARACTERISTICS

Satellite						
C/N	T_s	G/T	Meas G	Calc G	Range	El. Angle
14.0 db	74°K	32.0 db	50.9 db	51.8 db	38,887KM	31°
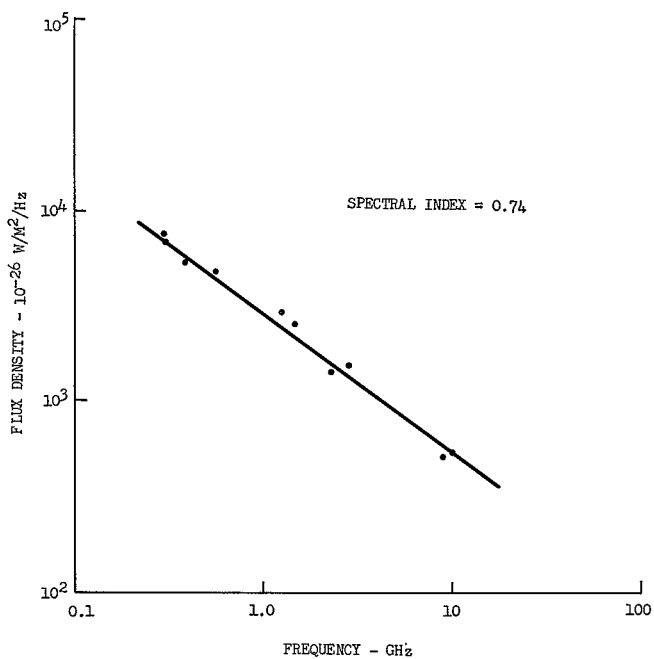
Figure 3.132.   Flux Density Versus Frequency for Radio Star Cassiopeia A
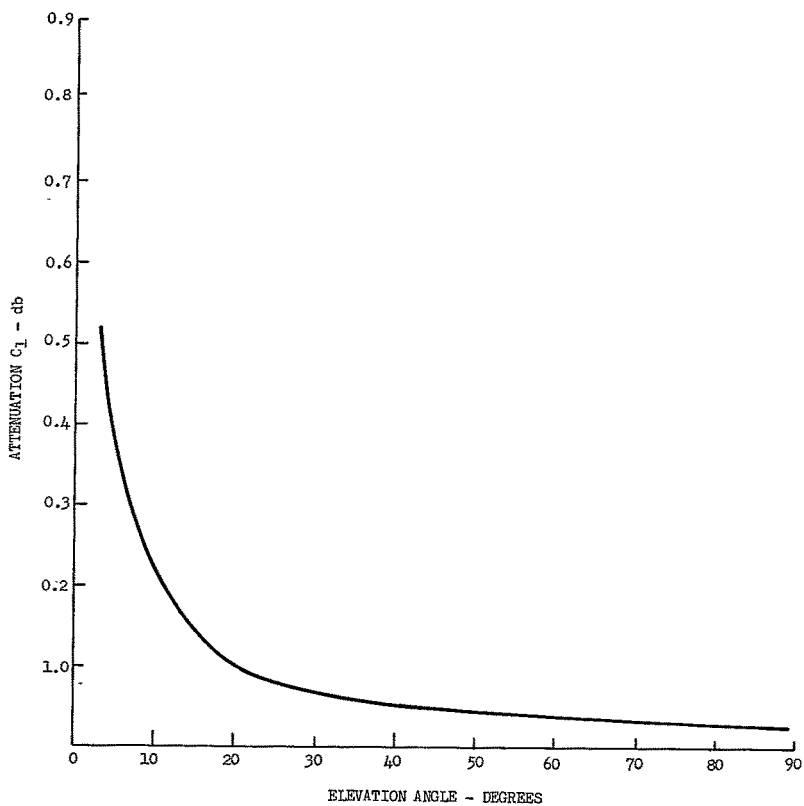
Figure 3.133. Atmospheric Attenuation at 4 GHz

3.316
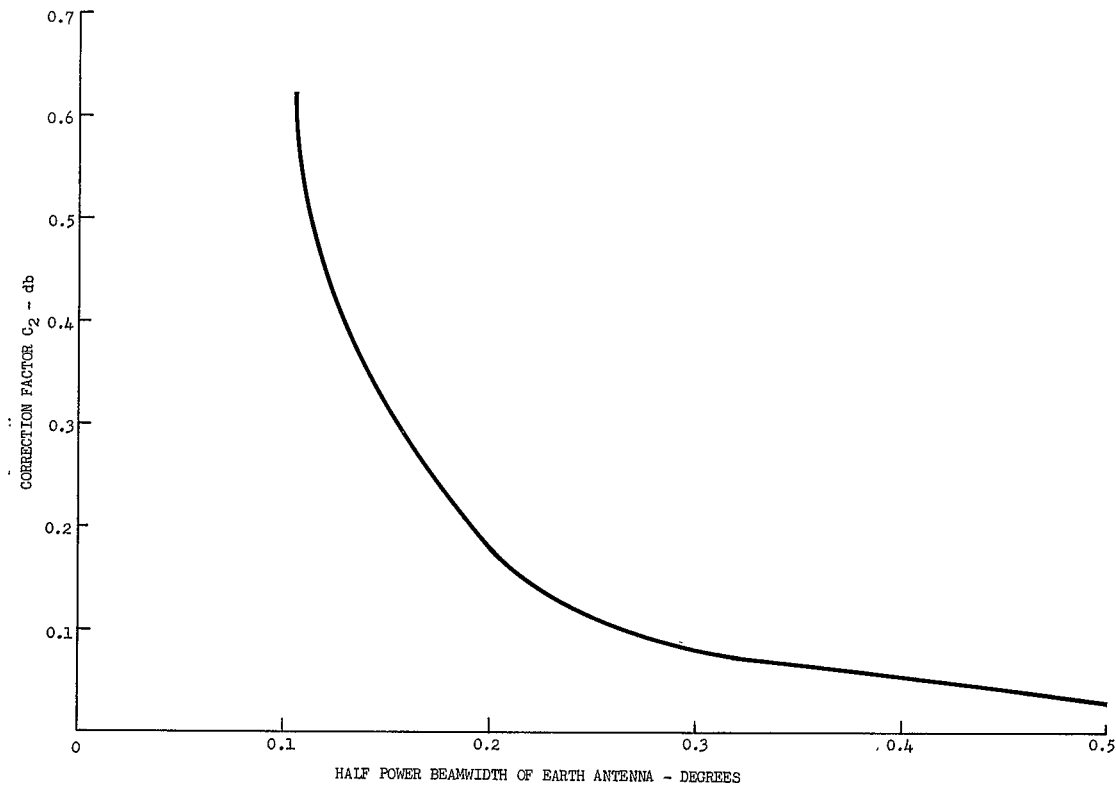
Figure 3.134.   Correction Factor for Angular Extension of Radio Star Cassiopeia A
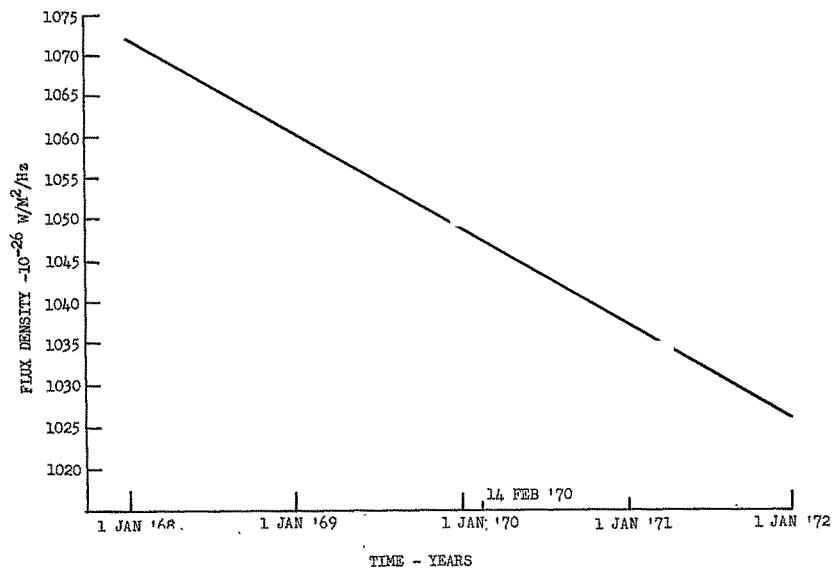
Figure 3.135.   Flux Density Versus Time of Cassiopeia A

3.7.2 EARTH-STATION TRANSMIT ANTENNA PATTERN (AN-SP-1.2) (H.J. Kochevar)

3.7.2.1 Descripton and Test Results

OBJECTIVE

The purpose of this experiment is to determine the transmit beam pattern of the earth station antennas and to present a three dimensional projection type of beam pattern display. Two types of system tests utilized to measure the antenna patterns consist of a one earth-station test and a two earth-station test. Both the one-and two-station tests require the use of an ATS satellite to provide a long-range antenna test facility to measure the antenna patterns. By comparing the results of the two techniques of testing the more informative method is clearly shown.

TEST CONDITIONS

The earth station antenna and the ATS satellite system have the capability of measuring the transmit and receive antenna patterns individually or simultaneously by utilizing a single earth station. However, test results indicate limitations exist in the magnitude of the scan angle that can be used for the transmit antenna pattern test. To obtain optimum test results each type of pattern test was conducted individually. Limitations in the test results of the transmit antenna pattern measurement were eliminated by using a two station system test. A two-station test requires the earth station whose antenna pattern is being measured to scan and transmit a signal to the ATS satellite. The retransmitted signal from the satellite is received by the second station antenna and recorded. An antenna pattern of the second station is obtained by reversing the process described above.

When either the single or two-station test is utilized, the transmit antenna pattern is measured by transmitting a test tone of 3.25 MHz in the SSB-FDMA/PhM mode to the satellite. The test tone signal received by the satellite phase modulates the downlink carrier of the satellite. The downlink PhM modulated carrier signal from the satellite is received by the earth station antenna where it is down-converted to a 70-MHz IF signal by the PhM receiver. Signal flow from this point is different for the two types of tests. For the single station test the 70-MHz signal from the PhM receiver is applied to the R/RR receiver. The 3.25-MHz tone signal is extracted from the IF signal by the R/RR receiver and applied to the Electrac demodulator from which an AGC signal output is provided. For the two-station test, the 3.25-MHz signal is obtained from the demodulation of the 70-MHz IF signal in the PhM receiver and applied to the Electrac demodulator. The AGC signal output from the Electrac demodulator is recorded for both tests.

Two receivers are required to perform the one-station test so that a sufficiently large range of signal level is obtained to maintain the signal level above threshold in the Electrac demodulator. This requirement is necessary because of the simultaneous variation

in the instantaneous gain of the transmit and receive antenna beams during the scanning period. For a two-station test the instantaneous gain of the transmit antenna beam varies with scanning while the receive antenna beam remains fixed. Therefore, only one receiver is required to maintain the signal level above threshold in the Electrac demodulator.

Test-tone power received at the satellite is a direct function of the earth-station transmit antenna pattern. The ground received test tone power is directly related to the PhM modulation of the satellite downlink carrier which is modulated by the satellite received test-tone signal. Therefore, the recorded AGC signal level developed from the 3.25-MHz tone is a direct representation of the earth station transmit antenna pattern. Time is also recorded concurrently with the AGC voltage on a strip-chart recorder.

A symmetrical antenna pattern measurement was achieved by using the autotrack coordinates as the reference position for the center point of the scanned frame. The raster scanning of a complete pattern frame by the antenna was automatically performed from a programmed tape. An entire pattern frame is produced by moving the antenna along the Y-axis at a rate of 0.05 degree per second and in steps of 0.05 degree along the X-axis after the completion of each Y-axis scan. This scanning rate was used for all tests performed at the Rosman and Mojave stations. The scanning characteristics for the tests conducted at Rosman and Mojave are summarized in Table 3.48.

Time and antenna X and Y-axes position angles for the complete coverage of a pattern frame were recorded on teletype tape. The recorded AGC voltage representing the relative antenna gain provides the information from which the three-dimensional projection display of the transmit pattern is developed.

The antenna pattern is constructed by first determining each recorded AGC voltage pattern representing one scan (see figure 3.137) with respect to its proper scan position in the pattern frame and its appropriate boundaries for each scan. Boundaries and the centerline for each scan are located by correlating the antenna position data and time as recorded on a print-out from the TTY tape with the time of the strip-chart recording of the AGC voltage.

A contour plot of the antenna pattern was developed by translating points of significant energy levels from the AGC voltage recording to a drawing representing a complete scanning frame and containing the number of scans shown in the above table. With a strip chart speed of 0.5 inch per second the scan length of the AGC voltage recording was sufficient to permit a direct full scale transfer of significant energy level points to the associated scan on the pattern frame drawing. By joining all of the plotted common points irregular contour lines are formed which represent the following antenna pattern characteristics:

a) Constant energy level lines of the main beam and cones of energy

b) Maximum energy levels of side lobes

c) Minimum energy levels of nulls

When a single station test is used to measure the transmit antenna pattern the system test capability is reduced resulting from the simultaneous variation of the transmit and receive instantaneous earth station antenna gain during the scanning period. This effect causes a small signal-to-noise ratio to be received by the earth station receivers resulting in the signal level falling below the threshold of the Electrac receiver. This condition causes the Electrac receiver to lose lock on the input signal whenever the antenna scans the low power level of the antenna beam. With this restriction a maximum peak-to-peak antenna scanning angle of 1.8 degrees was achieved for the Mojave station to cover a frame of the transmit pattern along both axes. Although a scan angle greater than 2 degrees is desirable, the maximum value of 1.8 degrees obtained with the one station test at Mojave includes all of the first side lobe. This amount of coverage normally provides sufficient information for most purposes.

With a two-station test, the transmit antenna patterns can be measured to a scan angle of 2.6 degrees (peak-to-peak) or greater which is sufficient to present the area considered to have the most significant information. Antenna patterns taken at the Rosman and Mojave stations used scan angles of 2.0 degrees and 2.6 degrees (peak-to-peak), respectively.

RESULTS

A transmit antenna pattern of the Mojave station was first measured by using the single station test in conjunction with the ATS-1 satellite. From the data obtained, a three-dimensional projection type of display of the transmit antenna pattern was developed and is illustrated in figure 3.136. A complete scan taken across the center of the main beam shown in figure 3.137 illustrates the configuration of the relative antenna gain for that particular cross section. The parameters defining the scanning characteristics for each antenna pattern test at Rosman and Mojave are given in table 3.48. The significant measured parameters presented in figures 3.138 and 3.140 for the Rosman and Mojave antenna patterns determined by the signal and two station tests are given in table 3.49.

Because of the advantages provided by the two station test, the antenna patterns for Rosman and Mojave were performed by this method and utilized the ATS-3 satellite. Three dimensional projection type of displays of both station's antenna pattern were developed from the two station test data obtained and are shown in figure 3.138 for Rosman and figure 3.140 for Mojave. The relative gain of each antenna pattern taken across the center of the beam is illustrated in figure 3.139 for Rosman and figure 3.141 for Mojave.

3.7.2.2 Analysis

The Mojave transmit antenna pattern presiented in figure 3.136 and derived by the single-station test essentially consists of contour lines indicating the following characteristics: the main beam at different relative power levels; maximum level of the side lobes and the minimum power levels or nulls. In figure 3.136, each side lobe and null is indicated by the average relative power level. Measured beamwidths of 0.24 and 0.27 degree at the half-power points (-3 db) in the X and Y-axes planes are in very close agreement with the predicted value of 0.28 degrees. The results verify this method of pattern measurement is very accurate in determining the antenna beamwidth.

Figure 3.136 presents the main beam in concentric constant level contours from the center of the beam to the first null. The contours vary in level from 0 db to an average value of -30 db at the first null. The first side lobe has an average power level of 18 db below the peak of the main beam. Measured angles for the first side lobe are 0.40 degree along the Y-axis and 0.48 degree along the X-axis. These value compare closely to the predicted value of 0.46 degrees.

A total of 18 scans were utilized to develop the transmit pattern illustrated in figure 3.136. Scans beyond the ninth from the beam center could not be used because sufficient data was not available. Useable data is limited in this pattern and is the result of the Electrac receiver loosing lock when the input signal level drops below the receiver threshold. This limitation in available data is a significant disadvantage in the use of a single-station test to obtain a transmit pattern of an earth station antenna.

The application of a two station test to measure the transmit antenna patterns provides useful data equally along both axes resulting in a symmetrical pattern around the main beam as illustrated in figures 3.138 and 3.139. The Rosman antenna with a diameter of 85 feet has a pattern as shown in figure 3.138 and indicates useful data was obtained for a beam angle coverage of 2 degrees (peak-to-peak) along both axes. This beam angle along the X-axis is twice the value as that provided by the single-station system test shown in figure 3.136. A total of 40 scans were utilized to complete one antenna pattern frame.

The Rosman pattern in figure 3.138 shows the main beam has a half-power (-3 db) beam width of 0.20 degree in the X-axis and 0.16 degree in the Y-axis. These values are in close agreement with the predicted value of 0.13 degrees. The first side lobe is located at an angle of 0.27 degree along the X-axis and 0.24 degree along the Y-axis. These values compare closely to the predicted value of 0.22 degrees. The level of the first side lobe has an average value of 18 db below the peak of the main beam.

A very interesting characteristic was revealed by the Rosman pattern presentation (figure 3.138) and shows the second side lobe consists of eight major irregular cones of energy located symetrically around the main beam. The relative peak magnitude of each energy cone in respect to the main beam varies over a range of -19 db to -26 db. This characteristic of energy cones, forming the second side lobe is contrary to the belief that the second side lobe forms a solid ring of energy surrounding the main beam similar to the first side lobe.

The configuration of each energy cone and the main beam are presented as constant level contours. These contours present a perspective view of the shape of the masses of energy in the direction of their height or magnitude.

To distinguish the different characteristics presented in the pattern illustrated in figure 3.138, three types of contours were used consisting of constant levels, peak levels and minimum levels. Constant level contours are used to represent irregular cones of energy and the main beam, the solid contour lines represent peak energy levels of the side lobes and the dotted contour lines represent the energy levels of the nulls.

Another important feature revealed by the pattern display is the distribution of energy in the side lobes and nulls beginning with the second null where irregular open contour lines diverge at the ends of the X-axis instead of forming closed concentric loops. Relative energy levels are indicated at different points along these contours to present the variation of the energy magnitude over the entire antenna pattern. The configuration of the energy cones and contours presents an overall picture of the energy distribution in the transmit antenna pattern. The first side lobe in the pattern is the only side lobe which forms a solid concentric ring of energy surrounding the main beam.

Additional cones of energy exist to that shown in the pattern of figure 3.138, however, their magnitude in respect to the adjacent nulls are so small their presentation was not considered significant. Irregular distribution of energy in the pattern shown by the contours beyond the first side lobe is the result of such factors as antenna reflector surface irregularities, misalignment of feeds and subreflector and interference from struts supporting the subreflector. The important measured parameters of the Rosman antenna pattern are summarized in table 3.49. Significant parameters defining the scanning characteristics for the Rosman pattern are presented in table 3.48. Relative gain of the Rosman antenna for one complete scan angle taken across the center of the main beam is shown in figure 3.139.

The ATS satellite not being a perfectly stationary geocentric spacecraft undergoes a small drift which creates a minor displacement of the center of each scan in respect to the previous scan. Maximum displacement will occur in the last scan with respect to the first scan where the total satellite drift is produced during the scanning period of one frame. In the development of the antenna pattern the center line of each recorded scan configuration is

aligned with the X-axis. This process eliminates the relative displacement of each scan therefore no errors are created in the construction of the pattern display.

The relationship of the satellite drift to the changes created in the X-and Y-axes coordinates of the Rosman antenna during autotrack is presented in figure 3.142. Time of start to finish in scanning one pattern frame results in a period of 27 minutes. For the period of 27 minutes, the graph indicates a change of 0.0025 degree occurs in the X-axis and a change of 0.070 degree in the Y-axis. This change in the X-and Y-axes is the displacement produced in the last scan with respect to the first of the antenna pattern. However, as mentioned above, this displacement causes negligible error or distortion in the developed pattern.

A difference between the values of the X-and Y-axes coordinates may occur as given above. This result is dependent on what section the scanning of one frame occurs on the figure eight pattern of motion the satellite produces during a 24-hour period. This difference factor has no effect in the development of the display pattern.

The Mojave antenna with a diameter of 40 feet has a pattern as shown in figure 3.140 and was measured with the two-station test. A scan covering 2.6 degrees was used with the Mojave antenna to provide a minimum of four side lobes in the pattern. Figure 3.140 shows the Mojave antenna main beam has a half power (-3 db) beamwidth of 0.29 degree in the X-axis and 0.26 degree in the Y-axis. A calculated beamwidth of 0.28 degree compares very closely to the two measured values. The first side lobe exhibits an average level of 18 db below the main beam and has an angle of 0.53 degree along the X-axis and 0.41 degree along the Y-axis. This measurement is in close agreement to the predicted value of 0.46 degrees. The measured parameters of the Mojave pattern are summarized in table 3.49 for the one-and two-station test and show a close agreement within the measuring tolerances between the two tests.

The second side lobe of the Mojave pattern also exhibits irregular cones of energy located symetrically around the main beam similar to that of the Rosman pattern. A total of ten major cones of energy occur in the second side lobe as shown in figure 3.140. The relative level of the peak of each cone of energy in respect to the main beam varies over a range of -21 db to -29 db. The first side lobe in the pattern is the only side lobe which forms a solid concentric ring of energy surrounding the main beam. An illustration of the relative gain of the Mojave antenna for a complete scan taken across the center of the main beam is shown in figure 3.141.

Contour construction of the Mojave transmit antenna pattern as presented in figure 3.140 was developed in the same manner as was done for the Rosman pattern. There are in existence additional low-level cones of energy in this pattern whose magnitudes are

3.324

too small to be considered significant for their presentation. The minor difference between the Rosman and Mojave antenna patterns is the result of their antenna parameters not being the same because of their basic difference in diameter. Struts supporting the subreflector will also have some effect on the pattern configuration. A quadripod (4 struts) is used to support the subreflector for the Rosman antenna and each pair is mounted in the plane of either the X-or Y-axes. For the Mojave antenna, each pair of a quadripod are mounted at 45 degrees to the planes of the X-and Y-axes.

Another factor effecting the pattern configuration is the surface tolerance of the parabolic antenna reflector. This tolerance normally expressed in rms deviation from an ideal parabola is very small for the Rosman and Mojave antennas and is given in table 3.50. The effect of the surface tolerance on the antenna gain for both stations is negligible and amounts to a reduction in gain of approximately less than 0.1 db. Some of the major characteristics for the Rosman and Mojave antennas are presented in table 3.50.

3.7.2.3 Conclusion

The two transmit antenna patterns presented as three dimensional projection displays and shown in figures 3.138 and 3.140 reveal information not normally seen in antenna pattern presentations. An important feature exhibited by the two patterns is the existance of irregular cones of energy for the second side lobe and beyond. With both antenna patterns exhibiting similar characteristics, the configuration becomes an example for a typical Cassegrainian antenna design. These characteristics are also similar to the results described in a publication on an antenna pattern measurement performed on a 30-ft Cassegrainian radar antenna. [50]

In addition to providing the above information, the two antenna patterns also present the following useful applications:

a) Provides a measure of the degree of circularity of any of the contours. Both patterns indicate the contours of the main beam through the first side lobe are slightly elliptical in form. This information is helpful when the gain of the antenna is to be measured by the pattern integration technique.

b) The antenna patterns being a three dimensional projection type of display are informative for investigation purposes on the energy distribution over an area of the antenna beam. Location of a cone of energy on a null can be quickly determined from the pattern presentation.

The large separation distance between the earth-station antenna and the satellite provides an ideal test range with which accurate measurements of the antenna far field pattern can be made. Accurate measurements are feasible because the primary degradation factors such as near field effects and multipath effects are essentially eliminated. Accuracy

of this method of measurement is verified by the close agreement of the measured beam angles and the first side lobe angles to their predicted values as shown in table 3.49. The method of measurement and presentation of the antenna pattern becomes informative by providing an accurate technique of measuring and by revealing the unique structure of the second side lobe as a ring of irregular energy cones surrounding the main beam.

TABLE 3.48. SCANNING CHARACTERISTICS

Station	Type of Test	Scan Angle	No. of Scans	One Scan Period	One Frame Period	AGC Volt. Chart Speed
Mojave	1 Station	1.8°	36	36 sec.	22 min.	0.2 in/sec
Mojave	2 Station	2.6°	52	52 sec.	45 min.	0.5 in/sec
Rosman	2 Station	2.0°	40	40 sec.	27 min.	0.5 in/sec

TABLE 3.49. TRANSMIT ANTENNA PATTERN CHARACTERISTICS

Station	System Test Used	Beamwidth (-3 db)			First Side Lobe Angle				First Null	No. Side Lobes
		X-Axis	Y-Axis	Theor.	X-Axis	Y-Axis	Theor.	Ave Level	Level (Ave.)	
Mojave	One Station	0.27°	0.24°	0.28°	0.48°	0.40°	0.46°	-18db	-30 db	3
Mojave	Two Station	0.29°	0.26	0.28°	0.53°	0.41°	0.46°	-18db	-36 db	3
Rosman	Two Station	0.20°	0.16	0.13°	0.27°	0.24	0.22°	-19db	-26 db	5

TABLE 3.50. CHARACTERISTICS OF EARTH STATION ANTENNAS

Characteristic	Earth-Station Antenna	
	Rosman	Mojave
Diameter (Cassegrain)	85 ft	40 ft
Gain Transmit (6.2 GHz)	61.5 db	54.6 db
Gain Receive (4:2 GHz)	58.5 db	51.0 db
Efficiency Transmit	47%	44%
Efficiency Receive	55%	46%
Polarization	Linear	Linear
Tracking Accuracy	±0.05°	±0.015°
Angular Velocity Range	0.005° to 3.0°/sec	0.04° to 5.0°/sec
RF Beamwidth Transmit (-3 db)	0.13°	0.28°
RF Beamwidth Receiver (-3 db)	0.20°	0.47°
System Noise Temp. (ZENITH)	63°K	63°K
Surface Tolerance	0.040 in. rms	0.031 in. rms
f/D Ratio	0.423	0.40
Subreflector Diameter (Hyperboloid)	11 ft	4 ft
Monopulse Feed	17-Horn Array	5 Dielectric Rods
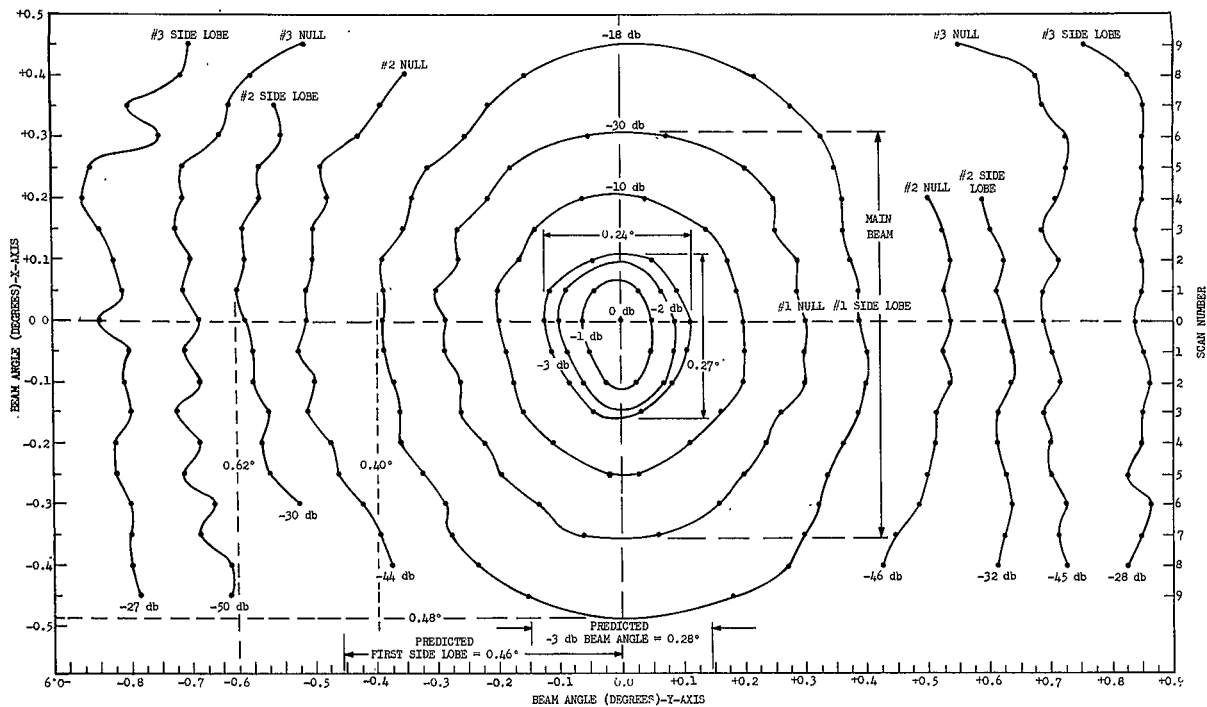
Figure 3.136.   Transmit Antenna Pattern - Mojave (Single Station)

3.328
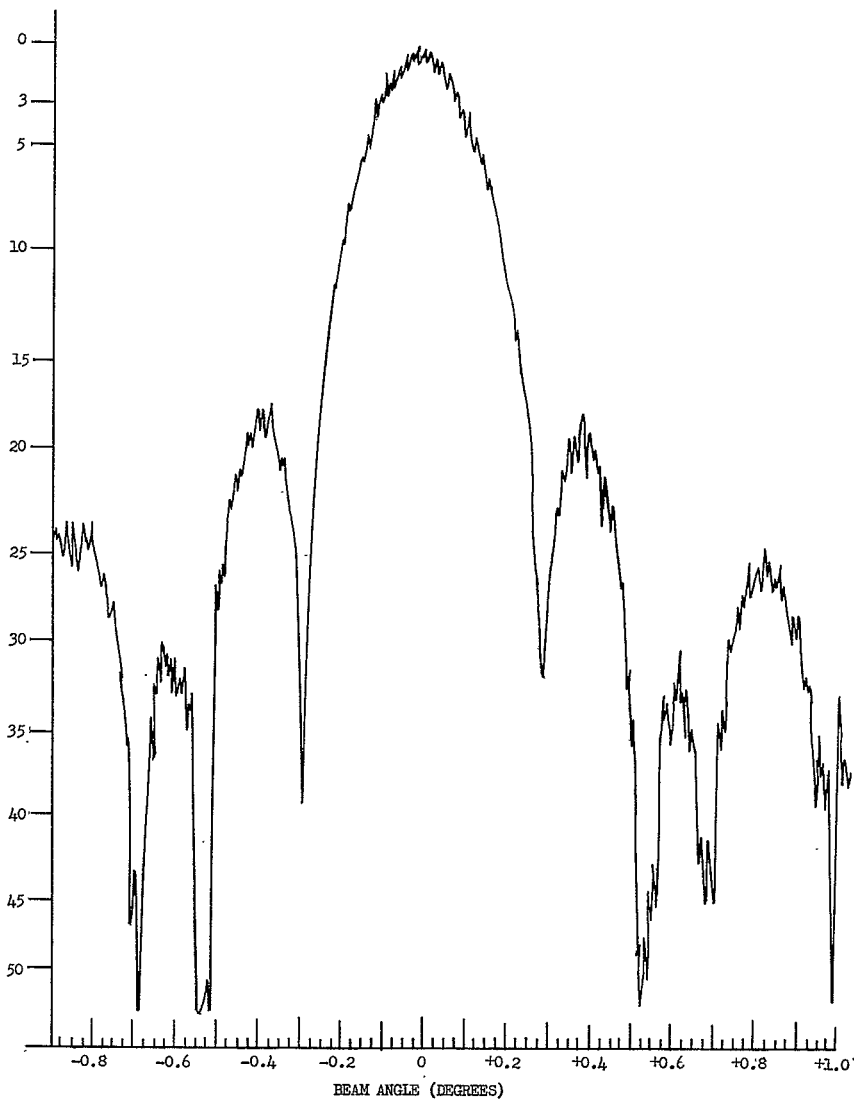
Figure 3.137.   Transmit Antenna Pattern – Center Scan (Mojave, Single Station)

3.329
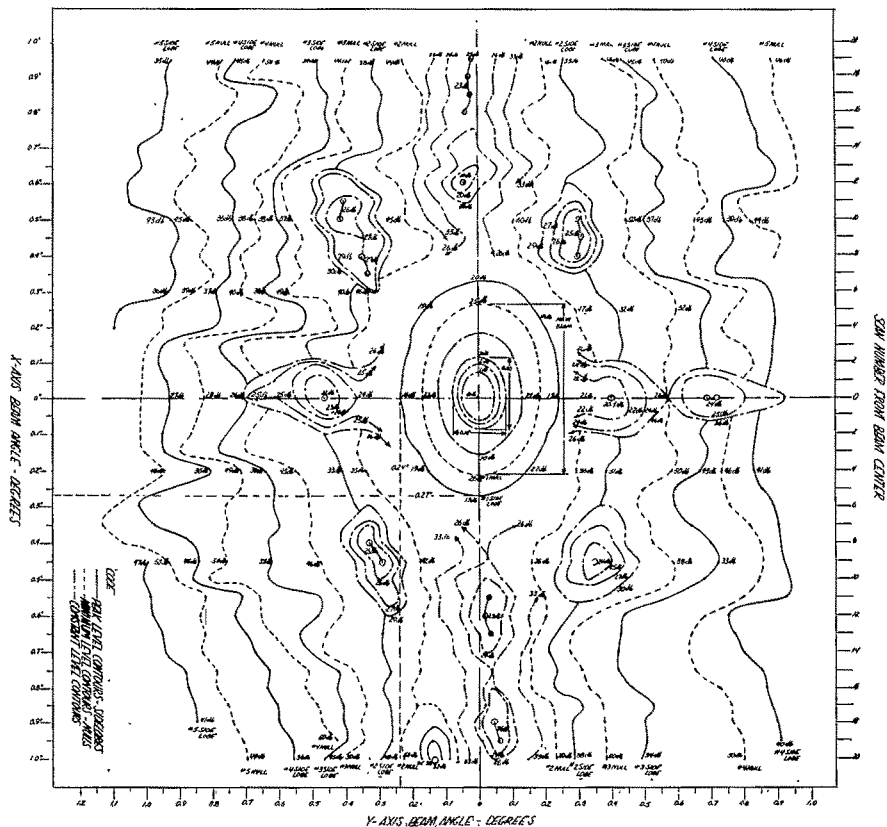
Figure 3.138. Transmit Antenna Pattern – Rosman (Two Stations)

3.330
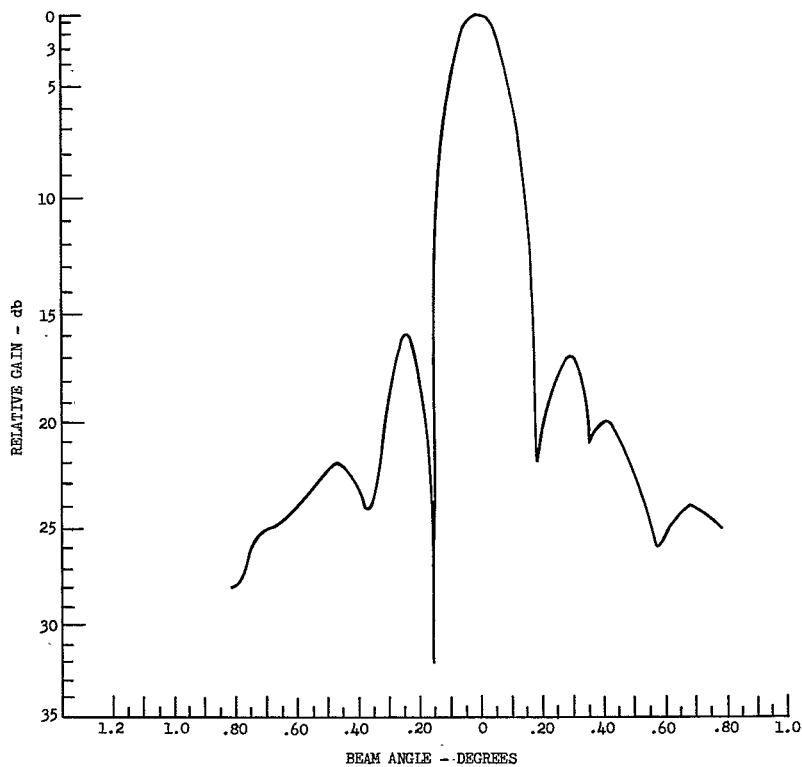
Figure 3.139.   Transmit Antenna Pattern - Center Scan (Rosman, Two Stations)

3.331
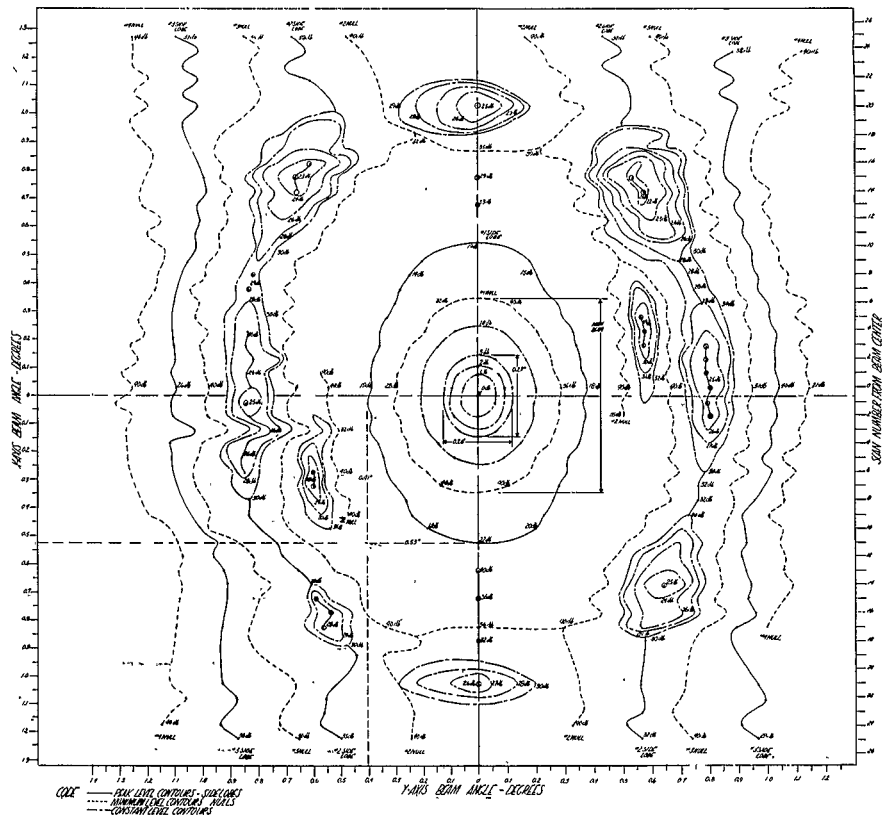
Figure 3.140. Transmit Antenna Pattern - (Mojave, Two Stations)
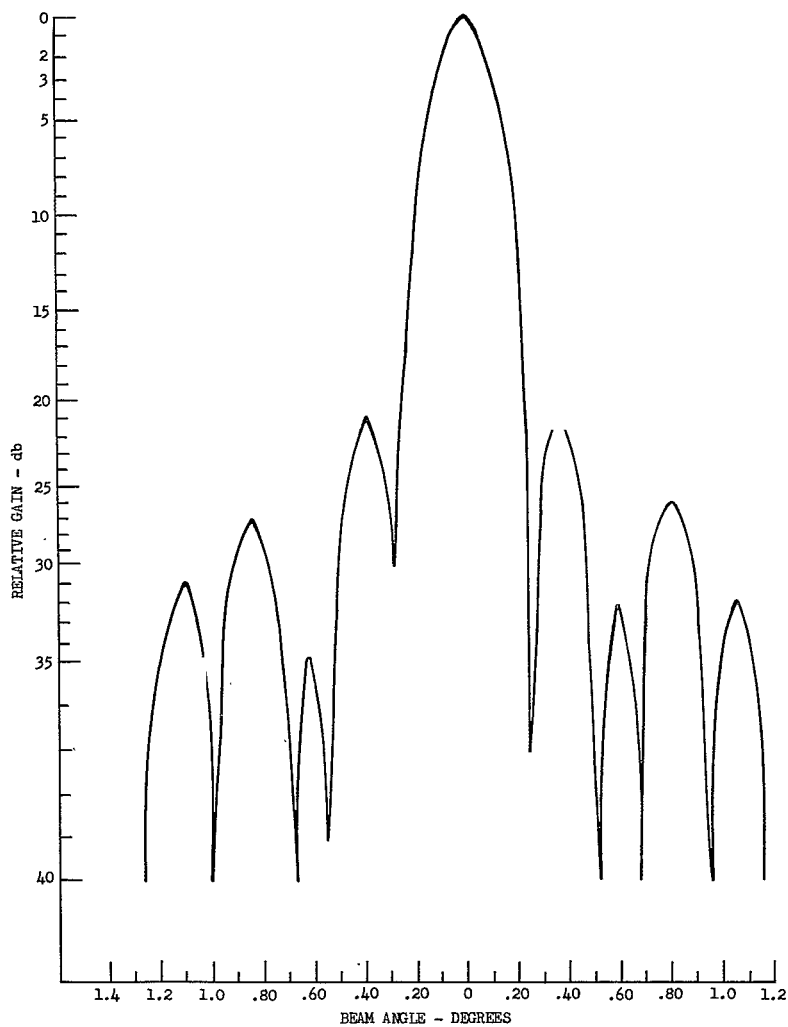
Figure 3.141. Transmit Antenna Pattern - Center Scan (Mojave, Two Stations)

3.333
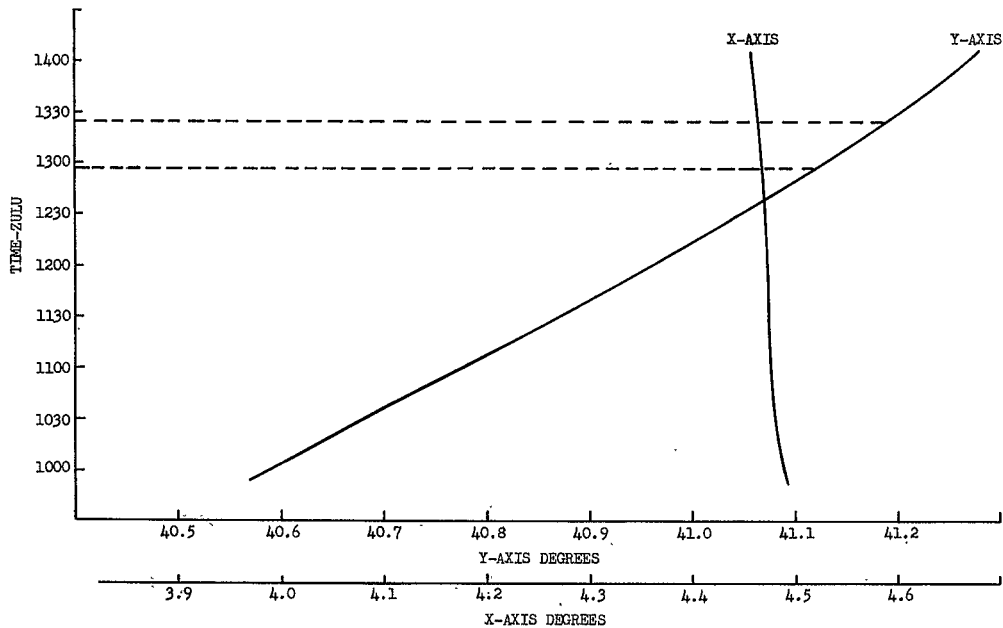
Figure 3.142. Rosman Antenna-Axes Change for Satellite Drift (ATS-3, March 31, 1970)

3.7.3 EARTH-STATION RECEIVE ANTENNA PATTERNS (AN-SP-1.2) (H.J. Kochevar)

3.7.3.1 Description and Test Results

OBJECTIVE

The purpose of this experiment is to determine the receive beam pattern of the earth-station antennas and to present a plot of the data obtained in a three-dimensional projection type of display similar to the one developed for the transmit antenna patterns described in section 3.7.2. A single earth station and an ATS satellite provide the long range test facility with which the antenna pattern measurements are performed.

TEST CONDITIONS

The earth receive antenna patterns were determined by utilizing a system configuration similar to that used for the transmit antenna patterns with the exception that the test signal was the satellite unmodulated downlink carrier. The resulting AGC signal developed in the R/RR receiver was recorded on a strip-chart recorder in conjunction with time information. Amplitude of the AGC signal varies as a direct function of the received carrier power level and conforms to the receive-antenna beam configuration.

Measurement of a symmetrical pattern around the main beam was achieved by using the autotrack coordinates as the reference position for the center point of the scanned frame. Negligible error is created in the antenna pattern presentation by the drift of the satellite during the time required to scan one complete frame.

A peak-to-peak scan angle of 2.6 degrees was utilized along both the X-and Y-axes to form one frame of the receive antenna pattern. This magnitude of scan angle was the same as that used for the two-station transmit antenna pattern test. A scan angle with this value can be used for the receive pattern because the downlink carrier level does not fall below the threshold of the R/RR receiver whenever the antenna scans the low power level of the antenna beam.

The raster scanning of a complete pattern frame by the antenna was automatically performed from a programmed tape. An entire pattern frame is produced by moving the antenna in steps of 0.05 degree along the X-axis after the completion of each scan of 2.6 degrees along the Y-axis. A total of 52 scans is provided along the X-axis for a peak-to-peak angular excusion of 2.6 degrees.

RESULTS

The receive antenna patterns were measured at the Mojave and Rosman stations in conjunction with the ATS satellite. Three-dimensional projection presentations of the antenna patterns were developed from the data obtained and are illustrated in figure 3.143 for Mojave and figure 3.145 for Rosman. A strip-chart recording of the AGC voltage

representing the relative antenna gain provided most of the data in developing the pattern presentations. A complete scan taken across the center of the main beam is shown in figure 3.144 for Mojave and figure 3.146 for Rosman and illustrates the configuration of the antenna pattern for that particular cross section.

Angular position and relative power level for each element presented in the antenna pattern illustrations can be located with reference to the center line and peak level, respectively, of the antenna main beam.

The contour lines shown in figure 3.143 and 3.145 represent the characteristics that are considered the most significant of the antenna pattern and consist of constant level contours of the main beam, the peaks of side lobes and the minimum power level or nulls. The antenna pattern presentations in figures 3.143 and 3.145 were developed by selecting points representing the significant features from each beam cross section shown in figures 3.144 and 3.146 and plotting them with respect to their scan number and beam angle. The antenna patterns indicate concentric contours are formed from the main beam through the first side lobe while open irregular contours are formed beyond the first side lobe.

The antenna X-and Y-axes coordinates and time recorded on teletype tape provide information with which the boundaries for each antenna scan angle presented on the AGC signal strip-chart recording can be accurately determined. The Y-axis servo-error signal was also recorded on the strip-chart recording of the AGC signal and provided additional information which aided in the location of the boundaries for each antenna scan angle.

Significant measured features shown in figures 3.143 and 3.145 of the antenna patterns at Rosman and Mojave are summarized in table 3.51.

3.7.3.2 Analysis

The Mojave receive antenna pattern presented in figure 3.143 consists of contour lines indicating constant levels of the main beam, peaks of the side lobes and minimum power levels or nulls, similar to that presented in the transmit patterns. The area scanned in the receive pattern extends beyond the range occupied by the second side lobe. Relative power levels over the entire antenna pattern at specific points on the contours representing the main beam, side lobes and nulls are indicated in the diagram. Measured beamwidths of 0.41 degree and 0.42 degree at the half-power points (-3 db) in the X-and Y-axes planes, respectively, have values very close to the calculated value of 0.47 degrees. This result indicates that a high degree of accuracy is obtained by using this method of measurement.

Figure 3.143 shows the main beam in five concentric contours, four of which are of constant level and vary for zero db at the beam center to -10 db. The first null is the fifth concentric contour and varies in level from -29 db to -48 db. The first side lobe which is also a closed concentric circle has a measured angle of 0.78 degree in the X-axis

3.336

and 0.71 degree   in the Y-axis as indicated in the diagram.   These values compare very closely to the calculated value of 0.68 degrees.

The results of the receive pattern obtained reveals an unsymmetrical distribution of energy occurs beyond the first side lobe.   Contours of the second side lobe form an open loop and diverge away from the center of the main beam at both ends of the X-axis.   Although the second null is a closed loop, it also has a diverging characteristic.   Between the diverging second null contours near the X-axis, points of maximum and minimum power were located as shown in figure 3.143.   One high-and one low-energy level exists in these two areas.   The diagram reveals the two high-energy level points are encircled by nulls of appreciably lower energy levels forming an approximate cone-shaped mass of energy.

With the contour configuration of the second null and second side lobe as shown in figure 3.143 and the forming of power level peaks it appears that many masses of energy in the form of cones are located around the antenna main beam along the second side lobe.   Additional scans may reveal the existence of a closure in the divergence of the diverging contours.   Irregular energy distribution in the antenna pattern is the result of such factors as, antenna reflector surface irregularities, interference from the struts supporting the subreflector, and mis-alignment of the feeds and subreflector.   Relative energy levels were indicated at different points along the contours to present the variation in energy level over the entire antenna pattern.   The magnitude of these energy points and their distribution presents an overall picture of the antenna pattern configuration relative to the center of the main beam.

The Rosman receive antenna pattern is also presented as a three dimensional projection display and is shown in figure 3.145.   With a larger antenna (85 ft) at this station then the Mojave (40 ft) antenna, a smaller beam angle is therefore produced.   This feature provides a greater coverage of the antenna pattern area for the same angle scanned.   A peak-to-peak scan angle of 2 degrees in the X-and Y-axes provides a pattern that displays contours through the third side lobe.

The measured beamwidth of the main beam at the -3 db level is 0.22 degree   in the X-axis and 0.19 degree   in the Y-axis.   These angles compare very closely to the calculated value of 0.20 degrees.

Rosman's pattern shows the contours of the side lobes and nulls beyond the second null also diverge and form discontinuous contour lines.   Location of high-and low-energy points at the ends of the X-axis between the second null contours reveals the existence of groups of energy in the form of irregular cones similar to the Mojave pattern.   The irregular configuration of the second null and side lobe and the forming of power level peaks indicates that there are in existence many individual masses of energy in the form of of cones surrounding the main beam along the second side lobe similar to the Mojave pattern.

The concentric contours of constant energy level of the main beam are also presented in figure 3.145 to provide a perspective view of the approximate shape of the center beam down to the first null. Variation of the energy level over the entire pattern is indicated by the relative levels located along each contour.

A comparison between the Rosman and Mojave antenna patterns indicates similar types of characteristics are obtained for a Cassegrainian antenna design regardless of the size of the antenna. A very interesting feature revealed by both antenna patterns is the existence of irregular shaped cones or masses of energy along the second side lobe and surrounding the main beam. This characteristic is similar to that given in a publication describing the results of an antenna pattern measurement performed on a 30 foot diameter Cassegrainian radar antenna[50]. The first side lobe for both antenna patterns is the only side lobe which forms a solid concentric ring of energy around the main beam. Remainder of the antenna pattern appears to consist of many masses of irregular energy cones surrounding the main beam similar to the transmit antenna patterns.

3.7.3.3 Conclusion

The receive antenna patterns shown in figures 3.143 and 3.145 presents a view of a three-dimensional projection display of the most significant characteristics of the RF beam for this particular design of a Cassegrainian antenna. The large separation distance between the earth station antenna and the satellite provides an ideal test range with which accurate measurements of the antenna far field pattern can be performed. Accurate measurements are feasible because the primary degradation effects such as the near field effects and multipath effects are essentially eliminated. This accuracy is verified by the close agreement of the measured main-beam angle and the location of the first side-lobe angle to their calculated values.

This antenna pattern test resulted in being very informative by revealing the unique structure of the side lobes and nulls beyond the first side lobe. Formation of irregular cones or masses of energy in the second side lobe proves to be a very interesting characteristic of the antenna. A list of the significant measured characteristics of the antennas at Rosman and Mojave shown in figures 3.143 and 3.145 are summarized in table 3.51.

TABLE 3.51.   RECEIVE ANTENNA-PATTERN CHARACTERISTICS

Station	Beamwidth (-3 db)			First Side-Lobe Angle				First Null Level (Av.)	No. of Side Lobes
	X-axis	Y-axis	Theor.	X-axis	Y-axis	Theor.	Av. Level		
Rosman	0.22°	0.19°	0.20°	0.31°	0.27°	0.32°	-20 db	-32 db	3
Mojave	0.41°	0.42°	0.47°	0.78°	0.71°	0.68°	-21 db	-44 db	2
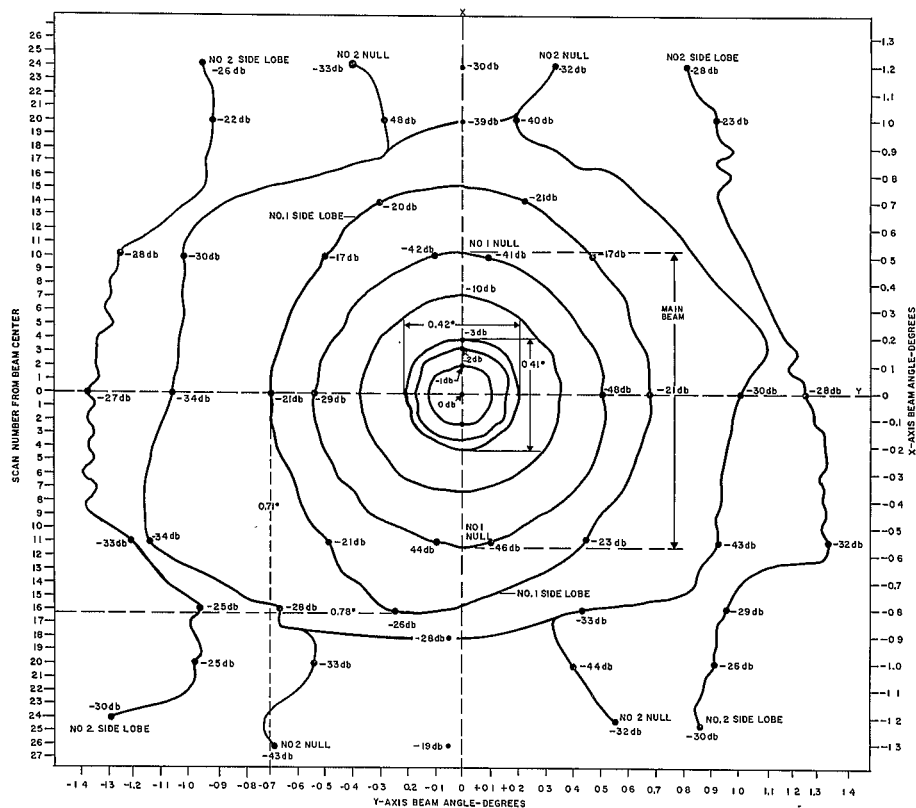
Figure 3.143. Receive Antenna Pattern-Mojave
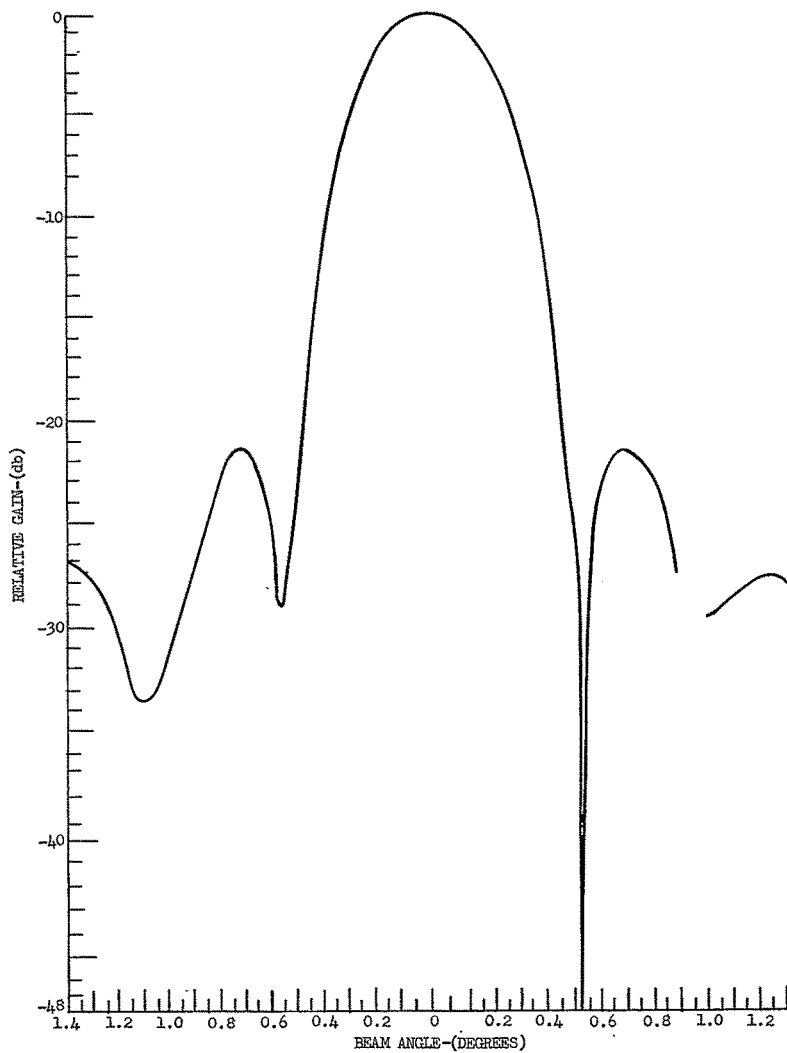
Figure 3.144. Receive Antenna Pattern-Center Scan (Mojave)
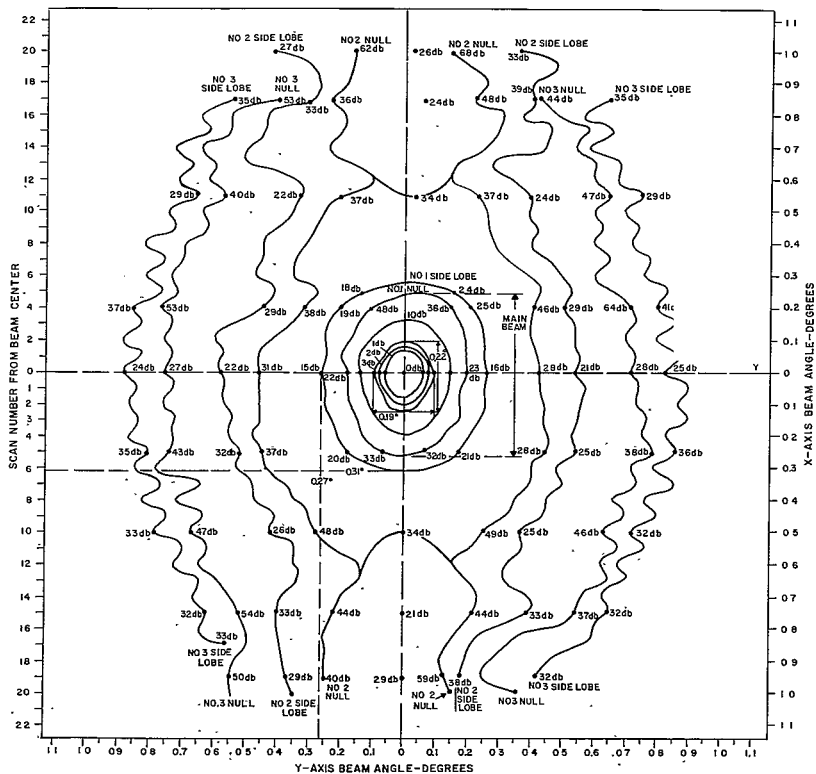
Figure 3.145.   Receive Antenna Pattern-Rosman
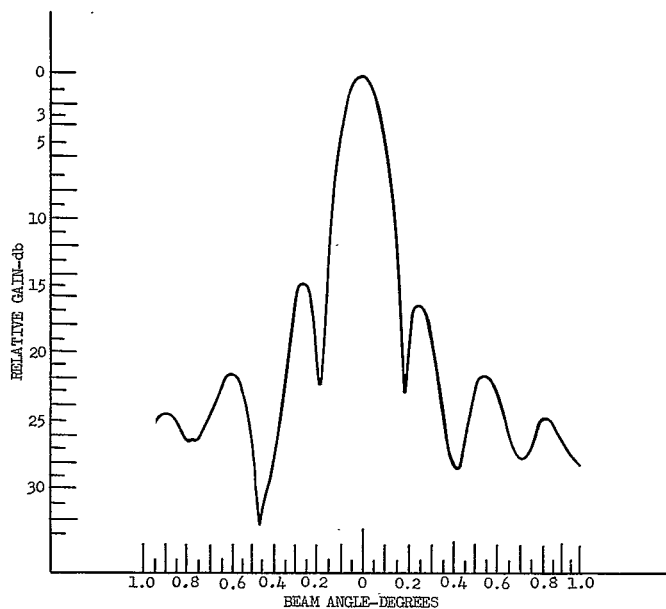
Figure 3.146.   Receive Antenna Pattern-Center Scan (Rosman)

5.1 MULTIPLEX-CHANNEL FREQUENCY STABILITY (R.J. Martel)

In the MA communications mode, it has been noted that,on strip-chart recordings, quite large instantaneous frequency deviations occur in the 1,000-Hz tone transmitted through a voice channel. The reasons for this have been investigated, and at present it appears that the deviations are due to the relatively poor inherent short-term stability of the 6-GHz standard in the SSB transmitter. Due to the propagation delays,the frequency-correction loop does not compensate for these effects, and in fact makes them worse.

The objectives of this investigation are to:

1) Consider how severe a problem this short-term frequency instability really is, from the viewpoint of system operation.

2) Examine the SSB-AFC system from an analytical point-of-view to determine its degree of expected performance in the presence of various input frequency disturbances, such as doppler, system-oscillator instability, etc.

3) Suggest experimental measurements which could be made to determine both the cause of the difficulty and its effects upon performance.

The CCIR Recommendations state that frequency error in any voice channel shall be not more than 2 Hz. They do not specify this as RMS, or peak or state what percentage of the time it may be exceeded. The implication is that it should never be exceeded. These recommendations are, however, a carryover from the old, and still valid, CCITT recommendations for carrier telephone systems; and they were intended to specify the required degree of long-term frequency stability or accuracy of frequency synchronization between the ends of a link, for the carrier oscillators in the multiplex equipment. These oscillators produce outputs at the carrier frequencies which, even in very high-capacity systems, are only a few megacycles, and which do not need to be moved to compensate for doppler shifts. Consequently there was never any need to allow the error to exceed 2 Hz for any portion of the time. Short-term stability was considered only in terms of the noise in a channel produced by it, which, together with all other sorts of noise, had a maximum permissible total value. In this system where the SSB signals are translated to over 6,000 MHz, and where, furthermore, doppler shifts must be compensated, the problem of short-term frequency stability becomes important.

Frequency stability in the channels is important because frequent errors can cause loss of intelligibility and data errors in the teletype and other digital messages. Although there is a great temptation to say that since the errors do exceed 2 Hz (peak),the system therefore does not meet CCIR specifications, and therefore needs improvement; we should first determine from experiments how bad the existing errors really are, in terms of

the system operation. As far as speech is concerned with its low data rate, it is quite debatable whether or not these errors of up to about 20-Hz peak would really cause a loss of intelligibility, or other objectionable characteristics. In the case of wideband FSK data, it is also unlikely that there would be much effect. If one tried to send DPSK or similar data signals the effect on the error rate would be disastrous, but these signals are not contemplated here; and in any event a short term jitter of ±2 Hz could also produce ill-effects. In the case of narrow band teletype, however, where the data rate is very low, the filters used in the teletype modem to recover the FSK signals will have quite narrow bandwidths. For 60 WPM teletype, with 120-Hz channel spacing for each of the filters, the FSK modem would have a bandwidth only in the order of 30 Hz. Therefore the 20-Hz peak frequency errors could severly affect this common method of transmitting teletype sub-multiplexed on voice channels. Also, if the multiplex channel is used to transmit musical programs, frequency offsets or errors would cause a constant displacement of the musical spectrum and thus destroy the necessary harmonic relationship between notes. If these errors approach or exceed 2 Hz the subjective effect on tonal quality of the musical sound will be quite noticeable.

In pursuing the multiplex channel frequency stability problem that appears to exist in the ATS single sideband system, it is highly desirable to first establish an analytical model of the frequency control loop which can serve as a basis for evaluation of subsequent experimental investigations. Frequency errors on the transmitted test tone in the multiplex channel could be due to any one or any combination of the following inputs which will in general be designated as R(s):

1. Receiver thermal or KTB noise
2. System oscillator FM noise (both short and long term)
3. Doppler
4. 60-Hz and other power line frequency modulation
5. 1.6-Hz modulation due to S/C spin
6. Noise contributed by other stations during multi-station tests.

It is presently reasoned that the two major sources of control loop frequency error (assuming a stable system) will be due to the time rate of change of the doppler shift and/or the frequency instability of the various oscillators associated with the SSB system. In the analysis that follows, these two sources of frequency error will be considered independently in the presence of a finite system transport lag. * Of particular interest in the proceeding presentation will be the effect of the so-called error cancellation circuits in the SSB transmitter on the MUX channel frequency error.

---

* The control loop transport lag is defined as the round trip delay through the satellite between the SSB transmitter and the ground PhM receiver.

The following subject matter will be treated in detail in the succeeding paragraphs:

1. Development of an AFC system model with error cancellation and transport lag.
2. The effect of doppler on the multiplex channel frequency error.
3. Derivation of the multiplex channel power density spectrum in terms of the system oscillator FM noise spectrum.
4. Development of alternate solutions to the AFC problem.
5. Determination of the normalized rms multiplex channel frequency error.
6. Derivation of the FSK modem error probability in terms of the channel frequency deviation and the rms frequency error.
7. Analysis of phase modulation due to 1.6-Hz S/C spin.
8. Analysis of 60 Hz angle modulation effect.
9. Analysis of 6-GHz phase lock klystron.
10. Presentation of experimental results from the computer programmed Fourie analysis and frequency distribution experiments.

5.1.1 DEVELOPMENT OF THE AFC SYSTEM TRANSFER FUNCTION

The baseband analogue of the present SSB AFC system including the error cancellation circuits can be represented in block diagram servo form as shown in figure 5.1. The open loop transfer function, KG(s), of the control loop can be written as the product of the individual subsystem functions as follows:

$$KG(s) = \frac{K_1 \, K_2 \, K_3}{\tau s + 1} \cdot e^{-sT} \tag{1}$$

where K_1 = Discriminator sensitivity = 40 millivolts per kHz.

K_2 = product of all open loop frequency independent gains = 2×10^3

K_3 = Voltage Controlled oscillator sensitivity = 12 kHz/Volt

Input R (s)

C(s)

$\mathcal{E}$(s) Control
Loop Error

Transport Lag
e^{-sT}

Control Loop
Error
Delayed

Discriminator .
K_1

$\mathcal{E}$'(s) MUX Channel
Error After Cancellation

Amplifier & Filter
$\dfrac{K_2}{\mathcal{T}s + 1}$

VCO
K_3
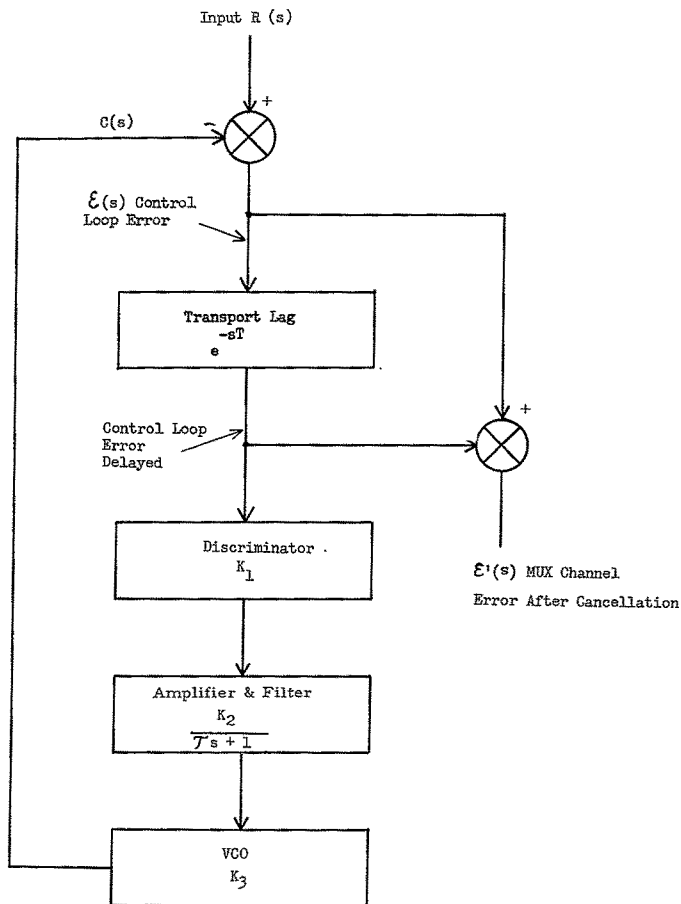
$$\mathcal{E}(s) = R(s) \cdot \left[\frac{\mathcal{T}s + 1}{\mathcal{T}s + 1 + Ke^{-sT}}\right]\left[1 - e^{-sT}\right]$$

where $K = K_1 K_2 K_3$

Figure 5.1. Baseband Analogue of the AFC System

5.4

T = loop time delay or transport lag

s = The Laplacean operator

$\tau = 1/\omega$ = Time constant of the loop filter = 590 second

The closed loop frequency error ε (s) can now be expressed in terms KG(s) and the input driving function R(s) as

$$\varepsilon(s) = \frac{R(s)}{1 + KG(s)} \qquad (2)$$

ε(s) actually represents the frequency error on the received pilot frequency. Referring again to figure 5.1 if the error cancellation circuit is considered, the resulting MUX channel frequency error ε'(s) can be expressed as

$$\varepsilon'(s) = \frac{R(s)}{1 + KG(s)} \cdot \left(1 - e^{-sT}\right) \qquad (3)$$

Now on substituting equation 1 into eq. 3 and letting $K_1 \cdot K_2 \cdot K_3 = K$, there results

$$\varepsilon'(s) = \overbrace{R_{(s)}}^{\text{Input}} \cdot \overbrace{\left[\frac{\tau s + 1}{\tau s + 1 + Ke^{-sT}}\right]}^{\text{AFC Loop Error}} \cdot \overbrace{\left(1 - e^{-sT}\right)}^{\text{Error Cancellation}} \qquad (4)$$

It will be recognized from the general expression of equation 4 that the MUX channel frequency error is a function of three distinctly separable items - the input variable R(s), the AFC loop error expression and the error cancellation expression. It is immediately obvious from equation 4 that for a system with zero transport lag $\varepsilon'(s) = 0$ since $e^{-sT} = 1$. However, for a system with T finite, which is the case for ATS-1 $\varepsilon'(s)$ will also be finite and its magnitude will be a non-monotonic function of frequency.

5.1.2 AFC ERROR DUE TO DOPPLER

It will be convenient at this point to first examine the error response of the AFC loop without the error cancellation circuits. The effect of error cancellation will be considered later.

It will be recognized from equation 1 that the e^{-sT} function merely introduces an additional phase shift of ω T radians (letting $s = j\omega$) into the overall phase of the open loop transfer function. Therefore the phase margin, θm, of the control loop can be expressed as

$$\theta m = 180 - (90 + 57\, \omega_n T) \qquad (5)$$

where θm is expressed in degrees

ω_n = frequency at which the KG(jω),function has a zero db value

For K = 1000 and τ = 590 seconds, from equation 1 letting $s = j\omega$, ω_n = 1.7 rps. Now from equation 5 for ATS-1 (T = 0.3 second[1]) θ_m = 61 degrees.

It can be shown that a phase margin of 61 degrees corresponds to a system damping ratio ζ of about 0.6.[2] For purposes of analysis, the open-loop transfer function KG(S) can be expressed in terms of ζ and ω_n as

$$KG(s) = \frac{\omega_n^2}{s(s + 2\zeta\omega_n) + \dfrac{\omega_n^2}{K}} \tag{6}$$

This expression includes the effect of transport lag since ζ is a function of T as shown earlier. Now writing the error function $\varepsilon(s)$ from equation 2, in terms of the open-loop gain value of equation 6, with K >> 1

$$H(s) = \frac{\varepsilon(s)}{R(s)} = \frac{s^2 + 2\zeta\omega_n s + \dfrac{\omega_n^2}{K}}{s^2 + 2\zeta\omega_n s + \omega_n^2} \tag{7}$$

It is of particular interest at this point to examine $\varepsilon(s)$ for a ramp input of frequency which is of course a range acceleration or a doppler rate.
Letting $R(s) = \dot{\omega}/s^2$ equation 7 becomes

$$\varepsilon(s) = \frac{\dot{\omega}\left(s^2 + 2\zeta\omega_n s + \dfrac{\omega_n^2}{K}\right)}{s^2\left(s^2 + 2\zeta\omega_n s + \omega_n^2\right)} \tag{8}$$

---

[1] 0.3 second is nominal value. Actual measured 2-way time delay for each station is 0.271, 0.254, and 0.263 seconds for Rosman, Mojave, and Cooby Creek, respectively.

[2] The relationship between ω_n and ζ can be derived to yield

$$\theta_m = \tan^{-1} 2\zeta = \left[\frac{1}{(4\zeta^4 + 1)^{1/2} - 2\zeta^2}\right]^{1/2}$$

(see C. J. Savant, "Basic Feedback Control System Design". McGraw-Hill Book Co., 1958, p. 391.)

From Laplace transform tables, the inverse Laplace transform of equation 8 can be obtained. Hence, the MUX channel frequency error as a function of time will be

$$E(t) = \mathcal{L}^{-1}\left[\varepsilon(s)\right] = \dot{\omega}\left\{10^{-3}t + 1.18\zeta - \frac{.59e^{-\zeta\omega_n t}}{\left(1-\zeta^2\right)^{1/2}} \cdot \right.$$
$$\left. \sin\left[1.7(1-\zeta^2)^{1/2}t - 2\tan^{-1}\frac{\left(1-\zeta^2\right)^{1/2}}{-\zeta}\right]\right\} \tag{9}$$

If one assumes a normalized input ramp of $\dot{\omega} = 1$ rps^2 for a system damped at 0.707 of critical and for $\omega_n = 1.7$ rps (the expected bandwidth for the ATS-1 system), equation 9 becomes

$$E(t) = 10^{-3}t + 0.83\left(1 - e^{-1.2t}\cos 68t\right) \tag{10}$$

This equation is plotted in figure 5.2 for a normallized input frequency ramp of 1 cps^2. It will be noted that for $t = 0$, $E(t) = 0$ and as t increases $E(t)$ increases to about 8 cps at $t = 1$ second, than $E(t)$ remains nearly constant until t increases beyond 100 seconds. It might also be of interest to note from equation 9 that as $\zeta \to 0*$, the AFC system would become oscillatory at a frequency of 1.7 rps. In this case, equation 9 reduces to

$$E(t)\Big|_{\zeta \to 0} = 10^{-3}t - 0.59\sin 1.7t \tag{11}$$

In order to appreciate more fully the net effect of the transport lag on the closed loop AFC system, it will be instructive to look at the loop performance as $T \to 0$. In this case, KG(s) will be

$$KG(s) = \frac{K}{\tau s + 1} \tag{12}$$

and the error function becomes

$$\varepsilon(s) = \frac{\dot{\omega}(s + \omega_1)}{s^2(s + \omega_2)} \tag{13}$$

where $\omega_2 = (K+1)\omega_1$
and $\omega_2 = 1.7 \times 10^{-3}$ rps.

* A reduction in ζ would occur if the system gain should increase, if the loop time constant should decrease, or if the transport lag should increase.

$$\mathcal{E}(s) = \frac{R(s)}{1 + KG(s)} \qquad \text{Where } KG(s) = \frac{K_1\, K_2\, K_3}{\tau s + 1}$$

R(s) → + Σ − → Disc. K_1 → $\dfrac{K_2}{\tau s+1}$ → VCO K_3 → C(s)

AFC LOOP REPRESENTATION WITH NO TRANSPORT LAG

$K = K_1\, K_2\, K_3$

For Frequency Ramp Input $R(s) = \dot{\omega}_o / s^2$

$$\mathcal{E}(s) = \frac{\dot{\omega}_o\,(s+1)}{s^2\,(s+\omega_2)} \qquad \text{Where } \omega_1 = 1/\tau_1$$
$$\omega_2 = \frac{K+1}{\tau_1}$$

For $K = 10^3$ $\omega_1 = 1.7 \times 10^{-3}$ rps

$E(t) = \mathcal{L}^{-1}\left[\mathcal{E}(s) = \dot{\omega}_o\,\left[10^{-3}t + .59\,(1 - e^{-1.7t})\right]\right]$

T = 0

Input Frequency Ramp
$\dot{\omega}_o = 1$ rps^2

Closed-Loop Error E(t) (T = 0)
For Normalized Input
$\dot{\omega}_o = 1$ rps^2

E(t) for Transport Lag = 0.3 sec
$\zeta = .707$

For System With Transport Lag

$$\frac{\epsilon(s)}{\omega} = \frac{(s^2 + 2\zeta \omega_{ns} + \omega^2\, nK^{-1})}{(s^2 + 2\zeta \omega_{ns} + \omega^2\, n)s^2}$$

$$\frac{E(t)}{\omega} = \zeta^{-1}\left[\frac{\epsilon(s)}{\omega}\right] = 10^{-3}t + 1.18\zeta\,\frac{-0.59\,e^{-\zeta \omega nt}}{[1-\zeta^2]^{1/2}}\,\sin\left[1.7\,(1-\zeta^2)^{1/2}t\, -2\,\tan^{-1}\frac{(1-\zeta^2)^{1/2}}{-\zeta}\right]$$

or $E(t) = 10^{-3}t + .83\left[1 - e^{-1.2t}\cos 68°\right]$

$\dot{\omega}_o = 1$ rps^2

$\zeta = .707$

Closed-Loop Frequency Error (Hz)

Real Time (Seconds)

10 hours

5.8

Figure 5.2. AFC Loop Error Versus Time for Frequency Ramp Input

Taking the inverse laplace transform of equation 13 yields

$$E(t) = \mathcal{L}^{-1}\left[\varepsilon(s)\right] = \frac{\dot{\omega}}{\omega_2}\left(\omega_1 t + 1 - e^{-\omega_2 t}\right)$$ (14)

and for a normalized input of $\ddot{\omega} = 1 \text{ rps}^2$
equation 14 takes the form

$$E(t) = 10^{-3}t + 0.59\left(1 - e^{-1.7t}\right)$$ (15)

This equation is also plotted in figure 5.2 and it will be noted that the transport lag of 0.3 second introduces only about a 0.2-Hz increase in the AFC loop-frequency error for an input ramp of 1 rps^2.

5.1.3 AFC DOPPLER ERROR WITH CANCELLATION

It will now be instructive to consider the effect of the error cancellation technique on the actual MUX channel frequency error. Referring again to the block diagram of figure 5.1 and recalling equation 4, one can write the MUX channel error E'(t) as

$$E'(t) = \mathcal{L}^{-1}\left[\varepsilon'(s)\right] = \mathcal{L}^{-1}\left[R(s) H(s)\right] - \mathcal{L}^{-1}\left[R(s) H(s) e^{-sT}\right]$$ (16)

where H(s) is the closed loop error transfer function as given in equation 7 and R(s) H(s) = $\varepsilon(s)$, the closed loop-error function as given in equations 8 and 13. Therefore E'(t) can be written:

$$E'(t) = \mathcal{L}^{-1}\left[\varepsilon(s)\right] - \mathcal{L}^{-1}\left[\varepsilon(s) e^{-sT}\right]$$ (17)

The first part of this expression, $\mathcal{L}^{-1}\left[\varepsilon(s)\right]$, is the solution which is given in equations 10 and 15 for T = 0.3 seconds and T = 0, respectively. The second part of equation 17 simply represents a time delay in the E(t) function beginning at a time T after the initial input or:

$$\mathcal{L}^{-1}\left[\varepsilon(s) e^{-sT}\right] = E(t - T) \quad \mu(t - T)$$ (18)

where $\mu(t - T)$ is a unit step function occurring at a time T seconds
and

$$E'(t) = E(t) - E(t - T) \mu(t - T)$$ (19)

substituting equation 10 input 19, after the 0.3-second time delay $E'(t)$ becomes

$$E'(t) = \left[10^{-3}t + 0.83\left(1 - e^{-1.2t}\cos 68t\right)\right] - \left\{10^{-3}(t - T) + \right.$$

$$\left. 0.83\left[1 - e^{-1.2(t - T)}68 \cos (t - T)\right]\right\} \tag{20}$$

on combining terms this becomes:

$$E'(t) = 10^{-3}T + 0.83\,e^{-1.2t}\left[e^{1.2T}\cos 68\,(t - T) - \cos 68t\right] \tag{21}$$

It can now be recognized from equation 20 that the maximum value of $E'(t)$ will occur at $t = 0.3$ second or

$$\begin{matrix}E'(t) & = & E(t) & = & 0.28 \text{ cps} \\ t = 0.3 \text{ sec} & & t = 0.3 \text{ sec} & & \end{matrix} \tag{.22}$$

and from equation 21 it is seen that as t becomes large the error will approach a limit at

$$\begin{matrix}E'(t) & = & 10^{-3}T & = & 0.0003 \text{ cps} \\ t \text{ large} & & & & \end{matrix} \tag{23}$$

It should be remembered of course that these errors are normalized to an input ramp function of 1 rps^2 and the actual error will be directly proportional to the input function.

Following this same procedure substituting equation 15 into equation 19 after the initial time delay, $E'(t)$ becomes

$$E'(t) = 10^{-3}t + 0.59e^{-1.7t}(e^{1.7t} - 1) \tag{24}$$

and the maximum value of the error for an input ramp of 1 rps^2 will again occur at $t = 0.3$ sec yielding

$$E'(t)_{max} = 0.24 \text{ cps} \tag{25}$$

as t becomes large, equation 24 will reduce to the same value as given in equation 23.

5.1.4 THE POWER DENSITY SPECTRUM OF THE AFC ERROR

It is desirable at this point to derive an expression for the one sided power density spectrum $G'_e(f)$ of the Multiplex Channel frequency error. This will prove to be extremely valuable in interpreting the results presently being obtained from the Fourier Analysis investigations being conducted through ATSOCC.

In general, the input driving function $R(s)$ can be expressed as

$$R(s) = D(s) + N(s) + Y(s) \tag{26}$$

where   D(s) = input due to doppler frequency changes.

N(s) = quadrature component of the thermal noise input

Y(s) = input due to system oscillator FM noise

For the case of a high input signal-to-noise ratio (Y(s) >> N(s)) and if doppler is not to be considered, the resulting MUX channel frequency error due to oscillator FM noise alone will be, from equation (4)

$$\varepsilon'(s) = Y(s) \, H(s) \left(1 - e^{-sT} \right) \tag{27}$$

where

$$H(s) = \frac{\tau \, s + 1}{\tau s + 1 + K e^{-sT}} \tag{28}$$

If the one-sided power-density spectrum of the oscillator FM noise input Y(s) is represented as $G_y(f)$, then from network theory, the one-sided density spectrum of the error $\varepsilon'(s)$ can be written as

$$G'_e(f) = G_y(f) \left| H(j\omega) \right|^2 \cdot \left| 1 - e^{-j\omega T} \right|^2 \tag{29}$$

Letting $S = j\omega$ in equation 28 $\left| H(j\omega) \right|^2$ becomes for $K \gg 1$

$$\left| H(j\omega) \right|^2 = \frac{1 + \omega^2 \, \tau^2}{K^2 + \omega^2 \tau^2 - 2K \, \omega \, \tau \, \sin \, \omega T} \tag{30}$$

It will be recalled that the last part of the $G_e'(f)$ function (equation 29) results from the error cancellation technique and can be expanded as a sine and cosine function to yield,

$$\left| 1 - e^{-j\omega T} \right|^2 = (1 - \cos \, \omega \, T)^2 + \sin \, \omega T \tag{31}$$

This can be trigonometrically simplified to give

$$\left| 1 - e^{-j \, \omega T} \right|^2 = 4 \sin^2 \frac{\omega \, T}{2} \tag{32}$$

The general expression for the one sided power density spectrum of the MUX channel error can now be written as

$$G'_e(f) = G_y(f) \, x \, \frac{1 + \omega^2 \, \tau^2}{K^2 + \omega^2 \tau^2 - 2K \, \omega \, \tau \, \sin \, \omega T} \, x \, 4 \sin^2 \frac{\omega T}{2} \tag{33}$$

It is necessary at this point to devise some model for $G_y(f)$ that is representative of the spectral density resulting from the composite contribution of the various oscillators

associated with the AFC system. Based on the stability analysis of oscillators in general, a reasonable assumption for the spectral density will be an inverse squared frequency relationship and can be expressed a

$$G_y(f) = \frac{C}{\omega 2} \text{ watts/cps} \tag{34}$$

where C is a constant of proportionality.

Now on substituting the assumed value of $G_y(f)$ from equation 34 into equation 33, the expression for the one-sided power-density spectrum of the MUX channel error will be

$$G'_e(f) = CT^2 \frac{\sin^2 \omega T/2}{(\omega T/2)^2} \cdot \frac{1 + \omega^2 \tau^2}{K^2 + \omega^2 \tau^2 - 2K\omega\tau \sin \omega T} \tag{35}$$

Particular note should be made of equation 35 because of its somewhat unexpected shape. It will be noted, for example, that as $\omega \longrightarrow o$, which is indicative of a long-term frequency drift $G'_e(f)$ has a finite value because of the $\sin^2 x/x^2$ term, or

$$G'_e(f)_{\omega \to 0} = \frac{CT^2}{K^2} \text{ watts} \tag{36}$$

In equation 35 if the values of $K = 10^3$, $\tau = 590$ seconds, $T = 0.3$ second and $\omega = 2\pi f$ are employed, the following expression is obtained:

$$G'_e(f) = 10^{-7} C \frac{\sin^2 .94 f}{f^2} \left[\frac{1 + 1.38 \times 10^7 f^2}{1 + 13.8 f^2 - 7.4 f \sin 1.88 f} \right] \tag{37}$$

The normalized value of this expression, $G'_e(f)/10^{-4}C$ was computer programmed, and the solution is plotted in figure 5.3. It will be noted that definite peaks occur at 0.57 cps, 4.73 cps and 8.15 cps, with progressively lower amplitudes. Also, the function goes to zero at multiples of about 3.34 cps.

To more closely relate the preceeding analysis with the actual frequency errors being measured at the stations, equation 37 might be written in terms of a voltage density, or a frequency density spectrum (assuming a frequency-discriminator type of detection). Therefore, taking the square root of $G_e'(f)$, assuming a normalized impedance level of 1 ohm, there results

$$\left[G'_e(f) \right]^{1/2} = 3.18 \times 10^{-4} C' \frac{\sin 0.94 f}{f} \left[\frac{1 + 1.38 \times 10^7 f^2}{1 + 13.8 f^2 - 7.4 f \sin 1.88 f} \right]^{1/2} \tag{38}$$
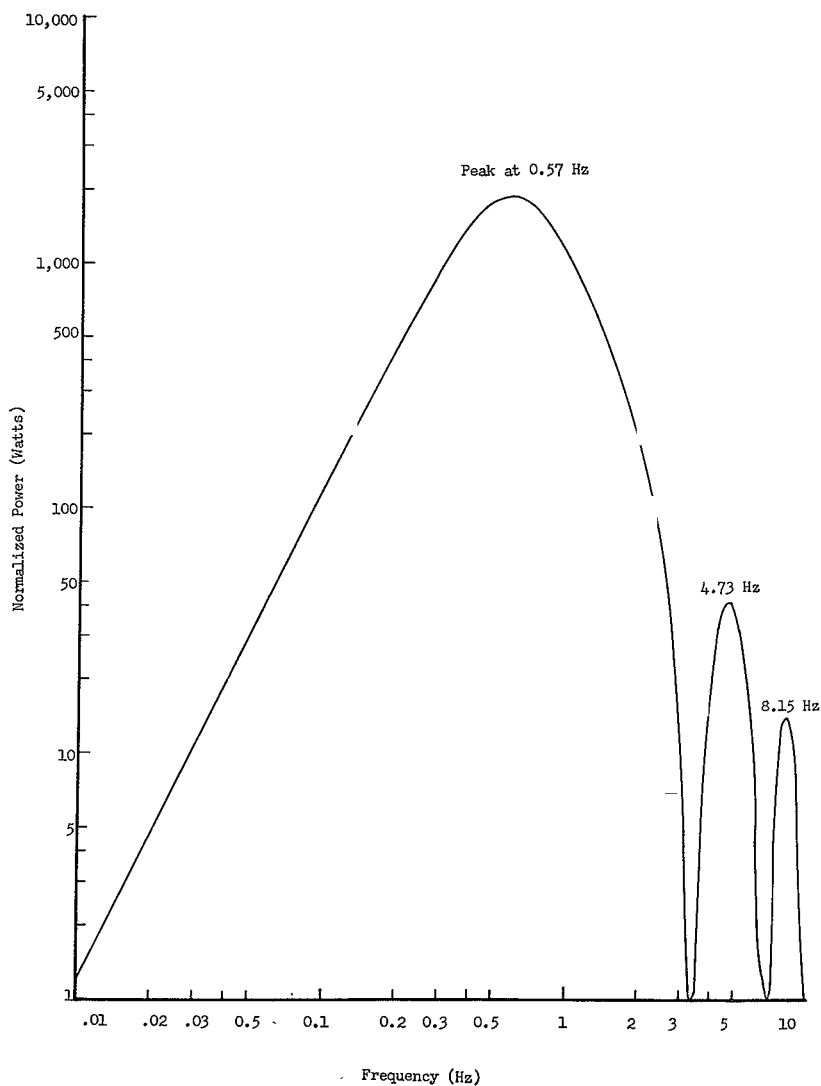
Figure 5.3. Power-Density Spectrum of Multiplex Channel-Frequency Error

5.13

Where C' is now a new constant taking into account the discriminator gain characteristic. This function was also computer programmed and plotted and is presented in figure 5.4. This same function is plotted on a linear scale in figures 5.5 and 5.6 along with experimentally obtained response from the Fourier series investigations. It is interesting to note the similarity between the two plots, particularly the peak which occurs at about 0.6 cps and the definite null that exists at about 3.3 cps. The experimental plots are the results of data obtained over a particular 16-second interval.

5.1.5 ALTERNATE SOLUTIONS TO THE AFC PROBLEM

The preceeding analysis has dealt almost exclusively with examination of the expected performance of the SSB-AFC system as it is presently configured. It will be instructive at this point to consider some possible alternate solutions to the frequency control problem which might yield an improvement in the multiplex channel frequency error.

A block diagram comparison of the most logical techniques which might be employed to achieve the desired frequency control of the SSB-MUX system is presented in diagrams A, B, C and D of figure 5.7. It will be recognized that the present AFC system, as represented by diagram B, is basically a type 0 system (diagram A) with the addition of the error cancellation function. The one-sided power-density spectrum of the multiplex channel error $G'_e(f)$ is given by either equation 35 or 37. It can be readily shown that if error cancellation is eliminated (diagram A) that equation 37 for the density spectrum will become

$$G_e(f) = \frac{0.25 \times 10^{-7} C}{f^2} \left[\frac{1 + 1.38 \times 10^7 f^2}{1 + 13.8 \ f^2 - 7.4f \sin 1.88f} \right] \tag{39}$$

5.14
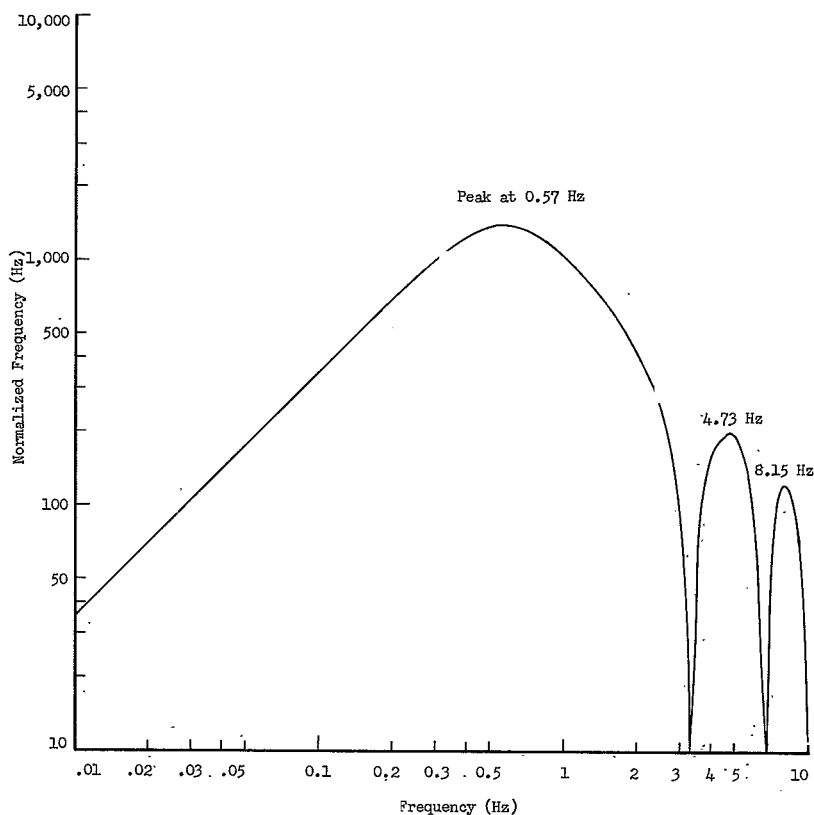
Figure 5.4. Frequency-Density Spectrum of Multiplex-Channel Error

5.15
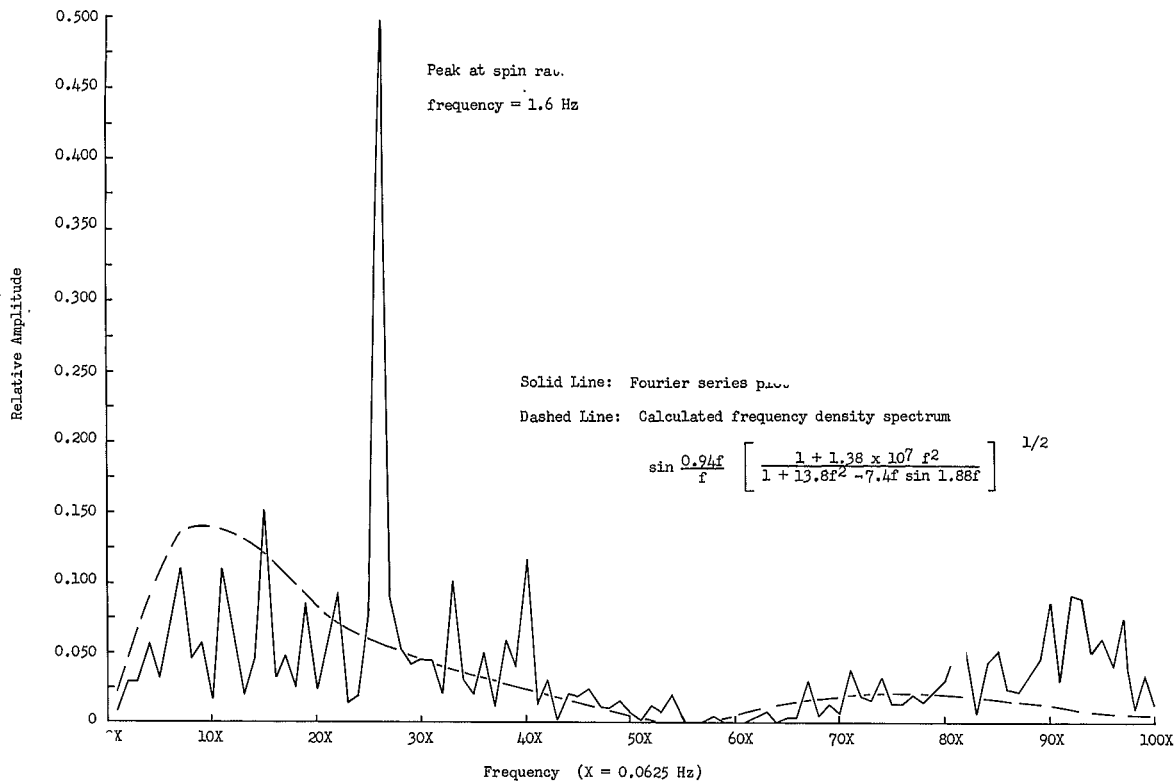
Figure 5.5. Fourier Series Plot of Frequency Error, (Rosman, 12 May 67, Cosine Function)
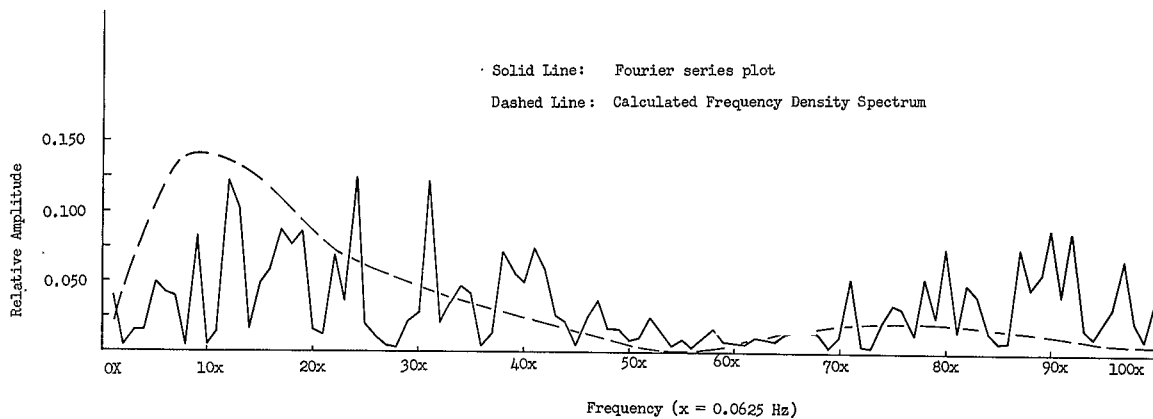
Figure 5.6. Fourier Series Plot of Frequency Error, (Rosman, 12 May 67, Sine Function)
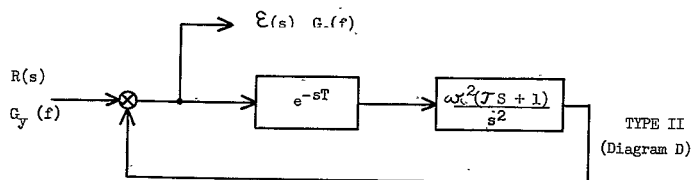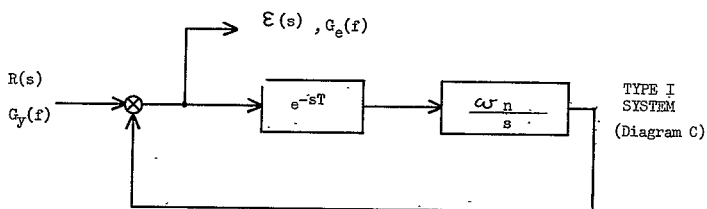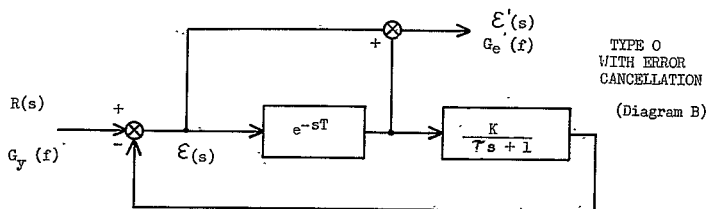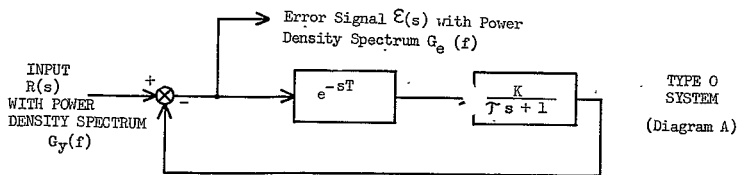
Figure 5.7. Comparison of Frequency Control Systems

Clearly, the type 0 system alone is not a good solution, since it cannot effectively compensate for long-term drift ($f \rightarrow 0$). A plot of the one-sided density spectrum for the type 0 system both with and without error cancellation (equations 37 and 39 respectively) is given in figure 5.8. Although not shown in this plot, it will be recognized that a zero occurs in equation 39 at a frequency of 0.00042 Hz, thus resulting in large frequency errors due to DC or very slow input-frequency variation.

A solution to this problem, other than error cancellation that will afford a considerable reduction in the DC frequency error, will be the use of a type I system as shown in figure 5.7, diagram C. Here a perfect integrator, ω_n/s, replaces the $K/(\tau s + 1)$ network of the type 0 system, and the open-loop transfer function becomes

$$KG(s) = \frac{\omega_n e^{-sT}}{s} \tag{40}$$

The closed-loop transfer function of the error signal will then be

$$H(s) = \frac{E(s)}{R(s)} = \frac{s}{s + \omega_n e^{-sT}} \tag{41}$$

Recalling now that the power-density spectrum of the error signal can be expressed as

$$G_e(f) = G_y(f) \left| H(j\omega) \right|^2 \tag{42}$$

Where, as before, $G_y(f)$ is the density spectrum of the input-frequency noise of the system oscillators as given by equation 34, equation 42 can be expressed as

$$G_e(f) = \frac{C}{\omega^2 + \omega_n^2 - 2K\omega \sin \omega T} \tag{43}$$

Where ω_n is the zero db crossover frequency of the open-loop response as obtained from equation 5. Now on letting $\omega_n = 1.7$ rps and $T = 0.3$ second, equation 43 can be written as

$$G_e(f) = \frac{0.35 C}{1 + 14 f^2 - 7.4 f \sin 1.88 f} \tag{44}$$
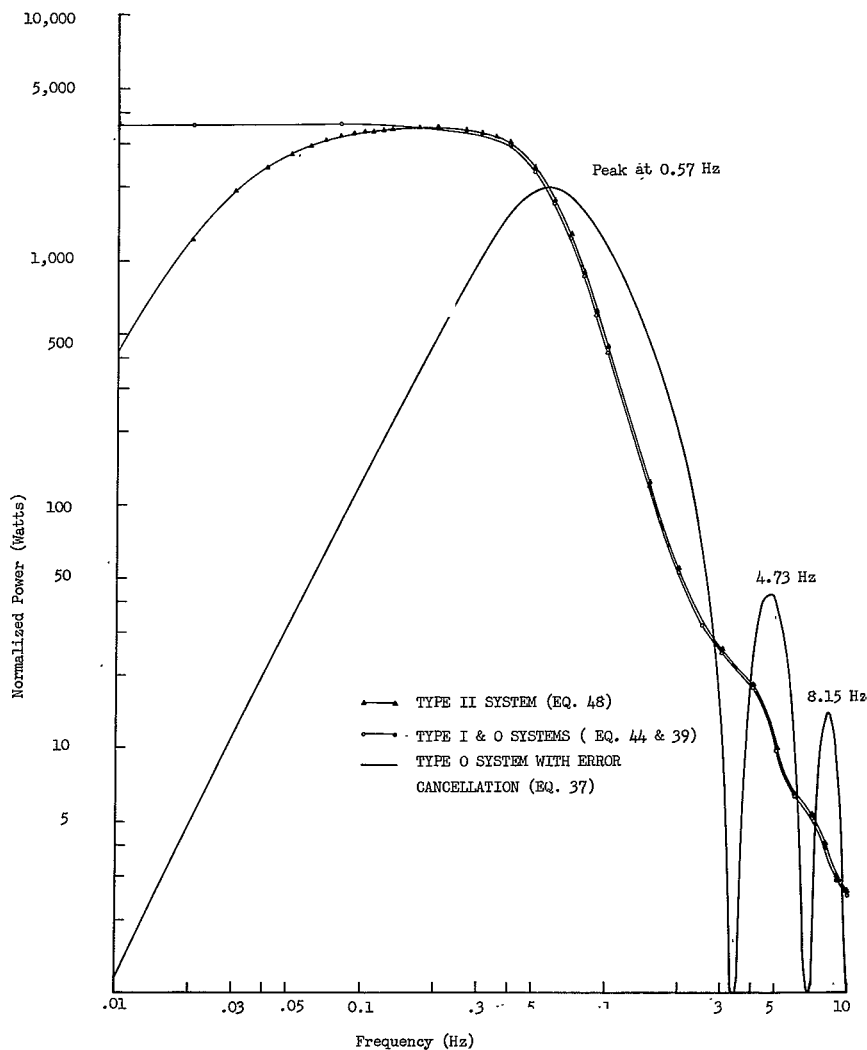
Figure 5.8.   Comparison of Power-Density Spectra

It is interesting to note the similarity between equations 39 and 44, the error density spectrums for the type-0 and type-I systems, respectively. In particular the error for the type-I system will have a finite value of C/ω_n^2 as $\omega \longrightarrow 0$, whereas the type-0 system error will approach infinity. As will be recognized from the comparative plots of figure 5.8, equation 39 and 44 are essentially identical for frequencies greater than .001 Hz.

Even further reductions in the DC value of the Mux Channel frequency error might be realized by employing a type-II system as represented in figure 5.7. Here, a double integration is employed and the open-loop transfer function takes the following form

$$KG(s) = \frac{\omega_c^2 (\tau_1 s + 1) e^{-sT}}{s^2} \tag{45}$$

The Bode plot of KG(s) is shown in figure 5.9, where τ_1 is the required time constant (5.9 seconds) of the lead network necessary to insure a reasonable phase margin (52.3 degrees from equation 5) at the crossover frequency of 1.7 rps. ω_c is the frequency at which the extension of the "2 slope" of the Bode plot crosses the zero-db axis and from figure 5.9, it is seen that $\omega_c = 0.535$ rps ($f_c = 0.0085$ Hz). Now on writing, the error transfer function as

$$H(s) = \frac{s^2}{s^2 + \omega_c^2 (\tau_1 s + 1) e^{-sT}} \tag{46}$$

and applying equation 42 the one-sided density spectrum of the error signal, for the type-II system for $G_y(f) = C/\omega^2$, becomes.

$$G_e(f) = C\omega^2 / \Big[\omega^4 - 2\omega_c^2 \tau_1 \omega^3 \sin \omega T + \omega_c^2 (\omega_c^2 \tau_1^2 + 2 \cos \omega T)\omega^2$$
$$- 2\omega_c^4 \tau_1 \omega \sin 2\omega T + \omega_c^4 \Big] \tag{47}$$

On letting $\omega = 2\pi f$ with $\omega_c = 0.535$ rps and $T = 0.3$ second, equation 47 reduces to

$$G_e(f) = Cf^2 / \Big[39.4f^4 - 21f^3 \sin 1.88f + (2.8 + 0.57 \cos 1.88f) f^2$$
$$0.15f \sin 3.76f + 2 \times 10^{-3} \Big] \tag{48}$$

.This equation is also plotted in figure 5.8 and it will be noted that the type-II system has the advantage of having a zero-frequency error as $f \longrightarrow 0$, and at frequencies above about 0.1 Hz, the error response is essentially identical to the type-I system. It
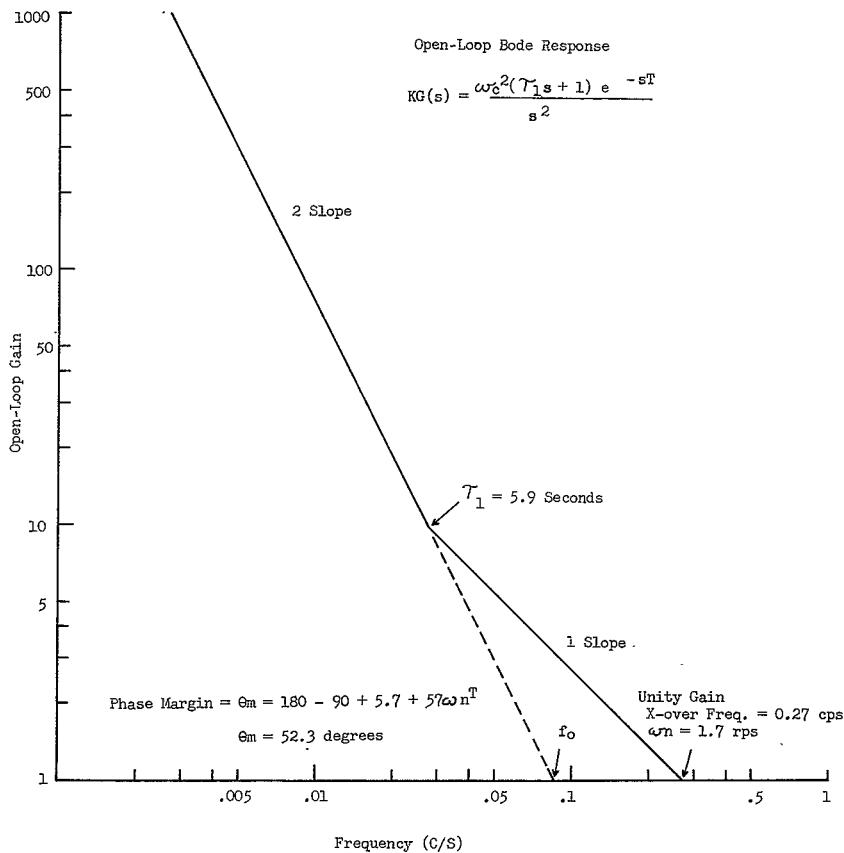
Figure 5.9. Open-Loop Bode Plot For Type-II System

The figure shows an Open-Loop Bode Response plot with the following labeled elements:

Open-Loop Bode Response

$$KG(s) = \frac{\omega_c^2(\tau_1 s + 1) e^{-sT}}{s^2}$$

2 Slope

$\tau_1 = 5.9$ Seconds

1 Slope

Phase Margin $= \theta_m = 180 - 90 + 5.7 + 57 \omega_n T$

$\theta_m = 52.3$ degrees

f_o

Unity Gain
X-over Freq. = 0.27 cps
$\omega_n = 1.7$ rps

Open-Loop Gain

Frequency (C/S)

5.22

might therefore be concluded, at least from a theoretical point of view, that the type-II system has the same basic advantages of the present type-0 system (with error cancellation) without the use of error cancellation.

5.1.6 DETERMINATION OF THE RMS FREQUENCY ERROR

The previous section has dealt with the derivation of the one sided power density spectra for various systems that might be considered for the SSB-AFC function and the conclusions to be drawn are mostly qualitative. It will be desirable at this point to show on a more quantitative basis the relative performance of these systems with respect to the system presently being used. The most meaningful yardstick by which to judge the AFC system performance is the magnitude of the RMS frequency error, σ (standard deviation), of the multiplex channel. It might also be recalled from network theory that the variance, σ^2, is directly obtainable from integration of the one sided density spectrum G_e (f) as follows

$$\sigma^2 = 2 \int_0^\infty G_e(f) \, df \qquad (49)$$

This integration was carried out for each system under consideration with the help of a digital computer over the limits of from 0.01 Hz to 10 Hz and from 1 to 10 Hz (short term) using Simpson's rule with increments of 0.01 Hz. The results of these integrations have been normalized with respect to the present system being used (type 0 with error cancellation) and are listed in table 5.1. The square root of the variance, which is the RMS or standard deviation, σ, is also tabulated.

Careful examination of table 5.1 will reveal several interesting points. First it might be concluded that the type-0 system with error cancellation will yield an RMS frequency error on a long term basis that is 0.9 db lower than any other system. This presupposes of course that the power density spectrum of the input source follows the assumed $1/\omega^2$ relationship. It can be observed from the power density plots of figure 5.8 that the reason for this 0.9 db difference in σ results largely from the reduction in the DC or very low-frequency (< 0.001 Hz) error reduction advantage of the type-0 system with error cancellation. This cannot be accomplished as effectively with the other systems under consideration. However it might also be reasonable to assume that the DC or very low-frequency input perturbations will not approach infinity as $\omega \to 0$ as indicated by the $1/\omega^2$ relationship assumed for the input spectrum. For this reason, it is also of interest to examine the shorter term effects ($\omega > 1$ Hz) on the frequency error for the systems in question. When the short-term error was examined by applying equation 49 over the limits of 1 to 10 Hz, it was noted that the present system showed an RMS frequency error that was 4.6 db greater than either the type-I or type-II systems.

TABLE 5.1.   DETERMINATION OF RMS FREQUENCY ERROR

AFC System Configuration	Spectrum $G_e(f)$ Power Density (Equation No)[2]	Variance (σ^2) Short[3] Term	Long[4] Term	Deviation σ Short[3] Term	Long[4] Term	$|G_e(f)|$ as f→o	Frequency Error For Doppler Offset (f_d)
Type 0	39	0.355	1.23	0.595	1.11	∞	$10^{-3}f_d$
Type 0[1] With E.C.	37	1	1	1	1	$10^{-6}T^2C$	0
Type I	44	0.355	1.23	0.595	1.11	0.35C	0
Type II	48	0.355	1.20	0.595	1.11	0	0

[1] Type 0 with Error Cancellation

[2] See Text

[3] Integration of $G_e(f)$ from 1 to 10 Hz

[4] Integration of $G_e(f)$ from 0.01 to 10 Hz

Some preliminary tests have been conducted at all three stations with the AFC system, both in the normal S/C configuration and with the error cancellation circuits bypassed. Indications, primarly from examination of the multiplex-channel strip-chart recording of frequency error, are that a noticeable reduction in the short-term rms error is realized when error cancellation is eliminated.

The overall conclusions to be drawn then from the foregoing analysis might be summarized as follows:

1) Some form of frequency control system must be employed at present to correct for both the fundamental stability limitation of the system oscillators as well as doppler, for both the synchronous and asynchronous satellites.

2) The Type-0 system alone is not sufficient since it cannot adequately compensate for DC or very long-term frequency drift.

3) The Type-0 system with error cancellation provides excellent cancellation of the low frequency (including doppler) frequency errors, however, its performance with regard to shorter term frequency inputs ($\omega > 1$ Hz) is some 4.6 db worse than the type-I or type-II systems.

4) The type-II system appears to give the best overall performance in the presence of both long-and short-term frequency perturbations (including doppler). However, in light of the complexity involved in implementation of such a scheme it is felt that the type-I system might be the optimum selection with some sacrifice in the long term frequency error. It might be recognized that the type-I system can be readily implemented as a phase lock loop, where a perfect integration can be obtained, rather that attempting to achieve integration in the basic AFC system.

5.1.7 DETERMINATION OF THE MULTIPLEX CHANNEL ERROR PROBABILITY

It is reasonable to assume that frequency instabilities or perturbation in the multiplex channel will have their most serious effect on the error rate or error probability of a low deviation FSK teletype modem. It will be instructive therefore to examine the error rate performance of this type of modem in light of the expected values of the RMS frequency error σ as determined in paragraph 5.1.6.

Assuming the oscillator noise statistics to be normally distributed with variance σ^2 and mean zero, the density function can be written in terms of the FSK channel frequency deviation, Δf, as follows:

$$\rho(\Delta f) = \frac{1}{\sigma\sqrt{2\pi}}\ e^{-\frac{1}{2}\left(\frac{\Delta f}{\sigma}\right)^2} \tag{50}$$

The probability of the oscillator noise exceeding some specified value Δf will then be the cumulative distribution from Δf to infinity or

$$P_e = \int_{\Delta f}^{\infty} \rho \, (\Delta f) \, d\Delta f \tag{51}$$

Changing variables and letting $x = \Delta f / \sqrt{2\sigma}$

equation 51 becomes

$$P_e = \frac{1}{\sqrt{\pi}} \int_x^{\infty} e^{-x^2} dx \tag{52}$$

This can be written in terms of the erf $(x)^*$ as

$$P_e = \frac{1}{2} \left[1 - \text{erf} (x) \right] \tag{53}$$

The error probability is easily computed for various $\Delta f / \sigma$ ratios using a table of error functions * and the approximation

$$P_e = \int_x^{\infty} e^{-x^2} dx = \frac{e^{-x^2}}{2x} \quad \text{for} \quad x \gg 1 \tag{54}$$

P_e is plotted as a function of the $\Delta f / \sigma$ ratio in figure 5.10.

One might now consider the case of an FSK modem with a 30-Hz deviation ($\Delta f = 30$ Hz). If the error probability is not to exceed 10^{-5}, then from figure 5.10 the allowable RMS frequency error, σ, (for $\Delta f / \sigma = 4.4$) will be 6.8 Hz. This number is particularly enlightening since only on a few occasions has the RMS frequency error been observed to be that high and this generally occurred when trouble was experienced in maintaining SSB-AFC lock. The test data has shown the RMS frequency error to be in the neighborhood of 2 to 3 Hz. It might therefore be tentatively concluded that the AFC system as it is presently configured will be more than adequate to insure bit error probabilities of less than 10^{-5} for low-deviation FSK modems.

If, however, as a result of experimentation it is found that σ is higher than the 6.8-Hz limit; it will be interesting to note from figure 5.10 and the results presented in table 5.1 that a significant decrease in the error rate can be achieved by using a type-I system in place of the present type-0 system with error cancellation. For example, this means that if the present system is operating with a error rate of 10^{-3} and an FSK deviation of 30 Hz, the value of σ from figure 5.10 will be 9.7 Hz. Recalling that the

---

* Harman, W.W., "Principles of the Statistical Theory of Communication," McGraw-Hill Book Company, Inc., New York, 1968, pp 114-115.

type-I system will reduce this error by a factor of 0.595, the RMS error will become 5.75 Hz. This corresponds to a $\Delta f/\sigma$ ratio of 5.2 or, from figure 5.10, an error rate of less than 3×10^{-7}. It will be noted, therefore, that the type-I system can yield a very significant improvement in the error rate of the FSK channel.

5.1.8 ANALYSIS OF THE 1.6-HZ S/C SPIN EFFECT ON THE MULTIPLEX CHANNEL FREQUENCY ERROR

It has been noted for some time that a very large frequency component exists at 1.6 Hz in the spectrum of the multiplex-channel frequency error, as determined by the Fourier analysis investigations. A typical Fourier plot of the density spectrum recorded at the Rosmar station on 4 July, 1967 is presented in figure 5.11. This plot clearly shows the predominance of the 1.6-Hz frequency component.

Data analyzed to date on both ATS-1 and ATS-3 has indicated a phase deviation in the order of 0.4 radian. Examination of the zero and first order Bessel functions $J_0(m)$ and $J_1(m)$, respectively) for m = 0.4 will indicate a multiplex channel S/N of only 14 db. The MUX channel voltage S/N for low-deviation ratios, m is approximated very closely by

$$S/N = \frac{J_0(m)}{J_1(m)} = \frac{2}{m} \tag{55}$$

Therefore, it is seen that the S/C spin modulation effect is a problem to be resolved in the future design of spin-stabilized communication satellites.

It might directly be concluded that this effect is in some way due to a phase modulation of the up-link 6-GHz signal caused by the 1.6-Hz spin rate of the satellite. The structure of the SHF S/C receiving antenna* is such that it will produce an omnidirectional doughnut-shaped pattern in a plane perpendicular to the S/C spin axis, and as such, should not normally be affected by the S/C spin.

It might be postulated, however, that for phase modulation to exist, there must be a displacement of the phase center of the antenna relative to the antenna spin axis as seen by an earth observer. This could possibly be caused by any one or a combination of the following:

1. A lateral displacement between S/C spin axis about its center of gravity and the antenna electrical axis.
2. A displacement of the antenna phase center relative to the S/C spin axis due to a mechanical tilt of the antenna relative to the S/C spin axis.

---

*Horizontally polarized 6-element cloverleaf array, coaxially driven, investment cast, and supported by a fiberglass structure. The antenna has an average gain of 6.2 db around the spin axis.

3. A gross misalignment or malfunction of one or more of the cloverleaf arrays which could result in an electrical displacement of the antenna phase center relative to the satellite spin axis.

If the phase perturbation is due to a lateral displacement of the antenna position as indicated by case 1 above, it is readily seen that the resultant peak phase deviation, μ, of
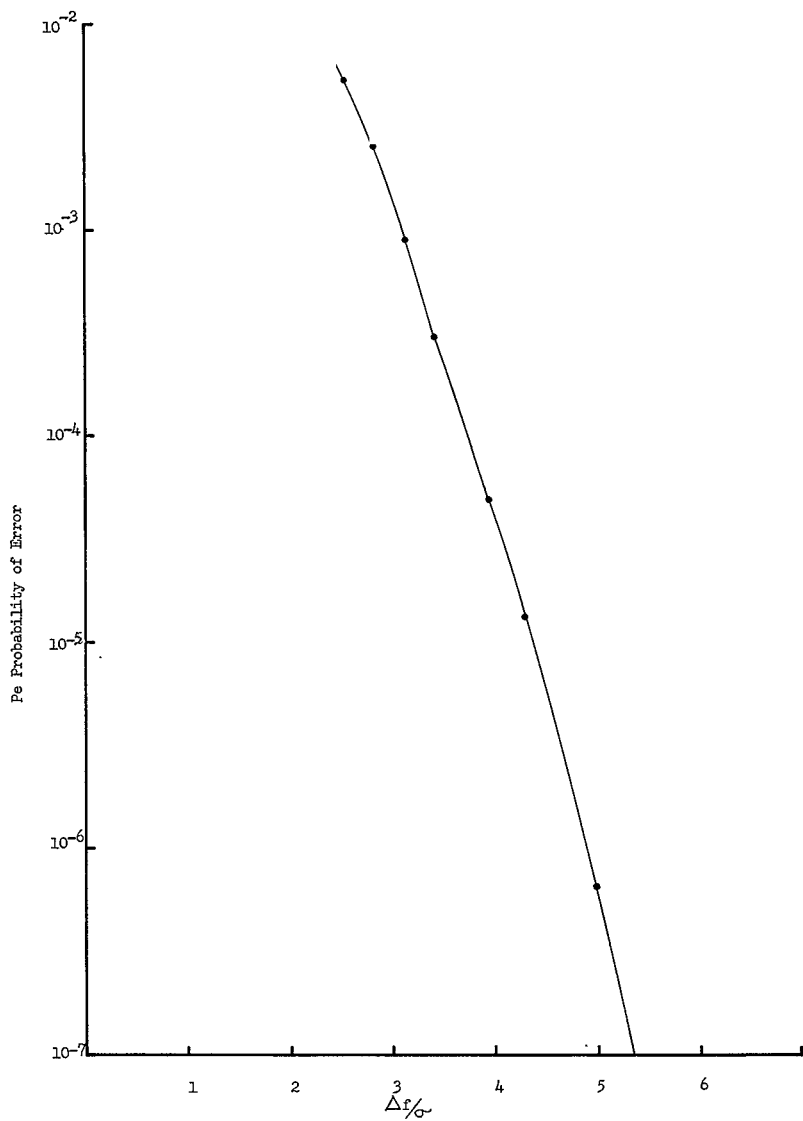
Figure 5.10. Error Probability Versus $\Delta f/\sigma$ Ratio

5.29
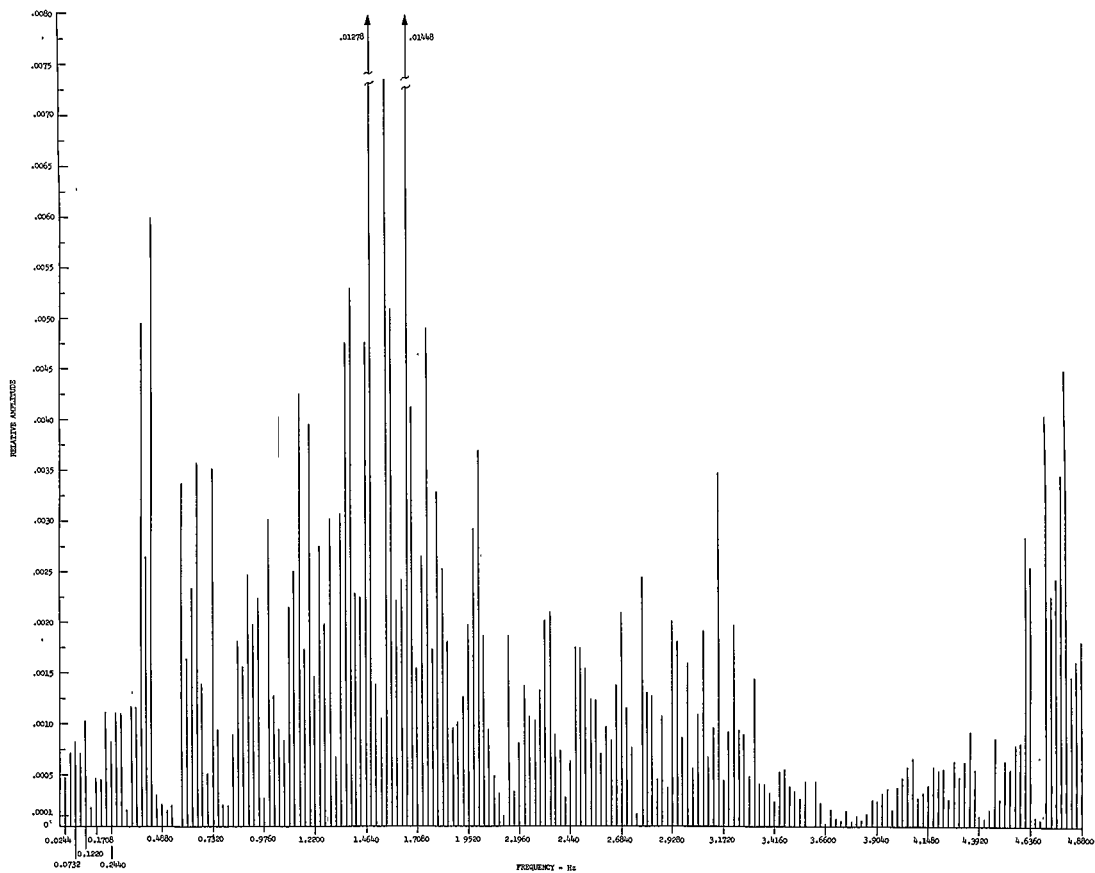
Figure 5.11. Amplitude Spectrum of Multiplex-Channel Frequency Error

the SHF received signal will be related to this physical displacement, δ , as follows:

$$\mu = \frac{2\pi\delta}{\lambda} \tag{55a}$$

where λ = wavelength of the SHF up-link frequency = 4.8 cm.

     The peak frequency deviation of the 1.6-Hz signal as shown by the Fourier analysis investigations has been about 0.65 Hz. This corresponds to a peak-phase deviation of about 0.41 radians. Recalling the transfer function of the AFC system and the error cancellation circuits as given by equations 30 and 32 respectively, and assuming the S/C spin rate to be large compared to the reciprocal of the AFC time constant, τ, the expected misalignment, δ, can be written as

$$\delta = \frac{\mu\lambda}{4\pi \sin\pi fT} \tag{56}$$

where $\hat{f}$ = spin frequency = 1.6 Hz

                 T = system transport time, nominally 0.26 second

     Evaluating equation 56 yields an expected displacement of 0.159 cm, or about 1/16 inch. It should be particularly noted that the transfer function of the error cancellation circuit is such that any phase modulation due to S/C spin at 1.6 Hz will fall right at the peak of the response curve defined by the (2 sinπfT) function and will consequently enhance or amplify the 1.6-Hz signal by about 6 db. This must be regarded as a true design anomaly, and every effort should be made in future satellite programs to either avoid the use of this spin rate, or use a different form of DC frequency error reduction in the AFC system. It might also be observed from equation 32 that if the satellite spin rate were chosen to be an exact integer multiple reciprocal of the system transport time, T, complete nulling of the 1.6-Hz signal could be realized.

     Again considering case 1, it will be observed that a lateral displacement of the antenna phase center will result in a phase modulation at only the 1.6-Hz fundamental (no higher harmonics), and furthermore, there will be no amplitude modulation of the received SHF signal.

     If case 2 is now considered, it might be visualized that a similar displacement, δ, of the antenna phase center as a result of the receiving antenna being tilted some angle, α, from the S/C spin axis will result in the same effect as described by equation 56. Assuming a displacement of 1/16 inch at the antenna phase center, and further assuming the antenna phase center to be at the physical center of the structure, which is about 12 inches in length, then the angle of misalignment will be given approximately by:

$$\alpha = \sin^{-1}\frac{\delta}{D} \tag{57}$$

where D is the distance from the point of tilt to the antenna phase center, which in this case is about 6 inches. Therefore, equation 57 indicates an angular misalignment of about 0.01 radian, or less than 0.6 degree.

This degree of misalignment, although resulting in a measurable phase modulation, should have only a very minor effect on the antenna amplitude response since the nominal antenna beamwidth is about 20 degrees.

If one now considers the cause of the phase modulation to be a result of some gross misalignment or malfunction of the colinear SHF receiving array, as indicated by case 3, one would indeed expect not only phase modulation but also a measurable degree of amplitude modulation. A quantitative analysis of this case in terms of the various malfunctions that may possibly exist could be a quite complicated and lengthy procedure, and does not appear warranted.

5.1.9 THE EFFECT OF 60-HZ MODULATION ON THE MUX CHANNEL FREQUENCY

It has been observed, as a result of spectral analysis of the received mux channel as well as the several MUX channel distortion tests conducted, that a considerable amount of test tone FM modulation by the power line frequency is present when the ATS-1 system is operated in the SSB/PhM mode. It will be of interest here not to suggest the orgin of this problem, but rather to indicate the effect of the AFC and error cancellation system on the relative magnitude of the resulting 60 Hz energy in the Mux channel.

Again recalling the transfer functions of the AFC system and the error cancellation circuits, as given by equations 30 and 32 respectively assuming $\omega\tau >> K$, the net response of the MUX channel as a result of quadrature modulation of the system oscillators will be given by

$$H(\omega) = 2 \sin\frac{\omega T}{2} = 2 \sin \ \pi f T \tag{58}$$

It will be recognized that equation 58 is the comb filter like response which is a result of the error cancellation circuit of the SSB transmitter. Now for f equal to 60 Hz, the magnitude of $H(\omega)$ will vary depending on the station transport lag T. These values are presented in table 5.2 along with the respective station delay times T. It is interesting to note that $H(\omega)$ will be zero when the argument of equation 58 is zero or any integer multiple of π. If both f and T are considered constants for a particular station then it is possible to add a small additional time delay ΔT such that

$$\sin \pi f(T + \Delta T) = 0 \tag{59}$$

when $f(T + \Delta T)\pi = n\pi$

or

$$\Delta T = \frac{n - fT}{f} \tag{60}$$

Station	Transport Lag. Time Delay, T (msec)	Frequency = 60 Hz		Frequency = 120 Hz		Additional Delay, ΔT To Null 60 Hz (msec)
		π f T (radians)	$\lvert 2 \sin \pi f T \rvert$ (db)	π f T (radians)	$\lvert 2 \sin \pi f T \rvert$ (db)	
Rosman	271	16.26 π	3.3	32.52 π	6 db	12.33
Mojave	254	15.24 π	2.7	30.48 π	6 db	12.66
Cooby	263	15.78 π	2.2	31.56 π	6 db	3.66

and n is the closest higher integer number to f T. For example, at Rosman the transport lag, T, is 271 milliseconds, therefore at 60 Hz f T = 16.26 and n will be 17. From equation 60, the required additional delay ΔT that must be added to null the 60 Hz will be 12.33 milliseconds. Using the same procedure the required additional delay, Δ T, for Mojave and Cooby Creek will be 12.66 milliseconds and 3.66 milliseconds respectively. It will also be of interest to note that the additional delay added to null the 60 Hz component will also null the harmonics of 60 Hz, i.e., 120 Hz, 180 Hz, etc. This is readily concluded from equations 59 and 60 since n will result in an integer number and the $\sin \pi$ f (T + ΔT) will be zero.

The foregoing analysis is not necessarily to be considered as a solution to the 60-Hz problem but rather was presented here to show the very pronounced effect that the error cancellation circuits will and could have on the ultimate performance and quality of the multiplex channel in the MA mode of operation.

5.1.10 AN ANALYSIS OF THE 6-GHZ KLYSTRON PHASE LOCK SYNCHRONIZER TECHNIQUE

A generalized block diagram of the phase lock system used to achieve a high degree of spectral purity for the 6-GHz uplink frequency for the ATS-SSB system is shown in figure 5.12. It will be subsequently shown here that the degree of frequency stability that can be attained in the 6-GHz signal will be limited almost exclusively by the degree of stability that can be achieved in the 7.413-MHz frequency standard. It will also be shown, contrary to some previous belief, that ripple on the klystron repeller high voltage supply, although of minor design interest, has little or no effect on the attainable spectral purity of the 6-GHz signal.

A baseband servo equivalent block diagram of figure 5.12 is shown in figure 5.13. It will be observed that changes in the controlled variable klystron output phase, C(s), can result from basically one or both of two possible sources. A disturbance or change in the klystron repeller voltage, R(s), will produce a phase change in the output

5.34
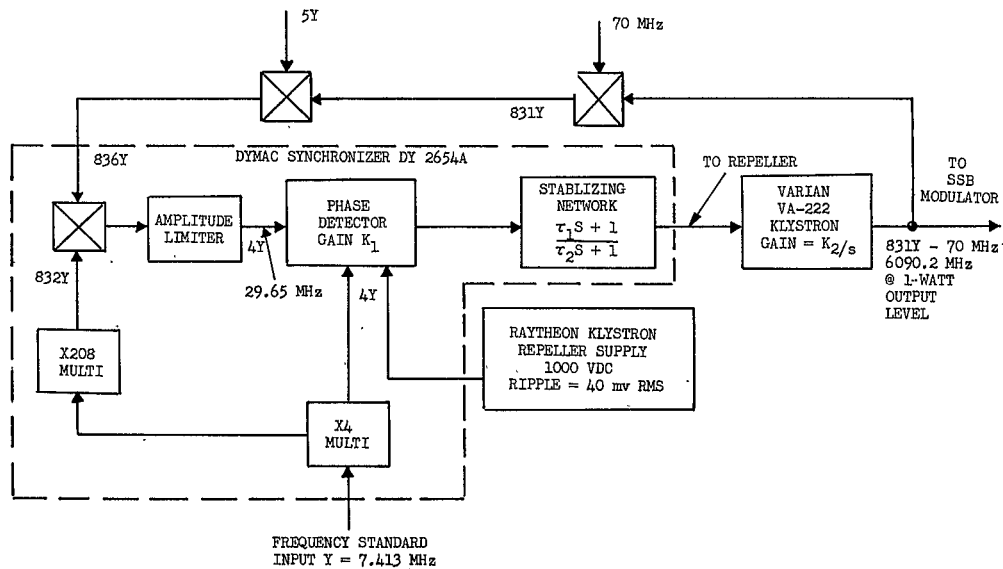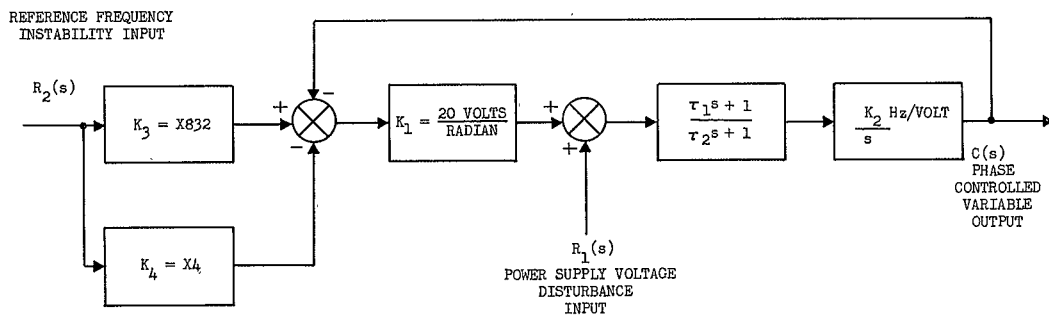
Figure 5.13. Baseband Servo Equivalent Block Diagram of Phase-Lock Synchronizer

frequency and/or frequency changes in the reference standard. $R_2(s)$ will produce corresponding changes in the klystron output frequency.

EFFECT OF POWER SUPPLY RIPPLE

It will be of interest to first consider the effect of power-supply voltage disturbances on the controlled variable output, $C(s)$. The voltage to phase closed loop transfer function can be written as follows:

$$\left. \frac{C(s)}{R_1(s)} \right|_{R_2(s) = 0} = \frac{1}{K_1} \times \frac{\tau_1 s + 1}{\tau_2 \tau_3 s^2 + (\tau_1 + \tau_3) s + 1} \tag{61}$$

where τ_1 = lead time constant of the stabilizing network

τ_2 = lag time constant of the stabilizing network

$\tau_3 = 1/K_1 K_2 = 1.59 \times 10^{-8}$ seconds, and

$K1$ = phase detector gain = 20 volts/radian

K_2 = klystron frequency sensitivity = 0.5 MHz/volt

Rewriting equation 61 in standard servo form and equating the denominator to the standard characteristic equation yields:

$$s^2 + \left(\frac{\tau_3 + \tau_1}{\tau_2 \tau_3} \right) s + \frac{1}{\tau_2 \tau_3} = s^2 + 2 \zeta \omega_n s + \omega_n^2 \tag{62}$$

where ζ is the system damping ratio which is generally specified at 0.707 of critical, and ω_n is the 3-db bandwidth of the closed-loop response. The Dymian DY-2654A handbook specifies the system 3-db bandwidth at about 100 kHz; therefore, on equating like terms of equation 62 with $\omega_n = 2\pi \times 100$ kHz and $\zeta = 0.707$, the following relationships can be shown to exist:

$$\left. \begin{array}{lll} & \tau_1 = \frac{1.4}{\omega_n} = 2.25 \times 10^{-6} \text{ seconds} \\ \text{or} & \omega_1 = 0.707 \, \omega_n \\ \text{and} & f_1 = 70.7 \text{ kHz} \end{array} \right\} \tag{63}$$

$$\left. \begin{array}{lll} \text{also} & \tau_2 = \frac{1}{\tau_3 \, \omega_n^2} = 1.59 \times 10^{-4} \text{ seconds} \\ \text{or} & \omega_2 = \omega_n^2 / K1 K2 \\ \text{and} & f_2 = 1 \text{ kHz} \end{array} \right\} \tag{64}$$

Now on substituting numerical values for τ_1, τ_2, τ_3 and K_1 into equation 61 there results:

$$\left. \frac{C(s)}{R_1(s)} \right|_{R_2(s) = 0} = \frac{1}{20} \times \frac{2.25 \times 10^{-6} \, s + 1}{2.53 \times 10^{-12} \, s^2 + 2.27 \times 10^{-6} \, s + 1} \tag{65}$$

The open-loop transfer function can now also be written and is presented along with the open-loop bode plot in figure 5.14.

It can be easily recognized therefore that for low frequency sinusoidal inputs the right side of equation 65 reduces to 1/20 and the resulting phase variation at the klystron output, θ out, will be a function of the input sinusoidal voltage amplitude, E_1, as follows:

$$\theta \text{ out} = \frac{E_1}{K_1} = \frac{E_1}{20} \text{ radians} \tag{66}$$

Referring again now to figure 5.12 and figure 5.13, it will be recognized that the output phase variation cannot be permitted to exceed $\pi/2$ radian if loop phase lock is to be maintained. In order to allow sufficient margin for noise and other disturbances that might arise, a phase error of $\pi/6$ will be specified. Therefore, from equation 66 a peak power supply ripple of $20 \times \pi/6 = 10.5$ volts is indicated. However, it will be subsequently shown that the peak 60-Hz frequency deviation cannot exceed 1.2 Hz if the 60-Hz special component in to be down at least 40 db from the carrier; therefore, the maximum peak phase excursion permitted will be only 0.02 radian ($m = \Delta f/f_a = 1.2/60$). Now again from equation 66, the maximum permitted repeller supply ripple will be $20 \times 0.02 = 400$ millivolts peak (284 millivolts RMS). Since the specified repeller supply ripple is only 40 millivolts RMS, no problem in maintaining acceptable frequency stability due to power supply ripple is anticipated.

EFFECT OF FREQUENCY-STANDARD INSTABILITY

It will now be of interest to examine the effect of frequency variations in the 7.413-MHz reference standard on the attainable spectrial purity of the 6-GHz-locked klystron. Again referring to the block diagram of figure 5.13, the closed-loop frequency transfer function can be written as:

$$\left. \frac{C(s)}{R_2(s)} \right|_{R_1(s) = 0} = \frac{(K_3 - K_4)(\tau_1 s + 1)}{\tau_2 \tau_3 s^2 + (\tau_1 + \tau_3) s + 1} \tag{67}$$

5.37

where τ_1, τ_2 and τ_3 are the same as defined previously,

K_3 = frequency multiplier gain = 832

K_4 = frequency multiplier gain = 4

Writing equation (67) in numerical form yields:

$$\left. \frac{C(s)}{R_2(s)} \right|_{R_1(s) = 0} = 828 \ \frac{2.25 \times 10^{-6} \ s + 1}{2.53 \times 10^{-12} \ s^2 + 2.27 \times 10^{-6} \ s + 1} \tag{68}$$

Again therefore, it is readily observed that for low-frequency sinusoidal input variations of peak deviation, Δf_i, the resultant peak-frequency deviation of the controlled variable output, Δf_o, will be multiplied by a factor of 828 or,

$$\Delta f_o = 828 \, \Delta f_i \tag{69}$$

From a table of first order Bessel functions for low values of deviation ratio, m, it will be observed that $J_1(m) = m/2$ where

m = Δ f/fa and fa is the modulating frequency of interest. Therefore,

$$\Delta f = 2 \ fa \ J_1(m) \tag{70}$$

As an example, if it is specified that the first 60-Hz sideband be down 40 db from the carrier ($J_1(m) = .01$), the maximum peak frequency deviation of the 6-GHz output will be only 1.2 Hz (2 x 60 Hz x 0.01). The corresponding peak frequency deviation of the 7.413-MHz y standard would then be only 1.45×10^{-3} Hz. This corresponds to a short-term operational frequency stability of about 2 parts in 10^{10} for a 60-Hz time period.

In summary then, it should be emphasized that the present approach of phase locking a reflect klystron to attain a reasonable drive power (1 watt) with a high degree of spectral purity is limited only by the attainable stability of the phase lock standard (in this case the 7.413-MHz Y-frequency that is derived from the 5-MHz Sulzer standard) and the subsequent frequency multiplier stages that follow.* In this regard, the present approach has no basic disadvantage over a direct higher power multiplier chain technique to achieve the desired frequency stability. Indeed the present design concept is not only capable of producing the desired results, but has the advantage of being able to operate the multiplier chain at lower power levels thus somewhat simplifing the incidental FM problem that would be more prevalent in a higher power multiplier chain.

---

*This assumes that the synchronizer PLL has sufficient gain to suppress the 60-Hz frequency component to a negligible level compared to the inherent noise of the standard.
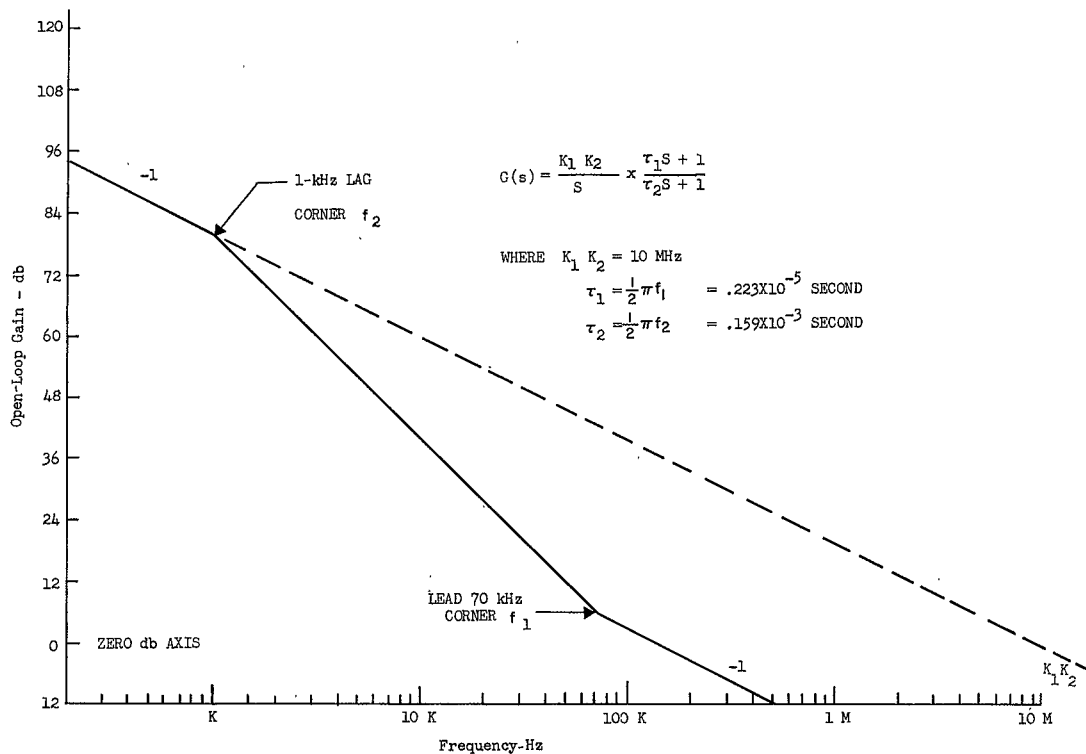
Figure 5.14. Bode Plot of Synchronizer Open-Loop Transfer Function, G(s

5.39

It can be seen from the generalized block diagram of figure 5.12 that amplitude modulation* of the reflex klystron, although appreciably reduced by the limiter, will be fed back, detected by the amplitude sensitivity phase detector, and ultimately result in an undesired frequency or phase modulation of the klystron. Assuming an inperfect limiter with a suppression ratio α; and a phase detector amplitude sensitivity of unity gain, K_6, the AM to PM baseband equivalent block diagram can be represented as shown in figure 5.15. The AM voltage to output phase transfer function can now be written as follows:

$$\frac{C(s)}{R_3(s)} = \frac{\alpha K_2 K_6 \ G(s)/s}{1 + K_1 \ K_2 \ G(s)/s} \tag{71}$$

where $C(s)$ = output phase variation

$R_3(s)$ = input voltage variation due to AMing of the reflex klystron

α = Limiter amplitude suppression factor

K_6 = Amplitude sensitivity of phase detector

$G(s) = \tau_1 \ s + 1/\tau_2 \ s + 1$

Now on letting $S = j\omega$, and assuming $\omega \ll K_1 K_2$, equation 71 can be simplified to yield

$$\theta \ out = \frac{\alpha K_6}{K_1} \quad E_3 \tag{72}$$

where θout is the output phase variation of the klystron corresponding to the complex variable $C(s)$, and E_3 is the input voltage disturbance corresponding to the complex quantity $R_3(s)$ resulting from klystron AM effects.

If a limiter suppression factor of -40 db ($\alpha = 0.01$) is assumed with K_6 = unity and K_1 = 20 volts/radian, equation 72 becomes

$$\theta \ out \ \bigg| = 5 \times 10^{-4} \ E_3 \tag{73}$$
$$(due \ to \ AM)$$

If θout at 60 Hz is again limited as before at a peak deviation 0.02 radian (Δf = 1.2 Hz for -40 db sidebands), than from equation 73, E_1 would have to be some 40 volts peak to produce 60-Hz sidebands greater than -40 db down from the carrier. This is clearly much larger than could possibly exist since the VA-222 klystron only has a nominal seven volt output level (1 watt into 50-ohm load). Even if the limiter suppression factor were

---

*Klystron amplitude modulation can for example result from a ripple or voltage variation primarily in the klystron beam supply. AM can also be caused by a mechanical vibration of the klystron.
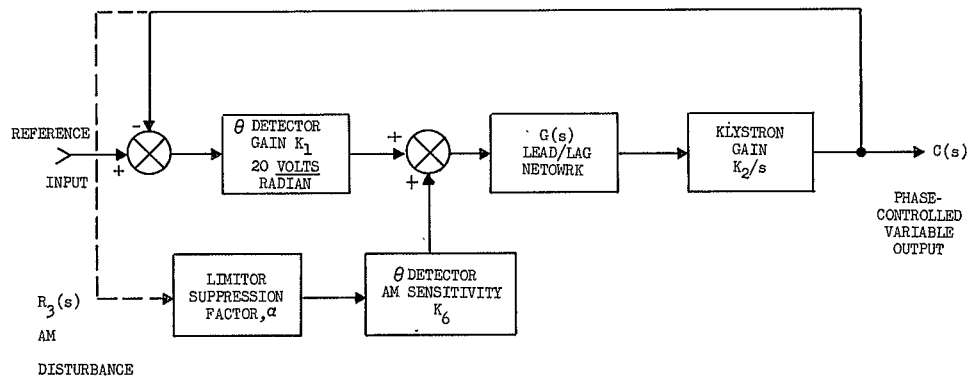
Figure 5.15. AM to PM Baseband Equivalent Block Diagram

reduced to -20 db, there would have to be some 60-percent AM modulation at 60 Hz to produce undesirable PhM effects. It might be concluded, therefore, that klystron AM produces negligible PhM of the locked klystron, assuming the limiter suppression to be at least -20 db or better.

PROBLEM SOLUTIONS

If the major source of frequency instability (in particular the incidental 60-Hz modulation) can in fact be isolated to the Dymec Synchronizer, the most probable source of trouble is in the basic stability of the 7.413-MHz Y standard and the subsequent X832 frequency multiplier chain. This could possibly necessitate the development of a new Y standard or a new ultrastable low-power multiplier chain, or it could involve a completely different approach to design of the 6-GHz frequency standard.

For example, one concept that has been suggested which would allow a significant improvement in both the basic 1/f noise of the standard as well as any 60-Hz discrete components that might be present, would be to achieve the 6-GHz reference frequency by a series of mixing operations where the sum frequency is extracted in place of the usual direct multiplication process. Whereas, direct frequency multiplication will result in a corresponding multiplication of any incidental FM effects by the multiplication factor n, the suggested approach would multiply the basic reference standard z by a factor of $n = 2^m$, where m is the number of mixing stages involved, but the incidental FM will only be multiplied by a factor of $2^{m/2}$. It can be reasoned therefore that the net oscillator noise spectrum will be reduced by a factor of $2^{m/2}$ relative to a direct multiplication approach as is presently employed. This could mean a reduction of over 13 db in the noise power density spectrum of the 6-GHz standard. Furthermore, it can be shown by proper decorrelation of the 60-Hz component that might be present in the oscillator standard, complete nulling of the 60-Hz FM sideband is possible using this approach.

Another possible solution that might be considered is the addition of gain in the feedback path (figure 5.13) between the controlled variable output C(s) and the input summing point. Designating this gain as K5, it can be readily shown that the resulting output frequency deviation as given by equation 69 will be reduced by a factor K5

or

$$\Delta f_o = \frac{828}{K_5} \ \Delta f_i \tag{74}$$

A practical implementation of this feedback gain is however, no simple consideration but could be achieved by cascading a frequency discriminator, a high gain DC amplifier, and a low power voltage controlled reflex klystron. The complexity of this solution lies in the ability to achieve this gain without introducing new instabilities, particularly those resulting from 1/f noise in the frequency discriminator diodes. This approach to improving the system stability, although theoretically sound, would require a development effort.

5.42

During March 1968, a special team met at NASA/GSFC to discuss, study, and plan a course of action that would lead to a rapid solution of the SSB/PhM mode frequency stability problem. Four consecutive days of presentation and study were begun on March 19, 1968 with the following persons participating: Messrs. E. Metzger and B. Perkins of NASA/GSFC; D. Harris -- Cooby Creek Systems Engineer and R. Parsons --Rosman Systems Engineer both of RCA; S. Ashford - Mojave Systems Engineer of Bendix; and T. Stores and R. Martel of Westinghouse. As a result of these meetings,it was generally reasoned that one of the principle sources of the 60-Hz problem existed in the fundamental purity of the 7.413-MHz Y standard.* It is unlikely that this Y-signal has the necessary 110-db, 60-Hz sidebands that are required.

As a result of these meetings,it was decided that the principle parties should visit the Rosman station so that the frequency stability problem might be further defined and specific solutions evolved. This trip was undertaken during the week of March 29, 1968 and extended into the following week. Upon arrival, initial tests were conducted in a normal simulator loop configuration which indicated that the 60-Hz sideband level was in the vicinity of -25 db below the 3-kHz test-tone level. This level was eventually reduced to better than 40 db by placing the 1A11 drawer (Y phase-lock loop) on batteries and disabling the PLL so that the Y VCXO now becomes the free-running system standard. The most significant result obtained from this test points up the importance of the Y reference standard on the ultimate stability of the 6-GHz frequency.

As an overall result of the knowledge gained during these two weeks of intensive investigation, the following recommendations are made in their order of anticipated cost:

1) Since it is now obvious that a major problem area exists in attempting to synthesize the Y-signal from the 5-MHz Sulzer standard, it is recommended that the entire synthesis process be bypassed (including the Y PLL) and replaced by a single fixed frequency Y crystal oscillator with the necessary short term stability (including 60 Hz, down by 110 db) that cannot be achieved in the present Y VCXO. In addition, eliminate the Y-distribution system presently used and place the new Y-fixed-frequency crystal in close proximity to the Dymec in the antenna assembly.

2) In lieu of the Y-crystal,it would be more desirable, but also more expensive, to build a 4Y-standard (or perhaps even higher) to reduce the multiplication factor necessary to achieve the desired 6-GHz output frequency.

* It is readily reasoned that if the 60-Hz sidebands must be down 50 db at 6 GHz, then the Y-standard must have (because of the 832 multiplication) sidebands down by some 110 db.

3) Replace the present Dymec unit with a new all solid-state phase lock synchronizer. This would be a complete self-contained unit (including the reference standard) independent of other system frequencies. It would be only necessary to specify the required long and short term frequency stability (including 60 Hz) of the 6-GHz output frequency. It should be emphasized that this may be possible by purchasing a state-of-the-art type off-the-shelf unit with a specially specified standard to yield the desired 6-GHz stability.

5.1.11 PRESENTATION OF THE FOURIER ANALYSIS EXPERIMENTATION RESULTS

This paragraph will describe the results of two Fourier Analysis experiments - one of these was conducted at Cooby Creek as a single station test on January 29, 1968, the other was a three-station test between Cooby Creek, Mojave and Rosman conducted on April 6, 1968. A comprehensive description of the SDS 910 digital computer program employed for collecting the data in these tests is presented in the "Short-Term Frequency Stability Experiment." Therefore, it will not be the intent of this section to discuss details involved in the implementation and execution of the experimental test plan but rather only to present and interpret the results in light of the theoretical expectations.

COOBY CREEK TEST OF JANUARY 29, 1968

This test was of particular significance since it was the first meaningful data obtained in both the normal ATS-1 loop configuration (AFC with error cancellation), and the ATS-1 loop with no error cancellation. The tests were run consecutively under exactly the same conditions at a sampling rate of 100 samples per second. Both frequency distribution plots and 200 Fourier coefficients for 0.1-Hz increments from 0.1 Hz to 20 Hz were produced for each test condition. The respective data is presented in figures 5.16 through 5.19.

The following salient characteristics can be noted from examination of these figures:

1) From the frequency spectrum (figure 5.17) obtained in the normal ATS-1 configuration, it can be observed that nulls exist at multiples of the reciprocal transport lag of 0.26 second or at frequencies of about 3.9 Hz, 7.8 Hz, 10.7 Hz, etc. This agrees almost exactly with the theory developed in previous paragraphs (ref. in particular, equation 58).

2) The standard deviation from the frequency density distribution of figure 5.16 is 3.53 Hz. This is again for the ATS-1 normal configuration.

3) Several interesting conclusions can be drawn from results of the Fourier
   analysis (figure 5.19) experiment conducted without the use of error
   cancellation:

   a) The distinct nulls present in the normal configuration are no longer
      present, thus confirming theory.

   b) The frequency deviation of the 1.6-Hz S/C spin modulation was reduced
      from 1.37 Hz to 0.82 Hz, which indicated that error cancellation is
      enhancing the effect of the S/C spin by some 4.5 db. This agrees very
      closely with the theory presented in paragraph 5.1.8 where an increase
      of 1.92 or 5.7 db is indicated.

   c) Also from figure 5.19 it can be seen that the measured deviation is a
      reasonably flat function of frequency, with an average deviation of about
      0.2 Hz. Also, since error cancellation is disabled, it can be reasoned
      that the result of this test represents the true picture of the composite
      system oscillators noise spectrum. Therefore, recalling the modulation
      index, m, given by $\Delta f/f_a$, and envoking equation 55, the normalized
      frequency density spectrum can be approximated as

      $$G_e \ (f) \ = \ \frac{\overline{\Delta f}}{2f} \tag{75}$$

      where $\overline{\Delta f}$ is the average deviation as determined from the Fourier
      analysis plot of figure 5.19. It appears then from the results of this
      single test at Cooby Creek that the normalized density spectrum follows
      a relationship given approximately by

      $$G_e \ (f) \ = \ \frac{0.1 \ Hz}{f} \tag{76}$$

4) It is readily seen from both the frequency distribution plot of figure 5.18
   and the Fourier analysis plot of figure 5.19, that there is a definite decrease
   in the system quadrature noise level when the error cancellation circuits are
   disabled. It will be recalled that this was predicted from the analysis of
   paragraph 5.1.6. This analysis predicted a 4.6-db decrease in the standard
   deviation, based on an integration over limits from 1 to 10 Hz. Unfortunately,
   the computer program effectively integrates from 0.1 to 20 Hz which pre-
   cludes a direct comparison. However, one would obviously expect the
   difference to be less, since the limits of integration are further separated.
   The computed value of σ for the no error cancellation test was 2.76 Hz, as
   compared to 3.53 Hz which represents a decrease of some 2.8 db. It should
   also be recognized that the presence of large discrete frequency components

such as 1.6-Hz spin modulation and power-line frequency modulation makes
a comparison of standard deviation values based on integration of the noise
spectrum somewhat unreliable.

MULTISTATION TEST OF APRIL 6 AND 7, 1968

This test was conducted as a three-station test with Cooby Creek receiving a
standard 3-kHz test tone first from its own transmitter, and then in turn from the Mojave
station and the Rosman station. In this manner, it is possible to analyze the frequency
stability of all three stations at a single receiving location - in this case Cooby Creek.
Unfortunately, the Mojave transmission was so poor for this test that meaningful data could
not be obtained. Frequency spectrum plots of Cooby Creek receiving Cooby Creek and Cooby
Creek receiving Rosman are shown in figures 5.20 and 5.21, respectively. Corresponding
frequency distribution curves for this test are given in figures 5.22 and 5.23. Also
presented in figure 5.24 is a frequency distribution curve for a Cooby Creek collimation
tower loop. The salient characteristics of this data are presented in table 5.3.

It should be pointed out that the Fourier Analysis of figures 5.20 and 5.21
differ somewhat from those obtained in the previous test conducted at Cooby Creek on
January 29, in that they are a result of averaging ten 10-second samples of data taken over a
particular test period. This was done in an attempt to smooth out the large noise variations
experienced on a single 10-second run. Also, in an attempt to show more clearly fluctuations
in the amplitude of the individual Fourier components as a function of time, the standard
deviation was computed and plotted as a function of frequency in figure 5.25. This plot is
particularly significant since it clearly indicates the time dependent amplitude of the
individual Fourier components.

SAMPLING RATE = 100 SAMPLES/SEC
STANDARD DEVIATION (1 σ) = 3.53 Hz
FREQUENCY SHIFT = 0.42 Hz

CPS
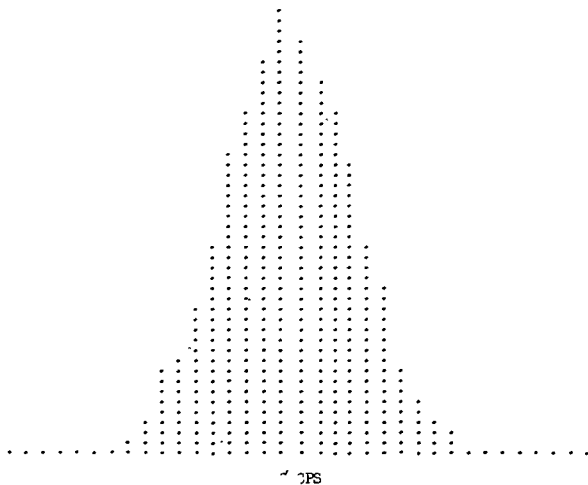
Figure 5.16. Frequency Distribution Function, ATS-1, Normal Configuration (Cooby Creek, 29 Jan. 68)

5.47
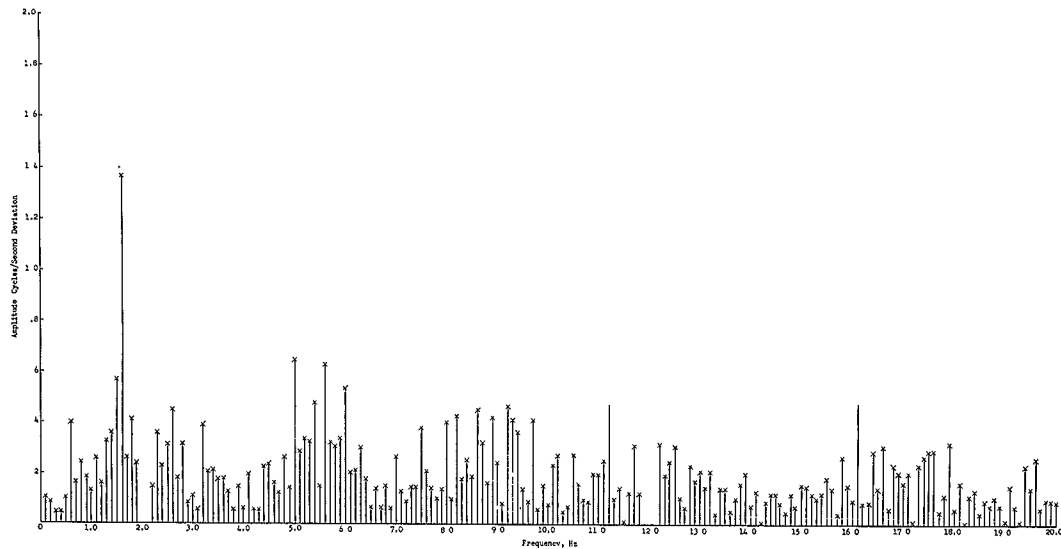
Figure 5.17.   Frequency Spectrum, ATS-1, Normal Configuration (Cooby Creek, 29 Jan 68)
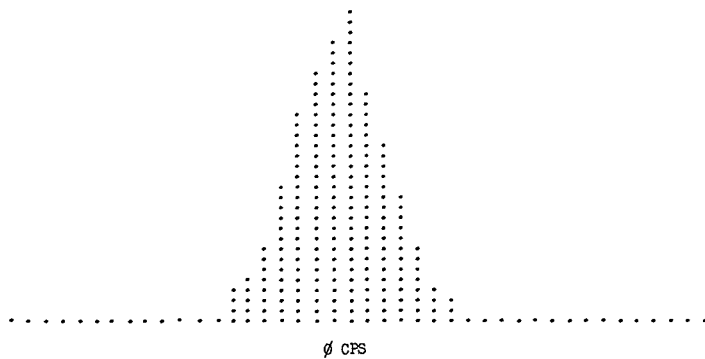
Figure 5.18. Frequency Distribution Function, ATS-1, No Error Cancellation
(Cooby Creek, 29 Jan 68)

5.49
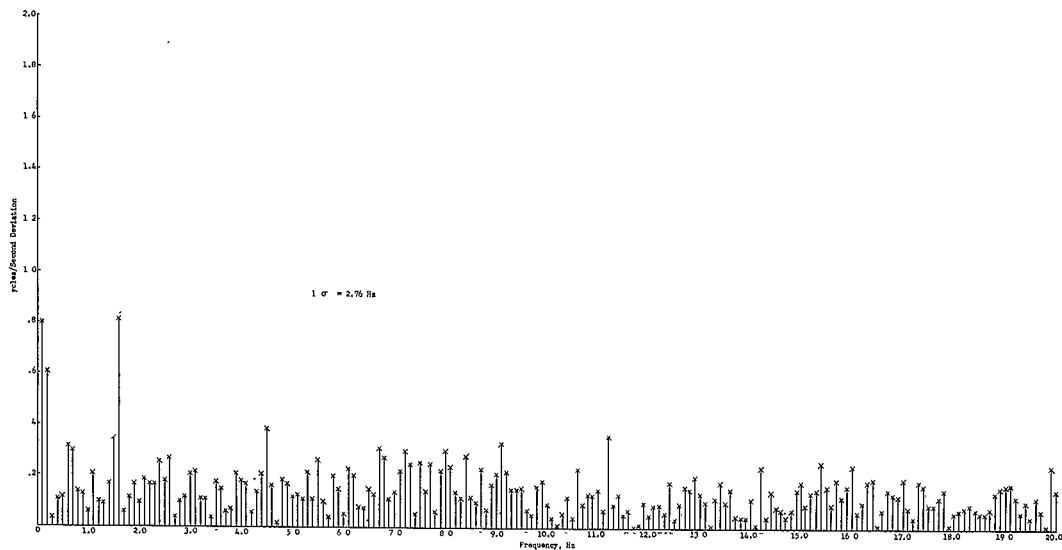
Figure 5.19.   Frequency Spectrum, ATS-1, No Error Cancellation (Cooby Creek, 29 Jan 68)

Receiving Station: Cooby Creek

Freq. (Hz)	Parameter	Coll. Tower	Transmitting Station		
			Cooby Creek	Rosman	Mojave
1.6 100 Sample per second	σ_1 (Hz)	0.001	0.0079	0.0073	Data not used
	Δf (Hz)	0.1380	1.265	1.138	
	m	0.086	0.790	0.711	
	R (db)	-27.4	-8	-9	
	δ		0.314	0.283	
60 100	σ_1 (Hz)	0.0005	0.0031	0.0055	Data not used
	Δf (Hz)	0.0418	0.2275	0.5069	
	m	0.000698	0.00379	0.00845	
	R (db)	-67	-51	-47.5	
120	σ_1 (Hz)	0.0009	0.0028	0.0859	Data not used
	Δf (Hz)	0.0739	0.6324	8.245	
	m	0.000316	0.00526	0.0687	
	R (db)	-72	-49	-29.1	
180	σ_1 (Hz)	0.0008	0.0015	0.0032	Data not used
	Δf (Hz)	0.0933	0.2723	0.2958	
	m	0.000518	0.00151	0.00164	
	R (db)	-69	-62.4	-61.7	
	Test σ	2.18	6.65	10.72	

σ_1 = Standard deviation of 10-second   values

Δf = Average deviation of 10-second   values

m   = Modulation index in radians

R   = Ratio of first sideband to carrier $= J_1/J_0$ (db)

δ = Expected misalignment of S/C antenna, cm
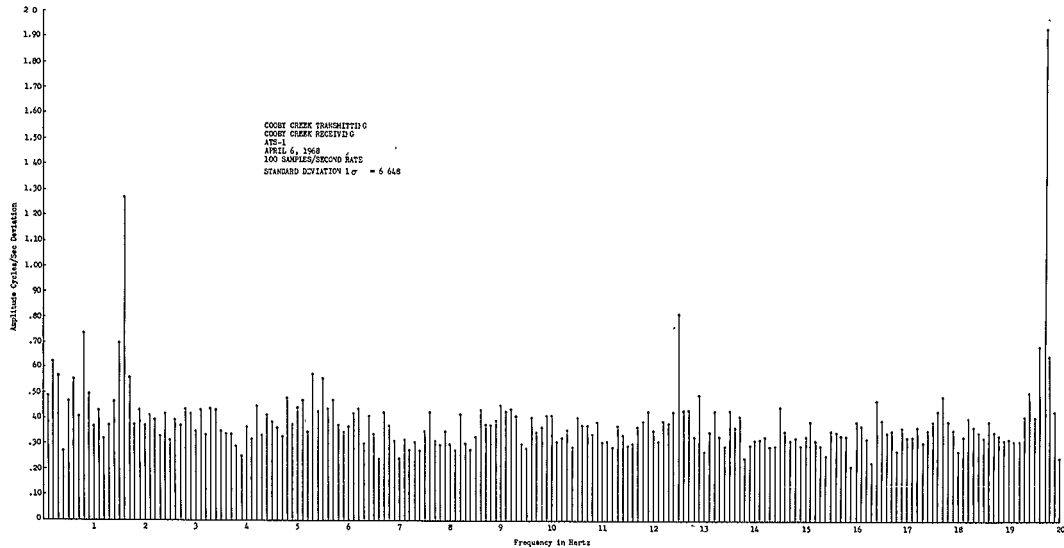
Figure 5.20. Fourier Analysis Frequency Spectrum, 10-Second Average
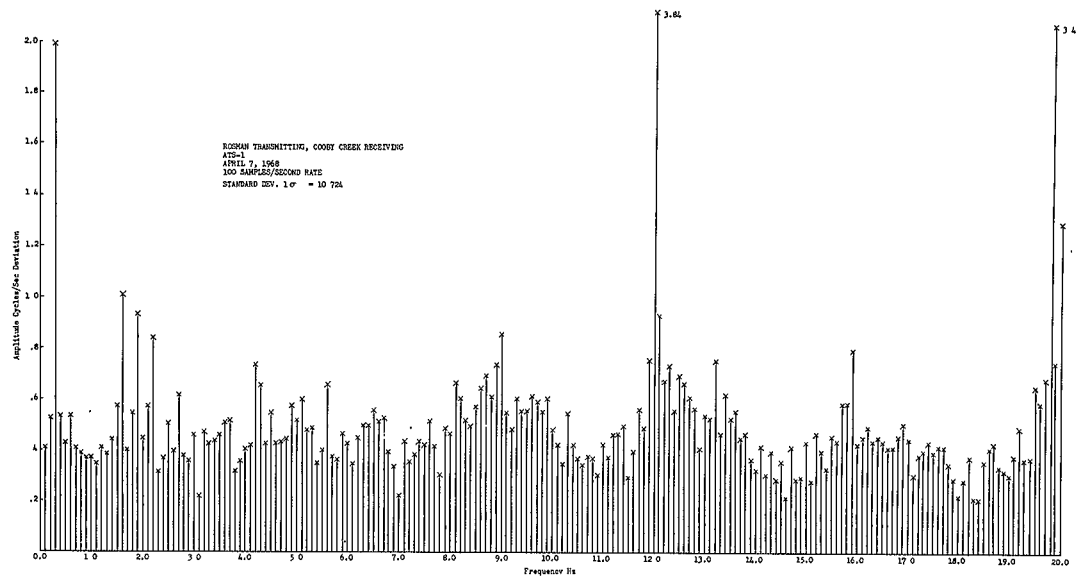
Figure 5.21. Fourier Analysis Frequency Spectrum, 10-Second Average

100 SAMPLE/SEC RATE
STANDARD DEV. 1σ = 6.648
FREQUENCY SHIFT = -1.442

$\emptyset$ CPS
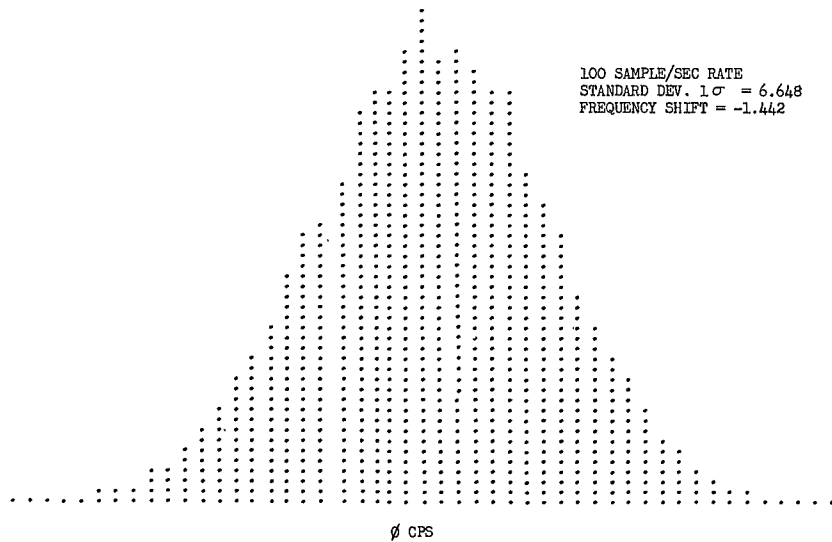
Figure 5.22.   Probability Density, Cooby Creek Recording Cooby Creek, 6 April 68 (ATS-1)
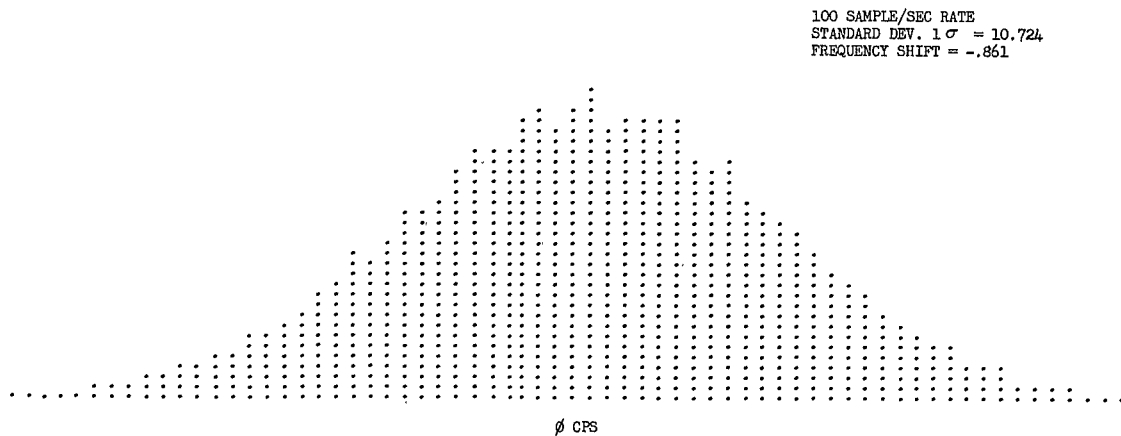
Figure 5.23. Probability Density, Cooby Creek Recording Rosman, 7 April 68 (ATS-1)

100 SAMPLE/SEC RATE
STANDARD DEV. 1σ = 2.175
FREQUENCY SHIFT = -.404

∅ CPS
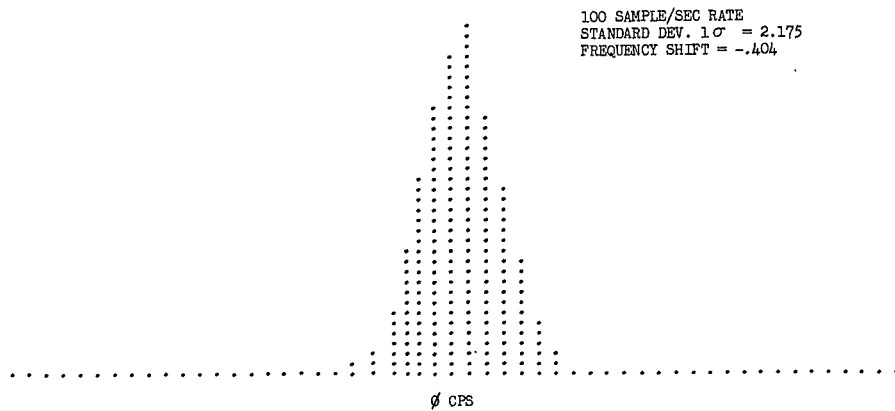
Figure 5.24. Probability Density, Cooby Creek Collimation Tower, 7 April 68
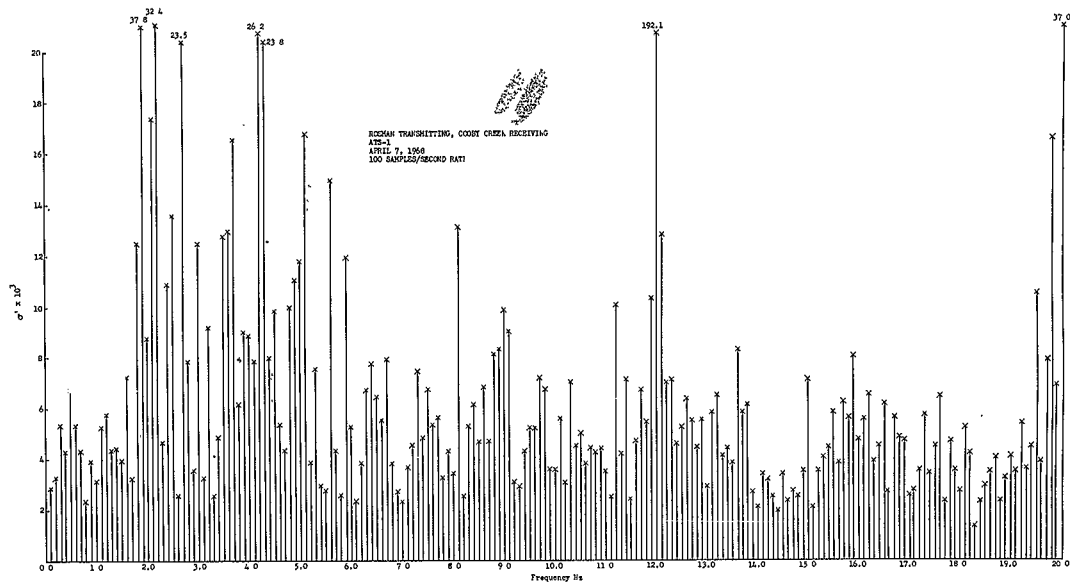
Figure 5.25. Standard Deviation of Secondly Values of Fourier Spectrum Amplitude Over 10-Second Interval

5.1.12 RESULTS OF SPECIAL LOW-DEVIATION FSK TESTS

To further evaluate the effect of the multiplex-channel frequency error in the SSB/PhM system, as well as to support the theoretical work presented in paragraph 5.1.7, regarding the multiplex-channel error probability performance, it was desirable to perform the special FSK test employing very low deviations.

The test was designed to be performed in six parts using the ATS-1 spacecraft and consists of one run through an RF loop at a deviation of ±5 Hz and five runs through the S/C loop at deviations of ±5 Hz, ±10 Hz, ±15 Hz, ±20 Hz, and ±25 Hz. All tests were to be performed at a standard bit rate of 100 bps and at a nominal multiplex-channel center frequency of 1 kHz. Data to be acquired consists of a digital error count with an accurately recorded test duration for each test deviation employed, and a representative sample strip chart or probability distribution of the multiplex-frequency variation recorded in a different channel during the test period.

The recommended test configuration employed for this test is outlined in the following paragraphs.

The Frederick model 600 Data-Transmission Test Set can be used to generate the basic digital pseudo-noise format, as well as to measure the error rate of the received data transmission from the multiplex channel discriminator. The actual binary FSK signal will be generated by a frequency synthesizer, such as the HP model 5102A. The synthesizer must be configured to be automatically driven by the digital pulse train of the Frederick 600 unit to deliver the desired FSK mark and space frequencies, f_m and f_s, respectively, such that $f_{m,s} = (1K \pm 5n)Hz$. Where n represents the test condition 1, 2, 3, 4, 5 corresponding to the desired deviation of ±5, ±10, ±15, ±20, and ±25 Hz, respectively.

The FSK signal from the synthesizer is then fed directly to a single multiplex channel and looped through the system (either an RF loop or S/C loop, as applicable). The recovered FSK signal from the receiver multiplex is fed to an appropriate frequency discriminator such as the GR1142A, IRIG, or the Halamore. The demodulated binary FSK signal is then sent to the Frederick 600 unit where comparison with the transmitted frequency yields the desired error count.

As auxiliary information to the FSK test, it is also desirable to transmit a multiplex channel test tone frequency in a different multiplex channel and either record on a strip chart or obtain a frequency distribution plot of the demodulated output from a suitable FM discriminator tuned to the test tone frequency to determine the standard deviation of the frequency instability for use in correlation with the FSK data.

It can be shown that the error probability, P_e, for this FSK test is related to the actual error count, N, measured in a specified time duration, D, and the bit rate, B, in the following manner:

$$P_e = \frac{N}{BD}$$

Therefore, for each test deviation employed, it is necessary to record the bit rate and also an accurate indication of the test period, so that the error probability can be predicted from equation (77).

Unfortunately, several difficulties have been encountered in attempting to perform a successful FSK test as described above. The major problem lies in the fact that as Δf increases much above 10 Hz, the error count drops very rapidly, as given by equation 54, and consequently the required test duration necessary to count a sufficiently large number of errors to establish a statistical average becomes unreasonably long. In fact, for all of the tests conducted to date, when the system was properly configured it was not possible to measure more than a few errors over a 1-hour period when the deviation approached a 15-Hz peak. Another problem encountered is that the theoretical error probability is based on an assumed normally distributed noise characteristic, and when only a few errors are counted over a very long period of time, it is likely that the measured errors are due to a noise source that does not follow this normally distributed noise characteristic. Still another problem encountered concerns the presence of discrete frequency components in the multiplex channel, particularly 1.6 Hz, and the 60 Hz and harmonically related frequency components. The presence of these components also tend to compromise the initial assumption of normally distributed noise.

A partially successful test was performed at Cooby Creek on 1 May 1968. At this time it was possible to measure a reasonable error rate of 240 errors per minute and 5 errors per minute at deviations of ±5 Hz and ±10 Hz, respectively, for a bit rate of 100 bits per second. At a deviation of ±15 Hz, no errors were recorded over a 50-minute interval. From equation (77), the error probability for the ±5-Hz and ±10-Hz deviations were determined as 0.04 and 0.000835, respectively. The corresponding channel rms frequency deviations (standard deviation) obtained from figure 5.10 or equation (53) can be determined as 2.9 Hz for the ±5-Hz deviation, and 3.1 Hz for the ±10 Hz deviation. The close proximity of these two values is some indication of the data quality; also, it is interesting to note that the σ value obtained from the Cooby Creek test of 29 January 1968, shows a σ value obtained from the probability distribution curve of 3.53 Hz, which is of the same order of magnitude as measured by this test.

5.1.13 SHORT-TERM FREQUENCY STABILITY IMPROVEMENT USING THE CARRIER REFERENCE TECHNIQUE

INTRODUCTION

The short-term instability presents a definite limitation to the usefulness of the system. Several methods have been considered to reduce the short-term instability. The classical approach is to use a "good tight" servo loop. This is not practical in this case because the large transport lag caused by the propagation delay precludes the use of sufficient bandwidth to materially reduce the instability. Other techniques must therefore be considered.

The technique used is based on the instantaneous compensation of the received FDM baseband. The point at which the frequency stability is really pertinent is at the demodulation point of the receive FDM unit. Therefore, it follows that if the received FDM baseband could be demodulated with respect to a reference carrier that contained the same abberations as those imposed on the FDM information signals, the resultant frequency distortion values would be reduced. A functional block diagram of the technique along with the method employed to measure frequency stability is shown in figure 5.26.

The method may be implemented by employing an appropriate receive filter and injecting a reference carrier at the group or supergroup sections of the receive multiplex unit. This method would apply, for example, to the 240-channel multiplex unit at the Mojave and Cooby Creek stations. A functional representation of the multiplex unit is shown in figure 5.27. In operating with supergroup 2, the group carrier (564 kHz) is employed as the reference (specific carrier for demodulating a given number of multiplex channels). For operation with supergroups 3 through 5, the respective super group carriers (1116, 1364, and 1612 kHz) must be employed. It is not permissible to employ the group reference carrier when operating with supergroups 3 through 5. In this case, the frequency error will double due to a reversal in sign caused by the numbers of mixing operations employed in generating these supergroups. In operating with the 1200-channel system at the Rosman station, four possible reference carriers can be used. These are the supermaster group, mastergroup, supergroup, and group carriers. The equivalent mixing operations are shown in figure 5.27. If four mixing operations are employed, only the supermaster and supergroup carriers can be the reference. From the above, it follows that the supergroup carriers will in general be employed for the reference. In this case, each station must transmit a carrier for each 60-channel group.

The major advantage of the carrier technique is that it can compensate for frequency variations regardless of the magnitude of the spacecraft transport lag and the magnitude of the incidental modulation present on the signal. The amount of rejection only depends on the difference in the modulation parameters on the FDM signal and carrier and on their relative time displacement, τ. Its major disadvantage is that it requires altering

MUX RCV
UNIT

PM
RCVR

300 - 3400
Hz FILTER

3-kHz TONE

REFERENCE
CARRIER

RCV
FILTER

$e^{-s\tau}$

(3-kHz)
DISCRIMINATOR

A/D
CONVERTER

SDS - 910
COMPUTER

FOURIER MEASUREMENT TECHNIQUE

τ- RELATIVE TIME
DISPLACEMENT BETWEEN
THE REFERENCE CARRIER AND
THE BASEBAND SIGNAL
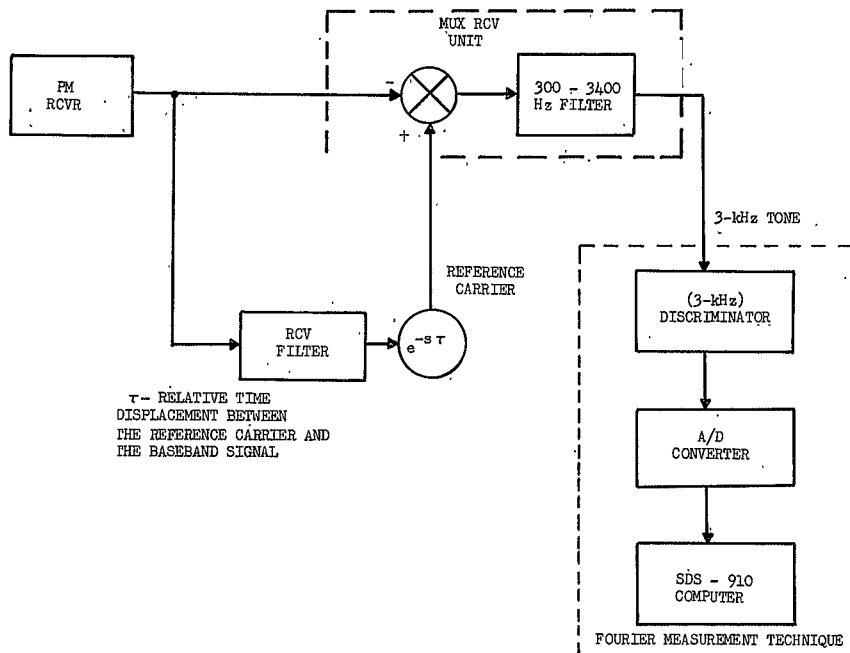
Figure 5.26.   Block Diagram Showing Frequency-Stability Measurement Technique
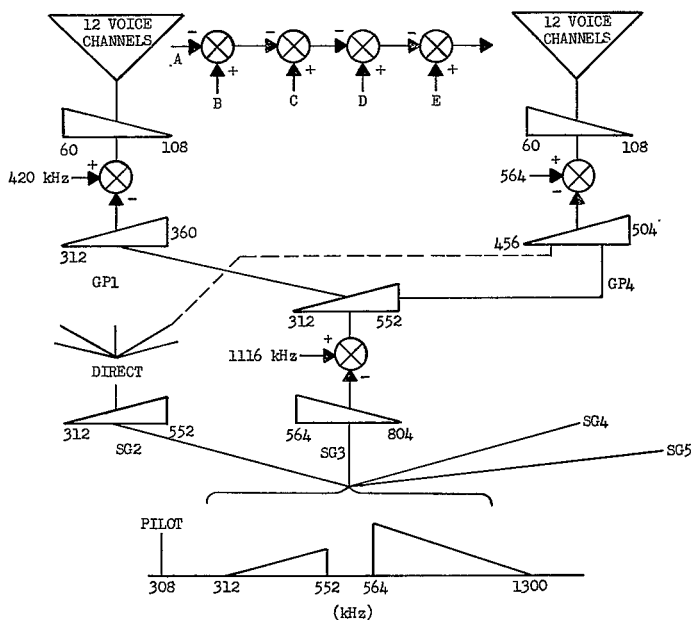
Figure 5.27.   Functional Representation of a Multiplex Unit

5.62

the standard receive multiplex units and it increases the operational complexity between participating stations. This complexity involves the choice of the correct carrier to transmit (group or supergroup) which is a function of the number and baseband location of the channel group. In particular, the following factors must be considered in implementing the technique:

1) In general, each originating station must transmit a carrier at nominal test tone level for each 60 channels that is transmitted (assuming supergroup correction). For 1200-channel system, supermaster group correction could be employed; however, this would assign as many as 900 channels to only one participating station. If greater flexibility is required for meeting changing peak load demands among the various stations, reference carrier assignments would have to be changed on an operational basis.

2) The required ground transmit power will increase by a factor of n Po (n is the number of carriers, Po is the transmit test tone level). For a large n factor the required reference carrier power can become a substantial part of the total transmit power. Tests have shown that a Po/10 carrier level can be employed with a proportionate increase in the test-tone short-term frequency instability. Hence, the actual carrier level will depend on the maximum permissible level of instability.

3) The standard receive multiplex unit must be altered to receive the desired reference carrier.

4) A frequency synthesizer must be added to the SSB transmitter to develop the desired carrier or carriers.

An alternate instrumentation procedure could be employed for the reference carrier technique. This would involve extracting the frequency abberations from one of the pilot tones and inserting them on a locally generated reference carrier. This would involve a frequency synthesizer, mixers, and selective amplifiers.

MATHEMATICAL DESCRIPTION OF REFERENCE CARRIER TECHNIQUE

As stated above, the technique consists of transmitting a reference carrier along with the desired signal. In transmission, the reference will be subjected to the same perturbations as the desired signal so that in the detection process the perturbations on the desired signal will be canceled out. Let the desired signal be noted as:

$$A_1 \cos \left[\omega_1 \tau + \theta_1 (\tau) \right] \tag{1}$$

and the reference carrier as,

$$A_2 \cos \left[\omega_2 (t - \tau) + \theta_2 (t - \tau) \right] \tag{2}$$

where:

$\theta_1(t)$ is the angular modulation applied to ω_1

$\theta_2(t)$ is the angular modulation applied to ω_2. For the general case assume

that $\dot{\theta}_1(t) \neq \dot{\theta}_2(t)$

$\quad$ τ is the relative time displacement between the two waves.

$\quad$ If the above two signals are applied to a mixer and the difference term extracted, it will be,

$$\frac{A_1 A_2}{2} \cos \left[(\omega_2 - \omega_1)t - \omega_2\tau + \theta_2(t - \tau) - \theta_1(t)\right] \qquad (3)$$

It is noticed that the difference term will consist of the difference frequency $\omega_2 - \omega_1$ a phase shift $\omega_2\tau$ and a difference term between the angle modulation functions.

Let $\qquad \theta_2(t - \tau) = M_2 \sin \omega_m (t - \tau) \qquad\qquad\qquad (4)$

$\qquad\qquad \dot{\theta}_1(t) = M_1 \sin \omega_m t \qquad\qquad\qquad\qquad (5)$

M_2 is the modulation index of the incidental modulation applied to ω_2.

M_1 is the modulation index of the incidental modulation applied to ω_1.

$\quad$ The resultant angle modulation term will be,

$$M_2 \sin \omega_m (t - \tau) + M_1 \sin (\omega_m t + \pi) \qquad (6)$$

Let $\omega_m t = \psi \quad$ and $\quad \omega_m \tau = \phi$

Equation (6) reduces to

$$M_2 \sin (\psi - \phi) + M_1 \sin (\psi + \pi) \qquad (7)$$

$\quad$ The above terms are two vectors whose magnitudes are M_2 and M_1 and whose arguments are $(\psi - \phi)$ and $(\psi + \pi)$, respectively. The resultant vector, $\overrightarrow{C}$, of the above vector addition will have the following components,

$$\text{Xcomp.} = M_2 \cos (\psi - \phi) - M_1 \cos \psi \qquad (8)$$
$$\text{Ycomp.} = M_2 \sin (\psi - \phi) - M_1 \sin \psi \qquad (9)$$

The magnitude of the resultant vector $\overrightarrow{C}$ is,

$$\sqrt{M_2^2 + M_1^2 - 2M_2 M_1 \cos \omega_m \tau} \qquad (10)$$

its argument is,

$$\tan^{-1}\left[\frac{M_2 \sin(\omega_m t - \omega_m \tau) - M_1 \sin \omega_m t}{M_2 \cos(\omega_m t - \omega_m \tau) - M_1 \cos \omega_m t}\right] \qquad (11)$$

If $\tau = 0$, the overall angle-modulation expression of equation (7) reduces to

$$(M_2 - M_1) \sin \omega_m t \qquad (12)$$

If τ is finite but $M_2 = M_1$ equation (7) reduces to,

$$(2M_2 \sin \frac{\omega_m \tau}{2}) \cos(\omega_m t - \frac{\omega_m \tau}{2}) \qquad (13)$$

From the above equations, it follows that perfect cancellation only occurs if $\tau = 0$ and $M_2 = M_1$. Equation (13) closely approximates the actual condition for the operational system. In this case it is expected that the angle-modulation sidebands will increase sinusoidally for increasing values of f_m where f_m is the baseband frequency. The M factor will be attenuated for f_m values of less than $1/6\tau$. For higher values of f_m there will be a gain in M reaching a maximum of 2M at an f_m of $1/2\tau$.

TEST RESULTS

The effect of the reference carrier technique on the test-tone short-term frequency stability was determined by utilizing the Fourier analysis method.

In order to determine the effect of the above technique on thermal noise, incidental modulation and the $1/f$ phase noise factors, tests were performed in various loops and test configurations. The effect of thermal noise was determined by instrumenting a loop consisting only of the transmit and receive multiplex units. At the transmit unit, thermal noise was injected into the system so that the exact S/N (test tone to thermal noise ratio) obtained in the S/C loop is realized. This value for the Mojave station, where the test was performed, is 37 db, flat weighted.

The response of the technique to the incidental modulation components was determined by impressing an FM signal of varying modulation frequencies on the test tone and reference carrier. The resulting response is shown in figure 5.28 for the conditions of no correction (error cancellation disabled), group correction and supergroup correction. Utilizing the response level at 100 Hz for the uncorrected condition as a reference, it was determined that the response for the group correction was -4.8 db and for the supergroup correction -48.5 db. The roll off in the response for all three conditions is due to the band pass and post detection filters shown in figure 5.26. The sinusoidal variation of attenuation with modulation frequency is evident as predicted by the mathematical description.

The 43.7-db difference in the attenuation factors is mainly due to the values of the τ factors for the two correction methods. A narrow-band filter is utilized with group

correction. The relative time delay caused by this filter is much greater than the value obtained for the wide band filter employed for the supergroup correction; hence, the difference in the τ values.

Characteristic error spectrums for normal system operation with the error cancellation unit disabled are shown in figures 5.29 and 5.30. For both examples the A/D sampling rate was set at 3000 to obtain the spectrum out to 600 Hz. As shown in figure 5.30, the various noise components are not as high as the corresponding components shown in figure 5.29. The latter test was performed on September 19, 1969, and the former on January 3, 1970. The reduction ($\sigma = 4.27$ Hz to $\sigma = 3.16$ Hz) is generally due to a decrease of the low-frequency components from the Y PLL and the $1/f$ phase noise. It has been found that the σ factor for the system is time variant. The main cause of this condition is the unexplainable variation in the levels of the noise components being emitted by the SSB transmitter.

As shown in the above figures, the resulting error spectrum is basically flat from 120 Hz to about 450 Hz. At higher frequencies the filters cause a definite roll-off. At lower frequencies the spectrum tends to increase due to the spin modulation components, $1/f$ phase noise and components being emitted by the Y PLL. Ideally, the spectrum should be triangular since the noise voltage at the output of an FM discriminator varies as kf (k is a constant and f is the baseband frequency). This triangular shape is realized in the multiplex back-to-back loop where only thermal noise is present.

Figure 5.31 is a representative plot of the error spectrum for supergroup correction of the normal condition shown in figure 5.30. Figure 5.32 is the corresponding histogram of the frequency distribution. Also shown in figure 5.31 are the lines that define the peak components of the error spectrums for the normal S/C loop and multiplex back-to-back loop configurations. From the figure, it is seen that the reference carrier technique eliminates all of the noise components in the lower part of the spectrum but has an amplification-effect on the thermal noise. This latter effect was checked by performing tests in the multiplex loop at an S/N of 37 db and 43 db with and without the reference carrier technique. In both S/N cases, the σ factors when using the technique were higher.

Table 5.4 lists the results of various tests conducted at different test tone frequencies, S/N values and in different loop configurations. The resulting σ's for normal and carrier reference conditions (supergroup and group corrections) are also listed. The resulting decrease in the σ factors for the decrease in test tone frequencies is mainly due to the decrease in the IF filter bandwidth. This bandwidth is always ±15 percent of the test tone frequency. In test run 2, only supergroup correction was employed since it is superior to group correction at S/N values of 37 db and 43 db and at two test tone frequencies. For both

conditions it is noticed that the σ values for the correction conditions are almost the same for the multiplex and S/C loop configurations. Hence, the thermal noise factor limits the final value of σ when employing the reference carrier technique in the S/C loop configuration. An increase of S/N of 6 db causes a reduction of 6.2 db in the σ factor (2.31 Hz to 1.12 Hz).

Figures 5.33 and 5.34 show the error spectrum for the frequency band of zero to 20 Hz for normal system operation and for operation with group correction. The sinusoidal response of the error correction loop is quite evident in the two figures. As shown in figure 5.34, the 1.6-Hz component and the other low-frequency factors other than thermal noise are eliminated by the above technique. It is also evident from figure 5.33 that the spin-modulation component falls near the peak of the first sinusoid as originally predicted.

The limitation in the improvement of the σ factor when employing the carrier correction technique is mainly due to two factors: (1) The apparent amplification of the thermal noise component by the technique and (2) The triangular shape of the baseband noise voltage. Both of these factors tend to increase the value of σ. This increase can be seen from the expression employed to compute σ :

$$\sigma^2 = \sum_{j=1}^{n} \frac{(x_j - \bar{x})^2}{n}$$

x_j are the sample values

$\bar{x}$ is the mean of the sample values

n is the number of sample points

From the above equation, it is noted that σ is a direct measure of the distance that the sample values are located from the mean. It follows that an x_j near the mean is not as critical as one that is a large distance from the mean. Hence, σ is heavily weighted by values at relatively large distances from the mean. Elimination of noise components in a given frequency interval near the mean is not as effective in reducing σ as elimination of the components in the same interval at a distance of 500 Hz from the mean. Since the baseband noise varies as kf, the increase in noise at the high end of the baseband region limits the amount that σ can be reduced. A direct reduction of this noise can only be realized by an increase in the test tone to spectral noise density ratio.

SUMMARY

The overall system AFC unit consists of a primary AFC loop and an open-loop system defined as an error correction loop. The latter loop has a sinusoidal response that is a function of the S/C transport lag. For the 0.27-second lag value obtained, it can be shown that the error correction loop amplifies the spin modulation components and the 60-Hz

components. It also attenuates the 1/f noise. From various tests, it has been shown that the overall AFC unit can compensate for long-term frequency drifts (S/C oscillator drifts and/or doppler).

A type-one AFC unit could replace the type-zero unit with error correction. Both systems produce a finite steady state error for an input frequency ramp of unit slope. The type one unit can eliminate the unwanted amplification of the 1.6-Hz and 60-Hz components. However, neither can eliminate or substantially reduce the factors that cause the short-term frequency instability.

A reference carrier technique was developed that could reduce the above instability irregardless of propagation time. This technique is based on the instantaneous compensation of the received FDM baseband. The major advantage of this technique is that the degree of reduction only depends on the difference in the modulation parameters on the FDM signal and carrier and on their relative time displacement, τ. Its disadvantages are as follows: (a) Must generate and transmit an additional carrier or carriers. (b) Requires an additional amount of transmitter power. (c) Increases system complexity by requiring a frequency synthesizer at the transmitter and an alteration of the standard receive multiplex unit. (d) Decreases the versatility of assigning multiplex channels for the participating stations. (e) Can cause a 6-db increase in the incidental modulation if the value of τ is high enough. (f) The technique causes an apparent amplification of the thermal noise in the baseband region.

The standard deviation (σ) of the frequency deviation histogram was chosen as the logical measure of the frequency instability. This factor weighs the noise components in the upper baseband region quite heavily. Because of the amplification effect and the fact that the baseband noise spectrum varies as kf, the limiting condition for the reduction of σ is the thermal noise component. Its reduction can be accomplished by an increase in the test tone to thermal noise ratio.

TABLE 5.4. REFERENCE CARRIER TEST DATA

TEST LOOP	TONE FREQ. (KHz)	MULTIPLEX S/N (db)	NORMAL SYSTEM CONFIGURATION (σ–Hz)	CARRIER REFERENCE		TEST RUN
				SUPER GROUP σ(Hz)	GROUP σ(Hz)	
MUX BB	2	37	1.33			1
S/C	2	37	3.07	1.91	2.98	1
MUX BB	2.5	37	1.63			1
S/C	2.5	37	3.7	2.4	3.43	1
MUX BB	3	37	1.78			1
S/C	3	37	3.98	2.52	3.57	1
MUX BB	2	37	1.26	1.72		2
S/C	2	37	2.88	1.66		2
MUX BB	2	43	0.69	0.93		2
S/C	2	43	2.72	0.89		2
MUX BB	3	37	1.66	2.36		2
S/C	3	37	3.16	2.31		2
MUX BB	3	43	0.91	1.23		2
S/C	3	43	3.0	1.12		2
S/C	3	37	3.74 (with error correction all other cases error correction is off)			

The figure shows a plot of DB (vertical axis, from −16 to 12) versus FREQUENCY IN Hz (horizontal axis, from 10 Hz to 1000 Hz) with curves labeled:

- S.G. CORRECTION
- GROUP CORRECTION
- NO CORRECTION – E OFF
- EMR POST DETECTION BW = 500 Hz

GROUP CORRECTION AT 100 Hz = −4.8 db
SUPERGROUP CORRECTION AT 100 Hz = −48.5 db
RELATIVE TO NO CORRECTION

FREQUENCY IN Hz
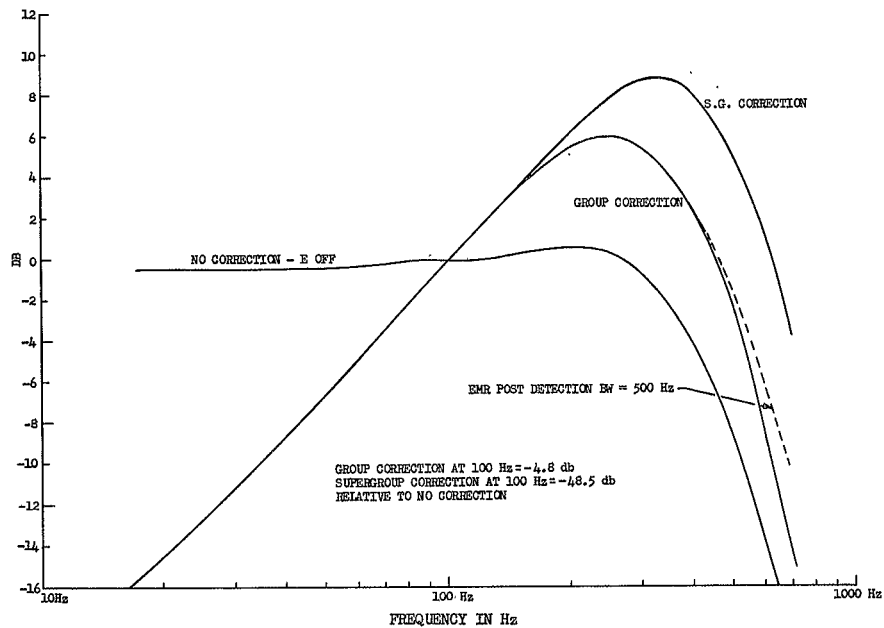
Figure 5.28. Carrier Correction Response
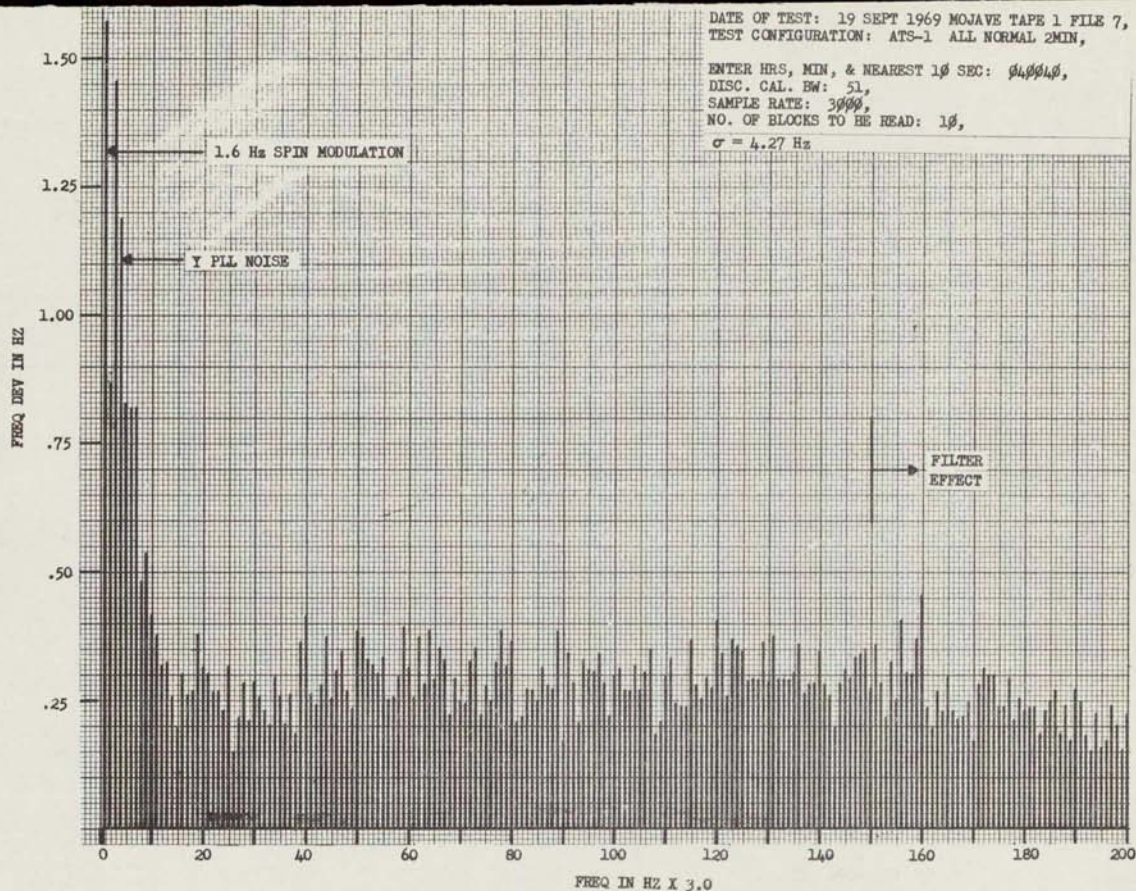
Figure 5.29. Normal System Configuration Error Spectrum ($\sigma = 4.27$ Hz)

Text within the figure:

DATE OF TEST: 19 SEPT 1969 MOJAVE TAPE 1 FILE 7,
TEST CONFIGURATION: ATS-1 ALL NORMAL 2MIN,

ENTER HRS, MIN, & NEAREST 1Ø SEC: Ø4ØØ4Ø,
DISC. CAL. BW: 51,
SAMPLE RATE: 3ØØØ,
NO. OF BLOCKS TO BE READ: 1Ø,

$\sigma = 4.27$ Hz

1.6 Hz SPIN MODULATION

Y PLL NOISE

FILTER EFFECT

FREQ IN HZ X 3.0

FREQ DEV IN HZ

5.71
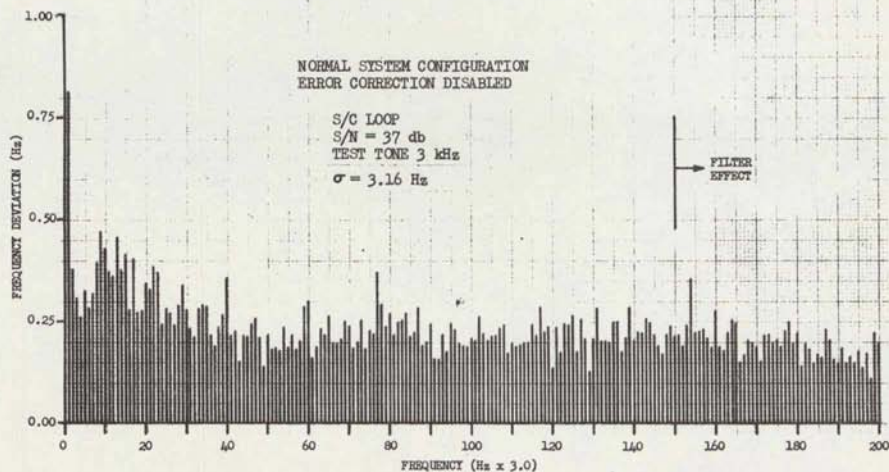
Figure 5.30. Normal System Configuration Error Spectrum (σ -3.16 Hz)
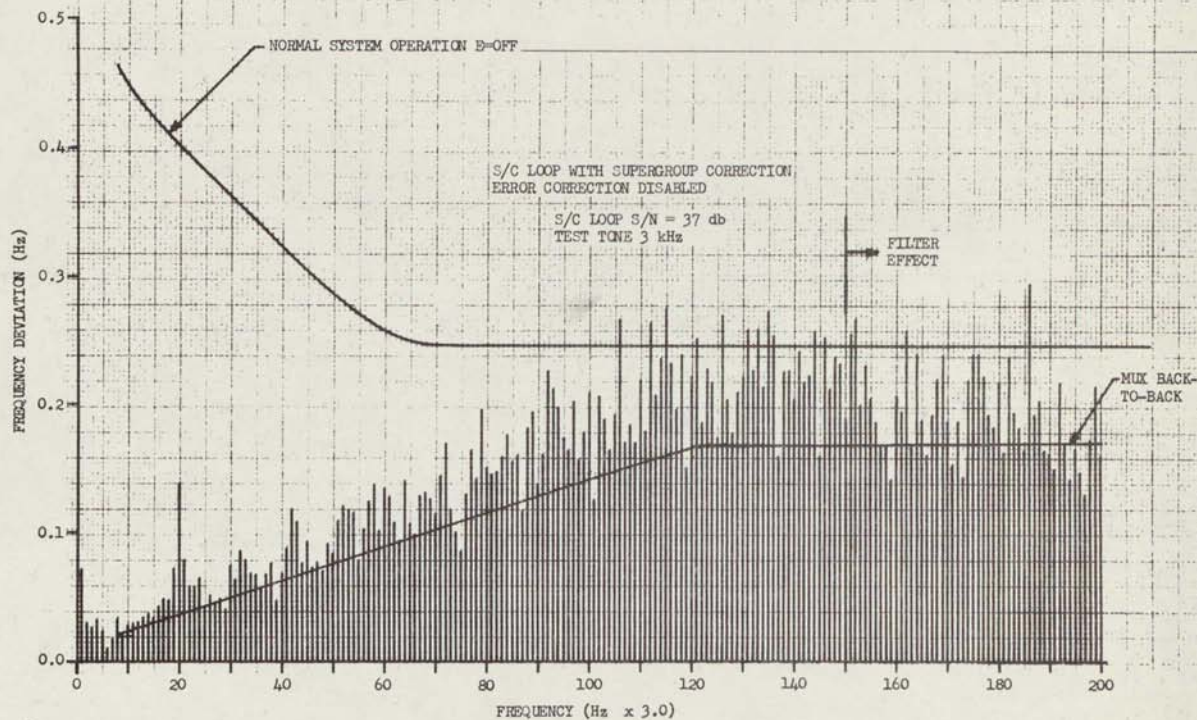
Figure 5.31. S/C Loop With Supergroup Correction (Error Correction Disabled) Error Spectrum
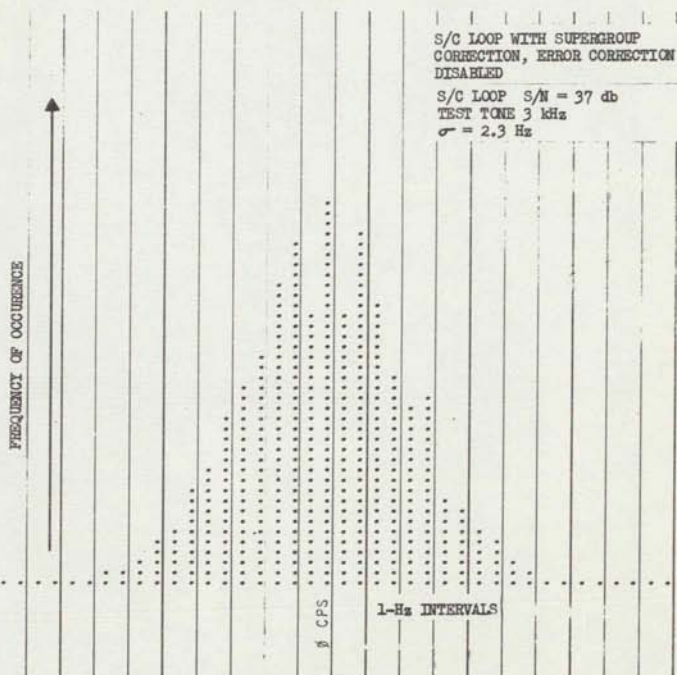
Figure 5.32. S/C Loop With Supergroup Correction (Error Correction Disabled) Frequency Deviation Histogram
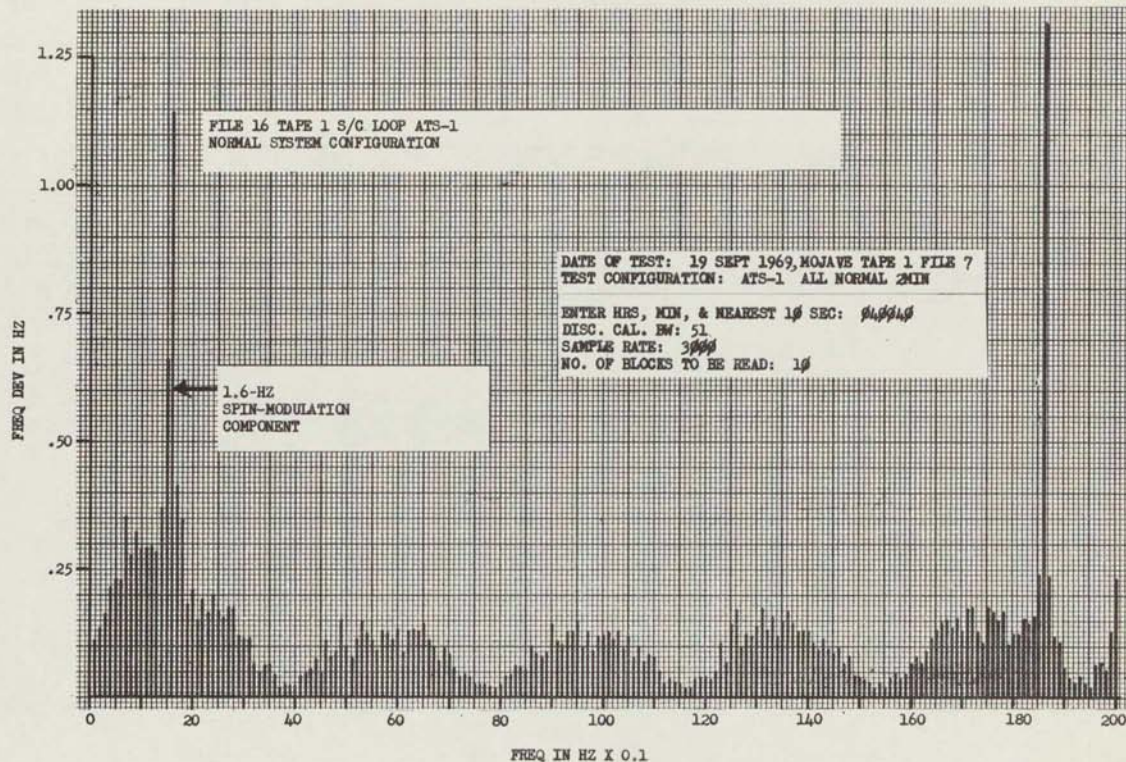
Figure 5.33. Error Spectrum in Frequency Range 0-20 Hz Without Reference Carrier Correction
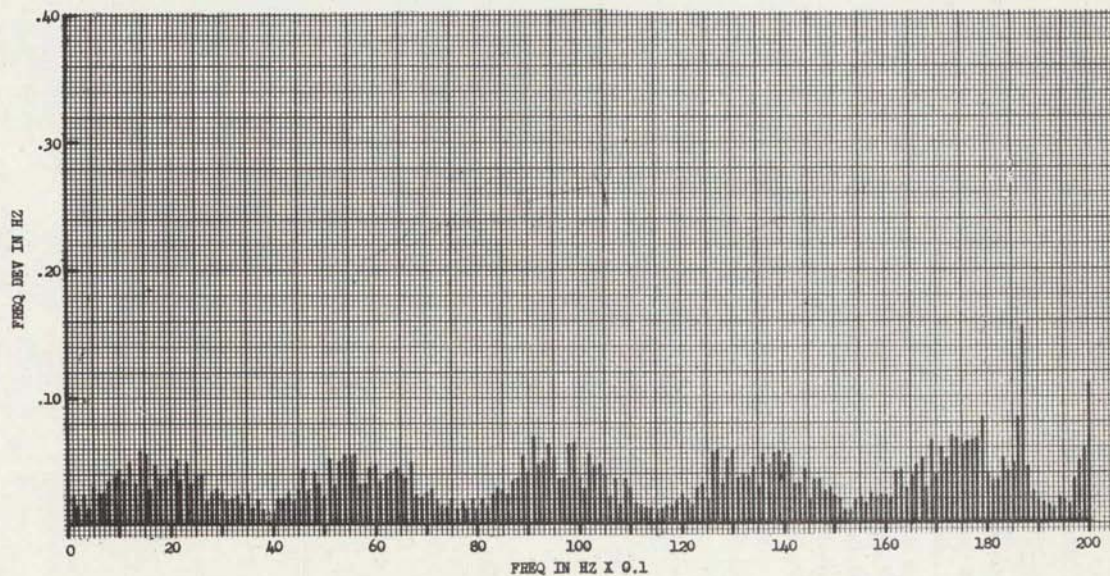
Figure 5.34. Error Spectrum in Frequency Range 0-20 Hz With Reference Carrier Correction

5.2 ANTENNA CHARACTERISTICS (J.G. McGillen)

5.2.1 INTRODUCTION

The communications equipment (receiver, transmitter, MUX, CTEC, etc) at the Rosman, Mojave, and Cooby Creek ATS ground terminals are almost identical, but the satellite tracking antennas at these stations utilized to support the communications experiments have a variety of performance characteristics which are descriptive of specific stations. These differences of the antenna characteristics, in some cases, affect the quantitative and qualitative results of much of the communications experimentation. In support of the Ground Terminal Antenna Patterns experiment (AN-AT-1.1) an investigation of the antenna positioning characteristics of the various ATS antenna systems has been initiated. As part of this program, a series of special tests are being conducted to determine the optimum test conditions under which the ground terminal antenna patterns experiment can be conducted. The results of this investigation will also aid other experiments where the antenna positioning performance is significant.

5.2.2 INITIAL INVESTIGATION

The ground-terminal antenna-pattern experiment requires the antenna under test to scan a raster pattern of specific dimensions at a controlled velocity to measure the RF characteristics of the directional RF patterns in the transmit (6 GHz) and receive (4 GHz) modes of operation. To develop a meaningful 3-dimensional RF antenna pattern, the angular excursions and the rate of scan which are selected to produce the raster scan positioning pattern are dependent upon: (a) the significant elements of the RF pattern that are desired; (b) the resolution required to define these elements; (c) the data sample rate; (d) the total time required to perform this measurement; and (e) the antenna positioning characteristics. The RF pattern significant elements that are of interest during this experiment have been specified, as that portion of the RF pattern that extends to the second side lobe. The data sample rate is fixed at one sample per second, and the time necessary to conduct this experiment has been kept to a minimum to satisfy system stability and operational requirements. The measured RF pattern resolution is mainly dependent on the data sample rate and the antenna positioning characteristics. It is the antenna positioning characteristics that will vary depending upon which antenna is used to perform this experiment. Since the data sample rate is low (1 per second) and a relatively high-resolution factor is desirable, the antenna scan rate is expected to approach the design limits of the system. With this in mind, a special test program was conducted at the Mojave ATS station on the 18th, 19th and 20th of July, 1967, to investigate the antenna positioning characteristics necessary to support the ground-terminal antenna-pattern experiment.

The antenna positioning test program began with an attempt to determine the smallest angular excursion that the antenna servo subsystem could respond to when a step positioning function was utilized. This test consisted of moving one axis of the antenna off boresignt in the manual mode and allowing an auto track mode error voltage, which was developed due to misalignment, to reposition the antenna. The servo-position and servo-error (velocity) voltages were recorded. Utilizing various angular offset positions, it was determined that the antenna would respond directly to a step function satisfactorily to offset angles of 0.06 degrees. These test results are not conclusive in themselves since the auto-track subsystem affected the test and the system was operated in a nonstandard environment.

Two methods were instrumented to position the axes of the antenna in a raster scan pattern to measure the receive antenna RF patterns. The X-axis (axis No. 1) was positioned using an analog scan voltage (sinusoidual) added to the X-axis servo-input circuitry. The Y-axis (axis No. 2) was positioned in discrete angular steps, utilizing the digital data positioning option, at the end of each excursion of the orthogonal plane (X-axis No. 1). The Y-axis was positioned utilizing the step function since this axis could not respond adequately at the required slow scan rate when an analog voltage was applied to the servo-drive circuitry. It was noted during this phase of the test that the X-axis responded adequately when this axis was moved in one direction, but when the axis reversed direction a considerable amount of X-axis striction was evident. This problem was analyzed and it was determined that a faulty servo valve was the major contributor. The servo valve was exchanged, but the new unit did not perform as well as the original unit. The servo system was optimized for best overall performance.

The Ground Terminal Antenna Receive Pattern experiment (AN-AT-1.1) was conducted on a preliminary basis to determine the capability of the antenna servo/drive subsystems to support this experiment. This experiment was performed on the 20th of July. Only one frame of the RF pattern was measured. During this exercise the servo drive voltage, servo error (velocity) voltage, and the analog equivalent of the received RF signal power were recorded as a function of time. A history tape of the antenna position was also recorded. The basic problem of unidirection antenna X-axis sticktion was observed throughout most of this experiment. The data obtained during this special test period was returned to Westinghouse for analysis.

The analysis of the data obtained during the special test program at the Mojave ATS station revealed several items of interest:

1) The test philosophy and the basic electronic instrumentation (receiving, transmitting, data collection) are adequate to support the Ground-Terminal Antenna Patterns experiment (AN-AT-1.1). In some cases, specific equipment items require further investigation to determine if their performance

can be improved. It was noted during the testing that the Electrac Receiver (model 215) did not have sufficient AGC range to support the experiment. The range and range rate receiver was substituted during this test. Additional tests of the Electrac Receiver are being requested to evaluate its usefulness in this experiment.

2) The antenna axis positioning methods have been exercised at Mojave and it is believed that under the right test environment the raster scan pattern necessary to perform the ground terminal antenna patterns experiment can be achieved. The scan velocity selected for the X-axis was nominally 0.1 degree per second. During this test the servo position voltage, servo error (velocity) voltage, AGC voltage, and antenna position (digital history tape) were recorded. Analysis of this test data, obtained utilizing a satellite to measure receive patterns, indicated that a <u>triangular</u> scan voltage should be used as a replacement for the sinusoidal antenna position voltage. The sinusoidal waveform produced a varying scan rate since the variable slope of the waveform continuously altered the antenna velocity. This condition is shown in figures 5.35 and 5.36 as antenna position $\Delta \theta$ angle as a function of time. The changing velocity is most undesirable from the data reduction point of view.

3) The test instrumentation necessary to perform the ground terminal antenna patterns experiment is complex and varied. The antenna servo/drive subsystems are considered part of this instrumentation. To measure meaningful RF patterns, based upon the experimental test criterion, the antenna positioning subsystems (servo/drive) are required to perform in a prescribed manner. The RF pattern measurements are affected by the antenna servo/drive subsystems design limitations and maintenance characteristics. The analysis of the test data obtained at the Mojave station, when the RF receive ground terminal antenna pattern measurement was conducted on a preliminary basis, indicated that the antenna could perform RF pattern measurements within its design limitations.

An example of the analog patterns that were measured and the servo/drive performance of the antenna in the form of servo position, servo error (velocity) and antenna-position error are shown in figure 5.36; data shown in the figure is representative of a single axis No. 1 (X-axis) line scan. The antenna RF response is of the classic type-and the servo/drive subsystems are operating adequately. It can be seen that the antenna position rate of scan is being altered as a function of the X-axis sine wave slope.

5.80
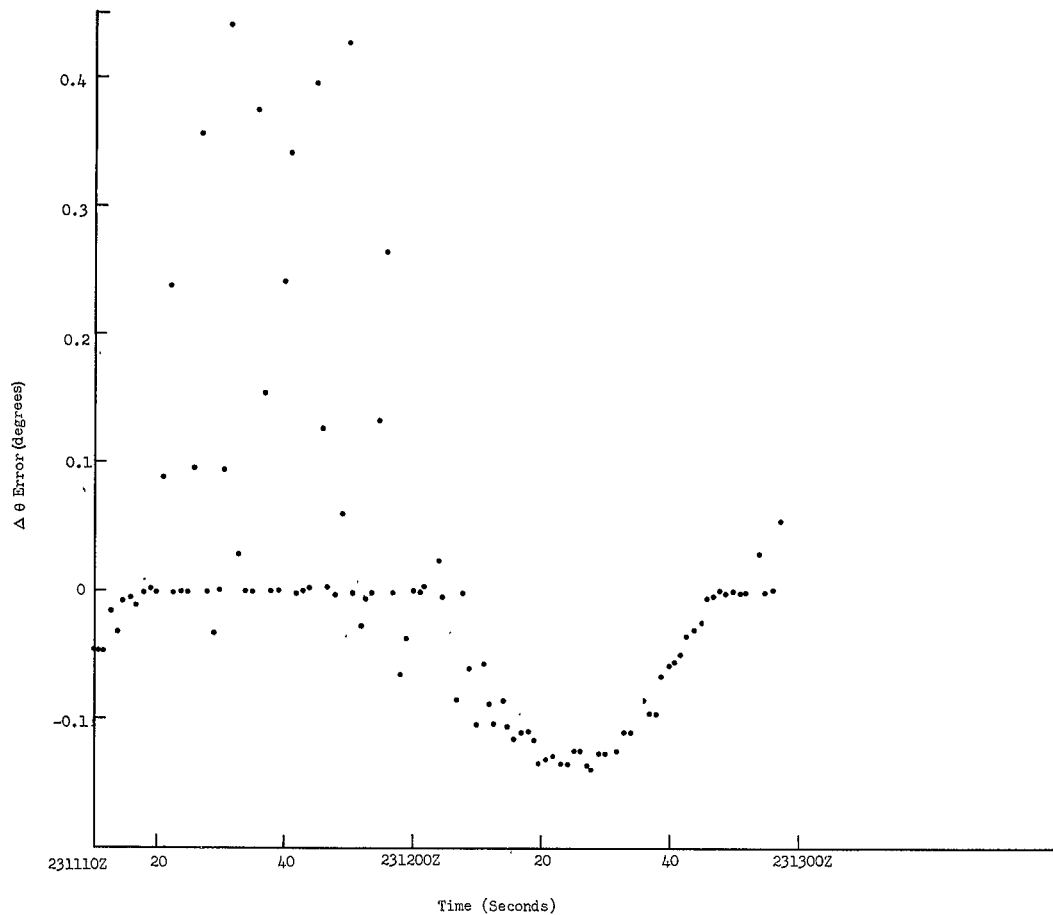
Figure 5.35. X-Axis Antenna Position Error
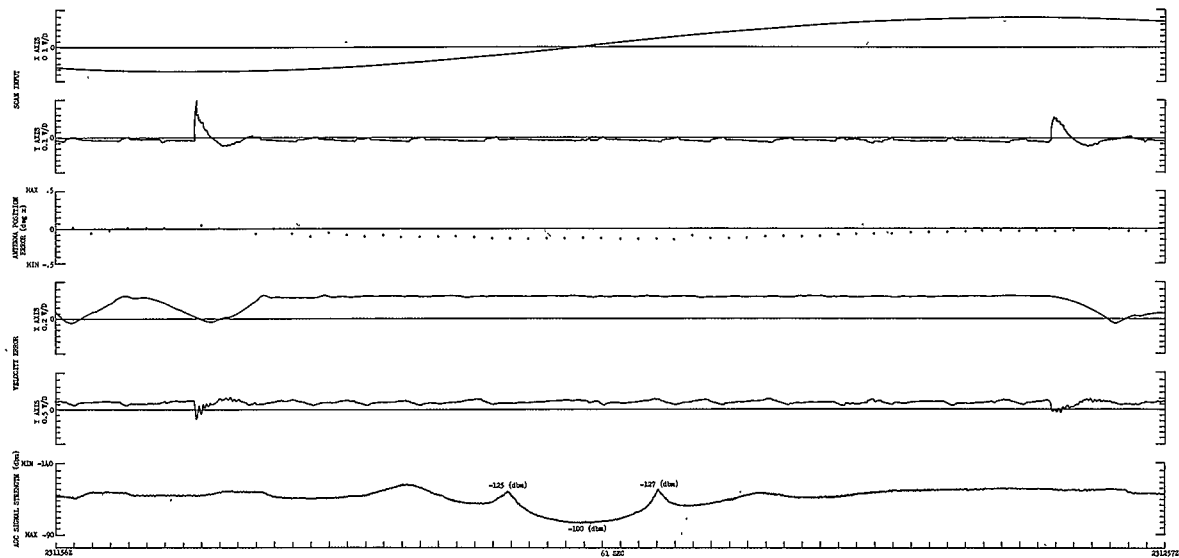
Figure 5.36. Antenna Performance Characteristics
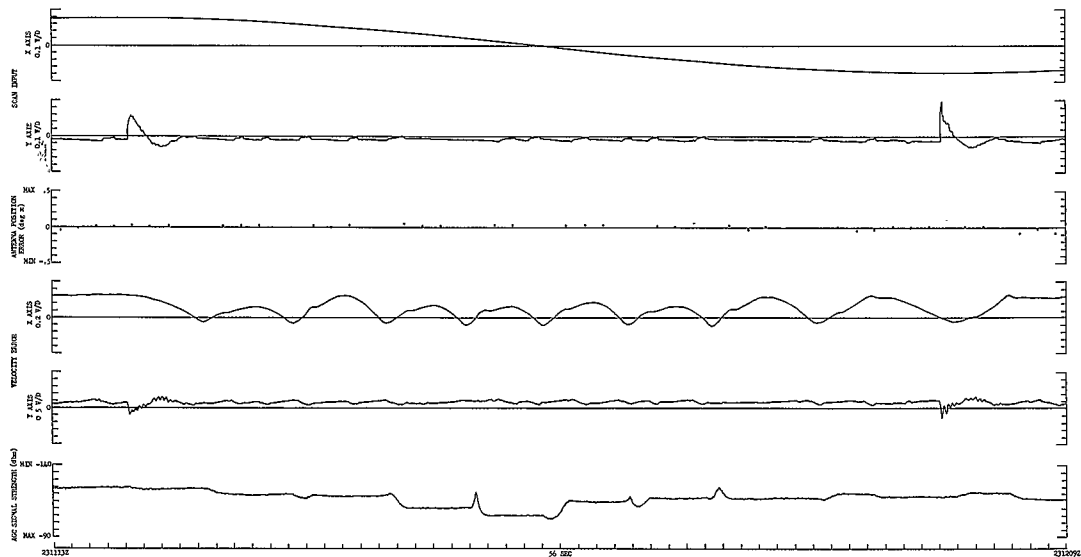
Figure 5.37. Antenna Performance Characteristics Depicting X-Axis Striction

The antenna position error was derived by noting the difference in antenna
position at 1-second intervals and plotting these values ($\Delta \theta$) as a function of
time. A expanded display of this data is shown in figure 5.35 which
was derived from the values presented in table 5.5. As indicated
previously, unidirectional X-axis sticktion was present during much of the
special test exercise and an example of this data is displayed in
figure 5.37. The analog presentation of the RF received signal level is a
distortion of the classic received antenna pattern shown in figure 5.36.
This distortion is due to the erratic positioning of the X-axis which is also
displayed as a function of X-axis velocity error. When the two examples of
antenna positioning characteristics are compared, the importance of antenna
performance on the Ground Terminal Antenna Pattern (AN-AT-1.1) experi-
ments is apparent.

TABLE 5.5. ANTENNA POSITION ERROR

Time (Zulu)	Antenna Position (θ)		Position Error ($\Delta \theta$)	
	X-Axis	Y-Axis	X-Axis	Y-Axis
231113	.043722	032325		
			-0.014	0
231114	043708	032325		
			-0.030	-0.003
23111	043678	032322		
			-0.008	-0.003
231116	043670	032319		
			-0.003	0
231117	043667	032319		
			-0.005	+0.090
231118	043662	032409		
			0	+0.058
231119	043662	032467		
			+0.002	-0.058
231120	043664	032409		
			0	+0.003
231121	043664	032412		
			+0.139	+0.008
231122	043725	032420		
			+0.236	0

5.83

TABLE 5.5. ANTENNA POSITION ERROR (Continued)

Time (Zulu)	Antenna Position (θ)		Position Error ($\Delta\theta$)	
	X-Axis	Y-Axis	X-Axis	Y-Axis
231123	043961	032420		
			0	0
231124	043961	032420		
			0	-0.003
231125	043961	032417		
			0	+0.003
231126	043961	032420		
			+0.097	-0.003
231127	044058	032417		
			+0.359	+0.003
231128	044417	032420		
			0	0
231129	044417	032420		
			-0.030	-0.003
231130	044387	032417		
			+0.002	+0.003
231131	044389	032420		
			+0.096	-0.006
231132	044483	032414		
			+0.443	+0.011
231133	044926	032425		
			+0.030	+0.003
231134	044956	032428		
			0	0
231135	044956	032428		
			0	0
231136	044956	032428		
			+0.377	-0.003
231137	045333	.032425		
			+0.154	-0.005
231138	045487	032420		
			0	0
231139	045487	032420		
			0	-0.003

TABLE 5.5. ANTENNA POSITION ERROR (Continued)

Time (Zulu)	Antenna Position (θ)		Position Error ($\Delta \theta$)	
	X-Axis	Y-Axis	X-Axis	Y-Axis
231140	045487	032417		
			+0.241	-0.006
231141	045728	032423		
			+0.341	-0.003
231142	046069	032420		
			0	0
231143	046069	032420		
			0	0
231144	046069	032420		
			+0.002	-0.003
231145	046071	032417		
			+0.398	+0.003
231146	046469	032420		
			+0.129	0
231147	046598	032420		
			+0.003	0
231148	046601	032420		
			-0.003	-0.003
231149	046598	032417		
			+0.061	-0.008
231150	046659	032425		
			+0.429	0
231151	047088	032425		
			0	0
231152	047088	032425		
			-0.025	0
231153	047063	032425		
			-0.005	0
231154	047058	032425		
			0	-0.005
231155	047058	032420		
			+0.136	0
231156	047194	032420		
			+0.267	+0.003

5.85

TABLE 5.5. ANTENNA POSITION ERROR (Continued)

Time (Zulu)	Antenna Position (θ)		Position Error (Δ θ)	
	X-Axis	Y-Axis	X-Axis	Y-Axis
231157	047461	032423		
			0	−0.003
231158	047461	032420		
			−0.063	+0.003
231159	047398	032423		
			−0.039	+0.005
231200	047356	032428		
			0	−0.003
231201	047359	032425		
			0	0
231202	047356	032425		
			+0.006	+0.105
231203	047362	032530		
			+0.104	+0.016
231204	047466	032546		
			+0.025	−0.038
231205	047491	032508		
			−0.003	+0.011
231206	047488	032519		
			−0.170	−0.005
231207	047318	032524		
			−0.083	−0.008
231208	047235	032516		
			0	0
231209	047235	032516		
			−0.060	+0.008
231210	047175	032524		
			−0.101	−0.005
231211	047074	032519		
			−0.055	0
231212 .	047019	032519		
			−0.088	+0.005

TABLE 5.5. ANTENNA POSITION ERROR (Continued)

Time (Zulu)	Antenna Position (θ)		Position Error (Δ θ)	
	X-Axis	Y-Axis	X-Axis	Y-Axis .
231213	.046931	032524		
			-0.110	-0.002
231214	046821	032522		
			-0.085	0
231215	046736	032522		

4) The central computer program that was written to display the RF antenna
patterns was dependent upon a smooth axis No. 1 (X-axis) scan of antenna
positions. The program as written can handle the sticktion of the antenna
axis internal to an active scan. An active scan is defined as being equal
to the total angular excursion minus 20 percent of the total excursion of
one scan.

At the extremities of a complete X-axis scan, where the definition of the
active scan is made, the program was dependent upon a smooth turn of this
axis. Not only was the transition not smooth, but at times it dwelled on the
same X-axis position for numerous consecutive seconds. The test data
taken at Mojave revealed these antenna scan characteristics and the central
computer program is now being modified to cope with these peculiarities.

5.2.3 PROPOSED INVESTIGATION

Based upon the analysis of the data obtained at the Mojave ATS station pre-
sented in paragraph 5.2.2, the impact of antenna positioning characteristics on the
Ground Terminal Antenna Pattern experiment (AN-AT-1.1) requires additional investigation.
The improvement of antenna pattern measurement and display resolution should be investi-
gated. This can be accomplished by performing additional special tests at all stations that
are intended to perform this experiment to determine the design limitations of the antennas
involved. The X-axis scan rate can then be tailored to produce the most acceptable antenna
pattern resolution factor at each station. In addition, the maintenance characteristics of
participating stations should be investigated so that the RF pattern experiments can be con-
ducted in an acceptable test environment. Test procedures are now being prepared to satisfy
the proposed investigations recommended in this report.

6. SUPPLEMENTARY INFORMATION

6.1 REFERENCE AND BIBLIOGRAPHY

1) NASA-GSFC: Operations Plan 13-66, Applications Technology Satellite ATS-B (November 1966)

2) GSFC-SII-012: Advanced Technological Satellite Experimental Communications System Description and Requirements (November 1966)

3) Westinghouse MDE 5857: Applications Technology Satellite SHF Communications Experimental Test Plan (November 1965)

4) C.C.I.R.: Documents of the Xth Plenary Assembly, Geneva, 1963 (Volumes IV & V)

5) Westinghouse DRA-R-1: ATS-B Communications Experiment Operations Requirements (June 1966)

6) Westinghouse DRA-R-2: ATS-B Communications Experiment Data Requirements (August 1966; revised November 1966)

7) Westinghouse DRA-R-3: ATS-B Communications Experiment Data Management Plan (August 1966; revised October 1966)

8) Westinghouse DRA-R-4: ATS-B Communications Experiment Computer Programming Specifications (September 1966; revised November 1966)

9) Hughes: Phased Array Transmitting Antenna and PACE (October 1966)

10) Westinghouse: ATS Communications System Phase II Integration Mojave Ground Station (November 1966)

11) Westinghouse: ATS Communications System Phase III Integration Mojave Ground Station (December 1966)

12) Westinghouse: ATS Communications System Phase II Integration Rosman Ground Station (December 1966)

13) Westinghouse: ATS Communications System Phase III Integration Rosman Ground Station (December 1966)

14) Westinghouse: Final Report, ATS Communications Integration Contract, Mojave Ground Station (June 1967)

15) Lanning, Ninth National Communications Symposium: Random Multiple Access (October 1963)

16) Schwartz, Aein, Kaiser, Proceedings of IEEE Vol. 54, No. 5: Modulation Techniques for Multiple Access to a Hard Limiting Satellite Repeater (May 1966)

17) Kaiser, Institute for Defense Analysis AD 457945: Multiple Access to a Communication Satellite With A Hard Limiting Repeater, Volume I Modulation Techniques and Their Applications (January 1965)

18) Aein, Schwartz, Report R-108 Institute for Defense Analysis: Multiple Access to a Communication Satellite With a Hard Limiting Repeater Volume II Proceedings of the IDA Multiple Access Summer Study April 1965

19) Wittman, Supplement to IEEE Trans. On Aerospace and Electronic Systems Vol. AED-3 No. 6: A Comparison of Multiple Access Techniques (November 1967)

20) ITT Federal Laboratories Task AD453730 Report, Task I: Anti Jamming Techniques Part II Hard Limiting Satellite Experiment (March 1966)

21) Prosser and Allnatt, Subjective Quality of Television Pictures Impaired by Random Noise, Prog. I.E.E. June 1965 (112) (6)

22) Pappenfus, Bruenc, and Shoenike: "Single Sideband Principles and Circuits".

23) Deleted

24) Walker: NAB Engineering Handbook 5th Edition 1960.

25) C.C.I.R.: Documents of XIth Plenary Assembly, Oslo, 1966, Study Program 5A/CMTT in Addendum No. 1 to Volume V.

26) Wass: A Table of Intermodulation Products, Journal of the IEE, Vol. 95, Part III, No. 33, January 1948.

27) Fletcher: Speech and Hearing, P. Van Nostrand Co. Vol. 1, pg. 145.

28) Wick: Ionospheric Abnormalities Affecting Earth - Satellite Paths at VHF, Document WP-4488, Collins Radio.

29) Westinghouse: ATS Technical Memo WATSTM No. 3, Comment on the Definative of Short Term Frequency Stability.

30) Deleted

31) "Application Technological Satellite Experimental Communication System Description and Requirements," ATS Project Office, Goddard Space Flight Center, Greenbelt, Md. GSFC-SII-012, November 1966, Revision C.

32) "Closed-Loop AFC System - SSB Transmitter," Prepared by Raytheon Company, Norwood, Mass. for NASA/GSFC, Contract No. NAS5-3464, Volume IV, January 1966.

33) "Operation and Maintenance - SSB Transmitter," Volume 1, Book 1, Prepared by Raytheon Company, Norwood, Mass. for NASA/GSFC, Contract No. NAS5-3464, September 1965.

34) "Short Term Frequency Stability," IEE-NASA Symposium, Goddard Space Flight Center, Greenbelt, Maryland. November 23-24, 1964.

35) "Frequency Stability," Special Issue Proceeding of the IEEE, February 1966.

36) "Frequency and Time Standards," Hewlett Packard Co. Application Note 52, November 1965.

37) "System Description of Syncom II Ground Stations," Prepared for GSFC by Lenkurt Electric Co., Inc., San Carlos, California, 1962, Appendix E.

38) "Final Report for ATS-SSB and FM Transmitters," Prepared for NASA/GSFC by Raytheon Company Equipment Division, Norwood, Massachusetts, Contract No. NAS5-3464.

39) Fedida and Palmer: Some Design Considerations for Links Carrying Multichannel Telephony, Marcini Review No. 120, Vol. XIX, First Quarter 1956.

40) Bennett and Davey: Data Transmission, McGraw - Hill.

41) Glen: Comparison of PSK vs. FSK and PSK-AM Binary Coded Transmission Systems, IRE Transactions on Comm. Systems, June 1960.

42) Rice: Noise in FM Receivers, Proc. Symposium on Time Series Analysis, Brown University, June 1962.

43) Hefferman: Analysis of Non-Linear Noise in FDM Telephony Transmission Over an SSB/PhM Satellite Communication System, NASA Goddard Space Flight Center.

44) Cohn: "A New Approach to the Analysis of FM Threshold Detection, Proc. NEC. Vol. 12pp. 221-36, 1956.

45) Rice: Noise in FM Receivers, M. Rosenblatt, el, in "Time Series Analysis", John Wiley & Son, Inc., New York, 1963

46) Documents of the XIth Plenary Assembly, Oslo, 1966, Volume IV.

47) Kuegler and Martel: "Short Term Frequency Stability Measurements of the ATS-1 MA Communication System" Proceeding of the International Conference on Communications, 1969.

48) Technical Staff, Bell Telephone Laboratories, Transmission Systems for Communications, Bell Telephone Laboratories, Inc., 1964.

49) Sullivan; "Intermodulation Distortion Study for FM Communications Satellite Systems, "Space Technology Laboratories, Inc, Redeno Beach, California, 1962.

50) Howard, Dean D., "Contour Pattern Analysis of a Radar Cassegrainian Antenna", The Microwave Journal, December 1968, pp 61-63.

51) Middleton, "An Introduction to Statistical Communication Theory, " pages 343 and 371, New York; McGraw Hill, 1960.

52) Papoulis, "Probability, Random Variables, and Stochastic Process, " page 317, New York; McGraw Hill, 1965.

53) Brockbank, R. A. and Wass, C.A.A.; "Nonlinear Distortion in Transmission Systems", Proc. IEE, Part 3, pages 45-56, January 1945.

6.2 GLOSSARY OF TERMINOLOGY

        An explanation of the approach to the definition of terms in this glossary is appropriate. The definitions presented on the following pages are specialized in that they relate to specific usage of the particular terms with regard to the analysis of ATS communcations experiments.

AFC System Closed Loop - The automatic control system of the SSB transmitter used to correct for long-term frequency variations of the 6 GHz up-link signal appearing at the satellite receiver.

Analyzer, Distortion, Total - An instrument measuring total harmonic distortion (T. H. D.) value of a complex or distorted wave by suppressing the fundamental component of the wave by means of a sharply tuned filter and permitting all unsuppressed components, both harmonic and non-harmonic, and including residual noise to be passed on to a metering circuit. The latter measures the RMS or equivalent RMS level of all unsuppressed components. The meter may be calibrated in either voltage or relative power (db) or both.

Analyzer, Wave - An instrument measuring the amplitudes of individual components of a complex or distorted wave by selecting each component, including the fundamental, individually in turn by means of a sharply tuned variable frequency filter and applying the selected component to a metering circuit. The latter measures the RMS or equivalent RMS level of the selected component. The meter may be calibrated in either voltage or relative power (db or both).

Antenna Gain, Ground Receive (G_{rg}) - The ratio of the voltage produced at the receiver terminals by a signal arriving from the direction of maximum sensitivity of the antenna to that produced by the same signal in an omnidirectional reference antenna. G_{rg} is the net antenna gain, that is the actual antenna gain minus plumbing losses.

Antenna Gain, Ground Transmit (G_{tg}) - The ratio of the field strength produced at a point along the line of maximum radiation by a given power radiated from the antenna to that produced at the same point by the same power from an omnidirectional antenna. G_{tg} is the net antenna gain, that is the actual antenna gain minus plumbing losses.

Antenna Gain, Satellite Receive (G_{rs}) - The ratio of voltage produced at the receiver terminals by a signal arriving from the direction of maximum sensitivity of the antenna to that produced by the same signal in an omnidirectional reference antenna. G_{rs} is the actual antenna gain minus plumbing losses.

Antenna Gain, Satellite Transmit (G_{ts}) – The ratio of the field strength produced at a point along the line of maximum radiation by a given power radiated from the antenna to the produced at the same point by the same power from an omnidirectional antenna. G_{tg} is the net antenna gain, that is the actual antenna gain minus plumbing losses.

ATSOCC – Operations control center for the ATS program.

Automated Test - Experimentation for which computerized techniques are used to facilitate data acquisition as well as subsequent reduction and analysis, because of the large number of measurements of time varying parameters required. The duration of a standard automated test may vary from 15 minutes to one hour.

Average Picture Level, Television (APL) - A measure of luminance of the raster, expressed in terms of percent of full white, 100% being full-white level, and 0% being full black.

Baseband, Multiplex - The frequency band occupied by the aggregate of the signals applied to (or received from) the facility interconnecting the multiplexing and radio equipments.

Baseband, Radio - The frequency band available for the transmission of all the combined telephone channels and/or other communication channels. This band is sometimes referred to as the "Video Baseband," but this use is depreciated.

Baseband, Video - The frequency band utilized to transmit and receive a composite video signal. The video signal is that electrical signal which results from the television scanning process, which is used at the receiving end of the communication system to reproduce the picture.

Best Estimate Value - The value that is obtained by averaging the measurements taken during all of the test runs which yielded reasonable results.

Calculated Value - An indicated result which is computed from both measured and calculated system parameters as defined in paragraph 7.1.

Carrier-to-Noise (C/N) - The ratio of the unmodulated carrier power level to the corresponding noise defined in the IF (predetection) bandwidth.

Cassegrain Subreflector - The second reflector on a Cassegrain antenna system.

CCIR - International Radio Consultive Committee.

CCITT - International Consultative Committee for Telephone and Telegraph

Closest Conjuction Period - Occurs when the S/C passes directly between the sun and earth where the sun falls directly within the beamwidth of the antenna. For communications experimentation analytical purpose, this is defined as starting when the S/N values are decreasing at a rate of greater than 3 db per minute and ending when they are increasing at a rate of less than 3 db per minute.

Communications Test and Evaluation Console (CTEC) - A coordinated set of test equipment, rack mounted, grouped to facilitate manual and semi-automated data acquisition and testing in the ATS communication system.

<u>Damping Ratio</u> (δ) - Used in specifying the stability of the closed loop AFC system. A nominal design values for δ is 0.707.

<u>Data Bit Error Rate (E)</u> - Percent of bits in error over a period of time, as measured through an FSK data modem. Errors in the digital data can also be expressed as an error number, which is the number of bits in error over a period of time.

<u>De-Spun</u> - The condition in which the effects of the satellite spinning motion on the gain of a satellite antenna are nullified.

<u>Differential Gain, Video</u> - The amplitude change, usually of the 3.58-MHz color subcarrier, introduced by the overall communications circuit as the subcarrier is varied from blanking to white level. Differential gain may be measured and expressed either in terms of decibels or percent.

<u>Differential Phase</u> - The phase change of the 3.58-MHz color subcarrier introduced by the overall circuit, measured in degrees, as the level of the video signal upon which it is superimposed is varied from blanking level to white level. In the ATS SHF frequency translation mode, the composite 81-Hz and 556-kHz signals are applied to the linear FM modulator and recovered from the linear FM discriminator. The variations in phase of the 556-kHz signal are measured and displayed as a function of the instantaneous value of intermediate frequency. From these differential phase readings, the differential time delay as a function of frequency may be obtained.

<u>Distortion, Single-Harmonic</u> - The ratio of the power at the fundamental frequency, measured at the output of the transmission system considered, to the power of any single harmonic observed at the output of the system because of its nonlinearity, when a single frequency signal of specified power is applied to the input of the system; expressed in db.

<u>Distortion, Total Harmonic</u> - The ratio of the power at the fundamental frequency, measured at the output of the transmission system considered, to the power of all harmonics observed at the system because of its nonlinearity, when a single frequency signal of specified power is applied to the input of the system; expressed in db.

<u>Doppler, Differential</u> - A fixed frequency error from the true frequency relationship existing between two or more lines of the transmitted RF spectrum due to a constant relative velocity between the earth transmitter and the satellite receiver.

<u>Doppler, Up-Link</u> - A fixed frequency offset from the nominal 6-GHz up-link signal produced by relative constant velocity between the earth transmitter and the satellite receiver.

<u>Effective Isotropic Radiated Power (EIRP)</u> - The amount of radiated power that is emitted by the combination of the transmitter and antenna which has a finite gain, P_t (dbm) + G_t (db).

<u>Experimental Test Plan (ETP)</u> - A document describing a communication test, outlining the test method, and specifying the data to be acquired.

Envelope Delay, Multiplex Channel – The envelope of the delay curve across the frequency passband of the channel that is obtained by referring the transit time delay of a signal at any specified frequency to the transit time of the frequency of minimum delay.

Equalization – The process of reducing frequency and/or phase distortion of a circuit by the introduction of networks to compensate for the difference in attenuation and/or time delay at the various frequencies in the transmission band.

Envelope Delay Distortion, Baseband – The variation in time delay of a given signal transmitted through the communications circuit as a modulation envelope of a subcarrier of any selected frequency when compared to the delay encountered by the same given signal when transmitted as the modulation envelope of a reference frequency subcarrier.

Error Cancellation – An open loop circuit implementation scheme by which the residual AFC frequency error is cancelled to yield a MUX channel signal free of all long-term frequency drifts.

Error Probability (P_e) – A term used to specify the number of probable bit errors for a given number of transmitted bits and the channel RMS frequency error. The term is normally used in conjunction with an FSK type of modem.

Faraday Rotation (Ω_M) – The rotation of the plane of polarization produced when a plane polarized wave is passed through the electric and magnetic fields of the ionosphere.

Field Test Procedure (FTP) – A document detailing, step-by-step, the procedure to perform specific communication tests in a controlled manner.

Frequency Error, Closed Loop, ϵ (s) – A frequency dependent term that specifies the amount of residual frequency error on the station pilot frequency after correction by the AFC loop.

Frequency Error, MUX, Channel, $\epsilon'(s)$ – The residual error on the transmitted MUX channel test-tone frequency after correction by the AFC system and the error cancellation circuits.

Frequency Response, Amplitude-Frequency Distortion – A measurement of the distortion of a transmission system caused by the non-uniform attenuation, or gain, of the system with respect to frequency.

Frequency Stability, Long Term – A term used to describe frequency variations of the system oscillator(s) occurring at rates within the correction bandwidth of the SSB-closed loop AFC system.

Frequency Stability, Short Term – A term used to describe frequency variations of the system oscillator(s) occurring at rates higher than the correction capability of the SSB-closed loop AFC system.

Frequency Translation (FT or FM/FM) - Frequency modulation for the ground-to-satellite link as well as for the satellite-to-ground link. The satellite transponder produces FM/FM frequency translation.

Ground Receiver System Noise Temperature (T_S) - The effective noise temperature in degrees Kelvin referred to the receiver input terminals, defined as $T_s = (F-1) T_o$, where noise factor F is the ratio of input to output signal-to-noise ratios of the receiver and T_o is the reference temperature. The T_s factor includes antenna temperature and all other noise sources common to the ground receiver.

Idle Noise (Idle Channel Noise) - The term "idle noise" is a shortened usage of "idle channel noise" and denotes the noise power measured in a channel (e. g., multiplex) in the absence of a signal.

Intermodulation Distortion, Video - As used in the ATS system, intermodulation distortion is that nonlinearity characterized by the appearance of frequencies in the output equal to the harmonics and the sums and difference of integral multiples of the component frequencies present in the input.

ITU - International Telecommunications Union.

Linearity, Multiplex Channel - A shortened form of the term "amplitude linearity response" denoting the input versus output power characteristic of an equipment. The power range (usually in dbm) over which output power increases 1 db for each 1-db increase of input power defines the linear operating range. Departure from this linear operating range is a measure of amplitude distortion of the unit under test.

Local Vertical Line - The line defined by the location of the particular ground station and a point that is defined by the intersection of the spin axis of the earth and the earth's equatorial plane.

Loop, Back-to-Back - A test set-up configuration in which transmitting or sending equipments are connected to the same station's receiving equipment by a local metallic circuit using interposed frequency translators, level adjusters and/or impedance matching when necessary. The interconnection may be made at any of several commonly designated equipment points; viz., RF or antenna terminals IF, baseband, or multiplex inputs or outputs.

Loop, Spacecraft (S/C) - In the ATS communications system, spacecraft loop (S/C loop) designates the system configuration in which intelligence is transmitted from an earth station to satellite bourne radio equipments from which the intelligence is retransmitted back to an earth receiving station. The latter may be the same station transmitting or another receiving station.

Manual Gain Control (MGC) - Mode of operation in which AGC (automatic gain control) is disabled and the gain of the controlled module (IF and/or RF) is adjusted by manual control(s).

Manual Test - Experimentation performed in support of related automated tests or for the determination of ground station equipment parameters. Categories satisfying the latter objective include baseband, multiplex channel, and video testing.

Measured Value - An experiment result that is directly obtained from measurements taken during a particular test run.

Modem - Acronym for modulator-demodulator.

Multiple Access (MA or SSB/PhM) - Single sideband modulation for the ground-to-satellite link and phase modulation for the satellite-to-ground link. The satellite transponder produces SSB/PhM translation.

Multi-Station Test - In the MA mode, each participating station transmits a specific noise-loading signal to the satellite, and each receives the return composite transmission. In the FT mode, only one station transmits to the satellite, while all of the participating stations receive the return transmission.

Noise Loading - The power in dbm of a Gaussian noise ("white noise") test signal which is considered to be equal to the power produced by a system containing a specified number of multiplex channels. In practice, the equivalent noise power is calculated as follows:

      1) For 12 to 240 channels - Equivalent Noise Power (i.e., noise loading) in dbm0 = (-1 +4 log N)

      2) For 240 to 1200 channels - Equivalent Noise Power (i.e., noise loading) in dbm0 = (-15 +10 log N)

where N = number of channels.

Noise Power Ratio (NPR) - The ratio of the noise in a slot channel when it is noise-loaded to the noise in a slot when the noise loading is removed from that channel. This factor is a measure of the intermodulation and idle noise present in the slot channel.

Noise Weighting - In measurement of circuit noise, a specific amplitude-frequency characteristic of a noise measuring set, designed to given numerical readings which approximate the amount of transmission impairment due to the noise, to an average listener using a particular class of telephone subset:

      1) F1A-line weighting - A noise weighting used in a noise measuring set to measure noise on a line that would be terminated by a 302-type or similar telephone subset. The meter scale readings are in dba(F1A), that is, weighted circuit noise power in db referenced to 3.16 picowatts (-85 dbm). Use of F1A-line weighting is indicated in parentheses.

2) Psophometric weighting - A noise weighting established by the International Consultative Committee for Telephony (CCIF, now CCITT), designated as CCIF-1951 weighting, for use in a noise measuring set of Psophometer. The shape of this characteristic is virtually identical to that of F1A weighting. The Psophometer is, however, calibrated with a tone of 800 cps, 0 dbm, so that the corresponding voltage across 600 ohms produces a reading called 0.775 volt. This introduces a 1-db adjustment in the formulas for conversion with dba.

Off-Beam Center Allowance, Receive Antenna Gain (B_r) - A reduction factor in db applied to the receive antenna gain due to an error in the pointing angle of the antenna.

Off-Beam Center Allowance, Transmit Antenna Gain (B_t) - A reduction factor in db applied to the transmit antenna gain due to an error in the pointing angle of the antenna.

Omni Mode - The mode of the spacecraft transmit antenna when the PACE system is not activated. The resultant pattern is omnidirectional.

Order-Wire or Order-Wire Channel - A voice frequency communication circuit or channel, either wire-line or radio, used for transmitting technical, operating or maintenance information between operating points. Order-wire channels are usually inferior in quality with respect to bandwidth and/or noise as compared with commercial grade voice and data channels. Order-wire channels are alternately called "service channels".

Quarter-Cycle - A 15-second time period utilized by the analog data-processing subroutine in which analog parameters are computed and recorded.

Path Loss, Actual (U_a) - Equal to E + L. This factor is the path loss value that exists, in fact, in the link.

Path Loss, Downlink (U_d) - Equal to $P_{ts} + G_{ts} - B_t - (P_{rg} - G_{rg})$. Computed or measured downlink path loss.

Path Loss, Free Space (E) - Attenuation suffered by an RF propagating wave because

of distance. It is equal to $\dfrac{16\pi^2 R^2}{\lambda^2}$.

Path Loss, Measured (U) - Computed from the expression $U - P_t + G_t - (P_r - G_r)$. It is equal to the ratio of transmit radiated power to the power received by an omni-directional antenna.

Path Loss, Uplink (U_u) - Equal to $P_{tg} + G_{tg} - (P_{rs} - G_{rs} + B_r)$. Computed or measured uplink path loss.

Phased Array Control Electronics (PACE) - Employed on the ATS-1 satellite transmit antenna to nullify the effects of the spinning satellite.

Pilot Frequency - A fixed frequency at the low end of the baseband spectrum that serves as the station reference frequency for the AFC loop.

Polarization Angle (Polang) - Polarization on angle measured about the line of sight, between the vertical plane containing the line of sight and the plane of polarization of the transponder signal (plane of electric vector and line of sight). If the polarization is vertical the polarization angle is zero; if the plane of polarization is rotated clockwise from the vertical as seen from the station, the polarization angle is positive.

Power Density Spectrum, $G_e(f)$ - A frequency dependent term used to describe the power spectrum of the MUX channel frequency as it is influenced by the system oscillator(s) long and short-term frequency stability.

Power Output, Ground Transmitter (P_{tg}) - For the FT mode of operation this value is the total output power. For the MA mode of operation this value is the test tone output power.

Power Output, Satellite Transmitter (P_{ts}) - The value is the total power output of the satellite transmitter.

Predicted Value - An indicated result which is computed from system parameter values stated for the FT or MA modes or other definitive documentation as modified by measurement of particular system conditions taken during the test run (principally, T_s). This applies mainly to the S/N values obtained from link calculations.

Propagation Loss (L) - This value is the loss in db suffered by a wave from the effects of atmospheric attenuation and scattering.

Range (R) - Line-of-sight range in nautical miles between the ground station and satellite.

Received Power, Ground Terminal (P_{rg}) - Power received at the input to ground receiver.

Received Power, Satellite (P_{rs}) - Power received at the input to satellite receiver.

Relative Transmission Level - The ratio of test-tone power at any point in a transmission system to the test-tone power at some point in the system chosen as a reference point (see zero transmission level reference point). This ratio is usually expressed in db units above (+) or below (-) the test tone power at the reference point and is then designated "dbm0". The "m" indicates that the basic reference power is 1 milliwatt. At times, in practice, liberty is taken with respect to referencing the test-tone power to a singular-system zero-reference level (or point) by referring the power under consideration at a particular point to the normal test-tone power at that same point and designating that ratio as dbm0. In such cases, it is important that the text clearly differentiates the reference level or point used. In noise-power measurements, noise power in dbm at a particular point is customarily expressed in dbm0 by referring the measured noise power in dbm to the zero reference-level value. The noise power is then in relative db units.

Single-Station Test - Where the site involved transmits to the satellite and receives the return transmission.

Signal-to-Noise Ratio (S/N) - The term signal/noise denotes the ratio of signal power to noise power in a given communications channel (e.g., multiplex channel) and is usually expressed in

db. The measured quantity is actually the ratio of signal-plus-noise to noise power. The quantity S/N is calculated from the measured (S + N)/N from S/N = $\left[(S + N)/N - 1\right]$. The quantity S/N is not the same as C/N (carrier-to-noise power ratio) and the two should not be used interchangeably.

Signal-to-Idle Noise Ratio, Multiplex Channel (MUX S/N) - The ratio of the test tone in a multiplex receive channel to the measured noise power present when the tone is not present. The technique that is employed is to compute the rms signal-to-rms noise ratios from the stated system parameters that are measured or known when the test was conducted.

Signal-to-Idle Noise Ratio, Video Weighted (TV S/N) - The ratio of the output signal (picture portion) to the rms noise level of the receiver baseband unit after filtering by a standard CCIR video filter.

Spin Modulation - Amplitude modulation impressed on the satellite and ground received input signals due to the spinning effect of the satellite.

Standard Deviation (σ) - Term used to describe the channel RMS frequency error. It is derived by taking the square root of the integral of the power density spectrum.

Standard Test Tone - For use at the 600-ohm audio portions of a circuit, shall be one mw (0 dbm) with a frequency of 1000 cps and shall be applied at a zero transmission-level reference point. (If applied to a point with a relative level other than zero, the absolute power of the tone shall be adjusted to suit the relative level at the point of application.)

Stiction - A Colloquial term used to describe static friction in axis bearings, gears,and drives where a small but finite torque is required to induce motion from a stationary position.

Switching Conference and Monitoring Arrangement (SCAMA) - Employed as a communications link between NASA, Goddard,and the ground-tracking stations under their control.

System Transport Lag (T) - The round trip RF propagation delay from the earth transmitter through the satellite and back to the ground receiver. For the synchronous satellite,this time is a nominal 0.27 seconds.

Thermal Power Ratio (TPR) · The ratio of the noise in a slot channel when the baseband is noise loaded to the noise in the slot when the noise loading is removed. This factor is a measure of the idle noise present in the slot channel.

Threshold, FM S/N - Defines a unique point in the input-output S/N relationship of an FM receiver at which there is a rapid non-linear degradation of the postdetection S/N as the received signal strength decreases.

Time Constant (τ) - Used in specifying the open-loop response of the AFC loop. τ is the reciprocal of the open-loop 3-db corner frequency.

Transfer Function, Open Loop, KG(s) - A frequency dependent equation that describes the voltage response of the open-loop AFC circuits.

Transmitter Power Output Rating - Whenever the power of a radio transmitter, etc., is referred to, it shall be expressed in one of the following forms: peak envelope power (pp, sometimes abbreviated pep), mean power (pm), or carrier power (pc). For different classes of emission, the relationships between peak envelope power, mean power, and the carrier power are defined as follows:

    1) Peak envelope power of a radio transmitter - The power supplied to the antenna transmission line by a transmitter during one radio frequency cycle at the highest crest of the modulation envelope, taken under conditions of normal operation.

    2) Mean power of a radio transmitter - The power supplied to the antenna transmission line by a transmitter during normal operation, averaged over a time sufficiently long compared with the period of the lowest frequency encountered in the modulation. A time of 1/10 second during which the mean power is greatest will be selected normally.

    3) Carrier power of a radio transmitter - The average power supplied to the antenna transmission line by a transmitter during one radio-frequency cycle under conditions of no modulation. This definition does not apply to pulse modulated emissions or FSK.

    4) Effective radiated power (ERP) - The power supplied to the antenna multiplied by the relative gain of the antenna in a given direction.

Vector-E - A vector that represents the direction and magnitude of the electric field component of an electromagnetic wave.

X-Y Plotter - An instrument which automatically plots the value of an independent variable versus a dependent variable directly on cartesian coordinate (X-Y) graph paper working from derived electrical signals.

Zero Transmission Level Reference Point - An arbitrarily chosen point in a circuit to which all relative transmission levels are referred. This point defined in the system is arbitrarily designated as "reference point"; thus the full designation or title above. It is not a power level or unit of measurement; hence, not dbm0. The "datum point" in surveying is analogous to the reference point in a communications system.

7. COMMON PERFORMANCE EQUATIONS AND CALCULATIONS

7.1 S/N LINK CALCULATIONS

In subsequent sections of this report, separate narratives are presented for each communications experiment. The description for each experiment contains data reduction and analysis techniques peculiar to those particular tests. However, certain information that applies to several experiments are presented here for convenience.

Throughout the narratives of the experiment descriptions, references are made to certain multiplex test channels, such as channels D and G. A definition of the frequencies for each of the channels at the three ground-tracking stations is presented in table 7.1.

TABLE 7.1. DEFINITION OF CHANNEL FREQUENCIES

Channel	Channel Frequency (kHz)	
	1200 Channels	240 Channels
Channel D (Low Signal)	336	336
Channel G (High Signal)	5340	1248
Channel H (Data)	344	344
Channel I (Low Noise)	340	340
Channel J (High Noise)	5336	1252
Channel C (See Note)*	2438	768
Low Slot	342	342
Center Slot	2438	768
High Slot	5340	1248

*NOTE: Channel C in data analysis is the hypothetical channel in the center slot.

To derive signal-to-idle noise ratios from acquired test data, as is done for both automated and manual experiment analyses, standard link-calculation procedures are normally used. These procedures are specified for both MA mode and FT mode link calculations in the paragraphs which follow. Symbols and definitions used in these link calculations apply equally to the experiment narratives in this report.

7.1.1 MA MODE LINK CALCULATIONS

This section concerns the details of the procedure employed to compute the factors for the MA-AT-1.1 experiment from various recorded factors and specified constants:

1) K_1 = Uplink test tone-to-idle noise level at satellite (weighted)

2) K_4 = Downlink test tone-to-idle noise level at earth receiver (weighted)

3) K_d = Downlink carrier-to-idle noise level

4) K_7 = Overall test tone-to-intermodulation noise ratio (weighted)

5) K_{80} = Overall link test tone-to-noise ratio (weighted) for the "noise loading off" condition

6) K_{8N} = Overall link test tone-to-noise (weighted) for the "noise loading on" condition

All of the above factors except K_d are defined in the F1A bandwidth of 1.55 kHz. K_d is defined in the ground receiver IF bandwidth. All factors are expressed in db.

The object of the following computations is to determine the overall link test tone-to-noise ratios for both noise loading conditions and prescribed multiplex channels in the MA-AT-1.1 automated test and the MA-MX-7.1 manual test. These ratios are measured in the above tests. Hence, a comparison of the measured and computed factors can be made as part of the analysis of the data from the Rosman(R), Mojave (M), and Cooby Creek (T) stations.

1) "Noise Loading Off" Computational Procedure:

a) Uplink, K_1 (db) = $P_{rs} - N_{rs} = P_{rs} - 10 \log (KB_{(F1A)} T_s)$

$\qquad = P_{rs} + 198.6 - 31.9 - 10 \log T_s$

$\qquad = P_{rs} + 166.7 - 10 \log T_s$

where

P_{rs} = Satellite receiver input test tone power

N_{rs} = Noise power at satellite receiver input

K = Boltzmann's constant = $1.38 (10)^{-23} \dfrac{\text{watts}}{\text{(°K) (Hz)}} = -198.6 \dfrac{\text{dbm}}{\text{(°K) (Hz)}}$

$B_{(F1A)}$ = Channel bandwidth (defined by an F1A weighted filter) = 1.55 kHz

T_s = Satellite receiver system noise temperature (°K) = $T_A + T_T + t (L-1) + L (T_R)$

where

T_A = Antenna noise temperature (°K) (only contributions received from the earth are considered)

T_T = Degradation due to transmitter noise (°K) due to the electrical isolation between transmit and receive feeds, (T_T is assumed to be insignificant)

t = Physical temperature of coupling network (°K)

L = Power loss of coupling network (total insertion loss from antenna to preamplifier)

T_R = Equivalent noise temperature of receiver preamplifier (°K) (referenced to 290°K)

	Transponder 1					Transponder 2				
Satellite	T_A (°K)	t (°K)	L (Numeric)	T_R (°K)	10 Log T_S (db)	T_A (°K)	t (°K)	L (Numeric)	T_R (°K)	10 Log T_S (db)
ATS-1	15	285	1.45	920	31.7	15	285	1.45	920	31.7
ATS-3	290	285	1.12	890	31.2	290	285	1.12	764	30.7

NOTE: T_A for ATS-1 is lower than for ATS-3, due to the receiver antenna pattern which results in the ATS-1 antenna seeing a large percentage of cold sky while the ATS-3 antenna is more nearly directed toward earth.

b) Downlink K_4 (db) = $P_{rg} - N_i + 10$ Log $M_s^2 - 3$

$$= P_{rg} - 10 \text{ Log } KT_s B_{(F1A)} + 10 \text{ Log } M_s^2 - 3$$

$$= P_{rg} + 198.6 - T_s \text{ (db)} - 31.9 - 9.1 - 3.0$$

$$= P_{rg} + 154.6 - T_s \text{ (db)}$$

P_{rg} = Ground receiver input power level in dbm

N_i = Noise at the ground receiver input due to the earth station receiver and antenna

T_s = Overall system ground receiver noise temperature (°K) measured in db (recorded daily at the site)

M_s = Peak channel test tone modulation index = 0.35 radian (numeric). A factor of 3 db is subtracted from the M_s^2 team (in db) in order to convert to the rms test tone value

c) Alternately, K_4 (db) = $10 \text{ Log } \dfrac{B_{IF}}{B_{F1A}} + 10 \text{ Log } M_s^2 - 3 + K_d$

$$= B_{IF} \text{ (db)} - 31.9 - 9.1 - 3.0 + K_d$$

$$= B_{IF} \text{ (db)} - 44.0 + K_d$$

$$= K_d + 31.5 \text{ (Rosman)}$$

$$= K_d + 27.9 \text{ (Mojave and Cooby Creek)}$$

B_{IF} = Receiver IF Bandwidth
Rosman, 30 MHz (nominal) 35.5 MHz actual (75.5 db Hz); Mojave and Cooby Creek, 12 MHz (nominal) 15.5 MHz actual (71.9 db Hz)

d) Overall Link K_{80} (numeric) = $\dfrac{K_1 \ K_4}{K_1 + K_4}$ (numeric) = $\dfrac{S}{N}$ (Noise off).

For RF Loop, K_{80} (db) = K_4

7.3

2) "Noise Loading On" Computational Procedure with 1200 (R) and 240 (M and T) Noise Channel Spectrum.

The overall Signal-to-noise for the full noise loading condition, K_{8N}, is given by:

$$K_{8N} = \frac{K_{80} \, K_7}{K_{80} + K_7} \quad \text{(numeric)}$$

K_7 (Overall test tone-to-intermodulation noise ratio, weighted) is given by;

$$K_7 = \frac{K_2 K_{ov}}{K_2 + K_{ov}} \quad \text{(numeric)}$$

where K_2 is the earth station transmitter test tone-to-intermodulation noise, and K_{ov} is the test tone-to-intermodulation noise due to the S/C and the earth station receiver. Figure 7.1 shows the K_2 factor for the Rosman station as a function of transmitter power output. Similar plots shown in figures 7.2 and 7.3 for the Mojave station and Cooby Creek Stations.

The K_{ov} term (MA Mode) is shown in figure 7.4 as a function of spacecraft loading. The K_{ov} factor is due primarily to the satellite transponder, and thus is the same for all three stations.

7.1.2 FT-MODE LINK CALCULATIONS

This paragraph deals with the details of the programming procedure that is employed to compute the signal-to-noise factors for the FT-AT-1.1 automated test and FT-MX-6.1 manual test. The following computed factors are employed in the analysis to determine the operational system characteristics at the time a test was conducted:

1) K_u = Overall uplink carrier-to-noise ratio per unit bandwidth

2) K_d = Overall downlink carrier-to-noise ratio per unit bandwidth

3) K_o = Overall link carrier-to-noise ratio per unit bandwidth

4) K_{LO} = Test tone-to-idle noise level ratio (weighted) in the 328-kHz channel for the "noise loading off" condition

5) K_{CO} = Test tone-to-idle noise level ratio (weighted) in the 768-kHz channel (M and T stations) and in the 2438-kHz channel (R station) for the "noise loading off" condition

6) K_{HO} = Test tone-to-idle noise level ratio (weighted) in the 1296-kHz channel (M and T stations) and in the 5560-kHz channel (R station) for the "noise loading off" condition

7) K_{LN} = Test tone-to-total noise level ratio (weighted) in the 328-kHz channel for the "noise loading on" condition

8) K_{CN} = Test tone-to-total noise level ratio (weighted) in the 768-kHz channel (M and T stations) and in the 2438-kHz channel (R station) for the "noise loading on" condition

9) K_{HN} = Test tone-to-total noise level ratio (weighted) in the 1296-kHz channel (M and T stations) and in the 5560-kHz channel (R station) for the "noise loading on" condition

The above factors can be computed from the following expressions:

1) "Noise Loading Off" computational Procedure:

   a) Uplink, K_u (db) $= P_{rs} - N_{rs}$

$$= P_{rs} - 10 \text{ Log} (KT_s)$$

$$= P_{rs} - 198.6 - 10 \text{ Log } T_s$$

where

P_{rs} = Satellite receiver total input power

N_{rs} = Noise power density at satellite receiver input

K = Boltzman constant = $1.38 (10)^{-23} \dfrac{\text{watts}}{(°K)(Hz)} = \dfrac{-198.6 \text{ dbm}}{(°K)(Hz)}$

T_s = Satellite receiver system noise temperature (°K) = $T_A + T_T + t(L-1) + L(T_R)$

where

T_A = Antenna noise temperature (°K) (only contributions received from the earth are considered)

T_T = Degradation due to transmitter noise (°K) (due to the electrical isolation between transmitter and receiver feeds, T_T is assumed to be insignificant)

t = Physical temperature of coupling network (°K)

L = Power loss of coupling network (total insertion loss from antenna to preamplifier)

T_R = Equivalent noise temperature of receiver preamplifier (°K) (referenced to 290°K)

Satellite	Transponder 1					Transponder 2				
	T_A (°K)	t (°K)	L (Numeric)	T_R (°K)	10 Log T_s (db)	T_A (°K)	t (°K)	L (Numeric)	T_R (°K)	10 Log T_s (db)
ATS-1	15	285	1.45	920	31.7	15	285	1.45	920	31.7
ATS-3	290	285	1.12	890	31.2	290	285	1.12	764	30.7

NOTE: T_A for ATS-1 is lower than for ATS-3 due to the receiver antenna pattern which results in the ATS-1 antenna seeing a large percentage of cold sky, while the ATS-3 antenna is more nearly directed toward earth.

b) Downlink, K_d (db) $= P_{rg} - N_i = P_{rg} - 10 \log KT_s$

$$= P_{rg} + 198.6 - T_s \text{ (db)}$$

P_{rg} = Ground receiver input level (dbm)

N_i = Noise power density at the ground receiver input from the ground receiver and ground antenna

T_s = Overall system ground receiver noise temperature (° K) measured in db

c) Alternately, for $K_u \gg K_d$

$$K_d = K_o$$

d) K_o (numeric) $= \dfrac{K_u \; K_d}{K_u + K_d}$ (numeric)

$$K_{LO} \text{ (db)} = -B_{F1A} + K_o + 10 \log M_1^2$$

$$K_{HO} \text{ (db)} = -B_{F1A} + K_o + 10 \log M_2^2$$

$$K_{CO} \text{ (db)} = -B_{F1A} + K_o + 10 \log M_3^2$$

B_{F1A} = F1A Bandwidth, 1.55 kHz (31.9 db Hz)

M = RMS test tone modulation index $= \dfrac{\Delta f}{F_{TT}}$

Δf = Test tone frequency deviation (rms value)

(490 kHz for 1200-channel station, 870 kHz for 240-channel station

F_{TT} = Multiplex channel frequency

Channel Spectrum	Channel	F_{TT} (kHz)	M (rms)	$10 \text{ Log } m^2$ (db)
1200 Channels	D (Low)	328	$M_1 = 1.48$	3.1
	G (High)	5340	$M_2 = 0.092$	-20.7
	C (Center)	2438.	$M_3 = 0.20$	-14.0
240 Channels	D (Low)	336	$M_1 = 2.53$	8.1
	G (High)	1248	$M_2 = 0.69$	-3.2
	C (Center)	768	$M_3 = 1.13$	1.1

For RF Loop, $K_o = K_d$

For 1200 Channels;

$$K_{LO} = K_o \text{ (db)} + (-28.8)$$
$$K_{HO} = K_o \text{ (db)} + (-52.6)$$
$$K_{CO} = K_o \text{ (db)} + (-45.9)$$

For 240 Channels;

$$K_{LO} = K_o \text{ (db)} + (-29.8)$$
$$K_{HO} = K_o \text{ (db)} + (-35.1)$$
$$K_{CO} = K_o \text{ (db)} + (-30.8)$$

2) "Noise Loading ON" Computational Procedure:

The test tone-to-total noise ratio for the noise loading "on" condition is determined by combining the effect of the overall test tone-to-intermodulation noise ratio (K_{ov}) with the test tone-to-total noise ratio for noise loading "off". Figure 7.5 shows the K_{ov} factor as a function of multiplex channel frequency for the nominal loading conditions used in the ATS-1 and ATS-3 missions. The change in K_{ov} due to using different baseband bandwidths (240-channel spectrum versus 1200-channel spectrum) was found to be within the spread of sampled data. Figure 7.5 shows the range of K_{ov} values which have been calculated using several samples of experimental data. The values used herein will be the average of the sampled data (shown as a heavy line in figure 7.5). From figure 7.5, the K_{ov} values for the FT Mode are, in db;

Channel	1200 Channels		240 Channels	
	ATS-1	ATS-3	ATS-1	ATS-3
LOW	61.5	65.2	61.5	65.2
center	46.8	49.9	55.5	58.9
HIGH	41.2	43.7	51.7	54.8

a) $K_{LN} = \dfrac{K_{LO} \, K_{OV}}{K_{LO} + K_{OV}}$ = S/N (Noise On, Channel D) (all numeric)

b) $K_{HN} = \dfrac{K_{HO} \, K_{OV}}{K_{HO} + K_{OV}}$ = S/N (Noise On, Channel G) (all numeric)

c) $K_{CN} = \dfrac{K_{CO} \, K_{OV}}{K_{CO} + K_{OV}}$ = S/N (Noise On, Channel C) (all numeric)

3) TV Weighted Noise Computational Procedure:

From Part (1);

a) Uplink, K_u (db) = P_{rs} + 100 - 10 Log (F-1)

b) Downlink, K_d (db) = P_{rg} + 198.6 - B_{IF} (db) - T_s (db)

$$= P_{rg} + 123.1 - T_s \text{ (db)}$$

From a) and b),

$$K_o = \frac{K_d \, K_u}{K_d + K_u} \qquad \text{(all numeric)}$$

c) Alternately, for $K_u \gg K_d$

$$K_d = K_o$$

For RF loop, $K_o = K_d$

d) $(S/N)_A$ +(db) = $K_o - B_{IF} + 10 \log \dfrac{B_{IF}}{B_V} + K_{FM} + K_{p-p} + K_w - K_s$

$$= K_o - 75.5 + 10 \log 7.32 + 8.4 + 9 + 10.6 - 2.9$$

$$= K_o - 41.8$$

$(S/N)_A$ = Post detection p-p signal to idle noise ratio (db) defined in a standard weighted filter for above threshold operation

B_{IF} = Receiver IF bandwidth = 35.5 MHz at R, M, and C (75.5 db Hz)

B_V = Video filter noise bandwidth = 4.85 MHz (66.9 db Hz)

K_{FM} = FM improvement factor (measured value) = 8.4 db

K_{p-p} = Factor required to convert S_{rms} to S_{p-p} = 9 db

K_w = Weighting factor = 10.6 db (measured)

K_s = Ratio of total video signal power (including sync pulses) to the useable video power, = 1.95 (ratio) = 2.9 db

4) TV Audio Channel Signal-to-noise computational procedure

a) Operation above Threshold

The subcarrier signal-to-noise ratio is given by;

$$(S/N)_s = K_o - B_{IF} + 10 \log \left[\left(\frac{B_{IF}}{B_s}\right) \left(\frac{f_{dc}}{f_s}\right)^2 \right] \qquad (1)$$

The demodulated audio channel signal-to-noise ratio is given by;

$$S/N = (S/N)_s + 10 \log \left[3 \left(\frac{B_s}{B_a}\right) \left(\frac{f_{ds}}{f_a}\right)^2 \right] \qquad (2)$$

substituting for $(S/N)_s$ from (1) gives:

$$S/N = K_o - B_{IF} + 10 \log \left[\left(\frac{B_{IF}}{B_s}\right) \left(\frac{f_{dc}}{f_s}\right)^2 \right] + 10 \log \left[3 \left(\frac{B_s}{B_a}\right) \left(\frac{f_{ds}}{f_a}\right)^2 \right] \qquad (3)$$

$$= K_o - 75.5 + 19.0 - 18.6 + 4.8 + 15.0 + 20.6 \qquad (4)$$

$$= K_o - 34.7 \qquad (5)$$

$(S/N)_s$ = Subcarrier Signal-To-Noise ratio

B_{IF} ≈ Receiver IF filter noise Bandwidth = 35.5 MHz (75.5 db Hz)

B_s = Subcarrier filter noise bandwidth = 445 KHz (56.5 db Hz)

f_{dc} = RMS deviation of carrier by subcarrier

= 707 kHz (58.5 db Hz) (with 6.0-mhz subcarrier)

= 885 kHz (59.5 db Hz) (with 7.5-MHz subcarrier)

f_s = Audio subcarrier frequency = 6.0 MHz or 7.5 MHz

$\left(\dfrac{f_{dc}}{f_s} = \text{RMS Carrier modulation index} = -9.3 \text{ db} \right)$

B_a = Audio channel filter noise bandwidth = 14.0 kHz (41.5 db Hz)

f_a = Peak modulating frequency = 13.0 kHz (41.1 db Hz)

f_{ds} = RMS deviation of subcarrier by audio signal

= 140 kHz (51.4 db Hz)

$\left(\dfrac{f_{ds}}{f_a} = \text{RMS subcarrier modulation index} = 10.3 \text{ db} \right)$

The factor 3 in equation (2) is due to the integration of the noise power density (N_d) over the audio channel bandwidth which is of the form:

$$N_d = Kf^2$$

where K is a constant of proportionality.

It should be noted that the S/N in the subcarrier is 0.4 db greater than the C/N in the IF BW.   From (1)

$$(S/N)_s = K_o - B_{IF} + 19.0 - 18.6 = K_o - B_{IF} + 0.4$$

By varying the deviation of the carrier by the subcarrier, the $(S/N)_s$ may be made greater or less than the C/N in the IF bandwidth, thus avoiding the possibility of causing the subcarrier detector to operate below threshold.
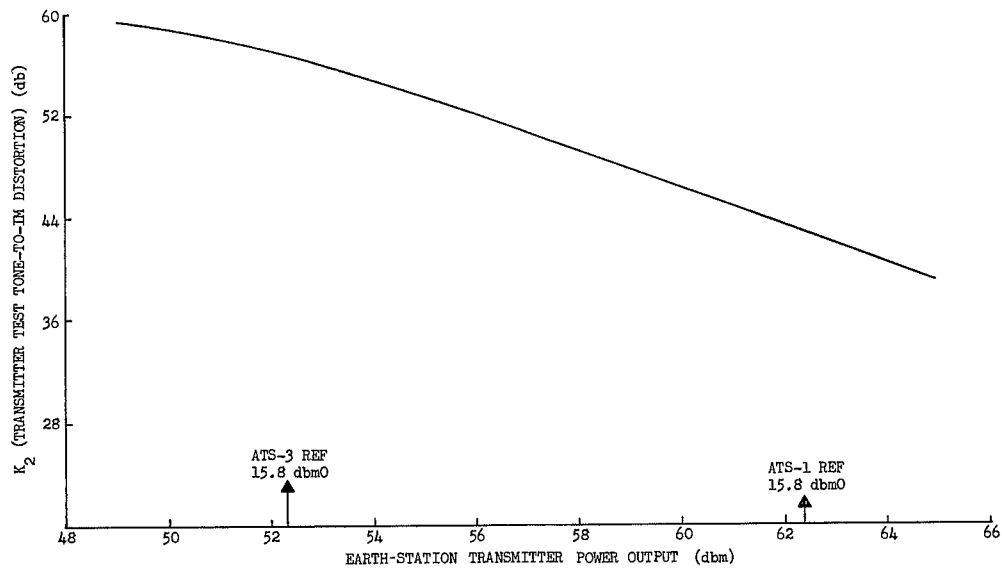
Figure 7.1. Test Tone-to-Intermodulation Distortion (K_2) Versus Transmitter Power Output (MA Mode, Rosman)
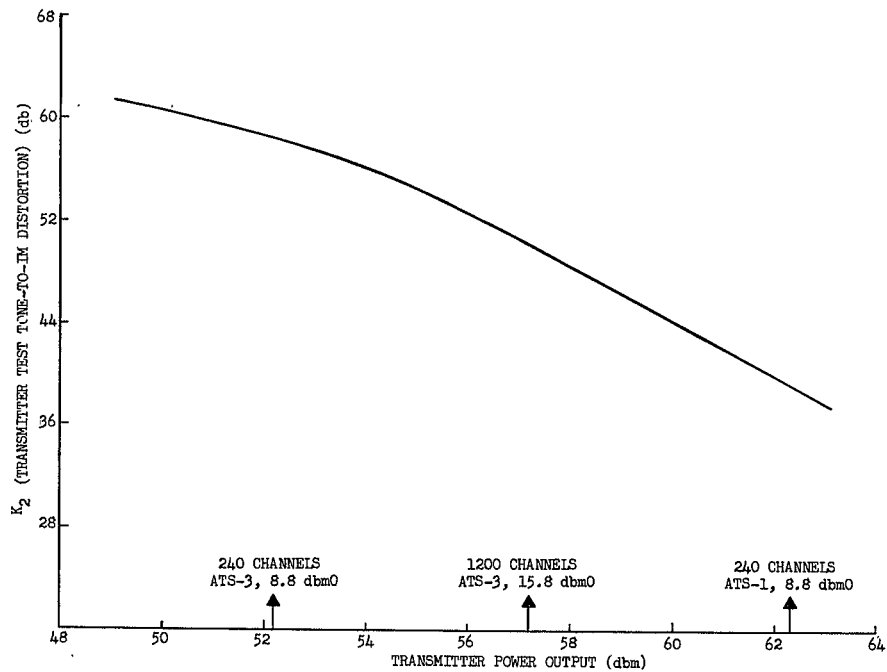
Figure 7.2. Test Tone-to-Intermodulation Distortion (K_2) Versus Transmitter Power Output (MA Mode, Mojave)
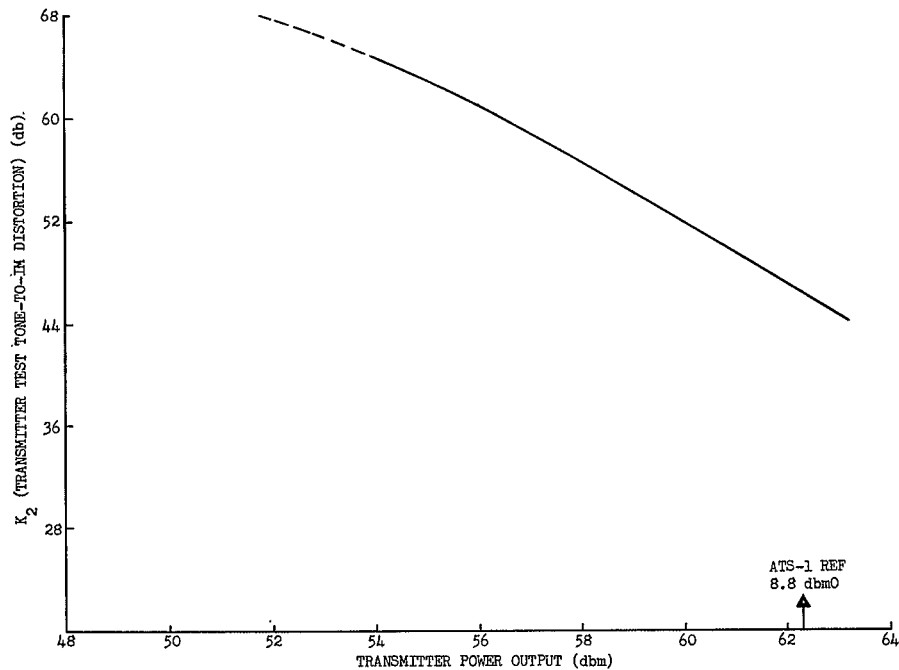
Figure 7.3. Test Tone-to-Intermodulation Distortion (K_2) Versus Transmitter Power Output (MA Mode, Cooby Creek)
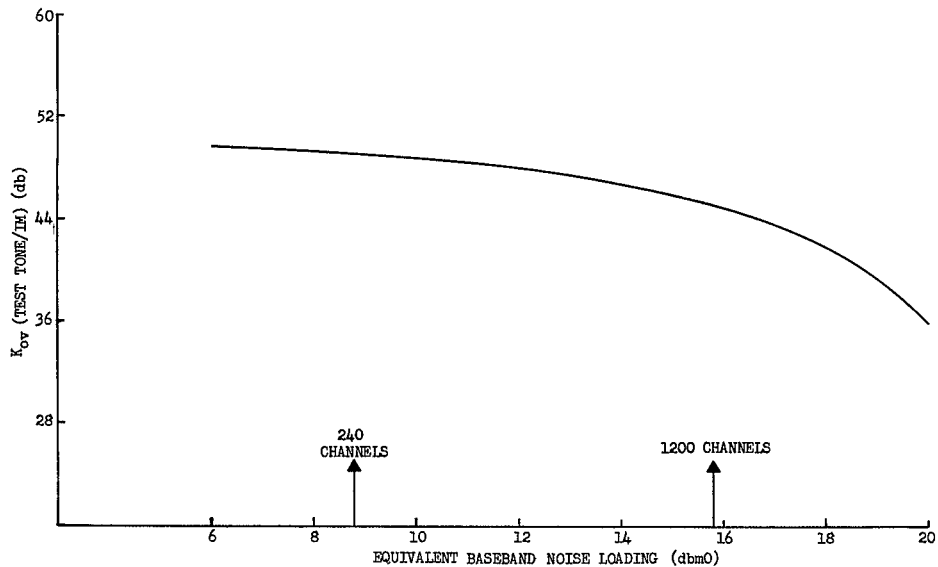
Figure 7.4.   Receiver and Transponder Test Tone-to-Intermodulation Noise Ratio (K_{ov}) Versus P_{tg} (db) (MA Mode)
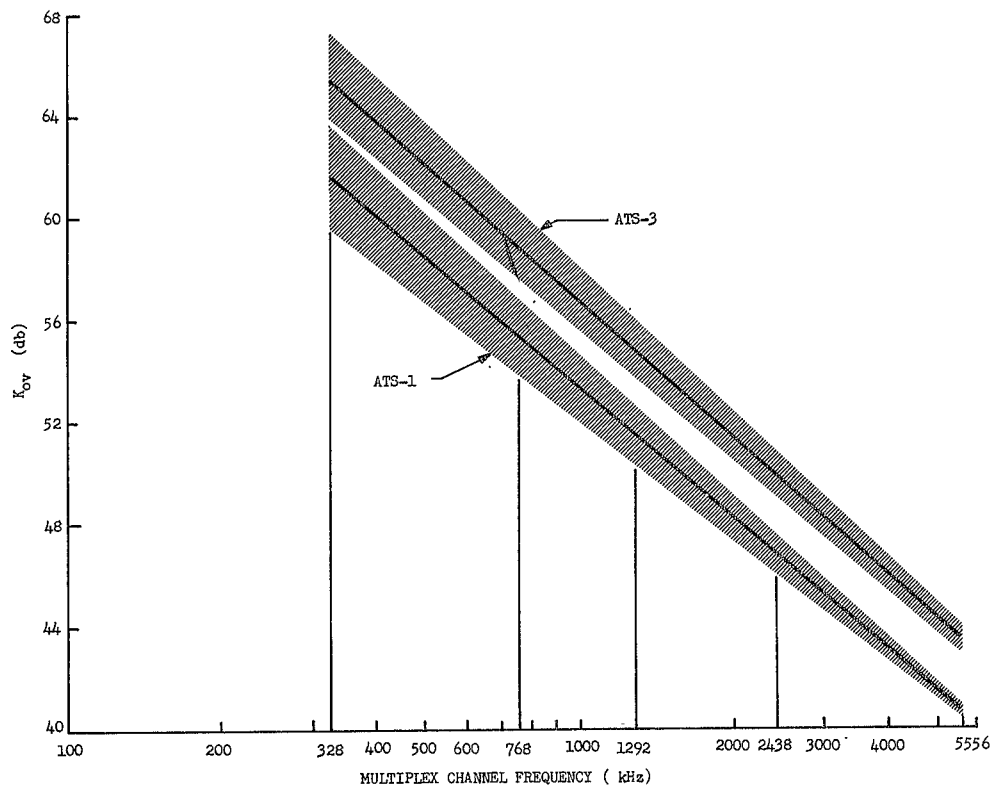
ire 7.5. Test Tone-To-Intermodulation Noise Ratio (K_{ov}) Versus Baseband Frequency (FT Mode)

7.2 PATH LOSS CALCULATIONS

This paragraph describes the method of determining both uplink and downlink path loss for experiments FT-AT-1.1, FT-RF-1.1, MA-AT-1.1 and MA-RF-1.1.

The relationship between transmitted and received powers in a communications link is as follows:

$$P_r = \frac{P_t \, G_t \, G_r \, \lambda^2}{16 \pi^2 \, R^2 \, L} = \frac{P_t \, G_t \, G_r}{U}$$

where:

P_r = Received power at the receiver input terminals

P_t = Transmitted power at the power amplifier output terminals

G_t = Transmitting antenna gain, including losses between the power ampli and the antenna

G_r = Receiving antenna gain, including losses between the antenna and the receiver input (e.g., maser input for the ground receiver)

λ = Wavelength

R = Range

$\dfrac{16 \pi^2 \, R^2}{\lambda^2}$ = Free-space loss

L = Other path losses, such as rain

$U = \dfrac{16 \pi^2 \, R^2 \, L}{\lambda^2}$

In decibels, the equation can be written

$$P_r = P_t + G_t + G_r - U$$

where U is regarded as a positive number (e.g., 150 db). From this equation

$$U = (P_t + G_t) - (P_r - G_r)$$

$$P_t - P_r = U - G_t - G_r$$

If R is expressed in nautical miles and the operating frequency in MHz, free space loss can be predicted as follows:

Free-space loss = 37.85 db + 20 log R + 20 log f.

Thus, the parameters and format treated and plotted in this experiment are:

1) SSB Transmitter Output $(P_t + G_t)_g$ - Effective radiated power per test tone (MA mode - SSB), effective total radiated power (FT mode - FM)

2) Satellite Received Power (P_{rs}) - Test-tone power at satellite receiver input terminals (MA mode), total power at satellite receiver input terminals (FT mode)
3) Uplink Path Loss (U_u)
4) Satellite Transmitter Power $(P_t + G_t)_s$ - Effective total radiated power
5) Ground Receiver Input Power (P_{rg}) - In dbm at receiver preamplifier input
6) Downlink Path Loss (U_d)

To illustrate the method of computation and the specific parameters that must be known to compute U accurately, an example will be shown. The following is the procedure for computing the uplink and downlink path-loss values for the Rosman station from the data in table 7.2.

UPLINK - MA MODE (ATS-1)

P_{tg} = 46.6 dbm - Ground transmitter test-tone output power

G_{tg} = 61.5 db - Ground transmit antenna gain minus plumbing losses

P_{rs} = -87.0 dbm - Spacecraft received test-tone power

G_{rs} = 6.2 db - Satellite receive antenna gain

$U = P_{tg} + G_{tg} - P_{rs} + G_{rs}$

U = Measured path-loss value

U = 46.6 + 61.5 + 87.0 + 6.2 = 201.3 db

E = 37.85 + 20 log R + 20 log F.

F = 6301.05 MHz - Transmit frequency

R = 22,000 N.M. - Line-of-sight range in nautical miles

E = 200.7 db

U_a = E + L

U_a = Actual path-loss value

L = Propagation loss (rain, etc.)

E = Free-space path loss

Where L ≈ 0 db

U = E

U - E = + 0.6 db

DOWNLINK - MA MODE (ATS-1)

P_{ts} = 37.9 dbm - Satellite transmit power output

G_{ts} = 13.6 db - Satellite transmit antenna gain minus plumbing losses

G_{rg} = 58.4 db - Ground antenna receive gain

P_{rg} = -89.4 dbm - Ground receiver input power

U = $P_{ts} + G_{ts} - P_{rg} + G_{rg}$

U = 37.9 + 13.6 + 89.4 + 58.4 = 199.3

E = 37.85 + 20 log R + 20 log F

F = 4178.591 MHz - Satellite transmit frequency

R = 22,000 N.M.

E = 197.1 db

$U - E$ = +2.2 db

The values of the constants utilized to compute U for the Mojave and Cooby Creek stations with ATS-1 are also shown in table 7.2. These constants are G_{tg}, G_{rs}, G_{ts}, and G_{rg}. The power-level values are measured during an actual test run. Also, the range value required to compute E is obtained for a given test run from computations of ephemeris data for the satellite.

Similar calculations are shown for ATS-3 in the following paragraph. It is based on the MA test performed at Mojave on May 1, 1968, shown in table 7.3

UPLINK - MA MODE (ATS-3)

P_{tg} = 42.9 dbm - Ground-transmitter output power

G_{tg} = 54.6 db - Ground-transmit antenna gain minus plumbing losses

P_{rs} = -87.0 dbm - Spacecraft received signal level

G_{rs} = 16.3 db - Satellite receive antenna gain

U = $P_{tg} + G_{tg} - P_{rs} + G_{rs}$

U = Measured path-loss value

U = 42.9 + 54.6 + 87.0 + 16.3 = 200.8 db

E = 37.85 + 20 log R + 20 log F

F = 6301 MHz - Transmit frequency

R = 20,500 N.M. = Line-of-sight range in nautical miles

E = 200.2 db

U_a = $E + L$

U_a = Actual path-loss value

L = Propagation loss (rain, etc.)

E = Free-space path loss

When $L \approx 0$ db

U = E

$U - E$ = + 0.6 db

DOWNLINK - MA MODE (ATS-3)

P_{ts} = 38.9 dbm - Satellite transmit power output

G_{ts} = 16.2 db - Satellite transmit antenna gain minus plumbing losses

G_{rg} = 51.0 db - Ground antenna receive gain

P_{rg} = -93.4 dbm - Ground receiver input power

U = $P_{ts} + G_{ts} - P_{rg} + G_{rg}$

U = 38.9 + 16.2 + 93..4 + 51.0 = 199.5

E = 37.85 + 20 log R + 20 log F

F = 4119.599 MHz - Satellite transmit frequency

R = 20,500 N.M.

E = 196.5 db

$U-E$ = +3.0 db

The power-level values are measured during actual test runs. The range value required to compute E is obtained for a given test run from computations of ephemeris data for the satellite. The constants employed and results of a similar calculation for Rosman are also presented in table 7.3.

7.19

TABLE 7.2. MEASURED AND PREDICTED RESULTS
OF RF SIGNAL POWER AND PATH LOSSES (ATS-1)

Station		Rosman	Mojave	Cooby Creek
FTP Number		MA-RF-1.1	MA-RF-1.1	MA-RF-1.1
Test Serial Number		R003	M001	T1020
Test Date		4/11/68	1/30/67	3/14/68
Test Duration		NA	NA	NA
SSB Ground Transmitter Test Tone Power Level	(dbm)	46.6	54.7	53.5
Ground Station Transmit Antenna Gain, Corrected	(db)	61.5	54.6	54.6
Ground Station ERP	(dbm)	108.1	109.3	108.1
Satellite Receiver Signal Level	(dbm)	-87.0	-87.0	-87.0
Satellite Receive Antenna Gain, Corrected	(db)	6.2	6.2	6.2
Satellite Net Received Signal Level	(dbm)	93.2	-91.9	93.2
Measured Uplink Path Loss	(db)	201.3	202.5	201.3
Predicted Uplink Path Loss	(db)	200.7	200.3	200.6
Difference (Δ) Between Predicted and Measured Uplink Path Loss	(db)	+0.6	+2.1	+0.7
Satellite Transmitter Power Level	(dbm)	37.9	35.6	35.6
Satellite Transmit Antenna Gain Corrected	(db)	13.6	13.6	13.6
Satellite EIRP	(dbm)	51.5	47.7	49.2
Ground Station Receiver Signal Level	(dbm)	-89.4	-96.0	-97.6
Ground Station Receive Antenna Gain	(db)	58.4	51.0	51.0
Ground Station Net Received Signal Level	(dbm)	147.8	-147.0	-148.6
Measured Downlink Path Loss	(db)	199.3	196.0	197.8
Predicted Downlink Path Loss	(db)	197.1	196.6	196.9
Difference (Δ) Between the Predicted and Measured Downlink Path Loss	(db)	+2.2	-0.6	+0.9

7.20

TABLE 7.3. MEASURED AND PREDICTED RESULTS
OF RF SIGNAL POWER AND PATH LOSSES (ATS-3)

Station		Rosman	Mojave	.
FTP Number		FT-RF-1.1	MA-RF-1.1	
Test Serial Number		R3-012	R3-007	
Test Date		2/27/68	5/1/68	
Test Duration		35 Min.	25 Min.	
SSB Ground Transmitter Test Tone Power Level	(dbm)	53.5	42.9	
Ground Station Transmit Antenna Gain, Corrected	(db)	62.1	54.6	
Ground Station ERP	(dbm)	115.6	97.5	
Satellite Receiver Signal Level	(dbm)	-70.6	-87.0	
Satellite Receive Antenna Gain, Corrected	(db)	16.3	16.3	
Satellite Net Received Signal Level	(dbm)	-86.9	-103.3	
Measured Uplink Path Loss	(db)	201.9	200.8	
Predicted Uplink Path Loss	(db)	200.0	200.2	
Difference (Δ) Between Predicted and Measured Uplink Path Loss	(db)	+1.9	+0.6	
Satellite Transmitter Power Level	(dbm)	40.2	38.9	
Satellite Transmit Antenna Gain Corrected	(db)	16.2	16.2	
Satellite EIRP	(dbm)	56.4	55.1	
Ground Station Receiver Signal Level	(dbm)	-83.6	-93.4	
Ground Station Receive Antenna Gain	(db)	58.4	51.0	
Ground Station Net Received Signal Level	(dbm)	-142.0	-144.4	
Measured Downlink Path Loss	(db)˙	198.4	199.5	
Predicted Downlink Path Loss	(db)	196.3	196.5	
Difference (Δ) Between the Predicted and Measured Downlink Path Loss	(db)	+2.1	+3.0	

7.3 EXPERIMENTAL ERROR ANALYSIS

The data analysis of the ATS-communications experiments described in section 3 is based on an evaluation of large quantities of data obtained under various controlled and uncontrolled conditions. This section describes the statistical approach used in obtaining meaningful conclusions from the mass of data in the light of the uncontrolled conditions.

The purpose of an experiment is to obtain knowledge of a specific parameter defined by the experimenter. The value of the defined parameter can vary with experimental conditions, resulting in some type of distribution. A set of distributed values for a defined parameter is referred to as a population. To gain knowledge of a population, a limited number of observations forming sample data is made. By using statistical inference methods explained below, conclusions concerning the population can be drawn from sample data.

The distribution of a population may be approximated by taking random samples of that population. Random sampling is a sampling procedure in which every member of the population has the same probability of being selected. Obtaining sample data by some procedure other than random sampling, can gather sample data which does not represent the population and results in incorrect conclusions about the population.

All sample data contains various levels of accuracy, and measured data only estimates the true value of the parameter at the time of measurement. Limited accuracy implies the presence of experimental error. The term "experimental error" varies in meaning from one person to another. For our purposes in this report we shall define it to mean all variability which exists among the results of independent experiments that are intended to be identical. Experimental errors can be classified into five types: systematic error, personal error, careless mistakes, assignable causes, and random error. Systematic errors are the same for each measurement or are a definite function of the value of the parameter being measured. An example of a systematic error is an imperfectly known constant, such as antenna gain, which is used to determine propagation path loss from received signal measurements. Personal errors are due to systematically different results obtained from personal judgment. Examples of personal errors are interpolating values on scales and rounding off numbers. Personal errors can be detected by having several individuals repeat the same measurement, and note the differences. Careless mistakes are caused by such things as not following the experimental procedures specified, errors in arithmetic, and reading the wrong scale. Assignable causes are variables which are left uncontrolled by the experimenter and have important effects on the parameter being measured. The experiment should be designed to control, if possible, all variables which have important effects on the outcome, leaving only the variables which individually influence the results very little. Random errors are variations caused by an accumulation of uncontrolled

variables, each of whose effects is individually small. If only random errors are present in the sample data, the sample data forms a random sequence which approximates a normal distribution. The presence of random errors can only be accepted when no more plausible explanation of the observed pattern of sample data is available. Statistical analysis can be correctly applied to sample data only when random errors are the only cause of experimental error. By analyzing a number of samples, the effects of random errors on the conclusions will be minimized. It is necessary to examine the sample data carefully before statistical analysis, looking for the presence of systematic errors and errors due to assignable causes. This is usually the most difficult phase of analysis since possible sources of error are often completely unknown to the analyst who was not present during the actual observation. Sample data should not be rejected solely because it does not fit the analyst's expectations. The only valid justification that can be used to reject sample data is when a source of experimental error other than random error has been located, and the effect of its presence cannot be removed.

To obtain the best conclusions about a population, the entire population should be analyzed. This is impossible since the population often has infinite size. Even when the population is of limited size, a small data sample is analyzed instead of the entire population because economy of time and money is an important factor. Analyzing small data samples usually brings adequate conclusions, making larger sample sizes unnecessary. In obtaining conclusions for a population, the properties of that population are usually estimated by one of two different estimate methods. One is called a point estimate and the other is called an interval estimate. A point estimate is a number obtained from computations or the sample values that serves as an approximation to the parameter being estimated. For example, a sample mean is a point estimate of the population mean. An interval estimate is usually constructed in such a manner that the probability of the intervals containing the parameter can be specified. The advantage of the interval estimate is that it shows how accurately the parameter is being estimated. If the length of the interval is very small, high accuracy has been achieved. Such interval estimates are called confidence intervals. A 90 percent confidence interval has been arbitrarily chosen as the basis for ATS analysis. This gives reasonable assurance that the interval contains the population mean, since the computed confidence interval is given a 0.9 probability of including the population mean.

The Student's t-distribution is a common statistical distribution used to calculate the confidence intervals when a small amount of sample data is available for data reduction. The Student's t-distribution is related to the normal distribution in such a way that when fewer and fewer datum values are used to calculate mean and standard deviation of the population, the confidence interval limits are increased. The theory behind the Student's t-distribution assumes that the population possesses a normal distribution. Therefore, the

confidence interval technique for the t-distribution should be used cautiously when it is not known if the population is actually normally distributed. The confidence interval limits for the Student's t-distribution are determined by:

$$\overline{X} \pm t \, S/n$$

where:

$\overline{X}$ = sample mean

t = Student's t-variable

S = sample standard deviation

n = number of samples

The sample mean is computed by:

$$\overline{X} = \frac{\sum\limits_{i=1}^{n} X_i}{n}$$

where X_i is a member of the sample data. The sample standard deviation is determined by the formula:

$$S = \left(\frac{\sum\limits_{i=1}^{n} (X_i - \overline{X})^2}{n-1} \right)^{1/2}$$

Note that this is slightly different from the formula for population standard deviation for normal distribution, which is:

$$\sigma = \left(\frac{\sum\limits_{i=1}^{n} (S_i - \mu)^2}{N} \right)^{1/2}$$

where μ is the population mean and N is the number in the population. The variable t is found from a Student's t-distribution table as follows: The degrees of freedom needed to read the distribution table is calculated by subtracting one from the sample size n. Locate the correct row corresponding to the number of degrees of freedom. The percentage points of the confidence limits are located across the top of the table. Therefore, each column corresponds to a specific confidence level. Care must be taken to understand which confidence interval the particular table labels across the top. Usually the analytic expression is written below the title of the table. An example of the Student's t-distribution is shown in figure 7.6. In figure 7.6, P(X) is the probability-density function, and F(X) is the cumulative-probability density function shown as the area under the probability-density curve from X = ∞ to X = a. The value of F(X) is the probability that X_i is less than a, likewise 1-F(X) is the probability that X_i is greater than a. The confidence interval used for the purpose of ATS analysis is illustrated in figure 7.7. The shaded area in figure 7.7 is the probability that X_i is within the confidence interval $(\overline{X}-b)$ to $(\overline{X} + b)$. This area is equal to 2F(X) - 1.

7.24
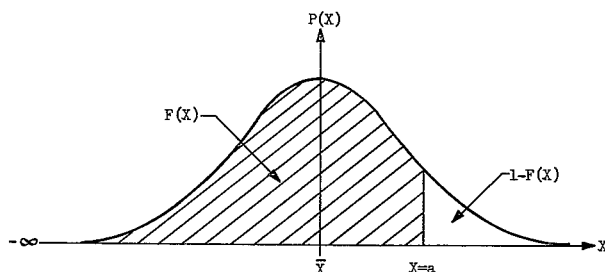
Figure 7.6.   Student's t-Distribution Probability Density Function
(F (X) = cumulative probability)
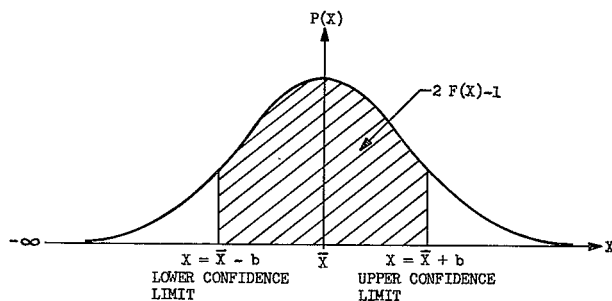
Figure 7.7.   Student's t-Distribution Probability Density Function
(2F (X) - 1= probability X_i is within confidence limits)

The column corresponding to $2F(X)-1$ equal to 0.90 is the column used to determine the value of $\underline{t}$ to be used in the confidence interval calculations for a 90-percent confidence level. For example, if there were 10 samples and a 90-percent confidence interval is to be computed, a $\underline{t}$ variable of 1.833 is selected from the distribution table.

Before applying the confidence interval analysis, at least three data values should be available. If there is less than three data values, the confidence interval will probably be so wide, that the conclusions are of little use. When used properly, the confidence interval method is a very useful inference technique.

The preceding discussion may be clarified by the following example wherein a random sample of four elements produces sample data values of 9, 10, 11, and 10 (sample A). The sample mean is calculated to be 10, and might be considered a fairly precise estimate of the population mean. On the other hand, we would consider the sample mean of 10 to be a less precise estimator of the population mean if the sample data values were 8, 9, 17, and 6 (sample B), since these values suggest greater population dispersion. For sample A, the 90-percent confidence limits are 9.04 and 10.96, while the confidence limits for sample B are 4.32 and 15.68. By comparing the confidence limits for both samples, it is apparent that sample A better estimates its own population mean since its confidence interval is smaller.

SAMPLE A

random samples: 9, 10, 11, 10

sample mean $= \overline{X} = \dfrac{9 + 10 + 11 + 10}{4} = 10.00$

sample standard deviation $= S =$

$$\left[\dfrac{(9 - 10)^2 + (10-10)^2 + (11-10)^2 + (10-10)^2}{\sqrt{3}} \right]^{1/2} = 0.816$$

t variable $= 2.353$

90% confidence limits $= 10 \pm \dfrac{2.353 \cdot 0.816}{\sqrt{4}} = 9.04 \ \& \ 10.96$

SAMPLE B

random samples: 8, 9, 17, 6

sample mean $= \overline{X} = \dfrac{8 + 9 + 17 + 6}{4} = 10.00$

sample standard deviation $= S =$

$$\left[\dfrac{(8-10)^2 + (9-10)^2 + (17-10)^2 + (6-10)^2}{\sqrt{3}} \right]^{1/2} = 4.830$$

t variable $= 2.353$

90% confidence limits $= 10 \pm \dfrac{2.353 \cdot 4.830}{\sqrt{4}} = 4.32 \& 15.68$

7.27

7.4 DERIVATION OF EXPRESSION FOR THE STABILITY OF AN OSCILLATOR WITH NOISE OF SPECTRAL DENSITY $G_e(f) = K/f$

7.4.1 RELATIONSHIP BETWEEN OSCILLATOR RMS FREQUENCY DEVIATION AND CARRIER TO PHASE JITTER NOISE RATIO*

Assume $1/f$ type oscillator phase noise in figure 7.8.

Under the above assumption, Δf, the rms frequency deviation is constant for all f_a, and the phase amplitude spectrum $G_e(f) = \dfrac{\Delta f}{f_a}$ rad/Hz. The power density spectrum is, therefore, $G'_e(f) = \left(\dfrac{\Delta f}{f_a}\right)^2 \dfrac{rad^2}{Hz}$.

Then, $\sigma_\phi^2 = 2 \displaystyle\int_{f_1}^{f_2} \left(\dfrac{\Delta f}{f_a}\right)^2 df_a = m^2$ where σ_ϕ^2 is the mean square phase deviation, or variance of the oscillator spectrum in radians. [2]

Solving, and assuming $f_2 \gg f_1$, we obtain:

$$m^2 = \frac{2(\Delta f)^2}{f_1} \ radians^2$$

$$and \quad m = \Delta f \sqrt{2/f_1} = \sigma_\phi \tag{1}$$

If $m < 1$, then the ratio of the first order Bessel function to the zero order function (the noise-to-carrier voltage ratio) is given by:

$$\frac{J_1(m)}{J_0(m)} = \upsilon_p \approx \frac{m}{2} \tag{2}$$

Substituting, $S_p = \dfrac{\Delta f \sqrt{2/f_1}}{2} = \dfrac{\Delta f}{\sqrt{2f_1}}$

The variance of the frequency deviation of the oscillator spectrum (again assuming $1/f$ type phase jitter) is given by:

$$\sigma_f^2 = 2 \displaystyle\int_{f'_1}^{f'_2} (\Delta f)^2 df_a = 2 (\Delta f)^2 f'_2 Hz^2, \text{ assuming } f'_1 \ll f'_2$$

$$\sigma_f = \Delta f \sqrt{2f'_2} = \Delta f \sqrt{2/T} \tag{3}$$

From equation (2), $\sigma_f = 2S_p \sqrt{f_1 f'_2} = 2S_p \sqrt{\dfrac{f_1}{T}}$

and $f'_2 = 1/T$ where T is the "averaging time", and f_1 is the lowest frequency of interest in the oscillator spectral density characteristic.

*This is a synopsis of "A Comment on the Definition of Short Term Frequency Stability", R. J. Martel, Westinghouse.

7.28

7.4.2 OSCILLATOR STABILITY CRITERION

Assuming the CCITT recommendation of 50-db total S/N ratio in a 3.1-kHz voice channel, and accepting the premise that, due to the constancy of test tone to phase jitter noise ratio, and due to the fact that phase jitter noise is not present when the test tone is absent, then it can be reasoned that the subjective effect is similar to perfect companding action, and a 23-db S/N improvement is realized. On this basis, a signal- to-phase-jitter noise ratio of 27 db will yield an effective 50-db S/N ratio. If 3 db is added to insure the total channel S/N will be better than 50 db, then a signal- to-oscillator phase-jitter noise ratio of 30 db will be the requirement. Assuming the maximum allowable carrier-frequency shift (f_1) to maintain naturalness of speech to be 20 Hz[22] and choosing an averaging time of one second in equation (3), then solving for σ_f, yields 0.286 Hz. The short-term carrier-frequency stability for a one-second averaging time is then $S = \dfrac{\sigma f}{f_c} = \dfrac{0.286}{6 \times 10^9} = 4.8 \times 10^{-11}$,

where f_c is the carrier frequency of the ATS uplink signal. In summary, the foregoing consideration requires that for a one-second averaging time and a maximum allowable oscillator frequency offset of ± 20 Hz, the oscillator stability S must be better than 4.8×10^{-11} and the suppression ratio S_p must be -30 db or better.

∞

TEST-TONE LEVEL

ϕ^2

G_e (f) $= \dfrac{\Delta f}{f}$

f_1 f_1 f_2
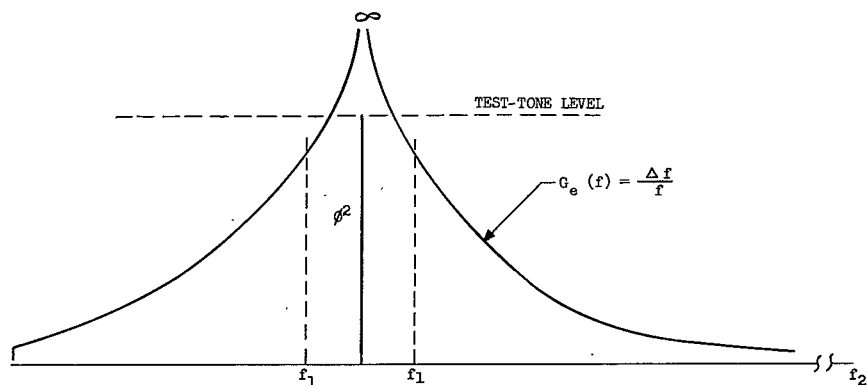
..NCY DEVIATION OF THE OSCILLATOR NOISE (CONSTANT FOR ALL f)

Figure 7.8. Derivation of Expression for the Stability of an Oscillator with Noise of
Spectral Density $G_e(f) = \Delta f/f$

7.30

7.5 DETERMINATION OF INTERMODULATION NOISE POWER CHARACTERISTIC FROM TEST DATA

The following items are contained in this paragraph:

1) Definitions of terms

2) Determination of $\dfrac{TT}{R}$ and $\dfrac{TT}{N}$

3) Determination of $\dfrac{TT}{I}$

4) Determination of TPR as a function of C/N.

7.5.1 DEFINITION OF TERMS

b   Bandwidth in which test-tone-to-noise ratios are defined. (3.1 kHz unweighted)

B   Total bandwidth of noise-loading spectrum (5248 kHz at Rosman, 984 kHz at Mojave and Cooby Creek)

B_{IF} Measured IF Noise bandwidth (15.5 MHz at Mojave and Cooby Creek, 35.5 MHz at Rosman)

$(C/N)_{IF}$ Pre-detection carrier-to-noise ratio (measured in the IF bandwidth, B_{IF})

f   Multiplex-channel test-tone frequency (at baseband)

Δf RMS test-tone frequency deviation (870 kHz at Mojave and Cooby Creek, 490 kHz at Rosman)

I   Intermodulation noise power

k   Transfer characteristic of FM demodulator

K   Loading factor (based upon CCIR recommendations as discussed in paragraph 7.6) Nominal loading is 8.8 db at Mojave and Cooby Creek, and is 15.8 db for the Rosman station.

N   Total noise power in multiplex channel (unweighted) = I + R.

N_o Noise power density in slot channel with noise loading removed from total baseband (noise generator turned off)

N_1 Noise power density in slot channel with noise loading removed from slot only (slot filter in noise generator output).

NPR   Noise-power ratio—Ratio of the noise-power density in a multiplex slot channel when it is noise-loaded to the noise-power density in the slot when the noise loading is removed by inserting a slot-rejection filter in the noise generator at the channel frequency.

P_o Signal power density

P_t Total signal power in baseband

R   Thermal noise power

S   Signal power in multiplex voice channel

TPR   Thermal noise-power ratio. Ratio of the noise-power density in a multiplex slot channel when it is noise-loaded to the noise-power density in the slot when the noise loading is removed by turning off the baseband noise source.

TT   Test-tone power level in one channel

7.5.2 DETERMINATION OF $\frac{TT}{R}$ and $\frac{TT}{N}$

By definition,

$$TPR = \frac{P_o}{N_o} \tag{1}$$

$$P_t = (TT)(K) = P_o B \tag{2}$$

Combining (1) and (2) gives:

$$(TPR)(N_o) = \frac{(TT)(K)}{B} \tag{3}$$

By definition,

$R = N_o b$

Combining with (3) gives:

$$\frac{(TPR)(N_o)}{N_o b} = \frac{(TT)(K)}{(B)\ R} \tag{4}$$

from which;

$$\frac{TT}{R} = \frac{(TPR)\ B}{b\ K}$$

Letting $Y = \frac{B}{b\,K}$ (for Rosman, Y= 22.5 db for 12.8 dbm0 loading, 19.5 for 15.8 dbm0 loading)
(for Mojave and Cooby Creek, Y= 20.7 db for 7.3 dbm0 loading 19.2 db for 8.8 dbm0 loading

$$\frac{TT}{R} = (TPR)\ Y \qquad \text{(numeric)} \tag{5}$$

In a similar manner,

$$\frac{TT}{N} = (NPR)\ Y \qquad \text{(numeric)} \tag{6}$$

For the channel loading used at Rosman, the baseband loading is 15.8 dbm0. Since the low-pass and high-pass filter corner frequencies are 5564 kHz and 316 kHz, respectively, the noise-loading bandwidth is 5248 kHz. The equivalent F1A filter noise bandwidth is 1.55 kHz. Using these values, the following conversion formulas are obtained:

$$\frac{TT}{N} \quad (WTD) \; = \; NPR + 19.5 \text{ db (For 15.8 dbm0 noise loading)}$$

$$\frac{TT}{R} \quad (WTD) \; = \; TPR + 19.5 \text{ db}$$

For the channel loading used at Mojave and Cooby Creek, the baseband loading is 8.8 dbm0. The low-pass and high-pass filter corner frequencies are 1300 kHz and 316 kHz, respectively, providing a noise-loading bandwidth of 984 kHz. The equivalent F1A filter noise bandwidth is 1.55 kHz. Using these values, the following conversion formulas are obtained:

$$\frac{TT}{N} \quad (WTD) \; = \; NPR + 19.2 \text{ db (For 8.8 dbm0 noise loading)}$$

$$\frac{TT}{R} \quad (WTD) \; = \; TPR + 19.2 \text{ db}$$

7.5.3 DETERMINATION OF $\frac{TT}{I}$

By definition:

$$NPR = \frac{P_o}{N_1} = \frac{P_o b}{N_1 b} = \frac{P_o b}{I + R} \tag{7}$$

from (7):

$$\frac{1}{NPR} = \frac{I}{P_o b} + \frac{R}{P_o b}$$

from which;

$$I = \frac{P_o b}{NPR} - R$$

Substituting (2) and (6) gives;

$$I = \frac{(TT)(K)}{B(NPR)} - \frac{TT}{(TPR)} Y$$

Letting $Y = \frac{B}{b K}$ gives;

$$I = \frac{TT}{Y(NPR)} - \frac{TT}{Y(TPR)}$$

from which;

$$\frac{TT}{I} = \frac{Y(TPR)(NPR)}{(TPR - NPR)} = \frac{(Y)(TPR)}{\frac{TPR}{NPR} - 1} \tag{8}$$

7.33

7.5.4 DETERMINATION OF TPR AS A FUNCTION OF C/N

(A) For the SSB-PhM (MA) mode:

The theoretical TPR value as a function of C/N can be computed by noting the relationship given in equation (6). It follows that:

$$\frac{TT}{R} = (TPR) + Y \ (db) \tag{9}$$

where

$$Y = 10 \log \left[B/Kb \right]$$

The TT/R is also a strict function of C/N and the rms test-tone modulation index m, which is $\frac{(0.35)}{\sqrt{2}}$ radian   rms. It follows that;

$$\frac{TT}{R} = \left(\frac{C}{N}\right)_{IF} \left(\frac{B_{IF}}{b}\right) \left(m^2\right) \quad \text{(numeric)} \tag{10}$$

where

B_{IF} is the measured IF Noise bandwidth (15.5 MHz at Mojave and Cooby Creek, and 35.5 MHz at Rosman).

Combining equations (9) and (10), expressed in db,

$$(TPR) = \left(\frac{C}{N}\right)_{IF} + B_{IF} + (m^2) - B + K \tag{11}$$

For Mojave and Cooby Creek, (in db),

$$(TPR) = \left(\frac{C}{N}\right)_{IF} + 8.7 \ \text{(for 8.8 dbm0 loading)} \tag{12}$$

For Rosman (in db),

$$\left(TPR\right) = \left(\frac{C}{N}\right)_{IF} + 12.0 \ \text{(for 15.8 dbm0 loading)} \tag{13}$$

B) For the FT mode:

The post-detection noise power density, N_o, of an FM system is given by Crosby in "Frequency Modulation Noise Characteristics" Proc. IRE 25, 472 (1937) as;

$$N_o = k \frac{f^2}{\left(\frac{C}{N}\right)_{IF} B_{IF}} \tag{14}$$

Substituting $k \ (\Delta f)^2 = TT$ into (2) gives;

$$P_o = \frac{k \ (\Delta f)^2 \ K}{B}$$

Dividing by (14) gives:

$$TPR = \frac{P_o}{N_o} = \frac{(\Delta f)^2 \ K\left(\frac{C}{N}\right)_{IF} (B)_{IF}}{B \ f^2} \tag{15}$$

For Mojave and Cooby Creek (8.8 dbm0 loading);

$$\text{TPR (db)} = 138.8 + \left(\frac{C}{N}\right)_{IF} - 20 \log (f) \qquad (16)$$

for Rosman (15.8 dbm0 loading);

$$\text{TPR (db)} = 137.9 + \left(\frac{C}{N}\right)_{IF} - 20 \log (f) \qquad (17)$$

from (16) and (17), the computed TPR values for various channel frequencies are;

$$\text{TPR (db)} = V + \left(\frac{C}{N}\right)_{IF}$$

where V is calculated to be:

Channel Frequency	Mojave and Cooby Creek (240 Channels, 8.8 dbm0)	Rosman (1200 Channels, 15.8 dbm0)
342	28.1	27.2
768	21.1	20.2
1002	18.6	17.7
1248	16.6	16.0
2438	-	10.2
3886	-	6.1
5340	-	5.2

7.6 BACKGROUND MATERIAL FOR ANALYSIS OF MULTIPLEX TEST DATA

The following items are contained in this paragraph:

1) Normalization of System Noise Temperature
2) FDM Multiplex User Requirements
3) System Loading
4) Calculation of Overall Carrier-to-Noise Ratio
5) Differential Doppler Effects

7.6.1 NORMALIZATION OF SYSTEM NOISE TEMPERATURE AND CARRIER TO NOISE RATIO

The normalization technique presented herein is applicable to both the loaded and unloaded conditions only as long as the system is thermal noise limited; i.e., the intermodulation noise is at least 10 db less than the thermal noise. For higher values of intermodulation noise, the loaded S/N or NPR values must be separated into thermal and intermodulation components. The thermal noise component is then normalized, and recombined with the intermodulation component (which is unchanged due to the normalization). The unloaded S/N or TPR value contains only thermal noise and may be normalized directly.

The loaded S/N (or NPR) may be separated into its thermal and intermodulation products by solving for K_2 as follows:

$$K_2 = \frac{K_1 K_3}{K_1 - K_3} \tag{1}$$

where: K_2 = intermodulation term (proportional to the reciprocal of the IM power)

K_1 = unloaded S/N (or NPR)

K_3 = loaded S/N (or NPR)

After normalizing the K_1 term (S/N or TPR) the normalized loaded S/N (or NPR) is determined as follows:

$$K_3 = \frac{K_1 K_2}{K_1 + K_2} \tag{2}$$

Note: Solutions to equations (1) and (2) for values expressed in db are shown in figures 7.10 and 7.11, respectively, presented in paragraph 7.6.4.

7.6.1.1 System Noise Temperature Normalization

It is desirable to normalize the measured and predicted values to account for known variations within a group of test runs in order to compare the results on a common basis. To this end, the test data may be normalized to a particular system noise temperature or CNR.

1) Calculate the change in the downlink carrier to noise ratio (ΔK_d) as follows (in db);

$$\Delta K_d = 10 \log_{10}\left(\frac{T_s}{76}\right)$$

2) To normalize the predicted value for $T_s = 76°K$, add ΔK_d to the downlink carrier-to-noise ratio and proceed to calculate the overall signal-to-noise ratio as described in paragraph 7.1 of this section.

3) To normalize the measured value for $T_s = 76°K$, add ΔK_d, (in db) to the measured value of S/N. The error introduced by adding ΔK_d to the overall S/N value rather than adding it to only the downlink component is less than ±0.05 db as long as the uplink S/N is at least 10 db greater than the downlink S/N. When this condition is not met the effect of the uplink S/N becomes significant and must be taken into account. In this event, the overall S/N is effected as follows:

Let k_o = overall signal-to-noise ratio (before normalization)

k_o' = overall signal-to-noise ratio (after normalization)

k_1 = uplink signal-to-noise ratio

k_2 = downlink signal-to-noise ratio

k_t = ratio of measured to normalized system noise temperature ($T_s/76$ for normalization to 76°K).

The above values are all numerical ratios

$$k_o = \frac{k_1 \, k_2}{k_1 + k_2} \tag{1}$$

$$k_o' = \frac{k_1 \, k_t \, k_2}{k_1 + (k_t k_2)} \tag{2}$$

From (1) and (2)

$$\frac{k_o'}{k_o} = \frac{k_t(k_1 + k_2)}{k_1 + k_2 \, k_t}$$

letting $\frac{k_1}{k_2} = k$ we have;

$$\frac{k_o'}{k_o} = \frac{k_t \, (k + 1)}{k + k_t} \tag{3}$$

for $k_t \ll k \gg 1$ $\quad \frac{k_o'}{k_o} = k_t$

for $k_t \gg k$

$$\frac{k_o'}{k_o} = k + 1$$

The change in multiplex-channel signal-to-noise ratio, $\triangle$ S/N, may be determined from equation (3). An approximation to equation (3) has been developed, which is accurate to within ±0.05 db for small changes in system noise temperature ($\triangle T_s < 2$ db); in db we have;

$$\triangle \frac{S}{N} = (0.05 \text{ K} + 0.5) \text{ K}_d \text{ for } 10 > \text{ K} > -10$$

$$\triangle \frac{S}{N} = \triangle K_d \text{ for K} \geqslant 10$$

$$\triangle \frac{S}{N} = 0 \text{ for K} < -10$$

where $\quad$ $K_d = 10 \log_{10} \triangle k_t$

$K = 10 \log_{10} k =$ uplink signal-to-noise ratio (in db) minus downlink signal-to-noise ratio.

Values of K are given in table 7.4. These values were calculated from the performance calculations presented in paragraph 2.4.

7.6.1.2 <u>CNR Normalization</u>

The S/N (or NPR) data is normalized for carrier-to-noise-ratio (CNR) in exactly the same manner as outlined above for the system noise temperature normalization, the only difference being that K_t is now equal to the ratio of the normalized CNR to the measured CNR (for a complete discussion of overall carrier-to-noise ratio, refer to paragraph 7.6.4).

7.6.2 FDM MULTIPLEX USER REQUIREMENTS

The user requirements are based upon CCIR and RETMA recommendations for FDM telephony. The recommendations are as follows;

1. RETMA recommendation TR-141 (par. 2.7) (Microwave Relay Systems for Communications)

TABLE 7.4. K FACTOR VARIATION

Station	Satellite	Transponder No.	TWT'S	K Factor (db)	
				SSB–PM (MA) Mode**	FT Mode*
Rosman	ATS–1	1 & 2	One	2.0	5.3
		1 & 2	Two	-0.8	2.5
	ATS–3	1	One	-0.3	1.6
		1	Two	-2.7	-0.6
		2	One	-4.1	-2.2
		2	Two	-6.9	-5.0
Mojave	ATS–1	1 & 2	One	9.4	11.4
and		1 & 2	Two	6.6	8.5
Cooby Creek	ATS–3	1	One	7.1	9.0
		1	Two	4.7	6.6
		2	One	3.3	5.5
		2	Two	0.5	2.4

*Uplink C/N - downlink C/N

** Uplink T T/N (idle) - downlink T T/N (idle)

"2.7.2 Standard:

The Telephone Channel rms signal-to-rms noise ratio shall be at least 35 db 95 percent of the time, and shall be at least 25 db 99 percent of the time. Unweighted in both cases.

As an option for telephone channel (voice) only, the rms signal-to-rms noise with FIA weighting shall be 45 db 95 percent of the time and 35 db 99 percent of the time."

2. CCIR recommendation 353-1 XI th Plenary Assembly, Oslo, 1966.

ACTIVE COMMUNICATION-SATELLITE SYSTEMS

FOR FREQUENCY-DIVISION MULTIPLEX TELEPHONY

(Question 2/1V)

"The CCIR,

CONSIDERING

(a) that the basic hypothetical reference circuit is intended as a guide to the design and construction of actual systems;

(b) that the costs of establishing and maintaining communication-satellite systems are critically dependent on the overall signal-to-noise performance requirements;

(c) that the total noise power in the basic hypothetical reference circuit should not be such, as would affect appreciably conversation in most telephone calls or the transmission of telephone signalling;

(d) that the extent of fading cannot be determined fully until more experimental data are available, but is not expected to be appreciable in active communication-satellite systems;

(e) that there may be other sources of noise of short duration;

UNANIMOUSLY RECOMMENDS

1. that the noise power, at a point of zero relative level in any telephone channel in the basic hypothetical reference circuit as defined in Recommendation 352 [1], should not exceed the provisional values given below:

1.1 10 000 pW psophometrically-weighted mean power in any hour; $\left(\dfrac{TT}{N} = 50 \text{ db}\right)$ TT = Test-tone power level.

1.2 10,000 pW psophometrically-weighted one-minute mean power for more than 20 percent of any month; $\left(\dfrac{TT}{N} = 50 \text{ DB}\right)$

_____

(1) The reference circuit is from ground station to satellite to ground station and does not include ground microwave or cable links.

7.40

1.3 50,000 pW psophometrically-weighted one-minute mean power for more than 0.3 percent of any month; ($\frac{TT}{N}$ = 42 db)

1.4 1,000,000 pW unweighted (with an integrating time of 5 ms), for more than 0.03 percent of any month; ($\frac{TT}{N}$ = 42 db)

2. that the following Notes should be regarded as part of the Recommendation:

Note 1. - Noise in the multiplex equipment is excluded from the above.

Note 2. - It is assumed that noise surges and clicks from power-supply systems and from switching apparatus (including switching from satellite to satellite) are reduced to negligible proportions and therefore will not be taken into account when calculating the noise power.

Note 3. - In applying the basic hypothetical reference circuit and the allowable circuit noise to the design of satellite and earth-station equipment for a given overall signal-to-noise performance, the system characteristics preferred by the CCIR, as found in its Recommendations, should be used where appropriate; where more than one value is recommended, the designer should indicate the value chosen; in the absence of preferred values, the designer should indicate the assumptions used. "

It should be noted that both the CCIR and RETMA recommendations are statistical in nature in so far as they recommend percentages of total time for which the TT/N is not to fall below a certain value. Since the number of test runs and the time base used for the ATS experiment is not sufficient to determine similar statistical performance, a conservative value of 50 db will be used as a nominal value of $\frac{TT}{N}$ which will satisfy the user requirements.

7.6.3 SYSTEM LOADING

The weighted TT plus noise-to-noise ratio is obtained by comparing the measured power present in a multiplex receive channel, when a standard channel test tone is transmitted in that channel, with the measured noise power present when the tone is removed. The satellite is noise-loaded by means of a white noise spectrum, adjustable in bandwidth and power level, to simulate up to a maximum of 1200 one-way voice channels, depending on the system configuration.

Since the satellite carries traffic in both directions, it is a two-wire device, at least in the same sense as is a single coaxial cable which carries traffic in two directions using different parts of the total available baseband for the two directions.

From the viewpoint of the satellite transponder, therefore, full loading is obtained with a total spectrum width of 1200 channels, and full loading of $(-15 + 10 \log_{10} 1200 = 15.8$ db) relative to test-tone level. In the case of <u>full</u> satellite loading and two ground stations, it makes no difference whether one considers the satellite to be loaded with 1200 channels in one direction, or 600 in each of two directions. As far as the ground station is concerned, it is carrying channels in one direction only through its transmitter, but <u>in both directions</u> (from itself as well as any other station), through its receiver. This is so because the PhM receiver receives and demodulates all the channels transmitted by the satellite, regardless of whether or not they are used at that station.

In single-station tests, it is sometimes desirable to load the satellite with "half" loading; i.e., N/2 channel loading for the N channel spectrum. It is for this reason that the <u>half</u> loading test with a 1200-channel spectrum, $(-18 + 10 \log_{10} 1200 = 12.8$ db loading) is used. Using ATS-3, with its higher receiving antenna gain, it is possible to fully load the satellite from either Mojave or Rosman, without exceeding the ground transmitter output power rating. The Mojave station, which has a smaller antenna than Rosman, in further limited in EIRP and thus, when running ATS-1 tests, must operate with a smaller number of channels even when using half-power loading. The tests are thus conducted with Mojave and Cooby Creek transmitting 120 one-way channels in a 240 spectrum $(-1 + 4 \log_{10} 120 = 7.3$ db loading) or 240 channels in a 240-channel spectrum (8.8 dbm0 loading). Using the ATS-3 satellite, it is possible to fully load the 1200-channel spectrum from Mojave and Rosman (15.8 dbm0 loading).

The channel loading from each earth station is determined according to the formula given in CCITT Recommendation G 222.

For systems amplifying in one direction only (as with the earth stations), we have:

$$n(\bar{P}) = -15 + 10 \log_{10} N \text{ db for } N \geq 240 \tag{1}$$

$$n(\bar{P}) = -1 + 4 \log_{10} N \text{ db for } 12 \leq N < 240 \tag{2}$$

for systems amplifying in two directions (as with the satellite in the MA Mode) we have;

$$n(\bar{P}) = -0.1 + 5 \log_{10} N \text{ db for } 12 \leq N \leq 240 \tag{3}$$

$$n(\bar{P}) = -12 + 10 \log_{10} N \text{ db for } N > 240 \tag{4}$$

where $n(\bar{P}) =$ white noise power

$N =$ number of one way channels

It should be noted that application of (1) and (4) yield the same result; for instance, simulation of 1200 one-way channels requires the same loading as 600 two-way channels.

Let us now consider cases where a station transmits a relatively small number of channels, less than 240 in one direction. If for example, there were two stations each sending 100 channels (that is there were two stations with a total of 100 two-way channels between them), then formula (3) would give a load of $(-0.1 + 5 \log_{10} 100) = +9.9$ db. This is not the same as for 200 one-way channels. For $N < 240$, formula (2) applies, and for 200 one-way channels this gives +8.2 db loading, which is quite significantly different from +9.9 db. If we had three stations, each sending say 100 one-way channels, we would get a yet different loading, not covered by any of the CCITT formulae.

Therefore, we can say that providing there is a limited number of stations, and that they are each transmitting a large number of channels (more than 240 one-way channels each) it is perfectly satisfactory to use loading of $(-15 + 10 \log_{10} N_r)$ db (where N_r is the number of channels for the rth station) for the ground transmitters at the N stations; and it is also satisfactory to use $(-15 + 10 \log_{10}(N_1 + N_2 \ldots + N_r \ldots))$ db total loading for the satellite and the receivers. Where there are stations using only a small number of channels, their ground transmitters, which carry traffic in one direction only, should be loaded as if they were each carrying the appropriate number of one-way channels. This will result in the satellite loading being somewhat incorrect. However, in our case where the satellite capacity is 1200 channels, and there are only three ground stations, the error will not greatly affect total performance.

7.6.4 CALCULATION OF OVERALL CARRIER-TO-NOISE RATIO

The overall carrier-to-noise ratio (CNR) of the ATS system is determined by the CNR's of the uplink as well as the downlink. The link with the smaller value will predominate, however, the effect of the larger value may be significant even with as much as 10-db difference between the links (a 10-db difference in CNR will result in an overall·CNR of 0.4 db less than that of the smaller link). As the difference between the CNR's becomes less, the larger value becomes even more significant. In many normalization processes, it is important to determine the overall CNR from measured values of received power. Since only the downlink CNR may be determined in this way, the uplink CNR must be calculated from theoretical values. The calculation of the overall CNR from measured data is further complicated by the fact that the received "carrier plus noise" power is measured with the earth station receiving satellite generated noise while the "noise only" power is measured with the earth station antenna pointed away from the satellite, thus receiving no satellite generated noise.

The symbols used in the following derivation are as follows:

$(C/N)_o$	Overall carrier-to-noise ratio
$(C/N)_u$	Uplink carrier-to-noise ratio (determined from system calculations) ·
N_i	Noise at the ground receiver input from the ground receiver and ground antenna
N_{rg}	Noise at the ground receiver input coming from the satellite
P_1	Rms power measured in the IF bandwidth with the ground station in normal operation
P_2	Rms power measured in the IF bandwidth with the ground station antenna pointed 5° to 10° off the satellite.
P_{rg}	Received signal power including satellite noise PhM sidebands (SSB-PhM mode) as well as signal sidebands

7.6.4.1 Determination of $(C/N)_o$ from Measured Data

The overall link carrier-to-noise ratio $(C/N)_o$ is found from measured values of P_1 and P_2 as follows:

1) The total rms power, P_1, in the IF bandwidth is measured with the system in normal operation (IF gain in AGC mode).

2) The total rms power, P_2, in the IF bandwidth is measured with the ground-station antenna pointed approximately 10° away from the spacecraft, and the IF gain set to MGC for the same AGC buss voltage that was used in step 1.

The power measured in step 1 consists of the following components:

$$P_1 = P_{rg} + N_{rg} + N_i \qquad (1)$$

The power measured in step 2 consists of the following components:

$$P_2 = N_i \qquad (2)$$

From (1) and (2);

$$\frac{P_1}{P_2} = \frac{P_{rg} + N_{rg} + N_i}{N_i} = \frac{P_{rg} + N_{rg}}{N_i} + 1 \qquad (3)$$

From which;

$$P_{rg} + N_{rg} = N_i \left(\frac{P_1}{P_2} - 1 \right) \qquad (4)$$

It may be shown that;

$$(C/N)_u = \frac{P_{rg}}{N_{rg}} \qquad (5)$$

Combining (4) and (5) gives;

$$N_{rg} (C/N)_u + N_{rg} = N_i \left(\frac{P_1}{P_2} - 1 \right)$$

This assumes no limiter enhancement;

From which;

$$\frac{N_{rg}}{N_i} = \frac{\left(\dfrac{P_1}{P_2} - 1 \right)}{(C/N)_u + 1} = A \qquad (6)$$

The actual overall carrier-to-noise ratio is given by;

$$(C/N)_o = \frac{P_{rg}}{N_i + N_{rg}} = \frac{\dfrac{P_{rg}}{N_i}}{1 + \dfrac{N_{rg}}{N_i}} = \frac{\dfrac{P_{rg}}{N_i}}{1 + A} \qquad (7)$$

From (4) and (6);

$$\frac{P_{rg}}{N_i} + \frac{N_{rg}}{N_i} = \frac{P_{rg}}{N_i} + A = \frac{P_1}{P_2} - 1 \qquad (8)$$

Combining (7) and (8) gives;

$$(C/N)_o = \frac{\dfrac{P_1}{P_2} - 1 - A}{1 + A} \qquad (9)$$

Combining (6) gives;

$$(C/N)_o = \frac{A(C/N)_u}{1 + A} \qquad (10)$$

7.45

Which is readily solved by substituting for A

From (6) which, for values of $(C/N)_u > 10$, becomes;

$$A = \frac{\left(\dfrac{P_1}{P_2} - 1\right)}{(C/N)_u}$$

So that $(C/N)_o = \dfrac{(C/N)_u \left(\dfrac{P_1}{P_2} - 1\right)}{(C/N)_u + \left(\dfrac{P_1}{P_2} - 1\right)}$ \hfill (11)

Which is of the form $K_3 = \dfrac{K_1 \ K_2}{K_1 + K_2}$

The solution of (11) is considerably aided by the use of the curves shown in figures 7.9 and 7.10, which present the solution of $\left(\dfrac{P_1}{P_2} - 1\right)$ and $\dfrac{K_1 \ K_2}{K_1 + K_2}$ in db form. The uplink carrier-to-noise ratio is determined from system calculations, reproduced for convenience in table 7.5. It may be desirable to determine the required CNR for one link (either uplink or downlink) in order to achieve a predetermined overall CNR with the other link CNR fixed. The solution is found to be of the form.

$$K_1 = \frac{K_3 \ K_2}{K_3 - K_2} \hfill (12)$$

where;

K_1 = unknown link CNR

K_2 = known link CNR

K_3 = overall CNR

Figure 7.11 presents the solution of (12) in db form.

TABLE 7.5. THEORETICAL UPLINK CARRIER-TO-NOISE RATIO

Satellite	ATS-1	ATS-3	
Transponder	No. 1 or 2	No. 1	No. 2
FT Mode (CNR in 35.5-MHz Noise BW) (CNR in 15.5-MHz Noise BW)	18.4 22.0	18.9 22.5	19.4 23.0
SSB-PhM Mode Equivalent CNR in 35.5-MHz Noise BW 15.5-MHz Noise BW	4.4+L 8.0+L	4.9+L 8.5+L	5.4+L 9.0+L
L = CCIR Loading 8.8db for 240 Channels 15.8db for 1200 Channels			
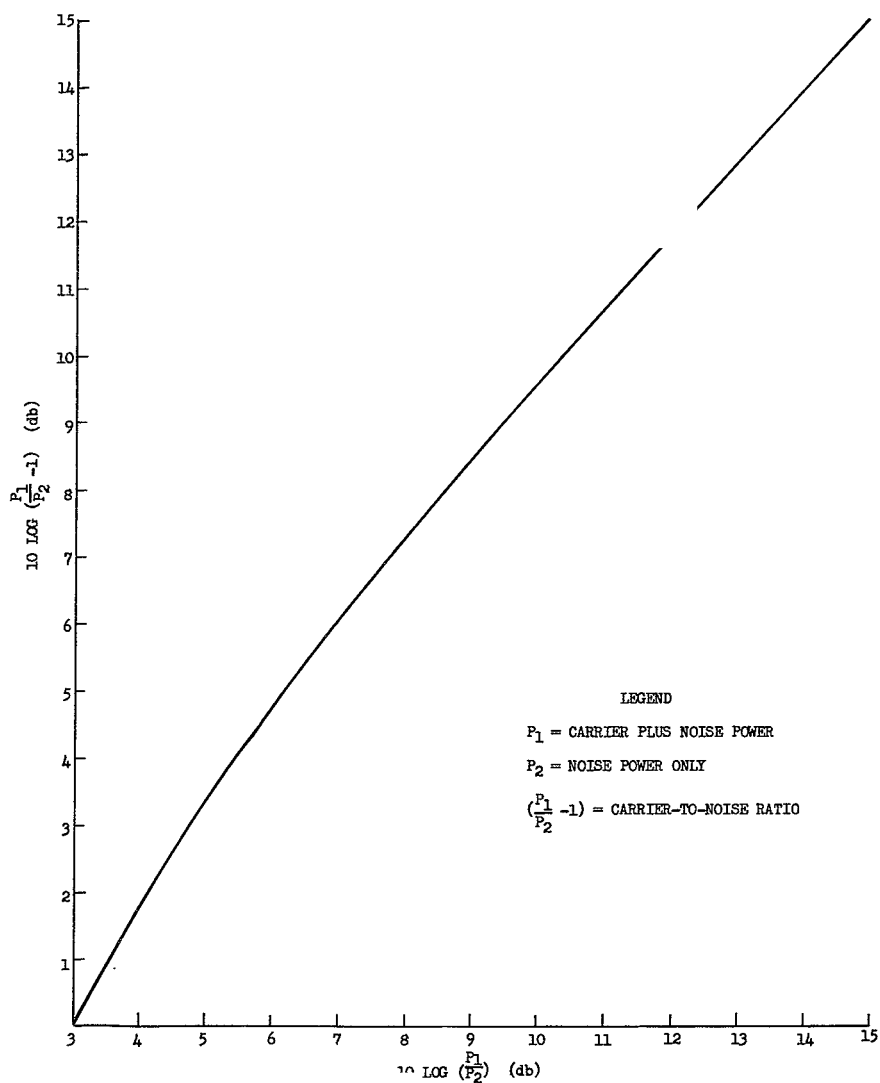
Figure 7.9. Carrier-to-Noise Ratio Conversion Nomogram

$$K_3 = \frac{K_1 \, K_2}{K_1 + K_2} \quad \text{(RATIO)}$$

$$K_3 = K_2 - \text{(C.F.)} \quad \text{(db)}$$

$$K_1 > K_2$$

K_1/K_2	C.F.
11db	0.34 db
12db	0.25 db
13db	0.20 db
16db	0.10 db
20db	0.04 db

EXAMPLE
LET $K_1 = 30$ db
       $K_2 = 21$ db
THEN $K_3 = K_2 - \text{(C.F.)} = 21 - 0.5 = 20.5$ db

LEGEND

K_1 = LINK "A" CNR

K_2 = LINK "B" CNR

K_3 = OVERALL CNR

C.F. IN db

K_1 (IN db) $-$ K_2 (IN db)
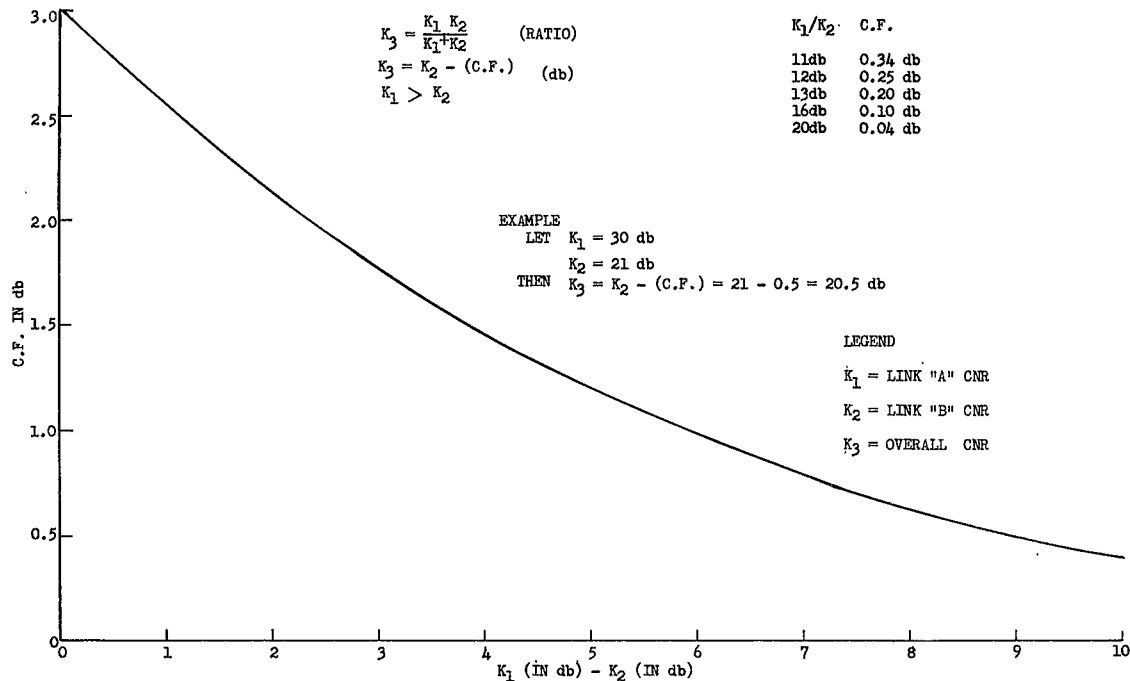
Figure 7.10. Overall Carrier-to-Noise Ratio Determination Nomog

$$K_2 = \frac{K_3 \quad K_1}{K_3 - K_1} \quad \text{(NUMERIC)}$$

$$K_2 = K_3 - \text{(C.F.)} \quad \text{(db)} \quad K_3 \geq K_1$$

LEGEND

K_1 = LINK "A" CNR

K_2 = LINK "B" CNR

K_3 = OVERALL CNR

EXAMPLE:
LET K_3 = 46.9 db
       K_1 = 40.9 db
THEN K_2 = K_3 - (C.F.)
       = 46.9 - 4.6 = 42.3 db
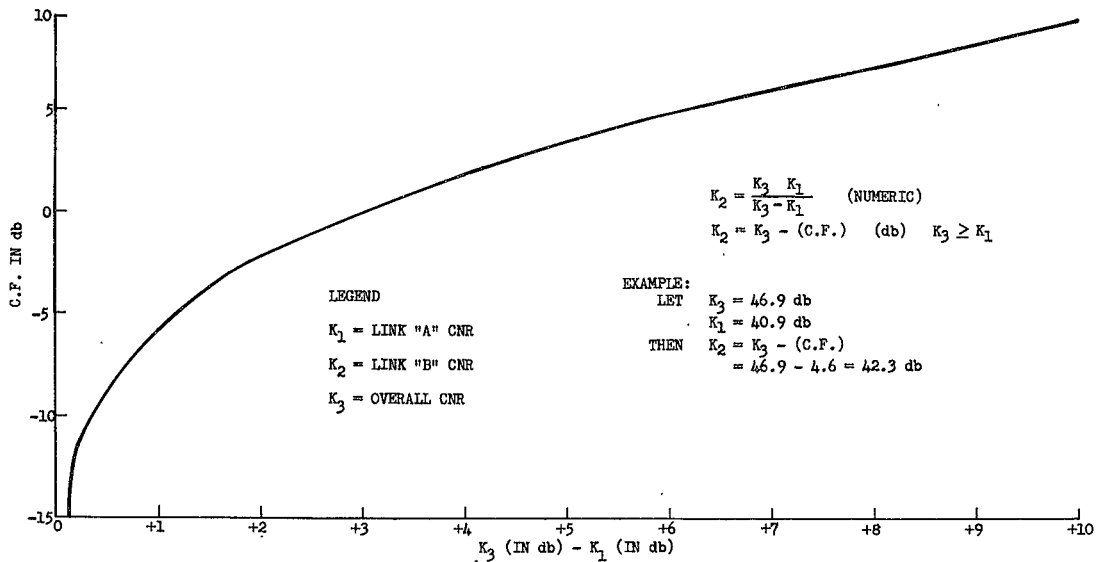
Figure 7.11. Link Carrier-to-Noise Ratio Determination Nomogram

7.6.5 DIFFERENTIAL DOPPLER EFFECTS

The derivations developed in this paragraph show the effects of satellite spin modulation (1.6 Hz for ATS-1 and ATS-3) on the frequency stability of an FDM voice channel subcarrier (7.6.5.1). The effect of observed range rate on the FDM channel frequency stability is also considered (7.6.5.2). Both effects contribute a negligible amount of instability as the following derivations show.

7.6.5.1   Determination of Peak-Frequency Deviation of an FM Signal Due to Satellite Spin (1.6-Hz phase modulation)

The theoretical magnitude of the frequency deviation of a multiplex-channel sub-carrier due to movement of the satellite receiver antenna phase center is derived in this paragraph. The derivation is based upon the 5-MHz FDM channel subcarrier, since it represents the worst case condition. As shown in figure 7.12, the satellite receive antenna phase center rotates about the satellite spin axis at the satellite spin rate.

From figure 7.12

D = distance from ground antenna to satellite geometric center (spin axis).

D_ϕ = distance from ground antenna to satellite receive antenna phase center.

δ = diameter of circle swept by rotation of satellite antenna phase center.

Then $D_\phi = D + \dfrac{\delta}{2} \cos \omega t$

and, assuming a satellite 1.6-Hz spin rate,

$$D_\phi = D + \frac{\delta}{2} \cos 10\, t \qquad\qquad (1)$$

To determine the maximum phase deviation due to δ ;

$$\mu = \frac{2\,\pi\,\delta}{\lambda}$$

$$\delta = \frac{\mu\,\lambda}{2\,\pi} \qquad\qquad (2)$$

where μ = maximum phase deviation

λ = wave length of uplink signal in question.

The ground-received signal with transmitter in normal AFC mode is effected by the error cancellation circuits, so that $\delta_{observed}$ differs from δ_{actual} in the following manner:

$$\delta_{actual} = \frac{\delta_{observed}}{2 \sin \frac{\omega T}{2}} = \frac{\lambda \mu}{4\,\pi \sin \pi f T} \quad \text{where } f = \text{satellite spin rate (1.6 Hz)}$$
$$T = \text{system transport Lag.}$$

From special Fourier Analysis Tests, the peak deviation observed in the MA mode at 1.6 Hz is 1.26 Hz. From this,

$$\mu = \frac{\Delta f}{f_a} = \frac{1.26}{1.6} = .79 \text{ radians.}$$

$\Delta f = 1.26$

$$\therefore \delta_{actual} = \frac{.79(4.8)}{4\pi \operatorname{Sin} \pi (1.6)(.26)} = \frac{3.78}{4(3.14) \operatorname{Sin} .42 \pi} = \frac{3.78}{12.56 (.98)} = .307 \text{ cm.}$$

Assuming a 5-MHz channel in the FT mode of operation,

$$\mu = \frac{2\pi(.307)}{\lambda_{5\ MHz}} = \frac{2\pi(.307)}{6000} = \frac{1.93}{6000} = 3.2 \times 10^{-4} \text{ rad.}$$

$f = 5$ MHz (uplink)

Assuming the same μ for downlink also,

$$\mu_{total} = 6.4 \times 10^{-4} \text{ radians}$$

$f = 5$ MHz

$$\Delta f_{total} = 1.6 \times 6.4 \times 10^{-4} = 10.24 \times 10^{-4} = .001 \text{ Hz}$$

It is concluded that the overall change in deviation of an FM signal due to the observed variation in phase center of the ATS-1 satellite is negligible for all practical purposes.

7.6.5.2   <u>Variations in Channel Test-Tone Frequency in FT Mode Due to Satellite Range Rate</u>

The purpose of this paragraph is to determine the theoretical effect of range acceleration of a synchronous satellite on the frequency stability of a multiplex-channel sub-carrier in the FT mode.

Actual range rate data of ATS-1 and ATS-3 is used to determine the effect on the worst case condition (FDM channel with a 5-MHz channel subcarrier).

From Figure 7.13

r = satellite range

$\dot{r}$ = rate-of-change of range (range rate) = $\frac{dr}{dt}$ = A Sin ωt

for $\omega t = \pi$ and t = 12 hours,

$\omega = \pi/12$ rad/hr

so that;

$\dot{r}$ = A Sin $\pi t/12$

Nominal Value of A for ATS-1: Between 3'/sec and 8'/sec

ATS-3: Between 3'/sec and 12'/sec

Assume nominal value of 6'/sec:

$$\dot{r} = 6 \, \text{Sin} \, (\pi t/12)$$

$$\ddot{r} = \pi/2 \, \cos \, \pi t/12$$

Now, $\delta f = 2\dot{r}f/c = \dfrac{2(6f)}{c} \text{Sin} \, \pi t/12$

$\delta_f^{\,\prime} = \ddot{r}f/c$

Subst: $\dot{\delta} f = \pi f/c \, \cos \, \pi t/12$

δf = frequency shift due to doppler

$\dot{r}$ = range rate

c = speed of light (9.84×10^8 ft/sec)

f = measurement frequency

Therefore, for a 5-MHz channel, over a test period of one hour, assuming the max $\dot{r}$ = 6 ft/sec for the 24-hour period encompassing the test, the expected rate of change of differential doppler δf is

$$\dot{\delta} f = \frac{\pi (5 \times 10^6)}{(9.84 \times 10^8)} \, \cos \, \pi t/12 = \frac{15.70 \times 10^6}{9.84 \times 10^8} \, \cos \frac{\pi t}{12}$$

the maximum rate of change of differential doppler occurs at t = 0

$$\dot{\delta} f = \frac{(5 \times 10^6) \pi}{(9.84 \times 10^8)} = \frac{15.70 \times 10^6}{9.84 \times 10^8} = 1.6 \times 10^{-2} = .016 \, \text{Hz/hr}$$

The δf occuring between t = 0 and t = 1 hour in figure 7.13 for a 5-MHz channel is:

$$\delta f \Big|_{t=0} - \delta f \Big|_{t=1} = \frac{2 \times 6 (5 \times 10^6)}{9.84 \times 10^8} \left[0 - \text{Sin} \, \pi/12 \right]$$

$$= \frac{2 \times .26 \times 30 \times 10^6}{9.84 \times 10^8} = \frac{15.60 \times 10^6}{9.84 \times 10^8} = .016 \, \text{Hz}$$

The maximum observable change in frequency over a six-hour period is:

$$\delta f \Big|_{t=0} - \delta f \Big|_{t=6} = \frac{2 \times 6 \, (5 \times 10^6)}{9.84 \times 10^8} = 6.0 \times 10^{-2} = .06 \, \text{Hz}$$

After station changing maneuvers, a range rate of 52 ft/sec (ATS-3) has been observed. The maximum change in frequency in a 5-MHz multiplex channel over a period of one hour is:

$$\delta f_{t=0} - \delta f_{t=1} = \frac{2 \times 52(5 \times 10^6)}{9.84 \times 10^8} \left[0 - \text{Sin } \pi/12 \right] = .138 \text{ Hz}$$

and over a six hour period:

$$\delta f_{t=0} - \delta f_{t=6} = \frac{2 \times 250}{9.84} \times 10^{-2} = .53 \text{ Hz}$$

From this brief consideration, it is concluded that the effects of range rate and range acceleration of the ATS synchronous satellites on multiplex-channel frequency stability in the FT mode is of no practical significance, even in the worst case observed thus far.
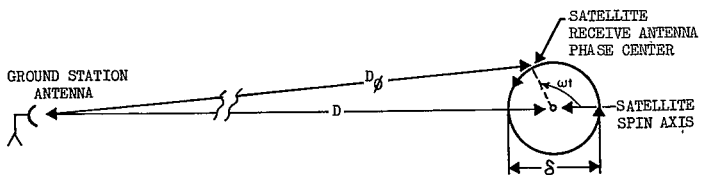
Figure 7.12. Satellite Phase Center Geometry
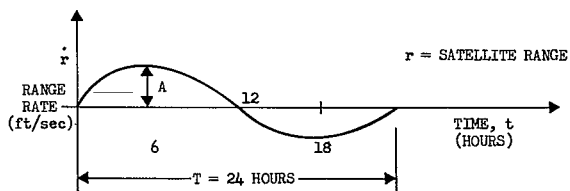
Figure 7.13. Time Variation of Range Rate

7.7 INTERMODULATION PREDICTION TECHNIQUE

The purpose of this section is to develop a technique for computing the inter-modulation (I) noise level from non-linear characteristics in a communication system that must handle a large number of telephony channels. This technique will involve theoretical results from several papers on intermodulation noise and the results from two-tone tests and group delay measurements conducted on the system under investigation. Also included in this section is an extention of the analysis technique developed in these papers for frequency-modulation systems to phase-modulation systems so that the SSB/PhM (MA) mode as well as the FT mode (frequency-modulation) can be analyzed.

7.7.1 FT MODE

In the FT mode, intermodulation noise in the receiver baseband output is primarily due to two factors: amplitude and phase non-linearities. Individual sources of amplitude non-linearities includes the FM modulator, FM demodulator, and baseband equipment. The system IF/RF sections of the earth station transmitter, S/C, and earth-station receiver are the primary sources of phase non-linearities.

7.7.1.1 Intermodulation Distortion Due to Amplitude Non-Linearity

If the transfer characteristics from the input to the modulator to the output of the receiver baseband amplifier (ignoring the effect of phase non-linearities which are considered separately) are expressed as a power series expansion in voltage, it can be shown that for a one-tone input, the following equation can be derived:

$$P_{hn} = t_n \, (P_f)_1^n \tag{1}$$

where:

P_{hn} = Individual harmonic power of order n.

t_n = Harmonic power of order n in milliwatts produced by that sinusoidal input which gives a fundamental output power of 1 milliwatt.

$(P_f)_1$ = Power of an individual fundamental output tone.

For a two-tone input, the following equation can be derived

$$P_{in} = K_1 \, t_n \, (P_f)_1^n \tag{2}$$

where:

K_1 = 4 for a $(f_2 \pm f_1)$ or $(f_1 \pm f_2)$ type 2nd-order product

= 9 for a $(2f_2 \pm f_1)$ or $(2f_1 \pm f_2)$ type 3rd-order product

= 16 for a $(3f_1 \pm f_2)$ or $(3f_2 \pm f_1)$ type 4th-order product

$$= \text{36 for a } (2f_1 \pm f_2) \text{ or } (2f_2 \pm 2f_1) \text{ type 4th-order product}$$

$$= \text{100 for a } (3f_1 \pm 2f_2) \text{ or } (3f_2 \pm 2f_1) \text{ type 5th-order product}$$

P_{in} = Individual intermodulation power of order n.

$(P_f)_1$ = Power of each individual fundamental output tone.

Brockbank and Wass[53] have shown that the total noise power, T_n, of order n for an input signal which is white noise between the limits $f_2 - f_1$ can be given by the following relationship:

$$T_n = 2^{n-1} \, n \, ! \, t_n \, P^n \qquad\qquad (3)$$

where

P = the total fundamental power of the output signal.

By a series of convolution integrals it is possible to develop the shape of the various n[th] order baseband noise spectra that show how T_n is distributed across the baseband. Figure 7.14 shows the second-and third-order intermodulation spectra $(F_n \ (\omega)$ for the 240-channel case. The area under these curves is normalized to unity while the abscissa frequency is normalized to the baseband signal bandwidth. Also shown is the baseband signal spectrum extending from 0.3 to 1.3 in normalized frequency units. Figure 7.15 shows the same spectra for the 1200-channel case. The input spectrum for the 1200-channel case extends from 0.06 to 1.06.

The total area under each curve represents the total distortion power for a given order. Hence, the nth order intermodulation power, d_n, in a certain multiplex channel, located at frequency f_1 with a frequency width of b (4 kHz) will be,

$$d_n = T_n \, F_n \ (\omega \ ) \, b^1 \qquad\qquad (4)$$

where b^1 is the normalized frequency width of the multiplex channel, since the frequency scale in figures 7.14 and 7.15 is normalized with respect to the signal bandwidth B. It follows that

$$b^1 = \frac{b}{B} = \frac{1}{N} \qquad\qquad (5)$$

where N is the total number of 4-kHz channels in the bandwidth B.

Therefore,

$$d_n = \frac{2^{n-1} \, n! \, t_n \, P^n \, F_n \ (\omega)}{N} \qquad\qquad (6)$$

The fundamental signal power in the same bandwidth, b^1, is $(\frac{b}{B})P$. The non-linear noise margin, S_n, of order n then becomes,

$$S_n = \frac{bP}{Bd_n} = \frac{1}{2^{n-1} \; n! \; t_n \; P^{n-1} \; F_n(\omega)} \tag{7}$$

This non-linear noise margin of order n is actually a signal density-to-n[th] order intermodulation noise density ratio. This ratio is similar to the well known NPR measurement. In the NPR measurements, all noise components make up the total noise level, rather than just a particular order of intermodulation noise given in equation (7).

If equation (1) or (2) is divided into the fundamental power used for each of the tones in the two tone input, the harmonic, H_{nr}, or intermodulation margin, I_{nr}, can be obtained. These results are given as follows,

$$H_{nr} = \frac{(P_f)_1}{P_{hn}} = \frac{1}{t_n \; (P_f)_1^{n-1}} \tag{8}$$

$$I_{nr} = \frac{(P_f)_1}{P_{in}} = \frac{1}{K_1 \; t_n \; (P_f)_1^{n-1}} \tag{9}$$

If the fundamental power of each tone, $(P_f)_1$, used in a two-tone test is equal to one-half of the total fundamental power, P, used in a noise-loading test, or $(P_f)_1$ used in a one-tone test, then equations (8) and (9) substituted into equation (7) yields a convenient relationship between two-tone test results (harmonic or intermodulation margins are obtained from two-tone tests) and S_n, the non-linear noise margin of order n. Thus for the condition $P/2 = (P_f)_1$

$$S_n = \frac{K}{2^{2n-2} \; n! \; F_n(\omega)} \; I_{nr} \tag{10}$$

$$S_n = \frac{1}{2^{2n-2} \; n! \; F_n(\omega)} \; H_{nr} \tag{11}$$

For a one-tone test where the fundamental power $(P_f)_1$ is equal to the total fundamental power, P, of a noise-loading test, the following relationship is obtained for the non-linear noise margin, S_n.

$$S_n = \frac{1}{2^{n-1} \; n! \, F_n(\omega)} \; H_{nr} \tag{12}$$

7.7.1.2 Intermodulation Distortion Due to Phase Non-Linearity

When the IF-RF phase transfer function of a system is not linear with frequency and an angle-modulated signal is being transmitted through the system, then intermodulation distortion will occur at the baseband output of the demodulator. The distortion caused by this phase non-linearity may be determined by assuming that the phase non-linearity distorts the instantaneous frequency deviation of the modulated signal, $\phi_i'(t)$, and that the non-linear phase transfer characteristics of the IF/RF sections may be represented as a power-series expansion of the above frequency deviation. For example, where $\phi_n(t)$ is the phase variation of the signal at the input to the demodulator and $\phi_i(t)$ is the phase variation of the signal at the modulator output, then $\phi_n(t)$ can be represented as

$$\phi_n(t) = \phi_i(t) + b_2 \left[\phi_i'(t)\right]^2 + b_3 \left[\phi_i'(t)\right]^3 + \ . \ . \ . \tag{13}$$

The terms b_2 and b_3 are constants of the IF/RF phase variation. The voltage output of the discriminator is proportional to the instantaneous frequency deviation, or $\phi_n'(t)$, the derivative of the signal phase variation $\phi_n(t)$. The following analysis is based upon the fact that equation (13) is a valid approximate model for phase non-linearities.

The actual harmonic power, P_{hn}, at the output of the discriminator for a single sinusoidal input tone can be shown to be

$$P_{hn} = \omega_f^2 \ n^2 t_n' \ (P_f)_1^n \tag{14}$$

where

ω_f = The frequency of the fundamental tone

$n^2 t_n'$ = Harmonic power in mW, of order n produced by that sinusoidal input, which gives a fundamental power output of 1mW, at an angular frequency W_f of unity.

Similarly, an intermodulation product, P_{in}, formed in a two-tone test can be shown to be for two equal power tones,

$$P_{in} = K_1 \ \omega^2 \ t_n' \ (P_f)_1^n \tag{15}$$

where

ω = the frequency at which the intermodulation tone occurs

K_1 = same as in equation (2)

Also it can be seen in equation (15) that the power of the intermodulation products vary directly with the square of the baseband frequency at which the product occurs.

.

7.59

For a white noise continuous input spectrum with normalized frequency limits of ω_1 to ω_2, the total distortion power of order n in a specific channel located at ω_3, is given by

$$d_n^1 = \frac{T_n F_n{'}(\omega_3)}{N} \qquad (16)$$

where

$$F_n{'}(\omega) = \omega^2 F_n(\omega)$$

The intermodulation spectra $F_n{'}(\omega)$ for the second and third order for the 240-and 1200-channel cases is given in figures 7.16 and 7.17, respectively. The intermodulation spectrum of a given order for the phase non-linearity can be derived from the amplitude spectrum by essentially multiplying each ordinate value by ω^2. This causes the phase intermodulation spectrum to be skewed to the higher frequency range. Hence, the intermodulation noise in the high channels will be mainly due to phase non-linearity.

Substituting equations (14) and (3) into equation (16), the following expression for the total distortion power of order n in a channel, d_n^1, is obtained. For the one-tone test case where $(P_f)_1 = P$

$$d_n^1 = \frac{2^{n-1} \, n! \, P_{hn} F_n{'}(\omega)}{\omega_f^2 \, N} \qquad (17)$$

The non-linear noise margin can now be calculated for phase nonlinearity. The fundamental power in a channel bandwidth is $(\frac{b}{B})P$.

The non-linear noise margin, S_n, of order n, then becomes for a one-tone test

$$S_n^1 = \frac{b}{B} \, \frac{P}{d_n^1} = \frac{f^2}{2^{n-1} \, n! \, F_n{'}(\omega)} \, H_{nr}^1 \qquad (18)$$

For a two-tone test where the fundamental power of each tone $(P_f)_1$ is equal to one-half of the total fundamental power, P, of a noise-loading test, then it can be shown that S_n^1, the non-linear noise margin can be given by the following relationships. These relationships are derived in a manner similar to the one-tone case. Thus for the condition $(P_f)_1 = (1/2)P$

$$S_n^1 = \frac{K}{2^{2n-1}} \, \frac{2}{(n)! \, F_n{'}(\omega)} \quad I_{nr}^1 \qquad (19)$$

$$S_n^1 = \frac{f^2}{2^{2n-1}(n)! \, F_n{'}(\omega)} \quad H_{nr}^1 \qquad (20)$$

7.7.2 SSB/PhM (MA) MODE

A block diagram of this system is shown in figure 7.25. The baseband input signal is translated to IF, amplified in the earth-station transmitter, and transmitted to the spacecraft. At the spacecraft the amplitude modulated signal is converted to a phase modulated signal by passing the amplitude modulated signal through a limiter. The carrier is multiplied and translated to the downlink transmission frequency. The IF/RF downlink transmission medium includes the spacecraft from the phase modulator to the earth-station demodulator input. The earth station demodulator consists of a discriminator which is then followed by a de-emphasis network.

In the following analysis, the non-linear transfer characteristics of the earth-station transmitter, S/C phase-modulator and earth-station discriminator are represented as power-series expansions with coefficients which are not a function of frequency. The transfer characteristics from the baseband input of the SSB transmitter to the input of the S/C phase-modulator will be expressed as:

$$V_o(t) = a_1 V_i(t) + a_3 V_i^3(t) + a_5 V_i^5(t) + \ldots \tag{21}$$

where $V_i(t)$ is the baseband input signal voltage, $V_o(t)$ is the output voltage and a_1 is the gain from the earth-station baseband input to the input of the spacecraft phase modulator. It is noted that all even order products fall out of band.

Since the S/C phase-modulator may be approximated by a dynamic phase transfer characteristic versus input voltage, the spacecraft-modulator can be represented in a way similar to the earth-station transmitter. The modulator output phase $\phi_m(t)$, is given by

$$\phi_m(t) = b_1 V_o(t) + b_2 V_o^2(t) + b_3 V_o^3(t) + \ldots \tag{22}$$

where b_1, b_2 and b_3 are constants of the spacecraft modulator. The effective frequency deviation, $\dot\phi_m(t)$, at the output of phase-modulator is given by

$$\dot\phi_m(t) = b_1 \frac{dV_o(t)}{dt} + b_2 \frac{dV_o^2(t)}{dt} + b_3 \frac{dV_o^3(t)}{dt} + \ldots \tag{23}$$

where $\dot\phi_m(t) = \omega(t) - \omega_c$, the instantaneous angular frequency deviation from the carrier, ω_c.

As was the case for phase distortion of an FM wave in the FT mode, distortion of the phase-modulated wave due to phase non-linearities is assumed to be represented as a power-series expansion of the effective frequency deviation of the phase-modulated signal. Thus, the phase variation to the input of the earth-station demodulator, ϕ_t, is represented by

$$\phi_t(t) = \dot\phi_m(t) + c_2 \left(\dot\phi_m(t)\right)^2 + c_3 \left(\dot\phi_m(t)\right)^3 + \ldots \tag{24}$$

where c_2 and c_3 are constants, representing the parabolic phase variation and the cubic phase variation of the IF/RF downlink section up to the input of the demodulator. A linear phase-variation term was not included, because linear phase variation only represents a constant delay of the signal and does not add distortion.

The discriminator also adds to the non-linear distortion, and the transfer characteristics of the discriminator is also represented as a power series expansion. The output voltage of the discriminator, V_d, is given by

$$V_d(t) = d_1 \phi_t'(t) + d_2 (\phi_t'(t))^2 + d_3 (\phi_t'(t))^3 + \ldots \tag{25}$$

where d_1, d_2, and d_3 are constants of the discriminator and ϕ_t' is the effective frequency deviation of the phase-modulated signal at the input to the discriminator.

Substituting each power series expansion into the subsequent equations allows the output voltage of the discriminator to be written in terms of the voltage input to the SSB transmitter. Ignoring higher order terms, the discriminator output voltage, $V_d(t)$, is given by

$$
\begin{aligned}
V_d(t) = \; & a_1 b_1 d_1 \frac{dV_i(t)}{dt} + a_3 b_1 d_1 \frac{dV_i^3(t)}{dt} + a_5 b_1 d_1 \frac{dV_i^5(t)}{dt} \\
& + a_1^2 b_2 d_1 \frac{dV_i^2(t)}{dt} + a_1^3 b_3 d_1 \frac{dV_i^3(t)}{dt} + a_1^2 b_1^2 c_2 d_1 \frac{d\left(\frac{dV_i(t)}{dt}\right)^2}{dt} \\
& + a_1^3 b_1^3 c_3 d_1 \frac{d\left(\frac{dV_i(t)}{dt}\right)^3}{dt} + a_1^2 b_1^2 d_2 \left(\frac{dV_i(t)}{dt}\right)^2 \\
& + a_1^3 b_1^3 d_3 \left(\frac{dV_i(t)}{dt}\right)^3 \tag{26}
\end{aligned}
$$

Also assumed in the above equation (26), is that the system has a relative low-intermodulation noise level. That is, harmonic or intermodulation margins for a particular device in the system are typically greater than 25 db. For example, if two tones are transmitted through the system and the lowest intermodulation margin is 25 db, then cross intermodulation spectra formed from two successive non-linear devices will be negligible with respect to the spectra of those terms listed in equation (26).

In equation (26), the first term of the discriminator output voltage represents the fundamental desired signal. The second through eighth terms of the discriminator output voltage in equation (26) represents distortion terms for each of the sources of intermodulation for dominant orders of intermodulation. In table 7.6, each of these terms are listed with the respective source of the distortion term.

The spectral shapes of the output intermodulation noise terms for a band limited white Gaussian noise input can be approximated by first finding the Fourier transform of the auto correlation function of those terms listed in table 7.6. Secondly, each of the power spectrums obtained must be multiplied by the magnitude of the transfer function squared, $\left|\frac{\omega_0}{\omega}\right|^2$, of the de-emphasis network.

As an example of how the spectrums are derived for the various noise terms, the spectral shape of the fourth term of equation (26), $\frac{d V_i^2(t)}{dt}$, will be calculated. This term corresponds to second-order, S/C, intermodulation noise. It will be assumed that the modulation consists of white, Gaussian noise, between the band limits of $f_1 = 0.316$ MHz and $f_2 = 5.564$ MHz (1200-channel spectrum).

The output spectrum from a process (stationary) which forms the product $X(t) Y(t)$ is given by the Fourier transform of the output autocorrelation of the product formed. In other words, if $W_z(\omega)$ is the spectrum of the product, then the following equation holds,

$$W_z(\omega) = F\left\{R(\tau)\right\} = F\left\{E\left[X(t) Y(t) X(t, +\tau) \; Y(t + \tau)\right]\right\} \tag{27}$$

The term $\frac{d V_i^2(t)}{dt}$ can be rewritten as $2 V_i(t) \frac{d V_i(t)}{dt}$. If we let $Y(t) = \frac{d V_i(t)}{dt}$ and $X(t) = V_i(t)$, then the following can be written for $W_z(\omega)$ equal to the power spectrum of the term $(1/2)\left(\frac{d V_i^2(t)}{dt}\right)$,

$$W_z(\omega) = F\left\{E\left[V_i(t) V_i'(t) V_i(t + \tau) \; V_i'(t + \tau)\right]\right\} \tag{28}$$

where $V_i'(t) = \frac{d V_i(t)}{dt}$.

Since the derivative of a Guassian function (namely $V_i(t)$) is also Gaussian,[51] equation (28) can be expanded as follows, [51]

$$\begin{aligned} W_z(\omega) = F\Big\{ &E\left[V_i(t) V_i'(t)\right] E\left[V_i(t + \tau) V_i'(t + \tau)\right] \\ &+ E\left[V_i(t) \; V_i'(t + \tau)\right] E\left[V_i'(t) \; V_i(t + \tau)\right] \\ &+ E\left[V_i(t) V_i(t + \tau)\right] E\left[V_i'(t) \; V_i'(t + \tau)\right] \Big\} \end{aligned} \tag{29}$$

TABLE 7.6. INTERMODULATION TERMS OF SSB/PhM (MA) MODE

Intermodulation Term at Discriminator Output (See Eq. 26)	Intermodulation Term Source	Spectrum at Baseband Output Shown in Figure
$a_3 b_1 d_1 \dfrac{dV_i^3(t)}{dt}$	Third Order, Uplink Amplitude Nonlinearity	Figure 7.18
$a_1^2 b_2 d_1 \dfrac{dV_i^2(t)}{dt}$	Second Order, S/C Modulator Nonlinearity (Amplitude)	Figure 7.19
$a_1^3 b_3 d_1 \dfrac{dV_i^3(t)}{dt}$	Third Order, S/C Modulator Nonlinearity (Amplitude)	Figure 7.20
$a_1^2 b_1^2 c_2 d_1 \dfrac{d\left(\dfrac{dV_i(t)}{dt}\right)^2}{dt}$	Second Order, Downlink Linear Group Delay (Phase Nonlinearity)	Figure 7.21
$a_1^3 b_1^3 c_3 d_1 \dfrac{d\left(\dfrac{dV_i(t)}{dt}\right)^3}{dt}$	Third Order, Downlink Parabolic Group Delay (Phase Nonlinearity)	Figure 7.22
$a_1^2 b_1^2 d_2 \left(\dfrac{dV_i(t)}{dt}\right)^2$	Second Order, Earth Station Discriminator Nonlinearity (Amplitude)	Figure 7.23
$a_1^3 b_1^3 d_3 \left(\dfrac{dV_i(t)}{dt}\right)^3$	Third Order, Earth Station Discriminator Nonlinearity (Amplitude)	Figure 7.24

If we can assume each of the above terms stationary, then the correlation functions are given as follows,

$$R_{vv'}(o) = E\left[V_i(t)\ V_i'(t)\right] = E\left[V_i(t+\tau)\ V_i'(t+\tau)\right] \tag{30a}$$

$$R_{vv'}(\tau) = E\left[V_i(t)\ V_i'(t+\tau)\right]' \tag{30b}$$

$$R_{vv'}(\tau) = E\left[V_i(t+\tau)\ \dot{V_i'}(t)\right] \tag{30c}$$

$$R_{v'}'R_{v}'(\tau) = E\left[V_i'(t)\ V_i'(t+\tau)\right] \tag{30d}$$

$$R_{vv}(\tau) = E\left[V_i(t)\ V_i(t+\tau)\right] \tag{30e}$$

Substituting equation (30) into equation (29) the following is obtained,

$$W_z(\omega) = F\left\{R_{vv'}^2(o)\right\} + F\left\{R_{vv'}(\tau)\ R_{vv'}(-\tau)\right\}$$
$$+ F\left\{R_{vv}(\tau)R_{v'v'}(\tau)\right\} \tag{31}$$

Since the baseband does not include zero frequency, the first term of equation (31) may be neglected because this term represents an impulse at zero frequency. The remaining terms may be determined from the derivation of $R_{xx'}(\tau)$ and $R_{x'x'}(\tau)$ given by ref. [52] where x is a random function and x^1 is the derivative of that random function x.

Results given by A. Papoulsis are,

$$R_{vv'}(\tau) = \frac{dR_{vv}(\tau)}{dt} \quad \text{and} \quad R_{v'v'}(\tau) = \frac{-d^2 R_{vv}(\tau)}{dt^2}$$

Since $R_{vv}(\tau)$ is an even function the derivative, $\dfrac{dR_{vv}(-\tau)}{dt}$, is negative with respect to $\dfrac{dR_{vv}(\tau)}{dt}$. That is,

$$R_{vv'}(-\tau) = \frac{dR_{vv}(-\tau)}{dt} = \frac{-dR_{vv}(\tau)}{dt} \tag{32}$$

Thus we have,

$$W_z(\tau) = F\frac{-dR_{vv}(\tau)}{dt} \cdot \frac{dR_{vv}(\tau)}{dt}$$
$$+ F\frac{-d^2R_{vv}(\tau)}{dt^2} \cdot R_{vv}(\tau) \tag{33}$$

The following Fourier transform theorems are used to obtain the output spectrum, $W_z(\omega)$, in terms of the input spectrum which is the Fourier transform of the autocorrelation of $V_i(t)$.

$$F\left\{\frac{d\,g\,(t)}{dt}\right\} = j\,2\pi f \;\; G(f) \tag{34}$$

$$F\left\{g_1(t)\,g_2(t)\right\} = \int_{\infty}^{\infty} G_1\,(y)\,G_2\,(f-y)\,dy \tag{35}$$

where $g(t)$, $g_1(t)$, and $g_2(t)$ are transformable and $G(f)$, $G_1(f)$, and $G_2(f)$ are the Fourier transforms of $g(t)$, $g_1(t)$ and $g_2(t)$, respectively.

If we let $X(f)$, $Y(f)$, $Z(f)$ be given by,

$$X(f) = F\left\{R_{vv}(\tau)\right\} \tag{36a}$$

$$Y(f) = F\left\{\frac{d\,R_{vv}(\tau)}{dt}\right\} = F\left\{R_{vv}{}'(\tau)\right\} \tag{36b}$$

$$Z(f) = F\left\{\frac{d^2 R_{vv}(\tau)}{dt^2}\right\} = F\left\{R_{vv}{}''(\tau)\right\} \tag{36c}$$

$Y(f)$ and $Z(f)$ can be written in terms of $X(f)$ using the theorem of equation (30) with equations (32b) and (32c).

$$Y(f) = j\,2\pi f \;\; X(f) \tag{37a}$$

$$Z(f) = (j2\pi f)^2 \;\; X(f) \tag{37b}$$

From equations (29), (31), and (32), the following expression for the spectrum $W_z(f)$ is obtained,

$$W_z(f) = \int_{-\infty}^{\infty} -Y\,(y) \cdot Y\,(f-y)\,dy$$
$$+ \int_{-\infty}^{\infty} -Z\,(y) \cdot X\,(f-y)\,dy \tag{38}$$

Substituting equation (33) into (34) and solving, $W_z(f)$ may be written

$$W_z(f) = (2\pi)^2 f \int_{-\infty}^{\infty} y\,X(y)\;X(f-y)\;dy \tag{39}$$

The input spectrum $X(f)$ is given by the following equation

$$X(f) = P_0\Big[u\,(f+5.564\ \text{MHz}) - u\,(f+0.316\ \text{MHz})$$
$$+ u\,(f-0.316\ \text{MHz}) - u\,(f-5.564\ \text{MHz})\Big] \tag{40}$$

where $u(f)$ is a step function defined as

$$u(f) = 1 \qquad f \geq 0$$
$$ = 0 \qquad f < 0 \tag{41}$$

and P_o is one-half the measured power density of the input noise spectrum.

If equation (36) is substituted into equation (35) and integration is carried out term by term, the following equation is obtained for the spectrum of the noise term $(1/2)\left(\dfrac{d\,v_i^2(t)}{dt}\right)$ at the output of the discriminator.

$$
\begin{aligned}
W_z(f) \;=\; P_o^2 \,(39.4)\Bigg[&\left(\frac{f^3}{2} + 5.564 \times 10^6\, f^2\right)\, u\,(f + 11.128 \text{ MHz}) \\
&- (f^3 + 5.88 \times 10^6\, f^2)\, u\,(f + 5.88 \text{ MHz}) \\
&+ (f^3 + 5.248 \times 10^6\, f^2)\, u\,(f + 5.248 \text{ MHz}) \\
&+ \left(\frac{f^3}{2} + 0.316 \times 10^6\, f^2\right)\, u\,(f + 0.632 \text{ MHz}) \\
&- (2f^3)\, u\,(f) \\
&+ \left(\frac{f^3}{2} + 0.316 \times 10^6\, f^2\right)\, u\,(f - 0.632 \text{ MHz}) \\
&+ (f^3 - 5.248 \times 10^6\, f^2)\, u\,(f - 5.248 \text{ MHz}) \\
&- (f^3 - 5.88 \times 10^6\, f^2)\, u\,(f - 5.88 \text{ MHz}) \\
&+ \left(\frac{f^3}{2} - 5.564 \times 10^6\, f^2\right)\, u\,(f - 11.128 \text{ MHz}) \Bigg]
\end{aligned}
\tag{42}
$$

The de-emphasis network is a linear network and thus does not contribute to any non-linear distortion. The effect of the de-emphasis network is taken into account by multiplying the square of the magnitude of the de-emphasis network transfer function $\left|\dfrac{\omega_o}{\omega}\right|^2$, times the signal spectrum and each intermodulation noise spectrum calculated at the output of the discriminator. In the case of each term of equation (26), the spectrum was calculated at the output of the discriminator with the technique used in the above example, and then multiplied by the transfer function of the de-emphasis filter. The power spectrum at the output of the de-emphasis network for each of the distortion terms in equation (26) is shown in figures 7.18 through 7.24.

The relationship between two-tone tests and downlink group delay in the (MA) mode can be calculated by referring to the equations that define the system model (21 through 25). If the non-linearities of the spacecraft modulator and the uplink from baseband input to the earth station transmitter to the input of the spacecraft modulator are ignored, then for a two-tone input, the phase-modulator output, $\phi_m(t)$, can be represented as

$$\phi_m(t) = \Delta\Omega \ (\sin \omega_1 t + \sin \ \omega_2 t) \tag{43}$$

where $\Delta\Omega$ is the radian deviation of each of the tones. The deletion of the non-linear distortion terms of the uplink and the modulator is justified for the calculation of distortion due to phase non-linearities of the IF/RF downlink transmission medium if the system two-tone inter-modulation margins are typically 25 db or greater.

The effective frequency deviation, $\dot{\phi}_t(t)$, at the output of the spacecraft modulator is given by

$$\phi_m'(t) = \Delta\Omega \ (\omega_1 \cos \omega_1 t + \omega_2 \cos \omega_2 t) \tag{44}$$

The phase variation at the input to the discriminator is obtained from equation (24) and is given as

$$\phi_t(t) = \phi_m(t) + c_2 \ (\phi_m'(t))^2 + c_3 \ (\phi_m'(t))^3 + \ldots \tag{45}$$

Thus, the frequency deviation of the signal at the input of the discriminator, $\phi_t'(t)$, is given by

$$\phi_t'(t) = \phi_m'(t) + 2 c_2 (\phi_m'(t)) (\phi_m''(t)) + 3 c_3 \ (\phi_m'(t)^2 (\phi_m''(t)) + \ldots \tag{46}$$

Substituting into equation (46) equations (43) and (44), the following is obtained

$$\phi_t'(t) = \Delta\Omega \, (\omega_1 \cos \omega_1 t + \omega_2 \cos \omega_2 t)$$

$$+ 2 c_2 \Delta^2 \Omega \, (\omega_1 \cos \omega_1 t + \omega_2 \cos \omega_2 t)$$

$$x \ (\omega_1^2 \sin \ \omega_1 t + \omega_2^2 \ \sin \omega_2 t)$$

$$+ 3 c_3 \Delta^3 \Omega \, (\omega_1 \cos \omega_1 t + \omega_2 \cos \omega_2 t)^2$$

$$x \ (\omega_1^2 \sin \omega_1 t + \omega_2^2 \sin \omega_2 t) \tag{47}$$

The voltage output of the discriminator, V_d, is equal to the frequency deviation at the input to the discriminator multiplied by the discriminator constant, d_1. Simplifying equation (47) and multiplying by the discriminator constant, d_1,

$$V_d = d_1 \left[\Delta\Omega \, \omega_1 \cos \omega_1 t + \Delta\Omega\omega_2 \cos \omega_2 t \right.$$

$$+ 2c_2 \Delta^2\Omega \left(\frac{\omega_1^3}{2} \sin 2\omega_1 t + \frac{\omega_2^3}{2} \sin 2\omega_2 t \right.$$

$$+ \frac{\omega_1\omega_2}{2} (\omega_2 - \omega_1) \sin (\omega_2 - \omega_1)t$$

$$\left. + \frac{\omega_1\omega_2}{2} (\omega_1 + \omega_2) \sin (\omega_1 + \omega_2)t \right)$$

$$+ 3c_3 \left(\frac{\omega_1^4}{4} \sin 3\omega_1 t + \frac{\omega_2^4}{4} \sin 3\omega_2 t \right.$$

$$+ \frac{\omega_1\omega_2^2}{4} (\omega_1 + 2\omega_2) \sin (\omega_1 + 2\omega_2)t$$

$$+ \frac{\omega_1\omega_2^2}{4} (2\omega_2 - \omega_1) \sin (2\omega_2 - \omega_1)t$$

$$+ \frac{\omega_1^2\omega_2}{4} (2\omega_1 + \omega_2) \sin (2\omega_1 + \omega_2)t$$

$$\left. \left. + \frac{\omega_1^2\omega_2}{4} (2\omega_1 - \omega_2) \sin (2\omega_1 - \omega_2)t \right) \right] \qquad (48)$$

The de-emphasis filter has a transfer function $\dfrac{\omega_0}{\omega}$ so that the voltage out of the de-emphasis network, V_{dn}, is given by

$$V_{dn} = \omega_0 d_1 \left[\Delta\Omega \, \cos \omega_1 t + \Delta\Omega \cos \omega_2 t \right.$$

$$+ 2c_2 \Delta^2\Omega \left(\frac{\omega_1^2}{4} \sin \omega_1 t + \frac{\omega_2^2}{4} \sin \omega_2 t \right.$$

$$\left. + \frac{\omega_1\omega_2}{2} \sin (\omega_2 - \omega_1)t + \frac{\omega_1\omega_2}{2} \sin (\omega_1 + \omega_2)t \right)$$

$$+ 3c_3 \Delta^3\Omega \left(\frac{\omega_1^3}{12} \sin 3\omega_1 t + \frac{\omega_2^3}{12} \sin 3\omega_2 t \right.$$

$$+ \frac{\omega_1\omega_2^2}{4} \sin (\omega_1 + 2\omega_2 t) + \frac{\omega_1\omega_2^2}{4} \sin (\omega_1 - 2\omega_2)t$$

$$\left. \left. + \frac{\omega_1^2\omega_2}{4} \sin (2\omega_1 + \omega_2)t + \frac{\omega_1^2\omega_2}{4} \sin (2\omega_1 - \omega_2)t \right) \right] \qquad (49)$$

The intermodulation margin can be obtained from equation (49) by dividing the respective intermodulation term into the fundamental term. Thus, second-and third-order intermodulation margins caused by phase non-linearities are given by

$$\frac{F}{I_2} = \frac{\Delta\Omega}{\frac{2}{2} c_2 \Delta^2\Omega\,\omega_1\omega_2} \tag{50a}$$

$$\frac{F}{I_3} = \frac{\Delta\Omega}{\frac{3}{4}(c_3)(\Delta^3\Omega)\omega_1^2\omega_2} \qquad \text{for a } (2f_1 \pm f_2) \text{ type product} \tag{50b}$$

$$\frac{F}{I_3} = \frac{\Delta\Omega}{\frac{3}{4}(c_3)(\Delta^3\Omega)\omega_1\omega_2^2} \qquad \text{for a } (f_1 \pm 2f_2) \text{ type product} \tag{50c}$$

The constants $2c_2$ and $3c_3$ are the linear group-delay and parabolic group-delay coefficients, respectively. The constant, $2c_2$, is the linear group delay in seconds/(radians/sec), and the constant, $3c_3$, is parabolic group delay in seconds/(radians/sec)^2. The angular frequencies ω_1 and ω_2 are given in radians/sec.

If ω_2 is the linear group delay in seconds over half the IF bandwidth, then the following equation holds,

$$2c_2 = \frac{\tau_2}{B/2} \tag{51}$$

where B is the IF bandwidth in radian/sec. Similarly, if τ_3 is the parabolic group delay in seconds over half the IF bandwidth, then $3c_3$ is given by

$$3c_3 = \frac{\tau_3}{(B/2)^2} \tag{52}$$

where B is again measured in radians/sec

Substituting equations (47) and (48) into equations (46a), (46b), and (46c), the following equations are obtained:

$$\frac{F}{I_2} = \frac{B}{\tau_2\Delta\Omega\omega_1\omega_2} \tag{53a}$$

$$\frac{F}{I_3} = \frac{B^2}{\tau_3\Delta\Omega\omega_1^2\omega_2} \qquad \text{for a } (2f_1 \pm f_2) \text{ type product} \tag{53b}$$

$$\frac{F}{I_3} = \frac{B^2}{\tau_3\Delta\Omega\omega_1\omega_2^2} \qquad \text{for a } (f_1 \pm 2f_2) \text{ type product} \tag{53c}$$

For example, suppose that it could be determined that the F/I_3 ratio due to phase non-linearities in the S/C loop is 28 db for fundamental tones of 3.886 MHz and 5.340 MHz, and that the intermodulation product is measured at 2.432 MHz. Further assume that each tone is transmitted 12.8 dbm0 above nominal test tone for the MA mode. The radian deviation for test tone is 0.35-radian peak. Thus for $(2f_1 \pm f_2)$ type product, equation (53b) becomes solving for group delay

$$\tau_3 = \frac{B^2}{\Delta^2 \Omega \omega_1^2 \omega_2 F} I_3 \tag{54}$$

where $B = 2\pi \ (30 \ \text{MHz})$.

The parabolic group delay becomes

$$\tau_3 = \frac{(2\pi \ (30 \times 10^6) \ )^2}{(2.34) \ (2\pi \ 3.886 \times 10^6)^2 \ (2\pi \ 5.34 \times 10^6) \ (25)} \tag{55}$$

$$= 46 \ \text{nsec.}$$
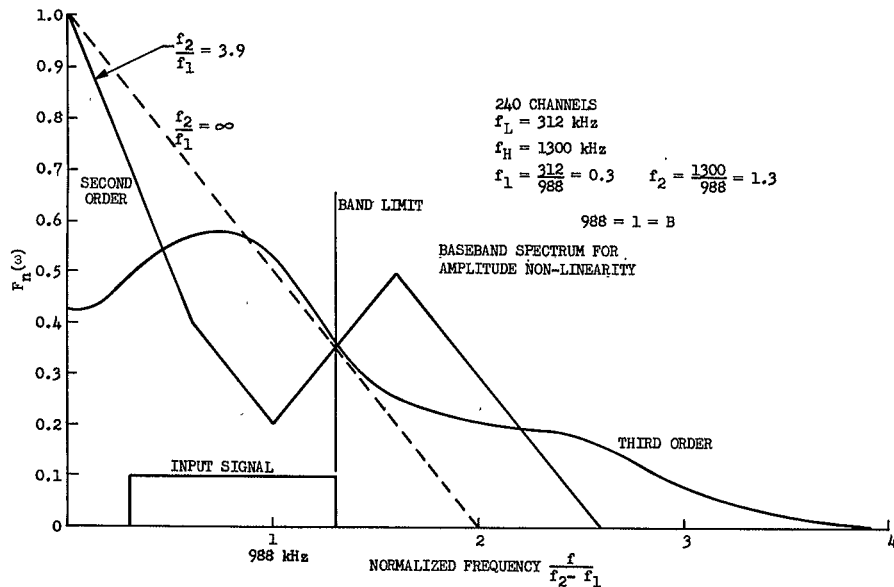
Figure 7.14. Baseband Spectrum for Amplitude Non-Linearity (FT Mode)(240 Channels)
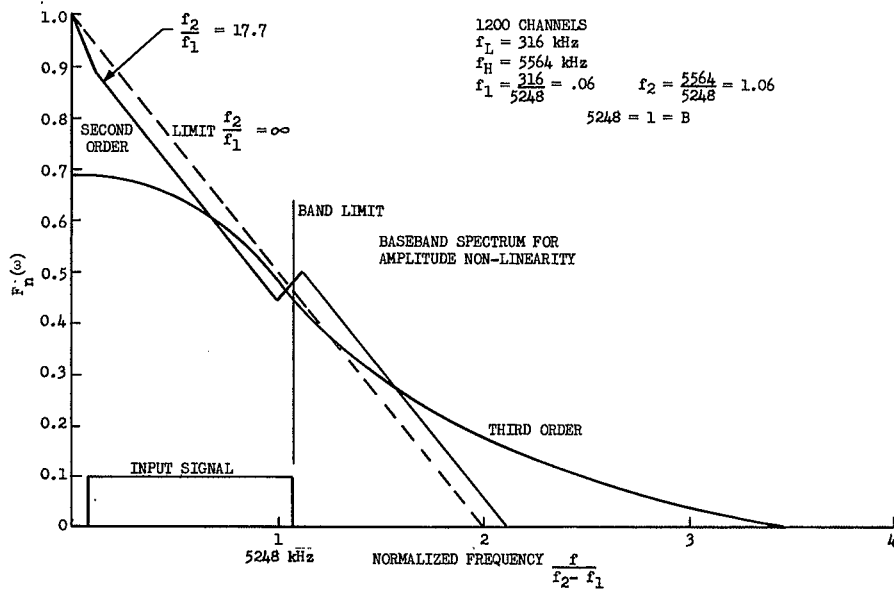
Figure 7.15. Baseband Spectrum for Amplitude Non-Linearity (FT Mode)(1200 Channels)
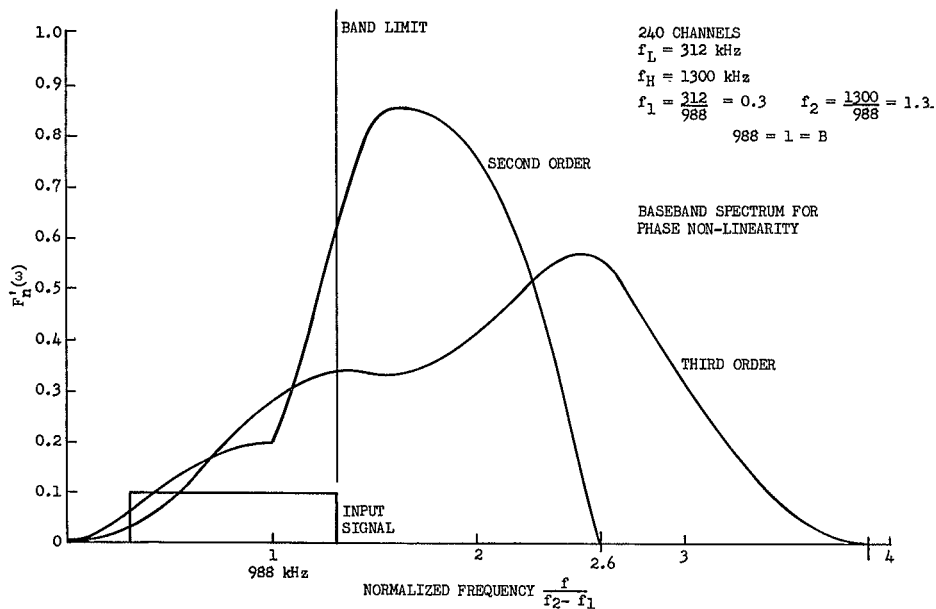
Figure 7.16. Baseband Spectrum for Phase Non-Linearity (FT Mode)(240 Channels)
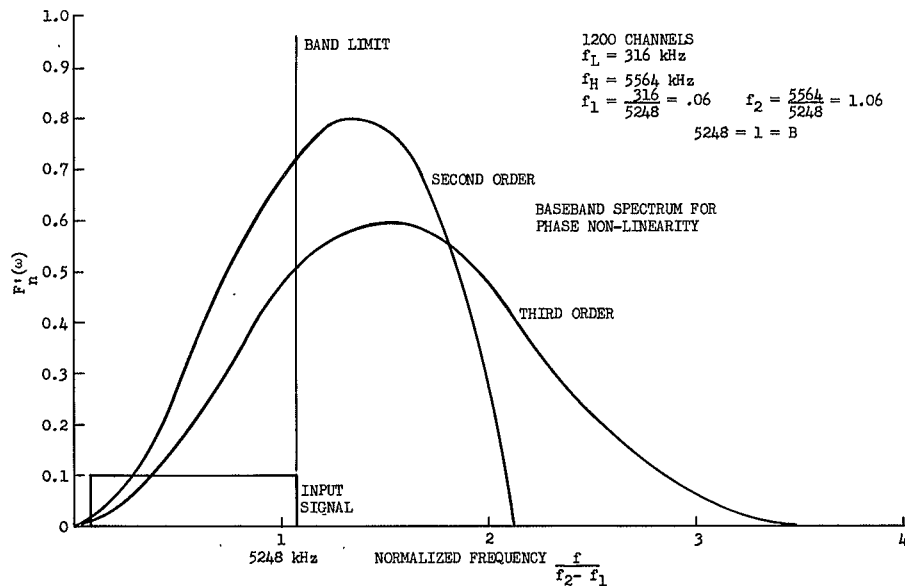
Figure 7.17. Baseband Spectrum for Phase Non-Linearity (FT Mode)(1200 Channels)

The figure shows a graph with y-axis labeled "RELATIVE INTERMODULATION NOISE, Y, (db)" ranging from 0 to -12, and x-axis labeled "FREQUENCY (MHz)" ranging from 0 to 12. A box labeled "BASEBAND SPECTRUM" appears at the bottom.

S_n = NONLINEAR NOISE MARGIN

I_3 = TWO-TONE INTERMODULATION MARGIN

S_n = K · (TWO-TONE INTERMODULATION MARGIN) · (RELATIVE NOISE)

 = K (db) + I_3 (db) + Y (db)
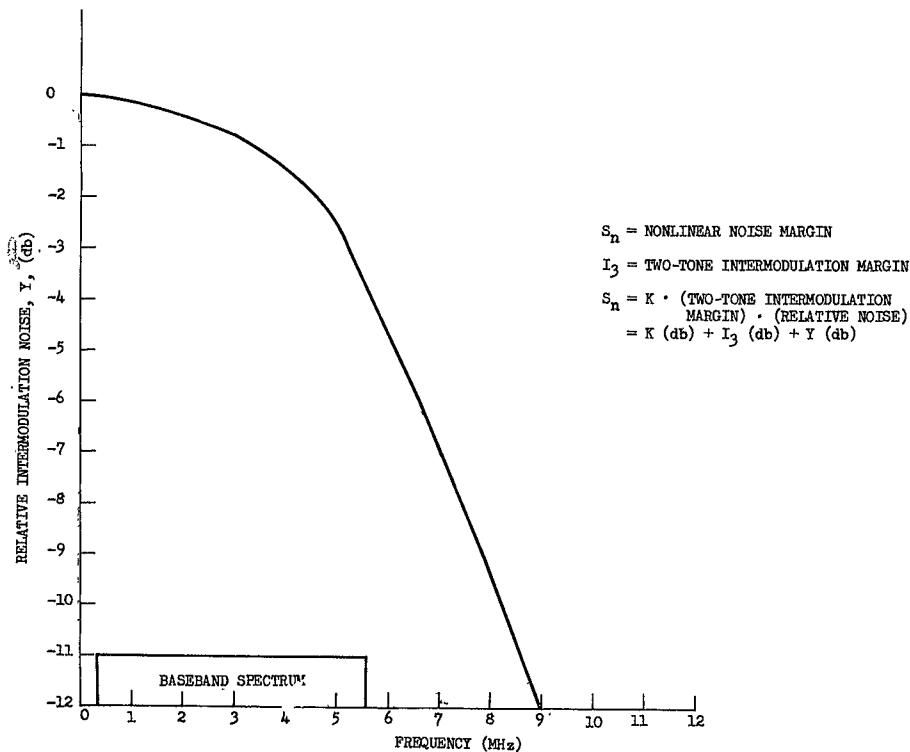
Figure 7.18. Third-Order Intermodulation Baseband Spectrum for SSB Transmitter (Amplitude, MA Mode)
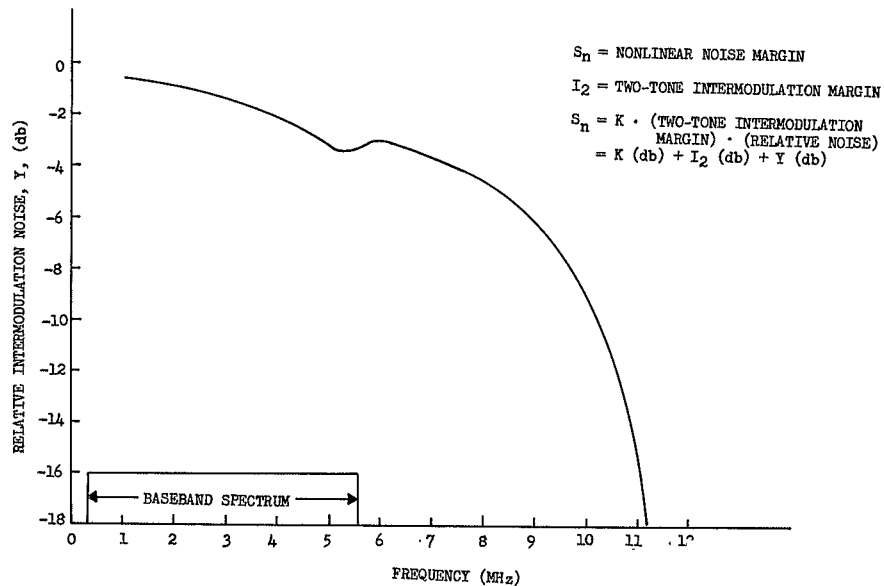
Figure 7.19. Second-Order Intermodulation Baseband Spectrum for S/C Modulator (Amplitude, MA Mode)
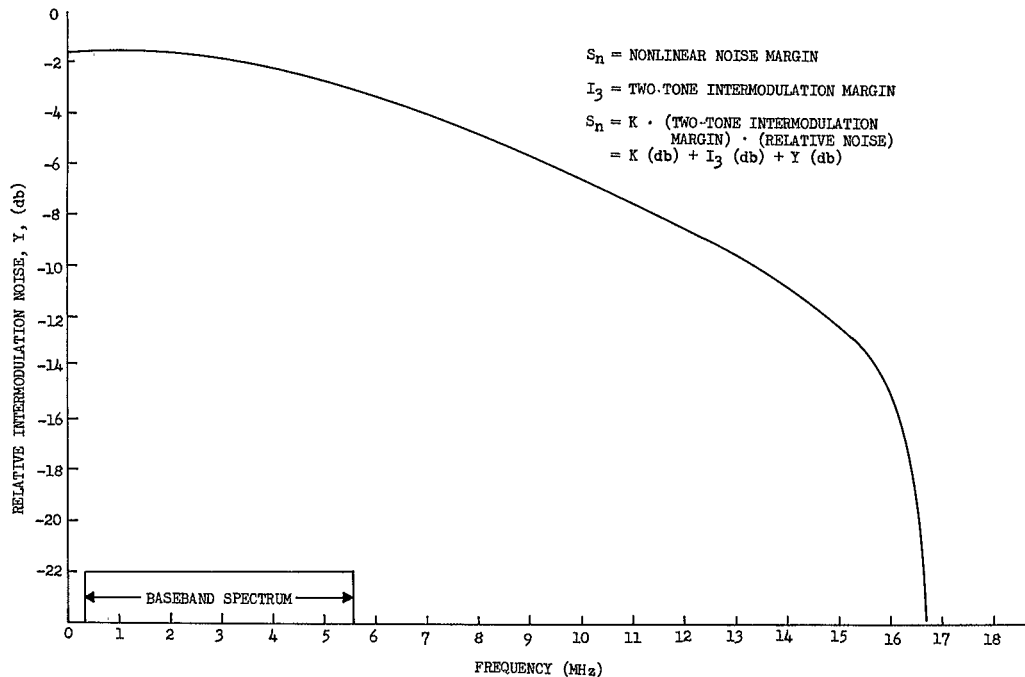
Figure 7.20. Third-Order Intermodulation Baseband Spectrum for S/C Modulator (Amplitude, MA Mode)
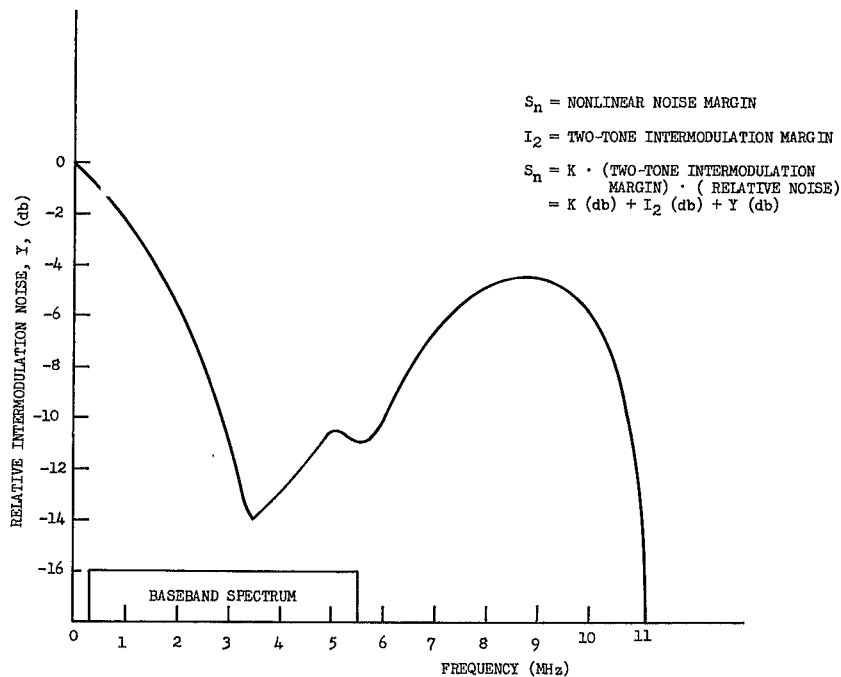
Figure 7.21. Second-Order Intermodulation Baseband Spectrum for IF-RF Downlink (Phase, MA Mode)
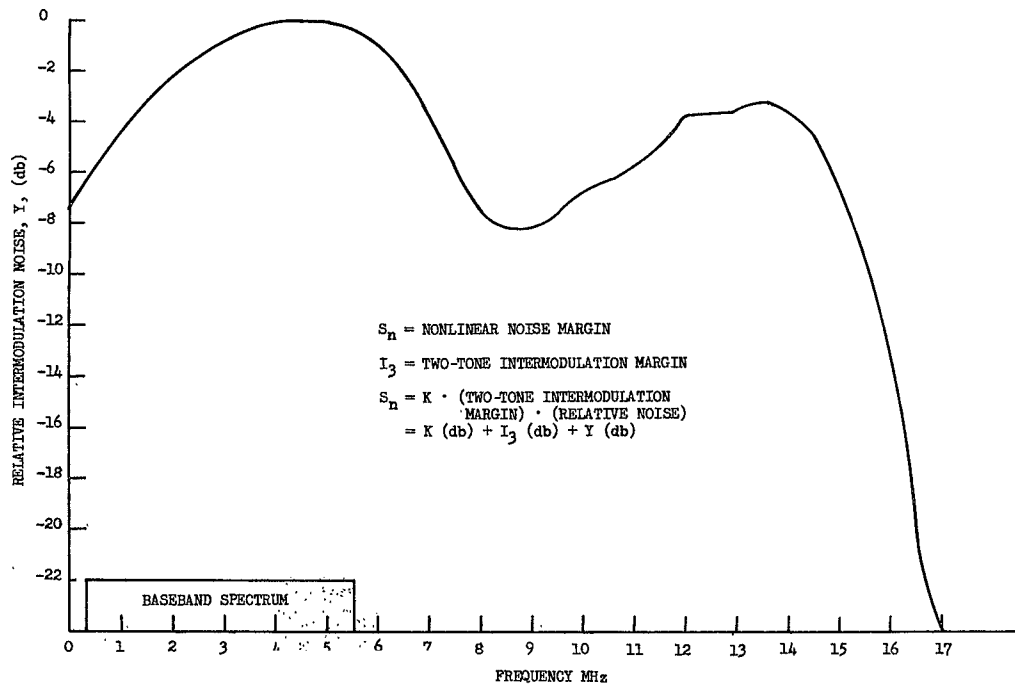
Figure 7.22. Third-Order Intermodulation Baseband Spectrum for IF-RF Downlink (Phase. MA Mod
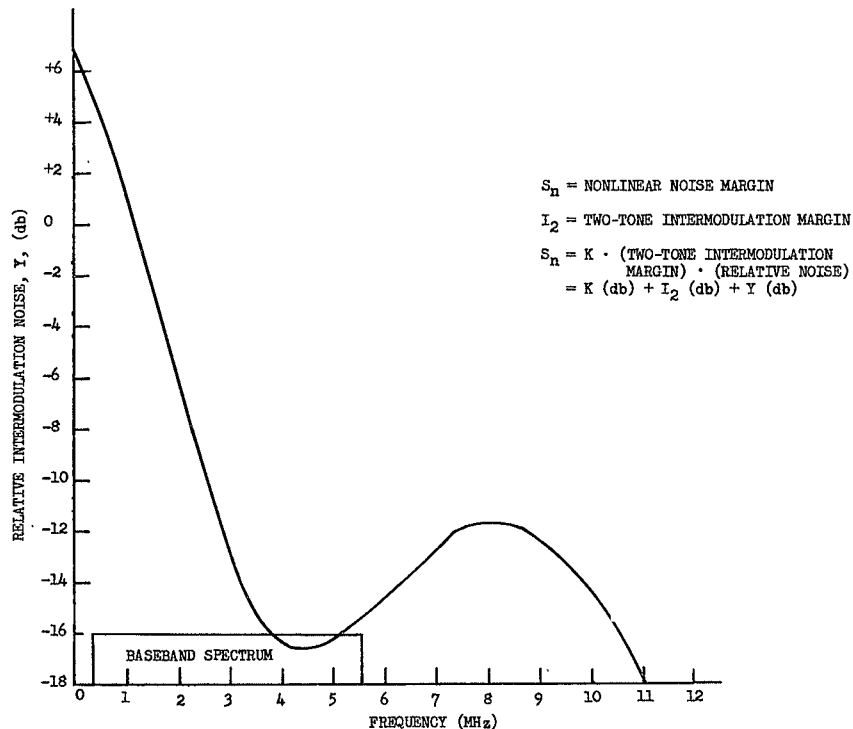
Figure 7.23. Second-Order Intermodulation Baseband Spectrum for Earth-Station Discriminator (Amplitude, MA Mode)
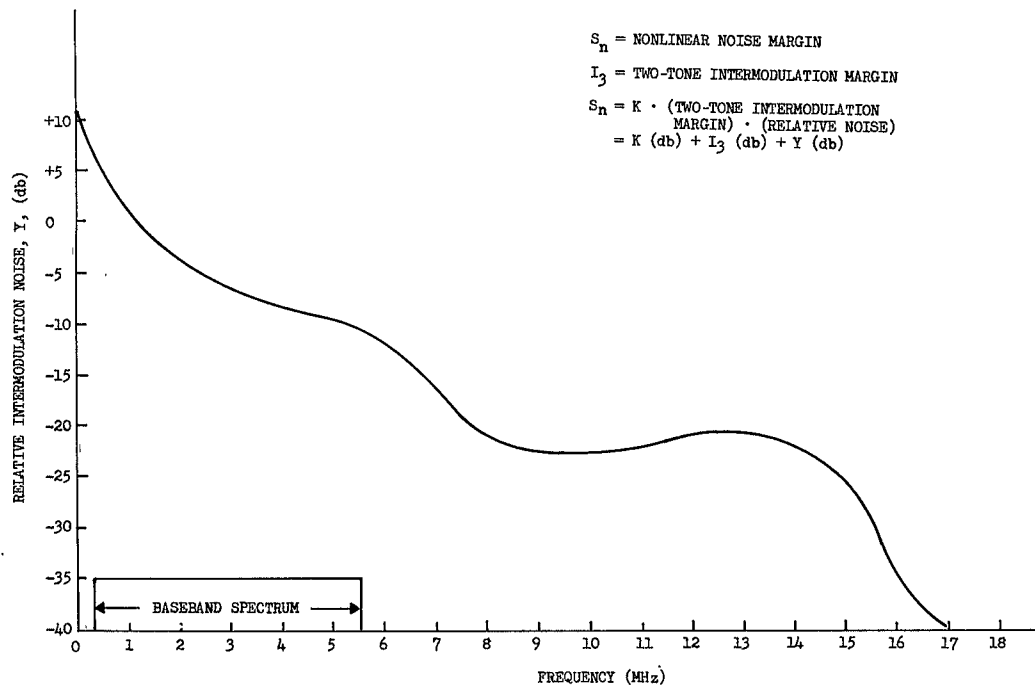
Figure 7.24. Third-Order Intermodulation Baseband Spectrum For Earth-Station Discriminator (Amplitude, MA Mode)

S_n = NONLINEAR NOISE MARGIN

I_3 = TWO-TONE INTERMODULATION MARGIN

S_n = K · (TWO-TONE INTERMODULATION MARGIN) · (RELATIVE NOISE)

= K (db) + I_3 (db) + Y (db)
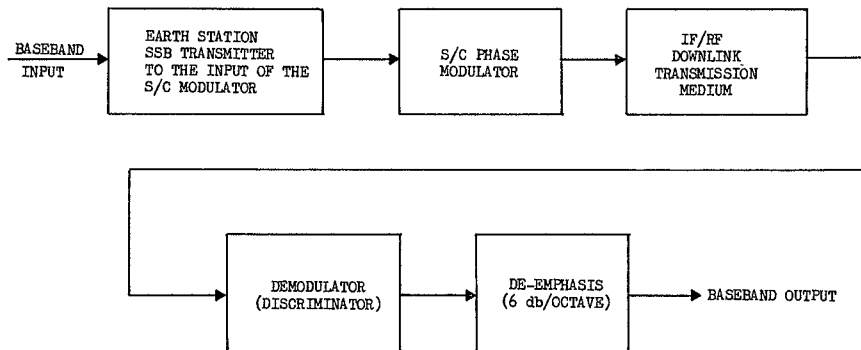
Figure 7.25. Block Diagram of MA Mode for Intermodulation Analysis

7.8 EXPERIMENT ORGANIZATION

The experiments are grouped into seven categories according to performance aspects:

Path Loss
IF/Baseband
Control Loop and Stability
Multiplex
Television
Spacecraft
Earth Station

There are over 50 Field-Test Procedures which fall into these performance aspects. Each procedure contains detailed instructions which permit station personnel to perform the tests as stated in the Experimental Test Plan. Each procedure is numbered according to an alphanumeric system which utilizes the two-letter groups and a number with a decimal. Example MA-MX-1.1.

The first two-letter group indicates the system operating mode as follows:

FT - Frequency Translation
MA - Multiple Access
AN - Antenna

The second two-letter group indicates the type of test and consists of the following:

AT - Tests performed in an automated mode
MX - Tests of multiplex-channel parameters
BB - Tests of baseband parameters
RF - Tests of radio-frequency parameters
SP - Special tests of unusual or complex sets of parameters
PA - Tests of antenna polarization

The first numeral in the numbered group is an arbitrary numbering of the tests following the categories defined by the two-letter groups. The second or (decimal) numeral is used to designate sub-tests under the first number wherein similar parameters are tested or similar techniques employed. Table 7.7, Experiment Grouping, categorizes the experiments (manual and automated) according to performance aspects, mode of operation (FT or MA) and satellite.

TABLE 7.7. SHF EXPERIMENT GROUPING

Performance Aspects	Type of Test and FTP Number		Applicable Satellites			
	Manual	Automated	ATS-1	ATS-3		
PATH LOSS EXPERIMENTS			.	.		
MA MODE						
RF Signal Power Level and Propagation Losses	MA-RF-1.1 MA-RF-1.2 MA-RF-1.3	MA-AT-1.1 MA-AT-1.2	X X X	X X X		
FT MODE						
RF Signal Power Level and Propagation Losses	FT-RF-1.1 FT-RF-1.2	FT-AT-1.1	X X	X X		
IF/BASEBAND EXPERI-MENTS						
MA MODE						
Baseband Frequency Response	MA-BB-2.1		X	X		
FT MODE						
Baseband Frequency Response	FT-BB-5.1		X	X		
Envelope Delay Dis-tortion	FT-BB-4.1		X	X		
Transmitter Receiver Linearity	FT-BB-2.1		X	X		
Differential Phase	FT-BB-3.1		X	X		
CONTROL LOOP AND STABILITY EXPERIMENTS						
MA MODE						
Multiplex-Channel Frequency Stability	MA-MX-1.1 MA-MX-1.2	MA-AT-1.1 MA-AT-1.2	X X X	X X X		
Multiplex-Channel Level Stability	MA-MX-2.1	MA-AT-1.1	X X	X X		
Ground-Transmitter Automatic-Level Control Loop	MA-SP-3.1		X	X		
FT MODE						
Multiplex-Channel Level Stability	FT-MX-1.1		X	X		

TABLE 7.7. SHF EXPERIMENT GROUPING (Continued)

Performance Aspects	Type of Test and FTP Number		Applicable Satellites	
	Manual	Automated	ATS-1	ATS-3
MULTIPLEX PERFOR-MANCE EXPERIMENTS				
MA MODE				
Channel S/N Ratio and Data-Error Rate	MA-MX-7.1 MA-MS-2.1	MA-AT-1.1 MA-AT-1.2	X X X	X X X
System Noise-Power Ratio	MA-BB-1.1	MA-AT-1.1 MA-AT-1.2	X X X	X X
Multiplex-Channel Linearity	MA-MX-4.1		X	X
Multiplex-Channel Audio Envelope Delay	MA-MX-5.1 MA-MS-1.1		X X	X X
Multiplex-Channel Harmonic Distortion	MA-MX-6.1		X	X
Multiplex-Channel Frequency Response	MA-MX-3.1		X	X
FT MODE				
Channel S/N Ratio and Data-Error Rate	FT-MX-6.1		X	X
		FT-AT-1.1	X	X
		FT-AT-1.1	X	X
System Noise-Power Ratio	FT-BB-1.1		X	X
Multiplex-Channel Linearity	FT-MX-3.1		X	X
Multiplex-Channel Audio Envelope Delay	FT-MX-4.1 FT-MS-1.1		X X	X X
Multiplex-Channel Harmonic Distortion	FT-MX-5.1		X	X
Multiplex-Channel Frequency Response	FT-MX-2.1		X	X
TELEVISION PERFORM-ANCE EXPERIMENTS				
FT MODE				
Video-Weighted Noise	FT-TV-1.1		X	X

TABLE 7.7. SHF EXPERIMENT GROUPING (Continued)

Performance Aspects	Type of Test and FTP Number		Applicable Satellites		
	Manual	Automated	ATS-1	ATS-3	
TELEVISION PERFORM-ANCE EXPERIMENTS (cont)					
FT MODE (cont)					
Video Channel Noise, Power Supply Hum, and Intermodulation Distortion	FT-TV-4.1		X	X	
Video Low-Frequency Response	FT-TV-2.3		X	X	
Video Transient Response	FT-TV-3.1		X	X	
Video Insertion Gain	FT-TV-2.2		X	X	
Video Differential Gain	FT-TV-2.1		X	X	
Color Vector Analysis	FT-TV-5.2		X	X	
TV Audio-Channel Idle Noise	FT-TV-6.1		X	X	
	FT-TV-6.2		X	X	
	FT-TV-6.4		X	X	
	FT-TV-6.5		X	X	
TV Audio Channel Periodic and Crosstalk Noise	FT-TV-6.1		X	X	
TV Audio-Channel Frequency Response	FT-TV-6.2		X	X	
TV Audio-Channel Harmonic Distortion	FT-TV-6.4		X	X	
TV Audio-Channel Amplitude Linearity	FT-TV-6.5		X	X	
SPACECRAFT EXPERI-MENTS					
MA MODE					
Carrier Modulation Due to Spin	MA-SP-1.1		X	X	
Spacecraft Transmit Antenna Pattern	AN-SP-2.1		X	X	
Spacecraft Receiver Antenna Pattern	AN-SP-2.2		X	X	

TABLE 7.7.   SHF EXPERIMENT GROUPING (Continued)

Performance Aspects	Type of Test and FTP Number		Applicable Satellites			
	Manual	Automated	ATS-1	ATS-3		
SPACECRAFT EXPERI-MENTS (cont)		-				
FT MODE						
Repeater Saturation Characteristics	FT-SP-1.1		X	X		
GROUND STATION EXPERIMENTS						
MA MODE						
Ground Terminal G/T	AN-SP-1.3		X	X		
Ground Terminal Trans-mitting Antenna Patterns	AN-SP-1.1		X	X		
Ground Terminal Receiving Antenna Patterns	AN-SP-1.2		X	X		
Earth Terminal Antenna Positioning Characteristics	AN-SP-1.4					

7.8.1 DESCRIPTION OF FIELD TEST PROCEDURES

Contained in subsequent paragraphs are individual writeups for each SHF test.

7.8.1.1 TEST FT-RF-1.1 RF SIGNAL POWER AND PATH LOSS

7.8.1.1.1 Objective

The objectives of this test are to measure the uplink and downlink path-loss values. The former factor is a function of the ground-radiated power and spacecraft received power. The latter is a function of the spacecraft radiated power and ground-received power.

Measurements of transmitter-output and receiver-input powers are made. The desired results are calculated using the measurements and the known characteristics of the antennas and feed systems. This is a single-station test and is performed with a synchronous or medium-altitude spacecraft.

7.8.1.1.2 Test Description

The ground-station FM transmitter power is measured by reading and recording the power monitor, built into the transmitter.

The spacecraft-received power and spacecraft-transmitter power is obtained from the data transmitted via the VHF telemetry.

The ground-station-receiver input power is computed from measurements of the I C/N and noise temperature (T_s) in the ground receiver.

The antenna gains are normalized at each site. The transmission line losses, diplexer losses, antenna feed-system losses, and all connector losses are measured. The resulting loss, in db, is subtracted from the calculated gain of the antenna.

In the above cases, the calculated antenna gains are those obtained by classical antenna gain computation which takes into account area, curvature, frequency, efficiency, and aperture-to-medium coupling losses. Actual gain is determined by measurement of each db gain or loss component.

7.8.1.2 TEST FT-RF-1.2 RF SIGNAL POWER AND PATH LOSS VARIATIONS

7.8.1.2.1 Objective

The objective of this test is to determine, for the FT mode, the variations of uplink and downlink path losses as a function of time. Strip-chart calibrated recordings of transmitter-output and receiver-input powers are made. The desired results are calculated using the measurements and the known characteristics of the antenna and feed systems. This is a single-station test and is performed with a synchronous or medium-altitude spacecraft.

7.8.1.2.2 Test Description

      The ground-station FM transmitter power is measured by reading and recording the power monitor, which is built into the transmitter.

      The spacecraft-received power and spacecraft-transmitter power is obtained from the data transmitted via the VHF telemetry.

      The ground-station-receiver input power is derived from continuous measurements of the AGC voltage developed in the ground receiver.

      The total uplink path loss is calculated from the power at the spacecraft-receiver input, the power at the ground-transmitter output, and the antenna gain characteristics.

      The total downlink path loss is calculated from the power at the ground-receiver input, the power at the spacecraft-transmitter output, and the antenna gain characteristics.

7.8.1.3 TEST FT-BB-1.1/MA-BB-1.1 SYSTEM NOISE-POWER RATIO

7.8.1.3.1 Objective

      The objective of this test is to measure the baseband noise-power ratio (NPR) as a function of test-slot frequencies and loading conditions. Both idle-noise and loaded-noise power ratios are measured. This test is performed in the MA and FT modes using a PhM demodulator. It is a single-station test, and is performed with either a medium-altitude or synchronous-altitude spacecraft.

7.8.1.3.2 Test Description

      This test consists of a noise-power ratio test, similar to that described in CCIR Recommendation 399. A continuous uniform spectrum of Gaussian noise, simulating various FDM baseband bandwidth spectra, is used to modulate the communications system. The above noise-power levels are utilized to simulate various loading conditions for the purpose of evaluating the system-intermodulation noise versus loading characteristics. Measurement is made at selected channels to determine system performance as a function of baseband frequency.

      Idle noise is measured for each of the channel capacity and baseband frequency options by completely removing the noise-loading modulating signal from the carrier.

7.8.1.4 TEST FT-BB-2.1 TRANSMITTER-RECEIVER LINEARITY

7.8.1.4.1 Objective

      The objective of this test is to measure the IF/RF amplitude characteristics versus IF frequency of the communication system operating in the FT Mode. Measurements are made between the transmitter video input and the receiver video output. This is a single-station test and is performed with a synchronous or medium-altitude spacecraft.

7.8.1.4.2 Test Description

This test is an amplitude linearity test of the entire FT Mode. For example, the amplitude of a signal inserted in the baseband may be distorted by baseband amplitude characteristics and by distortion in the modulator and demodulator portions of the system.

The sum of all distortions is measured by applying a low-amplitude high-frequency (556 kHz) tone to the modulator to produce a low-deviation FM signal, then "sweeping" this composite waveform through the IF/RF spectrum by applying a very low-frequency (81 cps) large-amplitude "bias" frequency to the modulator. The received signal is demodulated by the FM receiver. The low-frequency "sweep" is extracted to provide the horizontal sweep of an oscilloscope, and the high-frequency signal amplitude is detected and used for vertical deflection of the oscilloscope.

The oscilloscope display shows system-amplitude linearity.

7.8.1.5 TEST FT-BB-3.1 DIFFERENTIAL PHASE

7.8.1.5.1 Objective

The objective of this experiment is to evaluate the group-delay characteristics over the RF/IF bandwidth as a function of IF frequency. The test is run on the SHF equipment in the FT (video) mode, and is conducted on a single-station basis.

7.8.1.5.2 Test Description

The test is conducted by applying a high-amplitude 81-Hz signal to the transmitter video input. This signal sweeps the modulator at least ±15 MHz about the 70-MHz IF center frequency. A low-amplitude 556-kHz tone is superimposed which deviates the modulator approximately ±1.5 MHz. The received composite signal is demodulated and the 81 Hz component extracted for use as the horizontal sweep of an oscilloscope. The instantaneous phase of the 556-kHz tone is compared to a long-term average phase-locked local oscillator and displayed as the vertical deflection on the oscilloscope. The vertical scale is calibrated so that the deflection is proportional to group delay in nanoseconds. Markers are added on the scope graticule to indicate the 60, 65, 70, 75, and 80-MHz positions of the relative phase-delay trace.

7.8.1.6 TEST FT-BB-4.1 ENVELOPE-DELAY DISTORTION

7.8.1.6.1 Objective

The objective of this test is to measure the variations of envelope delay of the FT mode-transmission system as a function of video frequency. Measurements are made between the transmitter video input and the receiver video output. This is a single-station test and is performed with a synchronous or medium-altitude spacecraft.

7.8.1.6.2 Test Description

Envelope delay is measured using a group delay measuring set which switches at
a 597–Hz rate between a reference frequency of 200 kHz and a frequency which sweeps across
the video frequency range (100 kHz to 4.5 MHz). Both signals are amplitude modulated by a
20 kHz sine wave. When this signal is fed to a four-terminal network having different group
delays for the two carriers, a phase surge will appear in the signal envelope. The magnitude
of this surge is a measure of the difference in envelope delay presented by the system under
test to the different carrier signals.

The signal is evaluated in a special receiver where it is demodulated, and the
phase of the modulation on the swept frequency is compared with the phase of the modulation
on the reference frequency. The output of this unit is displayed on an x-y plotter envelope
versus baseband frequency.

7.8.1.7 TEST FT-BB-5.1/MA-BB-2.1 ·BASEBAND FREQUENCY RESPONSE

7.8.1.7.1 Objective

The objective of this test is to determine the frequency response from the
transmitter baseband input to the receiver baseband output in either the FT or MA mode.
This test in the FT mode employs a sweep technique above 100 KHz and a point-to-point
measurement below 100 kHz. In the MA mode, the sweep method is used from 0.3 kHz to
5.6 MHz. This is a single-station test and is performed with a synchronous or medium-
altitude spacecraft.

7.8.1.7.2 Test Description

The baseband frequency response in the MA mode and above 100 KHz in the FT
mode is measured using a swept oscillator, covering the baseband frequency range, connected to
the transmitter baseband input. The receiver baseband output is terminated in the receiver-
detector unit of the test set. The output of the detector is connected to the vertical
deflection input of the oscilloscope, in which the horizontal deflection is synchronized with
the sweep-oscillator rate. X-Y plots of the oscilloscope display are used for a permanent
record, and are identified by the time the plot was taken.

Below 100 kHz (FT mode only), point-to-point measurements are made.

7.8.1.8 TEST FT-TV-1.1 WEIGHTED NOISE

7.8.1.8.1 Objective

The objective of this test is to measure the peak-to-pe ↘ ↙gnal-to-idle noise
ratio in the FT mode baseband using a CCIR video-weighting filter. This is a single test and
is performed with a synchronous or medium-altitude spacecraft.

7.8.1.8.2 Test Description

   The system gain is set by transmitting a 1-volt peak-to-peak 15-KHz sine wave and setting the receiver output to 1-volt peak-to-peak.

   The output of the receiver-baseband unit is filtered with a standard CCIR video-weighting filter (525-line standard) and then measured on a true RMS voltmeter. (The HP 3400A will be used for this purpose, although its integrating time is somewhat different from that recommended by the CCIR) Signal-to-noise ratio will be calculated as peak-to-peak signal to weighted noise following CCIR recommendation 421 (Paragraph 3.3). The test is made in the absence of sync pulses.

7.8.1.9 TEST FT-TV-2.1 VIDEO DIFFERENTIAL GAIN

7.8.1.9.1 Objective

   The objective of this test is to measure variations in system video gain in the FT mode caused by changes of video-signal amplitude (differential gain), using a stairstep-pattern technique. This is a single-station test and is performed with a synchronous or medium-altitude spacecraft.

7.8.1.9.2 Test Description

   This test is performed by transmitting a stairstep pattern with a superimposed 3.58-MHz subcarrier; and by displaying both transmitted and received subcarrier amplitudes on waveform monitors. Both patterns will be photographed and differential gain will be determined from variations in the received subcarrier amplitude on the various steps. The test is performed with video-system loading at three different average-picture levels: (APL) 10-percent, 50-percent, and 90-percent APL. The 10-percent APL is obtained by transmitting the stairstep pattern on every fifth horizontal line with the four intervening lines at the black level. For 90-percent APL, the intervening lines are at the white level, while 50-percent APL utilizes the stairstep pattern on every horizontal line.

   This measurement corresponds to CCIR Recommendation 421,   paragraph no. 3.4.2.

7.8.1.10 TEST FT-TV-2.2 VIDEO-INSERTION GAIN (STABILITY)

7.8.1.10.1 Objective

   The objective of this test is to determine the video-system insertion gain stability in the FT mode-transmission system using the half-line bar technique. This is a single-station test and is performed with a synchronous or medium-altitude spacecraft.

7.8.1.10.2 Test Description

A half-line bar (window pattern) complete with sync pulses is transmitted over the system. Both the signal applied to the transmitter and the received signal are displayed on waveform monitors and the displays are photographed and evaluated.

The amplitude of both the transmitted and received half-line bar signals is monitored over a period of time to determine the insertion gain stability of the system.

This test is similar to CCIR Recommendation 421, paragraph 3.1.

7.8.1.11 TEST FT-TV-2.3 VIDEO LOW-FREQUENCY RESPONSE

7.8.1.11.1 Objective

This test will measure the low-frequency amplitude response of the video-transmission system operating in the FT mode. This is a single-station test and is performed with a synchronous or medium-altitude spacecraft.

7.8.1.11.2 Test Description

A test signal employing a window pattern complete with horizontal and vertical synchronizing and blanking pulses is transmitted over the system. Both the signal applied to the transmitter and the received signal are displayed and photographed. Distortion of the signal is determined from the display photographs by measuring the "tilt" on the white level of the signal. This test is similar to CCIR Recommendation 421, paragraph 3.5.1.2.

7.8.1.12 TEST FT-TV-3.1 VIDEO TRANSIENT RESPONSE

7.8.1.12.1 Objective

The objective of this test is to determine the video-system transient response in the FT mode-transmission system using a sine-squared pulse technique. This is a single-station test and is performed with a synchronous or medium-altitude spacecraft.

7.8.1.12.2 Test Description

A sine-squared pulse and a half-line bar (window pattern) complete with sync pulses are transmitted over the system. An expanded sine-squared pulse for both the signal applied to the transmitter and the received signal are displayed on waveform monitors and the displays are photographed.

Amplitude of the overshoot of 0.125-microsec (T pulse) and 0.25-microsec (2T pulse) sine-squared pulses will be measured to determine transient response.

This test is similar to CCIR Recommendation 421, paragraph 3.5.3.

7.8.1.13 TEST FT-TV-4.1 VIDEO CHANNEL NOISE, POWER-SUPPLY HUM AND INTER-MODULATION DISTORTION

7.8.1.13.1 Objective

The objective of this test is to measure the spurious signals, power-supply hum, and intermodulation noise present in the video channel using the FT mode. This is a single-station test and is performed with a synchronous or·medium-altitude spacecraft.

7.8.1.13.2 Test Description

The spurious signals present in the unmodulated video baseband are measured using a spectrum analyzer. The display is photographed and the ratio of the spurious signal level to the level of a calibrated reference tone is determined.

The intermodulation distortion in the video baseband is measured employing a two-tone method with the distortion products displayed on a spectrum analyzer. The display is photographed and the ratio of the level of the distortion products to the level of a calibrated reference tone is determined.

The power-supply hum signals and their harmonics from both the ground-station and the spacecraft power supplies are measured on a wave analyzer, and their amplitudes and frequencies recorded.

7.8.1.14 TEST FT-TV-5.2 COLOR VECTOR ANALYSIS

7.8.1.14.1 Objective

This test will measure the performance of the FT mode when a color-television test signal is transmitted. The quality of the color information sent over the system is analyzed. This is a single-station test and is performed with a synchronous or medium-altitude spacecraft.

7.8.1.14.2 Test Description

The signal used for this test consists of the six basic-color-bar composite chrominance signal generated by the color encoder. This test signal is transmitted over the system.

Vector presentations of the composite signal applied to the transmitter and the received video are displayed on the Vectorscope. H-Line display of composite color-bar signal applied to transmitter and the received video are displayed on a waveform monitor. Photographs are taken of the up-link and down-link signals.

Errors in hue and saturation will be read directly from the photographs as errors in vector phase and amplitude, respectively.

7.8.1.15 TEST FT-TV-6.1 TV AUDIO-CHANNEL PERIODIC & CROSSTALK NOISE

7.8.1.15.1 Objective

The objective of this test is to measure the spurious noise, video-audio crosstalk, and power-supply hum present in the audio channel of the FT transmission system when used for television. This is a single-station test and is performed with a synchronous or medium-altitude spacecraft.

7.8.1.15.2 Test Description

A reference test tone is inserted into the TV audio channel,and the video-channel input is terminated. The reference level is established on a spectrum analyzer during calibration after which the reference tone is removed. The audio channel is examined for hum and spurious signals. Modulation is then applied to the video channel, and the audio channel is re-examined for spurious and video-to-audio crosstalk noise.

7.8.1.16 TEST FT-TV-6.2 TV AUDIO-CHANNEL FREQUENCY RESPONSE

7.8.1.16.1 Objective

The objective of this test is to measure the amplitude versus frequency response of the TV audio channel in the FT mode. This is a single-station test and is performed with a synchronous or medium-altitude spacecraft.

7.8.1.16.2 Test Description

The TV audio-channel frequency response is measured by transmitting a constant level audio tone at several frequencies in the channel bandwidth and measuring the receiver output-power level at each frequency.

7.8.1.17 TEST FT-TV-6.4 TV AUDIO-CHANNEL HARMONIC DISTORTION

7.8.1.17.1 Objective

The objective of this test is to measure the harmonic distortion of the television audio channel. This is a single-station test and is performed with a synchronous or medium-altitude spacecraft.

7.8.1.17.2 Test Description

The TV-audio-channel harmonic distortion is measured by transmitting a constant level audio tone at different frequencies within the channel passband and measuring the levels of the harmonics of each fundamental present in the received signal.

The received power-output level for each fundamental is measured with an RMS voltmeter and a wave analyzer will be set for zero-db reference with this signal. The analyzer is then used to measure the level of each harmonic within the channel passband.

7.8.1.18 TEST FT-TV-6.5 TV AUDIO-CHANNEL AMPLITUDE LINEARITY

7.8.1.18.1 Objective

The objective of this test is to measure the amplitude linearity of the television audio channel. This is a single-station test, and is performed with a synchronous or mediun altitude spacecraft.

7.8.1.18.2 Test Description

The TV audio-channel linearity response is measured by transmitting a 1-kHz tone through the system at different amplitude levels, and measuring the output level at the receiving end of the loop. The received power-output level is measured with an RMS Voltmeter, and the harmonic distortion generated at the high-level input signals is measured with a Wave Analyzer.

7.8.1.19 TEST FT-MX-1.1/MA-MX-2.1 MULTIPLEX-CHANNEL LEVEL STABILITY

7.8.1.19.1 Objective

The objective of this test is to determine the short-term and long-term level stabilities of voice-channel test tones, in the FT or MA mode. This is a single-station test and is performed with a synchronous or medium-altitude spacecraft.

7.8.1.19.2 Test Description

Stability is measured by inserting a 1-kHz test tone in two multiplex channels, recovering the tone from the receive multiplex-channel output after transmission through the system, and measuring its output level. A VTVM (RMS) measures the output level, and provides a level-detection output (dc)

for recording the tone level on a strip recorder. One low and one high channel are tested and recorded simultaneously. The recording indicates maximum level fluctuations and short-term (less than two seconds) fluctuations of amplitude. Long-term stability may be determined from the readings taken over longer periods of time.

7.8.1.20 TEST FT-MX-2.1/MA-MX-3.1 MULTIPLEX-CHANNEL FREQUENCY RESPONSE

7.8.1.20.1 Objective

The objective of this test is to measure the amplitude versus frequency response of frequency division multiplex (FDM) voice channels, in either the FT or MA mode. This is a single-station test and is performed with a synchronous or medium-altitude spacecraft.

7.8.1.20.2 Test Description

A test tone of constant amplitude is inserted into designated multiplex channels. The frequency of the tone is then varied, and the output power level of the signal from the multiplex channel measured with an RMS voltmeter. Multiplex-channel output-signal amplitude versus input test-tone frequency describe the frequency response. The test result is presented as a normalized curve from which the degree of nonuniformity may be determined.

7.8.1.21 TEST FT-MX-3.1/MA-MX-4.1 MULTIPLEX-CHANNEL LINEARITY

7.8.1.21.1 Objective

The objective of this test is to measure the amplitude linearity of a frequency division multiplex (FDM) voice channel in either the FT or MA mode. This is a single-station test and is performed with a synchronous-altitude spacecraft.

7.8.1.21.2 Test Description

A constant-frequency test tone is inserted in a designated multiplex channel. The input-power level of the test tone is varied while the output-power level of the received signal is measured on an RMS voltmeter. The test result is presented in terms of output power versus input power from which the degree of nonlinearity may be determined.

7.8.1.22 TEST FT-MX-4.1/MA-MX-5.1 MULTIPLEX-CHANNEL ENVELOPE DELAY

7.8.1.22.1 Objective

The objective of this test is to measure the audio envelope relative delay, as a function of frequency, in a multiplex voice channel, in the FT or MA mode. This is a single-station test and is performed with a synchronous-altitude spacecraft.

7.8.1.22.2 Test Description

This test is performed by transmitting a "signal" tone of variable frequency and "reference" tone of fixed frequency through the communications system via two adjacent multiplex channels. The signals are recovered at the multiplex-channel outputs and inserted in the receive section of a delay measuring set.

The "signal" output is a variable audio frequency which is amplitude-modulated by 125 Hz. The "reference" tone is amplitude-modulated by the same 125 Hz. After demodulation, the two 125-Hz signals are phase-compared. When the "signal" frequency is equal to the "reference" frequency, the delay-measuring set is adjusted for a zero-relative phase reading. The phase of the 125 Hz recovered by demodulation of the several discrete audio frequencies, transmitted sequentially on the "signal" channel relative to the phase of the 125 Hz recovered from the "reference" channel, indicates the variations in delay time via the "signal" channel, relative to the delay at the frequency of minimum delay. The "signal" frequency is varied over the passband range of the multiplex channel. The test result is presented as relative delay of the test-signal-versus-frequency of this signal from which the degrees of variation may be determined.

7.8.1.23 TEST FT-MX-5.1/MA-MX-6.1 MULTIPLEX-CHANNEL HARMONIC DISTORTION

7.8.1.23.1 Objective

The objective of this test is to measure the received distortion level at spurious frequencies within a single multiplex channel, in the FT or MA mode. This is a single-station test and is performed with a synchronous or medium-altitude spacecraft.

7.8.1.23.2 Test Description

A test tone is inserted in the designated multiplex channel and the received audio-frequency spectrum is measured with a distortion meter. This meter suppresses the tone fundamental and measures the RMS total of all harmonic and distortion products within the channel passband. Normally two test-tone frequencies, 500 Hz and 1000 Hz, are used, sequentially. When requested, a wave analyzer is used to measure, separately, the amplitude of the harmonic and distortion products. The test results are presented as a table of measured harmonic and distortion products of the test tones. The test provides a measure of the distortion incurred by single tones in passage throught the system. The test also provides a measure of the signal-to-total noise ratio of the channel.

7.8.1.24 TEST FT-MX-6.1/MA-MX-7.1 MULTIPLEX-CHANNEL WEIGHTED NOISE MEASUREMEN
7.8.1.24.1 Objective

The objective of this test is to determine the signal-plus-weighted-noise to weighted-noise ratio in selected multiplex voice channels, under noise-loaded and non-noise-loaded conditions. The test is performed in either the MA or FT mode; it is a single-station test and may be performed with either a medium-altitude or synchronous-altitude spacecraft.

7.8.1.24.2 Test Description

The weighted signal-plus-noise-to-noise ratio is obtained by comparing the measured power present in a multiplex receive channel, when a standard-channel test tone is transmitted, with the measured noise power present when the tone is removed. The system is noise-loaded by means of a white noise spectrum, adjustable in bandwidth and power level, to simulate up to a maximum of 1200 one-way voice channels.

The multiplex transmitting equipment is connected to the up-link transmitter (FM or SSB) input, and the -16 dbm, 1-kHz test tone is applied to the inputs of the two multiplex channels, sequentially. A terminated F1A weighting filter and the RMS VTVM are connected to the output of the corresponding voice channel. While the test tone is being transmitted, the power level of the test-tone-plus-weighted noise is recorded. When the test tone is removed, weighted noise only is recorded. The VTVM reads directly in dbm with no external 600-ohm termination required. The weighted signal-plus-noise to noise ratio may be calculated from the VTVM readings. For values in excess of 15 db S/N, the S/N in db is given to sufficient accuracy by the difference of the two readings of the meter (in dbm). For low values of S/N, a calculation is required.

In the MA mode, the test is performed with the doppler- and level-correction loops in normal operation. Tests shall be made utilizing the PM discriminator in the ground receiver.

7.8.1.25 TEST FT-MS-1.1/MA-MS-1.1 MULTIPLEX-CHANNEL ENVELOPE DELAY (MULTI-STATION)

7.8.1.25.1 Objective

The objective of this test is to measure the relative audio-envelope delay as a function of frequency, in a multiplex channel, for the case of a multi-station communications link in the FT or MA mode. This is a multi-station test and is performed with a synchronous-altitude spacecraft.

7.8.1.25.2 Test Description

See Test Description FT-MX-4.1/MA-MX-5.1 (Para. 7.8.1.22.2)

7.8.1.26 TEST MA-MS-2.1 MULTIPLEX-CHANNEL WEIGHTED-NOISE MEASUREMENT (MULTI-STATION)

7.8.1.26.1 Objective

The purpose of this test is to determine the weighted signal plus noise-to-noise ratio in selected multiplex voice channels at the several stations, under simulated loaded and non-loaded conditions. The test is performed in the MA mode, and either as a two- or three-station test, depending on which stations are available at the time of test. This test may be performed with either a medium-altitude or synchronous-altitude spacecraft.

In conducting each of the tests herein described, each station will measure the characteristics of all channels visible at that station, including the locally received and locally generated channel test tones. Depending on time availability, as many options should be performed as is possible so as to obtain data under the maximum number of different conditions.

7.8.1.26.2 Test Description

See Test Description MA-MX-7.1 (Para. 7.8.1.24.2)

7.8.1.27 TEST MA-RF-1.1 RF SIGNAL POWER AND PATH LOSSES

7.8.1.27.1 Objective

The objective of this test is to measure the uplink and downlink path-loss values. The former factor is a function of the earth-radiated power and spacecraft-received power. The latter factor is a function of the spacecraft-radiated power and earth-received power. Measurements of transmitter-output and receiver-input power are made. The desired results are calculated using the measurements and the known characteristics of the antenna and feed systems. This is a single-station test and is performed with a synchronous- or medium-altitude spacecraft.

7.8.1.27.2 Test Description

The earth-station SSB transmitter power is measured on a single-channel test-tone basis by calibrating the transmitter, and by monitoring the voltage amplitude of the 308-kHz gain monitor pilot tone which is inserted in the transmitter baseband, and is recovered from the baseband of a monitor receiver connected to the transmitter output. This technique provides a measurement of transmitter single-channel test-tone power which is independent of the total transmitter noise-loading signal.

The power received at the spacecraft is measured on a single-channel test-tone basis. The station pilot tone, F_p, is present in the earth-transmitter baseband at a power equivalent to -10 db below the single-channel test tone. It will experience gain in the transmitter and loss in the propagation path before being converted to iPhM with a deviation proportional to the received power at the spacecraft transponder, for transmission on the down-link. This pilot is recovered from the earth PhM receiver baseband, and its voltage amplitude is calibrated as a measurement of the single-channel test-tone power received at the spacecraft receiver input.

The spacecraft PhM transmitter power is obtained from the data transmitted on the VHF telemetry channel from the spacecraft.

The earth-receiver input power is determined from C/N measurements made in the earth PhM receiver.

The effective radiated power, levels which would be received by isotropic antennas, and the path losses are calculated from the results of the above measurements, and a prior knowledge of the antenna characteristics and spacecraft modulator sensitivity. This data is normalized for aspect angle and range.

7.101

The antenna gains are normalized at each site. This will require, for the transmit antenna, measuring the transmission line losses, diplexer losses, antenna feed-system losses, and all connector losses. The resulting loss, in db, is then subtracted from the gain of the transmit antenna, in db.

For the receive antenna gain, subtract the transmission line losses, diplexer losses, antenna feed-system losses, and all connector losses, in db, from the calculated antenna gain.

The calculated antenna gains are those obtained by classical antenna gain computation which takes into account area, curvature, frequency, efficiency, and aperture-to-medium coupling losses. Actual gain is determined by measurement of each db gain or los component.

The actual spacecraft antenna gains shall be obtained by subtracting the known and calculated spacecraft cable losses from the computed antenna gain values.

7.8.1.28 TEST MA-RF-1.2 UPLINK RF SIGNAL POWER AND PATH-LOSS VARIATIONS

7.8.1.28.1 Objective

The objective of this test is to determine, for the MA mode, the variations of th spacecraft received signal and the earth-to-spacecraft path loss, as functions of time. Calibrated strip-chart recordings of earth-transmitter output-power and spacecraft-received input-power levels will permit calculation of the desired parameters. This is a single-station test and is performed with a synchronous or medium-altitude spacecraft.

7.8.1.28.2 Test Description

The earth-station SSB transmitter power is measured on a single-channel te. tone basis by calibrating the transmitter, and by continuously monitoring the voltage amplitude of the 308-kHz gain monitor pilot tone which is inserted in the transmitter baseband, and is recovered from the baseband of a monitor receiver connected to the transmit. output.

The power level received at the spacecraft is measured on a single-channel test tone basis. The station pilot, Fp, which is present in the earth-transmitter baseband at - below test-tone channel level, experiences gain in the transmitter and loss in the propagation path before being converted to PhM in the spacecraft transponder, and transmitted as PhM to the earth receiver. This pilot is recovered from the earth-receiver baseband. Its voltage amplitude shall be recorded on a strip-chart recorder, as a function of time, and will serve as a measurement of the single-channel test-tone power received at the spacecraft-receiver input.

7.8.1.29 TEST MA-RF-1.3 DOWNLINK RF SIGNAL POWER AND PATH-LOSS VARIATIONS

7.8.1.29.1 Objective

The objective of this test is to determine, for the MA mode, the variations of the earth-station receiver input power and the spacecraft-to-earth path loss, as functions of time. Discrete measurements of spacecraft-transmitter output power and continuous measurements of the earth-station receiver input-power levels will permit calculation of the desired parameters. This is a single-station test and is performed with a synchronous-or medium-altitude spacecraft.

7.8.1.29.2 Test Description

The spacecraft-transmitter output power is obtained from the data transmitted via the VHF telemetry. (The station pilot, Fp, will be present in the baseband of the earth-station transmitter and therefore, no provisions are necessary to insert a signal in the earth-station transmitter to perform this test.)

Variations of the earth-station receiver input power is derived from calibrated strip-chart recordings of the AGC voltage developed in the earth receiver.

The total downlink path loss and variations are calculated from the power at the earth-station receiver input, the spacecraft-transmitter output power, antenna gains, and feeder losses derived from meter readings and strip-chart recordings.

7.8.1.30 TEST MA-MX-1.1 MULTIPLEX-CHANNEL FREQUENCY STABILITY

7.9.1.30.1 Objective

The objective of this test is to measure the short-and medium-term frequency stability, and the phase noise (very short-term stability) of signals in a multiplex channel, operating in the Multiple Access (MA) mode. This is a single-station test and is performed with a synchronous-altitude spacecraft.

7.8.1.30.2 Description

This test is performed by inserting a 1-kHz test tone, from the station timing buffer, in the multiplex channel at an input level of -16 dbm per channel. The test-tone channel is transmitted through the system, in the MA mode, and demodulated back to 1 kHz (nominal). The frequency variation of the received test-tone frequency is then measured

7.8.1.31 TEST MA-SP-1.1 CARRIER MODULATION DUE TO SPIN

7.8.1.31.1 Objective

The objective of this test is to measure the effects produced by non-uniformities in the spacecraft antenna patterns in the case of the spin-stabilized spacecraft which is rotating at rates between 50 and 150 RPM. This test is made in the MA mode; it is a single-station test and is performed with a synchronous-altitude spacecraft.

7.8.1.31.2 Test Description

This test is performed by inserting a 1-kHz test tone in two multiplex channels and measuring the amplitude and phase variations of the received 1-kHz tones, and amplitude variations of the received RF signal level. Observation of the PhM receiver AGC will permit analysis of the spacecraft-transmitter antenna amplitude-modulation effect; observation of the test-tone frequency variation will permit analysis of the phase distortion caused by the space-craft-receive antenna non-uniform characteristics, and observation of the test-tone level variation will permit analysis of the amplitude-modulation of the test tone caused by the spacecraft-receive antenna modulation effect and the spacecraft-transmit antenna phase-modulation effect.

7.8.1.32 TEST MA-SP-3.1 EARTH TRANSMITTER (AUTOMATIC LEVEL-CONTROL LOOP)

7.8.1.32.1 Objective

This single-station test will obtain data for the evaluation of the performance of the automatic level-control (ALC) system for the SSB Transmitter as measured in terms of its response to transient disturbances while operating in the real environment with a space-craft MA transponder and with medium-or synchronous-altitude spatial geometry.

7.8.1.32.2 Background Information

In the MA mode, the spacecraft may receive SSB signals from many earth stations with variable but unique path attenuations between each earth station and the space-craft. The PhM deviation produced in the spacecraft SSB/PhM transponder is, ideally, pro-portional to the received SSB signal amplitude. In order to provide uniform deviation for all channels of the FDM. each earth station must, on an individual basis precorrect its transmitt power. ALC systems, at each earth station, operate by local measurement of the deviation, produced remotely at the spacecraft for the assigned pilot signal, Fp. The ALC adjusts the RF drive to the SSB power amplifier to compensate for long-term variations in channel deviation and to adjust the average power for the Fp pilot channel to the value specified for a standard test tone in the Operations Plan.

The ALC system has a control range of +6db and -24db about the nominal SSB transmitted power, and a response speed of 0.1db per second.

7.8.1.32.3 Test Description

      This test is performed in the multiple-access mode. The transient response, using a step function perturbation of the control loop, is a conventional test in feedback control circuits. Its use in this instance, for testing the automatic SSB level control, provides data on the complete circuit including the propagation paths through space. Analysis of the data permits evaluation of the suitability of the design concept for both medium and synchronous orbits and will furnish data for system optimization.

      The transient disturbances are applied to the level control system by stepping the level of the detected station pilot, Fp, prior to its summation with the level control reference voltage. The level of the detected return pilot (Fp) is stepped by inserting a precision attenuator before the pilot amplitude detector and the loop differential amplifier. Small transient disturbances of fractional db magnitude which are not possible with simple conventional attenuators are possible by use of the precision Daven V-225 attenuator.

      A specific method for applying the disturbance is used to simulate a transient change in propagation losses in the SSB uplink. To the level control reference comparator (differential amplifier), the change in received signal appears as a change in deviation in the PhM system which is assumed to be proportional to the received SSB level at the spacecraft.

      Manual switching of the inserted test attenuator will occur at intervals which are long compared to the settling time of the control system. A two-pole selector switch, S_1, is arranged so that the inserted attenuation can be varied and a simultaneous independent indication of the transient may be obtainable for recording reference. The switch is operated at intervals which are long compared to the settling time of the system considering the magnitude of the applied step. For example, at maximum speed for the motor-driven attenuator (which is the system level controller) of 0.1 db per second, steps of 1 and 6 db will require at least 10 and 60 seconds, respectively, plus the propagation delay and loop-settling times.

      Tests are performed for several incremental transient error levels to completely examine performance of the level control over its normal operating range.

      Recorded data during the test shall include the status of the attenuator and the response of the level control system as measured by detection of level changes of the 308-kHz SSB transmitter monitor pilot tone. For correlation purposes, the spacecraft-transmitted power level (obtained from the telemetry receiver) and PhM receiver AGC levels are desired.

      Analysis of these data will permit determination of the maximum rate of response of the level control for large errors, system dead time, rise time, overshoot, and total settling times.

7.8.1.33.1 Objective

The purpose of this test is to statistically determine the principle transmission characteristics of the Frequency-Translation (FT) mode for a single station. In order to obtain large samples of data, the test is performed automatically in a predetermined sequence and entered directly into a computer for data correlation and processing.

7.8.1.33.2 Test Description

The data to be acquired on an automated basis is listed below:

1. Earth-transmitter power output
2. Received carrier level, spacecraft and earth
3. Multiplex channel S/N ratio (top and bottom of spectrum)
4. Baseband response, level stability, and frequency stability
5. Baseband idle noise level, and loaded noise-power ratio
6. Baseband short-term discontinues and/or noise disturbances (Data channel error count)
7. Doppler measurement
8. Station time.
9. Earth-station antenna coordinates and polarization
10. Spacecraft attitude

This data is obtained for the frequency-translation mode of operation, and with a earth receiver utilizing an FM discriminator. Analog data will be sampled at a rate of about 8 samples per second and sequentially entered into the computer through a multiplexer and A/D converter. Digital data will be acquired through counters and entered directly into the computer through its parallel digital inputs. Additional input sources to the computer for communications experiment data are furnished by other subsystems. Data from these sources include spacecraft transmitted and received power levels obtained from the spacecraft telemetry (PCM-DHE) subsystem, antenna orientation coordinates from the tracking subsystem, and time-code data from the station clock.

The test equipment connection and configuration required for the data acquisition is automatically switched through a sequence-controlled relay matrix which is established by a plug-in patch board and computer program.

Equipment and bridging jacks are used to facilitate test program set-up and monitoring during a test run.

The Communications Test and Evaluation Console (CTEC) test equipment is connected to the ATS system equipment. The experimental performance data as delineated

above is then automatically acquired in accordance with the time sequence plan of the Sequence Timing System. An entire data-acquisition sequence is completed in 60 seconds. The analog multiplexer contains 16 input gates, 12 of which are sampled at a rate of 100·pps., with the remaining 4 available as spares for future expansion capability. Thus each of the nine analog data items will be sampled at a rate of about 8 samples per second for a total of 100 samples of each data item within the basic 15 seconds of data acquisition. (The first 3 seconds of each test sequence is reserved for matrix switching time and response time of the thermal RMS reading test equipments)

Data measurements at each end of the total baseband spectrum yield the F1A weighted noise and tone levels in two multiplex voice channels. Comparison of these two readings yield a measurement of channel S/N ratios in the two channels.

In the first 30 seconds of the sequence, the loaded slot-noise level and a reference reading of the total noise-power loading level are provided. The first reading is used to calculate the system noise-power ratio, and from this result the channel S/N ratio can also be calculated. This calculation may then be compared against other measurements as a check for equipment or system operational discrepancies. The long-term baseband response readings will normally vary directly with the thermal noise level of the ATS system. A comparison of the unloaded versus loaded readings reveal the individual contributions of thermal and intermodulation noise to the total system noise.

Data information concerning the long-term baseband response and overall system gain stability are provided. Unequal changes in level of these tones indicate changes in the baseband amplitude response curve, while equal changes indicate variations in system gain.

Determination of the path-loss values for both the up and down paths is accomplished. As indicated, the spacecraft-received carrier level from the Telemetry Subsystem is fed to the computer at 3-second intervals. (This information is read once a day for the MCC readout and is stored as a constant in the computer).

Frequency stability of the ATS system is also measured by monitoring the instabilities in the received test tone.

With the FT Mode of operation, there is no need for "gross-doppler" correction because the baseband is recovered with reference to a transmitted carrier. Therefore it is not recorded for the synchronous-altitude spacecraft. However, for the case involving the medium-altitude spacecraft, the "differential doppler" across the baseband will require correction. This is accomplished by inserting a 100-kHz pilot from the station synthesizer into the baseband (video) amplifier at the transmitters. This signal is then extracted from the output of the earth receiver and is used as the source of the 100-kHz master oscillator for the receiving section of the multiplex equipment. Thus each receiving-channel demodulator is shifted in proportion to its frequency allocation in the baseband to compensate for the total

doppler shift encountered in transmission (both up and down paths). It should be noted that the data now includes both components of the doppler shift. At a single-earth site, the signal will be 1000 Hz plus or minus $2\delta_1$, but for 2 earth sites, the signal would be 1000 Hz plus or minus δ_1 plus or minus δ_2.

Information on the short-term baseband discontinuities or noise disturbances is determined. Since the data can be sent at a rate of at least 1200 and probably 2400 bps, the accumulated error counts will monitor the system transmission stability over increments of time approaching 0.75 millisecond or less. Any system outage or impulse noise burst extending over this time period has a strong probability of causing an error in the data-transmission channel. A cyclic repetition of data error bursts can be correlated against other system variables in order to determine causes of the system disturbances.

"Noise-Loaded" system data is obtained for the first 30 seconds of each minute. The final 30 seconds of the data-acquisition sequence obtains data for an "unloaded" system.

7.8.1.34 TEST MA-AT-1.1 AUTOMATED STANDARD MA SINGLE-STATION TESTS

7.8.1.34.1 Objective

The purpose of this test is to statistically determine the principle transmission characteristics of the Multiple Access (MA) mode for a single station. In order to obtain large samples of data, the test is performed automatically in a predetermined sequence and entered directly into a computer for data correlation and processing.

7.8.1.34.2 Test Description

The data to be acquired on an automated basis is listed below:

1. Earth-transmitter power output
2. Received carrier level, spacecraft and earth
3. Multiplex channel S/N ratio (top and bottom of spectrum)
4. Baseband response, level stability, and frequency stability
5. Baseband idle noise level, and loaded noise-power ratio
6. Baseband short-term discontinuities and/or noise disturbances (Data channel error count)
7. Doppler measurement
8. Station time
9. Earth-station antenna coordinates and polarization
10. Spacecraft attitude

The data is obtained from the multiple-access mode of operation and from the earth receiver utilizing a PhM discriminator. Analog data is sampled at a rate of about 8 samples

per second and sequentially entered into the computer through a multiplexer and A/D converter. Digital data is acquired through counters and entered directly into the computer through its parallel digital inputs. Additional input sources to the computer for communications experiment data are furnished by other subsystems. Data from these sources include the spacecraft-transmitted power level obtained from the spacecraft telemetry (PCM-DHE) subsystem, antenna-orientation coordinates from the tracking subsystem, and time-code data from the station clock. The test-equipment connection and configuration required for the data acquisition is automatically switched through a sequence-controlled relay matrix which is established by a plug-in patch board and computer program.

Equipment and bridging jacks are used to facilitate test program set-up and monitoring during a test run.

The Communications Test and Evaluation Console (CTEC) test equipment is connected to the ATS system equipment. The experimental performance data as delineated above is then automatically acquired in accord with the time sequence plan. An entire data-acquisition sequence is completed in 60 seconds. The analog multiplexer contains 16 input gates, 12 of which are sampled at a rate of 100 pps., with the remaining 4 available as spares for future expansion capability. Thus each of the nine analog data items will be sampled at a rate of about 8 samples per second for a total of 100 samples of each data item within the basic 15 seconds of data acquisition. (The first 3 seconds of each test sequence is reserved for matrix switching time and response time of the thermal RMS reading-test equipments.)

Measurements at each end of the total baseband spectrum yield the F1A weighted noise and tone levels in two multiplex voice channels. Comparison of these two readings yields measurement of channel S/N ratios.

In the first 30 seconds of the sequence, the loaded slot noise level and a reference reading of the total noise-power loading level is measured. The first reading is used to calculate the system noise-power ratio and from this result, the channel S/N ratio can also be calculated. This calculation may then be compared against other measurements obtained as a check for equipment or system-operational discrepancies. During the final 30 seconds of the automated timing sequence, readings of the idle or unloaded, slot and total baseband noise levels are provided. These readings will normally vary directly with the thermal noise level of the ATS system. A comparison of the unloaded vs loaded readings reveals the individual contributions of thermal and intermodulation noise to the total system noise.

Data information concerning the long-term baseband response and overall system gain stability are furnished. Unequal changes in level of the 1-kHz tones indicate changes in the baseband amplitude response curve, while equal changes indicate variations in system gain. This latter item also directly monitors the performance of the pilot level-control loop.

Determination of the path-propagation conditions for both the up and down paths is furnished. It should be noted that in the SSB (multiple access) mode, there is no carrier for conventional earth– transmitting and spacecraft-receiving power measurements. The earth-transmitter power (data item 7) is obtained by monitoring the 308-kHz control-pilot sending level at the transmitted baseband recovery circuits. The spacecraft-received carrier power is obtained by monitoring the station pilot level as received back at the earth receiver. Since the satellite converts its received signals into a PhM signal, the pilot level as received at the earth is a direct measure of its signal strength in the satellite receiver.

The frequency stability of the ATS system is recorded. In the MA mode, the tone-frequency variations are directly related to the accuracy of the doppler-control system. Equal variations of these two frequencies from the 1-kHz tone standard will measure the gain accuracy of the "gross-doppler" correction loop. Unequal variations of these frequencies will measure the gain accuracy of the multiplex "differential-doppler" correction loop. Data information required to determine the actual system doppler, which is to be compensated by the correction loops, is supplied. Thus a correlation of frequency stability against system doppler yields a plot of doppler-correction accuracies (gross and differential) versus actual doppler.

Information on the short-term baseband discontinuities or noise disturbances is furnished. Since the data can be sent at a rate of at least 1200 bps, the accumulated error counts will monitor the system transmission stability over increments of time approaching 0.75 millisecond or less. Any system outage or impulse-noise burst extending over this time period has a strong probability of causing an error in the data-transmission channel. A cyclic repetition of data error bursts can be correlated against other system variables in order to determine causes of the system disturbances.

"Noise-Loaded" system data is obtained for the first 30 seconds of each minute. The final 30 seconds of the data-acquisition sequence obtains data for an "unloaded" system.

7.8.1.35 TEST MA-AT-1.2 AUTOMATED MULTIPLE STATION TESTS (MA MODE)

7.8.1.35.1 Objective

These tests will determine the performance of the system with two or more stations communicating with the spacecraft, simultaneously. Each station will statistically determine the principal transmission characteristics of the Multiple Access mode in the presence of modulation from other stations. In order to obtain large samples of data, the tests are performed automatically in a predetermined sequence and entered directly into a computer for data correlation and processing.

7.8.1.35.2 Test Description

See Test Description, Test MA-AT-1.1 (Para. 7.8.1.34.2)

In the tests to be described in the following section, reference is made to the Rosman, Mojave, and Cooby Creek stations. It should be noted that this is purely arbitrary and was done to more easily define station configurations. Channel-frequency assignments and noise-loading requirements may be interchanged, within the maximum capability of a station, based on station availability. Noise level for all configurations will be based on full-channel loading.

The tests are performed by loading the satellite with 1200 channels and varying the number of channels transmitted by the participating stations.

7.8.1.36 TEST AN-SP-2.1 SPACECRAFT TRANSMIT ANTENNA PATTERN

7.8.1.36.1 Objective

The objective of this test is to obtain data so that patterns of the spacecraft-transmitting-(4-GHz) phased array antenna, which is mechanically despun, can be made.

7.8.1.36.2 Test Description

It was desirable to obtain a complete spherical (three-dimensional) representation of the spacecraft antenna-radiation characteristics during the early drift periods of the satellites before the spacecraft spin-axis was reoriented into the normal operating position. In idealistic antenna test orientation, the spacecraft spin axis would be parallel to the earth equatorial plane. The satellite spin axis, when referenced to a point on the surface of the earth, revolves through 360 degrees in the earth's equatorial plane over a 24-hour period. This condition will permit the vertical plane of the space craft antenna pattern to be measured. The spacecraft transmit antenna can develop either an omnidirectional or a unidirectional pattern. The PACE (ATS-1) electrically despun antenna system is used to develop the unidirectional pattern. On ATS-1, the omnidirectional pattern is developed when the PACE system is not operating. Since the satellite is spin-stabilized (approximately 96 rpm), the omnidirectional pattern can be measured in the horizontal plane as the spacecraft rotates. The PACE system can be oriented and synchronized either manually via telemetry from an earth station, or automatically, by utilizing the sun as a reference. To measure the unidirectional pattern, the PACE system can be controlled so as to rotate the transmit beam slowly in 0.7-degree increments. By utilizing the natural rotation of the spacecraft spin axis in the vertical plane and the spin-stabilized, or synchronous-controlled PACE system in the horizontal plane, the spacecraft can be oriented so that a complete spherical radiation pattern can be measured.

On ATS-3, the MACE antenna system is used to control the position of the uni-directional beam developed by the reflector in a manner similar to the PACE system on ATS-1. A fail-safe mode can also be employed if the MACE system malfunctions. In this mode, the reflector is blown off and an omnidirectional pattern is obtained.

To perform a spacecraft-transmit antenna-pattern measurement, the spacecraft (ATS-1 or -3) generates a 4-GHz unmodulated test signal in the PhM transponder which is transmitted to earth.

The earth-station antenna is pointed at the spacecraft. The 4-GHz spacecraft-transmitted carrier is received at the earth station by the PhM receiver. The output is then fed to the tracking or R&RR receiver where a calibrated analog AGC voltage is developed which is a function of the earth-station RF-received power level. A calibrated strip-chart recorder is used to record the demodulator AGC voltage output. The recorded data can be utilized to develop a spacecraft antenna pattern.

When the unidirectional antenna patterns are measured, the PACE or MACE system is activated in the eclipse mode and appropriate commands are transmitted to step the main beam through 360 degrees of the spacecraft horizontal plane at a rate of approximately 6.0 degrees per second. To develop a full-spherical (three dimensional) representation of the spacecraft antenna pattern, the measurement is conducted continuously for a 12-hour period. As the spacecraft antenna pattern geometric form is altered, as a function of time (12 hours), the instantaneous gain factor of the spacecrafts transmitted energy (4 GHz) received at the earth station will vary proportionally. The earth-station measurement of received RF signal power is correlated with the measured aspect angle of the spacecraft to develop the three-dimensional spacecraft-transmit antenna pattern.

7.8.1.37 TEST AN-SP-2.2 SPACECRAFT RECEIVE ANTENNA PATTERN

7.8.1.37.1 Objective

The objective of this test is to obtain data so that patterns of the spacecraft receiving (6 GHz) collinear array antenna, which is mechanically despun, can be made.

7.8.1.37.2 Test Description

The ATS-3 spacecraft has a unidirectional receive antenna pattern similar to that of the transmit pattern. Measurements of the receive antenna pattern are obtained by utilizing the same procedures as that for the transmit antenna.

The pattern measurement consists of transmitting a 3.25-MHz test tone in the SSB-FDMA/PhM mode, from the earth station to the spacecraft. The signal received by the satellite phase-modulates the down-link carrier. The deviation is a direct function of the received signal power. This signal level varies in accordance with the instantaneous relative gain of the satellite receive antenna over the scan angle covered.

The resulting PhM carrier signal from the spacecraft is received by the same earth-station antenna where a 70-MHz IF signal is obtained from the IF output of the PhM receiver and applied to the R&RR receiver. The 3.25-MHz tone signal is extracted from the IF signal by the R&RR receiver and applied to the Electrac demodulator which provides an AGC signal output. The AGC signal level developed from the 3.25-MHz tone is a direct function of the PhM modulation or test-tone power and thus becomes a direct representation of the instantaneous relative gain of the antenna pattern. This AGC signal is recorded on a strip-chart recorder and provides data from which an antenna pattern can be developed.

7.8.1.38 TEST FT-SP-1.1 REPEATER SATURATION CHARACTERISTICS

7.8.1.38.1 Objective

The objective of this test is to determine the repeater saturation characteristics of the FT mode in terms of (1) spacecraft-carrier output power versus spacecraft-received power and (2) total link carrier-to-noise density as a function of spacecraft-received power.

7.8.1.38.2 Test Description

To determine the output carrier power as a function of input received carrier at the spacecraft, the overall (C+ N) is measured as a function of P_{rs} and then the (N) is subcontracted from (C+ N).

The P_{rs} is varied by changing the earth-station transmitter power. An unmodulated carrier is sent from the earth station to the spacecraft using the earth-station SSB transmitter. Transmitter linearity is such that it allows incremental change in transmitter power to be obtained at baseband without recalibrating the transmitter RF output power.

The overall (C+ N) is measured in a 2.16–MHz IF noise bandwidth at the earth station. The received carrier is then translated 10 MHz at IF such that it is outside of the 2.16-MHz filter bandwidth. Then the noise power in the 2.16-MHz noise bandwidth is measured in the absence of the carrier. This process is repeated for each incrementation of the earth-station transmitter. When measured noise power (N) is subtracted from (C+ N), an indirect measurement of the variation of transponder carrier output is obtained. The overall C/N ratio can also be obtained from this process. By multiplying the C/N ratio by 2.16 MHz, the carrier-to-noise density C/N_o may be obtained.

7.8.1.39 EARTH STATION ANTENNA PATTERN

7.8.1.39.1 Objective

The purpose of this test is to determine the transmit-and-receive beam pattern of the earth-station antennas and to present a three-dimensional projection type of display from a plot of the data obtained. Two earth stations and an ATS spacecraft provide the long-range test facilities with which the transmit antenna pattern measurements are

performed. A single earth station and an ATS spacecraft are utilized to perform the receive antenna-pattern measurements.

7.8.1.39.2 Test Description

Measurement of the transmit antenna pattern is performed by transmitting a test-tone signal to the spacecraft from one earth station and receiving the modulated signal transmitted from the spacecraft by the second earth station. For the receive antenna-pattern measurements,only one earth station is utilized to receive an unmodulated carrier signal from the spacecraft.

A symmetrical antenna-pattern measurement for both transmit and receive is achieved by using the autotrack coordinates as the reference position for the center point of the scanned frame. The raster scanning of a complete pattern frame by the antenna is obtained automatically from a programmed tape. An entire pattern frame is produced by moving the antenna in steps of 0.05 degree along the X-axis after the completion of each scan along the Y-axis. A small error in the antenna pattern is created by the drift of the spacecraft during the time required to scan one frame.

An excursion angle of approximately 2 degrees is used along the X and Y-axis to cover a complete frame for the transmit and receive patterns. This angular excursion is sufficient to provide data for several side lobes in both the transmit and receive antenna patterns.

7.8.1.39.2.1 Test AN-SP-1.1 Transmit Antenna Pattern

Measurement of the transmit antenna pattern is performed with two earth stations and the station whose antenna pattern is being determined transmits a test tone of 3.25 MHz in the SSB-FDMA/PhM mode to the spacecraft. The resulting PhM modulated carrier signal from the spacecraft is received by the second earth antenna where a 70-MHz IF signal is obtained from the IF output of the PhM receiver and applied to the R&RR receiver. The 3.25-MHz tone signal is extracted from the IF signal by the R&RR receiver and applied to the Electrac demodulator which provides an AGC signal output. The test-tone power received at the spacecraft is a direct function of the transmit antenna pattern. PhM modulation of the satellite down-link carrier by the test-tone signal is also a direct function of the test-tone power. The AGC signal level developed from the 3.25-MHz tone in the Electrac receiver is a direct function of the PhM modulation or test-tone power and thus becomes a direct representation of the antenna pattern.

The downlink-received carrier level from the spacecraft remains constant durin the scan and only the modulation is received as a variant. The AGC signal is recorded and provides data from which a plot of the antenna pattern can be constructed in the form of a three-dimensional projection type of display.

7.8.1.39.2.2 Test AN-SP-1.2 Receive Antenna Pattern

The earth-receive antenna patterns are determined by utilizing one earth station to receive an unmodulated PhM carrier from the ATS spacecraft. A similar system configuration as that for the transmit antenna pattern is used with the exception of the downlink carrier which is received by the R&RR receiver. The resulting AGC signal developed in this receiver is recorded on a strip-chart recorder in conjunction with time information. Amplitude of the AGC signal varies as a direct function of the received signal-power level and conforms to the receive antenna-beam configuration.

The data provided by the recorded AGC signal is used to construct a plot of the receive antenna pattern in the form of a three-dimensional projection type of display.

7.8.1.40 TEST AN-SP-1.3 EARTH TERMINAL G/T

7.8.1.40.1 Objectives

The purpose of this test is to determine accurately the G/T ratio of the earth terminal antennas by utilizing a radio star of known radiating power density as a signal source. Where an earth station which is capable of performing this measurement has established its G/T value, it becomes the standard with which other stations can determine their G/T ratio by a comparison method of their C/N ratio measurements performed with an ATS spacecraft.

With the establishment of the G/T ratio of an antenna, the gain can be obtained by simply measuring the system noise temperature and adding it (in db) to the G/T value.

7.8.1.40.2 Test Description

The establishment of the G/T ratio of an earth-station antenna by utilizing a radio star is performed at the Rosman station. With an 85-foot antenna, this station is the only one having sufficient gain to provide the minimum signal plus noise-to-noise ratio required from the low-radiation level emitted by the radio stars. If the S+N/N ratio is less than 2 db, the measurement accuracy is degraded considerably.

The radio star Cassiopeia A was selected for this measurement because it provides the largest power density level at the 4-GHz frequency than two other possible sources consisting of Cygnus A and Taurus A. Radiation level of the latter two stars is appreciably lower than Cassiopeia A and therefore they are not suitable for use in this test.

The G/T for the Rosman antenna is determined by first measuring the S+N signal with the antenna pointing at the Cassiopeia A star. With the antenna fixed in its position the antenna beam is moved approximately 10 degrees away from the star's position. At this antenna position, the receive noise level and the system noise

temperature are measured. With the measured S+ N/N and a calculated constant containing the established radiated power density of the star, the G/T ratio is determined.

After the G/T measurement is completed for the Rosman antenna, the next step is to measure the carrier-to-noise ratio of the signal received from one of the ATS spacecraft. The Rosman antenna was centered on the spacecraft (in this case the ATS-3) and the spacecraft's antenna beam centered on the earth-station antenna for a maximum received signal. The latter function is performed to normalize all parameters that may effect the measured carrier-to-noise ratio. An unmodulated carrier is provided by the spacecraft for this measurement. After the carrier- plus noise-to-noise ratio of the spacecraft received signal is measured, the Rosman antenna is moved about 10 degrees away from the spacecraft and the system noise temperature is measured. During this process, the elevation angle is kept constant to minimize the measuring errors.

The next procedure is to measure the carrier-to-noise ratio at the Mojave station antenna. This antenna is centered onto the same spacecraft and the spacecraft antenna beam oriented so that is is centered on the Mojave antenna for a maximum re-ceived signal. The carrier-plus-noise-to-noise ratio and the system noise temperature are measured by utilizing the same procedure as that performed on the Rosman antenna.

With data measured at Rosman and Mojave, the G/T and the antenna gain for both stations are computed.

7.8.1.41 TEST AN-SP-1.4 EARTH TERMINAL ANTENNA POSITIONING CHARACTERISTICS

7.8.1.41.1 Objective

The purpose of this test is to determine the performance of the dynamic posi-tioning characteristics of earth-station antennas. This test is primarily an evaluation of the complete antenna servo-system for each earth station.

7.8.1.41.2 Test Description

The antenna positioning characteristics of each earth station were investigated to establish the optimum performance obtainable from the antenna system under different modes of operation. Results of this test will aid other experiments such as antenna pat-tern measurements which require a high-quality performance.

The ground-terminal antenna-pattern experiment requires the antenna under test to scan a raster pattern of specific dimensions at a controlled velocity to measure the RF characteristics of the directional RF patterns in the transmit (6 GHz) and receive (4 GHz) modes of operation. To develop a meaningful RF antenna pattern, the angular excursions and the rate-of-scan which are selected to produce the raster-scan positioning pattern are dependent upon: (a) the significant elements of the RF pattern that are desired;

(b) the resolution required to define these elements; (c) the data-sample rate; (d) the total time required to perform this measurement; and (e) the antenna-positioning characteristics. The RF pattern significant elements that are of interest during this experiment have been specified as that portion of the RF pattern that extends to the second side lobe. The data-sample rate is fixed at one sample per second, and the time necessary to conduct this experiment has been kept to a minimum to satisfy system stability and operational requirements. The measured RF pattern resolution is mainly dependent on the data-sample rate and the antenna-positioning characteristics. It is the antenna positioning characteristics that will vary depending upon which antenna is used to perform this experiment. Since the data-sample rate is low (1 per second) and a relatively high-resolution factor is desirable, the antenna scan rate is expected to approach the design limits of the system. A test program was conducted at the Mojave ATS station to investigate the antenna-positioning characteristics necessary to support the ground-terminal antenna-pattern experiment.

The antenna-positioning test program began with an attempt to determine the smallest angular excursion that the antenna servo subsystem could respond to when a step-positioning function was utilized. This test consisted of moving one axis of the antenna off boresight in the manual mode and allowing an auto-track mode error voltage, which was developed due to misalignment, to reposition the antenna. The servo-position and servo-error (velocity) voltages were recorded. Utilizing various angular offset positions, it was determined that the antenna would respond directly to a step function satisfactorily to offset angles of 0.06 degrees. These test results are not conclusive in themselves since the auto-track subsystem affected the test and the system was operated in a non-standard environment.

Two methods were instrumented to position the axes of the antenna in a raster scan pattern to measure the receive antenna RF patterns. The X-axis was positioned using an analog scan voltage (sinusoidual) added to the X-axis servo-input circuitry. The Y-axis was positioned in discrete angular steps, utilizing the digital data-positioning option, at the end of each excursion of the orthogonal plane (X-axis). The Y-axis was positioned utilizing the step function since this axis could not respond adequately at the required slow scan rate when an analog voltage was applied to the servo-drive circuitry.

7.9 DATA-ACQUISITION TECHNIQUES

7.9.1 GENERAL

Communications experiments are performed in accordance with two categories of Field-Test Procedures, Automated and Manual; table 7.7 lists the type which is used for each experiment. In order to evaluate the voluminous amount of data produced from the experiments, a unique system was developed to automate the data-acquisition and data-reduction process by generating a series of automated tests. These tests are employed to determine the statistical characteristics of the variant properties of the dominant communication parameters.

The stations have been implemented with a special console, the Communication Test and Evaluation Console (CTEC), for each in performing both manual and automated tests and with a data-processing system for performing automated tests.

The overall cycle of data acquisition and reduction is based on a data-requirement plan on which the field-test procedures are based and from which the site computer programs were prepared and the manual data-reduction techniques outlined. Automated data in near final form and manual data in the form of curves and charts are routed, in accordance with a data plan, to an analysis team where the automated data is culled and refined and where manual data is analyzed and presented for this report.

The discussions which follow describe the automated data-processing system and the manual acquisition techniques employed in the analysis of the received data.

7.9.2 AUTOMATED ACQUISITION

7.9.2.1 The ATS Data-Processing System Approach

One of the objectives of the ATS communications experiments is to implement a data system which will automate the data-acquisition and data-reduction process for a series of automated experiments. This is accomplished by manually setting in the constants and starting the test. Data is acquired automatically and then the test is manually terminated. Communications experiments conducted with previous satellite systems developed voluminous amounts of manually acquired test data. The recording and reduction of this data was both time-consuming and tedious. This was especially true for experiments which measured system performance parameters by obtaining large amounts of time variant data for statistical evalation. To achieve a reasonable degree of confidence in statistical data, a large sample of individual time-correlated data values is desired; therefore, automated techniques of acquiring and processing data were necessary.

Automatic data acquisition and preliminary on-site data processing were achieved by utilizing the Communications Test and Evaluation Console and Data-Processing System (CTEC/DPS) at each of three ground stations. Basically, the CTEC/DPS functions under the control of a stored computer program, absorbing communications data inputs, reducing the data and performing real-time computations which yield system parameters in engineering units. The operation of a given experiment sequence or "run" is initiated and terminated manually by the operator; however, the functions of acquisition, processing, and recording of data are entirely automated. Computational results are recorded on digital magnetic tapes which are sent to a centralized data-reduction and analysis facility at GSFC. The central facility data processor is a Univac-1108 computer which is programmed to absorb the contents of the magnetic tapes to derive statistical and correlative information from the data, and to provide printed readouts to the data analysts.

The CTEC hardware consists of various communications test equipment, automatic switching and patching facilities, analog recorders, and special measuring devices. The DPS consists of an SDS-910 computer, its peripheral equipment (X-Y graph plotter, paper tape punch and reader, magnetic tape deck, and typewriter), various interface control, and ancillary equipments which are contained within the CTEC. The CTEC interfaces with the DPS via an automated test-patch panel through which control signal levels, supplied by the DPS flow to the automatic-switching circuitry of the CTEC. In turn these signals control relays which determine the test-equipment configuration within the CTEC. Thus the computer program may select a given test-equipment configuration, acquire a specified amount of data, and then automatically activate a new relay combination, thereby allowing data acquisition under a new system configuration. In addition to these requirements which are directly associated with the automated communications experiment, the computer program absorbs telemetry data in digital form from the station pulse-code-modulated data-handling equipment (PCM-DHE), converts the coded input data words to engineering units, and prepares teletype compatible punched paper tape for distribution in quasi real time to the various ATS experiments.

7.9.2.2 Processing Details

      In general, the computer-program routines perform the function of: 1) non-real-time testing of DPS operational hardware status, and 2) controlling the operation and real-time data processing of the automated communications experiments. With regard to the latter of these two functions, the specific functions are: 1) acquiring raw input data from the various data-generating devices in the CTEC, 2) reducing and processing the raw input data to produce computed communications system parameters in engineering units, and 3) recording of computed data values on digital-magnetic tape. These functions are performed on site.

      The primary function of the analog data-processing subroutines is to convert the averaged raw-data values to engineering units and then to perform arithmetic operations on the converted values to produce meaningful communications system characteristics. Data is acquired and processed under two different system conditions throughout the course of the cycle. Constants are added to adapt for measurement meter settings and calibration reference effects, thereby producing values in units of dbm.

      The following analog parameters are computed and recorded each quarter-cycle (15-second time period):

    1) Voice-Channel "D" signal level (Low channel)

    2) Voice-Channel "D" signal-to-noise ratio

    3) Voice-Channel "G" signal level (dbm) (High channel)

    4) Voice-Channel "G" signal-to-noise ratio

    5) Slot-Channel noise level (dbm)

    6) Slot-Channel noise-power ratio

    7) Baseband noise level

    8) SSB transmitter power level (dbm) (FM transmitter power level in FT mode)

    9) Uplink path loss (db)

   10) PM receiver AGC level (dbm) (FM receiver AGC level in FT mode)

   11) Downlink path loss (db)

From the digital-data inputs,the communications experiment processing routines derive information associated with signal doppler shift, satellite range rate, and signal-transmission error rate. The two digital counters located in the CTEC supply the data from which the range-rate and doppler shift values are obtained. The third digital-data input is derived in the following manner; the Frederick-600 Data-Transmission Set detects errors which occur in the transmission of a 1200-bit-per-second signal. Each detected error results in an interrupt to the computer. The interrupt circuitry is especially connected for this case such that a single instruction routine is executed every time an interrupt occurs.

Automated test data is processed at the central facility and displayed in the form of real-time plots of minutely or secondly values of the communication parameters discussed above. For statistical analysis, the displays consist of time availability plots and histograms. In addition, medians, means,and ten-and ninety-percent spread factors are also computed and displayed. These latter factors are the values equalled or exceeded ninety or ten percent of the time for a given sample of data.

7.9.3 MANUAL ACQUISITION

In the ATS program, standard manual data-acquisition techniques are employed to obtain data on standard communication (S/N, NPR, TPR) path-loss and system (noise temperatures, antenna gains) parameters. Basically, any one of 20 preset manual tests can be performed by inserting a plugboard (FT or MA mode) into the Communications Test and Evaluation Console (CTEC) and depressing switches. These switches connect the desired test equipment with the input and outputs of the subsystems. The test signals are divided, amplified, filtered, detected, switched etc., according to the particular field-test procedure being performed. In turn, data is obtained in the following forms; tables, graphs, strip charts,printouts, and photographs. The type of form that is employed depends mainly on the test parameter under consideration and the method that is employed in analyzing the resulting test data.

In the majority of manual tests, the resulting test data is recorded, on-site, on specific tabularized data sheets and on the various display forms listed above. The data sheets contain all of the supplementary system information that is required for correctly interpreting the test results. In certain tests,the actual test results are also recorded on the data sheets. In a majority of the manual tests, the specific display such as graphs, photo-graphs, strip-chart recordings, etc., are utilized along with the data sheets to completely present the test results and the system conditions that prevailed when the test was per-formed.

In tests (S/N, NPR, TPR) where discrete measurements are obtained,the data is presented in table form. In addition, this data is illustrated showing the data

plotted as a function of a specific parameter (time, frequency, etc.). In cases where a single measurement is obtained, the results are always presented in table form. For a baseband frequency response test, a direct graphical presentation is obtained by using an X-Y plotter to automatically trace (plot) out the amplitude response as a function of frequency.

Strip-chart recorders are used to record the ground-transmit and received power levels and also the satellite-received power level as a continuous function of time. These parameters are also measured on a discrete basis in most of the manual tests and inserted in tabular form on data sheets that are used by the stations to record the test results. The X-Y plotter and strip-chart recorder operations are quite similar except that with the recorder, time is always an independent variable. In the case of the strip-chart recorder, long-and short-term time variations of the test parameter can be precisely determined by varying the chart speed. For short-term variations, the chart moves at a rate of two inches per second while for long-term variations, the rate is two inches per minute.

In the majority of manual TV tests, a standardized test signal is utilized for testing the various system characteristics that are important for TV quality. These tests measure the degradation that occurs to the test signal when passing through the system. In order to perform this analysis, it is necessary to photograph the input-and output-test signals. Therefore, photographs provide the main data-acquisition source for the TV tests.